TEMPORAL DYNAMICS AND NUTRITIONAL TARGETING OF MULTI-ORGAN METABOLIC DYSFUNCTIONS IN NON-ALCOHOLIC FATTY LIVER DISEASE

EVELINE GART

Propositions

1. A multiple organ treatment approach is key in combatting non-alcoholic fatty liver disease.
   (this thesis)

2. Nutritional treatments course-correct metabolic dysfunctions in non-alcoholic fatty liver disease.
   (this thesis)

3. Evolutionarily conserved metabolic regulatory systems cultivate metabolic syndrome in societies with easily available food.

4. Insulin sensitivity is an excellent lifestyle-marker.

5. Nutritional and life-style changes have precedence above long-term pharmaceutical drug treatment of metabolic disease.

6. Celebration cakes make science sweet.

7. Everything goes differently than planned.

Propositions belonging to the thesis, entitled

Temporal dynamics and nutritional targeting of multi-organ metabolic dysfunction in Non-Alcoholic Fatty Liver Disease

Eveline Gart Wageningen, 10 May 2023

Temporal Dynamics and Nutritional Targeting of Multi-organ Metabolic Dysfunctions in Non-Alcoholic Fatty Liver Disease

Eveline Gart

Thesis committee

Promotor
Prof. Dr. J. Keijer
Professor of Human and Animal Physiology
Wageningen Universiteit & Research

Co-promotors
Dr. M.C. Morrison
Metabolic Health Research
TNO, Leiden

Dr. R. Kleemann
Metabolic Health Research
TNO, Leiden

Other Members
Prof. Dr. Eric Hazebroek, Wageningen University & Research
Prof. Dr. A.J. Han Moshage, UMC Groningen
Dr. H.A.M. Rick Mutsaers, Aarhus University, Denemarken
Dr. Debby P.Y. Koonen, University of Groningen

This research was conducted under the auspices of the Graduate School VLAG Graduate School (Biobased, Biomolecular, Chemical, Food, and Nutrition sciences).

Temporal Dynamics and Nutritional Targeting of Multi-organ Metabolic Dysfunctions in Non-Alcoholic Fatty Liver Disease

Eveline Gart

Thesis
submitted in fulfilment of the requirements for the degree of doctor
at Wageningen University,
by the authority of the Rector Magnificus,
Prof. Dr. A.P.J. Mol,
in the presence of the
Thesis Committee appointed by the Academic Board
to be defended in public
on Wednesday 10 May 2023
at 1:30 in the Omnia Auditorium.

Eveline Gart
Temporal Dynamics and Nutritional Targeting of Multi-organ Metabolic Dysfunctions in Non-Alcoholic Fatty Liver Disease

PhD thesis, Wageningen University, Wageningen, the Netherlands (2023)
With references, with summary in English

ISBN: 978-94-6447-574-6
DOI: https://doi.org/10.18174/586071

Table of contents

CHAPTER

General introduction and thesis outline

1.1 What is Non-alcoholic fatty liver disease?

Non-alcoholic fatty liver disease (NAFLD) is a chronic metabolic disorder characterized by excessive fat accumulation in the liver [1]. NAFLD is the hepatic manifestation of the metabolic syndrome and is characterized by obesity, visceral fat accumulation, hyperlipidemia and insulin resistance [1]. Overconsumption of energy-dense diets high in fat and sugar contribute to the development of NAFLD. Recently it has been suggested that metabolic (dysfunction) associated fatty liver disease (MAFLD) is a more relevant encompassing name for the liver disease. In addition, NAFLD excludes the role of alcohol consumption while it can be part of the unhealthy lifestyle [2].
Clinically, NAFLD includes a broad spectrum of liver damage, starting with fat accumulation (steatosis) in >5% of the hepatocytes which can progress to hepatic inflammation (non-alcoholic steatohepatitis; NASH) and fibrosis [1]. However, the pathophysiology of NAFLD development is still incompletely understood, which may contribute to the fact that at present no approved treatments are available. Therefore, NAFLD is currently considered to be one of the greatest global health problems and a disease area of unmet medical need. More specifically, there is an urgent need for innovative treatment strategies to correct metabolic dysfunctions that underlie NAFLD development.

1.2 Prevalence, public awareness, and diagnosis of NAFLD

The main risk factors for the development of NAFLD are obesity and insulin resistance [1]. As a result of the dramatic increase in obesity to epidemic proportions, the clinical and economic burden of NAFLD has also increased considerably [3]. NAFLD currently affects 25-30% of the adult population [4] and is the most common cause of liver transplants in young adults (<50 years) [5]. NAFLD is also becoming a rising problem in children, with a mean prevalence of 5-10% in the general population and up to 40% in obese children [3,6].
The prevalence may even be higher than the present estimations due to the difficulty of diagnosing NAFLD. The current “gold” standard for diagnosing and staging of NAFLD is a liver biopsy, an invasive procedure not without risk. As a consequence, population prevalence is usually estimated by circulating biomarkers (e.g. liver enzymes ALT and AST) and/or evidence of fatty liver on an ultrasound scan or via magnetic resonance imaging. However, these non-invasive techniques are less accurate to assess the severity of NAFLD and cannot distinguish between simple steatosis or NASH. In addition, hepatic steatosis generally does not lead to symptoms until the development of advanced fibrosis, therefore the disease may go undetected for years. Hence, there is a high need for more sensitive and specific non-invasive biomarkers [7]. A better understanding of the development of the disease may help to develop new, easily accessible, and specific biomarkers. Non-invasive biomarkers can be used for risk-stratification of adverse outcomes, improve monitoring of disease progression, and determine the response to treatments.
Another potential reason why NAFLD prevalence may be higher than current estimations and why treatments are still lacking is the insufficient public awareness of the severity of NAFLD development. Reports have shown that among 308 patients in those with major risk factors for NAFLD (overweight/obese, insulin resistant, or both overweight/obese and insulin resistant), the rates of awareness of NAFLD were low (19%, 23%, and 24%,

respectively) [8]. Supported by a recent study among young adults (43-55 years) that merely 16 of 667 (2.4%) participants with CT-defined NAFLD were aware of a NAFLD diagnosis [9]. More importantly, physicians see a substantial number of high-risk patients but are insufficiently aware of screening methods and diagnosis of NASH. A recent survey among physicians in the USA demonstrated that only 18% of primary care physicians and 30% of gastroenterologists were familiar with common NASH screening methods to assess NASH risk (e.g. blood test or liver scans) [10]. In addition, 46% of endocrinologists and 42% of primary care physicians would refer high-risk patients to a specialist [10]. This may thus contribute to low NASH diagnosis and the low referral rate indicates that also treatment necessity is underestimated.

Currently, NAFLD disease stage in liver biopsies is determined with the NAFLD activity score (NAS). The NAS score includes a semi-quantitative scoring of NASH, as well as a separate NASH fibrosis staging score. However, to determine biological effects, the NAS score is inadequate, the categorical system is too crude as sometimes improvements are seen *within* one stage which are not visible on the scale employed in the NAS score. Therefore, to assess biological effects a continues NAFLD scoring system would be better. Consequently, to enable a more accurate assessment of biological effects in preclinical studies a continuous NAFLD scoring system for rodent models has been developed [11] that is based on the human NAS scoring system [12]. To score NAFLD in rodent livers hematoxylin and eosin staining's are used to determine 1) macrovesicular steatosis: one large lipid droplet that fills the cytoplasm of hepatocytes, 2) microvesicular steatosis: multiple small lipid droplets that fill the hepatocytes, 3) hepatocellular hypertrophy: abnormally enlarged hepatocytes, which was added to replace the scoring of ballooned cells as they are hardly present in rodent models and subject to significant intra-observer and inter-observer variation - more specifically, the ballooning scores cannot be reproduced by expert pathologist themselves when inspecting a tissue specimen twice - [13], 4) lobular inflammation: infiltrates of immune cells. Liver fibrosis is scored separately using Sirius red staining to determine the hepatic collagen content. Besides the need for implementation and validation of non-invasive biomarkers, current scoring systems could also benefit from the application of digital scoring systems to better standardize histological outcomes.

1.3 Pathophysiology of NAFLD is incompletely understood

In humans, NAFLD is a disease that takes decades to develop with obesity as the main risk factor and insulin resistance as the main driving force. NAFLD is a multifactorial disease in which progression from simple steatosis to NASH and fibrosis is driven by a complex interplay between many molecular and cellular mechanisms [1]. The disease mechanisms are thought not be limited to the liver, but also extrahepatic signals originating from other key metabolic organs such as the adipose tissue and the gut may contribute [3]. Current knowledge on the contribution of other organs and driving factors is based mostly on studies that investigate these at a single time point (typically end-stage disease). However, such studies provide no insight into the temporal dynamics and chronology, which therefore remains poorly understood.

1.3.1 Liver pathophysiology in NAFLD

In the liver, lipids start to accumulate when the rates of hepatic lipid uptake and production exceed the rates of oxidation and export (e.g., via VLDL lipoprotein particles). The intrahepatic lipids that accumulate are predominantly triacylglycerides (TAGs) [14]. Insulin resistance in NAFLD patients can exacerbate hepatic lipid accumulation by stimulating de novo lipogenesis (DNL; via activation of SREBP1c, the master regulator of DNL) [4]. The development of insulin resistance of tissues may either involve local tissue inflammation or can be a consequence of lipid-induced insulin-resistance [14]. For example, specific bioactive lipids such as diacylglycerols (DAGs) [5] have been shown to directly interfere in insulin signaling at the level of its receptor. These DAGs are intermediate products of triacylglycerol (TAG) synthesis, in which free fatty acids (FFA) are incorporated into DAGs and consequently into TAGs. The latter are considered to be a safe storage form of lipids in contrast to the bioactive DAGs. The primary site of DAG synthesis is the endoplasmic reticulum (ER), an organelle that synthesizes, folds, and secretes various proteins, among which are proteins that enable the secretion of hepatic lipids (e.g., VLDL). The accumulation of DAGs in the ER can cause disruption of the endomembrane system, i.e., cause ER stress with diminished lipid mobilization and thereby exacerbate the accumulation of intrahepatic lipids.

The high liver lipid load in NAFLD also challenges the peroxisomes and mitochondria to utilize the excess fat. Excessive lipid oxidation in the peroxisomes and mitochondria gives rise to a chronic increase in reactive oxygen species (ROS) [15,16]. Elevated ROS production together with an impairment in antioxidant capacity can result in an imbalance that is harmful for the cell, a condition referred to as oxidative stress [16]. Mitochondria, as one of the major sources of ROS production, are particularly susceptible to oxidative damage. ROS species can also react with other critical cellular constituents including DNA, proteins and lipids which can result in the formation of for example 4-hydroxynonenal (4-HNE) [17].

Inflammation in the liver may develop as a consequence of cell damage that results from these metabolic dysfunctions. Normally, cells will prevent the overaccumulation of damaged mitochondria, ROS species or damaged ER to limit DNA damage and genomic instability by inducing autophagy or apoptosis. However in case of severe damage and a collapse in ATP levels, necrosis can occur which will trigger the immune system to remove the cell debris [18]. Furthermore, the activation of local macrophages into a proinflammatory phenotype will lead to the secretion of cytokines and chemokines that recruit monocytes and neutrophils to the liver causing mixed inflammatory infiltrates [9]. In addition, some lipids have been shown to directly trigger inflammation; 1) polyunsaturated fatty acids (PUFA) omega-6 and omega-3 can be metabolized to oxylipins which are implicated in the potentiation of pro- and anti-inflammatory responses [19], 2) saturated free fatty acids can bind and activate toll like receptor 4 [20], 3) cholesterol can induce the formation of cholesterol crystals which can activate the NLRP3 inflammasome [21], 4) lipid-oxidation induced formation of 4-HNE can bind and activate the inflammatory receptor Src, thereby activating Nf-kB signaling [22]. Conversely, inflammation can promote lipid accumulation as pro-inflammatory stimuli can activate and induce TBK1, which has been shown to represses energy expenditure by phosphorylating and inhibiting the key metabolic regulator AMPK [23].

Hepatocellular damage and inflammation can also activate repair mechanisms, i.e., stellate cells which are the main producers of extracellular matrix proteins including collagens. Persistent metabolic dysfunctions and thus consistent damage and inflammation, in case of NASH, can result in excessive collagen production by the stellate cells and subsequently scarring and liver fibrosis. During liver injury, transforming growth factor β (TGF-β) is the most potent fibrogenic cytokine and a key regulator in promoting HSC activation [24]. Quiescent HSC comprise 10% of the liver and, in response to chronic liver injury, HSC will be activated and can expand to approximately 15% of the total liver cells [25].
In addition to the reported metabolic dysfunctions in the liver of NAFLD patients, growing evidence suggests that the development of NAFLD is closely linked to the homeostasis of other organs, in particular other key metabolic organs such as white adipose tissue and the gut with its microbiota [26].

1.3.2 The role of adipose tissue in NAFLD pathophysiology
In obesity-associated NAFLD visceral white adipose tissue (WAT) accumulation has important clinical implications and is an independent risk factor of the metabolic syndrome [27]. In principle the main role of WAT is to store and release energy in the form of FFA when needed. The adipose tissue is also an endocrine organ, which produces adipokines such as leptin and adiponectin that are involved in the regulation of nutritional status, energy storage and interact with the immune system (e.g. adipogenesis, lipolysis, browning, inflammation, apoptosis) [28]. Increased WAT lipid storage during obesity can lead to hyperplasia (an increase in cell number via adipogenesis) or stimulate hypertrophy (an increase in adipocyte size). Especially the large hypertrophic adipocytes due to prolonged metabolic overload have been associated with adipose tissue dysfunction, characterized by the increase in secretion of adipokines and infiltration of immune cells and insulin resistance [29]. Typical for inflamed WAT is the clustering of immune cells around adipocytes, so called crown-like structures. Similar as described for the liver, inflammation and the accumulation of specific lipids, such as DAGs, can cause insulin resistance of the adipose tissue. In insulin-resistant adipose tissue the brake on lipolysis is impaired leading to an increased secretion of FFA which typically flux to the liver, thereby promoting NAFLD development. The FFA flux from adipose tissue has been shown to account for 60% of TAG accumulation in livers of NAFLD patients, while only 25% of the TAGs is derived from de novo lipogenesis and 15% from the diet [30].
Adipokine secretion from WAT may also affect homeostasis of other organs such as the liver, as leptin and adiponectin have pro- and anti-inflammatory potential, respectively [28]. In addition, leptin directly stimulate hepatic stellate cell activation in the liver [31,32], another direct link of how WAT can promote NAFLD progression. However, the temporal dynamics of metabolic dysfunctions/pathogenic events in visceral and subcutaneous WAT occur in relation to NAFLD development is unknown.

1.3.2 The role of the gut and its microbiota in NAFLD pathophysiology
The gut and its microbiota together form a homeostatic system to cope with metabolic factors (e.g., from diets) but it also forms a barrier to protect the host against detrimental external factors (e.g. pathogenic bacteria). A critical role of the microbiota in NAFLD development is likely, because mice without a gut microbiota were found to be resistant

to diet-induced obesity, insulin resistance and liver steatosis [33,34]. The microbiota generates a variety of metabolites from dietary products. These metabolites are, for example, produced via fermentation especially in the colon of complex digestible carbohydrates and proteins, forming short chain fatty acids (SCFAs), including acetate, propionate, caproate and butyrate. These SCFAs form an important energy source, but also function as signaling molecules via G-protein coupled receptors expressed on colonic cells, adipocytes and hepatocytes [35]. In addition, bile acids are produced in the liver, but are modified and metabolized by the gut microbiota. In the gut these bile acids mainly function as emulsifiers and allow the absorption of dietary fats, lipophilic vitamins, or drug molecules. In addition, bile acids can also activate the nuclear receptors in the intestine and liver and via these receptors regulate bile acid synthesis, lipid and glucose metabolism (e.g. via PPARGC1A and PPARα) [36].
In NAFLD patients an altered microbiota composition with reduced alpha-diversity (a measure of microbiome variety within one sample) has been reported. This altered microbiota of the gut may contribute to NAFLD development via an altered processing of diet components and subsequent changes in the production of SCFAs and bile acids [35]. Consequently, an alteration in microbiota composition and its microbial products can alter and impair gut barrier function [35]. This impairment in the gut can result in increased leakiness (e.g., translocation of bacteria, endotoxins, and other inflammatory mediators). Consequently, gut-derived metabolites can impact the liver, because approximately 70% of liver blood supply is derived from the intestines via the portal veins [37].
Despite the current knowledge on the potential role of many molecular and cellular mechanisms in NAFLD development, it remains unclear when specific pathogenic events in the liver itself, in the gut and in adipose tissue occur and contribute to NAFLD development (e.g., whether increased gut dysfunction precedes WAT dysfunction and NASH or whether the various organ dysfunctions develop simultaneously with NASH).

1.3.3 The use of the Ldlr-/-.Leiden mouse model to study NAFLD pathophysiology
To prevent severe disease, it is important to better understand the early phase of NAFLD development. In the early stages many metabolic derangements are likely reversible whereas late-stage disease (fibrosis) is more difficult to reverse. For early-stage NAFLD research and the development of biomarkers translational models play an important role. Translational models allow to follow disease development with time, under carefully controlled conditions and allow that the various implicated organs can be sampled and studied. Both aspects are very difficult or impossible to attain in humans. Ideally, animal models should mimic both the histopathology and pathophysiology of obesity associated NASH development observed in NASH patients.
The Ldlr-/-.Leiden mouse model when fed an energy dense diet (high in fat and sugar) develops obesity, dyslipidemia, and insulin resistance, essentially as observed in NASH patients. The translational value of this model has been demonstrated on NASH histology, molecular pathways and plasma metabolomics [38,39]. The mouse model is genetically modified in the low-density lipoprotein receptor (Ldlr) gene in such a way that it encodes a truncated non-functional Ldlr protein that will not bind LDL lipoproteins. As a consequence, the clearance of apoB containing lipoprotein particles (i.e., VLDL and LDL) by the liver is attenuated, resulting in a lipoprotein profile that reflects that of humans.

Therefore, the Ldlr-/- mouse model is a good candidate to study mechanisms, interventions and biomarkers in metabolic disease and their complications such as NAFLD/NASH. Preclinical research with this model aims to improve the predictability of efficacy and safety of NAFLD interventions by detailed knowledge of the dynamical multiple organ metabolic dysfunctions underlying NAFLD development.

1.4 Treatment of NAFLD

The pathophysiology of NAFLD is thus complex and still incompletely understood with no approved therapeutic treatments currently available. The advice for NAFLD patients is limited to changes in life-style, a situation that has altered little in over the past 10 years while the number of NAFLD patients continues to rise globally [28].

The heterogeneous mechanisms that are affected in NAFLD development has resulted in a wide range of drug classes (from small molecule inhibitors to antibodies) and drug targets. Interventions that are currently being developed target lipid metabolism, insulin signaling, inflammation, cell death, or fibrosis mechanisms [40]. Specifically fibrosis is associated with an excess all-cause mortality and liver related mortality in the general population [41]. Therefore, a lot of attention has been on management of this late stage process with encouragement of the Food and Drug Administration (FDA) and European Medicines Agency (EMA) in their guidelines and standards for drug development for NAFLD [40]. In the process of drug development, a treatment is reviewed on safety, dosage and target engagement based on preclinical and early clinical studies. Subsequently in phase 2 and 3 efficacy and side effects of interventions are investigated in clinical trials. Phase 3 approval by the FDA requires an improvement of either liver fibrosis without worsening of NASH or resolution of NASH with no worsening of liver fibrosis [40]. Unfortunately, with this focus on the late stage disease, mostly liver fibrosis, so far most of the current treatment approaches have failed and did not yet make it to the final phase 4, the post-marketing surveillance in public. In addition, interventions are currently not evaluated on cardiovascular disease effects. However, cardiovascular disease is driven by similar risk factors as NAFLD and is still the major overall cause of mortality in NAFLD patients independent of other metabolic comorbidities [39].

All in all, there is a very limited success in therapeutic approaches for NASH. This lack of success in combination with the high societal burden of the disease asks for alternative approaches. Maybe of even greater importance is the perception about the likelihood of disease progression to NASH. Simple steatosis in patients with metabolic syndrome is not considered a disease state, but preventive measures at this stage may hold the key to effective end stage disease reduction. The lack of success in combatting end stage disease, urges to focus more on prevention and on a more integrative approach in the development of treatments.

An alternative approach to more early disease stage or preventative strategies makes the use of nutritional strategies appealing. These nutritional strategies are more likely to correct metabolic derangements in multiple organs simultaneously when compared to a classical pharmacological ‘single target approach’. Especially considering the heterogenous mechanisms and multiple organs that are affected in NAFLD.

1.5 Aims and outline of this thesis

NAFLD is a complex disease and the lack of treatment options in combination with the high societal burden of NAFLD requires alternative treatment approaches. However, the pathophysiology of NAFLD development is still incompletely understood. Advancing our understanding of dysfunctional metabolic processes underlying NAFLD pathogenesis and their complex interplay is key for the development of successful interventions. In order to do this, we need translational models for NASH in which disease development and potential non-invasive biomarkers can be studied. At the same time, more knowledge about the dynamics of pathogenic processes enables optimal timing of the start of a treatment.

Therefore, the overall aims of this thesis were to gain more insight into the temporal development of metabolic dysfunctions that underlies obesity-associated NAFLD. More specifically the aims were:

1. To unravel the sequence of metabolic dysfunctions during NAFLD development in liver, gut and adipose tissue as well as relevant metabolites released by these organs.
2. To explore concepts to correct metabolic derangements in multiple organs using nutritional interventions and assess their potential to attenuate NAFLD development. Including the assessment of various anti-obesogenic hepatoprotective treatments to correct lipid processing, by increasing the oxidation of lipids or altering/reducing the storage of lipids.
3. To further investigate gut-WAT-liver crosstalk during NAFLD development by:
    a. Examining diet-independent correlations of organ dysfunction with the gut microbiota composition.
    b. Exploring whether a treatment that targets the gut microbiota could also have beneficial effects beyond the gut.
    c. Testing the effects of direct supplementation of microbiota-derived metabolites.

In **chapter 2** the aim was to gain insight into the temporal dynamics and chronology of metabolic dysfunctions in multiple organs (liver, adipose tissue, gut) during NAFLD development. Metabolic dysfunctions in the Ldlr-/-.Leiden mouse model were compared to those reported in NASH patients, to further assess the translational value of this NASH mouse model. These metabolic dysfunctions investigated were not limited to the liver itself, but also the role of the white adipose tissue and gut therein. Knowledge on the sequence of events will help define key pathogenic mechanisms and identify factors formed in these tissues that are relevant for fatty liver progression towards NASH and fibrosis.

Next, we aimed to study innovative nutritional treatment strategies and their potential mechanisms of action. For this, treatments were used that affected processes in the liver, white adipose tissue or gut/microbiota, or a combination of these, to restore organ homeostasis. In **chapter 3** we investigated nutrients that could potentially restore homeostasis by improving mitochondrial function and thereby increase lipid oxidation, using a combination of L-carnitine and nicotinamide riboside, with the respective monotreatments as reference groups. In **chapter 4** we studied the effects of long term

treatment with PUFA-rich krill oil on NAFLD development, because of the ability of krill oil to affect lipid composition and inflammatory signaling based on *in vitro* and/or short term studies. In **chapter 5**, we tested the hepatoprotective effects of the individual branched chain amino acids valine and isoleucine in a therapeutic setting, i.e., starting treatment when obesity associated NAFLD is already present.
Lastly, organ crosstalk in NAFLD development was investigated mainly focusing on the gut, WAT, and the liver and to a smaller extent on the brain. In **chapter 6** this last aim was addressed by examining diet-independent correlations of organ dysfunction with the gut microbiota composition at multiple sites, the mucosal and fecal compartment in the ileum and colon. In **chapter 7**, we tested whether prebiotic 2'-fucosyllactose, a human milk oligosaccharide, primarily thought to improve gut health, could also affect more distant organs like the liver. Furthermore, direct effects of supplementing microbiota-derived metabolites on NAFLD development were tested. In **chapter 8** this was investigated with the SCFA butyrate, which can exert metabolic improvements and has anti-inflammatory activities, but it was unknown whether it could also alleviate fibrosis in the context of obesity-associated NASH. Potential direct anti-fibrotic effects and mechanisms were further evaluated in primary human hepatic stellate cells. In **chapter 9** we tested the SCFAs caproate and propionate as therapeutic treatment in NASH and explored effects on more distant organs like the brain in the Ldlr-/-.Leiden mouse model, by evaluating SCFA effects on obesity-associated neuropathological changes.
Finally, the main findings of this thesis, its implications, and directions for future research are discussed in **chapter 10**, followed by a short summary of the thesis.
Taken together, in this thesis we provide new insights regarding the dynamics of metabolic dysfunctions in multiple organs during NAFLD development. The importance of these metabolic dysfunctions will be substantiated by investigation of nutritional strategies that target these key disease processes to attenuate NAFLD development.

References

[1] Loomba R, Friedman SL, Shulman GI. Mechanisms and disease consequences of nonalcoholic fatty liver disease. Cell 2021;184:2537–64. https://doi.org/10.1016/j.cell.2021.04.015.

[2] Eslam M, Newsome PN, Sarin SK, Anstee QM, Targher G, Romero-Gomez M, et al. A new definition for metabolic dysfunction-associated fatty liver disease: An international expert consensus statement. J Hepatol 2020;73:202–9. https://doi.org/10.1016/J.JHEP.2020.03.039/ATTACHMENT/C4E77195-9CBF-4F84-B420-5AFA6F53338D/MMC2.PDF.

[3] Anderson EL, Howe LD, Jones HE, Higgins JPT, Lawlor DA, Fraser A. The Prevalence of Non-Alcoholic Fatty Liver Disease in Children and Adolescents: A Systematic Review and Meta-Analysis. PLoS One 2015;10. https://doi.org/10.1371/JOURNAL.PONE.0140908.

[4] Younossi ZM, Koenig AB, Abdelatif D, Fazel Y, Henry L, Wymer M. Global epidemiology of nonalcoholic fatty liver disease—Meta-analytic assessment of prevalence, incidence, and outcomes. Hepatology 2016;64:73–84. https://doi.org/10.1002/HEP.28431/SUPPINFO.

[5] Doycheva I, Issa D, Watt KD, Lopez R, Rifai G, Alkhouri N. Nonalcoholic Steatohepatitis is the Most Rapidly Increasing Indication for Liver Transplantation in Young Adults in the United States. J Clin Gastroenterol 2018;52:339–46. https://doi.org/10.1097/MCG.0000000000000925.

[6] Yu EL, Schwimmer JB. Epidemiology of Pediatric Nonalcoholic Fatty Liver Disease. Clin Liver Dis 2021;17:196. https://doi.org/10.1002/CLD.1027.

[7] Singh SP, Barik RK. NonInvasive Biomarkers in Nonalcoholic Fatty Liver Disease: Are We There Yet? J Clin Exp Hepatol 2020;10:88. https://doi.org/10.1016/J.JCEH.2019.09.006.

[8] Wieland AC, Mettler P, McDermott MT, Crane LA, Cicutto LC, Bambha KM. Low awareness of nonalcoholic fatty liver disease among patients at high metabolic risk. J Clin Gastroenterol 2015;49:e6–10. https://doi.org/10.1097/MCG.0000000000000075.

[9] Cleveland ER, Ning H, Vos MB, Lewis CE, Rinella ME, Jeffrey Carr J, et al. Low Awareness of Nonalcoholic Fatty Liver Disease in a Population-Based Cohort Sample: the CARDIA Study 2019. https://doi.org/10.1007/s11606-019-05340-9.

[10] Wessels DH, Rosenberg Z. Awareness of non-alcoholic steatohepatitis and treatment guidelines: What are physicians telling us? World J Hepatol 2021;13:233. https://doi.org/10.4254/WJH.V13.I2.233.

[11] Liang W, Menke AL, Driessen A, Koek GH, Lindeman JH, Stoop R, et al. Establishment of a general NAFLD scoring system for rodent models and comparison to human liver pathology. PLoS One 2014;9. https://doi.org/10.1371/journal.pone.0115922.

[12] Brown GT, Kleiner DE. Histopathology of nonalcoholic fatty liver disease and nonalcoholic steatohepatitis. Metabolism 2016. https://doi.org/10.1016/j.metabol.2015.11.008.

[13] Pai RK, Jairath V, Hogan M, Zou G, Adeyi OA, Anstee QM, et al. Reliability of histologic assessment for NAFLD and development of an expanded NAFLD activity score. Hepatology 2022:1–14. https://doi.org/10.1002/hep.32475.

[14] Petersen MC, Shulman GI. Mechanisms of Insulin Action and Insulin Resistance. Physiol Rev 2018;98:2133. https://doi.org/10.1152/PHYSREV.00063.2017.
[15] Schrader M, Fahimi HD. Peroxisomes and oxidative stress. Biochim Biophys Acta - Mol Cell Res 2006;1763:1755–66. https://doi.org/10.1016/j.bbamcr.2006.09.006.
[16] Chen Z, Tian R, She Z, Cai J, Li H. Role of oxidative stress in the pathogenesis of nonalcoholic fatty liver disease. Free Radic Biol Med 2020;152:116–41. https://doi.org/10.1016/j.freeradbiomed.2020.02.025.
[17] Chen Z, Tian R, She Z, Cai J, Li H. Role of oxidative stress in the pathogenesis of nonalcoholic fatty liver disease. Free Radic Biol Med 2020;152:116–41. https://doi.org/10.1016/J.FREERADBIOMED.2020.02.025.
[18] Altman BJ, Rathmell JC. Metabolic Stress in Autophagy and Cell Death Pathways. Cold Spring Harb Perspect Biol 2012;4. https://doi.org/10.1101/CSHPERSPECT.A008763.
[19] Gart E, Salic K, Morrison MC, Caspers M, van Duyvenvoorde W, Heijnk M, et al. Krill oil treatment increases distinct pufas and oxylipins in adipose tissue and liver and attenuates obesity-associated inflammation via direct and indirect mechanisms. Nutrients 2021;13. https://doi.org/10.3390/nu13082836.
[20] Georgiadi A, Kersten S. Mechanisms of Gene Regulation by Fatty Acids. Adv Nutr 2012;3:127. https://doi.org/10.3945/AN.111.001602.
[21] Samstad EO, Niyonzima N, Nymo S, Aune MH, Ryan L, Bakke SS, et al. Cholesterol crystals induce complement-dependent inflammasome activation and cytokine release. J Immunol 2014;192:2837–45. https://doi.org/10.4049/JIMMUNOL.1302484.
[22] Jang EJ, Kim DH, Lee B, Lee EK, Chung KW, Moon KM, et al. Activation of proinflammatory signaling by 4-hydroxynonenal-Src adducts in aged kidneys. Oncotarget 2016;7:50864–74. https://doi.org/10.18632/ONCOTARGET.10854.
[23] Zhao P, Wong K in, Sun X, Reilly SM, Uhm M, Liao Z, et al. TBK1 at the crossroads of inflammation and energy homeostasis in adipose tissue. Cell 2018;172:731. https://doi.org/10.1016/J.CELL.2018.01.007.
[24] Dewidar B, Soukupova J, Fabregat I, Dooley S. TGF-β in Hepatic Stellate Cell Activation and Liver Fibrogenesis: Updated. Curr Pathobiol Rep 2015;3:291–305. https://doi.org/10.1007/s40139-015-0089-8.
[25] Kisseleva T, Cong M, Paik YH, Scholten D, Jiang C, Benner C, et al. Myofibroblasts revert to an inactive phenotype during regression of liver fibrosis. Proc Natl Acad Sci U S A 2012. https://doi.org/10.1073/pnas.1201840109.
[26] Kirpich IA, Marsano LS, McClain CJ. Gut-liver axis, nutrition, and non-alcoholic fatty liver disease. Clin Biochem 2015;48:923–30. https://doi.org/10.1016/j.clinbiochem.2015.06.023.
[27] Mirza MS. Obesity, Visceral Fat, and NAFLD: Queryingthe Role of Adipokines in the Progression ofNonalcoholic Fatty Liver Disease. ISRN Gastroenterol 2011;2011:1–11. https://doi.org/10.5402/2011/592404.
[28] Chait A, den Hartigh LJ. Adipose Tissue Distribution, Inflammation and Its Metabolic Consequences, Including Diabetes and Cardiovascular Disease. Front Cardiovasc Med 2020;7:22. https://doi.org/10.3389/FCVM.2020.00022/XML/NLM.
[29] Skurk T, Alberti-Huber C, Herder C, Hauner H. Relationship between adipocyte size and adipokine expression and secretion. J Clin Endocrinol Metab 2007;92:1023–

33. https://doi.org/10.1210/JC.2006-1055.
[30] Donnelly KL, Smith CI, Schwarzenberg SJ, Jessurun J, Boldt MD, Parks EJ. Sources of fatty acids stored in liver and secreted via lipoproteins in patients with nonalcoholic fatty liver disease. J Clin Invest 2005;115:1343–51. https://doi.org/10.1172/JCI23621.
[31] Ikejima K, Takei Y, Honda H, Hirose M, Yoshikawa M, Zhang Y-J, et al. Leptin receptor–mediated signaling regulates hepatic fibrogenesis and remodeling of extracellular matrix in the rat. Gastroenterology 2002;122:1399–410. https://doi.org/10.1053/gast.2002.32995.
[32] Choi SS, Syn WK, Karaca GF, Omenetti A, Moylan CA, Witek RP, et al. Leptin promotes the myofibroblastic phenotype in hepatic stellate cells by activating the Hedgehog pathway. J Biol Chem 2010;285:36551–60. https://doi.org/10.1074/jbc.M110.168542.
[33] Rabot S, Membrez M, Bruneau A, Gerard P, Harach T, Moser M, et al. Germ-free C57BL/6J mice are resistant to high-fat-diet-induced insulin resistance and have altered cholesterol metabolism. FASEB J 2010;24:4948–59. https://doi.org/10.1096/fj.10-164921.
[34] Bäckhed F, Manchester JK, Semenkovich CF, Gordon JI. Mechanisms underlying the resistance to diet-induced obesity in germ-free mice. Proc Natl Acad Sci 2007;104:979–84. https://doi.org/10.1073/pnas.0605374104.
[35] Dai X, Hou H, Zhang W, Liu T, Li Y, Wang S, et al. Microbial Metabolites: Critical Regulators in NAFLD. Front Microbiol 2020;11:2373. https://doi.org/10.3389/FMICB.2020.567654/BIBTEX.
[36] Sonne DP. MECHANISMS IN ENDOCRINOLOGY: FXR signalling: a novel target in metabolic diseases. Eur J Endocrinol 2021;184:R193–205. https://doi.org/10.1530/EJE-20-1410.
[37] Kalra A, Yetiskul E, Wehrle CJ, Tuma F. Physiology, Liver. StatPearls 2022.
[38] Morrison MC, Kleemann R, van Koppen A, Hanemaaijer R, Verschuren L. Key Inflammatory Processes in Human NASH Are Reflected in Ldlr−/−.Leiden Mice: A Translational Gene Profiling Study. Front Physiol 2018;9. https://doi.org/10.3389/fphys.2018.00132.
[39] Martínez-Arranz I, Bruzzone C, Noureddin M, Gil-Redondo R, Mincholé I, Bizkarguenaga M, et al. Metabolic subtypes of patients with NAFLD exhibit distinctive cardiovascular risk profiles. Hepatology 2022;00:1–14. https://doi.org/10.1002/HEP.32427.
[40] Fraile JM, Palliyil S, Barelle C, Porter AJ, Kovaleva M. Non-Alcoholic Steatohepatitis (NASH) – A Review of a Crowded Clinical Landscape, Driven by a Complex Disease. Drug Des Devel Ther 2021;15:3997. https://doi.org/10.2147/DDDT.S315724.
[41] Cianci N, Subhani M, Hill T, Khanna A, Zheng D, Sheth A, et al. Prognostic non-invasive biomarkers for all-cause mortality in non-alcoholic fatty liver disease: A systematic review and meta-analysis. World J Hepatol 2022;14:1025. https://doi.org/10.4254/WJH.V14.I5.1025.

CHAPTER

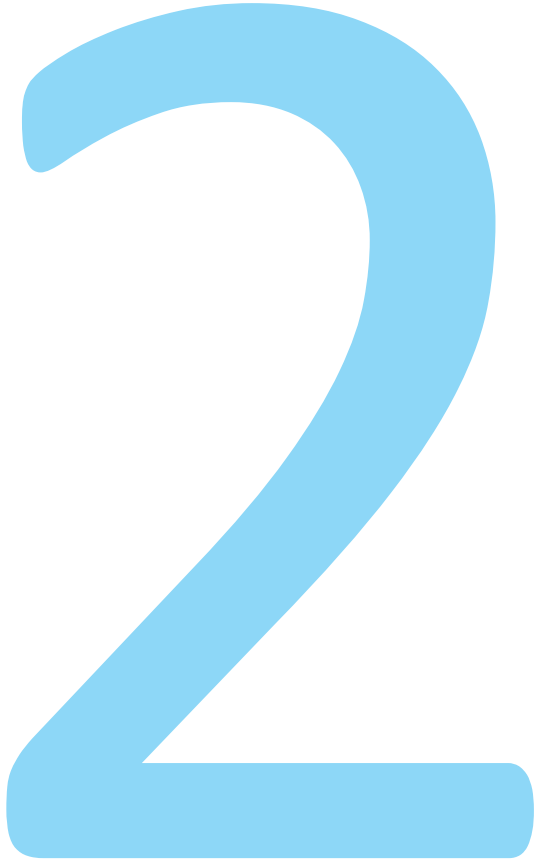

Translational characterization of the temporal dynamics of metabolic dysfunctions in liver, adipose tissue and the gut during diet-induced NASH development in Ldlr-/-.Leiden mice

Eveline Gart, Wim van Duyvenvoorde, Jessica M. Snabel, Christa de Ruiter, Joline Attema, Martien P.M. Caspers, Serene Lek, Bertie Joan van Heuven, Arjen G.C.L. Speksnijder, Martin Giera, Aswin Menke, Kanita Salic, Kendra K. Bence, Gregory J. Tesz, Jaap Keijer, Robert Kleemann, Martine C. Morrison

Heliyon. 2023 Feb 24;9(3):e13985.
doi: 10.1016/j.heliyon.2023.e13985. PMID: 36915476; PMCID: PMC10006542.

Abstract

Background: NAFLD progression, from steatosis to inflammation and fibrosis, results from an interplay of intra- and extrahepatic mechanisms. Disease drivers likely include signals from white adipose tissue (WAT) and gut. However, the temporal dynamics of disease development remain poorly understood.

Methods: High-fat-diet (HFD)-fed Ldlr-/-.Leiden mice were compared to chow-fed controls. At t=0, 8, 16, 28 and 38w mice were euthanized, and liver, WAT depots and gut were analyzed biochemically, histologically and by lipidomics and transcriptomics together with circulating factors to investigate the sequence of pathogenic events and organ cross-talk during NAFLD development.

Results: HFD-induced obesity was associated with an increase in visceral fat, plasma lipids and hyperinsulinemia at t=8w, along with increased liver steatosis and circulating liver damage biomarkers. In parallel, lipid catabolism regulators were deactivated and lipid synthesis regulators were activated. Subsequently, hepatocyte hypertrophy, oxidative stress and hepatic inflammation developed. Hepatic collagen accumulated from t=16w and became pronounced at t=28-38w. Epididymal WAT was maximally hypertrophic from t=8w, which coincided with inflammation development. Mesenteric and subcutaneous WAT hypertrophy developed slower and did not appear to reach a maximum, with minimal inflammation. In gut, HFD significantly increased permeability, induced a shift in microbiota composition from t=8w and changed circulating gut-derived metabolites.

Conclusion: HFD-fed Ldlr-/-.Leiden mice develop obesity, dyslipidemia and insulin resistance, essentially as observed in obese NAFLD patients, underlining their translational value. We demonstrate that marked epididymal-WAT inflammation, and gut permeability and dysbiosis precede the development of NAFLD stressing the importance of a multiple-organ approach in the prevention and treatment of NAFLD.

Graphical abstract

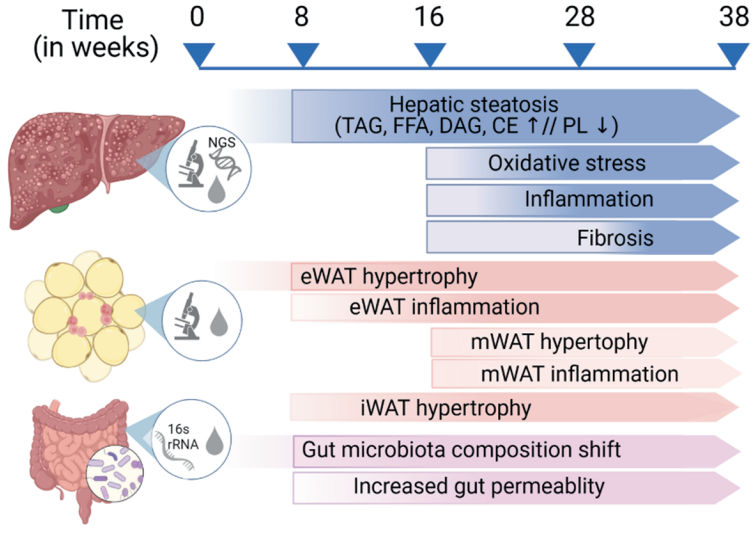

1. Introduction

Non-alcoholic fatty liver disease (NAFLD) is the most prevalent form of chronic liver disease worldwide. It is estimated to affect more than 20% of the adult population and is also becoming increasingly prevalent in children (1). The pathophysiology of NAFLD is incompletely understood, which may contribute to the fact that at present no approved therapeutic treatments are available. NAFLD is the hepatic manifestation of the metabolic syndrome, characterized by visceral fat accumulation, hyperlipidemia and insulin resistance (2). NAFLD is a complex multifactorial disease in which progression from simple steatosis to hepatic inflammation (non-alcoholic steatohepatitis; NASH) and fibrosis is driven by an intricate interplay between many molecular and cellular mechanisms (1). These are not limited to the liver, where processes such as lipid accumulation, inflammation and oxidative stress are potential disease drivers, but also originate from other key metabolic organs such as the adipose tissue and the gut (3). Current knowledge of the disease pathogenesis is based largely on studies that investigate a single time point (typically end-stage disease). However, such studies provide no insight into the temporal disease dynamics and chronology, which therefore remain poorly understood.
NAFLD is thought to begin with the accumulation of hepatic lipids, a condition known as steatosis. Hepatic lipids start to accumulate when the rates of lipid uptake and production exceed the rates of lipolysis and subsequent oxidation in peroxisomes and mitochondria, and lipid export (via VLDL). The excessive lipid load in the liver of NAFLD patients has been associated with increases in specific bioactive lipids such as diacylglycerols (DAGs) (4) - which can directly affect insulin signaling (5, 6) - and byproducts of oxidative-stress-induced lipid peroxidation (7). This metabolic dysfunctions can induce hepatocellular damage and may contribute to hepatic inflammation (infiltration of mixed inflammatory cells along with increases in proinflammatory cytokines and chemokines) (8), as well as hepatic fibrosis.

In addition to metabolic dysfunction in the liver of NAFLD patients, growing evidence suggests that the development of NAFLD is closely linked to the dysfunction of other metabolic organs, in particular the gut and adipose tissue (9). For example, NAFLD patients have an altered microbiota composition (10) and increased gut permeability (11). This altered microbiota composition may change nutrient processing, resulting in an altered production of short-chain fatty acids and bile acids, which can impact hepatic signaling pathways and metabolism (12). In obesity-associated NAFLD visceral fat has important clinical implications and is an independent risk factor of the metabolic syndrome (13, 14). White adipose tissue depots in obese subjects can become inflamed and can thus contribute to NAFLD, via lipid overflow which increases the lipid load on the liver, or via secretion of inflammatory cytokines and adipokines.

However, it is unclear when specific pathogenic events in the liver itself, and in gut and adipose tissue occur, what the sequence of these events is, and how they relate to NAFLD development (e.g., whether increased gut dysfunction precedes WAT dysfunction and NASH or whether the various organ dysfunctions develop simultaneously with NASH). Recent NAFLD research has mainly focused on the late stage of disease (e.g., fibrosis), however to prevent severe disease development more attention should be paid to the early phase of disease. For the latter, translational models for NASH in which the early phase of disease development and potential biomarkers can be studied play an important

role. Advancing our understanding of processes underlying NASH pathogenesis, the organ interactions and the complex interplay between them is crucial for the development of effective therapies.
Therefore, in this study we investigated temporal dynamics of metabolic dysfunctions in multiple organs (liver, adipose tissue, gut) during NAFLD development to investigate organ crosstalk. In particular, the sequence of pathogenic events as well as relevant metabolites released by these organs were studied. Knowledge on the disease dynamics will help define key pathogenic mechanisms and identify factors formed in these tissues that associate with fatty liver progression towards NASH and fibrosis. To study this we performed a longitudinal study to allow the study of both NASH (expected around 28 weeks) and liver fibrosis (evident around 38 weeks) as endpoint in the Ldlr-/-.Leiden mice. Ldlr-/-.Leiden mice display characteristics akin to NASH patients confirmed on the histopathological (15), metabolomic (16, 17) and transcriptional level (17, 18). Ldlr-/-.Leiden mice develop NAFLD in the context of obesity, hyperlipidemia with a humanized lipid profile, and hyperinsulinemia when fed energy-dense diets with a macronutrient composition comparable to natural human diets, thus eliminating the need to artificially modify the diets by adding cholesterol or lowering the methionine or choline content (18–20). A group of mice were euthanized at start point (t=0 weeks) and after 8, 16, 28 (NASH endpoint) and 38 weeks (liver fibrosis endpoint). At these time points features of HFD-induced metabolic dysfunction in liver, adipose tissue and the gut during NAFLD development were evaluated and compared with low-fat diet controls. Metabolic dysfunctions in the Ldlr-/-.Leiden mouse model were compared to those observed in NASH patients, to further assess the translational value of this NASH mouse model.

2. Materials and Methods

2.1. Animals, Diets and Study Design

Male Ldlr-/-.Leiden mice were bred and housed in the AAALAC-accredited SPF animal facility at TNO Metabolic Health Research (Leiden, the Netherlands). These mice are a substrain of the commercially available Ldlr-/- mouse (The Jackson Laboratory) and have a 94% C57BL/6J background and 6% 129S1/SvImJ background. The animals were used herein for a time course experiment in accordance with the rules and regulations set forward by the Animal Care and Use Committee and with ethical approval from an independent Animal Welfare Body (IVD TNO; approval number 3682/TNO-245). In addition, all procedures performed on these animals were in accordance with regulations and established guidelines and were reviewed and approved by Pfizer Institutional Animal Care and Use Committee. The mice were group-housed (four to five mice per cage) in Macrolon type 2L cages in a clean-conventional animal room (relative humidity 55 ± 10, temperature 20-24°C, light cycle 07:00 to 19:00) with ad libitum access to food and water. From weaning onwards all mice (n=103) were fed a standard laboratory low-fat control diet (chow; Sniff-R/M-V1530, Uden, the Netherlands). All mice were around the age of 14-16 weeks when the study started, and a group of these mice (n=6) was euthanized as a starting reference group (t=0). The remaining mice were divided into two different treatment arms, one part remained on chow while the others were fed an energy-dense high-fat diet (HFD; D12451, Research Diets Inc.; 20 kcal% protein, 35 kcal% carbohydrate

mainly from sucrose and 45 kcal% lard fat) to induce NAFLD. 5h-fasted blood samples for EDTA plasma preparation were collected from the tail vein at set intervals. Body weight and food intake measurements and body composition analyzed with echoMRI were acquired throughout the study. A few days before euthanasia, a functional gut permeability test was performed (details described below). Groups of n=6 chow and n=15 HFD fed mice were euthanized after 8, 16 and 28 weeks, and groups of n=15 chow and n=15 HFD fed mice after 38 weeks. Mice were euthanized by gradual-fill CO2 asphyxiation after a 5-h fast in the morning. At euthanasia blood for EDTA plasma and serum preparation was collected via heart puncture, organs were isolated and weighed, and mucosal microbiota from ileum and colon was collected. In addition, we included data from recent comparable studies using the same experimental conditions: male Ldlr-/-.Leiden mice of the same age fed the same diets (e.g. (20)).

2.2. Blood Chemistry

Analysis of cholesterol, triglycerides, insulin, adiponectin and leptin, alanine amine transferase (ALT), aspartate aminotransferase (AST), CK-18M30 and TIMP1 in EDTA plasma and whole blood glucose was performed as described previously (21, 22). 5-hours fasting plasma insulin and fasting blood glucose values were used to calculate IR = [insulin (ng/mL) × glucose (mM)]/22.5 (23). At t=20 weeks lipoprotein profiles were analyzed by separating plasma lipoproteins in fractions with fast protein liquid chromatography (FPLC) using (Pharmacia, Roosendaal, the Netherlands), as previously described (24). In the plasma fractions total cholesterol and triacylglycerols were measured with enzymatic assays (Roche diagnostics, Basel, CHF) (24). We also measured ApoB concentrations (t=24w) by ELISA following manufacturer instructions (ab230932, Abcam, Cambridge, UK).Gut-derived metabolites short-chain fatty acids (SCFAs; acetic acid, propionic acid, butyric acid, caproic acid, isobutyric acid, methylbutyric acid, isovaleric acid, and valeric acid) and bile acids (cholic acid, glycocholic acid, taurocholic acid, deoxycholic acid, taurodeoxycholic acid, chenodeoxycholic acid, β-murichолic acid, taurochenodeoxycholic acid, ursodeoxycholic acid, tauroursodeoxycholic acid, and hyodeoxycholic acid) were measured in 5-h-fasted terminal plasma at Triskelion (Utrecht, the Netherlands) as reported in (23).

2.3. Liver analysis

Liver histopathology was scored by a board-certified pathologist in Hematoxylin-Eosin (HE)-stained 3 µm cross sections of the medial lobe using a standardized method for rodents that is based on the human NAS scoring system (15). Total steatosis (macrovesicular and microvesicular) and hypertrophy (abnormally enlarged hepatocytes) for each mouse were determined as a percentage of total liver section affected. Hepatic inflammation was quantified by 1) counting the number of inflammatory aggregates in 5 fields per mouse at 100x magnification (field of view 4.15 mm^2) and expressed as the number of aggregates per mm^2 in the HE liver cross sections and 2) counting the number of F4/80-positive CLS per 3 µm liver cross of the medial lobe, which were F4/80 immunohistochemically stained as detailed in (17).
Intrahepatic cytokines (IL10, IL17, TNFα) and chemokines (MIP1a/CCL3, IP10/CXCL10, RANTES/CCL5, KC/CXCL1) were measured as previously described in (24) using a Simoa

multiplex immunoassay panel (3-plex 85-0450 and 4-Plex Developer Kit 100A-0497, Quanterix MA, USA) according to the manufacturer's protocol on an SP-X System (Quanterix). In the same liver homogenates cytokine MIF was measured following manufacturers protocol (Mouse MIF duoset DY1978, R&D systems, Abingdon, UK). Total protein concentrations were measured with the BCA Protein Assay Kit in the same homogenates (Thermo Fisher Scientific, Waltham, MA, USA) to normalize the inflammatory factors per mg of protein.

Hepatic fibrosis was analyzed in Sirius red-stained 3 µm cross sections of the sinister lobe and quantified by a board-certified pathologist as the percentage of hepatocytes affected. Hepatic total collagen content was quantified based on hydroxyproline residues obtained from acid hydrolysis (QZBtiscol, Quickzyme, Leiden, the Netherlands) of the sinister lobe. Collagen concentrations were normalized by protein concentrations, which were measured in the same hydrolysates (QZBtotprot, Quickzyme) according to manufacturer's instructions.

Fibrosis architecture was analyzed as detailed in (17) with multiphoton and second harmonic generation (SHG) imaging of hepatic collagen using a Genesis 200 imaging system and subsequent computer-assisted data analysis (HistoIndex, Singapore).

Liver vascular structures of mice fed a chow or HFD for 44 weeks were analyzed in the right and caudate liver lobe stained for 20h in a 1% iodine and 70% alcohol solution. The iodine-enhanced vascular structures were visualized by Micro-CT scanning (Zeiss Xradia Versa 520 with Zeiss Scout-and-Scan software, Carl Zeiss B.V., Breda, the Netherlands). The subsequent settings were used: 0.4x objective, pixel size 28.147 µm and 24.16 µm (chow and HFD, respectively), voltage 40/3 kV/W, camera binning 2, 801 views and 1201 views (chow and HFD, respectively) with angle range of 180°+fan.. Followed by 3D construction of the vascular structures with Zeiss XMReconstructor software.

The oxidative stress marker 4-hydroxynonenal (4-HNE) was analysed by immunohistochemistry in 4-HNE stained liver cross sections and quantified as previously described (25, 26).

Liver lipids were analysed with lipidomics on the lipidizer platform as detailed in (27). Lipids were grouped into classes: cholesterol esters (CE), ceramides (CER), dihydroceramides (DCER), hexosylceramides (HCER), lactosylceramides (LCER), lysophosphatidylcholines (LPC), lysophosphatidylcholines (LPE), phosphatidylcholines (PC), phosphatidylethanolamines (PE), sphingomyelins (SM), free fatty acids (FFA), diacylglycerols (DAGs), triacylglycerides (TAGs). The concentrations of the lipids were expressed as nmol/mg tissue, the total abundance of each lipid class is the sum of the respective lipid species concentrations.

Next generation sequencing was performed in RNA samples extracted from n=6 chow and n=10 HFD animals at 38 weeks. RNA concentration and RNA quality were determined as previously reported (24). RNA sequencing libraries for the Illumina (Ilumina NovaSeq6000, San Diego, CA) platform were generated Paired-End 150 bp for approximately 20 million Paired-End reads per sample at Genomescan BV (Leiden, the Netherlands). The sequences were filtered, trimmed and subjected to a QC procedure as described previously (28). These files were then merged and aligned to the reference genome "Mus_musculus.GRCm38.gencode.vM19". Htseq-count 0.6.1p1 was used to count the reads, these count files served as input for the differentially expressed genes (DEGs) analysis using the DESeq2-method (29). DEGs were used as an input for pathway analysis

through Ingenuity Pathway Analysis (IPA), accessed 12/21 (30). IPA uses gene expression data of all known downstream target genes to predict activation or deactivation of an upstream regulator as reported (22, 28).

2.4. Adipose tissue analysis

The perigonadal WAT (gWAT) and mesenteric WAT (mWAT) visceral white adipose tissue depots and the inguinal subcutaneous WAT (iWAT) were isolated and weighed. All three depots were paraffin-embedded and cross sections (5-µm thick) were stained with hematoxylin-phloxine-saffron. Adipocyte morphometry (cell size and count) was analyzed using the automated image analysis plug-in Adiposoft (31) in ImageJ (32). Inflammation was quantified by scoring the amount of crown-like structures (CLS) in the same fields as the morphometry analyses and expressed as number of CLS/1000 adipocytes as described in detail elsewhere (33).

2.5. Gut analysis

Gut permeability was assessed using a functional *in vivo* assay that measures the ability of fluorescein isothiocyanate (FITC)-labelled dextran (3-5kDa FD4; Sigma, St. Louis, MO, USA) to cross from the intestinal lumen into the circulation as described previously (21). A baseline blood sample was taken after a 4h fast, then FD4 was administered by oral gavage (900 mg/kg). Four hours after FD4 administration a second plasma sample was collected to measure FD4 concentrations using a fluorometer (FLUOstar Galaxy, BMG labtech, Offenburg, Germany). The baseline blood sample was used to correct for autofluorescence.
Microbiota DNA was isolated from samples collected from the mucosa layer from both the ileum and the colon using the AGOWA mag mini kit (DNA Isolation Kit, AGOWA, Berlin, Germany) according to the manufacturer's instructions. Metagenomic sequencing of 16S rRNA gene (~270 bp), spanning the V4 hypervariable regions, and subsequent data analysis was performed as described previously (21).

2.6. Statistics

The present study tested the null hypothesis whether HFD feeding increased disease parameters relative to the lean chow controls for the respective HFD and chow groups per time point (8, 16, 28 and 38 weeks). Statistical analysis was performed with IBM SPSS statistics version 25.0 (SPSS Inc., Chicago, Illinois, USA). Data was tested for normality with the Shapiro-Wilk test and for equal variance with Levene's test ($\alpha = 0.05$). For normally distributed variables, and independent sample t-test was used (1-sided). In case the data was not normally distributed, a Mann-Whitney test was used (1-sided). P-values <0.05 were considered statistically significant. Correlations were studied by Pearson's correlation analysis. IPA analysis to determine differentially expressed genes were based on Fisher's exact test ($\alpha = 0.01$).

3. Results

3.1. HFD fed Ldlr-/-.Leiden mice develop features of the metabolic syndrome: obesity associated with increased visceral fat mass, hyperlipidaemia and hyperinsulinemia

As expected, HFD-feeding induced robust weight gain over the course of the 38-week diet study, inducing significantly increased body weight compared to chow fed mice already after 8 weeks. Fat mass was significantly elevated, primarily driven by an increase in visceral adiposity. Lean mass and caloric intake remained largely comparable between the two groups (Figure 1A-C).

In chow-fed animals, the metabolic risk factors plasma cholesterol, triglycerides and insulin increased slightly over time while glucose and HOMA-IR remained stable (Figure 1D-F). In contrast, HFD induced pronounced hyperlipidaemia as observed by a doubling of plasma cholesterol concentrations after 8 weeks that kept on rising until 28 weeks and then levelled-off. Plasma triglycerides showed a comparable pattern over time. The HFD-induced increases in plasma cholesterol and triglycerides are mainly confined to the atherogenic apoB-containing (V)LDL lipoprotein particles as can be appreciated from the lipoprotein profiles in figure 1G-H essentially as observed in dyslipidemic humans (35, 36) and in subjects with NASH (37). In line with this, circulating apoB plasma concentrations were significantly increased by HFD relative to chow (figure 1I).

HFD feeding induced pronounced hyperinsulinemia after 8 weeks and fasting insulin levels continued to rise and were four-fold higher than chow at 38 weeks. Glucose levels remained similar over time in both chow and HFD animals. Together with the high insulin concentrations, this indicates a pronounced decrease in systemic insulin sensitivity with HFD. Consistent with this, HOMA-IR as a measure of insulin resistance was also found to be significantly increased with HFD.

The liver damage markers ALT and AST in plasma (Figure 1J-K), routinely used as clinical liver function markers, were determined on the group level demonstrating low levels in chow while in HFD they gradually continued to increase. Consistent with this, plasma concentrations of the liver integrity marker CK18-M30 and the liver fibrosis marker TIMP1 slightly increased with chow over time whereas HFD feeding significantly increased both biomarkers.

These data indicate that HFD-induced obesity is associated with an early (t=8 weeks) increase in visceral fat mass, development of dyslipidemia and hyperinsulinemia, accompanied by an increase in circulating ALT, AST, CK-18 and TIMP1 levels. The latter plasma markers are indicative of liver damage as is typically observed in NAFLD/NASH patients (38, 39).

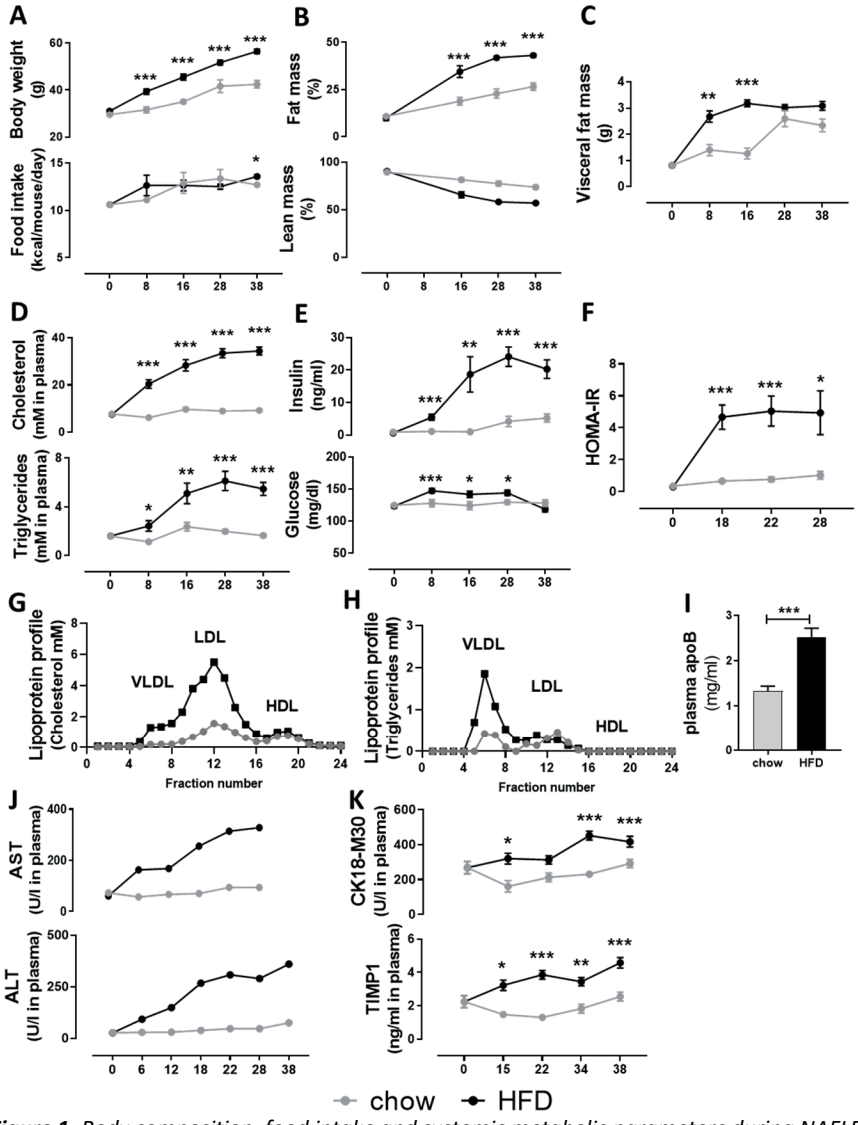

Figure 1. *Body composition, food intake and systemic metabolic parameters during NAFLD development. Groups of Ldlr-/-.Leiden mice fed a chow or a high-fat (HFD) diet were euthanized over time up to 38 weeks. (**A**) body weight and caloric food intake, (**B**) Fat mass and lean mass determined with echoMRI, (**C**) visceral fat mass is a composite of the visceral epididymal and mesenteric fat mass. In 5-h fasted plasma (**D**) cholesterol and triglyceride concentrations were determined as well as (**E**) insulin and glucose in whole blood. Insulin and glucose concentrations were used to calculate the (**F**) HOMA-IR. Lipoprotein profiles were analyzed in fasting plasma pools (n = 15/grp) and fractionated with FPLC, in the respective fractions (**G**) cholesterol and (**H**) triglyceride concentrations were determined at t=20 and plotted as profiles. (**I**) plasma apoB concentrations. Circulating liver integrity markers (**J**) AST and ALT were determined in plasma pools (n≥8/grp). Liver damage markers including (**K**) CK-18M30 and TIMP1 were analyzed in 5-h fasted plasma. The x-axis indicates the time in weeks and data represent mean ± SEM with * p < 0.05, ** p < 0.01, *** p < 0.001 vs. HFD.*

3.2. Obesity-associated NASH and liver fibrosis progression are associated with increases in intrahepatic cytokines and chemokines

To investigate the temporal development of liver dysfunction in more detail, histopathological analysis of NASH and liver fibrosis was combined with biochemical analysis of intrahepatic cytokines, chemokines and collagen content. Chow-fed animals developed minimal hepatic steatosis and hepatocellular hypertrophy, with these features being only observed to a small extent at the later timepoints, after 28 and 38 weeks (Figure 2A-F). In contrast, HFD feeding resulted in pronounced development of total hepatic steatosis already from 8 weeks onwards (Figure 2A-B), represented by equal increases in both micro- (Figure 2C) and macrovesicular steatosis (Figure 2D), and increased hepatocellular hypertrophy (Figure 2E-F).
In addition, hepatic inflammation scored by histological quantification of the inflammatory aggregates and F4/80-positive crown-like structures (CLS) was practically absent in the chow fed-mice (Figure 2G-J). HFD-feeding increased hepatic inflammation after 8 weeks, an effect which became pronounced after 16 weeks of HFD and kept rising both in the number of inflammatory cell clusters (Figure 2G-H) as well as in the formation of F4/80-positive CLS (Figure 2I-J). These hepatic CLS are a hallmark of NASH that has been shown to correlate with fibrosis development in NASH patients (40). Histological observations of hepatic inflammation were supported by biochemical analysis of intrahepatic chemokines and cytokines (Table 1). HFD feeding induced increases in the pro-inflammatory cytokine IL-17 after 8 and 38 weeks, but did not significantly affect intrahepatic TNFα and MIF relative to chow. The chemokines CCL3, CCL5, CXCL1, CXCL10 on the other hand were all significantly increased by HFD feeding, and these chemokines are important for the infiltration of immune cells typically observed in NASH patients (41). The anti-inflammatory cytokine IL-10 as potential counter-regulator response was significantly upregulated with HFD after 8 weeks and remained elevated at 16 weeks, though thereafter became comparable to chow levels.
In parallel, an NGS analysis and subsequent upstream regulator analysis was performed, which integrates changes in the expression of all known target genes downstream from a particular regulator. The upstream regulator analysis predicts the activity of an upstream regulator unrelated to its expression on protein level. HFD activated the pathways controlled by IL-17A, TNF, MIF, CCR2, CCL2 and CCL5 and IL-10 (Table 2). The activation of TNFα and MIF by HFD signaling was not associated with an increased hepatic protein expression of the respective cytokine/chemokine, which may be caused by downstream changes in signaling/activity.
Liver fibrosis was quantified by measuring the intrahepatic collagen content (Figure 2K) and histologically by quantification of the Sirius-red (SR) positive area in liver cross-sections (Figure 2L-M). The hepatic collagen concentrations and Sirius-red positive area remained low on chow diet. By contrast, HFD feeding induced liver fibrosis from 16 weeks onwards as observed by a doubling of the intrahepatic collagen content and an increased SR-positive area after 38 weeks. HFD feeding also induced changes in the fibrosis architecture over time as observed by significant increases in collagen area ratio, fiber density, reticulation index, number of fibers per area, mean fiber thickness and mean fiber length (supplemental figure 1).

These data provide substantial context regarding the temporal development of NASH. Together this data indicates that the steep increase in body fat mass with HFD feeding is accompanied by an early accumulation of fat in the liver, followed by abnormal enlargement of hepatocytes. After 16 weeks, hepatic inflammation and hepatic collagen are slightly increased, and this becomes particularly prominent around the time hepatocyte expansion plateaus (28-38 weeks).

The comparison with mice on a chow diet shows that HFD-induced NASH and fibrosis results in profound changes in liver histology, suggesting an impact on the functionality and architectural characteristics of the organ. To illustrate this, livers from chow and HFD-treated mice were analyzed by Micro-CT followed by 3D reconstruction (Supplemental video 1). This analysis showed that vascular structures, enhanced with iodine contrast, are clearly visible on a chow diet (Figure 2N), while they were hardly visible anymore after HFD treatment (Figure 2O), suggesting that the flow of blood and possibly also bile through the organ may be disrupted on a HFD.

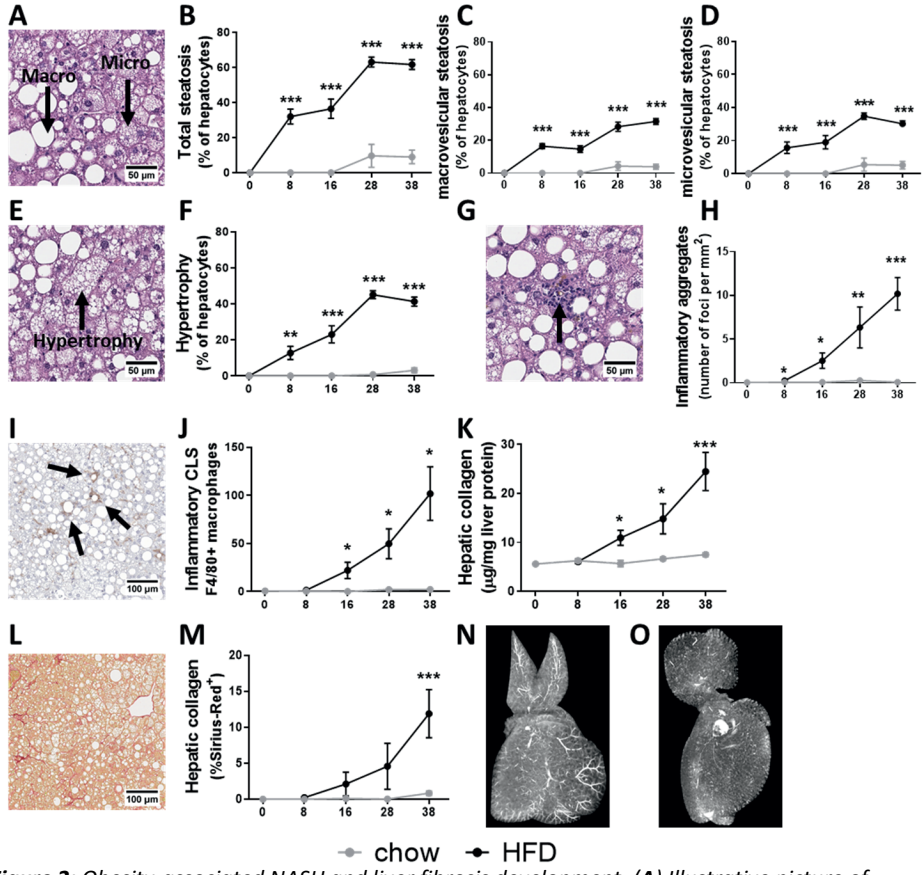

Figure 2: *Obesity-associated NASH and liver fibrosis development. (**A**) Illustrative picture of haematoxylin-eosin (HE) stained liver cross sections of HFD-induced NASH and scored for over time development of (**B**) total steatosis, a sum of (**C**) macrovesicular steatosis and (**D**) microvesicular steatosis. In the same HE cross sections (**E**) hepatocellular hypertrophy was (**F**) quantified. (**G**) Illustration of inflammatory aggregates (indicated by arrow) to score (**H**) hepatic inflammation of mixed inflammatory cell infiltration per mm^2, alongside analysis of (**I**) F4/80 immunoreactivity as marker of macrophages to score (**J**) inflammatory crown-like structures per cross section. Liver fibrosis was scored biochemically by quantification of (**K**) collagen content per mg protein and (**L**) histologically in Sirius-red stained liver cross-sections by (**M**) quantification of the percentage of Sirius-Red positive area. The x-axis indicates the time in weeks and data are presented as mean ± SEM. * p<0.05, ** p<0.01, *** p<0.001 compared to the chow control group. Representative images from the 3D reconstruction supplemental videos of vascular structures analyzed by Micro-CT are demonstrated for (**N**) chow and (**O**) HFD.*

Table 1. Intrahepatic chemokines and cytokines concentrations

	Chow					HFD			
	T=0	**T=8**	**T=16**	**T=28**	**T=38**	**T= 8**	**T=16**	**T=28**	**T=38**
IL-17 (pg/mg)	1.0 ± 0.4	0.9 ± 0.4	1.6 ± 0.3	2.0 ± 0.7	1.0 ± 0.5	1.4 ± 0.5	1.7 ± 0.9	2.3 ± 0.7	1.8 ± 0.6
TNF-α (pg/mg)	7.0 ± 2.3	5.8 ± 3.5	8.6 ± 0.7	11.1 ± 3.7	7.7 ± 3.2	10.6 ± 4.4	9.9 ± 4.0	12.4 ± 2.3	9.1 ± 2.3
MIF (ng/mg)	111.1 ± 15.9	101.7 ± 27.4	96.0 ± 13.9	125.9 ± 26.2	101.3 ± 28.6	116.2 ± 24.4	120.1 ± 28.4	140.8 ± 33.3	123.7 ± 20.6
CCL3 (pg/mg)	1.0 ± 0.2	1.6 ± 1.2	1.3 ± 0.1	2.1 ± 1.1	2.2 ± 1.4	2.6 ± 1.5	9.7 ± 11.3	12.6 ± 8.3	19.6 ± 8.3
CCL5 (pg/mg)	14.9 ± 4.0	11.5 ± 8.3	27.3 ± 15.0	40.3 ± 17.7	28.6 ± 15.8	28.5 ± 16.2	92.1 ± 87.9	122.6 ± 132.6	189.5 ± 102.3
CXCL1 (pg/mg)	1.6 ± 0.4	9.4 ± 14.5	2.2 ± 1.2	2.4 ± 0.7	2.3 ± 0.8	3.0 ± 0.8	4.9 ± 4.2	6.3 ± 3.1	5.4 ± 1.7
CXCL10 (pg/mg)	2.6 ± 1.0	2.5 ± 0.6	2.9 ± 0.7	5.6 ± 1.6	3.1 ± 1.2	3.9 ± 1.4	7.3 ± 5.2	9.4 ± 6.0	7.4 ± 2.2
IL-10 (pg/mg)	15.8 ± 4.6	16.3 ± 5.7	18.7 ± 2.8	27.5 ± 6.5	19.3 ± 8.9	24.3 ± 6.3	25.5 ± 10.1	30.0 ± 6.5	24.7 ± 6.5

IL-10 = Interleukin-10; IL-17 = Interleukin-17; TNF-α = tumor necrosis factor-α; MIF = macrophage migration inhibitory factor; MIP-1α= Macrophage inflammatory protein-1 alpha, also known as CCL3 = chemokine (C-C motif) ligand 3; RANTES = Regulated on Activation, Normal T cell Expressed and Secreted, also known as CCL5 = chemokine (C-C motif) ligand 5, KC = keratinocytes-derived chemokine, also known as CXCL1 = chemokine (C-X-C motif) ligand 1; IP-10 = interferon gamma-induced protein 10, also known as CXCL10 = chemokine (C-X-C motif) ligand 10. Data represents mean ± SD with significant differences between HFD and chow per time point (p<0.05) were indicated in the HFD-fed groups, with significant increases shown in red.

Table 2. Upstream regulators involved in inflammation

	HFD vs chow	
Upstream regulator	***Z-score***	***p-value***
IL10	1.6	0.000
IL17A	2.4	0.000
TNF	7.3	0.000
MIF	1.9	0.033
CCR2	5.0	0.000
CCL2	1.5	0.000
CCL3	-	-
CCL5	1.9	0.000
CXCL10	-	-

Upstream regulator analysis used gene expression data after 38 weeks of diet to predict the activity of an upstream regulator unrelated to its expression on protein level. The analysis integrates changes in the expression of all known target genes downstream from a particular regulator. The activity of an upstream regulator is represented by a Z-score, a negative Z-score indicates inhibition of the respective regulator, and a positive Z-score indicates activation (shown in red). The p-value < 0.05 in grey indicates significant enrichment of the genes downstream of a regulator, i.e., that more downstream genes are affected than can be expected by chance. N/A indicates an insufficient number of differentially expressed genes to predict the activation state of an upstream regulator.

3.3. NASH and liver fibrosis development associated with accumulation of specific lipids and the oxidative stress marker 4-HNE in the liver

As demonstrated by the histological analysis above, steatosis continuously increased during NAFLD progression. The accumulation of lipids in liver is mostly attributable to a significant increase in TAGs: at start, approximately 15% of total liver fat were TAGs which increased to 70% of total liver fat at 38 weeks in HFD fed mice (supplemental figure 2). In addition, HFD feeding also significantly increased the concentrations of the neutral lipids DAGs, CE and to some extend FFAs. In line with the HFD-induced increase of intrahepatic lipids and swelling of hepatocytes (steatosis & hypertrophy), the concentrations of intrahepatic phospholipids decreased: PC, PE, LPC, LPE, SM (Table 3), many of which are membrane lipids. The ceramide phospholipids HCER and LCER on the other hand, were increased in HFD relative to chow.
Consistent with the development of steatosis in the HFD-fed animals, important upstream regulators involved in lipid catabolism (PPARA, AMPK, CLUH, SIRT1, UCP1), peroxisomal lipid catabolism (ACOX1) and mitochondrial biogenesis (PPARGC1A, PPARGC1B, ESSRA, NRF1, CLUH) were all inactivated with HFD feeding after 38 weeks (Table 4). At the same time, the activity of SREBF1, a positive regulator of fatty acid synthesis genes, was increased with HFD, which is in line with the pronounced elevation of plasma insulin (which activates SREBF1). While TAG accumulation is considered a safe storage form of lipids, diacylglycerols (DAGs) block insulin signaling via protein kinase C (PRKC) at the level of the insulin receptor (41). In line with the accumulation of DAGs the activity of protein kinase C delta (PRKCD) was also higher with HFD, indicating the development of lipid-induced hepatic insulin resistance essentially as observed in humans (5).

In NAFLD, a high lipid load can lead to increased lipid oxidation and subsequently higher rates of reactive oxygen species (ROS) production. When elevated, ROS production together with an impairment in antioxidant capacity can result in an redox imbalance and oxidative stress which is harmful for hepatocytes (42). To understand the level oxidative stress in our model, the lipid peroxidation marker 4-HNE was longitudinally analyzed by immunostaining of liver cross-sections (Figure 3). HFD feeding increased 4-HNE positive immunoreactivity inside hepatocytes after 12 weeks, especially in the pericentral area in hypertrophic hepatocytes and those containing microvesicular steatosis (representative images in figure 3A). The latter is associated with mitochondrial dysfunction and oxidative stress (43, 44), and these observations are consistent with the view that oxidative stress leads to 4-HNE formation prior to cell death and inflammation. In addition to this intrahepatocellular immunoreactivity, 4-HNE positivity was also observed in immune cell clusters and crown-like structures. Quantification of these structures demonstrated that 4-HNE immunoreactivity was practically absent in chow, whereas HFD feeding induced 4-HNE immunoreactivity after 16 weeks progressed up to 38 weeks (Figure 3B). 4-HNE positive immunoreactivity significantly correlated with microvesicular steatosis, inflammation and hepatic collagen content (supplemental figure 3).
In line with these histological observations, the upstream regulator analysis of hepatic gene expression demonstrated that HFD feeding reduced the activity of anti-oxidant enzymes catalase (CAT), Glutathione peroxidase 1 (GPX1), superoxide dismutase 1 (SOD1) and glutathione reductase (GR) (Table 4). In addition, NGS pathway analysis demonstrated

that the biological pathway 'mitochondrial dysfunction' was significantly affected in HFD animals.

Taken together, after 8 weeks HFD feeding increased intrahepatic concentrations of specific bioactive lipids such as FFAs, CE and DAGs as well as the oxidative stress marker 4-HNE. Specifically, the early observed 4-HNE immunoreactivity in (enlarged) hepatocytes is indicative of metabolic dysfunction in NAFLD development, while the 4-HNE immunoreactivity associated with inflammatory cells and CLS is indicative of either clearance of 4-HNE positive debris by immune cells, or the formation of ROS and lipid oxidation products by immune cells themselves.

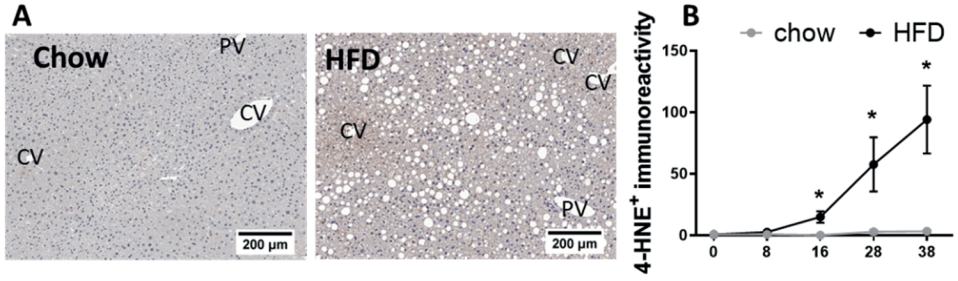

Figure 3: *Hepatic oxidative stress induced lipid peroxidation. (**A**) Illustrative pictures of 4-HNE with indications for the central veins (CV) and portal veins (PV). (**B**) 4-HNE quantification. The x-axis indicates the time in weeks and data are presented as mean ± SEM. * p<0.05 compared to the chow control group.*

Table 3. Intrahepatic lipid class concentrations

	Chow					HFD			
	T=0	**T=8**	**T=16**	**T=28**	**T=38**	**T=8**	**T=16**	**T=28**	**T=38**
Neutral lipids									
TAG	11.8 ± 3.0	20.6 ± 10.9	19.3 ± 9.4	53.1 ± 35.7	43.1 ± 28.8	76.9 ± 27.8	132.4 ± 54.7	178.9 ± 33.3	156.6 ± 31.0
DAG	2.6 ± 0.6	3.2 ± 1.1	2.7 ± 1.0	4.7 ± 1.9	4.0 ± 1.6	8.3 ± 7.3	7.2 ± 2.9	7.6 ± 3.3	5.6 ± 2.6
FFA	22.9 ± 5.6	21.1 ± 3.0	20.0 ± 3.4	23.4 ± 4.0	25.6 ± 4.6	33.3 ± 11.9	26.0 ± 3.7	26.9 ± 2.7	26.1 ± 3.4
CE	1.4 ± 0.5	1.3 ± 0.3	1.3 ± 0.3	1.9 ± 0.5	2.2 ± 0.6	6.3 ± 1.6	10.7 ± 4.7	12.7 ± 5.0	13.4 ± 3.2
Phospholipids									
PC	15.5 ± 1.3	15.7 ± 1.2	14.8 ± 1.0	15.4 ± 0.7	14.7 ± 2.3	14.3 ± 1.4	13.8 ± 2.1	12.6 ± 1.0	12.1 ± 1.2
PE	9.6 ± 2.1	9.5 ± 1.6	8.9 ± 1.6	8.7 ± 1.0	9.3 ± 2.1	8.2 ± 1.9	7.2 ± 2.3	6.4 ± 0.9	5.6 ± 1.3
LPC	2.9 ± 0.9	2.6 ± 0.9	2.5 ± 1.2	2.1 ± 0.5	2.8 ± 0.7	2.6 ± 0.7	2.2 ± 0.6	1.7 ± 0.4	2.0 ± 0.5
LPE	0.9 ± 0.4	0.8 ± 0.6	0.7 ± 0.4	0.5 ± 0.2	0.9 ± 0.4	0.7 ± 0.3	0.5 ± 0.2	0.4 ± 0.2	0.5 ± 0.2
SM	9.5 ± 1.3	8.9 ± 1.6	8.5 ± 2.3	7.7 ± 1.2	7.6 ± 1.6	6.3 ± 0.8	5.3 ± 1.0	4.3 ± 0.8	4.5 ± 0.7
CER	0.5 ± 0.0	0.5 ± 0.1	0.6 ± 0.3	0.4 ± 0.1	0.5 ± 0.1	0.4 ± 0.1	0.4 ± 0.1	0.5 ± 0.1	0.5 ± 0.1
DCER	0.028 ± 0.003	0.031 ± 0.005	0.040 ± 0.022	0.024 ± 0.004	0.031 ± 0.008	0.029 ± 0.006	0.027 ± 0.006	0.024 ± 0.006	0.027 ± 0.005
HCER	0.035 ± 0.003	0.030 ± 0.003	0.030 ± 0.007	0.032 ± 0.004	0.036 ± 0.008	0.042 ± 0.008	0.045 ± 0.007	0.045 ± 0.006	0.050 ± 0.006
LCER	0.005 ± 0.001	0.004 ± 0.002	0.005 ± 0.002	0.004 ± 0.002	0.005 ± 0.002	0.005 ± 0.002	0.008 ± 0.003	0.008 ± 0.002	0.008 ± 0.002

Lipid class concentrations in nmol/mg liver. TAG = Triacylglycerols, DAG = Diacylglycerols, FFA = free fatty acids, CE = Cholesterol esters, PC = Phosphatidylcholines, PE = Phosphatidylethanolamines, LPC = Lysophosphatidylcholines, LPE = Lysophosphatidylethanolamines, SM = Sphingomyelins, CER = Ceramides, DCER = Dihydroceramides, HCER = Hexosylceramides, LCER = lactosylceramide. Data represents mean ± SD with significant differences between HFD and chow per time point ($p<0.05$) were indicated in the HFD-fed groups, with significant increases shown in red and significant decreases shown in green.

Table 4. upstream regulators involved in lipid metabolism

	HFD vs chow	
Upstream regulator	***Z-score***	***p-value***
PPARGC1A	-4.7	0.000
PPARGC1B	-2.3	0.064
ESRRA	-0.9	0.000
NRF1	-1.0	0.027
CLUH	-1.9	0.000
AMPK	-1.8	0.017
SIRT1	-3.7	0.000
UCP1	-1.4	0.000
PPARA	-0.8	0.000
ACOX1	-5.6	0.000
SREBF1	1.4	0.000
PRKCD	4.2	0.059
PRKCE	0.7	0.001
SOD1	-1.7	0.000
SOD2	-0.2	0.000
CAT	-2.2	0.000
GPX1	-1.2	0.000
GR	-2.4	0.000

Upstream regulator analysis used gene expression data after 38 weeks of diet to predict the activity of an upstream regulator unrelated to its expression on protein level. The analysis integrates changes in the expression of all known target genes downstream from a particular regulator. The activity of an upstream regulator is represented by a Z-score, a negative Z-score indicates inhibition of the respective regulator (shown in green), and a positive Z-score indicates activation (shown in red). The p-value < 0.05 in grey indicates significant enrichment of the genes downstream of a regulator, i.e., that more downstream genes are affected than can be expected by chance. N/A indicates an insufficient number of differentially expressed genes to predict the activation state of an upstream regulator.

3.4. Visceral white adipose tissue dysfunction but not subcutaneous white adipose tissue dysfunction precedes the development of NASH and liver fibrosis

To determine whether adipose tissue (dys)function might contribute to liver disease development, histological analyses of visceral and subcutaneous WAT depots as well as analysis of circulating adipokines over time was performed. In both chow and HFD-fed mice early body fat mass increases were associated with an early expansion of the eWAT, a visceral depot that seemed to reach its maximum expansion capacity after 8 weeks of HFD, while in chow-fed animals it took 28 weeks to reach a similar weight (Figure 4A). By contrast, the visceral mWAT depot expansion was minimal in both chow and HFD fed mice, although significantly higher with HFD (Figure 4B). The subcutaneous inguinal white adipose tissue (iWAT) continued to rise in mass and this increase was linear during 38 weeks of HFD resulting in a 3-fold higher weight gain compared to chow (Figure 4C). These observations are comparable to the changes in average adipocyte cell size, with the

strongest increase in cell size in the eWAT depot in both chow and HFD fed animals (Figure 4D-F).

Adipose tissue inflammation, scored by the number of crown-like structures, was very low in chow-fed animals with incidental CLS apparent after 28 weeks in the eWAT depot while they were almost entirely absent in the mWAT and iWAT depot (Figure 4G-I). In contrast, HFD increased CLS numbers in eWAT after 8 weeks and this reached significance from 16 weeks onwards. mWAT inflammation was overall much lower than in eWAT, though HFD feeding still significantly increased the number of CLS at 16 and 38 weeks. HFD also slightly increased the number of CLS in subcutaneous iWAT, but this depot did not become significantly inflamed compared to chow (Figure 4I) which is in line with its presumed role as a safe storage depot.

In line with these data, plasma levels of the pro-inflammatory adipokine leptin only slightly increased with chow, while HFD increased leptin levels early with tripled concentrations after 16 weeks after which they remained high (Figure 4J). Plasma levels of the anti-inflammatory adipokine adiponectin remained comparable in chow and HFD mice until 28 weeks, after which adiponectin continued to rise in chow but significantly declined in HFD fed mice (Figure 4K).

These data indicate that the time point of maximal eWAT expansion coincides with the development of CLS in adipose tissue. Hypertrophy in mWAT and sWAT is a much slower process and these depots do not appear to reach maximal expansion within the period studied. These depots start to become inflamed once NASH is established. Therefore, it is possible that circulating factors that may affect NAFLD progression are mainly derived from an early hypertrophic inflamed visceral eWAT depot, although it cannot be excluded that lipids draining from the mesenteric depot into the liver also contribute to the lipid load during the course of disease.

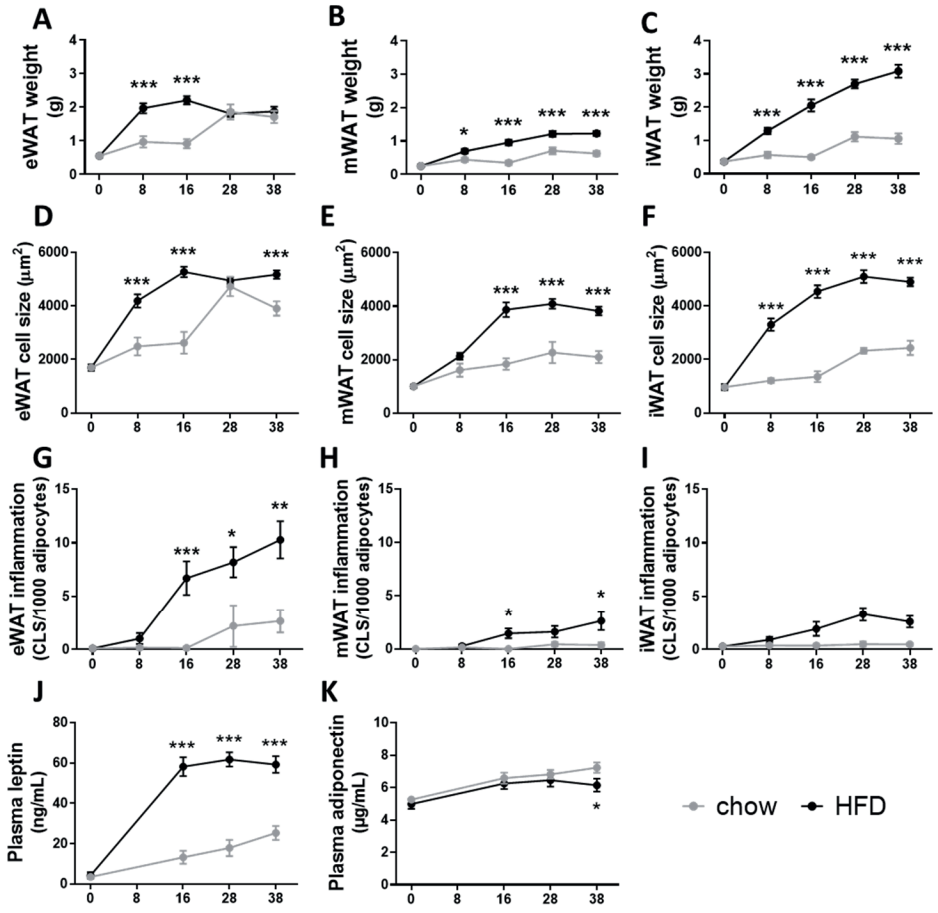

Figure 4: *Obesity-associated white adipose tissue dysfunction during NAFLD development. Adiposity scored in visceral (**A**) epididymal white adipose tissue (eWAT) weight, (**B**) mesenteric WAT (mWAT), and subcutaneous (**C**) inguinal WAT (iWAT). Cell morphometry analysis to determine average cell sizes of (**D**) eWAT, (**E**) mWAT and (**F**) iWAT. The number of crown-like structures (CLS) per 1000 adipocytes was scored to determine (**G**) eWAT inflammation, (**H**) mWAT inflammation and (**I**) iWAT inflammation. Circulating adipokine concentrations*

3.5. Increased gut permeability and microbiota dysbiosis associated with altered plasma bile acid and SCFA concentrations precede the development of NASH and liver fibrosis

To investigate gut dysfunction during NASH development, microbiota composition, gut permeability and circulating gut-derived metabolites (SCFAs and bile acids) were analyzed. Mucosal microbiota composition changes were analyzed with 16sRNA in the mucosa of the ileum and colon and are visualized by non-metric multidimensional scaling (NMDS) (Figure 5). Every dot in this NDMS graph represents the total microbiota composition of one mouse and close distances between dots represent similarity in microbiota

composition. All mice were on a chow diet at t=0 indicated by the black circle in the ileum and colon, over time the chow-fed mice remained clustered together with more diverse compositions in the ileum compared with the colon compartment. In contrast, HFD feeding induced a pronounced shift in microbiota composition within 8 weeks. Thereafter, HFD-fed mice continued to overlap in both the ileum (Figure 5A) and colon compartment (Figure 5B). HFD feeding significantly increased the abundance of many genera including for instance *Allobaculum, Clostridium_IV* and *Clostridium_XI*. A complete overview of time-resolved changes in both compartments is provided/visualized in supplemental figure 4. Statistical analysis of microbiota compositions using permutation tests confirmed that the microbiota composition of HFD-fed mice was significantly altered from 8 weeks onwards.

Gut permeability was assessed by the ability of FITC-labelled dextran to pass from the intestinal lumen into the circulation, which is thought to reflect paracellular permeability (FD4 test) (Figure 5C). Gut permeability in chow-fed animals remained low and stable over time, whereas HFD feeding significantly increased gut permeability already after 8 weeks and continued to increase over time.

To investigate whether the gut microbiota and gut permeability changes associated with alterations in circulating levels of gut-derived metabolites, we analysed the levels of SCFAs and bile acids in fasting plasma. Total plasma SCFA concentrations were not affected during HFD-induced NASH development (Supplemental figure 5A), but the SCFA composition did shift with HFD feeding (Table 5). Specifically, a rise in the less abundant SCFA caproate, isobutyrate, methylbutyrate, valerate and isovalerate were observed. Circulating total bile acids in chow-fed mice decreased over time while in HFD-fed mice they increased towards the end of the study (Supplemental figure 5B). After 38 weeks of HFD total bile acids were significantly elevated compared to chow (Table 6), including specific bile acids G-CA, T-CA, DCA, T-CDCA and T-UDCA that were reportedly elevated in NASH patients (underlined in table 7)(45).

In conclusion, the observed early increase in gut permeability is in line with the significant change in microbiota composition as well as changes in circulating gut-derived metabolites involved in organ crosstalk. Gut dysfunction including microbiota dysbiosis, increased gut permeability and altered gut-derived metabolites precede hepatic inflammation and fibrosis.

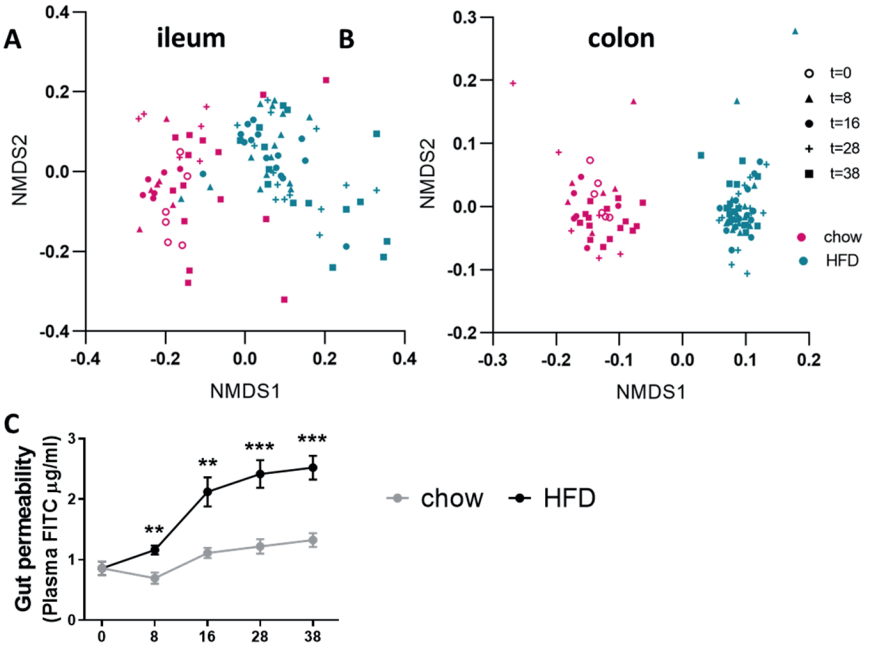

Figure 5: *Gut dysbiosis, increased gut permeability and altered circulating microbiota derived metabolites during NAFLD development. Microbiota composition was studied using 16s rRNA gene analysis in the mucosal compartments of both the ileum and colon over time. The microbiota composition was visualized by non-metric multidimensional scaling (NMDS), using the Bray–Curtis index, of the (**A**) the ileum and (**B**) colon: every dot represents the microbiota composition of one mouse and the distance between dots represents how (dis)similar the microbiota composition is between these mice. (**C**) Functional gut permeability was determined using fluorescent labelled dextran's (FD4 test). The x-axis represents the time in weeks and data are presented as mean ± SEM. * p<0,05, ** p<0,01, *** p<0,001 compared to the chow control group.*

Table 5. Circulating short-chain fatty acid (SCFA) concentrations as gut-liver crosstalk mediator

	Chow					HFD			
	T=0	**T=8**	**T=16**	**T=28**	**T=38**	**T=8**	**T=16**	**T=28**	**T=38**
Acetate	2.556 ± 0.797	4.098 ± 1.522	3.832 ± 2.019	2.866 ± 0.676	3.423 ± 1.117	5.383 ± 1.997	3.456 ± 1.034	2.726 ± 0.818	3.392 ± 0.544
Butyrate	0.083 ± 0.053	0.086 ± 0.041	0.082 ± 0.029	0.043 ± 0.019	0.050 ± 0.023	0.060 ± 0.025	0.056 ± 0.030	0.049 ± 0.017	0.048 ± 0.019
Caproate	0.075 ± 0.017	0.101 ± 0.032	0.103 ± 0.032	0.092 ± 0.025	0.091 ± 0.025	0.191 ± 0.092	0.205 ± 0.082	0.307 ± 0.126	0.164 ± 0.074
Isobutyrate	0.025 ± 0.012	0.024 ± 0.007	0.038 ± 0.009	0.027 ± 0.008	0.024 ± 0.012	0.028 ± 0.008	0.033 ± 0.013	0.043 ± 0.015	0.028 ± 0.006
Methylbutyrate	0.027 ± 0.006	0.032 ± 0.010	0.043 ± 0.007	0.033 ± 0.008	0.024 ± 0.004	0.030 ± 0.010	0.041 ± 0.013	0.050 ± 0.015	0.033 ± 0.008
Valerate	0.003 ± 0.005	0.005 ± 0.003	0.006 ± 0.002	0.006 ± 0.003	0.001 ± 0.001	0.006 ± 0.003	0.009 ± 0.007	0.013 ± 0.005	0.007 ± 0.003
Isovalerate	0.011 ± 0.002	0.010 ± 0.035	0.013 ± 0.004	0.011 ± 0.004	0.014 ± 0.006	0.019 ± 0.008	0.020 ± 0.008	0.027 ± 0.010	0.020 ± 0.008

Fasted plasma SCFA concentrations in µg/ml. Data represent mean ± SD with significant differences between HFD and chow per time point ($p<0.05$) were indicated in the HFD-fed groups, with significant increases shown in red.

Table 6. Circulating bile acid concentrations as gut-liver crosstalk mediator

	Chow					HFD			
	T=0	T=8	T=16	T=28	T=38	T=8	T=16	T=28	T=38
Primary BA									
Cholic acid (CA)	0.638 ± 0.312	0.496 ± 0.141	0.433 ± 0.251	0.388 ± 0.358	0.280 ± 0.164	0.061 ± 0.050	0.124 ± 0.097	0.252 ± 0.168	0.295 ± 0.241
Taurocholic acid (T-CA)	0.167 ± 0.082	0.255 ± 0.116	0.139 ± 0.070	0.203 ± 0.246	0.202 ± 0.184	0.343 ± 0.406	0.743 ± 1.108	1.589 ± 1.823	1.692 ± 1.569
Glycocholic acid (G-CA)	0.005 ± 0.003	0.005 ± 0.002	0.003 ± 0.002	0.003 ± 0.001	0.003 ± 0.002	0.002 ± 0.001	0.004 ± 0.004	0.010 ± 0.011	0.011 ± 0.010
Chenodeoxycholic acid (CDCA)	0.022 ± 0.003	0.018 ± 0.002	0.017 ± 0.013	0.014 ± 0.021	0.011 ± 0.007	0.001 ± 0.003	0.007 ± 0.009	0.013 ± 0.009	0.012 ± 0.005
Taurochenodeoxycholic acid (T-CDCA)	0.005 ± 0.002	0.011 ± 0.005	0.005 ± 0.001	0.007 ± 0.008	0.009 ± 0.007	0.020 ± 0.012	0.038 ± 0.045	0.077 ± 0.061	0.074 ± 0.042
Secondary BA									
Deoxycholic acid (DCA)	1.223 ± 0.185	0.305 ± 0.192	0.729 ± 0.150	0.292 ± 0.216	0.377 ± 0.155	0.263 ± 0.163	0.487 ± 0.205	0.525 ± 0.228	0.527 ± 0.212
Taurodeoxycholic acid (T-DCA)	0.096 ± 0.020	0.082 ± 0.066	0.069 ± 0.011	0.034 ± 0.015	0.055 ± 0.042	0.184 ± 0.131	0.206 ± 0.151	0.319 ± 0.314	0.203 ± 0.092
Ursodeoxycholic acid (UDCA)	0.081 ± 0.016	0.098 ± 0.016	0.102 ± 0.040	0.045 ± 0.039	0.056 ± 0.035	0.008 ± 0.010	0.042 ± 0.021	0.035 ± 0.021	0.044 ± 0.028
Tauro-ursodeoxycholic acid (T-UDCA)	0.030 ± 0.020	0.021 ± 0.004	0.015 ± 0.004	0.015 ± 0.010	0.018 ± 0.009	0.048 ± 0.022	0.063 ± 0.055	0.098 ± 0.068	0.100 ± 0.056

Fasted plasma bile acid concentrations in µM. Data represent mean ± SD with significant differences between HFD and chow per time point ($p<0.05$) were indicated in the HFD-fed groups, with significant increases shown in red and significant decreases shown in green.

4. Discussion

In the current study we extensively characterized the sequence of pathogenic events during NAFLD development in multiple organs (liver, gut, adipose tissue) as well as circulating metabolites implicated in organ crosstalk. Ldlr-/-.Leiden mice on a HFD develop obesity, plasma dyslipidemia (e.g., increased cholesterol and triglycerides, mainly confined to the atherogenic apo-B containing lipoproteins) and insulin resistance, as observed in NASH patients. In this translational context we observed that WAT dysfunction (specifically eWAT inflammation) and gut dysfunction (microbiota dysbiosis, increased gut permeability, and altered composition of gut-derived metabolites) precede the development of NASH and liver fibrosis. In the liver, early metabolic dysfunction manifests as an increase in lipid accumulation (steatosis), mainly in the form of triglycerides but also FFA, cholesterol esters and low abundant bioactive lipids such as DAGs. Intrahepatic hits from free cholesterol, FFA and oxidative stress-induced 4-HNE can promote hepatic inflammation and fibrosis.

In humans, NAFLD develops over decades, with obesity and insulin resistance as the main risk factors for progression (1). Likewise, diet-induced liver disease progression is relatively slow in mouse models that use translational experimental set-ups to mimic human pathophysiology (e.g., using diets that have human-like macronutrient composition), such as reported herein for the Ldlr-/-.Leiden model. Other NASH models using experimental diets that contain high concentrations of cholesterol up to 1% or even 2% (w/w of diet) may develop liver pathology faster, however this is at the cost of translational value. Treatment with exogenous dietary cholesterol increases intrahepatic free cholesterol, but shuts down endogenous cholesterol synthesis in the liver (47–49). The excess cholesterol in these models is the single driver of the NASH pathology (i.e. it is required for disease induction)(50). In contrast, increased intrahepatic free cholesterol in NASH patients is due to endogenous increase in hepatic cholesterol synthesis and is one of many pathways involved in the complex multi-organ disease progression of NAFLD (these intrahepatic free cholesterol concentrations in NASH patients are reflected in the Ldlr-/-.Leiden mouse (17)). Another frequently-used NASH model is based on the restriction of dietary choline and methionine, which leads to impairment in the assembly and secretion of VLDL particles by the liver. Intrinsic to this strategy to experimentally induce steatosis, these models lack dyslipidemia and are normolipidemic, and are characterized by severe body weight loss which contrasts NASH patients. Of note, although dietary methionine and choline deficiency is not translational to NASH patients, these mouse models may be relevant for a specific subset of NASH patients that have impaired VLDL secretion (16).

In Ldlr-/-.Leiden mice, HFD-feeding induced a pronounced increase in plasma cholesterol and TAGs mainly confined in the atherogenic apoB-containing (V)LDL lipoprotein particles. This reduced clearance of apoB-containing lipoprotein particles in the Ldlr-/-.Leiden model is akin to the human situation and results in similar lipoprotein profiles as observed in subjects with NASH (51). In addition, the HFD-induced increases in (V)LDL in the Ldlr-/-.Leiden mouse are accompanied by a pronounced increase in oxLDL (52). The genetic alteration of the LDL receptor in this model is not the driver of NAFLD/NASH development (which is induced by HFD feeding in the model, not by the genetic alteration in itself), but

rather it is a tool to establish a lipid environment in the liver and plasma compartment that mimics the human situation, with vascular complications that affect vessels and capillaries in- and outside the liver. A consequent limitation of this genetic alteration is that the Ldlr-/-.Leiden mouse is unsuitable to study the effects therapeutics requiring a functional ldl-receptor. Diet-induced dyslipidemia promotes the development of atherosclerosis, the major underlying cause of cardiovascular disease (CVD) and this is typically also observed in the HFD-treated Ldlr-/-.Leiden model (16, 20). The presence of atherosclerosis in conjunction with NAFLD/NASH is important because cardiovascular disease (CVD) is the major overall cause of mortality in NASH patients. This is also reflected in a head-to-head metabolomics comparison of HFD-treated Ldlr-/-.Leiden mice with n=1099 NASH patients, demonstrating that a large portion of NASH patients is at risk of CVD disease and the metabolome of these patients corresponds with that of the Ldlr-/-.Leiden mice (16).

Hepatic fat accumulation during NAFLD development was mainly attributable to an increase in triglyceride content in the HFD-fed mice. These triglycerides are considered an inert and safe storage form of energy (53). At the same time HFD feeding significantly elevated hepatic CE, DAGs and temporarily increased FFA during early NASH development. In line with our data a recent cohort of 365 biopsies ranging from non-steatosis obesity to NASH found that TAGs, DAGs and CE were significantly increased in NASH patients (54). Specifically, the accumulation of the less abundant lipid species seems detrimental for cell function. In sedentary humans, even in young individuals, DAGs and CER have been shown to directly bind to protein kinase C and block insulin receptor function (5, 6), (55, 56). Importantly, DAGs were found to correlate best with insulin resistance (compared to for example body mass index and ceramides) (42, 57). This correlation of DAGs and insulin resistance has been confirmed in both mice (53) and humans (58) in clamp experiments specifically examining insulin sensitivity.

The high liver lipid load in NAFLD challenges the peroxisomes and mitochondria to utilize the excess fat. Excessive lipid oxidation gives rise to a chronic increase in reactive oxygen species (ROS) (43, 59). In HFD-fed Ldlr-/-.Leiden mice, we demonstrated that already after 12 weeks of HFD feeding, 4-HNE positive immunoreactivity is observable inside hepatocytes that are often hypertrophic, thus lending support to the notion that they are overloaded by lipids and oxidative stress. In the current study we showed that 4-HNE immunoreactivity continuously increased during NAFLD development, together with a predicted deactivation of anti-oxidant enzymes (CAT, GPX1, SOD1, GSR) after 38 weeks of HFD. This suggests that persistent oxidative stress causes damage to the hepatocyte, consistent with the view that oxidative stress occurs prior to inflammation and cell death and may deplete the anti-oxidant safeguards. Our data is also consistent with findings in NAFLD patients, in which ROS and byproducts of ROS-induced lipid peroxidation are elevated and are associated with disease severity (7, 60). Furthermore, intrahepatic glutathione content and anti-oxidant enzyme activity of SOD and catalase are significantly decreased in NAFLD patients (60, 61).

NAFLD progression from lipid accumulation to hepatic inflammation together with increases in 4-HNE immunoreactivity are potentially directly linked. Many examples of this

link exist: 1) activation of TLR4 by saturated FFA (62) 2) accumulation of intrahepatic cholesterol and subsequent formation of cholesterol crystals which activate the NLP3 inflammasome (63) 3) formation of 4-HNE which can bind and activate the inflammatory receptor SRC, thereby activating NF-kB signaling (64). Conversely, inflammation may also stimulate hepatic lipid accumulation: TKB1, activated by pro-inflammatory stimuli, has been shown to repress energy expenditure by phosphorylating and inhibiting the key metabolic regulator AMPK (65). Although beyond the scope of the current study, the muscle may also affect the inflammatory status of the liver as exercise improved muscle health in HFD fed Ldlr-/-.Leiden mice and associated with improvements in hepatic inflammation (3). The activation of local macrophages and their shift towards a proinflammatory phenotype promotes the secretion of cytokines and chemokines to recruit monocytes and neutrophils to the liver and amplify the inflammatory response. Indeed, 8 weeks of HFD resulted in an increase in cytokine IL-17 and chemokines MIP1a (CCL3), RANTES (CCL5), KC (CXCL1), IP-10 (CXCL10), all of which are critical for immune cell infiltration and also observed in human livers. The rise in intrahepatic cytokines and chemokines resulted in mixed inflammatory infiltrates in the liver as observed in HE sections and by increased F4/80 positive CLS, essentially as observed in NASH patients (8).

It is thought that persistent hepatocellular damage and inflammation are drivers of fibrosis, which is by itself a key prognostic marker of all-cause mortality in NAFLD patients (66). The signals that can activate hepatic stellate cells, the main producers of extracellular matrix proteins including collagens, are manifold (67). These include cytokines such as TGF-β but also metabolites such as 4-HNE from oxidative stress-induced lipid peroxidation. The observed early increases in leptin from adipose tissue can also directly stimulate hepatic stellate cell activation (68, 69). These extrahepatic signals such as leptin that can promote fibrosis in the liver suggest that treatment for NAFLD should not be limited to the liver but should also correct dysmetabolic states in distant organs with metabolic crosstalk to the liver.

Adipose tissue hypertrophy and inflammation, particularly in the eWAT depot, preceded evident NASH development in the current study. During diet-induced metabolic overload WAT depots can expand by adipocyte hyperplasia (an increase in cell number via adipogenesis) and adipocyte hypertrophy (an increase in cell size). Both processes are thought to have physiological limits, and in this study we demonstrate that these vary between different WAT depots, as was also observed in C57BL/6J mice fed the same HFD (70). In this study, we have shown that the time point of maximal eWAT expansion coincides with the development of CLS in adipose tissue indicating that processes occurring at maximal hypertrophy form triggers for immune cell infiltration and cellular inflammation. This is supported by the observation that particularly the large (hypertrophic) adipocytes are the main source of inflammatory mediators while smaller adipocytes hardly release inflammatory factors in *ex vivo* cultured adipocytes from obese men (71). Hypertrophic inflamed eWAT in Ldlr-/-.Leiden mice is associated with predicted activation of inflammatory upstream regulators including cytokines and chemokines (3, 22) as well as increases in circulating levels of SAA, E-selectin and TNFα (3). The development of adipocyte hypertrophy in mWAT and sWAT is a slower process, and these depots became inflamed when NASH is already histologically manifest. Therefore, it is

likely that circulating factors that may affect NASH development in mice are mainly derived from an early hypertrophic inflamed eWAT depot. Consistent with this observation, we also demonstrated that the surgical removal of inflamed eWAT in C57BL/6J mice on a HFD resulted in a significant reduction in NASH (70). The visceral adipose tissue in humans is also considered to be the most detrimental and visceral obesity is associated with a predisposition for developing disorders including insulin resistance, CVD and NAFLD, while storing fat in the subcutaneous depot is considered a more safe way and does not associate with insulin resistance (72). This is further supported by higher cytokine secretion by cultured visceral derived adipocytes compared with subcutaneous adipocytes (73). Subcutaneous adipocytes on the other hand, secrete more adiponectin and may therefore be more beneficial (73). A potential link between NAFLD and dysfunctional WAT is an elevated lipolysis in these depots as they become insulin resistant. Impaired insulin action can increase the flux of FFA towards the liver. This notion is further supported by the fact that the degree of insulin resistance in adipose tissue is tightly associated with NAFLD severity (74). Of note, the FFA influx has been shown to account for 60% of TAG in livers of NAFLD patients, while only 25% of the TAGs is derived from DNL and 15% from the diet (75).

In this study, HFD feeding induced an early shift in microbiota composition, altered circulating microbiota derived metabolite concentrations BA and SCFA and increased gut permeability before NASH developed. Therefore it seems likely that the gut could play a role in NAFLD development, consistent with reports of mice without gut microbiota that were resistant to diet-induced obesity, liver steatosis and insulin resistance (76, 77). The microbiota regulates bile acid homeostasis (78), is involved in metabolic processes such as glucose, lipid and energy homeostasis (79), and it produces (via fermentation of carbohydrates and proteins) short chain fatty acids (SCFAs)(80, 81). After the major shift in microbiota composition at t=8w, we observed only minor changes in microbiota composition during NAFLD progression. Nonetheless, It is possible that changes in microbiota function (i.e. diet processing and metabolite production) may have changed over time and in that respect were able to affect NASH progression. This notion is in line with our observations that circulating levels of microbiota-derived metabolites (SCFA, BCFA, secondary bile acids) change over time throughout the study. These microbiota-derived metabolites may impact NAFLD/NASH progression because they have roles in energy metabolism and can modulate inflammation (25, 34). Nonetheless, the extent to which these changes over time contribute to experimental NASH/fibrosis development cannot be determined based on the currently available data. Interestingly, the increase in total circulating bile acids of T-CA, G-CA, T-CDCA, DCA and T-UDCA with HFD, were also reported to be elevated in plasma of NASH patients (46). Fecal transplantation of microbiota from healthy lean subjects into NAFLD patients improved intestinal permeability, confirming that microbiota composition and gut barrier function are linked (82). Similarly, it was demonstrated that fecal transplantation had beneficial effects on liver markers including gamma-glutamyl transferase and tended to improve ALT which also suggest a link between gut and the liver. Indeed increases in intestinal permeability have also been shown to correlate with liver disease severity (83). In a recent study, we increased Bifidobacterium and transiently improved gut permeability (FD4 test) using the prebiotic 2'-fucosyllactose. This improvement of dysbiosis and gut permeability was

accompanied by lower LPS binding protein levels, reduced liver steatosis and reductions in DAGs, further supporting the role of the gut and its microbiota in the control of metabolic homeostasis (24).

Intrinsic to the setup of the study we cannot demonstrate causation of metabolic dysfunction in the liver or dysfunctional WAT or gut/microbiota during the development of NAFLD. The potential role of metabolic dysfunctions in these organs in NAFLD development have been reported previously using interventions that targeted the white adipose tissue (70, 84), the gut (24, 85), the liver (17, 29, 86), or multiple organs simultaneously (3, 22, 25, 26, 34). However, this study does provide insight into the temporal dynamics and chronology of these processes and how they interact with each other during the development NAFLD. It is obvious that only processes that proceed a particular biochemical or histological hallmark in liver can contribute to the initiation of this disease hallmark. Nonetheless, we cannot exclude that processes that occur at a relatively late time point in the pathogenesis may still further aggravate the disease from the time point of their occurrence. For instance, changes to the overall anatomical architecture of the liver as demonstrated by Micro-CT may affect the flow properties of the organ at a relatively late stage and thereby may impair both nutrient and oxygen supply as well as hamper bile secretion which will aggravate the pathogenesis.

In conclusion, Ldlr-/-.Leiden mice fed a HFD develop obesity, dyslipidemia and insulin resistance, and the underlying processes involve molecular changes in visceral depots, dyslipidemia with increased atherogenic apoB-containing lipoproteins, and lipid-induced insulin resistance, essentially as observed in obese NASH patients. These obesity-associated NAFLD features (including a humanized lipid profile and translational dietary conditions) in the Ldlr-/-.Leiden mouse model are comparable to NASH patients, which emphasizes the translational value of the mouse model. In this NAFLD/NASH model we provide temporal insight into the dynamic metabolic dysfunctions underlying NAFLD in the liver, visceral (eWAT and mWAT) and subcutaneous WAT (iWAT) depots and the gut (microbiota). In the liver, metabolic dysfunction manifests as an early accumulation of specific bioactive lipids (DAGs and CER) which can directly promote insulin resistance. This experimental condition is relevant for the study of treatments because additional hits from intrahepatic free cholesterol, FFA and oxidative stress-induced 4-HNE can promote hepatic inflammation and fibrosis. In addition to these intrahepatic triggers, the experimental conditions employed herein also take into account the role of distant organs with metabolic-inflammatory cross-talk to the liver. For instance, epididymal WAT inflammation and gut dysfunction (microbiota dysbiosis and gut permeability) preceded the development of NASH and liver fibrosis and appeared to contribute to NAFLD/NASH on basis of aforementioned published studies. Hence, new strategies aiming at prevention, or attenuation of NAFLD/NASH development should not be limited to the liver but also should consider correcting dysmetabolism and inflammation in other organs that affect metabolic homeostasis in the liver.

Acknowledgements
We would like to thank Elsbet Pieterman, Nanda Keijzer, Nicole Worms, Anita van Nieuwkoop, Nikki van Trigt, Simone van der Drift and Marijke Voskuilen for their excellent technical assistance.

References

1. Loomba R, Friedman SL, Shulman GI. Mechanisms and disease consequences of nonalcoholic fatty liver disease. *Cell* 184: 2537–2564, 2021. doi: 10.1016/j.cell.2021.04.015.
2. Polyzos SA, Kang ES, Boutari C, Rhee E-J, Mantzoros CS. Current and emerging pharmacological options for the treatment of nonalcoholic steatohepatitis. *Metabolism* 111: 154203, 2020. doi: 10.1016/j.metabol.2020.154203.
3. van den Hoek AM, de Jong JCBC, Worms N, van Nieuwkoop A, Voskuilen M, Menke AL, Lek S, Caspers MPM, Verschuren L, Kleemann R. Diet and exercise reduce pre-existing NASH and fibrosis and have additional beneficial effects on the vasculature, adipose tissue and skeletal muscle via organ-crosstalk. *Metabolism* 124: 154873, 2021. doi: 10.1016/J.METABOL.2021.154873.
4. Gorden DL, Ivanova PT, Myers DS, McIntyre JO, VanSaun MN, Wright JK, Matrisian LM, Brown HA. Increased diacylglycerols characterize hepatic lipid changes in progression of human nonalcoholic fatty liver disease; comparison to a murine model. *PLoS One* 6, 2011. doi: 10.1371/JOURNAL.PONE.0022775.
5. Lyu K, Zhang Y, Zhang D, Kahn M, ter Horst KW, Rodrigues MRS, Gaspar RC, Hirabara SM, Luukkonen PK, Lee S, Bhanot S, Rinehart J, Blume N, Rasch MG, Serlie MJ, Bogan JS, Cline GW, Samuel VT, Shulman GI. A Membrane-Bound Diacylglycerol Species Induces PKCε-Mediated Hepatic Insulin Resistance. *Cell Metab* 32: 654-664.e5, 2020. doi: 10.1016/J.CMET.2020.08.001.
6. Magkos F, Su X, Bradley D, Fabbrini E, Conte C, Eagon JC, Varela JE, Brunt EM, Patterson BW, Klein S. Intrahepatic Diacylglycerol Content Is Associated With Hepatic Insulin Resistance in Obese Subjects. *Gastroenterology* 142: 1444-1446.e2, 2012. doi: 10.1053/J.GASTRO.2012.03.003.
7. Koliaki C, Szendroedi J, Kaul K, Jelenik T, Nowotny P, Jankowiak F, Herder C, Carstensen M, Krausch M, Knoefel WT, Schlensak M, Roden M. Adaptation of Hepatic Mitochondrial Function in Humans with Non-Alcoholic Fatty Liver Is Lost in Steatohepatitis. *Cell Metab* 21: 739–746, 2015. doi: 10.1016/j.cmet.2015.04.004.
8. Ibrahim SH, Hirsova P, Gores GJ. Non-alcoholic steatohepatitis pathogenesis: sublethal hepatocyte injury as a driver of liver inflammation. *Gut* 67: 963, 2018. doi: 10.1136/GUTJNL-2017-315691.
9. Kirpich IA, Marsano LS, McClain CJ. Gut-liver axis, nutrition, and non-alcoholic fatty liver disease. *Clin. Biochem.* 48: 923–930, 2015.
10. Lee G, You HJ, Bajaj JS, Joo SK, Yu J, Park S, Kang H, Park JH, Kim JH, Lee DH, Lee S, Kim W, Ko GP. Distinct signatures of gut microbiome and metabolites associated with significant fibrosis in non-obese NAFLD. *Nat Commun* 11, 2020. doi: 10.1038/S41467-020-18754-5.
11. Luther J, Garber JJ, Khalili H, Dave M, Bale SS, Jindal R, Motola DL, Luther S, Bohr S, Jeoung SW, Deshpande V, Singh G, Turner JR, Yarmush ML, Chung RT, Patel SJ.

Hepatic Injury in Nonalcoholic Steatohepatitis Contributes to Altered Intestinal Permeability. *Cell Mol Gastroenterol Hepatol* 1: 222, 2015. doi: 10.1016/J.JCMGH.2015.01.001.

12. Hu H, Lin A, Kong M, Yao X, Yin M, Xia H, Ma J, Liu H. Intestinal microbiome and NAFLD: molecular insights and therapeutic perspectives. *J Gastroenterol* 55: 142, 2020. doi: 10.1007/S00535-019-01649-8.
13. Mirza MS. Obesity, Visceral Fat, and NAFLD: Queryingthe Role of Adipokines in the Progression ofNonalcoholic Fatty Liver Disease. *ISRN Gastroenterol* 2011: 1–11, 2011. doi: 10.5402/2011/592404.
14. Taylor RS, Taylor RJ, Bayliss S, Hagström H, Nasr P, Schattenberg JM, Ishigami M, Toyoda H, Wai-Sun Wong V, Peleg N, Shlomai A, Sebastiani G, Seko Y, Bhala N, Younossi ZM, Anstee QM, McPherson S, Newsome PN. Association Between Fibrosis Stage and Outcomes of Patients With Nonalcoholic Fatty Liver Disease: A Systematic Review and Meta-Analysis. *Gastroenterology* 158: 1611-1625.e12, 2020. doi: 10.1053/J.GASTRO.2020.01.043.
15. Liang W, Menke AL, Driessen A, Koek GH, Lindeman JH, Stoop R, Havekes LM, Kleemann. R, Van Den Hoek AM. Establishment of a general NAFLD scoring system for rodent models and comparison to human liver pathology. *PLoS One* 9, 2014. doi: 10.1371/journal.pone.0115922.
16. Martínez-Arranz I, Bruzzone C, Noureddin M, Gil-Redondo R, Mincholé I, Bizkarguenaga M, Arretxe E, Iruarrizaga-Lejarreta M, Fernández-Ramos D, Lopitz-Otsoa F, Mayo R, Embade N, Newberry E, Mittendorf B, Izquierdo-Sánchez L, Smid V, Arnold J, Iruzubieta P, Castaño YP, Krawczyk M, Marigorta UM, Morrison MC, Kleemann R, Martín-Duce A, Hayardeny L, Vitek L, Bruha R, Fuente RA de la, Crespo J, Romero-Gomez M, Banales JM, Arrese M, Cusi K, Bugianesi E, Klein S, Lu SC, Anstee QM, Millet O, Davidson NO, Alonso C, Mato JM. Metabolic subtypes of patients with NAFLD exhibit distinctive cardiovascular risk profiles. *Hepatology* 00: 1–14, 2022. doi: 10.1002/HEP.32427.
17. Morrison MC, Verschuren L, Salic K, Verheij J, Menke A, Wielinga PY, Iruarrizaga-Lejarreta M, Gole L, Yu W, Turner S, Caspers MPM, Martínez-Arranz I, Pieterman E, Stoop R, van Koppen A, van den Hoek AM, Mato JM, Hanemaaijer R, Alonso C, Kleemann R. Obeticholic Acid Modulates Serum Metabolites and Gene Signatures Characteristic of Human NASH and Attenuates Inflammation and Fibrosis Progression in Ldlr-/-.Leiden Mice. *Hepatol Commun* 2: 1513–1532, 2018. doi: 10.1002/hep4.1270.
18. Morrison MC, Kleemann R, van Koppen A, Hanemaaijer R, Verschuren L. Key Inflammatory Processes in Human NASH Are Reflected in Ldlr−/−.Leiden Mice: A Translational Gene Profiling Study. *Front Physiol* 9, 2018. doi: 10.3389/fphys.2018.00132.
19. van Koppen A, Verschuren L, van den Hoek AM, Verheij J, Morrison MC, Li K, Nagabukuro H, Costessi A, Caspers MPM, van den Broek TJ, Sagartz J, Kluft C, Beysen C, Emson C, van Gool AJ, Goldschmeding R, Stoop R, Bobeldijk-Pastorova I, Turner SM, Hanauer G, Hanemaaijer R. Uncovering a Predictive Molecular Signature for the Onset of NASH-Related Fibrosis in a Translational NASH Mouse Model. *Cell Mol Gastroenterol Hepatol* 5: 83-98.e10, 2018. doi: 10.1016/j.jcmgh.2017.10.001.

20. van den Hoek AM, Verschuren L, Worms N, van Nieuwkoop A, de Ruiter C, Attema J, Menke AL, Caspers MPM, Radhakrishnan S, Salic K, Kleemann R. A Translational Mouse Model for NASH with Advanced Fibrosis and Atherosclerosis Expressing Key Pathways of Human Pathology. *Cells* 9: 1–21, 2020. doi: 10.3390/cells9092014.
21. Gart E, Souto Lima E, Schuren F, de Ruiter C, Attema J, Verschuren L, Keijer J, Salic K, Morrison M, Kleemann R. Diet-Independent Correlations between Bacteria and Dysfunction of Gut, Adipose Tissue, and Liver: A Comprehensive Microbiota Analysis in Feces and Mucosa of the Ileum and Colon in Obese Mice with NAFLD. *Int J Mol Sci* 20: 1, 2018. doi: 10.3390/ijms20010001.
22. Gart E, Salic K, Morrison MC, Caspers M, van Duyvenvoorde W, Heijnk M, Giera M, Bobeldijk-Pastorova I, Keijer J, Storsve AB, Hals PA, Kleemann R. Krill oil treatment increases distinct pufas and oxylipins in adipose tissue and liver and attenuates obesity-associated inflammation via direct and indirect mechanisms. *Nutrients* 13, 2021. doi: 10.3390/nu13082836.
23. Morrison MC, Gart E, van Duyvenvoorde W, Snabel J, Nielsen MJ, Leeming DJ, Menke A, Kleemann R. Heat-Inactivated Akkermansia muciniphila Improves Gut Permeability but Does Not Prevent Development of Non-Alcoholic Steatohepatitis in Diet-Induced Obese Ldlr−/−.Leiden Mice. *Int J Mol Sci* 23: 1–17, 2022. doi: 10.3390/ijms23042325.
24. Gart E, Salic K, Morrison MC, Giera M, Attema J, de Ruiter C, Caspers M, Schuren F, Bobeldijk-Pastorova I, Heer M, Qin Y, Kleemann R. The Human Milk Oligosaccharide 2'-Fucosyllactose Alleviates Liver Steatosis, ER Stress and Insulin Resistance by Reducing Hepatic Diacylglycerols and Improved Gut Permeability in Obese Ldlr-/-.Leiden Mice. *Front Nutr* 0: 1215, 2022. doi: 10.3389/FNUT.2022.904740.
25. Gart E, Duyvenvoorde W van, Toet K, Caspers MPM, Verschuren L, Nielsen MJ, Leeming DJ, Lima ES, Menke A, Hanemaaijer R, Keijer J, Salic K, Kleemann R, Morrison MC. Butyrate Protects against Diet-Induced NASH and Liver Fibrosis and Suppresses Specific Non-Canonical TGF-β Signaling Pathways in Human Hepatic Stellate Cells. *Biomedicines* 9: 1954, 2021. doi: 10.3390/BIOMEDICINES9121954.
26. Salic K, Gart E, Seidel F, Verschuren L, Caspers M, van Duyvenvoorde W, Wong KE, Keijer J, Bobeldijk-Pastorova I, Wielinga PY, Kleemann R. Combined Treatment with L-Carnitine and Nicotinamide Riboside Improves Hepatic Metabolism and Attenuates Obesity and Liver Steatosis. *Int J Mol Sci* 20, 2019. doi: 10.3390/IJMS20184359.
27. Gart E, Duyvenvoorde W van, Caspers MPM, Trigt N van, Snabel J, Menke A, Keijer J, Salic K, Morrison MC, Kleemann R. Intervention with isoleucine or valine corrects hyperinsulinemia and reduces intrahepatic diacylglycerols, liver steatosis, and inflammation in Ldlr−/−.Leiden mice with manifest obesity-associated NASH. *FASEB J* 36: e22435, 2022. doi: 10.1096/FJ.202200111R.
28. Ghorasaini M, Mohammed Y, Adamski J, Bettcher L, Bowden JA, Cabruja M, Contrepois K, Ellenberger M, Gajera B, Haid M, Hornburg D, Hunter C, Jones CM, Klein T, Mayboroda O, Mirzaian M, Moaddel R, Ferrucci L, Lovett J, Nazir K, Pearson M, Ubhi BK, Raftery D, Riols F, Sayers R, Sijbrands EJG, Snyder MP, Su B, Velagapudi V, Williams KJ, De Rijke YB, Giera M. Cross-Laboratory Standardization of Preclinical Lipidomics Using Differential Mobility Spectrometry and Multiple

Reaction Monitoring. *Anal Chem* 93: 16369–16378, 2021. doi: 10.1021/ACS.ANALCHEM.1C02826.

29. Mueller AM, Kleemann R, Gart E, van Duyvenvoorde W, Verschuren L, Caspers M, Menke A, Krömmelbein N, Salic K, Burmeister Y, Seilheimer B, Morrison MC. Cholesterol Accumulation as a Driver of Hepatic Inflammation Under Translational Dietary Conditions Can Be Attenuated by a Multicomponent Medicine. *Front Endocrinol (Lausanne)* 12, 2021. doi: 10.3389/fendo.2021.601160.
30. Love MI, Huber W, Anders S. Moderated estimation of fold change and dispersion for RNA-seq data with DESeq2. *Genome Biol* 15, 2014. doi: 10.1186/s13059-014-0550-8.
31. Krämer A, Green J, Pollard J, Tugendreich S. Causal analysis approaches in Ingenuity Pathway Analysis. *Bioinformatics* 30: 523–530, 2014. doi: 10.1093/BIOINFORMATICS/BTT703.
32. Galarraga M, Campión J, Muñoz-Barrutia A, Boqué N, Moreno H, Martínez JA, Milagro F, Ortiz-de-Solórzano C. Adiposoft: automated software for the analysis of white adipose tissue cellularity in histological sections. *J Lipid Res* 53: 2791–2796, 2012. doi: 10.1194/jlr.D023788.
33. Schneider CA, Rasband WS, Eliceiri KW. NIH Image to ImageJ: 25 years of Image Analysis. *Nat Methods* 9: 671, 2012. doi: 10.1038/NMETH.2089.
34. Tengeler AC, Gart E, Wiesmann M, Arnoldussen IAC, van Duyvenvoorde W, Hoogstad M, Dederen PJ, Verweij V, Geenen B, Kozicz T, Kleemann R, Morrison MC, Kiliaan AJ. Propionic acid and not caproic acid, attenuates nonalcoholic steatohepatitis and improves (cerebro) vascular functions in obese Ldlr-/- .Leiden mice. *FASEB J* : 1–19, 2020. doi: 10.1096/fj.202000455R.
35. Liangsupree T, Multia E, Metso J, Jauhiainen M, Forssén P, Fornstedt T, Öörni K, Podgornik A, Riekkola ML. Rapid affinity chromatographic isolation method for LDL in human plasma by immobilized chondroitin-6-sulfate and anti-apoB-100 antibody monolithic disks in tandem. *Sci Reports 2019 91* 9: 1–10, 2019. doi: 10.1038/s41598-019-47750-z.
36. Kennedy AJ, Ellacott KLJ, King VL, Hasty AH. Mouse models of the metabolic syndrome. *Dis Model Mech* 3: 156, 2010. doi: 10.1242/DMM.003467.
37. Zhang QQ, Lu LG. Nonalcoholic Fatty Liver Disease: Dyslipidemia, Risk for Cardiovascular Complications, and Treatment Strategy. *J Clin Transl Hepatol* 3: 78, 2015. doi: 10.14218/JCTH.2014.00037.
38. Kawanaka M, Nishino K, Nakamura J, Urata N, Oka T, Goto D, Suehiro M, Kawamoto H, Yamada G. Correlation between serum cytokeratin-18 and the progression or regression of non-alcoholic fatty liver disease. *Ann Hepatol* 14: 837–844, 2015. doi: 10.5604/16652681.1171767.
39. Tincopa MA. Diagnostic and interventional circulating biomarkers in nonalcoholic steatohepatitis. *Endocrinol Diabetes Metab* 3: e00177, 2020. doi: 10.1002/EDM2.177.
40. Itoh M, Kato H, Suganami T, Konuma K, Marumoto Y, Terai S, Sakugawa H, Kanai S, Hamaguchi M, Fukaishi T, Aoe S, Akiyoshi K, Komohara Y, Takeya M, Sakaida I, Ogawa Y. Hepatic crown-like structure: A unique histological feature in non-alcoholic steatohepatitis in mice and humans. *PLoS One* 8, 2013. doi: 10.1371/journal.pone.0082163.

41. Wu L, Gao X, Guo Q, Li J, Yao J, Yan K, Xu Y, Jiang X, Ye D, Guo J. The role of neutrophils in innate immunity-driven nonalcoholic steatohepatitis: lessons learned and future promise. *Hepatol Int* 14: 652–666, 2020. doi: 10.1007/S12072-020-10081-7/FIGURES/4.
42. Petersen MC, Shulman GI. Roles of Diacylglycerols and Ceramides in Hepatic Insulin Resistance. *Trends Pharmacol. Sci.* 38: 649–665, 2017.
43. Chen Z, Tian R, She Z, Cai J, Li H. Role of oxidative stress in the pathogenesis of nonalcoholic fatty liver disease. *Free Radic Biol Med* 152: 116–141, 2020. doi: 10.1016/j.freeradbiomed.2020.02.025.
44. Natarajan SK, Eapen CE, Pullimood AB, Balasubramanian KA. Oxidative stress in experimental liver microvesicular steatosis: Role of mitochondria and peroxisomes. *J Gastroenterol Hepatol* 21: 1240–1249, 2006. doi: 10.1111/j.1440-1746.2006.04313.x.
45. Fromenty B, Pessayre D. Impaired mitochondrial function in microvesicular steatosis effects of drugs, ethanol, hormones and cytokines. *J Hepatol* 26: 43–53, 1997. doi: 10.1016/S0168-8278(97)80496-5.
46. Puri P, Daita K, Joyce A, Mirshahi F, Santhekadur PK, Cazanave S, Luketic VA, Siddiqui MS, Boyett S, Min HK, Kumar DP, Kohli R, Zhou H, Hylemon PB, Contos MJ, Idowu M, Sanyal AJ. The presence and severity of nonalcoholic steatohepatitis is associated with specific changes in circulating bile acids. *Hepatology* 67: 534–548, 2018. doi: 10.1002/HEP.29359.
47. Jones PJH, Pappu AS, Hatcher L, Li ZC, Illingworth DR, Connor WE. Dietary Cholesterol Feeding Suppresses Human Cholesterol Synthesis Measured by Deuterium Incorporation and Urinary Mevalonic Acid Levels. *Arterioscler Thromb Vasc Biol* 16: 1222–1228, 1996. doi: 10.1161/01.ATV.16.10.1222.
48. Lecerf JM, De Lorgeril M. Dietary cholesterol: from physiology to cardiovascular risk. *Br J Nutr* 106: 6–14, 2011. doi: 10.1017/S0007114511000237.
49. Kleemann R, Verschuren L, Van Erk MJ, Nikolsky Y, Cnubben NHP, Verheij ER, Smilde AK, Hendriks HFJ, Zadelaar S, Smith GJ, Kaznacheev V, Nikolskaya T, Melnikov A, Hurt-Camejo E, Van der Greef J, Van Ommen B, Kooistra T. Atherosclerosis and liver inflammation induced by increased dietary cholesterol intake: A combined transcriptomics and metabolomics analysis. *Genome Biol* 8: 1–16, 2007. doi: 10.1186/GB-2007-8-9-R200/TABLES/4.
50. Gallage S, Avila JEB, Ramadori P, Focaccia E, Rahbari M, Ali A, Malek NP, Anstee QM, Heikenwalder M. A researcher's guide to preclinical mouse NASH models. *Nat Metab* 4: 1632–1649, 2022. doi: 10.1038/s42255-022-00700-y.
51. Kooistra T, Verschuren L, De Vries-Van Der Weij J, Koenig W, Toet K, Princen HMG, Kleemann R. Fenofibrate reduces atherogenesis in ApoE*3Leiden mice: Evidence for multiple antiatherogenic effects besides lowering plasma cholesterol. *Arterioscler Thromb Vasc Biol* 26: 2322–2330, 2006. doi: 10.1161/01.ATV.0000238348.05028.14.
52. Seidel F, Kleemann R, Duyvenvoorde W van, Trigt N van, Keijzer N, Kooij S van der, Kooten C van, Verschuren L, Menke A, Kiliaan AJ, Winter J, Hughes TR, Morgan BP, Baas F, Fluiter K, Morrison MC. Therapeutic Intervention with Anti-Complement Component 5 Antibody Does Not Reduce NASH but Does Attenuate Atherosclerosis and MIF Concentrations in Ldlr-/-.Leiden Mice. *Int J Mol Sci 2022,*

Vol 23, Page 10736 23: 10736, 2022. doi: 10.3390/IJMS231810736.
53. Petersen MC, Shulman GI. Mechanisms of Insulin Action and Insulin Resistance. *Physiol Rev* 98: 2133, 2018. doi: 10.1152/PHYSREV.00063.2017.
54. Vvedenskaya O, Rose TD, Knittelfelder O, Palladini A, Wodke JAH, Schuhmann K, Ackerman JM, Wang Y, Has C, Brosch M, Thangapandi VR, Buch S, Züllig T, Hartler J, Köfeler HC, Röcken C, Coskun Ü, Klipp E, Von Schoenfels W, Gross J, Schafmayer C, Hampe J, Pauling JK, Shevchenko A. Nonalcoholic fatty liver disease stratification by liver lipidomics. *J Lipid Res* 62: 100104, 2021. doi: 10.1016/J.JLR.2021.100104.
55. Turban S, Hajduch E. Protein kinase C isoforms: Mediators of reactive lipid metabolites in the development of insulin resistance. *FEBS Lett* 585: 269–274, 2011. doi: 10.1016/J.FEBSLET.2010.12.022.
56. Hajduch E, Lachkar F, Ferré P, Foufelle F. Roles of Ceramides in Non-Alcoholic Fatty Liver Disease. *J Clin Med* 10: 1–19, 2021. doi: 10.3390/JCM10040792.
57. Samuel VT, Shulman GI. Mechanisms for insulin resistance: Common threads and missing links. *Cell* 148: 852–871, 2012. doi: 10.1016/j.cell.2012.02.017.
58. Magkos F, Su X, Bradley D, Fabbrini E, Conte C, Eagon JC, Varela JE, Brunt EM, Patterson BW, Klein S. Intrahepatic diacylglycerol content is associated with hepatic insulin resistance in obese subjects. *Gastroenterology* 142, 2012. doi: 10.1053/J.GASTRO.2012.03.003.
59. Schrader M, Fahimi HD. Peroxisomes and oxidative stress. *Biochim. Biophys. Acta - Mol. Cell Res.* 1763: 1755–1766, 2006.
60. Chen Z, Tian R, She Z, Cai J, Li H. Role of oxidative stress in the pathogenesis of nonalcoholic fatty liver disease. *Free Radic Biol Med* 152: 116–141, 2020. doi: 10.1016/J.FREERADBIOMED.2020.02.025.
61. Videla LA, Rodrigo R, Orellana M, Fernandez V, Tapia G, Quiñones L, Varela N, Contreras J, Lazarte R, Csendes A, Rojas J, Maluenda F, Burdiles P, Diaz JC, Smok G, Thielemann L, Poniachik J. Oxidative stress-related parameters in the liver of non-alcoholic fatty liver disease patients. *Clin Sci (Lond)* 106: 261–268, 2004. doi: 10.1042/CS20030285.
62. Georgiadi A, Kersten S. Mechanisms of Gene Regulation by Fatty Acids. *Adv Nutr* 3: 127, 2012. doi: 10.3945/AN.111.001602.
63. Samstad EO, Niyonzima N, Nymo S, Aune MH, Ryan L, Bakke SS, Lappegård KT, Brekke O-L, Lambris JD, Damås JK, Latz E, Mollnes TE, Espevik T. Cholesterol Crystals Induce Complement-Dependent Inflammasome Activation and Cytokine Release. *J Immunol* 192: 2837–2845, 2014. doi: 10.4049/jimmunol.1302484.
64. Jang EJ, Kim DH, Lee B, Lee EK, Chung KW, Moon KM, Kim MJ, An HJ, Jeong JW, Kim YR, Yu BP, Chung HY, Jang EJ, Kim DH, Lee B, Lee EK, Chung KW, Moon KM, Kim MJ, An HJ, Jeong JW, Kim YR, Yu BP, Chung HY. Activation of proinflammatory signaling by 4-hydroxynonenal-Src adducts in aged kidneys. *Oncotarget* 7: 50864–50874, 2016. doi: 10.18632/ONCOTARGET.10854.
65. Zhao P, Wong K in, Sun X, Reilly SM, Uhm M, Liao Z, Skorobogatko Y, Saltiel AR. TBK1 at the crossroads of inflammation and energy homeostasis in adipose tissue. *Cell* 172: 731, 2018. doi: 10.1016/J.CELL.2018.01.007.
66. Cianci N, Subhani M, Hill T, Khanna A, Zheng D, Sheth A, Crooks C, Aithal GP. Prognostic non-invasive biomarkers for all-cause mortality in non-alcoholic fatty

liver disease: A systematic review and meta-analysis. *World J Hepatol* 14: 1025, 2022. doi: 10.4254/WJH.V14.I5.1025.
67. Tsuchida T, Friedman SL. Mechanisms of hepatic stellate cell activation. *Nat Rev Gastroenterol Hepatol* 14: 397–411, 2017. doi: 10.1038/NRGASTRO.2017.38.
68. Ikejima K, Takei Y, Honda H, Hirose M, Yoshikawa M, Zhang Y-J, Lang T, Fukuda T, Yamashina S, Kitamura T, Sato N. Leptin receptor–mediated signaling regulates hepatic fibrogenesis and remodeling of extracellular matrix in the rat. *Gastroenterology* 122: 1399–1410, 2002. doi: 10.1053/gast.2002.32995.
69. Choi SS, Syn WK, Karaca GF, Omenetti A, Moylan CA, Witek RP, Agboola KM, Jung Y, Michelotti GA, Diehl AM. Leptin promotes the myofibroblastic phenotype in hepatic stellate cells by activating the Hedgehog pathway. *J Biol Chem* 285: 36551–36560, 2010. doi: 10.1074/jbc.M110.168542.
70. Mulder P, Morrison MC, Wielinga PY, Van Duyvenvoorde W, Kooistra T, Kleemann R. Surgical removal of inflamed epididymal white adipose tissue attenuates the development of non-alcoholic steatohepatitis in obesity. *Int J Obes* 40: 675–684, 2016. doi: 10.1038/ijo.2015.226.
71. Skurk T, Alberti-Huber C, Herder C, Hauner H. Relationship between adipocyte size and adipokine expression and secretion. *J Clin Endocrinol Metab* 92: 1023–1033, 2007. doi: 10.1210/JC.2006-1055.
72. Espinosa De Ycaza AE, Søndergaard E, Morgan-Bathke M, Lytle K, Delivanis DA, Ramos P, Carranza Leon BG, Jensen MD. Adipose Tissue Inflammation Is Not Related to Adipose Insulin Resistance in Humans. *Diabetes* 71: 381–393, 2022. doi: 10.2337/DB21-0609.
73. Małodobra-Mazur M, Cierzniak A, Pawełka D, Kaliszewski K, Rudnicki J, Dobosz T. Metabolic Differences between Subcutaneous and Visceral Adipocytes Differentiated with an Excess of Saturated and Monounsaturated Fatty Acids. *Genes (Basel)* 11: 1–16, 2020. doi: 10.3390/GENES11091092.
74. Lomonaco R, Ortiz-Lopez C, Orsak B, Webb A, Hardies J, Darland C, Finch J, Gastaldelli A, Harrison S, Tio F, Cusi K. Effect of adipose tissue insulin resistance on metabolic parameters and liver histology in obese patients with nonalcoholic fatty liver disease. *Hepatology* 55: 1389–1397, 2012. doi: 10.1002/hep.25539.
75. Donnelly KL, Smith CI, Schwarzenberg SJ, Jessurun J, Boldt MD, Parks EJ. Sources of fatty acids stored in liver and secreted via lipoproteins in patients with nonalcoholic fatty liver disease. *J Clin Invest* 115: 1343–1351, 2005. doi: 10.1172/JCI23621.
76. Rabot S, Membrez M, Bruneau A, Gerard P, Harach T, Moser M, Raymond F, Mansourian R, Chou CJ. Germ-free C57BL/6J mice are resistant to high-fat-diet-induced insulin resistance and have altered cholesterol metabolism. *FASEB J* 24: 4948–4959, 2010. doi: 10.1096/fj.10-164921.
77. Bäckhed F, Manchester JK, Semenkovich CF, Gordon JI. Mechanisms underlying the resistance to diet-induced obesity in germ-free mice. *Proc Natl Acad Sci* 104: 979–984, 2007. doi: 10.1073/pnas.0605374104.
78. Aron-Wisnewsky J, Doré J, Clement K. The importance of the gut microbiota after bariatric surgery. *Nat. Rev. Gastroenterol. Hepatol.* 9: 590–598, 2012.
79. Carr RM, Reid AE. FXR Agonists as Therapeutic Agents for Non-alcoholic Fatty Liver Disease. *Curr. Atheroscler. Rep.* 17: 2015.

80. den Besten G, Lange K, Havinga R, van Dijk TH, Gerding A, van Eunen K, Muller M, Groen AK, Hooiveld GJ, Bakker BM, Reijngoud D-J. Gut-derived short-chain fatty acids are vividly assimilated into host carbohydrates and lipids. *AJP Gastrointest Liver Physiol* 305: G900–G910, 2013. doi: 10.1152/ajpgi.00265.2013.
81. den Besten G, van Eunen K, Groen AK, Venema K, Reijngoud D-J, Bakker BM. The role of short-chain fatty acids in the interplay between diet, gut microbiota, and host energy metabolism. *J Lipid Res* 54: 2325–2340, 2013. doi: 10.1194/jlr.R036012.
82. Craven L, Rahman A, Nair Parvathy S, Beaton M, Silverman J, Qumosani K, Hramiak I, Hegele R, Joy T, Meddings J, Urquhart B, Harvie R, McKenzie C, Summers K, Reid G, Burton JP, Silverman M. Allogenic Fecal Microbiota Transplantation in Patients With Nonalcoholic Fatty Liver Disease Improves Abnormal Small Intestinal Permeability: A Randomized Control Trial. *Am J Gastroenterol* 115: 1055–1065, 2020. doi: 10.14309/AJG.0000000000000661.
83. Miele L, Valenza V, La Torre G, Montalto M, Cammarota G, Ricci R, Mascianà R, Forgione A, Gabrieli ML, Perotti G, Vecchio FM, Rapaccini G, Gasbarrini G, Day CP, Grieco A. Increased intestinal permeability and tight junction alterations in nonalcoholic fatty liver disease. *Hepatology* 49: 1877–87, 2009. doi: 10.1002/hep.22848.
84. Mulder P, Morrison MC, Verschuren L, Liang W, Van Bockel JH, Kooistra T, Wielinga PY, Kleemann R. Reduction of obesity-associated white adipose tissue inflammation by rosiglitazone is associated with reduced non-alcoholic fatty liver disease in LDLr-deficient mice. *Sci Rep* 6, 2016. doi: 10.1038/SREP31542.
85. Salic K, Kleemann R, Wilkins-Port C, McNulty J, Verschuren L, Palmer M. Apical sodium-dependent bile acid transporter inhibition with volixibat improves metabolic aspects and components of non-alcoholic steatohepatitis in Ldlr-/-.Leiden mice. *PLoS One* 14, 2019. doi: 10.1371/JOURNAL.PONE.0218459.
86. Morrison MC, Mulder P, Salic K, Verheij J, Liang W, van Duyvenvoorde W, Menke A, Kooistra T, Kleemann R, Wielinga PY. Intervention with a caspase-1 inhibitor reduces obesity-associated hyperinsulinemia, non-alcoholic steatohepatitis and hepatic fibrosis in LDLR−/−.Leiden mice. *Int J Obes* 40: 1416–1423, 2016. doi: 10.1038/ijo.2016.74.

Supplemental information

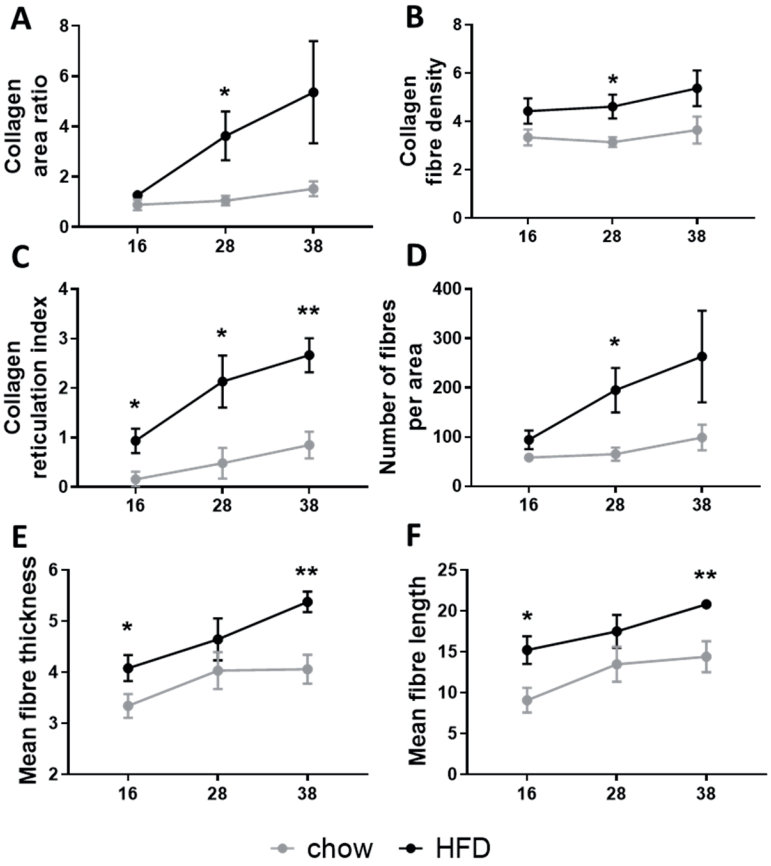

***Supplemental figure 1**: Fibrosis architecture measured with multiphoton and second harmonic generation imaging in liver cross sections from week 16 until week 38 in chow and HFD-fed Ldlr-/-.Leiden mice. (**A**) Collagen area ratio, (B) collagen fiber density, (**C**) collagen reticulation index, (**D**) number of fibers per area, (**E**) mean fiber thickness and (**F**) mean fiber length. The x-axis indicates the time in weeks and data are presented as mean ± SEM. * p<0.05, ** p<0.01 compared to the chow control group.*

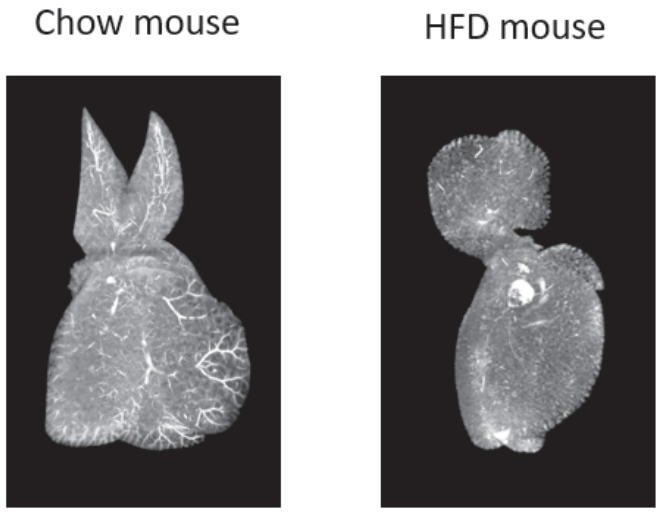

***Supplemental video 1**: Illustration of vascular structures after 44 weeks of chow or HFD-feeding in Ldlr-/-.Leiden mice. The vascular structures were enhanced with iodine contrast and visualized with Micro-CT and subsequent 3D reconstruction of the liver.*

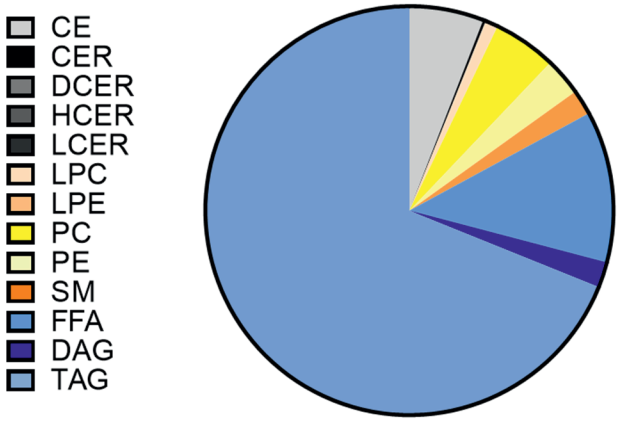

***Supplemental figure 2**: Intrahepatic lipid composition after 38 weeks of HFD-feeding in Ldlr-/-.Leiden mice: 5.9% cholesterol esters (CE), 0.2% ceramides (CER), 0.01% dihydroceramides (DCER), 0.02% hexosylceramides (HCER),0.00% lactosylceramides (LCER), 1.0% lysophosphatidylcholines (LPC), 0.00% lysophosphatidylcholines (LPE), 5.0% phosphatidylcholines (PC), 3.0 % phosphatidylethanolamines (PE), 2.0% sphingomyelins (SM), 12.0% free fatty acids (FFA), 2.0% diacylglycerols (DAGs), 69.0 % triacylglycerides (TAGs).*

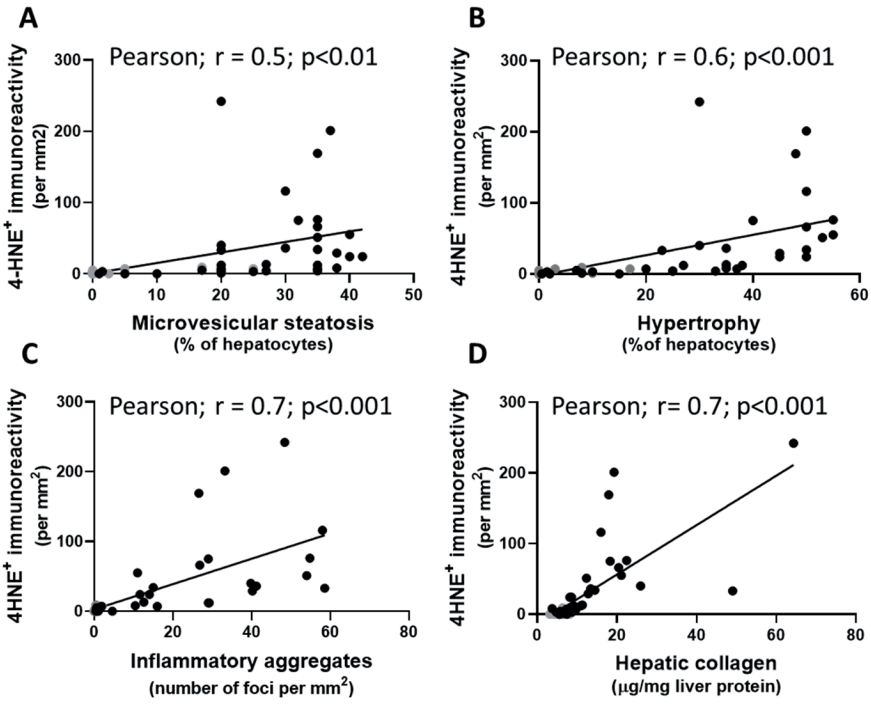

***Supplemental figure 3**: Pearson's correlation analysis of hepatic 4-HNE positive immunoreactivity and (**A**) microvascular steatosis, (**B**) hypertrophy, (**C**) inflammatory aggregates and (**D**) collagen content.*

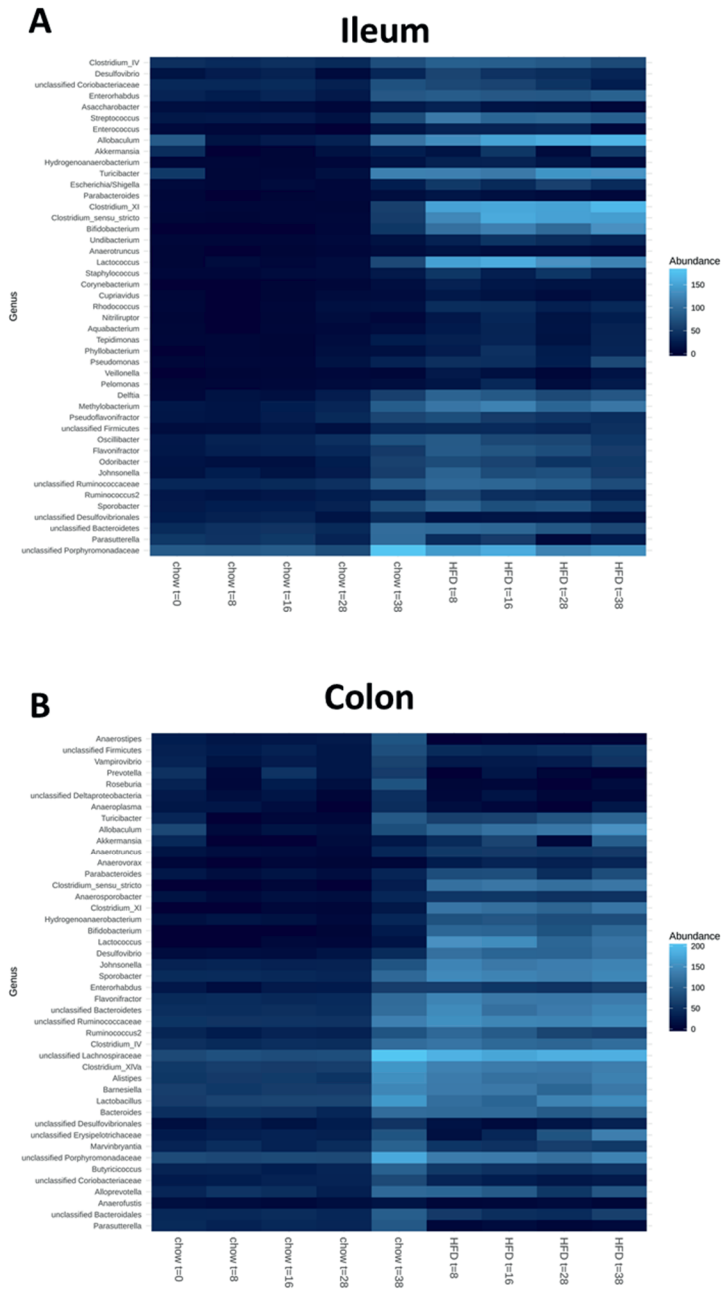

Supplemental figure 4: *List of genera of which the abundance was significantly affected by HFD compared to chow over time in the mucosal layer of the (**A**) ileum and (**B**) colon in Ldlr-/-.Leiden mice.*

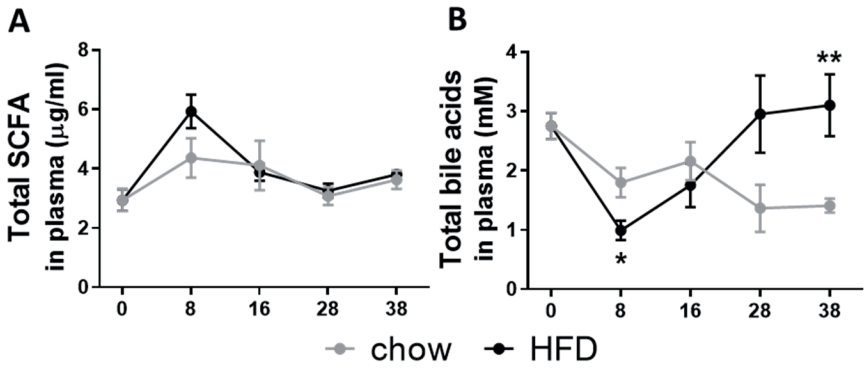

Supplemental figure 5: *Circulating microbiota derived metabolites including (**A**) total short-chain fatty acids (SCFAs) and (**B**) total bile acids were determined in plasma. The x-axis represents the time in weeks and data are presented as mean ± SEM. * p<0,05, ** p<0,01 compared to the chow control group.*

CHAPTER

Combined treatment with L-Carnitine and Nicotinamide Riboside improves hepatic metabolism and attenuates obesity and liver steatosis

Kanita Salic, Eveline Gart, Florine Seidel, Lars Verschuren, Martien Caspers, Wim van Duyvenvoorde, Kari E. Wong, Jaap Keijer, Ivana Bobeldijk- Pastorova, Peter Y. Wielinga, Robert Kleemann

Int J Mol Sci. 2019 Sep 5;20(18):4359.
doi: 10.3390/ijms20184359. PMID: 31491949; PMCID: PMC6770226.

Abstract

Obesity characterized by adiposity and ectopic fat accumulation is associated with the development of non-alcoholic fatty liver disease (NAFLD). Treatments that stimulate lipid utilization may prevent the development of obesity and comorbidities. This study evaluated the potential anti-obesogenic hepatoprotective effects of combined treatment with L-carnitine and nicotinamide riboside, i.e., components that can enhance fatty acid transfer across the inner mitochondrial membrane and increase nicotinamide adenine nucleotide (NAD+) levels, which are necessary for β-oxidation and the TCA cycle, respectively. Ldlr −/−.Leiden mice were treated with high-fat diet (HFD) supplemented with L-carnitine (LC; 0.4% w/w), nicotinamide riboside (NR; 0.3% w/w) or both (COMBI) for 21 weeks. L-carnitine plasma levels were reduced by HFD and normalized by LC. NR supplementation raised its plasma metabolite levels demonstrating effective delivery. Although food intake and ambulatory activity were comparable in all groups, COMBI treatment significantly attenuated HFD-induced body weight gain, fat mass gain (−17%) and hepatic steatosis (−22%). Also, NR and COMBI reduced hepatic 4-hydroxynonenal adducts. Upstream-regulator gene analysis demonstrated that COMBI reversed detrimental effects of HFD on liver metabolism pathways and associated regulators, e.g., ACOX, SCAP, SREBF, PPARGC1B, and INSR. Combination treatment with LC and NR exerts protective effects on metabolic pathways and constitutes a new approach to attenuate HFD-induced obesity and NAFLD.

Graphical abstract

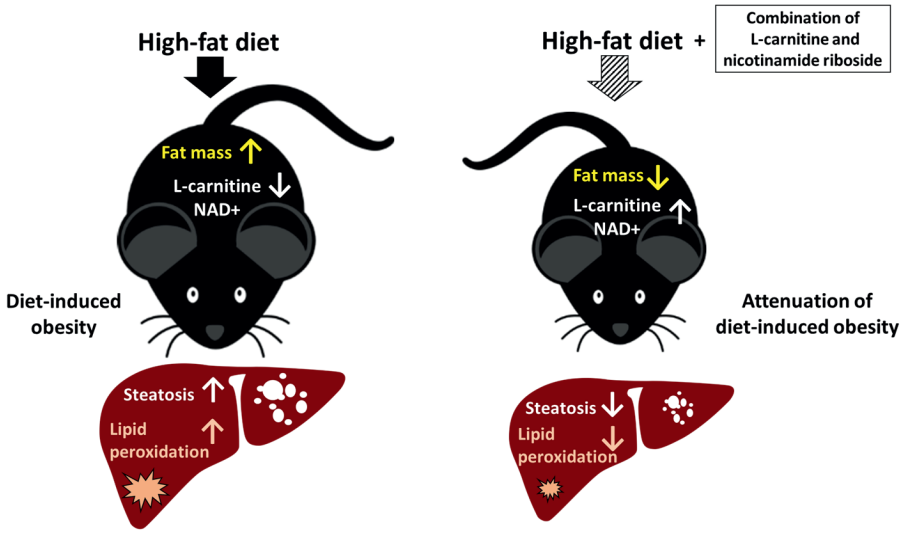

1. Introduction

Worldwide, the prevalence of overweight and obesity in both adults and children has increased dramatically over the last decades and has become a major health concern [1]. Adiposity and ectopic fat accumulation are characteristics of obesity that can cause comorbidities. In recent years non-alcoholic fatty liver diseases (NAFLD) has emerged as the most common chronic liver disease associated with obesity [2]. Current concepts for treatment of obesity focus on lifestyle changes and include dietary advice combined with exercise. Despite lifestyle and dietary advice, obesity rates have not declined in the last three decades [1]. Also, current treatments are insufficient to accomplish sustained weight loss for the majority of obese patients [3]. Hence, there is a need for new strategies that stimulate energy metabolism in other ways [4].

L-carnitine (LC) plays an important role in oxidative metabolism, since it is required for the transfer of long-chain fatty acids (FAs) from the cytosol into the mitochondrial matrix, where β-oxidation occurs. These FAs need to be activated as acyl-CoAs and transformed into acylcarnitines to be transported across the mitochondrial membrane. Acylcarnitines < C22 in length can enter the mitochondrial matrix [5], in exchange for free carnitine, where they are reconverted to acyl-CoAs and can be used for β-oxidation [6]. Similarly, carnitine is also required for the transport of end products of peroxisomal β-oxidation, medium and short-chain acyl-CoAs, out of the peroxisomes to allow further processing in the mitochondria [7]. A decline in carnitine levels has been associated with insulin resistance and diet-induced obesity and was suggested to be a consequence of long-term lipid overload, dysfunction of energy metabolism and incomplete fat oxidation [8]. Conversely, LC supplementation in obese rats was shown to restore carnitine levels and improve metabolic function [8].

Nicotinamide ribose (NR) is a dietary precursor molecule of nicotinamide adenine nucleotide (NAD+) and has been shown to enhance oxidative metabolism and protect mice against high-fat diet (HFD) induced obesity [9]. NAD+ provides reducing equivalents that fuel oxidative phosphorylation, crucial for oxidative metabolism and metabolic homeostasis. It has been shown that NAD+ levels decline in obesity and closely related metabolic disorders, such as diabetes and NAFLD [10,11], suggesting that treatments which enhance NAD+ content may moderate the development of these disorders. NAD+ has also been shown to play a role in limiting oxidative stress damage [10]. Oxidative stress has been implicated during obesity and in human NAFLD development [12]. Several studies have reported increased levels of 4-hydroxynonenal (4-HNE), a marker of oxidative stress-induced lipid peroxidation [13] in NAFLD patients [14–16].

The properties of LC and NR that improve oxidative metabolism and enhance FA utilization prompted us to study their effects in a chronic model of high-fat diet-induced obesity, insulin resistance and NAFLD. More specifically, we evaluated the long-term effects of combined LC and NR treatment as a novel strategy for reducing obesity and NAFLD and used respective mono-treatments as a reference. To do so, Ldlr−/−.Leiden mice received HFD with and without LC, NR and their combination (COMBI) for 21 weeks. At this time point the Ldlr−/−.Leiden mice developed obesity and hepatic steatosis, the main endpoints of this study. Moreover, this diet-induced mouse model recapitulates specific molecular

metabolomic and transcriptomic signatures of NAFLD patients [17–19]. Body composition, plasma metabolic parameters and acylcarnitines, hepatic histology, lipid peroxidation and genome-wide liver *transcriptomics* were analyzed. These analyses were used to evaluate combined and individual effects of LC and NR on obesity, NAFLD development and hepatic oxidative stress-related damage.

2. Materials and Methods

2.1. Animals and Diets

All animal experiments were performed according to the rules and regulations set out by the Netherlands Law on Animal Experiments and were approved by an independent Committee on Animal Care and Experimentation (approval reference number DEC-3383, Date: 25 February 2013, DEC-Zeist, The Netherlands).

Male Ldlr−/−.Leiden mice [17,18] were bred by TNO Metabolic Health Research (Leiden, The Netherlands). Mice were housed in Makrolon® cages at approximately 21 °C, with a 12-h daily light cycle and relative humidity of 50–60%. The mice were supplied with food and tap water ad libitum and mice were fed standard lab chow (Ssniff R/M diet V1530, Uden, The Netherlands) until they were 12–15 weeks old. Subsequently, 74 mice were divided into five experimental groups. The healthy reference group continued to receive a chow diet (n = 13) and the high-fat diet control group (HFD) received a NAFLD inducing diet (45 kcal% fat from lard, 35 kcal% from carbohydrates, primarily sucrose and 20% kcal from protein; D12451, Research Diets, New Brunswick, NJ, USA) as described previously [17] (n = 16). L-carnitine (0.4% *w*/*w*, Sigma-Aldrich, Zwijndrecht, The Netherlands; LC group; n = 15), nicotinamide riboside (0.3% *w*/*w*, NovAlix, Cedex, France; NR group; n = 15) and the combination of both (COMBI group, n = 15) were mixed through the HFD and the respective groups were treated with these diets for 21 weeks.

In order to measure ambulatory locomotor activity in the different treatment groups, mice (n = 8 per group) were single housed in metabolic cages (Phenomaster, TSE systems) at approximately 21 °C, with a 12-h daily light cycle for 48 h in weeks 19–21. The metabolic cages measured ambulatory locomotor activity using infrared beams along the x and y axis. Beam interruptions caused by movement of the mice were registered every 30 minutes during the 48-h timeframe and represented as counts.

2.2. Food Intake, Body Composition

Food intake and body weight were monitored every three weeks of the study. Total body fat mass was assessed with EchoMRI at the start and in week 9, 15 and 21 of the study as previously described [42].

2.3. Plasma Measurements

Blood samples were collected after 5 h fast via tail vein bleeding for isolation of EDTA plasma for evaluation of total cholesterol, triglycerides and insulin as described [17]. Plasma HDL-cholesterol was determined after precipitation as described earlier [43] with enzymatic

assays (CHOD-PAP, Roche Diagnostics, Almere, the Netherlands). Non-HDL cholesterol was calculated by subtracting HDL-cholesterol levels from total plasma cholesterol levels. Blood glucose was measured using a hand-held glucometer in tail blood during blood collection (FreeStyle Lite, Abbott, Alameda CA, USA).

2.4. Sacrifice and Analysis of Fat and Liver Tissue

All animals were sacrificed under non-fasted conditions by CO2 asphyxiation after 21 weeks of dietary treatment. Blood was collected via cardiac puncture for EDTA-plasma collection. White adipose tissue (WAT) was collected from gonadal and mesenteric WAT, abdominal fat mass, and the subcutaneous fat depot. The liver was weighed and divided into different parts. The medial lobe was fixed in formalin and embedded in paraffin. Development of NAFLD was analyzed in 3-µm liver hematoxylin-eosin stained sections and analyzed by a board-certified pathologist using a well-established adapted scoring method for human NAFLD [44] as described [17]. Briefly, the level of total steatosis per mouse was expressed as a percentage of the total liver section affected by microvesicular or macrovesicular steatosis. Similarly, hypertrophy was expressed as the affected percentage of the total liver section. Steatosis and hypertrophy were scored in the liver sections at a 50x magnification. The HE stained liver sections were digitalized with a 20 × magnification (Aperio AT2, Leica Biosystems, Amsterdam, The Netherlands) and used for the representative images.

2.5. 4-HNE Oxidative Stress-Related Marker Staining and Quantification in Liver Tissue

Oxidative stress-related marker 4-hydroxynonenal (4-HNE) was analyzed in 3-µm paraffin liver sections. After deparaffinization of the liver sections, heat-induced epitope retrieval was performed with a PH 6 citrate buffer (PT link, Dako, Denmark). Subsequently, sections were washed with 0.05% Tween-20 in phosphate-buffered saline (PBS) and blocked for 30 min at room temperature (RT) with 5% normal goat serum in PBS. Staining was performed by overnight incubation at 4 °C with Rabbit anti-4-HNE Michael adducts primary antibody (1:1000 in PBS, ref.393207, Millipore Corporation, Billerica, MA, USA PBS). The next day these sections were washed and blocked for endogenous peroxidase with 3% H2O2 during 20 min, and subsequently incubated for 45 min with a BrightVision poly-HRP-anti-rabbit secondary antibody (1:1 in PBS, Immunologic, Duiven, The Netherlands;) all at RT. Lastly, after washing the sections, Diaminobenzidine (DAB) was used for color development by 5 min incubation and nuclei were stained with hematoxylin for 30 s at RT.

The 4-HNE stained liver sections were digitalized with a 20 × magnification (Aperio AT2, Leica Biosystems, Amsterdam, The Netherlands). In these scans 4-HNE positive immunoreactivity was scored in two different liver sections in five nonoverlapping fields per liver section and expressed as amount of 4-HNE positive immunoreactivity structures per mm^2.

2.6. LC-MS/MS

Sacrifice plasma samples were used to measure L-carnitine, nicotinamide and several acylcarnitine levels. The metabolites were measured with the Metabolon analytical system (Metabolon, Inc., Durham, NC, USA). A non-targeted semiquantitative liquid chromatography–tandem mass spectrometry (LC-MS/MS) platform was applied for the identification of structurally named and unknown molecules [45,46]. All normalized relative ion counts were log transformed, and the remaining data were imputed with the minimum value on a per metabolite basis and reported in relative units (RU).

2.7. Gene Expression and Pathway Analysis

Total-RNA isolation kit (Bio-connect, Huissen, The Netherlands) was used to extract RNA from snap-frozen livers. The RNA concentration was measured spectrophotometrically using a NanoDrop 1000 (Isogen Life Science, De Meern, The Netherlands). To assess the quality of the isolated RNA, the 2100 Bioanalyzer (Agilent Technologies, Amstelveen, The Netherlands) was used. Next, messenger RNA (mRNA) library was produced for next generation sequencing following the manufacturer's protocol NEBNext Ultra Directional RNA Library Prep Kit for Illumina (New England Biolabs, Ipswich, MA, USA). The quality and yield of the PCR products were consistent with the expected size distribution (300–800 base pairs). Clustering and DNA sequencing were performed by GenomeScan BV (Leiden, The Netherlands) using a NextSeq 500 sequencer (Illumina, San Diego, CA, USA). The sequences were directly aligned with the mouse reference genome (GRCm38p4) using the Start 2.5 algorithm with default settings. Gene expression data is accessible at Gene Expression Omnibus (https://www.ncbi.nlm.nih.gov/geo/) under GSE136821. The DESeq-method [47] was used to evaluate differential expressed genes between treatment groups with a cut-off at $p < 0.01$. Effects of LC, NR and the COMBI treatment on hepatic gene expression was analyzed by gene enrichment analysis across pathways and biological processes with the Ingenuity Pathway Analysis suite (IPA; www.ingenuity.com). The upstream regulator analysis tool of IPA was used to assess the activity of upstream regulators essentially as reported in [48]. Briefly, the gene expression levels of all known target genes of an upstream regulator of interest are analyzed together. A Z-score less than -2 indicates a significantly reduced transcriptional activity, while a Z-score greater than 2 indicates a significant activation based on the direction of gene expression changes of target genes essentially as reported in translational studies [17]. In addition, the software also analyses whether the observed effects are statistically significant (p-value), i.e., whether a greater number of target genes are modulated than can be expected to occur by chance.

2.8. Statistical Analysis

All data are presented as mean ± standard error of the mean (SEM) or as indicated otherwise. This study investigated the hypothesis that L-carnitine, nicotinamide riboside and their combination attenuate the development of disease relative to the untreated HFD control group. Data distribution was tested with the Shapiro-Wilk test ($p < 0.05$) and for equal variances with Levene's test ($p < 0.05$). For normally distributed data with equal

variances, a one-way analysis of variance (ANOVA) was used, if the F-statistic was significantly different Dunnett's post hoc test was used one-sided compared to HFD (α = 0.05). A Kruskal–Wallis test was used for data sets that were not normally distributed or did not have equal variances. If the Kruskal–Wallis test indicated a significant difference (p < 0.05), a Mann–Whitney U test was used to compare groups one sided to HFD. For the pathway analysis of differentially expressed genes, P values were based on Fisher's exact test (α = 0.01).

3. Results

3.1. Experimental Diets Induce Carnitine and Nicotinamide Plasma Levels

Plasma L-carnitine levels were higher in chow than in the high-fat diet (HFD) treated mice (1.2 ± 0.1 RU vs 0.9 ± 0.1 RU; p < 0.05) (Figure 1A). Plasma L-carnitine levels in the NR group (0.7 ± 0.0 RU) were comparable to the HFD control group. L-carnitine treatment in the LC and the COMBI groups restored carnitine levels to 1.1 ± 0.1 RU (p < 0.05) and 1.3 ± 0.1 RU (p < 0.001), respectively, i.e. comparable to the chow healthy reference group.

Plasma nicotinamide concentrations, a metabolite of NR were similar in the chow, HFD and LC groups (0.8 ± 0.1 RU; 0.9 ± 0.0 RU and 0.9 ± 0.1 RU, respectively) (Figure 1B). Nicotinamide riboside treatment in the NR and COMBI groups significantly elevated plasma nicotinamide levels to 1.9 ± 0.1 RU and 1.9 ± 0.3 RU, respectively (both p < 0.001).

Overall, these data show that dietary supplementation with LC and NR in an HFD resulted in a normalization or modest increase of the respective circulating metabolites, indicating effective delivery into the circulation.

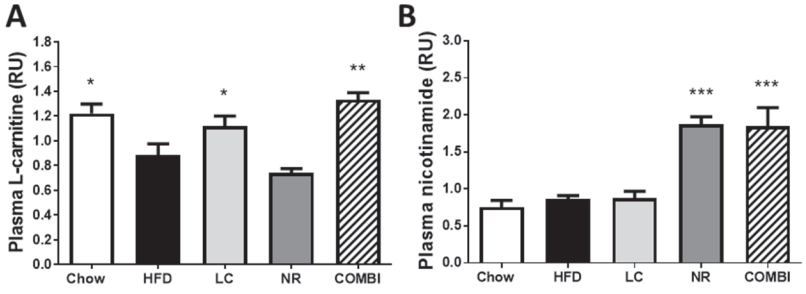

Figure 1. Dietary L-carnitine (LC), nicotinamide riboside (NR) or both (COMBI) supplementation to a high-fat diet (HFD) increased the plasma levels of L-carnitine and nicotinamide after 21 weeks of treatment, indicating effective delivery via the diet. LC-MS was used to measure plasma levels of (**A**) L-carnitine and (**B**) nicotinamide. Data are presented in relative units (RU) as mean ± SEM, * p < 0.05 or ** p < 0.01 or *** p < 0.001 compared to the HFD control group.

3.2. Combined Treatment with L-Carnitine and Nicotinamide Riboside Attenuates HFD-Induced Obesity Independent of Food Intake or Activity

To evaluate the effect of LC and NR and their combination on the development of obesity, food intake (FI), activity and body weight (BW) were monitored during the study, and fat mass was determined by EchoMRI at set time points.

Average FI during the study (Figure 2A) was similar in all groups. Ambulatory activity was measured during 48 h in metabolic cages, in which the counts are a measure for beam interruptions caused by movement (Figure 2B,C). These results showed no significant differences in activity between the groups.

Even though FI and activity were similar, the average BW gain in the HFD control group was 21.4 ± 0.9 g after 21 weeks, which indicated the development of obesity. By contrast, the average BW gain in the chow group was only 12.8 ± 0.9 g ($p < 0.001$) (Figure 2D). Mono-treatment with LC or NR affected BW only slightly, and the BW gain was comparable in these groups (19.7 ± 0.7 g and 19.3 ± 1.4 g, respectively). Notably, BW gain was significantly reduced in the COMBI group (18.1 ± 1.1 g; $p < 0.05$) compared to HFD, indicating that combination therapy attenuated obesity development.

Consistent with this observation, the total gain in fat mass in the HFD group was 17.5 ± 0.6 g whereas mice in the chow group gained significantly less fat (7.0 ± 0.8 g; $p < 0.001$) (Figure 2E). LC and NR alone resulted in 10% reduction in fat gain (15.8 ± 0.6 g; $p = 0.13$ in the LC group and 15.9 ± 0.7 g; $p = 0.17$ in the NR group). COMBI treatment resulted in 17% reduced fat gain (14.5 ± 1.0 g; $p < 0.01$). A more refined longitudinal analysis with EchoMRI revealed that the COMBI treatment was most effective in attenuating fat mass in the period between 15 weeks and 21 weeks (Figure 2F) when obesity was already established. Consistent with the EchoMRI data, the weight of the abdominal white adipose tissue (WAT) depots were significantly reduced by COMBI treatment (Figure 2G), and similar fat mass-lowering effects were observed for the subcutaneous WAT depot (Figure 2H).

These data demonstrate that COMBI treatment significantly attenuated HFD-induced obesity and adiposity independent of food intake or activity, an effect that could not be achieved with the individual components.

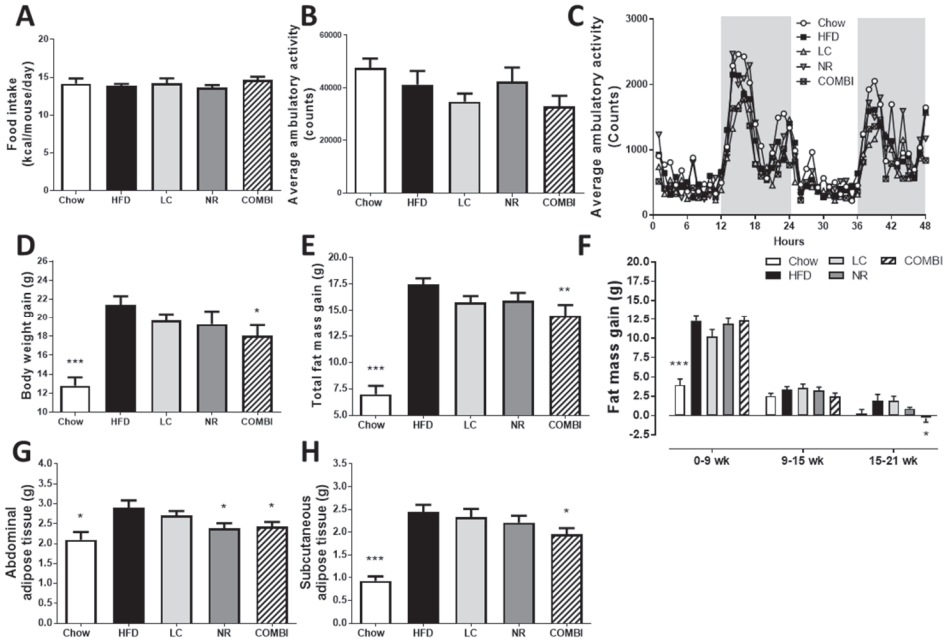

Figure 2. Effect of LC, NR and COMBI treatment on obesity after 21 weeks of treatment. (**A**) Food intake, (**B**) average ambulatory activity represented in counts, i.e., amount of infrared beam interruptions caused by movement, (**C**) average ambulatory activity during 48 hours, (**D**) body weight gain, (**E**) total fat mass gain, (**F**) fat mass gain over time, (**G**) abdominal tissue mass and (**H**) subcutaneous adipose tissue mass. Data are presented as mean ± SEM, * $p < 0.05$ or ** $p < 0.01$ or *** $p < 0.001$ compared to the HFD control group.

3.3. COMBI Treatment Attenuates Metabolic Risk Factors and Liver Integrity Marker ALT

Compared to the HFD group, fasting plasma cholesterol, high-density lipoprotein (HDL)-cholesterol and non-HDL cholesterol, triglycerides, insulin, blood glucose and alanine aminotransferase (ALT) levels were not significantly lowered with the treatments, although the COMBI treatment had the most reducing effects on these metabolic risk factors (Table 1). We subsequently performed an extensive plasma metabolomics analysis to profile plasma acylcarnitines, which inform on the effects related to fatty acid processing and β-oxidation.

We observed a significant increase in long-chain acylcarnitines in plasma of HFD-treated mice compared to the chow group (Table 2), indicating an elevation of these lipid species in HFD-induced obesity. When compared to HFD, LC and COMBI treatments resulted in a shift towards more medium-chain acylcarnitines, while NR consistently lowered plasma acylcarnitines concentrations (all values < 0).

Collectively, these data show that metabolic risk factors and liver integrity marker ALT were partially yet not significantly reversed by LC and NR and the most pronounced lowering effects were observed in the COMBI treatment group.

Table 1. Metabolic parameters.

	Chow	HFD	LC	NR	COMBI
Cholesterol (mM)	11.0 ± 3.3 ***	32.2 ± 14.4	28.6 ± 12.5	30.3 ± 10.6	25.4 ± 10.2
HDL-cholesterol (mM)	1.2 ± 0.6 ***	3.2 ± 1.4	2.5 ± 1.0	2.8 ± 1.3	2.5 ± 1.2
Non-HDL cholesterol (mM)	9.8 ± 3.6 ***	27.4 ± 12.3	26.1 ± 12.3	26.1 ± 8.9	22.9 ± 9.4
Triglycerides (mM)	2.6 ± 1.1 **	6.1 ± 5.4	4.9 ± 2.3	5.3 ± 3.9	3.7 ± 2.1
Glucose (mM)	7.6 ± 1.5	8.1 ± 2.1	7.5 ± 1.1	7.9 ± 1.6	7.4 ± 1.0
Insulin (ng/mL)	7.3 ± 7.1 **	24.8 ± 21.0	21.9 ± 18.7	28.0 ± 14.8	15.0 ± 7.7
ALT (U/L)	117 ± 83 ***	368 ± 249	330 ± 132	293 ± 127	267 ± 142

Blood glucose and plasma metabolic risk factors after 21 weeks of diet feeding. Values are mean ± SD, * $p < 0.05$ or ** $p < 0.01$ or *** $p < 0.001$ compared to the HFD control group.

Table 2. Plasma acylcarnitines.

	Acylcarnitines	HFD vs Chow	LC vs HFD	NR vs HFD	COMBI vs HFD
Short-chain	3-hydroxybutyrylcarnitine (C4-1)	0.1	0.5	−0.9	−0.5
	3-hydroxybutyrylcarnitine (C4-2)	−0.6	0.6	−0.3	0.3
	valerylcarnitine (C5)	−0.8	−0.1	−0.4	0.2
Medium-chain	hexanoylcarnitine (C6)	−0.4	−0.0	−0.5	0.4
	octanoylcarnitine (C8)	−0.2	0.3	−0.5	0.4
	decanoylcarnitine (C10)	0.3	0.7	−0.4	0.3
	laurylcarnitine (C12)	0.2	0.3	−0.5	0.3
	cis-4-decenoylcarnitine (C10:1)	0.2	0.4	−0.5	0.4
	5-dodecenoylcarnitine (C12:1)	0.3	0.3	−0.6	0.1
Long-chain	myristoylcarnitine (C14)	0.2	0.2	−0.4	0.2
	pentadecanoylcarnitine (C15)	0.8	0.2	−0.4	0.1
	palmitoylcarnitine (C16)	0.8	0.1	−0.3	−0.1
	margaroylcarnitine (C17)	1.7	0.2	−0.3	−0.0
	stearoylcarnitine (C18)	2.1	0.1	−0.2	0.0
	oleoylcarnitine (C18)	1.5	0.0	−0.4	−0.3
	arachidoylcarnitine (C20)	1.8	0.4	−0.1	0.2
	myristoleoylcarnitine (C14:1)	0.5	0.3	−0.5	0.2
	palmitoleoylcarnitine (C16:1)	0.3	0.1	−0.6	−0.4
	linoleoylcarnitine (C18:2)	0.8	0.2	−0.4	−0.1
	linolenoylcarnitine (C18:3)	0.0	0.3	−0.4	−0.0
	eicosenoylcarnitine (C20:1)	2.0	−0.1	−0.3	−0.4
	dihomo-linoleoylcarnitine (C20:2)	1.4	0.1	−0.3	−0.1
	arachidonoylcarnitine (C20:4)	0.6	0.4	−0.4	0.1
	dihomo-linolenoylcarnitine (20:3n3 or 6)	0.9	0.2	−0.3	0.0

Values present 2log transformed ratios between the groups compared and specified in the top row, positive values represent an increase and negative values a decrease. Green indicates a significant decrease, conversely, orange indicates a significant increase, with $p < 0.05$ considered as significant.

3.4. COMBI Treatment Reduces HFD-Induced Liver Steatosis

Next, we examined whether the adiposity-attenuating effects of the COMBI treatment had consequences for ectopic fat deposition in the liver. Liver weight was 3.0 ± 0.2 g in the HFD group and 2.0 ± 0.1 in the chow group ($p < 0.001$) (Figure 3A). COMBI treatment significantly reduced liver weight (2.4 ± 0.2 g; $p < 0.05$), which suggested an effect on hepatic steatosis while the mono-treatments had a less pronounced effect (LC 2.6 ± 0.1 g; $p = 0.07$, and NR 2.7 ± 0.2 g; $p = 0.29$). To investigate this in more detail, cross-sections of livers were analyzed for histopathological features of NAFLD (Figure 3B) and scored using a human-based grading system as described in the Materials and Methods section.

Steatosis in the HFD treated mice contained on average 62.8 ± 3.0% of the cross-sectional area, whereas the chow group hardly displayed steatosis (7.7 ± 3.7%; $p < 0.001$) (Figure 3C). The mono-treatments did not affect total steatosis (58.7 ± 3.3%; $p = 0.18$ in LC and 64.3 ± 2.8%; $p = 0.32$ in the NR groups), while COMBI treatment significantly reduced steatosis by 22% (49.1 ± 5.0%; $p < 0.05$).

Consistent with the steatosis-inducing effect of HFD, abnormally enlarged hypertrophic hepatocytes covered 40.0 ± 3.6% of the cross-sectional area in the HFD group while such cells were hardly observed in mice on the chow diet (2.1 ± 1.3%; $p < 0.001$) (Figure 3D). Neither LC nor NR affected HFD-induced hypertrophy (LC 38.3 ± 3.4%, and NR 38.9 ± 2.7%), but the COMBI treatment showed a significant reduction in hepatocellular hypertrophy (31.1 ± 4.2% of the liver area; $p < 0.05$).

Collectively, these data show that the adiposity-attenuating effects of the COMBI treatment are associated with a reduction in NAFLD development.

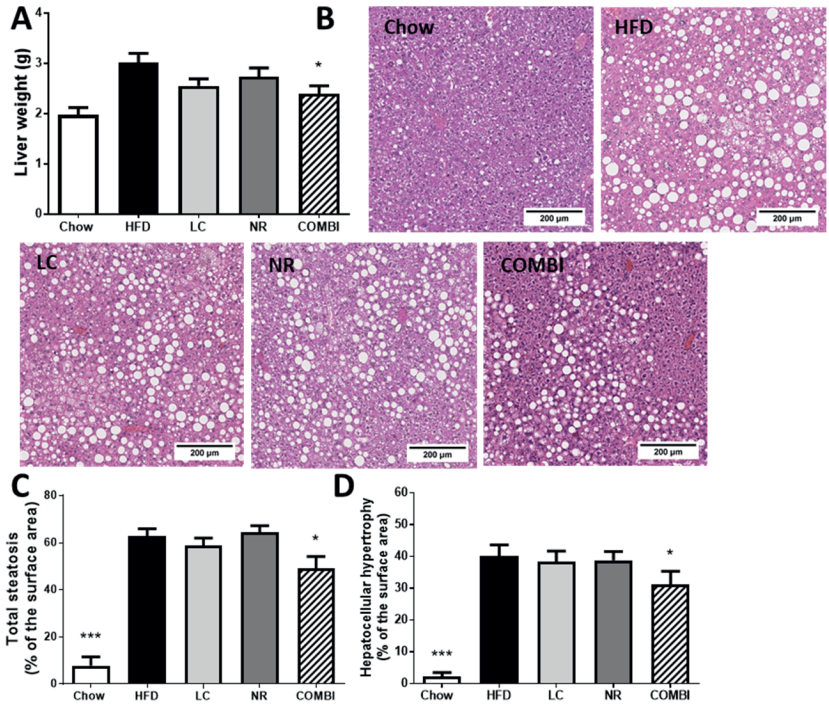

Figure 3. Liver analysis after 21 weeks of LC, NR and COMBI treatment. (**A**) Liver weight, (**B**) representative images of hematoxylin-eosin stained liver sections, (**C**) total steatosis, (**D**) hepatocellular hypertrophy. Data are presented as mean ± SEM, * $p < 0.05$ or ** $p < 0.01$ or *** $p < 0.001$ compared to the HFD control group.

3.5. NR and COMBI Attenuate Hepatic Lipid Peroxidation

Next, we investigated whether the observed hepatoprotective effects may be associated with an attenuation of oxidative stress induced lipid peroxidation. To this end we used 4-HNE as a marker and quantified the amount of 4-HNE positive structures by immunohistochemistry (Figure 4A,B).

The amount of positive 4-HNE structures in the HFD treated mice was high (9.6 ± 2.4 per mm^2), whereas the chow group scarcely showed any 4-HNE structures (0.3 ± 0.1; $p < 0.001$). LC only demonstrated a trend in lowering 4-HNE immunoreactivity (5.9 ± 2.0; $p = 0.09$), while both the NR and COMBI treatment revealed a significant decrease in 4-HNE immunoreactivity (4.7 ± 1.8 and 4.3 ± 2.0; both $p < 0.05$).

In conclusion, NR and COMBI treatment significantly attenuated the amount of 4-HNE adducts, suggesting that these treatments could reduce oxidative stress-related lipid peroxidation.

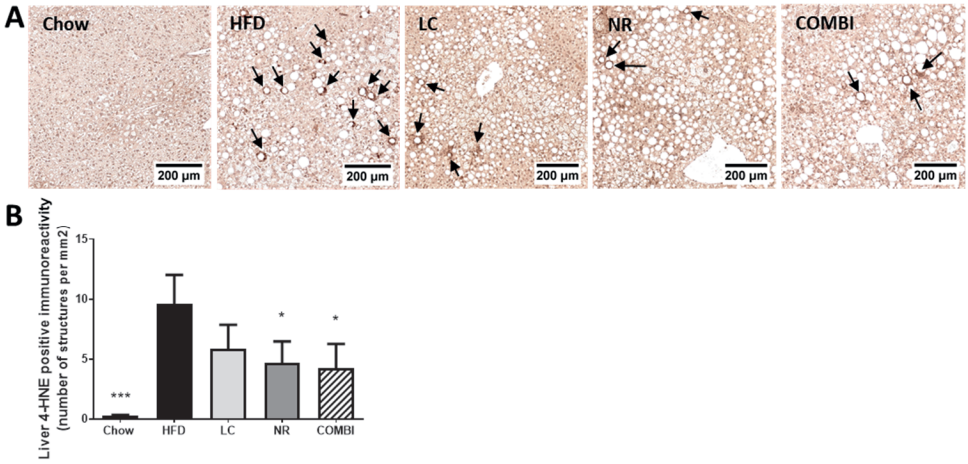

Figure 4. The 4-hydroxynonenal (4-HNE) marker for oxidative stress-related lipid peroxidation was analyzed in the liver using immunohistochemistry after 21 weeks of LC, NR and COMBI treatment. Stained liver sections were used for (**A**) representative images of 4-HNE, and quantification of (**B**) 4-HNE-positive immunoreactivity indicated here by arrows per mm^2. Data are presented as mean ± SEM, * $p < 0.05$ compared to the HFD control group.

3.6. COMBI Counteracts Effects of HFD on Metabolic Pathways in the Liver

A genome-wide gene expression profiling analysis was performed to gain insight into the molecular processes underlying the observed hepatoprotective effects of the COMBI treatment. HFD treatment resulted in 3914 differentially expressed genes (DEGs) compared to chow. The significant changes were used as input for an upstream regulator analysis, as described in the Materials and Methods section. HFD treatment strongly and significantly activated upstream regulators of chemokine and cytokine signaling (e.g., CCL5 and CXCL2, IL1b, IL4, IFNγ); transcriptional inflammatory control (e.g., AP1, JNK, NFκB); TRL signaling (e.g., TRL2, TRL4); metabolic control and hepatic insulin signaling (e.g., ACOX1, INSIG1, INSR, PPARGC1B, FOXO1, TP53, SIRT2) and oxidative stress response (e.g., NOS2, SOD).

LC resulted in 175 DEGs, NR in 208 DEGs and the COMBI treatment had the greatest effect on gene expression with 332 DEGs compared to HFD (Supplementary Material, Figure S1). A subsequent upstream regulator analysis showed that the majority of the above-mentioned regulators were not significantly affected by the mono-treatments (indicated by n/a in Table 3). By contrast, COMBI reversed numerous HFD-induced upstream regulators linked to metabolic control and insulin signaling (Table 3). For instance, HFD inhibited the enzyme ACOX1, involved in the first step of the peroxisomal fatty acid β-oxidation pathway, which was reversed by COMBI treatment. Similar counter-regulatory effects were found for regulators involved in lipid metabolism (SCAP, SREBF1, SREBF2), glucose uptake (SIRT2) and insulin signaling (INSR), which were inactivated by HFD and activated in the COMBI group. Together, this analysis demonstrates that COMBI treatment counteracted the detrimental effects of HFD in the liver and mainly affected master regulators relevant to metabolic control, thereby providing a rationale for its hepatoprotective effects.

Table 3. Upstream regulator analysis based on hepatic gene expression of metabolism related genes.

Upstream Regulator	HFD vs Chow		LC vs HFD		NR vs HFD		COMBI vs HFD	
	Activation z-score	p-value	Activation z-score	p-value	Activation z-score	p-value	Activation z-score	p-value
Metabolism-related								
ACOX1	-7,1	0,000	n/a	n/a	n/a	n/a	2,7	0,000
ATP7B	-3,2	0,000	n/a	n/a	n/a	0,03	2,0	0,001
INSIG1	-2,1	0,000	n/a	n/a	n/a	n/a	-1,9	0,000
INSR	-2,3	0,000	n/a	n/a	n/a	n/a	1,7	0,000
NR3C1	-2,1	0,000	n/a	n/a	n/a	n/a	-1,6	0,036
PPARGC1B	-3,3	0,035	n/a	n/a	n/a	n/a	2,2	0,000
SCAP	-4,8	0,000	n/a	n/a	n/a	n/a	3,3	0,000
SREBF1	-1,1	0,000	n/a	n/a	n/a	n/a	2,7	0,000
SREBF2	-3,0	0,000	n/a	n/a	n/a	n/a	2,6	0,000
SIRT2	-3,2	0,000	n/a	n/a	n/a	n/a	2,2	0,000
TSC2	-4,7	0,000	n/a	n/a	n/a	n/a	2,0	0,009
CDKN2A	0,0	0,000	n/a	n/a	n/a	n/a	-2,4	0,040
CNR1	2,7	0,007	n/a	n/a	n/a	n/a	n/a	n/a
CYP51A1	3,0	0,000	n/a	n/a	n/a	n/a	n/a	0,000
CYP2E1	2,1	0,000	n/a	n/a	n/a	n/a	n/a	n/a
EP300	4,5	0,000	n/a	n/a	n/a	n/a	-2,2	0,003
FOXO1	4,5	0,000	n/a	n/a	n/a	n/a	-2,1	0,015
FOXO3	0,6	0,000	n/a	n/a	n/a	n/a	-2,2	0,043
MAT1A	2,4	0,090	n/a	n/a	n/a	n/a	n/a	n/a
NR3C2	2,1	0,000	n/a	n/a	n/a	n/a	-2,0	0,006
TP53	2,2	0,000	n/a	n/a	n/a	n/a	-2,0	0,002

Changes in upstream regulator are predicted from changes in transcription factors or key regulators with a Z-score. $Z < -2$ indicates a relevant inhibition (shown in orange) and $Z > 2$ indicates a relevant activation (shown in green). Significant changes with $Z > 1.5$ are shown in light orange. The *p*-value indicates significant enrichment of the genes downstream of a regulator ($p < 0.01$ was considered statistically significant). n/a indicates an insufficient number of differentially expressed genes to link gene effects to an upstream regulator.

4. Discussion

The objective of the present study was to evaluate the anti-obesogenic and hepatoprotective effects of a novel treatment using a combination of LC and NR. We found that dietary supplementation with LC and NR was efficient because it elevated L-carnitine and nicotinamide plasma levels. Furthermore, the COMBI treatment attenuated HFD-induced body weight gain and total fat mass. The observed reduction in obesity development in the COMBI group was independent of food intake or locomotor activity, and was associated with an attenuation of metabolic risk factors and liver integrity marker ALT. COMBI treatment also reduced total steatosis, lipid peroxidation associated damage and affected several upstream regulators involved in liver metabolism. Hardly any of these anti-obesogenic or hepatoprotective effects were observed with the mono-treatments. Studies investigating combinations of LC and NR have not been reported so far, therefore, we used literature describing the effects of the individual components to discuss our findings.

Measures of adiposity were significantly reduced in the COMBI group. Interestingly, longitudinal Echo-MRI measurements showed that COMBI treatment reduced fat mass development specifically after week 15 (between 15–21 weeks), i.e., when obesity was already established. Since prolonged periods of nutrient excess result in a gradual accumulation of lipids, which may impair mitochondrial metabolism [12] at a certain stage, it is possible that carnitine and NAD+ become essential at the later timepoints when mitochondrial dysfunction and associated oxidative stress is more likely to occur. Indeed, there was pronounced 4HNE-positive immunoreactivity in HFD livers at the end of the study, and this immunoreactivity was lower in the COMBI group indicating reduced oxidative stress-associated lipid peroxidation [13]. We found that mono-treatment with LC did not result in a significant reduction in body weight and fat mass, and similar findings were reported by others studying body composition in rodents [20–22] or BMI in healthy and obese humans [23]. Also, short time studies using NR up to 15 weeks in rodents [20,24] and up to 12 weeks humans [25–28] did not report effects on body weight or body composition. In contrast, Canto et al. and Gariani et al. showed that 12 and 18 weeks of NR 400 mg/kg supplementation in C57Bl/6J mice reduced body weight due to a reduction in fat mass [9,29], respectively. Consistent with these reports, we observed a significant reduction in abdominal fat mass by NR in the present study. However, we did not found effects on total body fat mass, which could potentially be a consequence of a lower NR concentration used in our study.

We did not observe significant effects of the mono-treatments and the COMBI treatment on fasting total cholesterol, triglycerides, glucose and insulin, still the COMBI group showed consistently lower levels in all metabolic risk factors and plasma ALT. In particular the trend towards lower insulin and glucose suggests an effect on insulin signaling. Indeed, hepatic upstream regulator gene analysis predicted that HFD treatment significantly reduced glucose uptake (SIRT2) [30] and insulin receptor activity (INSR), and also revealed the counter-regulatory effects of the COMBI treatment on both processes, suggesting an improvement in the sensitivity of hepatic insulin.

Both LC and NR effects on plasma metabolic risk factors may be dose dependent. LC with 2000 mg daily for 24 weeks resulted in lower glucose and plasma lipid levels in NASH patients [31] as well as improved insulin sensitivity [32], whereas 19 months treatment with a very low dose of 100 mg/kg LC daily in mice did not reveal any significant effects on plasma lipid levels [33]. Similarly, studies in mice reported lowering effects of 400 mg/kg NR on ALT [27], fasting glucose and an improvement in insulin sensitivity [9,29]. By contrast, a very recent human study employing 2000 mg NR daily supplementation, which is approximately 2–3 times lower in concentration compared to the animal studies, could not reproduce the positive effects on insulin sensitivity and whole-body glucose metabolism in obese insulin resistant men [26].

Plasma acylcarnitines are often increased in obese patients with type 2 diabetes [34] and in high-fat diet induced animal models [8,35,36]. Acylcarnitines are typically formed in the cytosol to shuttle FAs across the mitochondrial membrane into the matrix, thereby providing substrate for β-oxidation. The observation that acylcarnitines are elevated in plasma of subjects with metabolic disease suggest that in the case of chronic oversupply with FAs, the capacity to further process these FAs has been reached and their metabolites also ultimately accumulate in plasma. Shuttling these acylcarnitines to the plasma could potentially prevent the buildup of possibly toxic acyl-CoA species inside the cell [37]. In line with this view, we also observed increased plasma acylcarnitines concentrations in the HFD group when compared to chow, in particular long-chain acylcarnitines. COMBI treatment increased plasma medium-chain acylcarnitines compared to the HFD. The increase of these acyl carnitine species could reflect incomplete β-oxidation. However, this does not seem to be in line with our other findings that COMBI treatment attenuated obesity, fat mass gain and hepatic steatosis, which all suggest an improvement in fatty acid catabolism and β-oxidation rather than worsening. An explanation for the seemingly discordant observations is provided by Lehman et al. who showed that medium chain acylcarnitines increase after exercise and acylcarnitines may enhance lipid oxidation [38]. Although the mice in the COMBI group were not more active relative to the HFD group, they gained 17% less fat mass. Therefore, it is possible that the COMBI treatment mimics some processes that are also activated during exercise leading to a higher metabolic rate.

The adiposity-attenuating effects of the COMBI treatment were associated with a reduction in NAFLD development, i.e., a reduction in both total steatosis and hepatocellular hypertrophy. Moreover, the liver weight was lower in mice treated with the COMBI. Collectively, the reduction in weight gain and improved liver health may be a result of improved hepatic metabolism and processing of fatty acids. Indeed, among the molecular processes underlying the observed hepatoprotective effects of the COMBI treatment were multiple pathways and upstream regulators critical for metabolic homeostasis. For example, COMBI treatment reversed HFD-induced deactivation of PPARGC1B involved in mitochondrial biogenesis and the increase of oxidative phosphorylation [39]. COMBI also reversed HFD-induced SREBF2 and SCAP modulation important players in lipid metabolism [40] and counteracted the HFD-induced inactivation of the enzyme ACOX1, which controls the first step of the peroxisomal FA β-oxidation pathway [41].

In conclusion, we showed that a novel treatment with a combination of LC and NR, but not the mono-treatments, significantly attenuated obesity, fat mass, hepatic steatosis and exerted beneficial effects on metabolic control pathways and upstream regulators (ACOX, SCPAP, SREBF2, PPARGC1B, INSR) in the liver. Dietary supplementation with LC and NR could constitute a new therapeutic approach to prevent obesity and its complications in the liver.

Acknowledgments: We would like to thank Teake Kooistra for scientific discussions and Karin Toet for her excellent technical assistance.

References

1. Ng, M.; Fleming, T.; Robinson, M.; Thomson, B.; Graetz, N.; Margono, C.; Mullany, E.C.; Biryukov, S.; Abbafati, C.; Abera, S.F.; et al. Global, regional, and national prevalence of overweight and obesity in children and adults during 1980-2013: A systematic analysis for the Global Burden of Disease Study 2013. *Lancet* **2014**, 6736, 1–16. doi:10.1016/S0140-6736(14)60460-8.
2. Younossi, Z.M.; Koenig, A.B.; Abdelatif, D.; Fazel, Y.; Henry, L.; Wymer, M. Global epidemiology of nonalcoholic fatty liver disease—Meta-analytic assessment of prevalence, incidence, and outcomes. *Hepatology* **2016**, doi:10.1002/hep.28431.
3. Fildes, A.; Charlton, J.; Rudisill, C.; Littlejohns, P.; Prevost, A.T.; Gulliford, M.C. Probability of an obese person attaining normal body weight: Cohort study using electronic health records. *Am. J. Public Health* **2015**, doi:10.2105/AJPH.2015.302773.
4. Lee, Y.; Kwon, E.Y.; Choi, M.S. Dietary isoliquiritigenin at a low dose ameliorates insulin resistance and NAFLD in diet-induced obesity in C57BL/6J mice. *Int. J. Mol. Sci.* **2018**, 19, doi:10.3390/ijms19103281.
5. Schrader, M.; Costello, J.; Godinho, L.F.; Islinger, M. Peroxisome-mitochondria interplay and disease. *J. Inherit. Metab. Dis.* **2015**, doi:10.1007/s10545-015-9819-7.
6. Wijburg, F.A.; Wüst, R.C.I.; Visser, G.; Wanders, R.J.A.; Knottnerus, S.J.G.; IJlst, L.; Houtkooper, R.H.; Ferdinandusse, S.; Bleeker, J.C . Disorders of mitochondrial long-chain fatty acid oxidation and the carnitine shuttle. *Rev. Endocr. Metab. Disord.* **2018**, 19, 93–106. doi:10.1007/s11154-018-9448-1.
7. Antonenkov, V.D.; Hiltunen, J.K. Transfer of metabolites across the peroxisomal membrane. *Biochim. Biophys Acta. – Mol. Basis. Dis.* **2012**, doi:10.1016/j.bbadis.2011.12.011.
8. Noland, R.C.; Koves, T.R.; Seiler, S.E.; Lum, H.; Lust, R.M.; Ilkayeva, O.; Stevens, R.D.; Hegardt, F.G.; Muoio, D.M . Carnitine insufficiency caused by aging and overnutrition compromises mitochondrial performance and metabolic control. *J. Biol. Chem.* **2009**, doi:10.1074/jbc.M109.032888.
9. Cantó, C.; Houtkooper, R.H.; Pirinen, E.; Youn, D.Y.; Oosterveer, M.H.; Cen, Y.; Fernandez-Marcos, P.J.; Yamamoto, H.; Andreux, P.A.; Cettour-Rose, P.; et al . The NAD+ precursor nicotinamide riboside enhances oxidative metabolism and protects against high-fat diet-induced obesity. *Cell Metab.* **2012**, 15, 838–847, doi:10.1016/j.cmet.2012.04.022.

10. Garten, A.; Schuster, S.; Penke, M.; Gorski, T.; De Giorgis, T.; Kiess, W.Physiological and pathophysiological roles of NAMPT and NAD metabolism. *Nat. Rev. Endocrinol.* **2015**, doi:10.1038/nrendo.2015.117.
11. Yoshino, J.; Baur, J.A.; Imai, S.I. NAD + Intermediates: The Biology and Therapeutic Potential of NMN and NR. *Cell Metab.* **2018**, doi:10.1016/j.cmet.2017.11.002.
12. Bournat, J.C.; Brown, C.W. Mitochondrial Dysfunction in Obesity. *Curr. Opin. Endocrino.l Diabetes Obes*. **2016**, doi:10.1097/MED.0b013e32833c3026.Mitochondrial.
13. Zhong, H., Yin, H. Role of lipid peroxidation derived 4-hydroxynonenal (4-HNE) in cancer: Focusing on mitochondria. *Redox. Biol.* **2015**, doi:10.1016/j.redox.2014.12.011.
14. Loguercio, C.; De Girolamo, V.; De Sio, I.; Tuccillo, C.; Ascione, A.; Baldi, F.; Budillon, G.; Cimino, L.; Di Carlo, A.; Pia Di Marino, M.; et al . Non-alcoholic fatty liver disease in an area of southern italy: Main clinical, histological, and pathophysiological aspects. *J. Hepatol.* **2001**, doi:10.1016/S0168-8278(01)00192-1.
15. Seki, S.; Kitada, T.; Yamada, T.; Sakaguchi, H.; Nakatani, K.; Wakasa, K. In situ detection of lipid peroxidation and oxidative DNA damage in non-alcoholic fatty liver diseases. *J. Hepatol.* **2002**, doi:10.1016/S0168-8278(02)00073-9.
16. Ore, A., Akinloye O.A. Oxidative Stress and Antioxidant Biomarkers in Clinical and Experimental Models of Non-Alcoholic Fatty Liver Disease. *Medicina* **2019**, 55, 26, doi:10.3390/medicina55020026.
17. Morrison, M.C.; Verschuren, L.; Salic, K.; Verheij, J.; Menke, A.; Wielinga, P.Y.; Iruarrizaga-Lejarreta, M.; Gole, L.; Yu, W.; Turner, S.; et al . Obeticholic Acid Modulates Serum Metabolites and Gene Signatures Characteristic of Human NASH and Attenuates Inflammation and Fibrosis Progression in Ldlr-/-.Leiden Mice. *Hepatol. Commun.* **2018**, 2, 1513–1532, doi:10.1002/hep4.1270.
18. Morrison, M.C.; Kleemann, R.; van Koppen, A.; Hanemaaijer, R.; Verschuren, L. Key inflammatory processes in human NASH are reflected in Ldlr-/-.Leiden mice: A translational gene profiling study. *Front. Physiol.* **2018**, doi:10.3389/fphys.2018.00132.
19. van Koppen, A.; Verschuren, L.; van den Hoek, A.M.; Verheij, J.; Morrison, M.C.; Li, K.; Nagabukuro, H.; Costessi, A.; Caspers, M.P.M.; van den Broek, T.J.; et al . Uncovering a Predictive Molecular Signature for the Onset of NASH-Related Fibrosis in a Translational NASH Mouse Model. *Cell Mol. Gastroenterol. Hepatol.* **2018**, 5, 83-98.e10, doi:10.1016/j.jcmgh.2017.10.001.
20. Ishikawa, H.; Takaki, A.; Tsuzaki, R.; Yasunaka, T.; Koike, K.; Shimomura, Y.; Seki, H.; Matsushita, H.; Miyake, Y.; Ikeda, F.; et al . L-carnitine prevents progression of non-alcoholic steatohepatitis in a mouse model with upregulation of mitochondrial pathway. *PLoS ONE* **2014**, doi:10.1371/journal.pone.0100627.
21. Melton, S.A.; Keenan, M.J.; Stanciu, C.E.; Hegsted, M.; Zablah-Pimentel, E.M.; O'Neil, C.E.; Gaynor, P.; Schaffhauser, A.; Owen, K.; Prisby, R.D.; et al . L-carnitine supplementation does not promote weight loss in ovariectomized rats despite endurance exercise. *Int. J. Vitam. Nutr. Res.* **2005**, doi:10.1024/0300-9831.75.2.156.
22. Fujisawa, K.; Takami, T.; Matsuzaki, A.; Matsumoto, T.; Yamamoto, N.; Terai, S.;

Sakaida, I. Evaluation of the effects of L-carnitine on medaka (Oryzias latipes) fatty liver. *Sci. Rep.* **2017**, doi:10.1038/s41598-017-02924-5.

23. Del Vecchio, F.; Coswig, V.; Galliano, L. Comment on 'The effect of (L-)carnitine on weight loss in adults: A systematic review and meta-analysis of randomized controlled trials. *Obes. Rev.* **2016**, doi:10.1111/obr.12436.
24. Shi, W.; Hegeman, M.A.; van Dartel, D.A.M.; Tang, J.; Suarez, M.; Swarts, H.; van der Hee, B.; Arola, L.; Keijer, J . Effects of a wide range of dietary nicotinamide riboside (NR) concentrations on metabolic flexibility and white adipose tissue (WAT) of mice fed a mildly obesogenic diet. *Mol. Nutr. Food Res.* **2017**, doi:10.1002/mnfr.201600878.
25. Martens, C.R.; Denman, B.A.; Mazzo, M.R.; Armstrong, M.L.; Reisdorph, N.; McQueen, M.B.; Chonchol, M.; Seals, D.R. Chronic nicotinamide riboside supplementation is well-Tolerated and elevates NAD+ in healthy middle-Aged and older adults. *Nat. Commun.* **2018**, doi:10.1038/s41467-018-03421-7.
26. Dollerup, O.L.; Christensen, B.; Svart, M.; Schmidt, M.S.; Sulek, K.; Ringgaard, S.; Stødkilde-Jørgensen, H.; Møller, N.; Brenner, C.; Treebak, J.T.; et al . A randomized placebo-controlled clinical trial of nicotinamide riboside in obese men: Safety, insulin-sensitivity, and lipid-mobilizing effects. *Am. J. Clin. Nutr.* **2018**, doi:10.1093/ajcn/nqy132.
27. Villani, R.G.; Gannon, J.; Self, M.; Rich, P.A. L-Carnitine Supplementation Combined with Aerobic Training Does Not Promote Weight Loss in Moderately Obese Women. *Int. J. Sport. Nutr. Exerc. Metab.* **2016**, doi:10.1123/ijsnem.10.2.199.
28. Rafraf, M.; Karimi, M.; Jafari, A. Effect of L-carnitine supplementation in comparison with moderate aerobic training on serum inflammatory parameters in healthy obese women. *J. Sports Med. Phys. Fitness.* **2015,** 55, 1363–1370.
29. Gariani, K.; Menzies, K.J.; Ryu, D.; Wegner, C.J.; Wang, X.; Ropelle, E.R.; Moullan, N.; Zhang, H.; Perino, A.; Lemos, V.; et al . Eliciting the mitochondrial unfolded protein response by nicotinamide adenine dinucleotide repletion reverses fatty liver disease in mice. *Hepatology* **2016**, doi:10.1002/hep.28245.
30. Watanabe, H.; Inaba, Y.; Kimura, K.; Matsumoto, M.; Kaneko, S.; Kasuga, M.; Inoue, H . Sirt2 facilitates hepatic glucose uptake by deacetylating glucokinase regulatory protein. *Nat. Commun.* 2018. doi:10.1038/s41467-017-02537-6.
31. Malaguarnera, M.; Gargante, M.P.; Russo, C.; Antic, T.; Vacante, M.; Malaguarnera, M., et al. L-carnitine supplementation to diet: A new tool in treatment of nonalcoholic steatohepatitisa randomized and controlled clinical trial. *Am. J. Gastroenterol.* **2010**, doi:10.1038/ajg.2009.719.
32. Ruggenenti, P.; Cattaneo, D.; Loriga, G.; Ledda, F.; Motterlini, N.; Gherardi, G.et al. Ameliorating hypertension and insulin resistance in subjects at increased cardiovascular risk: Effects of acetyl-l-carnitine therapy. *Hypertension* **2009**, doi:10.1161/HYPERTENSIONAHA.109.132522.
33. Cheema, U.B.; Most, E.; Eder, K.; Ringseis, R. Effect of lifelong carnitine supplementation on plasma and tissue carnitine status, hepatic lipid metabolism and stress signalling pathways and skeletal muscle transcriptome in mice at advanced age. *Br. J. Nutr.* **2019**, doi:10.1017/S0007114519000709.

34. Malaguarnera, M.; Gargante, M.P.; Russo, C.; Antic, T.; Vacante, M.; Malaguarnera, M.; Avitabile, T.; Li Volti, G.; Galvano, F . Increased levels of plasma acylcarnitines in obesity and type 2 diabetes and identification of a marker of glucolipotoxicity. *Obesity* **2010**, doi:10.1038/oby.2009.510.
35. Koves, T.R.; Li, P.; An, J.; Akimoto, T.; Slentz, D.; Ilkayeva, O.; Dohm, G.L.; Yan, Z.; Newgard, C.B.; Muoio, D.M. Peroxisome proliferator-activated receptor-γ co-activator 1α-mediated metabolic remodeling of skeletal myocytes mimics exercise training and reverses lipid-induced mitochondrial inefficiency. *J. Biol. Chem.* **2005**, doi:10.1074/jbc.M507621200.
36. Koves, T.R.; Ussher, J.R.; Noland, R.C.; Slentz, D.; Mosedale, M.; Ilkayeva, O.; Bain, J.; Stevens, R.; Dyck, J.R.B.; Newgard, C.B.; et al. Mitochondrial Overload and Incomplete Fatty Acid Oxidation Contribute to Skeletal Muscle Insulin Resistance. *Cell Metab.* **2008**, doi:10.1016/j.cmet.2007.10.013.
37. Li, L.O.; Klett, E.L.; Coleman, R.A. Acyl-CoA synthesis, lipid metabolism and lipotoxicity. *Biochim. Biophys. Acta. – Mol. Cell Biol. Lipids* **2010**, doi:10.1016/j.bbalip.2009.09.024.
38. Lehmann, R.; Zhao, X.; Weigert, C.; Simon, P.; Fehrenbach, E.; Fritsche, J.; Machann, J.; Schick, F.; Wang, J.; Hoene, M.; et al. Medium chain acylcarnitines dominate the metabolite pattern in humans under moderate intensity exercise and support lipid oxidation. *PLoS ONE* **2010**, doi:10.1371/journal.pone.0011519.
39. St-Pierre, J.; Lin, J.; Krauss, S.; Tarr, P.T.; Yang, R.; Newgard, C.B.; Spiegelman, B.M. Bioenergetic analysis of peroxisome proliferator-activated receptor γ coactivators 1α and 1β (PGC-1α and PGC-1β) in muscle cells. *J. Biol. Chem.* **2003**, doi:10.1074/jbc.M301850200.
40. Cheng, X.; Li, J.; Guo, D. SCAP/SREBPs are Central Players in Lipid Metabolism and Novel Metabolic Targets in Cancer Therapy. *Curr. Top Med. Chem.* **2018**, doi:10.2174/1568026618666180523104541.
41. Hu, T.; Foxworthy, P.; Siesky, A.; Ficorilli, J. V.; Gao, H.; Li, S.; Christe, M.; Ryan, T.; Cao, G.; Eacho, P.; et al. Hepatic peroxisomal fatty acid β-oxidation is regulated by liver X receptor α. *Endocrinology* **2005**, doi:10.1210/en.2005-0591.
42. choemaker, M.H.; Kleemann, R.; Morrison, M.C.; Verheij, J.; Salic, K.; Van Tol, E.A.F.; Kooistra, T.; Wielinga, P.Y. A casein hydrolysate based formulation attenuates obesity and associated nonalcoholic fatty liver disease and atherosclerosis in LDLr-/-.Leiden mice. *PLoS ONE* **2017**, doi:10.1371/journal.pone.0180648.
43. Kühnast, S.; Van Der Tuin, S.J.L.; Van Der Hoorn, J.W.A.; Van Klinken, J.B.; Simic, B.; Pieterman, E.; Havekes, L.M.; Landmesser, U.; Lüscher, T.F.; Van Dijk, K.W.; et al. Anacetrapib reduces progression of atherosclerosis, mainly by reducing non-HDL-cholesterol, improves lesion stability and adds to the beneficial effects of atorvastatin. *Eur. Heart J.* **2015**, doi:10.1093/eurheartj/ehu319.
44. Liang, W.; Menke, A.L.; Driessen, A.; Koek, G.H.; Lindeman, J.H.; Stoop, R.; Havekes, L.M.; Kleemann., R.; Van Den Hoek, A.M. Establishment of a general NAFLD scoring system for rodent models and comparison to human liver pathology. *PLoS ONE* **2014**, doi:10.1371/journal.pone.0115922.
45. Evans, A.M.; DeHaven, C.D.; Barrett, T.; Mitchell, M.; Milgram, E. Integrated,

nontargeted ultrahigh performance liquid chromatography/ electrospray ionization tandem mass spectrometry platform for the identification and relative quantification of the small-molecule complement of biological systems. *Anal. Chem.* **2009**, doi:10.1021/ac901536h.

46. Evans, A.; Bridgewater, B.; Liu, Q.; Mitchell, M.; Robinson, R.; Dai, H.; Stewart, S.; DeHaven, C.; Miller, L . High Resolution Mass Spectrometry Improves Data Quantity and Quality as Compared to Unit Mass Resolution Mass Spectrometry in High-Throughput Profiling Metabolomics. *J Postgenomics Drug Biomark Dev.* **2015**, doi:10.4172/2153-0769.1000132.
47. Anders, S.; Huber, W. Differential expression analysis for sequence count data. *Genome Biol.* **2010**, doi:10.1186/gb-2010-11-10-r106.
48. Liang, W.; Tonini, G.; Mulder, P.; Kelder, T.; van Erk, M.; van den Hoek, A.M.; Mariman, R.; Wielinga, P.Y.; Baccini, M.; Kooistra, T.; et al . Coordinated and Interactive Expression of Genes of Lipid Metabolism and Inflammation in Adipose Tissue and Liver during Metabolic Overload. *PLoS ONE* **2013**, doi:10.1371/journal.pone.0075290.

Supplemental information

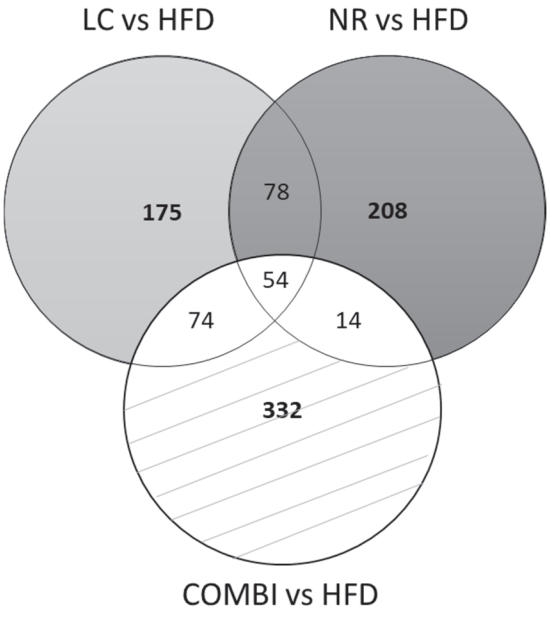

***Figure S1**. Total number of differentially expressed genes and overlap of the different dietary treatment comparisons.*

CHAPTER

4

Krill oil treatment increases distinct PUFAs and oxylipins in adipose tissue and liver and attenuates obesity-associated inflammation via direct and indirect mechanisms

Eveline Gart, Kanita Salic, Martine C. Morrison, Martien Caspers, Wim van Duyvenvoorde, Marieke Heijnk, Martin Giera, Ivana Bobeldijk-Pastorova, Jaap Keijer, Andreas B. Storsve, Petter-Arnt Hals and Robert Kleemann

Nutrients. 2021 Aug 18;13(8):2836.
doi: 10.3390/nu13082836. PMID: 34444996; PMCID: PMC8401900.

Abstract

The development of obesity is characterized by the metabolic overload of tissues and subsequent organ inflammation. The health effects of krill oil (KrO) on obesity-associated inflammation remain largely elusive, because long-term treatments with KrO have not been performed to date. Therefore, we examined the putative health effects of 28 weeks of 3% (*w*/*w*) KrO supplementation to an obesogenic diet (HFD) with fat derived mostly from lard. The HFD with KrO was compared to an HFD control group to evaluate the effects on fatty acid composition and associated inflammation in epididymal white adipose tissue (eWAT) and the liver during obesity development. KrO treatment increased the concentrations of EPA and DHA and associated oxylipins, including 18-HEPE, RvE_2 and 14-HDHA in eWAT and the liver. Simultaneously, KrO decreased arachidonic acid concentrations and arachidonic-acid-derived oxylipins (e.g., HETEs, PGD_2, PGE_2, $PGF_2\alpha$, TXB_2). In eWAT, KrO activated regulators of adipogenesis (e.g., PPARγ, CEBPα, KLF15, STAT5A), induced a shift towards smaller adipocytes and increased the total adipocyte numbers indicative for hyperplasia. KrO reduced crown-like structures in eWAT, and suppressed HFD-stimulated inflammatory pathways including TNFα and CCL2/MCP-1 signaling. The observed eWAT changes were accompanied by reduced plasma leptin and increased plasma adiponectin levels over time, and improved insulin resistance (HOMA-IR). In the liver, KrO suppressed inflammatory signaling pathways, including those controlled by IL-1β and M-CSF, without affecting liver histology. Furthermore, KrO deactivated hepatic REL-A/p65-NF-κB signaling, consistent with increased PPARα protein expression and a trend towards an increase in IkBα. In conclusion, long-term KrO treatment increased several anti-inflammatory PUFAs and oxylipins in WAT and the liver. These changes were accompanied by beneficial effects on general metabolism and inflammatory tone at the tissue level. The stimulation of adipogenesis by KrO allows for safe fat storage and may, together with more direct PPAR-mediated anti-inflammatory mechanisms, attenuate inflammation.

Graphical abstract

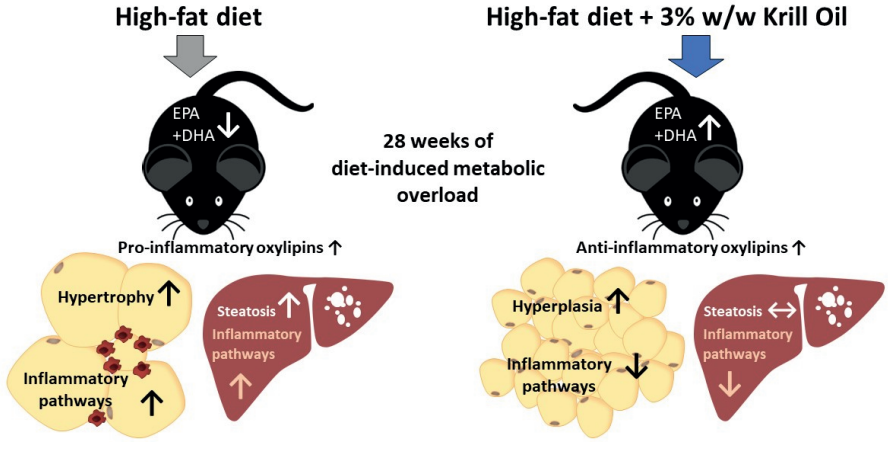

1. Introduction

Metabolic overload caused by excessive intake of energy-dense foods promotes the development of obesity, which is characterized by inflammation in white adipose tissue (WAT) and the liver [1]. During the development of obesity, WAT expands to store the energy surplus. This WAT expansion involves two processes: adipocyte hyperplasia (an increase in the cell number via adipogenesis) and adipocyte hypertrophy (an increase in cell size) [2]. Both processes have a physiological limit, and these vary between different WAT depots. The epididymal WAT (eWAT) of mice, for example, predominantly responds to metabolic overload with hypertrophy [3]. We and others have shown that the time point of maximal eWAT expansion coincides with the development of adipose tissue inflammation [3,4]. eWAT is thought to be particularly susceptible to becoming inflamed because of its limited ability to initiate the adipogenesis program required for hyperplasia. The development of hypertrophic and inflamed WAT is typically paralleled by changes in systemic inflammation markers, including cytokines (e.g., TNF-α, Il-6) and adipokines [5]. These circulating factors can contribute to the development of insulin resistance as well as liver steatosis and inflammation in obese subjects [6]. Treatments that could correct metabolic imbalances and exert anti-inflammatory activities would be beneficial for all obesity-associated disorders.

Krill oil (KrO), a marine oil extracted from Antarctic krill, is rich in phospholipids (>55% of total lipids), most of which are phosphatidylcholines (>85%). KrO has a high content of long-chain omega-3 polyunsaturated fatty acids (PUFAs), in particular eicosapentaenoic acid (EPA) and docosahexaenoic acid (DHA) [7]. Lipids from KrO can be stored in cells or converted intracellularly into a variety of bioactive oxylipins that can act as direct inflammatory modulators [8]. Many of the fatty acids (FAs) present in KrO, as well as their metabolites, are ligands of transcriptional regulators, including peroxisome-proliferator-activated receptors (PPARs) [9]. PPARα and PPARγ are predominately expressed in the liver and WAT, respectively, where they control the expression of genes that are critical for metabolism and adipogenesis. In addition, PPARs have anti-inflammatory properties, and can repress NF-κB-mediated transcription via multiple mechanisms (including direct physical association and upregulation of the IκBα protein) [10–12]. Besides being a ligand for PPARs, KrO-derived EPA and DHA can displace arachidonic acid (ARA), an omega-6 FA with proinflammatory properties, from membranes and may also compete with ARA for further enzymatic processing [13]. Via these indirect mechanisms, EPA and DHA can attenuate the pro-inflammatory effects of ARA and its downstream metabolites, such as hydroxyeicosatetraenoic acids (HETEs), oxoeicosanoids (KETEs), prostaglandins (PGs), thromboxanes (TXs) and leukotrienes (LTs) [14]. Furthermore, EPA and DHA themselves can be enzymatically converted into inflammation-resolving mediators, including hydroxyeicosapentaenoic acids (HEPEs), hydroxy docosahexaenoic acids (HDHAs) and further into resolvins (RVs), protectins (PDs) and maresins (MaRs) [14].

In this study, our aim was to examine the putative health effects of long-term (28 weeks) KrO supplementation (3% *w*/*w*) in mice, since the health effects of KrO on obesity-associated organ inflammation remain largely elusive due to the lack of long-term treatment studies using physiologically relevant KrO concentrations. A small number of

relatively short studies (less than 12 weeks of KrO treatment [15–19]) consistently point to an improvement of metabolic homeostasis and metabolic risk factors. To gain a better mechanistic insight into how KrO exerts its effects, we analyzed WAT and the liver by means of genome-wide mRNA sequencing to identify molecular pathways and critical upstream regulators. Furthermore, both tissues were subject to a comprehensive fatty acid composition analysis, including oxylipins using LC-MS/MS. Ldlr-/- Leiden mice were chosen as a model because these mice develop obesity in combination with pronounced hyperinsulinemia and adipose tissue and liver inflammation when treated with energy-dense diets for 28 weeks (to allow for the histological analysis of organ inflammation) with a human-diet-like macronutrient composition, not requiring dietary supplementation with cholesterol [20–23]. Under the experimental conditions employed herein, Ldlr-/- Leiden mice have been shown to develop histopathological features similar to humans and they recapitulate human disease pathways, as demonstrated by recent comparative transcriptomics, metabolomics and proteomics studies [22,24,25]. We show that long-term KrO treatment markedly affects the tissue levels of PUFAs and oxylipins, and consistently with this, reduces their inflammatory tone.

2. Materials and Methods

2.1. Animals, Diets and Study Design

All animal experiments were performed in accordance with the Animal Care and Use Committee and ethical approval by an independent Animal Welfare Body (IVD TNO; approval number 3682/TNO-274). Male Ldlr-/- Leiden mice were obtained from the breeding facility of TNO Metabolic Health Research, Leiden, The Netherlands. All mice were group-housed in an AAALAC-accredited animal facility (relative humidity 50%–60%, temperature ~21 °C, light cycle 7 am to 7 pm) and had ad libitum access to food and water. Body weight and blood glucose data obtained before the start of dietary treatment were used to match mice into three comparable groups, to ensure that group differences at the end were attributable to the treatment they received during the study and not due to differences at baseline. The control group (n = 15) was treated with an energy-dense high-fat diet (HFD; D12451, Research Diets Inc.; 20 kcal% protein, 35 kcal% carbohydrate, 45 kcal% fat, with 39 kcal% from lard and 6 kcal% from soybean oil). The KrO treatment group received an HFD in which 3% of the total diet was replaced with KrO (KrO diet). The KrO (Superba Boost, Aker BioMarine Antarctic ASA, Lysaker, Norway) itself contained EPA ≥150 mg/g and DHA ≥70 mg/g, which is approximately 20% of EPA and DHA fatty acids in KrO. Fatty acids are structural components of lipid species that are efficiently taken up in the intestine (phospholipids). KrO is a marine oil that is particularly rich in phospholipids and the KrO used in this study contained ≥560 mg/g phospholipids, of which ≥480 mg was phosphatidylcholine. At an expected average daily intake of 3 g diet per mouse, the dietary intake of KrO was 0.09 g/mouse/day on average. HFD and KrO diets were isocaloric. A reference group remained on a low-fat control chow diet (n = 6) (chow; Ssniff-Spezialdiäten GmbH, Soest, Germany).

Body weight and food intake were measured regularly, and body composition was determined using echoMRI (EchoMRI-LLC, Houston, TX, USA). Blood samples were taken from the tail vein at the start of the study and after 8 weeks, 16 weeks and 28 weeks. In week 28, animals were terminated after 5 h fasting via gradual-fill CO_2 asphyxiation and a terminal blood sample was collected via cardiac puncture. Isolated adipose and liver tissues were fixed in formalin and paraffin-embedded for histological analysis, or snap-frozen and stored at −80°C for gene expression, lipid and protein analyses.

2.2. Blood Chemistry

Analyses of cholesterol, triglycerides, insulin, leptin, adiponectin, ALAT in fasting EDTA plasma and blood glucose were performed as described previously [22]. The blood sampling over time allowed us to calculate area under the curve (AUC) values of plasma parameters (GraphPad Prism, version 8 for Windows, GraphPad Software, La Jolla, CA, USA, www.graphpad.com). Free fatty acids (FFAs) were measured in orlistat (1 mg/L; Sigma-Aldrich, St. Louis, MO, USA) [26]-treated plasma and quantified with the NEFA-HR kit (Instruchemie, Delfzijl, The Netherlands).

2.3. Total Fatty Acid Composition Analysis in Dry Blood Spots, White Adipose Tissue and Liver

Dry blood spots (DBSs) collected during blood sampling, as well as tissue collected at sacrifice from eWAT and the liver, were analyzed for their fatty acid composition (OmegaQuant Analytics, Sioux Falls, SD, USA). Briefly, blood was collected during blood sampling after 28 weeks of treatment on filter paper pre-treated with an antioxidant cocktail (Fatty Acid Preservative Solution) and dried at room temperature for 15 min. Tissue samples were weighed and transferred into screw-cap glass vials that contained tritricosanoin as an internal standard (tri-C23:0 TG) (NuCheck Prep, Elysian, MN, USA). These tissues were homogenized and then extracted with a modified Folch extraction. A portion of the organic layer was transferred to a screw-cap glass vial and dried in a speed vac. The dried tissue samples and a punch of the DBS filter paper in screw-cap glass vials were treated with BTM solution (methanol containing 14% boron trifluoride, toluene, methanol; 35:30:35 *v*/*v*/*v*) (Sigma-Aldrich). The vial was briefly vortexed and heated (100 °C for 45 min). After cooling, hexane (EMD Chemicals, New Hampshire, MA, USA) and HPLC-grade water were added, and samples were vortexed and centrifuged to separate layers. An aliquot of the hexane layer was used for gas chromatography (GC). GC was carried out using a GC-2010 (Shimadzu Corporation, Columbia, MD, USA) equipped with a SP-2560, 100-m fused silica capillary column (0.25 mm internal diameter, 0.2 µm film thickness; Supelco, Bellefonte, PA, USA). Fatty acids were identified and calibrated using a standard mixture of defined fatty acids (GLC OQ-A, NuCheck Prep). Fatty acid composition was expressed relatively (percentage of total identified fatty acids) and given in absolute concentrations (µg fatty acid per mg WAT or liver tissue).

2.4. Free Fatty Acids and Lipid Mediator Composition in White Adipose Tissue and Liver

White adipose and liver tissues from sacrificed mice were homogenized in water at a concentration of 0.33 mg/µL (Biosolve, Valkenswaard, The Netherlands). WAT (10 mg) or liver tissue (2.7 mg) homogenates were mixed with 600 µL MeOH (Merck, Darmstadt, Germany) containing internal standards (0.33 ng/mL PGE_2-d4, LTB_4-d4, 15-HETE-d8, 14(15)-EET-d11, 0.66 ng/mL 8-iso-PGF_2 alpha-d4 and 3.3 ng/mL DHA-d5, all Cayman Chemical, Ann Abor, MI, USA) and 200 µL water was added to the mixture. Samples were incubated for 20 min at −20 °C and centrifuged (10 min at 16.100× *g*, 4 °C). Supernatant was diluted with water, acidified to pH ±3.0 using formic acid (VWR, Darmstadt, Germany) and applied to C18 SPE cartridges (Sep-Pak C18, 200 mg, 3 cc, Waters, Milford, MA, USA). The obtained samples were cleaned consecutively with water and *n*-hexane (VWR) and eluted using methyl formate (Sigma-Aldrich). The eluate was dried at 40 °C under a stream of nitrogen and reconstituted in 40% MeOH. Samples were analyzed using an LC-MS/MS system consisting of two LC-30AD pumps, a SIL-30AC autosampler and a CTO-20AC column oven (All Shimadzu, Hertogenbosch, The Netherlands). Samples were injected with an autosampler (at 6 °C) and separated on a Kinetex C18 column (Phenomenex, Aschaffenburg, Germany, 50 × 2.1 mm, 1.7 µm) using a gradient of 0.01% acetic acid (Fluka, Darmstadt, Germany) in water (Honeywell-Riedel de Haën, Seelze, Germany; eluent A) and 0.01% acetic acid in MeOH (eluent B) with the oven at 50 °C. The gradient was as follows: 0.0–1.0 min constant at 30% B, 1.0–1.1 min linear increase to 45% B, 1.1–2.0 min linear increase to 53.5% B, 2.0–4.4 min linear increase to 55.5% B, 4.0–7.0 min linear increase to 90% B, 7.0–7.1 min linear increase to 100% B, 7.1–9.0 min constant at 100% B, 9.0–9.5 min linear decrease to 30% B, 9.5–11.5 min constant at 30% B. Detection was achieved on a Qtrap 6500 (Sciex Nieuwerkerk a/d, IJssel, The Netherlands) equipped with an ESI source. The MS was operated in negative scheduled MRM mode, with the source needle voltage at −4500 V, drying temperature of 450 °C, ion source gas 1 and 2 (both air) at respectively 40 and 30 psi and the nitrogen nebulizer gas at 30 psi. The entrance potential was set to 10 V and the collision gas flow to 'medium'. Individually optimized parameters for each compound can be found in Supplementary Table S1.

The detected lipid mediators PDX and RvE_2 were identified based on comparisons with authentic standard material. Both substances showed closely matching (<0.5% deviation) relative retention times between samples and authentic standard material. Furthermore, the tandem mass spectra for PDX were closely matched (Supplementary Figure S1). In the case of RvE_2, we monitored four characteristic fragment ions of RvE_2 by means of a dedicated product ion scan LC-MS/MS method. The obtained relative retention times and ion ratios were also compared with authentic standard material (Supplementary Figure S2). Standards of RvE_1, RvE_2, 18(R)-RvE_3 and 18(S)-RvE_3 were gifts from Dr. Makoto Arita (Tokyo, Japan); all other standards were obtained from Cayman Chemicals.

2.5. Histological Analysis of Adipose Tissue and Liver

Paraffin-embedded 5-µm-thick cross sections of eWAT were stained with hematoxylin-phloxine-saffron and scanned for digital analysis (Aperio AT2, Leica Biosystems, Amsterdam,

The Netherlands). Cell size and counts of adipocytes were analyzed using Adiposoft [27]. Inflammation was quantified by scoring the amount of crown-like structures (CLS) and expressed as the number of CLS/1000 adipocytes, as described previously in detail [28]. The calculation of total eWAT cell numbers as a measure of hyperplasia was performed using a well-established mathematical model [29].

The histopathological analysis of liver steatosis and hypertrophy was performed on 3-µm-thick hematoxylin-eosin-stained cross sections of the medial lobe using a standardized method for rodent liver histopathology, based on the human NAS scoring system [30,31]. The percentages of the total liver sections affected by steatosis and hypertrophy translate into the NAS categories of severity as follows: 0 (<5%), 1 (5%–33%), 2 (34%–66%) and 3 (>66%) [30]. In addition, F4/80 immunostaining was performed on the liver sections as detailed in [24] and the number of F4/80-positive CLSs was counted in three nonoverlapping fields and expressed per mm^2.

2.6. Liver Biochemistry

Total hepatic triglyceride content was determined in crude liver homogenates by following the Bligh and Dyer method for lipid extraction with methanol and chloroform [32]. In the same liver homogenates, protein levels were determined, using a Lowry protein assay. The lipids were separated by means of high-performance liquid chromatography (HPTLC) on silica gel plates and stained with color reagent (5 g of $MnCl_2$•4 H_2O, 32 mL of 95%–97% H_2SO_4 added to 960 mL of CH_3OH:H_2O 1:1 *v*/*v*). The liver triglyceride bands were quantified with a ChemiDoc Touch Imaging System (Bio-Rad, Hercules, CA, USA) using Image-lab version 5.2.1 software (Bio-Rad) and were expressed per mg protein.

2.7. Genome-Wide Gene Expression Analysis

Next generation sequencing (NGS) was performed essentially as described [24]. Briefly, total RNA was extracted from eWAT using an Ambion RNAqueous total RNA isolation kit (Thermo Fisher Scientific, Waltman, MA, USA) and from the liver using the RNA-Bee total-RNA isolation kit (Bio-Connect, Huissen, The Netherlands), and was subsequently purified using PureLink RNA Mini Kit (Thermo Fisher Scientific). The RNA concentration was determined spectrophotometrically using a Nanodrop 1000 (Isogen Life Science, De Meern, The Netherlands), and RNA quality was assessed using a 2100 Bioanalyzer (Agilent Technologies, Amstelveen, The Netherlands). Strand-specific messenger RNA sequencing libraries were multiplexed, clustered and sequenced on a Nextseq500 V2 system (Illumina, San Diego, CA, USA) at Genomescan (Leiden, The Netherlands). The sequenced, annotated and aligned gene counts served as inputs for the differentially expressed gene (DEG) analysis using the Deseq2-method [33]. The integrity of the gene expression datasets from eWAT and the liver were analyzed (e.g., distance matrix and principal component analysis) and 10% technical outliers were excluded. For the subsequent bioinformatical analysis, n = 5 chow, n = 9 HFD and n = 9 KrO liver samples, as well as n = 5 chow, n = 8 HFD and n = 10 KrO eWAT samples, were used. DEGs were used as inputs for pathway analysis through Ingenuity Pathway Analysis (IPA; www.ingenuity.com). IPA uses gene expression data of all

known downstream target genes to predict the activation or deactivation of an upstream regulator. Z-scores greater than 2 indicate the enhanced activity of an upstream regulator, whereas a Z-score less than −2 indicates the reduced activity of an upstream regulator [24]. The *p*-value indicates the significance of the gene enrichment of these upstream regulators.

2.8. Western Blot Analysis

Liver tissue from HFD- and KrO-treated mice (*n* = 4/group) were homogenized in lysis buffer containing 150 mM NaCL, 1 mM EDTA PH = 8, 50 mM Tris-HCL PH = 7.4, 1% Igepal, 0.25% deoxycholate, 0.1% SDS, 1 mM PMSF, 1 mM Na_3VO_4 and complete mini EDTA-free protease inhibitor (Roche, Mannheim, Germany). Homogenates were centrifuged at 13,000 rpm for 15 min at 4 °C, and the protein content of the supernatant was determined using the BCA Protein Assay Kit (Thermo Fisher Scientific). Proteins (50 ug) in 2× SDS Laemmli Sample Buffer (1:1 *v*/*v*; Sigma-Aldrich) were boiled for 5 min at 95 °C. Subsequently, samples were separated on a 4%–20% (*w*/*v*) SDS-page gel (mini-Protean TGX stain-free precast gels; Bio-Rad). Proteins were transferred onto Trans-blot Turbo mini PVDF blotting membranes (Bio-Rad) using the MIXED MW program on the Trans-blot Turbo Bio-Rad machine. The blotting membranes were blocked for 1 h with 5% (*w*/*v*) milk powder in tris-buffered saline with 0.1% Tween 20 and incubated overnight at 4 °C with either the primary antibody IκBα (#9242S–1:1000 *v*/*v*; Cell Signaling, Leiden, The Netherlands), PPARα (ab24509–1:1000 *v*/*v*; Abcam, Cambridge, UK) or αTubulin (T5168-1:1000 *v*/*v*; Sigma-Aldrich). Secondary antibody (anti-mouse HRP conjugate #7076S-1:2000 *v*/*v* or anti-rabbit HRP conjugate #7074S-1:2000 *v*/*v*; Cell Signaling) was added and SuperSignal West Femto (Thermo Fisher Scientific) was used to visualize protein bands. Blots were analyzed with a ChemiDoc Touch Imaging system (Bio-Rad) and band intensities were normalized to αTubulin.

2.9. Statistical Analysis

All data shown are presented as mean ± standard deviation (SD). The experiments investigated the null hypothesis that KrO does not have beneficial effects on disease parameters relative to controls (HFD). Therefore, KrO was compared to the HFD control group, and data from chow mice were provided as a reference. The significance of differences between KrO and HFD was tested using one-sided *t*-tests (α = 0.05) if the data were normally distributed with equal variances. Data sets that were not normally distributed or with unequal variances were tested with a Mann–Whitney U test. IPA analysis to determine differentially expressed genes were based on Fisher's exact test (α = 0.01).

3. Results

3.1. Long-Term KrO Treatment Improves Lipid Composition in Blood, eWAT and Liver Tissue

During 28 weeks of HFD feeding, body weight increased from 29.4 g to 52.7 g in the HFD control group. EchoMRI analysis showed that the observed weight gain relative to chow could mainly be ascribed to an increase in fat mass (Table 1). KrO treatment had no effect on body weight development, total fat mass or absolute mass of eWAT or subcutaneous

WAT (sWAT), whereas the mesenteric WAT (mWAT) mass was significantly lower than in HFD. The energy intake was comparable in all groups. Plasma lipids were significantly elevated by the HFD compared with chow, indicating a state of hyperlipidemia, and were not affected by KrO (Table 1).

Table 1. Body composition, energy intake and plasma lipids.

	Chow	HFD	KrO
BW (g)	41.6 ± 6.6 *	52.7 ± 4.4	50.9 ± 2.9
Fat mass (g)	11.0 ± 3.3 *	23.2 ± 2.9	21.4 ± 2.4
Lean mass (g)	29.0 ± 3.6 *	29.6 ± 2.7	29.9 ± 1.8
eWAT (g)	1.9 ± 0.5	2.0 ± 0.5	1.9 ± 0.3
sWAT (g)	1.1 ± 0.3 *	2.5 ± 0.6	2.4 ± 0.4
mWAT (g)	0.7 ± 0.3 *	1.2 ± 0.3	0.9 ± 0.2*
EI (kcal/mouse/day)	13.1 ± 1.1	13.9 ± 1.1	14.2 ± 0.5
FI (g/mouse/day)	4.3 ± 0.4 *	2.9 ± 0.2	3.0 ± 0.1
Cholesterol (mM)	7.6 ± 2.2 *	34.2 ± 13.0	43.3 ± 18.5
Triglycerides (mM)	1.7 ± 0.6 *	6.0 ± 3.4	6.6 ± 4.8

Body composition, food intake and plasma lipids after 28 weeks of dietary treatment. BW: body weight; EI: energy intake; FI: food intake; eWAT: epididymal white adipose tissue (WAT); sWAT: subcutaneous WAT; mWAT mesenteric WAT. In the left column, data from the chow group are provided for reference. Data are presented as mean ± SD, * $p < 0.05$ compared to HFD.

To assess whether KrO altered the omega-3 FA content in the circulation, we analyzed the FA composition in dry blood spots (Supplementary Table S2). Compared to HFD, KrO treatment significantly increased the relative amounts of omega-3 FAs, with marked effects on EPA (19.8-fold) and DHA (1.5-fold).

We next examined whether similar changes would occur at the tissue level (Table 2). In eWAT, KrO treatment increased the absolute tissue concentrations of EPA (13.7-fold) and DHA (3.6-fold) and other omega-3 FAs measured. KrO had comparable effects in the liver, where it increased EPA (10.8-fold) and DHA (2.0-fold) concentrations. Table 2 also demonstrates that the absolute concentrations of EPA and DHA were lower in eWAT than in the liver.

Table 2. Fatty acid concentrations in eWAT and the liver.

	eWAT			Liver		
Fatty Acids (Ug/Mg Tissue)	**Chow**	**HFD**	**KrO**	**Chow**	**HFD**	**KrO**
Omega-3						
Alpha-Linolenic (ALA) C18:3n3	11.0 *	4.8	5.5 *	0.7	0.7	0.9 *
Eicosapentaenoic (EPA) C20:5n3	0.3 *	0.1	1.5 *	0.3 *	0.2	2.5 *
Docosapentaenoic n3 C22:5n3	0.8	0.5	1.6 *	0.5 *	0.6	2.0 *
Docosahexaenoic (DHA) C22:6n3	1.9 *	1.1	4.0 *	3.7	3.9	7.6 *
Omega-6						
Linoleic (LA) C18:2n6	214.0 *	169.3	173.5	16.7 *	28.1	25.2
gamma-Linolenic C18:3n6	0.7	0.7	0.6	0.3 *	0.6	0.3 *
Eicosadienoic C20:2n6	1.1 *	2.5	2.4 *	0.3 *	0.7	0.6 *
Dihomo-g-linolenic C20:3n6	1.9 *	1.3	1.1 *	1.0 *	1.6	1.2 *
Arachidonic (ARA) C20:4n6	3.6 *	3.2	1.3 *	5.3 *	6.6	3.2 *
Docosatetraenoic C22:4n6	0.5 *	0.7	0.2 *	0.3 *	1.0	0.3 *
Docosapentaenoic n6 C22:5n6	0.3	0.3	0.1 *	0.1	0.5	0.0 *
Cis-Monosaturated						
Palmitoleic C16:1n7	79.8 *	32.8	34.1	5.0	5.9	6.8
Oleic C18:1n9	288.8 *	427.2	411.8	29.2 *	86.1	72.5
Eicosenoic C20:1n9	4.9 *	3.9	3.5 *	0.7 *	2.1	1.7 *
Nervonic C24:1n9	0.1 *	0.1	0.1	0.1	0.1	0.1 *
Saturated						
Myristic C14:0	7.7 *	5.5	6.4 *	0.5 *	1.0	0.8 *
Palmitic C16:0	152.6	133.4	130.3	21.4 *	46.4	38.6 *
Stearic C18:0	9.0 *	21.9	20.6	5.0 *	5.9	5.4 *
Arachidic C20:0	0.3 *	0.2	0.2	0.2	0.2	0.3
Behenic C22:0	0.1	0.0	0.0	0.1 *	0.0	0.1 *
Lignoceric C24:0	0.0 *	0.0	0.0	0.0 *	0.0	0.0 *
Trans						
Palmitelaidic C16:1n7t	0.8	0.7	0.9 *	0.1 *	0.1	0.2 *
Elaidic C18:1t	0.7 *	1.9	1.6 *	0.1 *	0.3	0.2 *
Linoelaidic C18:2n6t	2.0	1.6	1.5	0.3 *	0.5	0.3 *

Fatty acid concentrations determined in eWAT and liver tissue after 28 weeks of dietary treatment. The types of fatty acids are indicated in bold. In the left column, data from the chow group are provided for reference. Average fatty acid concentrations significantly higher compared to the HFD control group are shown in orange, and significantly lower concentrations are shown in green ($p < 0.05$).*

By contrast, KrO treatment significantly reduced ARA concentrations in the circulation by 59% compared to HFD (0.4-fold reduction), i.e., below the levels of chow reference mice (Supplementary Table S2). In WAT and the liver, KrO had similar effects and strongly reduced ARA tissue concentrations by 59% and 52%, respectively. Other omega-6 FAs were also lowered by KrO, with the exception of linoleic acid and gamma-linolenic acid. The concentrations of monosaturated, saturated and trans FAs were scarcely changed by KrO.

Collectively, these data indicate that KrO treatment affected the lipid composition in the circulation, eWAT and the liver in a comparable way: all tissues showed a marked increase in omega-3 FAs and a decrease in ARA concentrations. The highest absolute concentrations of omega-3 FAs were observed in the liver.

3.2. KrO Reduces WAT Inflammation, Improves Adipocyte Size Distribution and Increases Inflammation-Resolving Lipid Mediators Derived from EPA and DHA

We next investigated the possible effects of KrO on WAT histology, and analyzed adipocyte cell size, WAT inflammation (CLS) and the total number of adipocytes in eWAT.

The average adipocyte cell size of the HFD control group (5063.1 ± 518.7 µm^2) was similar to that of the chow reference group (4724.4 ± 891.1 µm^2). Treatment with KrO significantly reduced the average adipocyte size (4200.1 ± 709.6 µm^2) relative to HFD (Figure 1A,B). A subsequent, more refined, analysis of the cell size distribution revealed that this effect was attributable to an increase in the number of very small adipocytes (<2000 µm^2) by KrO, whereas the number of large adipocytes (>8000 µm^2), which reportedly release many inflammatory mediators [34], decreased (Figure 1C).

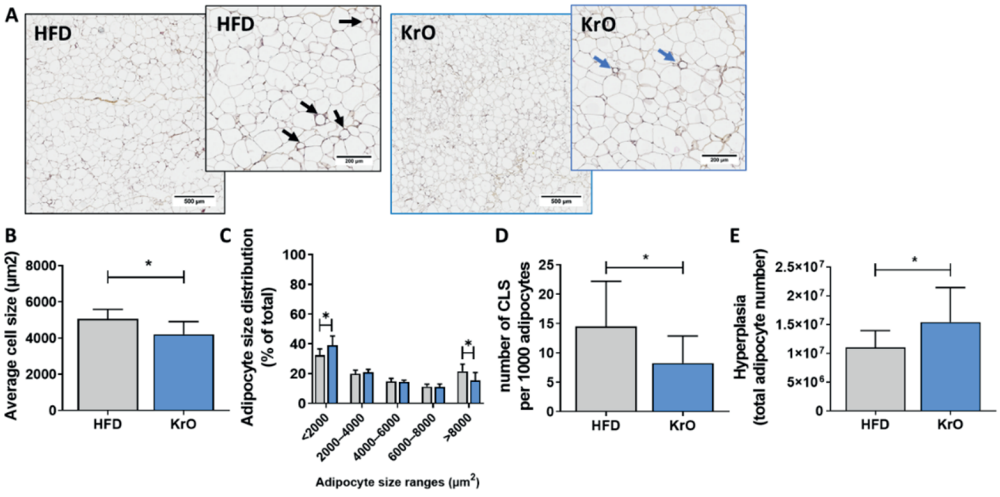

Figure 1. *Effect of KrO on eWAT. (**A**) Representative images of HPS-stained eWAT, one low magnification image and one high magnification image per treatment, with arrows to indicate crown-like structures (CLS). eWAT sections were analyzed to determine (**B**) average adipocyte cell size, (**C**) adipocyte size distribution, (**D**) number of CLS per 1000 adipocytes, and (**E**) total number of eWAT cells as a measure of hyperplasia. Data are presented as mean ± SD, *p < 0.05 compared to HFD.*

In the HFD control group, many immune cells were observed, and a substantial portion of inflammatory cells formed CLSs (14.5 ± 7.7 per 1000 adipocytes). The number of CLSs in HFD was strongly increased relative to chow (2.2 ± 4.8 CLSs per 1000 adipocytes). Treatment with KrO prevented HFD-induced CLS formation and significantly reduced CLS numbers by approximately 42% (Figure 1D), demonstrating that KrO reduces tissue inflammation. This histological effect was substantiated by the results of a genome-wide gene expression analysis and subsequent upstream regulator analysis of eWAT. This analysis predicts the activation state of an upstream regulator (e.g., cytokines, signaling molecules, transcription factors) based on the expression pattern of genes downstream from this regulator. HFD activated multiple upstream regulators relative to chow, including TNFα, TRAP1, CCL2/MCP-1, IL-1β, IL-6 and MIF, indicating the activation of a broad spectrum of proinflammatory signaling pathways. KrO significantly suppressed many of these inflammatory pathways, as demonstrated by the deactivation of the respective upstream regulators/cytokines (Table 3).

Table 3. Upstream regulator analysis in eWAT.

	HFD vs. Chow		KrO vs. HFD	
	Z-Score	***p*-Value**	**Z-Score**	***p*-Value**
Proinflammatory				
CCL2	3.4	0.000	−2.2	0.013
IL1B	6.7	0.000	−2.3	0.306
IL4	3.2	0.000	−0.1	0.016
IL6	3.5	0.000	−1.1	0.027
IL17A	2.5	0.000	−1.9	1.000
MIF	4.2	0.000	−1.9	1.000
TNF	9.5	0.000	−4.5	0.001
TRAP1	3.5	0.015	−2.4	0.001
TGFB1	4.7	0.000	−1.0	0.009
Adipogenesis—Clonal Expansion				
AP1	3.3	0.001	n/a	1.000
CEBPB	1.7	0.000	1.4	0.004
CEBPD	2.2	0.000	n/a	1.000
Adipogenesis—Differentiation				
PPARG	−4.9	0.000	5.0	0.000
RB1	−6.5	0.000	5.1	0.000
CEBPA	0.7	0.000	1.1	0.018
KLF4	−1.1	0.004	2.0	1.000
KLF5	−0.8	0.006	n/a	1.000
KLF15	n/a	1.000	3.0	0.000
SREBF1	−1.5	0.000	1.3	0.002
STAT5A	−1.2	0.000	2.8	0.004
STAT5B	−0.7	0.000	2.1	0.427

Negative Regulators of Adipogenesis				
KDM5A	4.6	0.000	−5.2	0.000
STK11	3.5	0.000	−4.6	0.000
KLF2	−1.2	0.000	n/a	1.000
GATA3	1.0	0.000	n/a	1.000
WNT5a	−0.5	0.000	n/a	1.000
Metabolism-Related				
PPARGC1A	−4.5	0.000	4.8	0.000
PPARGC1B	−2.6	0.018	2.6	0.001
ESRRA	−3.5	0.000	2.5	0.000
NRF1	−0.7	0.031	2.2	0.003
INSR	−3.4	0.000	3.9	0.000
IGF1R	−2.6	0.000	3.4	0.056
IRS1	−0.5	0.000	1.6	0.001

The activity of upstream regulators in eWAT was calculated based on gene expression changes of all downstream target genes. A Z-score < −2 indicates inhibition of the respective pathway (shown in orange) and Z > 2 indicates activation (shown in green). The p-value < 0.05 indicates significant enrichment of the target genes downstream of a regulator, i.e., that more downstream genes are affected than can be expected by chance. n/a indicates an insufficient number of differentially expressed genes to predict the activation state of an upstream regulator.

Intracellular free PUFAs and their respective oxylipin metabolites directly involved in regulating inflammatory responses were measured in eWAT homogenates. A schematic overview of oxylipins that can be synthesized from EPA, DHA and ARA is provided in Figure 2A, together with the tissue concentrations of these three precursors (Figure 2B). Feeding with the HFD lowered the levels of omega-3-derived mediators 13-HoTre and 19,20 DiHDPA and increased 18-HEPE and 4-HDHA, 10-HDHA and 17-HDHA (Table 4). Simultaneously, HFD increased intracellular ARA and many pro-inflammatory omega-6-derived oxylipins, including 9-HoDE, 8–11- and 15-HETE and prostaglandin D2 (PGD_2). By contrast, KrO upregulated all EPA- and DHA-derived oxylipins, whereas almost all omega-6 derived pro-inflammatory oxylipins were significantly suppressed with the KrO diet (Table 4).

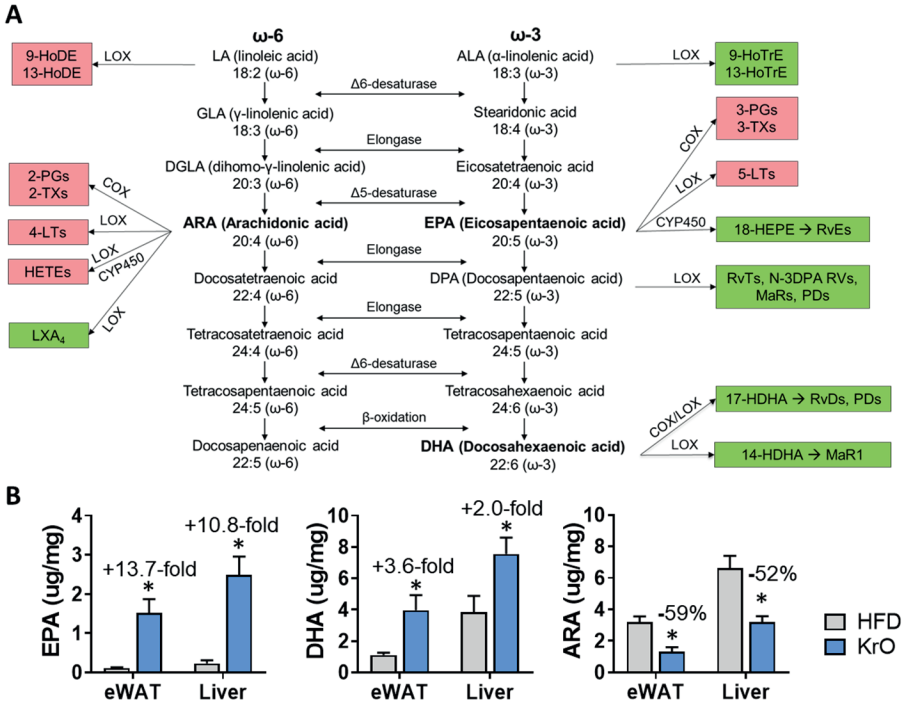

Figure 2. *(**A**) Overview of omega-6 (ω-6) and omega-3 (ω-3) FA synthesis pathways with linoleic acid (LA) and α-linolenic acid (ALA) constituting the upstream precursors, respectively. PUFAs compete for the same desaturase and elongase enzymes during the synthesis of eicosapentaenoic acid (EPA), docosahexaenoic acid (DHA) and arachidonic acid (ARA). These PUFAs can further be metabolized by the COX/LOX/CYP450 enzymes into oxylipins. Oxylipins that are typically implicated in the potentiation of inflammatory responses are highlighted in red, whereas oxylipins typically involved in the resolution of inflammatory responses are shown in green. (**B**) Effect of KrO on the tissue concentrations of EPA, DHA and ARA, determined by GC. Data are presented as mean ± SD, * $p < 0.05$ compared to HFD.*

Table 4. Oxylipin analysis in eWAT.

	Chow	HFD	KrO
Omega-3 Lipid Mediators			
ALA/GLA	0.025	0.024	0.021
9-HoTrE	0.011	0.020	0.012
13-HoTrE	0.027 *	0.017	0.011
EPA	0.005	0.010	0.074 *
5-HEPE	0.001 *	0.001	0.011 *
12-HEPE	0.012	0.017	0.067 *
15-HEPE	0.003	0.005	0.026 *
18-HEPE	0.002 *	0.005	0.029 *
RvE2	ND	ND	ND
18R-RvE3	0.002	ND	ND
DPAn-3	0.003	0.006	0.018 *
DHA	0.019	0.042	0.099 *
4-HDHA	0.000 *	0.002	0.003 *
7-HDHA	0.001	0.002	0.004 *
10-HDHA	0.001 *	0.007	0.016 *
17-HDHA	0.002 *	0.007	0.013 *
PDX	0.001	0.002	0.004 *
14,15-diHETE	ND	0.002	0.004
14(S)-HDHA	0.007	0.013	0.024 *
19,20-DiHDPA	0.013 *	0.007	0.015 *
Omega-6 Lipid Mediators			
LA	0.059	0.060	0.074
9-HoDE	0.269 *	0.662	0.362 *
13-HoDE	0.506	0.959	0.569 *
DGLA	0.003 *	0.006	0.006
ARA	0.015 *	0.046	0.018 *
5-HETE	0.005 *	0.028	0.006 *
LXA4	0.001	0.002	ND
5-KETE	0.002 *	0.011	0.003 *
8-HETE	0.005 *	0.042	0.008 *
11-HETE	0.030 *	0.290	0.051 *
12-HETE	0.065	0.247	0.046 *
12-KETE	0.003	0.006	0.002
15-HETE	0.015 *	0.111	0.024 *
15-KETE	0.003 *	0.016	0.005 *
8S,15S-diHETE	0.001	0.002	0.000 *
17-OH-DH-HETE	0.001 *	0.005	0.001 *
PGD_2	0.042 *	0.311	0.028 *
PGE_2	0.057	1.226	0.052 *
$PGF_{2\alpha}$	0.006	0.034	0.004 *
PGJ_2	ND	0.017	ND
8-iso- $PGF_{2\alpha}$	0.001 *	0.003	0.001 *
13,14 dihydro-15 keto- $PGF_{2\alpha}$	ND	0.009	ND

TxB_2	0.012	0.051	0.005 *
6-tra-LTB_4	0.001	0.003	0.001
6t,12 epi-LTB_4	0.001	0.004	0.001
AdA	0.001 *	0.004	0.001 *
DPAn-6	0.002 *	0.011	0.002 *

Lipid mediator levels (area ratios relative to the class-specific internal standard) measured in eWAT tissue are expressed as mean area ratios. Area ratios significantly higher compared to the HFD control group are shown in orange, and significantly lower ratios are shown in green ($p < 0.05$). In the left column, data from the chow group are provided for reference. ND = not detectable.*

Pathway analysis of the gene expression data also revealed that apelin signaling, an insulin-dependent adipocyte differentiation pathway [35], was strongly activated by KrO and that the activity of important upstream regulators of adipogenesis, including PPARγ, RB1, CEBPα, KL4, KL15, STAT5A and STAT5B (Table 3), was stimulated by KrO. Conversely, negative regulators of differentiation, such as KDM5A and STK11, were activated by HFD and suppressed with KrO. To corroborate this finding with histology results, we calculated the total number of adipocytes present in eWAT using an established method [29]. The adipocyte number in eWAT of HFD-fed animals (1.10×10^7) was similar to that of the chow reference group (1.08×10^7). Interestingly, KrO-fed mice showed a significant 1.4-fold increase in adipocyte numbers (1.54×10^7), which is clearly indicative of hyperplasia (Figure 1E) and which supports the results of the upstream regulator analysis.

Furthermore, HFD deactivated PPARGC1A, PPARGC1B, ESRRA and NRF1, whereas KrO strongly induced these upstream regulators, pointing to a beneficial effect on mitochondrial biogenesis.

Collectively, these data show that treatment with KrO reduced CLSs and increased the number of adipocytes in eWAT. In line with these histological results, KrO prevented the activation of inflammatory regulators by HFD, increased PUFA concentrations and stimulated the formation of anti-inflammatory bioactive lipids. KrO treatment also resulted in a shift towards smaller adipocytes and fewer large adipocytes, possibly as a consequence of its adipogenesis-stimulating effect.

3.3. Effect of KrO on Adipokines and Metabolic Risk Factors

We next investigated whether the observed histological changes in WAT were accompanied by effects on adipokine levels and insulin resistance (HOMA-IR).

Plasma leptin levels were 2.5 ± 2.0 ng/mL at t = 0 and were increased by HFD, reaching 58.1 ± 10.8 ng/mL in week 28, which differed significantly from the chow reference group (26.6 ± 8.0 ng/mL). KrO significantly attenuated this HFD-evoked increase in leptin (37.7 ± 6.4 ng/mL). Furthermore, the total leptin exposure over time (AUC from data at 0, 8, 16 and 28 weeks) was significantly reduced by KrO (Table 5). Plasma adiponectin levels were higher with KrO compared to HFD at the beginning of the treatment until week 16 and this difference became smaller towards the end of the study. The total adiponectin exposure over time (AUC) was significantly higher in KrO compared to HFD (Table 5).

Table 5. Effect of KrO on adipokines, metabolic risk factors and transaminases.

	Chow	HFD	KrO
AUC leptin	32.3 ± 16.4 *	114.2 ± 15.4	100.4 ± 0.4 *
AUC adiponectin	18.5 ± 1.8 *	22.5 ± 2.5	25.19 ± 2.3 *
Glucose (mM)	7.2 ± 0.8	7.6 ± 0.9	6.9 ± 0.9 *
Insulin (ng/mL)	4.1 ± 3.9 *	20.4 ± 14.4	12.4 ± 7.1 *
HOMA-IR	34.1 ± 33.9 *	170.2 ± 116.3	92.2 ± 46.8 *
Free fatty acids (mM)	1.1 ± 0.2	1.3 ± 0.4	2.4 ± 1.0 *
ALT (U/l)	66.6 ± 21.5 *	391.9 ± 258.2	277.9 ± 170.7
AST (U/l)	17.8 ± 3.9 *	491.1 ± 497.2	264.2 ± 104.1

*AUC: area under the curve, HOMA-IR: homeostatic model assessment for insulin resistance, ALT: alanine aminotransferase, AST: aspartate aminotransferase. In the left column, data from the chow group are shown for reference. Data are presented as mean ± SD, * $p < 0.05$ compared to HFD.*

Fasting blood glucose levels and HFD-induced increases in plasma insulin levels were reduced with KrO. Subsequently, the HOMA-IR values were significantly lower in the KrO group, indicating that KrO improved insulin resistance. Genome-wide gene expression analysis showed that HFD inactivated upstream regulators that are important in insulin signaling (INSR and IGF1R) in both the liver and eWAT, and KrO counteracted this effect in eWAT (Table 3).

Free fatty acid (FFA) plasma concentrations were not significantly raised with HFD, whereas KrO significantly increased FFAs compared to the HFD in line with the lower insulin concentrations.

Plasma ALT and AST levels were significantly increased by the HFD compared to the chow reference diet. This increase in both ALT and AST tended to be less pronounced in the KrO group.

Taken together, KrO reduced leptins and increased adiponectin exposure, which was paralleled by an improvement in HOMA-IR.

3.4. Effects of Krill Oil in the Liver

HFD treatment resulted in the development of hepatic steatosis, hepatocellular hypertrophy and the formation of F4/80-positive CLSs, indicating macrophage aggregation around dying hepatocytes (Figure 3A–D). These histological characteristics were practically absent in the chow group . The liver histology and the lipid content of the KrO group was comparable to that of the HFD group. On a molecular level, however, gene expression profiling and subsequent upstream regulator analysis demonstrated the activation of many proinflammatory pathways by HFD, which were reversed by KrO (Table 6). More specifically, KrO quenched the HFD-induced activation of proinflammatory cytokine signaling (e.g., by IL-1β, IFN-A2 and CSF1) and proinflammatory transcription factors (e.g., REL-A/p65-NF-κB and STAT1). Critical upstream regulators of metabolism, including the β-oxidation enzyme ACOX1 and the mitochondrial biogenesis activator PPARGC1A, were deactivated with HFD, and KrO attenuated this effect, suggesting a reactivation of lipid processing. Moreover, HFD

activated SREBF1 as key regulator of de novo lipogenesis, whereas KrO deactivated SREBF1 and thereby seemed to suppress lipid synthesis. Furthermore, cholesterol synthesis regulators deactivated by HFD (e.g., SCAP, SREBP2) were even further suppressed with KrO (Table 6).

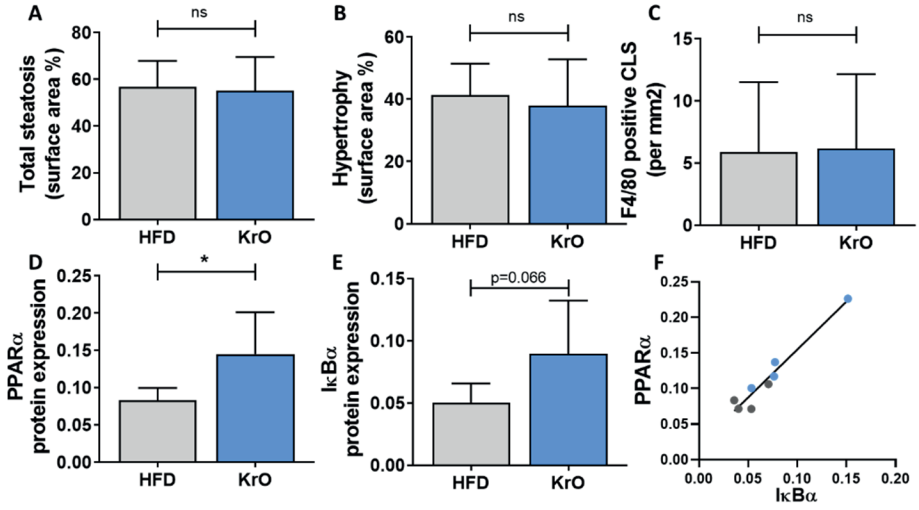

Figure 3. *Effect of KrO on the liver—(**A**) total steatosis, (**B**) triglyceride content expressed per mg of liver protein (**C**) hepatocellular hypertrophy and (**D**) F4/80-positive crown-like structures (CLSs). Liver protein levels of (**E**) PPARα and (**F**) IκBα normalized for αTubulin expression, and (**G**) correlation between PPARα and IκBα. (**H**) representative images of the Western blot bands. Data are presented as mean ± SD, * p < 0.05 compared to HFD.*

Table 6. Upstream regulator analysis in the liver.
The activity of an upstream regulator in the liver was calculated based on gene expression

	HFD vs. Chow		KrO vs. HFD	
Proinflammatory	**Z-Score**	***p*-Value**	**Z-Score**	***p*-Value**
CCL2	1.8	0.000	−2.0	0.171
CXCL12	4.2	0.000	−0.3	0.011
IL1B	7.9	0.000	−2.1	0.001
IFNA2	4.7	0.002	−1.9	0.036
IFNB1	2.7	0.000	−0.5	0.006
IFNG	6.1	0.000	−0.6	0.001
CSF1	5.1	0.000	−3.2	0.000
TNF	9.7	0.000	−1.1	0.000
NFKB1	4.8	0.000	−1.3	0.042
NFKBIA	3.2	0.000	0.2	0.029
RELA	4.9	0.000	−1.5	0.006
REL	3.2	0.000	−2.0	0.074
STAT1	6.4	0.000	−1.7	0.000
TICAM1	4.8	0.000	−2.6	0.068
Metabolism-Related				
ACOX1	−5.4	0.000	1.7	0.000
PPARGC1A	−2.7	0.000	1.7	0.004
SCAP	−3.2	0.000	−3.8	0.000
SREBF1	1.0	0.000	−2.6	0.000
SREBF2	−1.7	0.001	−3.2	0.000

changes of all downstream target genes. A Z-score < −2 indicates inhibition of the respective pathway (shown in orange) and Z > 2 indicates activation (shown in green). The p-value < 0.05 indicates significant enrichment of the target genes downstream of a regulator, i.e., that more downstream genes are affected than can be expected by chance. n/a indicates an insufficient number of differentially expressed genes to predict the activation state of an upstream regulator.

When compared to its anti-inflammatory activities in WAT, KrO attenuated different pro-inflammatory pathways and a different set of transcriptional regulators in the liver. Many of the KrO-modulated signaling pathways in the liver converge in transcriptional regulation by NF-κB family members, and KrO significantly deactivated REL-A/p65-NF-κB, for instance. In line with this, Western blot analysis of liver tissue homogenates revealed an increase in PPARα protein expression and a trend (p = 0.066) towards an increase in IκBα protein levals by KrO relative to HFD. PPARα protein expression was significantly correlated with IκBα protein expression (R^2 = 0.9) (Figure 3D–F).

Next, we investigated whether KrO affected the intrahepatic levels of bioactive lipids using the same oxylipin platform as before. Table 7 shows that HFD significantly decreased the levels of ALA-, EPA- and DHA-derived lipid mediators (e.g., 15- and 18-HEPE, involved in inflammation resolution), while increasing many LA- and ARA-derived lipid species known to promote inflammation (e.g., HETEs, PGD_2, PGE_2, PGF_2 and TXB_2). By contrast, KrO-treated livers exhibited lower levels of ALA and higher levels of LA, suggesting that the processing of omega-3 FAs is enhanced in the presence of KrO. Indeed, all detectable EPA- and DHA-derived metabolites (except 14-HDHA, a precursor of MaR_1) were significantly increased with KrO and a strong signal corresponding to genuine resolvin RvE_2 (same MS/MS transition, identical retention time) was only detectable in KrO-fed mice. Strikingly, KrO suppressed the formation of oxylipins with proinflammatory properties downstream of ARA to such an extent that they were no longer detectable.

Table 7. Oxylipin analysis in the liver.	**Chow**	**HFD**	**KrO**
Omega-3-Derived			
ALA/GLA	0.208 *	0.304	0.143 *
9-HoTrE	0.070 *	0.016	0.022 *
13-HoTrE	0.036 *	0.015	0.013
EPA	0.283	0.267	1.765 *
5-HEPE	0.033 *	0.007	0.096 *
12-HEPE	0.559 *	0.172	1.077 *
15-HEPE	0.029 *	0.011	0.126 *
18-HEPE	0.052 *	0.012	0.169 *
RvE_2	ND	ND	0.004
18R-RvE_3	ND	ND	ND
DPAn-3	0.110 *	0.157	0.525 *
DHA	0.858 *	1.419	2.920 *
4-HDHA	0.037 *	0.015	0.039
7-HDHA	0.014	0.010	0.027 *
10-HDHA	0.066	0.049	0.122 *
17-HDHA	0.052	0.044	0.074 *
PDX	0.013	0.014	0.027 *
14,15-diHETE	0.062 *	0.028	0.206 *
14(S)-HDHA	0.123	0.126	0.155
19,20-DiHDPA	0.303 *	0.517	0.643 *
Omega-6-Derived			
LA	0.296	0.339	0.420 *
9-HoDE	1.567 *	0.935	0.746
13-HoDE	2.399*	1.367	1.167
DGLA	0.095 *	0.189	0.215
ARA	0.372 *	0.658	0.348 *
5-HETE	0.150 *	0.083	0.037 *
LXA_4	0.008	0.015	0.004
8-HETE	0.070	0.069	0.032 *
11-HETE	0.555	0.675	0.222 *
12-HETE	1.146	1.255	0.308 *
15-HETE	0.491	0.418	0.172 *
15-KETE	0.045	0.030	0.016 *
8S,15S-diHETE	0.005	0.006	0.002 *
17-OH-DH-HETE	0.016	0.019	0.004 *
PGD_2	0.039 *	0.105	0.016 *
PGE_2	0.068	0.103	0.023 *
$PGF_{2\alpha}$	0.041 *	0.095	0.012 *
PGJ_2	ND	ND	ND
8-iso- $PGF_{2\alpha}$	0.003	0.004	0.002
13,14 dihydro-15 keto- $PGF_{2\alpha}$	ND	0.005	ND

TxB_2	0.049 *	0.133	0.017 *
6-tra-LTB_4	0.004	0.003	ND
6t,12epi-LTB_4	0.006	0.004	ND
AdA	0.028 *	0.110	0.039 *
DPAn-6	0.073 *	0.323	0.047 *

Lipid mediator levels measured in liver tissue are expressed as mean area ratios. Area ratios significantly higher compared to the HFD control group are shown in orange, and ratios that are significantly lower are depicted in green (* $p < 0.05$). In the left column, data from the chow group are provided for reference. ND = not detectable.

Altogether, KrO quenched inflammatory signaling pathways and upregulated the expression of proteins that can interfere with NF-κB signaling (e.g., PPARα. It also suppressed the accumulation of lipids and oxylipins with pro-inflammatory properties and strongly induced the presence of lipid species that contribute to an anti-inflammatory milieu.

4. Discussion

This study shows that the fatty acid and oxylipin content of adipose tissue and the liver can be strongly modulated with KrO during the development of obesity, and that KrO treatment attenuates inflammatory processes, resulting in a reduced inflammatory tone. Lipidomic analyses, in conjunction with functional regulator analyses of signaling pathways in adipose tissue and the liver, provided rationales for possible direct and indirect mechanisms by which KrO exerts its effects. One of the direct effects is the increase in anti-inflammatory oxylipins. An important indirect effect is the activation of adipogenic gene expression programs in adipose tissue, accompanied by WAT hyperplasia. The observed increase in WAT storage capacity and the associated decrease in inflammation can contribute to whole-body metabolic health, which is consistent with the observed improvement in insulin resistance (i.e., HOMA-IR) and adipokine concentrations.

A general FA compositional analysis revealed that KrO strongly increased the omega-3 PUFA content in the circulation, WAT and the liver (especially that of EPA and DHA), while simultaneously decreasing the omega-6 PUFA content in these organs, with pronounced reductions in ARA. The observed fatty acid composition changes were grosso modo comparable for both organs, yet the absolute omega-3 PUFA concentrations per milligram of tissue were clearly higher in the liver. Importantly, a refined oxylipin LC-MS/MS analysis showed that KrO strongly increased lipid species with anti-inflammatory properties [36–38] derived from EPA and DHA (e.g., 18-HEPE, RvE_2, 14-HDHA, 17-HDHA, PDX/10S,17S-diHDHA), whereas it suppressed the HFD-induced formation of ARA-derived oxylipins (e.g., HETEs, PGD_2, PGE_2, PGF_2 and TXB_2), which often exert pro-inflammatory effects [38–42]. Notably, the results of the two independent lipidomics approaches employed herein (the fatty acid composition analysis and the oxylipin analyses) were in line with each other. Both approaches consistently indicated that KrO treatment altered the organ lipid environment in favor of PUFAs and oxylipins that can resolve inflammation, while lowering ARA and ARA-derived oxylipins that can promote inflammation. For instance, HFD-feeding increased

PGD_2, PGE_2 and PGF_2 levels in both WAT and the liver, which can stimulate chemotaxis of immune cells [43,44] by increasing local cytokine release and the endothelial expression of adhesion molecules to facilitate immune cell tissue infiltration [39,45]. KrO blunted this HFD-evoked effect, and the observed PGD_2, PGE_2 and PGF_2 levels were even lower with KrO compared to the chow diet. Conversely, HFD feeding diminished the levels of anti-inflammatory oxylipins such as 18-HEPE, a precursor for E series resolvins, and 17-HDHA in liver [37]. KrO counteracted this detrimental effect, resulting in an increase of 18-HEPE and 17-HDHA levels in WAT and the liver. Notably, 17-HDHA treatment has been shown to reduce WAT inflammation, increase adiponectin expression and improve glucose tolerance in obese mice [37]. 18-HEPE, RvE_2, 14-HDHA, 17-HDHA, PDX and other anti-inflammatory oxylipins were increased with KrO in this study and are thought to be directly involved in inflammation resolution mechanisms, as reported by [36–38,46–49], and hence may contribute to a lipid environment in WAT and the liver that protects against chronic inflammation.

It is likely that inflammation-resolving oxylipins were formed from their precursor fatty acids present in KrO (EPA and DHA), but these precursors themselves can also be enzymatically synthesized from ALA. The enzymes responsible for omega-3 PUFA processing are the same as those for omega-6 processing but the rate-limiting enzyme, delta-6-desaturase, has a higher preference for omega-3 FAs relative to omega-6 FAs [50,51]. Thus, an enhanced conversion of ALA in the presence of KrO may also explain the pronounced increases in anti-inflammatory oxylipins.

The observation that the levels of most PUFAs and oxylipins are higher in the liver than in WAT is consistent with metabolic studies in mice [52]. These tissue differences may have multiple causes, including the expression or activity of the aforementioned enzymes that ultimately determine the extent to which substrates (EPA, DHA, ARA) are available for subsequent enzymatic conversions (e.g., by Cyp450, COX, LOX and auto-oxidation) into the respective oxylipins [42,53]. Collectively, the lipidomic analyses demonstrate that KrO can directly affect the inflammatory milieu in WAT and the liver by modulating PUFA and oxylipins in these organs, suggesting beneficial effects on inflammatory pathways and processes.

Indeed, pathway and upstream regulator analyses clearly demonstrated a suppression of HFD-induced inflammatory pathways by KrO in WAT and the liver. For example, KrO deactivated multiple inflammatory HFD-stimulated pathways, including those controlled by TNFα, TNF receptor-associated protein 1 (TRAP1) and CCL2 in eWAT, as well as the IL-1β and M-CSF pathways in the liver. Attenuation of TNFα/IL-1β/CCL2-mediated inflammation in metabolic organs has been shown to improve insulin resistance [54–56], consistent with the observed reduction of fasting insulin and HOMA-IR in KrO-treated mice. For instance, TNFα inhibits insulin signaling by stimulating the phosphorylation of inhibitory residues on the insulin receptor substrates (IRS1 and IRS2) and impairs IRS-mediated phosphatidylinositol 3-kinase activation [57,58]. KrO appeared to interfere with this process in our study, because we observed significantly increased upstream regulator activities of INSR, IGF1R and IRS1 in eWAT. This effect is consistent with reduced CLS counts in eWAT and was paralleled by decreased leptin and increased adiponectin concentrations in plasma.

The KrO-dependent adipokine changes point to an improvement in whole-body homeostasis, including the neuroendocrine circuits affecting adipocytes [59]. Observed elevations in adiponectin can directly affect immune cells, mediating anti-inflammatory activities [60], as well as affecting general metabolism by inhibiting gluconeogenesis and stimulating lipid utilization/b-oxidation [61,62], which is consistent with our pathway analyses.

The deactivation of TRAP1 by KrO points to reduced oxidative-inflammatory stress in eWAT because TRAP1 is a mitochondrial heat shock protein involved in the maintenance of mitochondrial integrity under stress or pathological conditions [63].

In addition, KrO stimulated the activity of PPARγ, RB1, CEBPα, KLF15 and STAT5A, all of which are transcriptional master regulators that orchestrate adipogenesis [64,65], and it suppressed negative regulators of adipogenesis (KDM5A and STK11). Consistently with the KrO-induced proadipogenic gene expression program in eWAT, the absolute number of adipocytes increased in this depot, and so did the proportion of small adipocytes, together indicating KrO-induced hyperplasia. WAT hyperplasia constitutes a mechanism by which the total storage capacity for fat is increased, allowing the body to cope with metabolic overload from HFD [3]. This indirectly prevents adipocyte hypertrophy and tissue inflammation and attenuates the effect of cytokines implicated in insulin resistance (e.g., TNFα and MIF signaling [4]), as observed herein. Furthermore, KrO also activated PGC1A, PGC1B, ESSRA and NRF1, which are indicative of increased mitochondrial biogenesis (growth and division of pre-existing mitochondria) in eWAT, which is in line with the reported effects of PUFAs during adipocyte differentiation [66,67]. The activation of PPARγ by KrO-derived lipids may, at least partly, explain the effects observed in eWAT, as well as the observed increase in adiponectin, a PPARγ target gene [60,68]. PPARγ activation could also be responsible for the decrease in leptin, because PPARγ antagonizes CEBPα-mediated leptin mRNA transcription [69]. The activation of PPARγ and PPARα by PUFAs and oxylipins from KrO may contribute to the anti-inflammatory effects observed in WAT and the liver. Activated PPARs can negatively interfere with proinflammatory transcription factors such as NF-κB in several ways: PPARs can directly interact with NF-κB proteins [70] or increase the cytosolic inhibitor, IκBα, thereby preventing nuclear translocation and NF-κB-mediated gene expression [10,11]. The observed increase in PPARα protein levels and high concentrations of potential ligands in KrO-treated livers support the possibility of anti-inflammatory mechanisms involving direct PPARα interaction, [70] and complementary indirect mechanisms (e.g., an increase in IκBα) that negatively interferes with NF-κB signaling. Although KrO attenuated CLS formation in eWAT, there was no effect on F4/80-positive CLSs in the liver. This may be explained by a fundamental difference in plasticity between these organs: although the WAT can respond with hyperplasia and expand further (or redistribute fat among its depots) [71], the liver is anatomically restricted, with a limited storage capacity so that even lipids that are beneficial in nature may cause physical damage to cells when present in excess amounts. In addition, the higher circulating FFAs with KrO may result in a higher influx of fat to the liver, thereby counteracting the beneficial effects on hepatic fat oxidation (i.e., PPARA, ACOX1, PPARGC1A), altogether leading to comparable hepatic steatosis as in the HFD controls. Of note, the steatosis observed in the KrO group is unlikely to be a

consequence of increased de novo lipogenesis, because KrO significantly suppressed SREBF1 activity—the key regulator of hepatic lipid synthesis. This is also in line with the observed reduced fasting insulin concentrations with KrO. By contrast, at least a part of the steatosis observed in the HFD control group may be due to increased *de novo* lipogenesis because SREBF1 is significantly activated, and insulin, the transcriptional inducer of Srebp1c, is elevated.

This study has limitations and strengths. Intrinsic to the set-up of the study, we cannot distinguish whether the replacement of HFD by KrO *per se*, or specific KrO components or metabolites formed from KrO, or a combination of the above, are responsible for the beneficial effects observed in KrO-treated mice. We could have included additional groups to substantiate these findings, for instance, groups in which KrO was administered orally superimposed on the HFD. Another limitation is that we cannot estimate the contribution of the PUFAs attached to phospholipids relative to those in other lipid classes. It is possible that the profound effects of KrO are related to its high phospholipid content and the increased bioavailability of EPA and DHA [72], which consequently also affects oxylipin availability. Important strengths of this study are the long period of KrO treatment (28 weeks), resulting in relevant endpoints; the use of large treatment groups (n = 15 mice) for high statistical power; the extensive molecular (omics) analyses of adipose tissue and the liver using next-generation sequencing technology to identify activated pathways and upstream regulators in both organs; the profiling of fatty acids in three compartments (plasma, adipose tissue, liver), which provides information on the relative enrichment of PUFAs in each of these tissues; and one of the most comprehensive oxylipin analysis reported so far, including adipose tissue and the liver. Our oxylipin profiling analyses at the tissue level showed that HFD treatment markedly increased oxylipins with proinflammatory properties, whereas oxylipins with inflammation-resolving properties were reduced. KrO treatment appeared to counteract these HFD-evoked changes. These KrO-dependent changes of the inflammatory tone within eWAT and the liver can, at least partly, be explained by the ingested PUFAs, and similar effects may occur in other species. In a human study, it has been shown that a linear dose–response relationship exists between the intake of EPA and DHA and the levels of anti-inflammatory oxylipins measured in plasma [73]. This suggests that the direct effects of KrO on oxylipin tissue concentrations observed herein may also be achievable with dietary regimens in humans.

In conclusion, we have demonstrated that long-term KrO treatment (28 w) improves the fatty acid composition in the circulation, WAT and the liver. This improvement is characterized by marked elevations in omega-3 FAs and associated oxylipins, which can exert beneficial effects on metabolism (e.g., fasting insulin, adipokines) and tissue inflammation. Functional gene expression and pathway analyses, combined with lipidomic analyses, provide rationales for direct and indirect effects of KrO-derived PUFAs and oxylipins on metabolic and inflammatory pathways controlled by PPARα/PPARγ. The stimulatory effect of KrO on adipogenesis and hyperplasia allows for the safe storage of excess fat in adipose tissue and contributes indirectly to the suppression of inflammation. This indirect effect complements the more direct mechanisms that intercept inflammatory pathways on the molecular level.

Acknowledgments: We would like to thank Christa de Ruiter and Joline Attema for their technical assistance with the in-life experiment.

References

1. Hotamisligil, G.S. Inflammation, metaflammation and immunometabolic disorders. *Nature* **2017**, *542*, 177–185.
2. Longo, M.; Zatterale, F.; Naderi, J.; Parrillo, L.; Formisano, P.; Raciti, G.A.; Beguinot, F.; Miele, C. Adipose tissue dysfunction as determinant of obesity-associated metabolic complications. *Int. J. Mol. Sci.* **2019**, *20*, 2358.
3. Mulder, P.; Morrison, M.C.; Wielinga, P.Y.; Van Duyvenvoorde, W.; Kooistra, T.; Kleemann, R. Surgical removal of inflamed epididymal white adipose tissue attenuates the development of non-alcoholic steatohepatitis in obesity. *Int. J. Obes.* **2016**, *40*, 675–684.
4. Morrison, M.C.; Kleemann, R. Role of macrophage migration inhibitory factor in obesity, insulin resistance, type 2 diabetes, and associated hepatic co-morbidities: A comprehensive review of human and rodent studies. *Front. Immunol.* **2015**, *6*, 308.
5. Ellulu, M.S.; Patimah, I.; Khaza'ai, H.; Rahmat, A.; Abed, Y. Obesity & inflammation: The linking mechanism & the complications. *Arch. Med. Sci.* **2017**, *13*, 851–863.
6. Shashaj, B.; Bedogni, G.; Graziani, M.P.; Tozzi, A.E.; DiCorpo, M.L.; Morano, D.; Tacconi, L.; Veronelli, P.; Contoli, B.; Manco, M. Origin of cardiovascular risk in overweight preschool children: A cohort study of cardiometabolic risk factors at the onset of obesity. *JAMA Pediatr.* **2014**, *168*, 917–924.
7. Winther, B.; Hoem, N.; Berge, K.; Reubsaet, L. Elucidation of phosphatidylcholine composition in krill oil extracted from Euphausia superba. *Lipids* **2011**, *46*, 25–36.
8. Bannenberg, G.L.; Chiang, N.; Ariel, A.; Arita, M.; Tjonahen, E.; Gotlinger, K.H.; Hong, S.; Serhan, C.N. Molecular Circuits of Resolution: Formation and Actions of Resolvins and Protectins. *J. Immunol.* **2005**, *174*, 4345–4355.
9. Krey, G.; Braissant, O.; L'Horset, F.; Kalkhoven, E.; Perroud, M.; Parker, M.G.; Wahli, W. Fatty acids, eicosanoids, and hypolipidemic agents identified as ligands of peroxisome proliferator-activated receptors by coactivator-dependent receptor ligand assay. *Mol. Endocrinol.* **1997**, *11*, 779–791.
10. Korbecki, J.; Bobiński, R.; Dutka, M. Self-regulation of the inflammatory response by peroxisome proliferator-activated receptors. *Inflamm. Res.* **2019**, *68*, 443–458.
11. Ricote, M.; Glass, C.K. PPARs and molecular mechanisms of transrepression. *Biochim. Biophys. Acta-Mol. Cell Biol. Lipids* **2007**, *1771*, 926–935.
12. Gervois, P.; Fruchart, J.C.; Staels, B. Drug insight: Mechanisms of action and therapeutic applications for agonists of peroxisome proliferator-activated receptors. *Nat. Clin. Pract. Endocrinol. Metab.* **2007**, *3*, 145–156.
13. Surette, M.E. The science behind dietary omega-3 fatty acids. *CMAJ* **2008**, *178*, 177–180.
14. Calder, P.C. Omega-3 polyunsaturated fatty acids and inflammatory processes: Nutrition or pharmacology? *Br. J. Clin. Pharmacol.* **2013**, *75*, 645–662.
15. Tillander, V.; Bjørndal, B.; Burri, L.; Bohov, P.; Skorve, J.; Berge, R.K.; Alexson, S.E. Fish oil and krill oil supplementations differentially regulate lipid catabolic and synthetic pathways in mice. *Nutr. Metab.* **2014**, *11*, 20.
16. Tou, J.C.; Altman, S.N.; Gigliotti, J.C.; Benedito, V.A.; Cordonier, E.L. Different sources of omega-3 polyunsaturated fatty acids affects apparent digestibility, tissue

deposition, and tissue oxidative stability in growing female rats. *Lipids Health Dis.* **2011**, *10*, 179.
17. Fenton, J.I.; Gurzell, E.A.; Davidson, E.A.; Harris, W.S. Red blood cell PUFAs reflect the phospholipid PUFA composition of major organs. *Prostaglandins Leukot. Essent. Fat. Acids* **2016**, *10*, 179.
18. Burri, L.; Johnsen, L. Krill Products: An Overview of Animal Studies. *Nutrients* **2015**, *7*, 3300–3321.
19. Sun, D.; Zhang, L.; Chen, H.; Feng, R.; Cao, P.; Liu, Y. Effects of Antarctic krill oil on lipid and glucose metabolism in C57BL/6J mice fed with high fat diet. *Lipids Health Dis.* **2017**, *16*, 218.
20. van den Hoek, A.M.; Verschuren, L.; Worms, N.; van Nieuwkoop, A.; de Ruiter, C.; Attema, J.; Menke, A.L.; Caspers, M.P.M.; Radhakrishnan, S.; Salic, K.; et al. A Translational Mouse Model for NASH with Advanced Fibrosis and Atherosclerosis Expressing Key Pathways of Human Pathology. *Cells* **2020**, *9*, 2014.
21. Morrison, M.C.; Verschuren, L.; Salic, K.; Verheij, J.; Menke, A.; Wielinga, P.Y.; Iruarrizaga-Lejarreta, M.; Gole, L.; Yu, W.-M.; Turner, S.; et al. Obeticholic Acid Modulates Serum Metabolites and Gene Signatures Characteristic of Human NASH and Attenuates Inflammation and Fibrosis Progression in Ldlr-/-.Leiden Mice. *Hepatol. Commun.* **2018**, *2*, 1513–1532.
22. Gart, E.; Lima, E.S.; Schuren, F.; De Ruiter, C.G.F.; Attema, J.; Verschuren, L.; Keijer, J.; Salic, K.; Morrison, M.C. Diet-Independent Correlations between Bacteria and Dysfunction of Gut, Adipose Tissue, and Liver: A Comprehensive Microbiota Analysis in Feces and Mucosa of the Ileum and Colon in Obese Mice with NAFLD. *Int. J. Mol. Sci*. **2019**, *20*, 1.
23. Mueller, A.M.; Kleemann, R.; Gart, E.; Van Duyvenvoorde, W.; Verschuren, L.; Caspers, M.; Menke, A.; Krömmelbein, N.; Salic, K.; Burmeister, Y.; et al. Cholesterol Accumulation as a Driver of Hepatic Inflammation Under Translational Dietary Conditions Can Be Attenuated by a Multicomponent Medicine. *Front. Endocrinol*. **2021**, *12*, 156, doi:10.3389/fendo.2021.601160.
24. Morrison, M.C.; Verschuren, L.; Salic, K.; Verheij, J.; Menke, A.; Wielinga, P.Y.; Iruarrizaga-Lejarreta, M.; Gole, L.; Yu, W.; Turner, S.; et al. Obeticholic Acid Modulates Serum Metabolites and Gene Signatures Characteristic of Human NASH and Attenuates Inflammation and Fibrosis Progression in Ldlr-/-.Leiden Mice. *Hepatol. Commun.* **2018**, *2*, 1513–1532.
25. van Koppen, A.; Verschuren, L.; van den Hoek, A.M.; Verheij, J.; Morrison, M.C.; Li, K.; Nagabukuro, H.; Costessi, A.; Caspers, M.P.M.; van den Broek, T.J.; et al. Uncovering a Predictive Molecular Signature for the Onset of NASH-Related Fibrosis in a Translational NASH Mouse Model. *Cmgh* **2018**, *5*, 83–98.e10.
26. Krebs, M.; Stingl, H.; Nowotny, P.; Weghuber, D.; Bischof, M.; Waldhäusl, W.; Roden, M. Prevention of in vitro lipolysis by tetrahydrolipstatin. *Clin. Chem.* **2000**, *46*, 950–954.
27. Galarraga, M.; Campión, J.; Munõz-Barrutia, A.; Boqué, N.; Moreno, H.; Martínez, J.A.; Milagro, F.; Ortiz-de-Solórzano, C. Adiposoft: Automated software for the analysis of white adipose tissue cellularity in histological sections. *J. Lipid Res.* **2012**, *53*, 2791–2796.
28. Tengeler, A.C.; Gart, E.; Wiesmann, M.; Arnoldussen, I.A.C.; van Duyvenvoorde, W.; Hoogstad, M.; Dederen, P.J.; Verweij, V.; Geenen, B.; Kozicz, T.; et al. Propionic acid

and not caproic acid, attenuates nonalcoholic steatohepatitis and improves (cerebro) vascular functions in obese Ldlr-/- .Leiden mice. *FASEB J.* **2020**, *34*, 9575–9593.
29. Jo, J.; Gavrilova, O.; Pack, S.; Jou, W.; Mullen, S.; Sumner, A.E.; Cushman, S.W.; Periwal, V. Hypertrophy and/or hyperplasia: Dynamics of adipose tissue growth. *PLoS Comput. Biol.* **2009**, *5*, e1000324.
30. Liang, W.; Menke, A.L.; Driessen, A.; Koek, G.H.; Lindeman, J.H.; Stoop, R.; Havekes, L.M.; Kleemann., R.; Van Den Hoek, A.M. Establishment of a general NAFLD scoring system for rodent models and comparison to human liver pathology. *PLoS ONE* **2014**, *9*, e115922.
31. Kleiner, D.E.; Brunt, E.M. Nonalcoholic fatty liver disease: Pathologic patterns and biopsy evaluation in clinical research. *Semin. Liver Dis.* **2012**, *32*, 3–13.
32. Bligh, E.G.; Dyer, W.J. A Rapid Method of Total Lipid Extraction and Purification. *Can. J. Biochem. Physiol.* **1959**, *37*, 911–917.
33. Love, M.I.; Huber, W.; Anders, S. Moderated estimation of fold change and dispersion for RNA-seq data with DESeq2. *Genome Biol.* **2014**, *15*, 550.
34. Skurk, T.; Alberti-Huber, C.; Herder, C.; Hauner, H. Relationship between adipocyte size and adipokine expression and secretion. *J. Clin. Endocrinol. Metab.* **2007**, *92*, 1023–1033,.
35. Boucher, J.; Masri, B.; Daviaud, D.; Gesta, S.; Guigné, C.; Mazzucotelli, A.; Castan-Laurell, I.; Tack, I.; Knibiehler, B.; Carpéné, C.; et al. Apelin, a newly identified adipokine up-regulated by insulin and obesity. *Endocrinology* **2005**, *146*, 764–1771.
36. White, P.J.; Arita, M.; Taguchi, R.; Kang, J.X.; Marette, A. Transgenic restoration of long-chain n-3 fatty acids in insulin target tissues improves resolution capacity and alleviates obesity-linked inflammation and insulin resistance in high-fat-fed mice. *Diabetes* **2010**, *59*, 3066–3073.
37. Neuhofer, A.; Zeyda, M.; Mascher, D.; Itariu, B.K.; Murano, I.; Leitner, L.; Hochbrugger, E.E.; Fraisl, P.; Cinti, S.; Serhan, C.N.; et al. Impaired local production of proresolving lipid mediators in obesity and 17-HDHA as a potential treatment for obesity-associated inflammation. *Diabetes* **2013**, *62*, 1945–1956.
38. Serhan, C.N. Pro-resolving lipid mediators are leads for resolution physiology. *Nature* **2014**, *510*, 92–101.
39. Morimoto, K.; Shirata, N.; Taketomi, Y.; Tsuchiya, S.; Segi-Nishida, E.; Inazumi, T.; Kabashima, K.; Tanaka, S.; Murakami, M.; Narumiya, S.; et al. Prostaglandin E 2 –EP3 Signaling Induces Inflammatory Swelling by Mast Cell Activation . *J. Immunol.* **2014**, *192*, 1130–1137.
40. Caussy, C.; Chuang, J.-C.; Billin, A.; Hu, T.; Wang, Y.; Subramanian, G.M.; Djedjos, C.S.; Myers, R.P.; Dennis, E.A.; Loomba, R. Plasma eicosanoids as noninvasive biomarkers of liver fibrosis in patients with nonalcoholic steatohepatitis. *Therap. Adv. Gastroenterol.* **2020**, *13*, 13.
41. Maciejewska, D.; Drozd, A.; Skonieczna-Zydecka, K.; Skórka-Majewicz, M.; Dec, K.; Jakubczyk, K.; Pilutin, A.; Stachowska, E. Eicosanoids in nonalcoholic fatty liver disease (NAFLD) progression. Do serum eicosanoids profile correspond with liver eicosanoids content during NAFLD development and progression? *Molecules* **2020**, *25*, 2026.
42. Musso, G.; Gambino, R.; Cassader, M.; Paschetta, E.; Sircana, A. Specialized Proresolving Mediators: Enhancing Nonalcoholic Steatohepatitis and Fibrosis Resolution. *Trends Pharmacol. Sci.* **2018**, *39*, 387–401.
43. Hirai, H.; Tanaka, K.; Yoshie, O.; Ogawa, K.; Kenmotsu, K.; Takamori, Y.; Ichimasa, M.; Sugamura, K.; Nakamura, M.; Takano, S.; et al. Prostaglandin D2 selectively induces

chemotaxis in T helper type 2 cells, eosinophils, and basophils via seven-transmembrane receptor CRTH2. *J. Exp. Med.* **2001**, *193*, 255–262.
44. Weller, C.L.; Collington, S.J.; Hartnell, A.; Conroy, D.M.; Kaise, T.; Barker, J.E.; Wilson, M.S.; Taylor, G.W.; Jose, P.J.; Williams, T.J. Chemotactic action of prostaglandin E2 on mouse mast cells acting via the PGE2 receptor 3. *Proc. Natl. Acad. Sci. USA* **2007**, *104*, 11712–11717.
45. Tsuge, K.; Inazumi, T.; Shimamoto, A.; Sugimoto, Y. Molecular mechanisms underlying prostaglandin E2-exacerbated inflammation and immune diseases. *Int. Immunol.* **2019**, *31*, 597–606.
46. Titos, E.; Rius, B.; González-Périz, A.; López-Vicario, C.; Morán-Salvador, E.; Martínez-Clemente, M.; Arroyo, V.; Clària, J. Resolvin D1 and Its Precursor Docosahexaenoic Acid Promote Resolution of Adipose Tissue Inflammation by Eliciting Macrophage Polarization toward an M2-Like Phenotype. *J. Immunol.* **2011**, *187*, 5408–5418.
47. González-Périz, A.; Planagumà, A.; Gronert, K.; Miquel, R.; López-Parra, M.; Titos, E.; Horrillo, R.; Ferré, N.; Deulofeu, R.; Arroyo, V.; et al. Docosahexaenoic acid (DHA) blunts liver injury by conversion to protective lipid mediators: Protectin D1 and 17S-hydroxy-DHA. *FASEB J.* **2006**, *20*, 2537–2539.
48. González-Périz, A.; Horrillo, R.; Ferré, N.; Gronert, K.; Dong, B.; Morán-Salvador, E.; Titos, E.; Martínez-Clemente, M.; López-Parra, M.; Arroyo, V.; et al. Obesity-induced insulin resistance and hepatic steatosis are alleviated by ω-3 fatty acids: A role for resolvins and protectins. *FASEB J.* **2009**, *23*, 1946–1957.
49. Meijerink, J.; Poland, M.; Balvers, M.G.J.; Plastina, P.; Lute, C.; Dwarkasing, J.; Van Norren, K.; Witkamp, R.F. Inhibition of COX-2-mediated eicosanoid production plays a major role in the anti-inflammatory effects of the endocannabinoid N-docosahexaenoylethanolamine (DHEA) in macrophages. *Br. J. Pharmacol.* **2015**, *172*, 24–37.
50. Shi, H.; Chen, H.; Gu, Z.; Zhang, H.; Chen, W.; Chen, Y.Q. Application of a delta-6 desaturase with α-linolenic acid preference on eicosapentaenoic acid production in Mortierella alpina. *Microb. Cell Factories* **2016**, *15*, 117.
51. Olga, L.; van Diepen, J.A.; Bobeldijk-Pastorova, I.; Gross, G.; Prentice, P.M.; Snowden, S.G.; Furse, S.; Kooistra, T.; Hughes, I.A.; Schoemaker, M.H.; et al. Lipid ratios representing SCD1, FADS1, and FADS2 activities as candidate biomarkers of early growth and adiposity. *EBioMedicine* **2021**, *63*, 103198.
52. Picklo, M.J.; Idso, J.; Seeger, D.R.; Aukema, H.M.; Murphy, E.J. Comparative effects of high oleic acid vs high mixed saturated fatty acid obesogenic diets upon PUFA metabolism in mice. *Prostaglandins Leukot. Essent. Fat. Acids* **2017**, *119*, 25–37.
53. Strassburg, K.; Huijbrechts, A.M.L.; Kortekaas, K.A.; Lindeman, J.H.; Pedersen, T.L.; Dane, A.; Berger, R.; Brenkman, A.; Hankemeier, T.; Van Duynhoven, J.; et al. Quantitative profiling of oxylipins through comprehensive LC-MS/MS analysis: Application in cardiac surgery. *Anal. Bioanal. Chem.* **2012**, *404*, 1413–1426.
54. Morrison, M.C.; Mulder, P.; Salic, K.; Verheij, J.; Liang, W.; Van Duyvenvoorde, W.; Menke, A.; Kooistra, T.; Kleemann, R.; Wielinga, P.Y. Intervention with a caspase-1 inhibitor reduces obesity-associated hyperinsulinemia, non-alcoholic steatohepatitis and hepatic fibrosis in LDLR-/-.Leiden mice. *Int. J. Obes.* **2016**, *40*, 1416–1423.
55. Hotamisligil, G.S.; Shargill, N.S.; Spiegelman, B.M. Adipose expression of tumor necrosis factor-α: Direct role in obesity-linked insulin resistance. *Science* **1993**, *259*, 87–91.

56. Duffaut, C.; Zakaroff-Girard, A.; Bourlier, V.; Decaunes, P.; Maumus, M.; Chiotasso, P.; Sengenès, C.; Lafontan, M.; Galitzky, J.; Bouloumié, A. Interplay between human adipocytes and T lymphocytes in obesity: CCL20 as an adipochemokine and T lymphocytes as lipogenic modulators. *Arterioscler. Thromb. Vasc. Biol.* **2009**, *29*, 1608–1614.
57. Ruan, H.; Lodish, H.F. Insulin resistance in adipose tissue: Direct and indirect effects of tumor necrosis factor-α. *Cytokine Growth Factor Rev.* **2003**, *14*, 447–455.
58. Hers, I.; Tavaré, J.M. Mechanism of feedback regulation of insulin receptor substrate-1 phosphorylation in primary adipocytes. *Biochem. J.* **2005**, *388*, 713–720.
59. Larabee, C.M.; Neely, O.C.; Domingos, A.I. Obesity: A neuroimmunometabolic perspective. *Nat. Rev. Endocrinol.* **2020**, *16*, 30–43.
60. Fang, H.; Judd, R.L. Adiponectin regulation and function. *Compr. Physiol.* **2018**, *8*, 1031–1063.
61. Liu, Y.; Turdi, S.; Park, T.; Morris, N.J.; Deshaies, Y.; Xu, A.; Sweeney, G. Adiponectin corrects high-fat diet-induced disturbances in muscle metabolomic profile and whole-body glucose homeostasis. *Diabetes* **2012**, *62*, 743–752.
62. Park, S.K.; Oh, S.Y.; Lee, M.Y.; Yoon, S.; Kim, K.S.; Kim, J.W. CCAAT/enhancer binding protein and nuclear factor-Y regulate adiponectin gene expression in adipose tissue. *Diabetes* **2004**, *53*, 2757–2766.
63. Matassa, D.S.; Amoroso, M.R.; Maddalena, F.; Landriscina, M.; Esposito, F. New insights into TRAP1 pathway. *Am. J. Cancer Res.* **2012**, *2*, 235–248.
64. Rosen, E.D.; MacDougald, O.A. Adipocyte differentiation from the inside out. *Nat. Rev. Mol. Cell Biol.* **2006**, *7*, 885–896.
65. Moseti, D.; Regassa, A.; Kim, W.K. Molecular regulation of adipogenesis and potential anti-adipogenic bioactive molecules. *Int. J. Mol. Sci.* **2016**, *17*, 124.
66. Flachs, P.; Horakova, O.; Brauner, P.; Rossmeisl, M.; Pecina, P.; Franssen-Van Hal, N.; Ruzickova, J.; Sponarova, J.; Drahota, Z.; Vlcek, C.; et al. Polyunsaturated fatty acids of marine origin upregulate mitochondrial biogenesis and induce β-oxidation in white fat. *Diabetologia* **2005**, *48*, 2365–2375.
67. Cho, E.; Jung, W.; Joo, H.-Y.; Park, E.-R.; Kim, M.-Y.; Kim, S.-B.; Kim, K.S.; Bin Lim, Y.; Lee, K.H.; Shin, H.J. Cluh plays a pivotal role during adipogenesis by regulating the activity of mitochondria. *Sci. Rep.* **2019**, *9*, 6820.
68. Mulder, P.; Morrison, M.C.; Verschuren, L.; Liang, W.; Van Bockel, J.H.; Kooistra, T.; Wielinga, P.Y.; Kleemann, R. Reduction of obesity-associated white adipose tissue inflammation by rosiglitazone is associated with reduced non-alcoholic fatty liver disease in LDLr-deficient mice. *Sci. Rep.* **2016**, *6*, 31542.
69. Zhang, Y.; Chua, S. Leptin function and regulation. *Compr. Physiol.* **2018**, *8*, 351–369.
70. Delerive, P.; De Bosscher, K.; Besnard, S.; Vanden Berghe, W.; Peters, J.M.; Gonzalez, F.J.; Fruchart, J.C.; Tedgui, A.; Haegeman, G.; Staels, B. Peroxisome proliferator-activated receptor α negatively regulates the vascular inflammatory gene response by negative cross-talk with transcription factors NF-κB and AP-1. *J. Biol. Chem.* **1999**, *274*, 32048–32054.
71. Cinti, S. Adipose Organ Development and Remodeling. *Compr. Physiol.* **2018**, *8*, 1357–1431.
72. Rossmeisl, M.; Macek Jilkova, Z.; Kuda, O.; Jelenik, T.; Medrikova, D.; Stankova, B.; Kristinsson, B.; Haraldsson, G.G.; Svensen, H.; Stoknes, I.; et al. Metabolic effects of n-3 PUFA as phospholipids are superior to triglycerides in mice fed a high-fat diet: Possible role of endocannabinoids. *PLoS ONE* **2012**, *7*, e38834.

73. Ostermann, A.I.; West, A.L.; Schoenfeld, K.; Browning, L.M.; Walker, C.G.; Jebb, S.A.; Calder, P.C.; Schebb, N.H. Plasma oxylipins respond in a linear dose-response manner with increased intake of EPA and DHA: Results from a randomized controlled trial in healthy humans. *Am. J. Clin. Nutr.* **2019**, *109*, 1251–1263.

Supplemental information

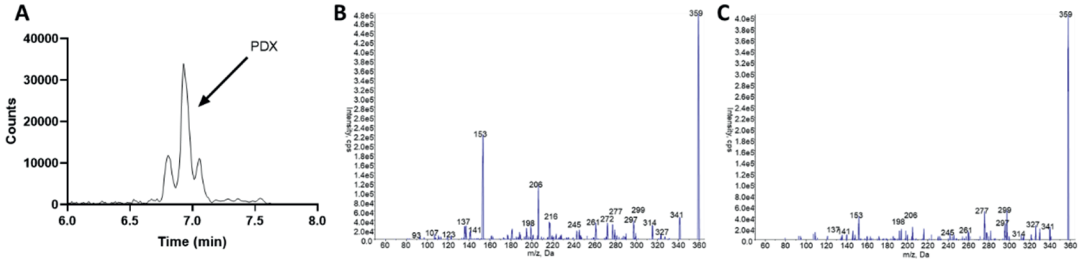

Supplemental figure S1. *PDX identification based on comparisons with a standard for PDX. A) Chromatogram of PDX in a representative eWAT sample, B) PDX authentic standard material MS/MS spectrum, C) MS/MS spectrum obtained from representative WAT sample.*

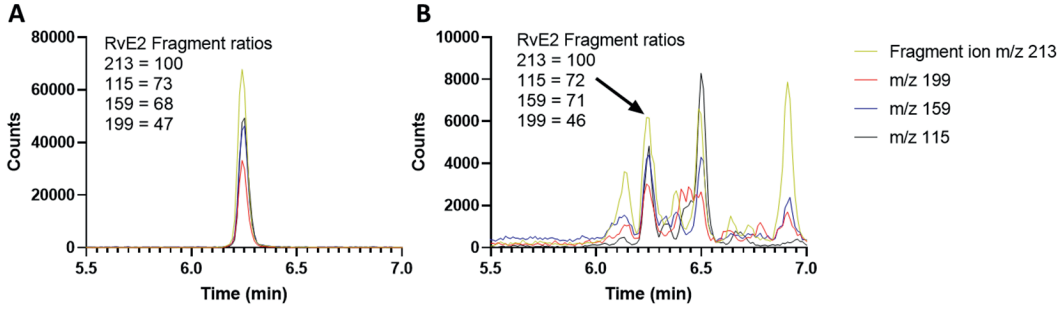

Supplemental figure S2. *RvE2 identification based on comparisons with a RvE2 standard. The graphs show characteristic fragment ions of RvE2 with a dedicated product ion scan LC-MS/MS: A) 1ng/ml authentic standard material, B) RvE2 fragments from a representative liver sample.*

Supplemental Table 1. Individually optimized LC-MS/MS parameters for each compound.

ID	m/z in Q1	m/z in Q3	Time (min)	DP (volts)	EP (volts)	CE (volts)	CXP (volts)
LXA4	351.1	114.8	5.5	-40	-10	-20	-11
5-HETE	319.1	115.0	8.0	-65	-10	-18	-11
8-HETE	319.1	154.9	7.9	-70	-10	-20	-19
11-HETE	319.1	167.0	7.9	-70	-10	-22	-15
12-HETE	319.1	179.0	7.9	-65	-10	-20	-23
15-HETE	319.1	219.1	7.8	-55	-10	-18	-9
15-HEPE	317.1	219.0	7.5	-65	-10	-18	-19
18-HEPE	317.1	259.0	7.4	-5	-10	-16	-7
LXB4	351.1	220.9	5.1	-60	-10	-22	-13

Leukotriene B4	335.1	195.0	6.9	-65	-10	-22	-21
17-HDHA	343.1	245.0	7.9	-65	-10	-16	-15
14,15-diHETE	335.1	207.0	7.0	-65	-10	-24	-21
19,20-DiHDPA	361.1	273.0	7.4	-55	-10	-22	-15
RvE1	349.1	195.0	3.8	-95	-10	-22	-13
RvE2	333.1	114.9	6.1	-35	-10	-18	-15
18S-RvE3	333.1	245.2	6.7	-25	-10	-16	-17
18R-RvE3	333.1	245.0	7.1	-55	-10	-18	-23
TxB2	369.1	169.0	4.6	-55	-10	-24	-15
6-trans-LTB4	335.1	194.9	6.7	-105	-10	-22	-11
20-OH LTB4	351.1	195.0	4.0	-60	-10	-24	-17
PGD2	351.1	233.0	5.0	-30	-10	-16	-13
PDX	359.1	153.0	6.8	-70	-10	-22	-9
PD1	359.1	153.0	6.9	-70	-10	-22	-9
MaR1_2	359.2	250.2	7.0	-65	-10	-20	-13
LTE4	438.1	333.1	7.0	-55	-10	-26	-15
8S,15S-diHETE	335.1	207.9	6.7	-55	-10	-22	-17
LTD4	495.1	177.0	6.7	-70	-10	-28	-19
Leukotriene B4 d4	339.1	196.9	6.9	-70	-10	-22	-19
15-HETE d8	327.2	226.0	7.8	-85	-10	-18	-11
PGE2-d4	355.1	193.0	4.9	-50	-10	-26	-17
7,17-DiHDPA	361.1	198.9	7.0	-45	-10	-26	-23
RvD1	375.1	215.0	5.6	-50	-10	-26	-11
RvD2	375.1	277.1	5.3	-60	-10	-18	-15
6t,12epi-LTB4	335.1	194.9	6.8	-80	-10	-22	-25
PGF2a	353.1	193.0	5.2	-80	-10	-34	-11
PGE2_2	351.2	271.1	4.9	-50	-10	-22	-21
17-OH-DH-HETE	347.1	247.0	8.2	-110	-10	-22	-27
13-HoTrE	293.0	195.0	7.4	-45	-10	-24	-19
13-HoDE	295.0	194.9	7.7	-110	-10	-24	-21
7S-MaR1	359.1	249.9	6.6	-20	-10	-20	-19
15-Keto-PGE2	349.0	234.9	4.5	-65	-10	-20	-13
13,14dihydro-15keto-PGF2a	353.1	195.0	5.4	-110	-10	-32	-11
8-iso-PGE2	351.1	271.0	4.6	-5	-10	-24	-19
8-iso-PGF2a	353.1	193.0	4.5	-135	-10	-34	-11
9-HoTrE	293.0	170.9	7.4	-75	-10	-20	-15
9-HoDE	295.0	171.0	7.7	-130	-10	-22	-7
AA	303.0	205.1	8.8	-155	-10	-20	-11
DHA	327.1	229.2	8.8	-115	-10	-18	-11
EPA	301.0	202.9	8.6	-125	-10	-18	-21
AdA	331.1	233.0	9.1	-130	-10	-22	-11
DPAn-3	329.1	231.1	9.0	-50	-10	-20	-17
DHAd5	332.0	288.1	8.8	-75	-10	-16	-13
LA	279.0	261.0	8.8	-115	-10	-28	-13
ALA/GLA	277.0	233.0	8.6	-90	-10	-22	-29
PGJ2	333.0	271.0	6.1	-30	-10	-22	-17

5,15-diHETE	335.0	173.1	6.8	-55	-10	-20	-11
10-HDHA	343.1	153.0	7.9	-25	-10	-20	-15
7-HDHA	343.1	141.1	8.0	-85	-10	-18	-23
14(15)EET	319.0	218.9	8.1	-5	-10	-16	-55
11(12)EET	318.9	166.9	8.2	-90	-10	-18	-19
8(9)EET	319.0	154.9	8.2	-60	-10	-18	-13
15Deoxy PGJ2	315.0	203.0	7.3	-50	-10	-28	-19
20-HETE_2	319.0	289.1	7.7	-70	-10	-24	-15
4-HDHA	343.1	101.0	8.2	-50	-10	-18	-9
14(S)-HDHA	343.1	204.9	8.0	-60	-10	-18	-27
5-HEPE	317.0	114.9	7.7	-55	-10	-18	-11
12-HEPE	317.0	179.0	7.6	-60	-10	-18	-17
5-KETE	317.0	203.1	8.1	-70	-10	-24	-11
12-KETE	317.0	153.0	7.9	-60	-10	-22	-9
15-KETE	317.0	113.0	7.8	-10	-10	-22	-5
19(20)-EpDPA	343.1	281.1	8.1	-70	-10	-16	-11
DGLA	305.1	261.2	9.0	-85	-10	-22	-13
8-iso-PGF2alpha-d4	357.3	197.0	4.5	-110	-10	-34	-20
14(15)-EET-d11	330.2	219.0	8.1	-85	-10	-15	-15

Table S2. Fatty acid composition of dried blood spots, eWAT and liver tissue.

	Dried blood spots			eWAT			Liver		
Fatty acids (% of all FA measured)	**chow**	**HFD**	**KrO**	**chow**	**HFD**	**KrO**	**chow**	**HFD**	**KrO**
Omega-3									
alpha-Linolenic C18:3n3	0.2%*	0.2%	0.3%*	1.5%*	0.6%	0.7%*	0.8%*	0.4%	0.5%*
Eicosapentaenoic (EPA) C20:5n3	0.6%*	0.3%	6.6%*	0.1%*	0.0%	0.2%*	0.4%*	0.1%	1.6%*
Docosapentaenoic n3C22:5n3	0.6%*	0.3%	0.8%*	0.1%*	0.1%	0.2%*	0.6%*	0.3%	1.2%*
Docosahexaenoic (DHA) C22:6n3	5.7%*	4.5%	6.7%*	0.3%*	0.1%	0.5%*	4.5%*	2.0%	4.7%*
Omega-6									
Linoleic C18:2n6	18.4%	18.1%	18.7%	27.1%*	20.8%	21.6%*	18.6%*	14.7%	15.0%
gamma-Linolenic C18:3n6	0.3%	0.3%	0.2%*	0.1%*	0.1%	0.1%	0.3%	0.3%	0.2%*
Eicosadienoic C20:2n6	0.2%*	0.3%	0.4%*	0.1%*	0.3%	0.3%	0.3%*	0.4%	0.3%*
Dihomo-g-linolenic C20:3n6	1.4%	1.3%	1.3%	0.3%*	0.2%	0.1%*	1.1%*	0.9%	0.7%*
Arachidonic (ARA) C20:4n6	18.9%*	20.7%	8.4%*	0.6%*	0.4%	0.2%*	6.6%*	3.5%	2.0%*
Docosatetraenoic C22:4n6	0.9%*	0.6%	0.1%*	0.1%*	0.1%	0.0%*	0.3%*	0.5%	0.2%*

Docosapentaenoic n6C22:5n6	0.5%	0.4%	0.0%*	0.0%	0.0%	0.0%*	0.2%*	0.3%	0.0%*
Cis-Monosaturated									
Palmitoleic C16:1n7	2.2%*	1.6%	3.1%*	10.4%	4.0%*	4.3%*	5.1%*	3.0%	3.9%*
Oleic C18:1n9	15.6%*	20.2%	23.0%*	36.5%	52.6%*	51.3%*	29.7%*	44.4%	41.8%*
Eicosenoic C20:1n9	0.4%	0.4%	0.4%	0.6%	0.5%*	0.4%*	0.7%	1.1%	1.0%*
Nervonic C24:1n9	0.5%*	0.2%	0.3%*	0.0%	0.0%*	0.0%	0.1%*	0.0%	0.1%*
Saturated									
Myristic C14:0	0.2%	0.1%	0.2%*	1.0%	0.7%*	0.8%*	0.5%	0.5%	0.5%*
Palmitic C16:0	21.8%*	18.7%	19.3%	19.6%	16.4%*	16.2%	23.5%	23.9%	22.6%*
Stearic C18:0	10.3%	10.7%	9.0%*	1.2%	2.7%*	2.7%	6.1%*	3.1%	3.5%
Arachidic C20:0	0.2%*	0.2%	0.2%	0.0%	0.0%*	0.0%	0.3%*	0.1%	0.2%*
Behenic C22:0	0.5%*	0.2%	0.2%	0.0%	0.0%	0.0%	0.1%*	0.0%	0.0%*
Lignoceric C24:0	0.5%*	0.2%	0.2%	0.0%	0.0%*	0.0%	0.1%*	0.0%	0.0%*
Trans									
Palmitelaidic C16:1n7t	0.1%	0.1%	0.1%*	0.1%	0.1%*	0.1%*	0.1%	0.1%	0.1%*
Elaidic C18:1t	0.2%*	0.2%	0.2%	0.1%	0.2%*	0.2%*	0.1%*	0.1%	0.1%*
Linoelaidic C18:2n6t	0.2%	0.2%	0.2%*	0.3%	0.2%*	0.2%	0.3%*	0.3%	0.2%*

*Average fatty acid percentages after 28 weeks of dietary treatment are shown (percentage of totally identified fatty acids) with *p<0.05 compared to HFD. Data of the chow group was provided for reference.*

CHAPTER

5

Intervention with isoleucine or valine corrects hyperinsulinemia and reduces intrahepatic diacylglycerols, liver steatosis and inflammation in Ldlr-/-.Leiden mice with manifest obesityassociated NASH

Eveline Gart, Wim van Duyvenvoorde, Martien P. M. Caspers, Nikki van Trigt, Jessica Snabel, Aswin Menke, Jaap Keijer, Kanita Salic, Martine C. Morrison, Robert Kleemann

FASEB J. 2022 Aug;36(8):e22435.
doi: 10.1096/fj.202200111R. PMID: 35830259.

Abstract

Non-alcoholic steatohepatitis (NASH) is associated with a disturbed metabolism in liver, insulin resistance and excessive accumulation of ectopic fat. Branched-chain amino acids (BCAAs) may beneficially modulate hepatic lipids, however it remains unclear whether individual BCAAs can attenuate already established NASH and associated oxidative-inflammatory stress. After a 26 weeks run-in on fast food diet (FFD), obese Ldlr-/-.Leiden mice were treated for another 12 weeks with either valine or isoleucine (3% of FFD) and then compared to FFD controls. Valine and isoleucine did not affect obesity, dyslipidemia, gut permeability or fecal fatty acid excretion, but significantly reduced hyperinsulinemia. Valine and isoleucine reduced ALT, CK-18M30, and liver steatosis with a particularly pronounced suppression of the microvesicular component (-61% by valine and -71% by isoleucine). Both BCAAs decreased intrahepatic diacylglycerols and 4-hydroxynonenal immunoreactivity, a marker for oxidative stress-induced lipid peroxidation. Functional genomics analysis demonstrated that valine and isoleucine affected BCAA metabolism genes, deactivated master regulators of anabolic pathways related to steatosis (e.g. SREBPF1) and activated master regulators of mitochondrial biogenesis (e.g. PPARGC1a) and lipid catabolism (e.g. ACOX1, AMPK). This correction of critical metabolic pathways on gene expression level was accompanied by a significant decrease of histological liver inflammation, and suppression of FFD-stimulated cytokine and chemokine proteins KC/CXCL1, MCP-1/CCL2 and MIP-2/CXCL2 and their pathways. In conclusion, a dietary intervention with either valine or isoleucine corrected liver diacylglycerols, gene expression of multiple metabolic processes and reduced NASH histology with profound hepatoprotective effects on oxidative stress and inflammatory proteins.

1. Introduction

Non-alcoholic fatty liver disease (NAFLD) is the hepatic manifestation of the metabolic syndrome, which is characterized by obesity, dyslipidemia, hyperinsulinemia and insulin resistance.[1,2] The strong association between NAFLD, insulin resistance and dyslipidemia is thought to be causal to the increased risk of atherosclerosis in NAFLD patients.[3] The relationship between hyperinsulinemia NAFLD and atherosclerosis has been explained by an insulin-mediated upregulation of SREBF1 (*SREBP-1c*). This upregulation stimulates hepatic *de novo* fatty acid (FA) synthesis[4,5] and thereby the excessive accumulation of fat (steatosis), while at the same time promoting hepatic VLDL secretion and dyslipidemia. Hepatic steatosis in NAFLD is typically associated with disturbed lipid handling processes among which increased FA synthesis and diminished FA oxidation.[6] These disturbances in lipid handling are also associated with hepatic insulin resistance mediated by diacylglycerols (DAGs),[7] increased oxidative stress and hepatocellular damage.[8,9] Together they promote the development of non-alcoholic steatohepatitis (NASH) characterized by liver inflammation and activated inflammatory cytokine signaling pathways stimulated by TNF-α, IL-1β, KC/CXCL1, MCP1/CCL2 and others.[10] In particular the accumulation of small lipid droplets in hepatocytes, referred to as microvesicular steatosis, is thought to be related to impaired lipid processing and mitochondrial dysfunction.[11] Also, deactivation of AMP-activated protein kinase (AMPK), a major regulator of energy homeostasis and lipid catabolism, is frequently observed in NASH.[12,13] This deactivation drives anabolic processes including lipogenesis via SREBF1, while impairing peroxisomal β-oxidation (e.g. ACOX1 activity).

Therapeutic strategies for NAFLD/NASH that have been developed during the past several years do not or only partially correct the aforementioned complex disturbances of liver lipid metabolism.[9] Hence, there is a great interest in new approaches, including nutritional treatments, that may restore metabolic homeostasis and reduce liver inflammation. A recent study showed that a mix of equal amounts of the branched-chain amino acids (BCAAs) leucine, isoleucine and valine administered via the diet, can prevent hepatic steatosis in mice fed a choline-deficient high-fat diet.[14] However, choline deficiency is a physiologically artificial condition and is mainly used experimentally to inhibit the assembly and secretion of VLDL particles in the liver.[15] As a consequence, also the development of dyslipidemia is prevented under such experimental conditions which contrasts the situation in NASH patients. Furthermore, it is unclear how these BCAA effects are achieved and studies investigating whether individual BCAA can correct the multiple metabolic pathways affected in NASH have not been performed.

It is also unknown whether the individual BCAAs can attenuate NASH development in a therapeutic setting, i.e. starting treatment when obesity, dyslipidemia, hyperinsulinemia, and liver steatosis are already established. To study the potential hepatoprotective effects of a therapeutic intervention with single BCAAs, we employed dietary supplementation with valine or isoleucine in an established mouse model for diet-induced NAFLD/NASH with atherosclerosis, Ldlr-/-.Leiden mice.[16–19] These mice exhibit hyperinsulinemia, obesity and human-like pathological hallmarks of NASH[20] in combination with hepatocellular damage from oxidative stress.[21] These mice also express key inflammatory pathways

observed in NASH patients[18,19] when fed a fast-food diet (FFD) with a macronutrient composition and cholesterol content comparable to human diets.[22] Next-generation sequencing (NGS) and ingenuity pathway analysis provides a possibility to comprehensively analyze metabolic and inflammatory pathways including their upstream regulators based on integrated gene expression analysis of downstream target genes. We employed this technique in conjunction with hepatic protein analysis by Western blot and multiplex assays to support histological and immunohistochemical observations made in liver and to identify the metabolic processes and inflammatory pathways that were affected by the individual BCAAs.

2. Materials and methods

2.1 Animal experiment

The animal experiment was performed according to standards of the Animal Care and Use Committee and ethical approved by an independent Animal Welfare Body (IVD TNO; approval number 20172064/TNO-439) and the ARRIVE guidelines were followed. Male Ldlr-/-.Leiden mice (genetic background 94% C57BL/6J and 6% 129S) obtained from the breeding stock at TNO Metabolic Health Research (Leiden, the Netherlands) were group-housed (four to five mice per cage) in Macrolon cages in clean-conventional animal rooms (relative humidity 50–60%, temperature ~21C, light cycle 7a.m. to 7 p.m.) in an animal facility accredited by the American Association for Accreditation of Laboratory Animal Care (AAALAC) at TNO Metabolic Health Research with *ad libitum* access to food and water.

During a 26 week run-in period, three groups of mice were fed a fast-food diet (FFD; 41 kcal% fat from milk fat, 44 kcal% from primarily fructose as carbohydrate, and 14 kcal% from mainly casein as protein source; Research Diets, new Brunswick, NJ,USA). After 26 weeks two FFD groups started with a 12-week intervention in which FFD was supplemented with 3% (w/w) valine (FFD+Val) or isoleucine (FFD+Iso) and these two treatment groups were compared to a FFD control group. Mice were matched into these three treatment groups of n=15 mice per group, based on body weight, plasma cholesterol and triglycerides and blood glucose. N=15 mice are required to detect statistical differences in NASH (at α=0.05 and power = 0.8), the main end-point. The concentration of valine and isoleucine was based on a long-term dietary supplementation study with BCAAs.[23] Of note, in the BCAA intervention groups the casein content was lowered to make sure that the intake of total protein was comparable between the groups. In addition, levels of other essential amino acids were supplemented to bring them back up to the same level as in the FFD control group. Adjustments were made following the guidelines of the National research council, and the requirements put forward by the subcommittee on laboratory animal nutrition.[24] During the whole study period of 26 weeks run-in plus 12 weeks of intervention, thus 38 weeks, a reference group (n=8) remained on a low-fat chow diet (chow; Sniff-R/M-V1530, Uden, the Netherlands). Blood samples were obtained from the tail vein in 5h-fasted mice, and body weight, food intake and body composition measurements were acquired at set time points during the study. After 38 weeks mice were sacrificed by gradual-fill CO_2 exposure and liver tissues were collected for biochemical measurements and histopathology (snap frozen and formalin fixation, respectively). Effects of the valine and isoleucine interventions were

evaluated using histological and biochemical techniques on features of the metabolic syndrome and NASH. To gain insight into the molecular processes affected by valine and isoleucine, we performed NGS and subsequent bioinformatical analysis to study entire metabolic and inflammatory pathways and the respective activity of upstream regulators.

2.2 Blood chemistry

Analysis of cholesterol, triglycerides (TGs), insulin, alanine amine transferase (ALT), tissue inhibitor of metalloproteinases-1 (TIMP-1) in EDTA plasma and glucose in whole blood was performed as described previously.[25] In addition, cytokeratin 18-M30 (CK18-M30) and apolipoprotein B (ApoB) were measured in EDTA plasma according to manufacturer's instructions (Cusabio CSB-E14265m, Houston, USA, and Abcam Ab230932, Cambridge, UK, respectively).

For lipoprotein profiles analysis, lipoproteins were first separated via fast protein liquid chromatography (FPLC) using an AKTA apparatus (Pharmacia, Roosendaal, the Netherlands), as previously described.[26,27] Subsequently, total cholesterol and triglycerides were measured in the fractions collected for profiling with enzymatic assays (Roche diagnostics, Basel, CHF).

Plasma amino acids were extracted and derivatized with AccQTag reagent (Waters). The derivatized amino acids were then analyzed by LC-MS. For quantification of the 20 normal amino acids (including the branched-chain amino acids), calibration curve standards prepared in albumin solution were measured. Nitrogen-15, carbon-13 amino acid internal standards were added to all samples before extraction.

2.3 Fecal fatty acid excretion

Fatty acid excretion was determined in feces collected from cages over a 3-day time period. These feces were freeze-dried and weighed. An aliquot of these lyophilized feces (15 mg) was derivatized as previously reported[28] using pentadecanoic acid (C15:0) as internal standard. The samples were prepared as previously described[28] and applied on a GC column (CP Sil88, Chrompack International) in a Scion 436-GC (Goes, the Netherlands) equipped with a flame ionization detector. Quantification the fecal fatty acids (C14:0, C16:0, C16:1, C18:0, C18:1, C18:2, C18:3, as these are the major FA present) were based on the area ratio to the internal standard and expressed as µmol/mouse/day.

2.4 Liver histopathology

NASH was scored in hematoxylin-Eosin-stained cross sections based on the human NAS scoring system using a standardized method for rodents.[20] Briefly, for each mouse the percentage of total liver section affected by steatosis (macrovesicular and microvesicular) and hypertrophy (abnormally enlarged hepatocytes) was determined. Hepatic inflammation was quantified by counting the number of inflammatory aggregates in 5 fields per mouse at 100x magnification (field of view 4.15 mm2) and expressed as the number of aggregates per mm^2 as reported.[25]

Oxidative stress-induced lipid peroxidation marker 4-hydroxynonenal (4-HNE) was analyzed in 4-HNE-stained liver sections (with Rabbit anti-4-HNE 1:2000, ref.393207, Millipore Corporation, Billerica, MA, USA PBS) as previously described,[29] for n = 5 chow, and n = 8 FFD, FFD + valine and FFD + isoleucine. 4-HNE-positive immunoreactive structures were counted in three non-overlapping fields and expressed per mm^2.

2. 5 Intrahepatic diacylglycerol content determination
Diacylglycerol (DAG) content was quantified in crude liver homogenates according to manufacturer's instructions (ab242293, Abcam, Cambridge, UK). In short, this assay extracts cellular lipids using methanol, chloroform and NaCl. Extracted lipids are treated with a kinase that phosphorylates DAGs to yield phosphatidic acid (PA). A lipase then hydrolyzes PA into glycerol-3-phosphate, which is subsequently oxidized by glycerol-3-phosphate oxidase (GPO) to produce hydrogen peroxide that reacts with a fluorometric probe.

2.6 Hepatic genome-wide gene expression analysis
Briefly, liver total RNA was isolated using RNA-Bee (Bio-Connect, Huissen, the Netherlands) and purified using PureLink RNA Mini Kit (Thermo Fisher Scientific, Waltman, USA). RNA concentration was determined spectrophotometrically using the Nanodrop 1000 (Isogen Life Science, De Meern, the Netherlands), and RNA quality was assessed using the 2100 Bioanalyzer (Agilent Technologies, Amstelveen, the Netherlands). Strand-specific messenger RNA sequencing libraries for the Illumina (Ilumina NovaSeq6000, San Diego, CA) platform were generated paired-End 150 bp for approximately 20 million Paired-End reads per sample at Genomescan (Leiden, the Netherlands).
The sequences were filtered, trimmed and subjected to a quality control as described previously.[30] These files were then merged and aligned to the reference genome "Mus_musculus.GRCm38.gencode.vM19". To count the read mapping frequency per gene Htseq-count 0.6.1p1 was used, and resulting count files served as input for the differentially expressed genes (DEGs) analysis using the Deseq2-method.[31] DEGs were used as an input for pathway and upstream regulator analysis through Ingenuity Pathway Analysis (IPA).[32] IPA also uses gene expression data of all known downstream target genes to predict activation or deactivation of an upstream regulator as reported.[25]

2.7 Hepatic protein expression analysis
Protein expression of phosphorylated-BCKDH, total-BCKDH, phosphorylated-AMPK and tubulin was determined using Western blot analysis. Liver homogenates were made with ice cold lysis buffer as previously described,[25] and protein content was determined (BCA Protein Assay Kit, Thermo Fisher Scientific). Protein samples (40 µg) were separated and blotted as previously reported.[25] The blotting membranes were treated with block buffer for 1 h (5% (*w*/*v*) milk powder in tris-buffered saline with 0.1% Tween 20 (TBST)) and incubated overnight in at 4 °C in block buffer with either the primary antibody targeting phosphorylated-BCKDH (# A304-672A-M 1:1000; Thermo Fisher Scientific), total-BCKDH (# A303-790A, Thermo Fisher Scientific), phosphorylated-AMPK-threonine172 (#2531-1:1000 v/v; Cell signaling, Leiden, the Netherlands) or αTubulin (T5168-1:1000 v/v; Sigma-Aldrich). The next day, blots were washed in TBST and incubated for 1 h in block buffer with the secondary antibody (#7074S-1:2000 *v*/*v*; Cell Signaling). Blots were washed again and treated with Super Signal West Femto (Thermo Fisher Scientific) to visualize protein bands. Blots were analyzed with a ChemiDoc Touch Imaging system (Bio-Rad) and band intensities were normalized to tubulin.

2.8 Intrahepatic cytokines and chemokines

Intrahepatic concentrations of cytokines (IL-1b, IL-4, IL-6, IL-10, IL-15, IL-17A/F, IL-33, IFNy and TNFa) and chemokines (MIP1a/CCL3, IP10/CXL10, KC/CXCL1, MIP-2/CXCL2) were measured in liver biopsies homogenized in lysis buffer as previously reported.[33] The cytokines and chemokines in liver were measured using a multiplex immunoassay panel (#KH152AOH; V-PLEX Custom Mouse Biomarker, Mesoscale Discovery (MSD), Maryland, USA) according to the manufacturer's protocol on a MESO QuickPlex SQ 120 reader (MSD). Total protein concentrations in the same homogenates were assessed with a BCA Protein Assay Kit (Thermo Fisher Scientific, Waltham, MA, USA) to determine the inflammatory factors per mg of protein.

2.9 Statistics

Statistical analysis was performed with IBM SPSS statistics version 25.0 (SPSS Inc., Chicago, Illinois, USA). Data was tested for normality with the Shapiro-Wilk test and for homoscedasticity with Levene's test ($\alpha = 0.05$). Normally distributed data with equal variance was tested with an one-way analysis of variance (ANOVA) with a Dunnet's post hoc test using FFD as the control group. Not normally distributed data and/or data with non-equal variances were tested with the Kruskal-Wallis test and Mann-Whitney post hoc test.

3. Results

3.1 Valine and isoleucine decreased FFD-induced hyperinsulinemia and improved circulating liver damage markers independent of effects on body composition

After 38 weeks on FFD, mice developed pronounced obesity with a significantly increased body weight and fat mass and a reduced lean mass, relative to chow (Table 1). Valine or isoleucine did not affect these endpoint readouts. Average caloric intake during the 12-week intervention period was comparable between FFD and chow, and valine and isoleucine did not affect caloric intake.

FFD feeding induced hyperlipidemia with pronounced increases in plasma cholesterol and TGs, which were non-significantly lowered by valine and isoleucine. Plasma lipoprotein profiles demonstrated that the FFD-induced increase in plasma TGs can mainly be ascribed to an increase in VLDL lipoprotein particles and the increase in plasma cholesterol to an increase in (V)LDL sized particles (Figure 1A-B). Valine had no marked effect on the lipoprotein profiles, while isoleucine seemed to lower TG in VLDL and cholesterol in VLDL/LDL. Indeed, fasted plasma ApoB mainly present on (V)LDL particles was significantly increased with FFD, while valine did not affect ApoB concentrations and isoleucine significantly lowered ApoB (Table 1).

To analyze whether the BCAAs would affect uptake of dietary fat, fecal fatty acid concentrations were determined. Treatment with FFD resulted in an average fatty acid excretion of 32.8 µmol/mouse/day. Valine and isoleucine did not affect the excretion of fecal fatty acids showing comparable values (27.8 and 19.8 µmol/mouse/day, respectively) (Figure 1C).

Fasting glucose was lower in the FFD group compared to chow, and valine reversed this FFD effect non-significantly whereas this reversal reached significance in the isoleucine group (Table 1). FFD strongly induced hyperinsulinemia compared to chow-fed mice.

Valine and Isoleucine significantly reduced fasting insulin concentrations compared to FFD, indicative of an BCAA-induced improvement in insulin resistance.
Gut permeability, assessed by analysis of orally administered FD4 and subsequent uptake in plasma, was non-significantly elevated with FFD relative to chow, and not affected by either of the BCAAs (Table 1).
FFD and chow feeding groups demonstrated comparable BCAA concentrations in fasting plasma. Consistent with the dietary supplementation of valine and isoleucine, a few mice of the respective treatment groups showed modest elevations of these BCAA an effect which became significant for isoleucine. Leucine concentrations were comparable in all groups (Supplemental figure 1).
Circulating markers of liver injury ALT and CK18-M30 were significantly elevated with FFD relative to chow (Table 1). Valine tended to lower these markers. Isoleucine had a more pronounced lowering effect and significantly decreased ALT and CK18-M30. Together these biomarker analyses indicate potential hepatoprotective effects of valine and isoleucine independent of effects on body composition.

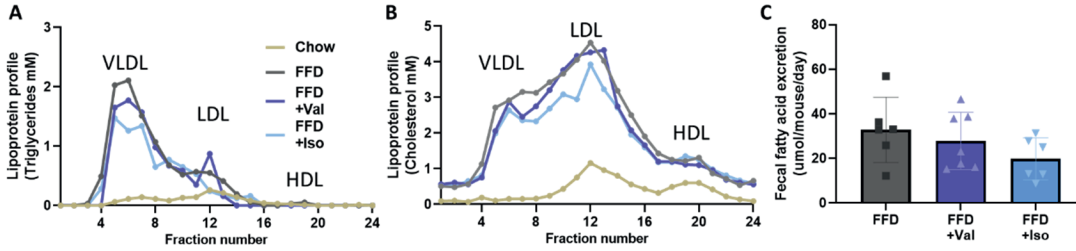

***Figure 1**. Lipoprotein profiles were analyzed in plasma (pooled from n=15 mice per treatment group) by fast protein liquid chromatography (FPLC). In the obtained fractions total (**A**) cholesterol and (**B**) triglycerides were measured and the results were plotted as profiles. (**C**) Fecal fatty acid excretion. Data presented as mean ± SD.*

Table 1. Body weight, body composition and risk factors of metabolic disease.

	Chow	FFD	FFD +Val	FFD +Iso
Body weight (g)	34.0 ± 3.7*	46.2 ± 5.0	45.0 ± 5.2	43.4 ± 6.0
Fat mass (% of BW)	11.2 ± 4.3*	37.9 ± 4.2	36.6 ± 6.8	34.7 ± 7.1
Lean mass (% of BW)	85.4 ± 4.1*	59.9 ± 4.1	61.5 ± 5.7	63.8 ± 7.1
12-week avg food intake (Kcal/mouse/day)	12.6 ± 1.4	13.8 ± 1.0	16.4 ± 2.0	15.0 ± 1.7
Cholesterol (mM)	9.2 ± 1.0*	50.0 ± 10.1	46.3 ± 10.5	42.0 ± 15.9
Triglycerides (mM)	1.6 ± 0.3*	10.3 ± 2.4	8.6 ± 2.6	7.7 ± 4.4
ApoB (mg/ml)	0.4 ± 0.1*	0.7 ± 0.1	0.7 ± 0.1	0.6 ± 0.1*
Glucose (mM)	7.9 ± 0.6*	6.9 ± 0.7	7.6 ± 1.0	7.5 ± 1.3*
Insulin (ng/ml)	0.9 ± 0.3*	4.7 ± 2.0	3.3 ± 1.3*	3.2 ± 1.5*
FD4 (ug/ml)	1.3 ± 0.3	1.7 ± 0.3	1.8 ± 0.6	1.9 ± 1.1
ALT (U/l)	39.6 ± 9.6*	304.8 ± 106.8	251.2 ± 108.7	196.9 ± 90.7*
CK18-M30 (mU/ml)	219.1 ± 39.6*	383.6 ± 59.2	343.3 ± 42.7	310.5 ± 69.9*

*Plasma readouts were determined in endpoint plasma (t=38) collected after dietary intervention with valine (FFD + Val) or isoleucine (FFD + Iso) for 12 weeks. * asterisk indicates significance of difference compared to the FFD control group with p<0.05, data shown here as mean ± SD.*

3.2 Valine and isoleucine upregulate BCAA metabolism genes

We next evaluated whether BCAA treatment affected the hepatic gene expression program that controls BCAA metabolism using NGS.

FFD strongly decreased the hepatic mRNA expression of BCAT and genes that encode for the BCKDH complex (BCKDHA, BCKDHB, DBT, DLD), and many related genes (PPM1K, ACADSB, ECHS1, HIBADH, ALDH6A1; Figure 2A) that encode for proteins required for BCAA catabolism (graphical overview in figure 2B). Valine, and to an even greater extent, isoleucine reversed the FFD-induced effects resulting in upregulation of many of these genes (Figure 2A). Taken together, gene expression data indicate that treatment with valine and isoleucine stimulates genes involved in the catabolism of BCAAs in the liver, thereby counteracting the effect of FFD feeding during NASH development. Hepatic protein expression analysis demonstrated that FFD significantly increased the ratio between phosphorylated-BCKDH and total-BCKDH, yet valine and isoleucine did not significantly lower this ratio (Supplemental figure 2).

A

	FFD vs Chow		Valine vs FFD		Isoleucine vs FFD	
	2logR	P-value	2logR	P-value	2logR	P-value
BCAT2	-0.57	0.000	0.14	0.114	0.18	0.031
BCKDK	0.18	0.062	-0.13	0.114	-0.14	0.076
PPM1K	-0.87	0.000	0.27	0.036	0.55	0.000
BCKDHA	-0.12	0.167	0.08	0.305	0.12	0.091
BCKDHB	0.00	0.971	0.08	0.258	0.19	0.008
DBT	-0.79	0.000	0.17	0.057	0.21	0.012
DLD	-0.16	0.034	0.15	0.016	0.00	0.987
ACADSB	-1.11	0.000	0.26	0.009	0.23	0.018
ECHS1	-0.21	0.002	0.11	0.057	0.11	0.055
HIBCH	-0.02	0.779	0.13	0.093	0.19	0.010
HIBADH	-0.59	0.000	0.18	0.008	0.23	0.000
ALDH6A1	-0.84	0.000	0.19	0.056	0.20	0.043
PCCB	-0.26	0.000	0.17	0.007	0.11	0.078
HSD17B10	-0.27	0.013	0.20	0.029	0.19	0.032
ACAT1	0.03	0.712	0.13	0.082	0.12	0.097
ACAT2	0.10	0.517	0.05	0.711	0.00	0.985

B

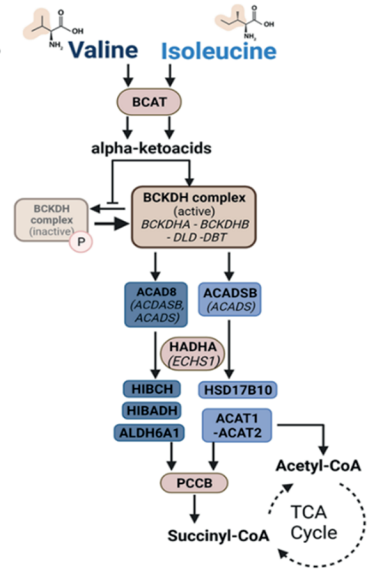

Figure 2. *Changes in expression of genes involved in BCAA metabolism. (**A**) Gene expression changes are expressed in 2log fold-change (2logR), red indicates upregulation in gene expression, green indicates downregulation and P-values indicate significant changes marked in grey. (**B**) Graphical overview of valine and isoleucine catabolism. Valine and isoleucine can promote their own breakdown via the branched-chain α-ketoacid dehydrogenase (BCKDH) complex. Valine can further be metabolized into succinyl-CoA while isoleucine provides acetyl-CoA or succinyl-CoA, which can enter the tricarboxylic acid (TCA) cycle.*

3.3 Valine and isoleucine reduced hepatic lipid accumulation associated with an improvement in lipid metabolism

To investigate potential hepatoprotective effects of valine and isoleucine on tissue level, we examined liver weight and histopathological features of NASH. FFD feeding increased liver weight and induced pronounced steatosis with comparable induction of macro- and microvesicular steatosis and increased hepatocellular hypertrophy (Figure 3A-F). Valine and isoleucine-treated livers were lower in weight, showing a reduction of 15% and 25%, respectively (Figure 3B). Macrovesicular steatosis was decreased by 28% with valine and by 24% with isoleucine (Figure 3C-D). The decrease in microvesicular steatosis was even more pronounced, with marked reductions by 61% (valine) and 71% (isoleucine) relative to FFD (Figure 3E). Hepatocellular hypertrophy was lowered by 47% and 60% with valine and isoleucine, respectively (Figure 3F).

Consistent with the histological steatosis effects, FFD markedly increased intrahepatic diacylglycerols (DAGs) (Figure 3G), a lipid that blocks insulin action at the level of its receptor.[7] The FFD-induced accumulation was significantly suppressed by both valine and isoleucine, providing a mechanistic rationale for the significant reduction of hyperinsulinemia observed with both BCAAs.

The pronounced effects on liver histology were substantiated by NGS and subsequent upstream regulator analyses (IPA bioinformatics tool [32]). The IPA analysis predicts the activation state of an upstream regulator (e.g. transcription factor, metabolic enzyme, signaling cytokine) based on the expression pattern of (target) genes downstream from

this regulator (Table 2). FFD affected lipid metabolism in multiple ways and several regulators of lipid synthesis (e.g. SREBF1) and anabolic processes (e.g. IGF1, AGT), were activated, whereas regulators involved in energy homeostasis and lipid catabolism (e.g. AMPK, ACOX1, EHHADH) as well as mitochondrial biogenesis (PPARGC1A, CLUH) and energy dissipation (UCP1) were deactivated. In line with this FFD lowered pThr172-AMPK with borderline significance (p=0.06) (Supplemental figure 3). Valine and isoleucine counter-regulated many of these FFD gene expression effects (Table 2), which was further supported by canonical pathway analysis. For example, valine and isoleucine stimulated the canonical triglyceride degradation pathway (Z=2.0; p<0.05 and Z=3.0; P<0.05, respectively) and especially isoleucine affected the canonical fatty acid β-oxidation pathway (Z=2.2; p<0.05) and canonical AMPK signaling (Z=1.9; p<0.05). Taken together, valine and isoleucine supplementation inhibits lipid synthesis pathways and stimulates hepatic lipid catabolism pathways in line with the observed reduction of liver steatosis.

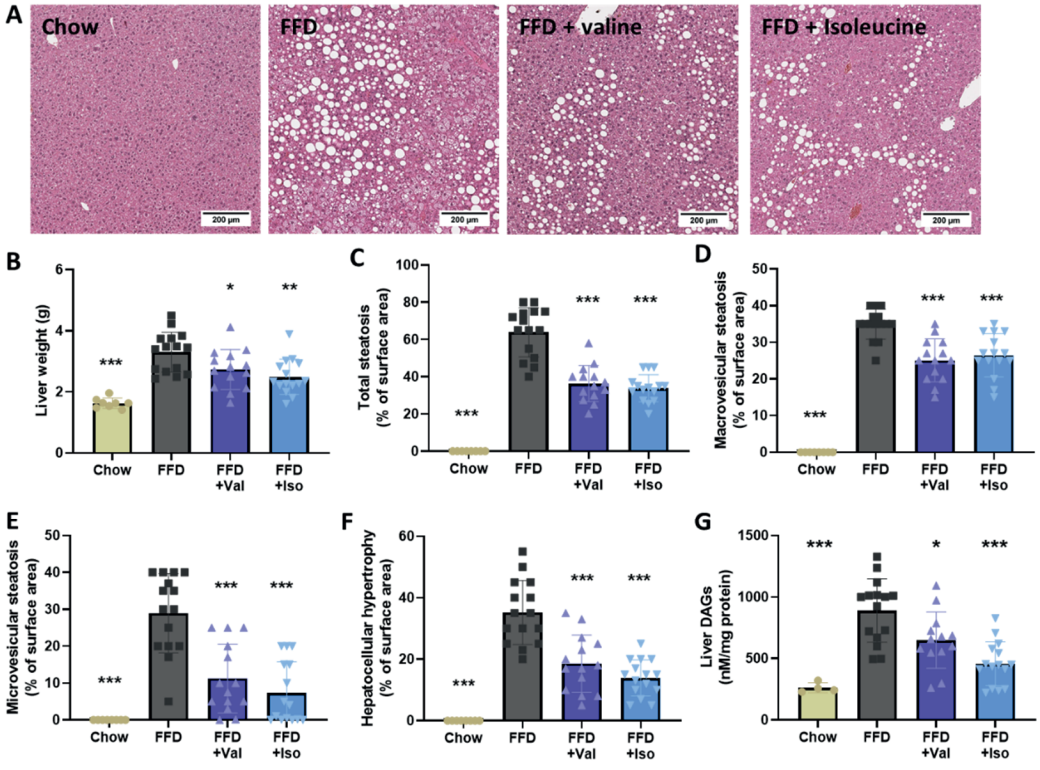

Figure 3: *(**A**) Representative images of hematoxylin and eosin (H&E) stained liver cross-sections, (**B**) liver weight, histological analysis of the HE stained liver cross-section for: (**C**) total steatosis, (**D**) macrovesicular steatosis, (**E**) microvesicular steatosis, (**F**) hepatocellular hypertrophy. (**G**) intrahepatic diacylglycerol (DAG) lipids expressed per mg protein. Data are presented as mean ± SD, * p < 0.05 or ** p < 0.01 or *** p < 0.001 compared to the FFD control group.*

Table 2. Upstream regulator analysis of key lipid metabolism regulators

	FFD vs Chow		Valine vs FFD		Isoleucine vs FFD	
	Z-score	**p-value**	**Z-score**	**p-value**	**Z-score**	**p-value**
Lipid synthesis						
SREBP	2.1	0.002	N/A	1.000	-1.4	0.001
SREBF1	2.7	0.000	N/A	1.000	-1.6	0.000
NR1H3	0.8	0.000	N/A	1.000	-0.6	0.001
AGT	9.6	0.000	-4.1	0.000	-6.4	0.000
IGF1	4.0	0.000	-1.6	0.001	-0.9	0.000
Lipid oxidation						
PPARGC1A	-2.7	0.000	2.1	0.004	3.9	0.000
CLUH	-1.6	0.012	1.6	0.000	1.0	0.048
AMPK	-2.0	0.000	N/A	1.000	1.9	0.005
SIRT1	-3.9	0.000	N/A	1.000	1.9	0.000
UCP1	-1.3	0.000	2.3	0.017	2.0	0.001
ACOX1	-6.2	0.000	4.0	0.000	6.1	0.000
EHHADH	-2.3	0.001	N/A	1.000	1.0	0.010

The activity of an upstream regulator was calculated based on gene expression changes of all downstream target genes. A negative Z-score indicates inhibition of the respective regulator or pathway (green color) and a positive Z-score indicates activation (red color). The p-value < 0.05 in grey indicates significant enrichment of the target genes downstream of a regulator, i.e. that more downstream genes are affected than can be expected by chance. N/A indicates an insufficient number of differentially expressed genes to predict the activation state of an upstream regulator.

3.4 Valine and isoleucine attenuate hepatic lipid peroxidation, a hallmark of oxidative stress

The pronounced effect of BCAA on microvesicular steatosis, a form of steatosis that is associated with mitochondrial dysfunction,[8] prompted us to examine oxidative stress in the liver as mitochondria are the main producers of reactive oxygen species. 4-hydroxynonenal (4-HNE) is a marker for lipid peroxidation induced by oxidative stress, and 4-HNE-positive immunoreactivity (IR) was analyzed in the liver by counting the number of 4-HNE positive structures (typical examples shown in Figure 4A). Notably, closer inspection revealed that 4HNE positive immunoreactivity was also present in enlarged hepatocytes (as exemplified in Supplemental Figure 4). This observation is consistent with the view that oxidative stress associated 4HNE formation is a pathophysiological hallmark already observable in hepatocytes prior to cell death and inflammation. 4-HNE-positive IR was practically absent in chow and FFD feeding strongly increased the 4-HNE-positive IR (Figure 4B). This FFD-induced increase was significantly suppressed with both valine and isoleucine. Interestingly, the number of 4-HNE positive structures also significantly correlated with microvesicular steatosis (Pearson correlation; R = 0.57, p = 0.0012) (Figure 4C).

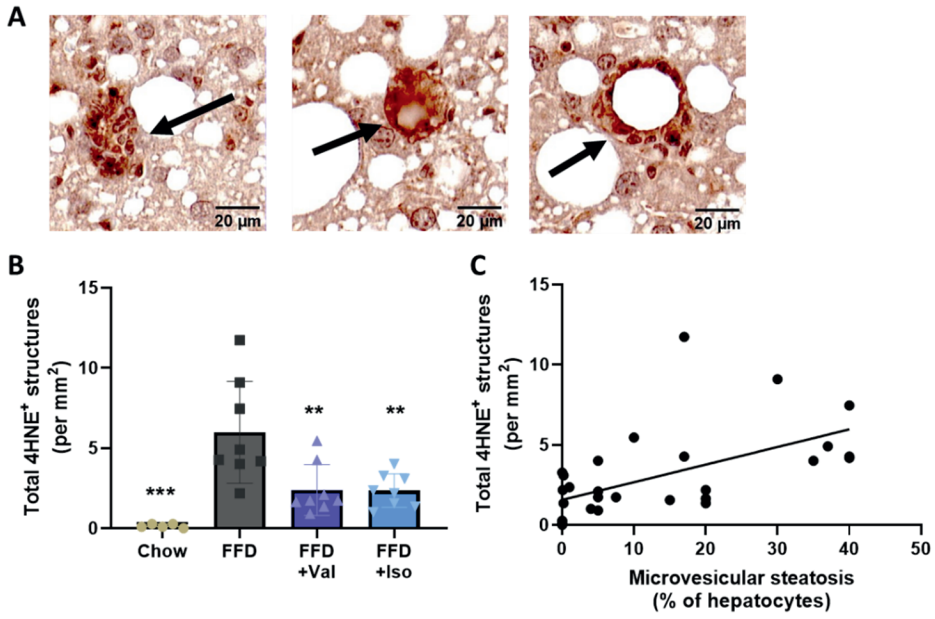

Figure 4: *The oxidative-stress induced lipid peroxidation marker 4-hydroxynonenal (4-HNE) was analyzed in liver cross sections using immunohistochemistry. (**A**) Representative photomicrographs of structures with 4-HNE-positive immunoreactivity. (**B**) Quantification of the 4-HNE-positive structures (**C**). Correlation of 4-HNE-positive structures with microvesicular steatosis. Data are presented as mean ± SD, * p < 0.05 or ** p < 0.01 or *** p < 0.001 compared to the FFD control group.*

5

Valine and isoleucine attenuate hepatic inflammation

Hepatic inflammation was histologically analyzed (Figure 5A-D) and complemented by gene expression analysis of inflammatory pathways using NGS datasets.

Liver inflammation expressed as the number of inflammatory aggregates per mm^2 was practically absent in the chow fed animals, whereas FFD-mice developed pronounced hepatic inflammation. Valine suppressed the number of inflammatory aggregates by 36% and isoleucine even by 51% (Figure 5B). The histological analysis of lobular inflammation was supported by immunohistochemical staining of F4/80, a macrophage marker, (Figure 5C) and GR-1, a neutrophil marker (Figure 5D). F4/80 and GR-1 immunoreactivity was strongly increased by FFD feeding and less pronounced in the groups treated with valine and isoleucine.

Consistent with this marked suppression of lobular inflammation, upstream regulator analysis indicated that FFD-feeding resulted in a pronounced activation of several proinflammatory cytokine pathways, including the signaling cascades downstream of IL-1β, CSF1 and TNF-α (Table 3). FFD also activated chemokine signaling implicated in NASH development among which the inflammatory pathways controlled by CCL2, CCR2 and CXCL12. Both valine and isoleucine deactivated specific proinflammatory signaling pathways, including IL-1β, TNF-α, CCR2 and CXCL12. The anti-inflammatory effects of isoleucine were often more pronounced and included suppression of IL17A signaling which was not affected by valine. Subsequent analysis of canonical pathways associated with inflammation revealed that FFD activated NF-κB signaling (Z=2.4; p<0.05), chemokine

signaling (Z=3.0; p<0.05), MIF regulation of innate immunity (Z=3.2; p<0.05), IL-8/KC signaling (Z=4.7, p<0.05) and fMLP signaling in neutrophils (Z=3.4 and p<0.05). The observed downregulation of CXCL12 with both BCAAs indicates an attenuation of neutrophil chemotaxis. Indeed, valine and isoleucine decreased IL-8/KC signaling (both with Z=-2.5 and p<0.05) and non-significantly lowered fMLP signaling in neutrophils. Consistent with the increase in liver inflammation with FFD on histological and transcriptomics level, FFD increased the intrahepatic protein concentrations of pro-inflammatory cytokines IL-1β, IL-6, IL-15, IL-17A/F, IL-33 and TNFα and chemokines KC/CXCL1, MIP-2/CXCL2 and IP10/CXL10 (Table 4). At the same time FFD also increased cytokines IL-4 and IL-10 with anti-inflammatory properties. Isoleucine but not valine significantly attenuated the expression of the pro-inflammatory chemokines MCP1/CCL2, KC/CXCL1 and MIP-2/CXCL2. In addition, valine and isoleucine further increased IL-4 concentrations indicating an hepatoprotective effect of both BCAA.

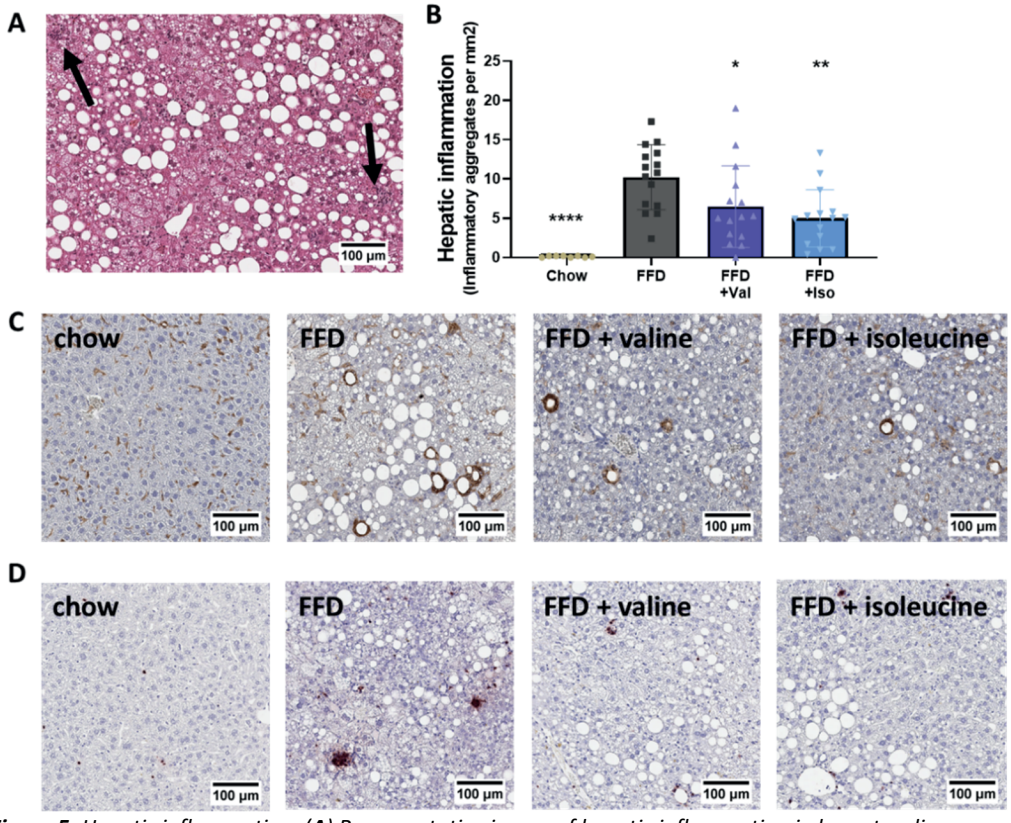

Figure 5: *Hepatic inflammation. (**A**) Representative image of hepatic inflammation in hematoxylin and eosin (H&E) stained liver cross-sections, quantified by counting (**B**) the number of inflammatory aggregates and expressed per mm^2. Representative photomicrographs of (**C**) F4/80 immunoreactivity and (**D**) GR-1 immunoreactivity in the different treatment groups. Data are mean ± SD, * p < 0.05 or ** p < 0.01 or *** p < 0.001 compared to the FFD control group.*

Table 3. Upstream regulator analysis of inflammatory regulators

	FFD vs Chow		Valine vs FFD		Isoleucine vs FFD	
	Z-score	p-value	Z-score	p-value	Z-score	p-value
Cytokines						
IL1	4.7	0.000	-1.3	0.005	-2.5	0.000
IL1A	5.3	0.000	-2.1	0.018	-2.3	0.000
IL1B	7.5	0.000	-1.8	0.000	-4.1	0.000
IL2	5.0	0.000	-1.4	0.000	-3.2	0.000
IL3	3.7	0.000	-1.8	0.004	-0.9	0.004
IL5	5.0	0.000	-2.2	0.004	-2.4	0.001
IL6	2.3	0.000	-1.5	0.000	-2.4	0.000
IL12B	2.6	0.002	N/A	1.000	-2.2	0.263
IL13	3.7	0.000	-2.4	0.000	-1.7	0.000
IL15	4.8	0.000	-2.0	0.072	-1.0	0.022
IL17A	3.8	0.000	N/A	1.000	-2.9	0.017
IL27	3.9	0.001	N/A	1.000	-2.3	0.149
IL33	6.4	0.000	-3.4	0.001	-2.0	0.022
IFNG	6.7	0.000	-2.7	0.000	-2.7	0.000
CSF1	4.7	0.000	-3.4	0.002	-3.2	0.000
CSF2	7.9	0.000	-2.9	0.000	-3.1	0.000
CSF3	1.9	0.000	-2.0	0.004	-0.4	0.000
MIF	3.1	0.003	N/A	1.000	-0.8	0.002
OSM	2.4	0.000	-1.4	0.005	-2.3	0.000
TNF	7.6	0.000	-3.2	0.000	-4.2	0.000
Chemokines						
CCL2	2.2	0.000	N/A	1.000	N/A	1.000
CCR2	5.8	0.000	-4.0	0.000	-4.2	0.000
CCL5	2.2	0.000	N/A	1.000	N/A	1.000
CCL6	2.2	0.019	N/A	1.000	N/A	0.013
CXCL3	3.1	0.001	N/A	1.000	N/A	1.000
CXCL8	1.7	0.000	N/A	1.000	-1.1	0.047
CXCL10	2.6	0.017	N/A	1.000	N/A	1.000
CXCL12	4.2	0.000	-2.5	0.210	-2.0	0.000

The activity of an upstream regulator was calculated based on gene expression changes of all downstream target genes. A negative Z-score indicates inhibition of the respective regulator or pathway (green color) and a positive Z-score indicates activation (red color). The p-value < 0.05 in grey indicates significant enrichment of the target genes downstream of a regulator, i.e. that more downstream genes are affected than can be expected by chance. N/A indicates an insufficient number of differentially expressed genes to predict the activation state of an upstream regulator.

Table 4. Intrahepatic cytokines and chemokines

	Chow	FFD	FFD +Val	FFD +Iso
IL-1β	4.2 ± 1.1*	16.9 ± 4.3	19.5 ± 11.1	13.9 ± 7.7
IL-4	0.02 ± 0.01*	0.07 ± 0.02	0.12 ± 0.03*	0.11 ± 0.04*
IL-6	3.5 ± 0.7*	6.5 ± 0.9	6.6 ± 1.1	6.6 ± 1.4
IL-10	0.4 ± 0.1*	1.0 ± 0.3	1.0 ± 0.2	1.2 ± 0.4
IL-15	5.2 ± 1.9*	15.0 ± 3.7	12.8 ± 2.5	15.2 ± 4.0
IL17A/F	0.2 ± 0.1*	0.4 ± 0.0	0.3 ± 0.0	0.4 ± 0.1
IL-33	6.7 ± 0.9*	20.7 ± 7.1	23.5 ± 10.4	22.9 ± 11.3
TNF-a	0.2 ± 0.1*	0.9 ± 0.2	1.3 ± 0.7	0.9 ± 0.4
IFNγ	0.0 ± 0.0	0.1 ± 0.0	0.1 ± 0.1	0.1 ± 0.0
MCP-1/CCL2	1.5 ± 0.6*	12.8 ± 2.9	13.5 ± 3.4	9.5 ± 4.2*
MIP-1a/CCL3	3.5 ± 3.7	13.0 ± 7.2	14.6 ± 15.0	11.5 ± 10.1
KC/CXCL1	1.6 ± 0.3*	6.1 ± 1.2	6.2 ± 2.0	4.3 ± 1.2*
MIP-2/CXCL2	0.6 ± 0.4*	5.5 ± 2.4	4.8 ± 2.6	3.0 ± 1.1*
IP-10/CXCL10	4.7 ± 1.2*	15.8 ± 4.2	18.3 ± 8.1	14.1 ± 5.4

*The concentrations of cytokines and chemokines are expressed in pg per mg protein, determined in liver homogenates after dietary intervention with valine (FFD + Val) or isoleucine (FFD + Iso) for 12 weeks. * asterisk indicates significance of difference compared to the FFD control group with p<0.05, data shown here as mean ± SD.*

4. Discussion

The objective of this study was to investigate potential hepatoprotective effects of valine and isoleucine individually, and to study whether these BCAAs can attenuate NASH development when administered therapeutically, i.e. starting treatment when features of the metabolic syndrome and NASH are already established. NGS was used to gain insight into the comprehensive effects of the BCAAs on canonical pathways critical for liver metabolism and the activation state of upstream regulators, which exceeds conventional mRNA expression analysis. Supplementation of FFD with valine or isoleucine reduced liver steatosis and associated oxidative stress as demonstrated by an attenuated formation of the lipid peroxidation marker 4-HNE. Both BCAAs restored the detrimental effects of FFD feeding on hepatic metabolic homeostasis: they corrected the expression of BCAA metabolism genes and counter-regulated FFD effects on key regulators involved in energy homeostasis and lipid metabolism (e.g. AMPK, SREBPF1). These beneficial metabolic effects were accompanied by a pronounced reduction of immune cell-mediated liver inflammation. These cellular effects were further substantiated by a suppression of critical inflammatory pathways (e.g. IL1β and TNFα signaling) known to be upregulated in NASH patients.[18]

The observed hepatoprotective effects of valine and isoleucine were independent of changes in body weight or body composition and gut permeability, consistent with

previous reports demonstrating no effect of BCAA on body weight development in obesity.[14,34] Cardiovascular risk factors such as plasma total cholesterol and triglycerides were non-significantly lowered with valine and isoleucine, in line with a slightly lower TG in VLDL and cholesterol in VLDL/LDL in the lipoprotein profiles. These results suggest that the observed reduction of liver steatosis is not due to an enhanced hepatic lipid output, i.e. enhanced assembly and secretion of VLDL particles from the liver into the circulation, as the lipid output was in fact lowered by the BCAAs. These observations are in line with an *in vitro* study which demonstrated that BCAAs had minor effects on apoB (primary protein on VLDL and LDL lipoprotein particles) secretion by hepatocytes.[35] In addition, we showed that fecal fatty acid output was comparable between groups indicating that the decrease in liver steatosis can also not be explained by an enhanced fatty acid excretion via the feces, implying an effect on hepatic lipid handling and utilization.

Interestingly, the microvesicular form of steatosis was most strongly decreased with valine and isoleucine. The development of microvesicular steatosis is related to mitochondrial dysfunction and impaired FA oxidation, which in turn promotes the accumulation of hepatic FA in small lipid droplets.[11] The observed decrease in microvesicular steatosis therefore suggests an improvement of lipid handling related to mitochondrial function.[36,37] Interestingly, we found that valine and isoleucine promoted mitochondrial biogenesis as both PPARGC1α[38] and CLUH,[39] which were suppressed by FFD were reactivated with the BCAAs. In line with these data, also hepatic lipid metabolism appears to be stimulated with valine as well as isoleucine, because key metabolic regulators involved in lipid oxidation (ACOX1, EHHADH) and energy homeostasis (AMPK) were activated and key regulators involved in fatty acid synthesis (SREBF1) and anabolic processes (IGF1, AGT) were conversely inactivated. The NGS upstream regulator effects on AMPK were more pronounced than the Western blot analyses, i.e. a trend decrease in AMPK-phospho-Threonine 172 and no effect with the BCAAs. However, in contrast to the Western blot analysis, an upstream regulator analysis uses gene expression data of *all known* downstream target genes of AMPK to predict its state of activation or deactivation. The NGS analysis thus indirectly involves all possible protein modifications, including potential AMPK deactivations regulated by diacylglycerols[40,41] and inflammation [12], and is per definition also not limited to a particular type of protein modification (e.g. phosphorylation, acetylation, allosteric inhibition/activation). The lipids in the smaller lipid droplets, which manifest as microvesicular steatosis, are thought to be easier metabolizable than large droplets.[42] When lipids are used to meet energy demands of the liver smaller lipid droplets are thought to be metabolized first, which decreases the likelihood that larger intracellular lipid droplets (macrovesicular steatosis) are being formed.[42] Macrovesicular steatosis impairs hepatocellular function and activates stellate cells,[43] which is supported by the correlation between macrovesicular steatosis and fibrosis in rodent models of disease.[44]

Moreover, oxidative stress has been linked to the manifestation of microvesicular steatosis[8] and increased lipid peroxidation from ROS species with the formation of 4-HNE adducts in liver.[21,29] Mitochondria are among the main producers of ROS, which increase

when mitochondria become dysfunctional, as has been reported in NASH patients.[45] The observed decrease in 4-HNE immunoreactivity in the valine and isoleucine treated groups indicates less oxidative stress and less hepatic lipid peroxidation, which could be a consequence of better functioning mitochondria and/or greater numbers of mitochondria because valine and isoleucine activated PPARGC1α and CLUH which control critical steps in mitochondrial biogenesis.[38,39] This study also confirmed the presumed positive association between oxidative stress and microvesicular steatosis showing a significant correlation between 4-HNE immunoreactivity and microvesicular steatosis. Our results are also in line with a recent study which demonstrated that a mixture of BCAA prevented fat accumulation and mitochondrial dysfunction in hepatocytes of alcohol-consuming rodents.[46] These protective effects on mitochondria appear to be specific for BCAAs as shown in a rodent study comparing a mixture of BCAAs to a mixture of amino acids from casein.[46]

Besides improving mitochondrial functioning, valine and isoleucine may alleviate the accumulation of lipids in the liver via their effect on insulin. Fasting insulin was strongly increased by FFD feeding and this induction was significantly lowered with both BCAAs. Moreover, insulin promotes SREBP1-mediated *de novo* lipogenesis[4,5] in liver and upstream regulator analysis indeed demonstrated that FFD feeding strongly enhanced SREBP1 activity. By contrast, valine and isoleucine lowered circulating plasma insulin and deactivated SREBP1. This effect on insulin and SREBP1 may contribute to reduction of steatosis. Besides these direct effects in liver, insulin also has extrahepatic effects on lipases and in the adipose tissue.[7] Improved insulin action can lower fat fluxes from the adipose tissue to the liver which also reduces metabolic overload and fat accumulation in liver, including intrahepatic DAGs which can build-up when fatty acid fluxes become too high or fatty acid catabolism is impaired. In the present study, FFD treatment indeed resulted in a significant increase of liver DAGs and this FFD effect was counter-regulated by valine and isoleucine.

DAGs are causal to insulin resistance, because DAGs impair insulin signaling at the level of its receptor via recruitment of novel PKCs (in liver and other organs including skeletal muscle and WAT).[47] Importantly, also in humans it has been shown that DAGs correlate with insulin sensitivity measured by clamp technique.[47] Hence, it is amenable that intercepting with BCAA adjusts the overall metabolism and thereby reduces the build-up of DAGs and associated insulin resistance, a key driver of NAFLD development.

AMPK is one of the major regulators of energy homeostasis and activated AMPK inhibits fatty acid synthesis (by phosphorylating and inhibiting SREBP1)[48] at the same time stimulating β-oxidation (e.g. directly via PCG1a and indirectly via ACOX1).[49] Furthermore, AMPK is a ROS and nutrient sensor and also controlled by diacylglycerols and inflammatory signaling pathways (TNF-α /TBK1), which were increased and activated by FFD in the present study and suppressed by valine and isoleucine on pathway level. In essence, the observed attenuation of inflammation with valine and isoleucine and the improvement of lipid metabolism should not be interpreted as separate observations. Because metabolism and inflammation are evolutionarily interconnected via enzymes such as AMPK and transcriptional regulators such as peroxisome proliferator activated receptors (PPARs),[12,50] it is likely that an improvement of metabolic processes by BCAAs attenuated the induction of inflammatory pathways and, vice versa. Quenching of

inflammatory cytokine or chemokine signaling cascades with valine or isoleucine allowed metabolism to function closer to optimal homeostasis. It is difficult to disentangle metabolic processes and low-grade chronic inflammation during the development of NAFLD/NASH. Mitochondria with their primary function in metabolism, could however be implicated in the initiation of chronic inflammation, in particular once they disintegrate together with the cells in which they reside. Mitochondrial proteins contain n-formyl-met-leu-pheu (fMLP) peptides which exert chemotactic function for neutrophils once released from necrotic cells.[51] It has been demonstrated that human mitochondrial formyl-peptides promoted chemotaxis of immune cells and oxidative burst of neutrophils *in vitro.*[52] Interestingly, FFD feeding activated the canonical pathways relevant for neutrophil recruitment (e.g. IL-8/KC and fMLP signaling) and valine and isoleucine attenuated these canonical pathways, consistent with a decrease in hepatic immunoreactivity of GR-1 with valine and isoleucine, and indicative of decreased neutrophil infiltration. This observation is noteworthy because neutrophils are components of the inflammatory aggregates that were reduced with valine and isoleucine, and they constitute a hallmark of human NASH and drivers of the pathogenesis.[53,54] In line with histology and the NGS-based predictions, KC/CXCL1 protein levels were strongly increased by FFD and reduced with isoleucine. At this point we would like to emphasize that the NGS-based prediction of an entire proinflammatory cytokine/chemokine signaling cascade may deviate from the protein expression level of the respective cytokine/chemokine. The reason is that the NGS-approach predicts the signaling cascade on basis of dozens of downstream target genes of a cytokine/chemokine whereas the protein concentration of this cytokine/chemokine *per se* does not inform on the activity of its downstream signaling cascade.

Published rodent studies investigating the effect of BCAA restriction and BCAA supplementation may seem contradictory because one might expect opposite effects. In general, both strategies can improve metabolic processes depending on the type and stage of dysmetabolism at start of the treatment and how metabolic disturbances are induced. Published studies vary strongly regarding diets and their composition, the study design (prevention of diseases versus intervention in already deranged metabolism), the condition under which tissues were collected (feeding vs fasting state), and the readouts.[23,55,64–73,56,74–76,57–63] BCAA restriction is not necessarily the opposite of supplementing a high caloric diet with BCAAs because BCAA restriction can affect body weight[73–76] which was not observed in the present study. In BCAA restriction experiments, White et al.,[75] Fontana et al.[76] and Yu et al.[74] reported improvements in metabolic health readouts including improvements in hepatic insulin sensitivity and energy expenditure. However BCAA restricted animals in these studies were significantly lower in weight compared to their respective controls and health effects may thus be a consequence of weight loss.

In the present study we examined the effect of valine and isoleucine in FFD-pretreated mice that were in a particular dysmetabolic state at the start of the intervention, i.e. obese mice with associated dyslipidemia and hyperinsulinemia[77] exhibiting elevated diacylglycerol concentrations at tissue level which we and others[78–80] consider to be critical for the development of insulin resistance. Herein, BCAA affected the accumulation

of DAGs at tissue level and improve insulin resistance assessed by HOMA. In Ldlr-/-.Leiden mice, DAGs accumulate specifically in response to FFD feeding but not in mice fed chow diet despite comparable calorie intake. The accumulation is thus very likely a consequence of both higher fatty acid fluxes from chronically inflamed WAT depots and a higher intake of calories from fat because the total caloric intake was comparable among the groups. It is possible that under experimental studies in which DAGs do not accumulate (e.g. chow feeding in general), effects on insulin resistance cannot be found which may explain at least some of the discordant observations. For instance, a study by White et al demonstrated that BCAA supplementation in healthy chow fed rats did not induce insulin resistance[81], possibly because DAGs are not increased (neither by chow nor by the BCAA themselves). Rising circulating BCAA concentrations via the drinking water in high fat/high sucrose or high fat diet treated mice did not modulate insulin resistance in obese mice.[60] This observation differs from our finding which could be related to the differences regarding the administration route (via drinking water versus dietary ad mix), differences in doses and treatment time, and alternative DAG-independent mechanisms. For example, BCAAs can activate mTOR/p70S6 kinase and potentially affect insulin receptor phosphorylation.[82] In general it can be said that lipid-induced insulin resistance is predominantly mediated by DAGs, in addition to this lipid-mediated mechanism also chronic tissue inflammation (e.g. cytokines and chemokines) can impair insulin signaling.[78–80] In many published high fat diet-induced obesity studies, information about DAG concentrations on the tissue level is not available, and it is therefore difficult to provide an overall explanation for discrepancies between studies.

A limitation of the current study is that we did not sacrifice a group of mice at 26 weeks, i.e. the time point at which interventions were started, to assess the level of NASH and liver fibrosis prior to treatment which would have allowed us to assess a putative regression of histological features. Therefore, we cannot differentiate whether valine and isoleucine merely inhibited further NASH progression from 26 weeks onwards or whether they were even able to regress the disease. Based on extensive time course studies in the same mouse strain (same age, same sex, same diets) the expected level of total steatosis at 26 weeks is 50-60% as reported.[16] This then would point to a regression of the disease with valine and isoleucine within 12 weeks of treatment because both treatment arms displayed only about 34% total steatosis. The sacrifice conditions (5h fasting in the present experiment) were probably not optimal to determine circulating BCAA because dietary BCAA seemed to be rapidly metabolized and only a few mice exhibited elevated levels in the fasting state. Similarly, fasting conditions may have compromised the assessment of protein modifications with short half-life such as the phosphorylation status of BCKDH. More comprehensive analyses that rely on counts of mRNA transcripts with longer half-life and that involve dozens of genes of a pathway or signaling cascade may therefore be more accurate under our sacrifice circumstances. Leucine was not included in this study because leucine reportedly reduces food intake,[83] therefore it would not have been possible to dissociate specific metabolic effects of leucine from its effects on food intake given the diet-induced nature of the model used herein. Another limitation of the study is the absence of metabolic flux measurements, which were beyond the initial scope.

In conclusion, intervention with dietary valine or isoleucine attenuated already established obesity and insulin resistance-associated NASH. The BCAAs do not affect a specific disease pathway but affect multiple metabolic and inflammatory processes simultaneously as summarized in figure 6. The marked decrease in microvesicular steatosis may at least partly be explained by improved lipid processing and oxidation in the liver and concomitant suppression of *de novo* lipid synthesis as determined indirectly by NGS on pathway level. An improved catabolism of hepatic lipids is further supported by a slight reduction in apoB and lipoproteins (reflecting lower hepatic lipid output) as well as the absence of fatty acid excretion via the feces. Improvement of hepatic lipid metabolism is also supported by the pronounced reduction in plasma insulin, hepatic diacylglycerols, lipid peroxidation and lobular inflammation, the latter being substantiated by a profound suppression of critical inflammatory proteins and pathways. Altogether this study demonstrates that valine and isoleucine constitute nutritional treatments that can help restore metabolic and inflammatory homeostasis in steatotic livers and that such dietary strategies could be combined with pharmaceutical interventions directed at fibrosis.

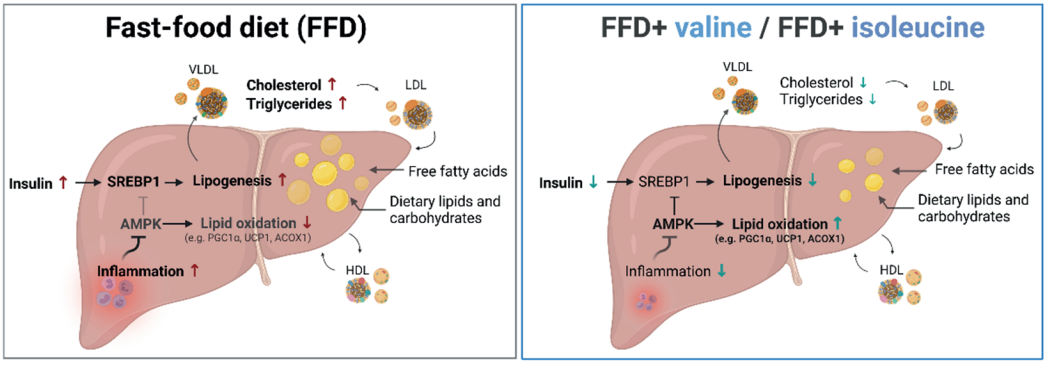

***Figure 6**: Overview of the different mechanisms which promote NASH development during FFD feeding and were corrected with valine or isoleucine supplementation, including multiple lipid metabolism processes resulting in reduced NASH-associated steatosis and inflammation.*

Acknowledgments: We would like to thank Jessica Snabel and Marijke Voskuilen for their excellent technical assistance, and Christa G. F. de Ruiter and Joline Attema for their support with coordination and conduct of the animal studies.

References

1. Perumpail BJ, Khan MA, Yoo ER, Cholankeril G, Kim D, Ahmed A. Clinical epidemiology and disease burden of nonalcoholic fatty liver disease. *World J Gastroenterol*. Published online 2017. doi:10.3748/wjg.v23.i47.8263
2. Diehl AM, Day C. Cause, Pathogenesis, and Treatment of Nonalcoholic Steatohepatitis. *N Engl J Med*. Published online 2017. doi:10.1056/nejmra1503519
3. Zhou YY, Zhou XD, Wu SJ, Fan DH, Van Poucke S, Chen YP, Fu SW, Zheng MH. Nonalcoholic fatty liver disease contributes to subclinical atherosclerosis: A systematic review and meta-analysis. *Hepatol Commun*. 2018;2(4):376. doi:10.1002/HEP4.1155
4. Smith, G. I., Shankaran, M., Yoshino, M., Schweitzer, G. G., Chondronikola, M., Beals, J. W., Okunade, A. L., Patterson, B. W., Nyangau, E., Field, T., Sirlin, C. B., Talukdar, S., Hellerstein, M. K., & Klein S. Insulin resistance drives hepatic de novo lipogenesis in nonalcoholic fatty liver disease. *J Clin Invest*. Published online 2020. doi:10.1172/JCI134165
5. Yecies JL, Zhang HH, Menon S, Liu S, Yecies D, Lipovsky AI, Gorgun C, Kwiatkowski DJ, Hotamisligil GS, Lee CH, Manning BD. Akt stimulates hepatic SREBP1c and lipogenesis through parallel mTORC1-dependent and independent pathways. *Cell Metab*. 2011;14(1):21-32. doi:10.1016/j.cmet.2011.06.002
6. Cusi K. Role of obesity and lipotoxicity in the development of nonalcoholic steatohepatitis: Pathophysiology and clinical implications. *Gastroenterology*. Published online 2012. doi:10.1053/j.gastro.2012.02.003
7. Petersen MC, Shulman GI. Mechanisms of Insulin Action and Insulin Resistance. *Physiol Rev*. 2018;98(4):2133. doi:10.1152/PHYSREV.00063.2017
8. Natarajan SK, Eapen CE, Pullimood AB, Balasubramanian KA. Oxidative stress in experimental liver microvesicular steatosis: Role of mitochondria and peroxisomes. *J Gastroenterol Hepatol*. 2006;21(8):1240-1249. doi:10.1111/j.1440-1746.2006.04313.x
9. Loomba R, Friedman SL, Shulman GI. Mechanisms and disease consequences of nonalcoholic fatty liver disease. *Cell*. 2021;184(10):2537-2564. doi:10.1016/j.cell.2021.04.015
10. Niederreiter L, Tilg H. Cytokines and fatty liver diseases. *Liver Res*. 2018;2(1):14-20. doi:10.1016/J.LIVRES.2018.03.003
11. Fromenty B, Pessayre D. Impaired mitochondrial function in microvesicular steatosis effects of drugs, ethanol, hormones and cytokines. *J Hepatol*. 1997;26:43-53. doi:10.1016/S0168-8278(97)80496-5
12. Zhao P, Sun X, Chaggan C, Liao Z, Wong K in, He F, Singh S, Loomba R, Karin M, Witztum JL, Saltiel AR. An AMPK–caspase-6 axis controls liver damage in nonalcoholic steatohepatitis. *Science*. 2020;367(6478):652. doi:10.1126/SCIENCE.AAY0542
13. Garcia D, Shaw RJ. AMPK: Mechanisms of Cellular Energy Sensing and Restoration of Metabolic Balance. *Mol Cell*. 2017;66(6):789-800. doi:10.1016/J.MOLCEL.2017.05.032
14. Honda T, Ishigami M, Luo F, Lingyun M, Ishizu Y, Kuzuya T, Hayashi K, Nakano I, Ishikawa T, Feng GG, Katano Y, Kohama T, Kitaura Y, Shimomura Y, Goto H,

Hirooka Y. Branched-chain amino acids alleviate hepatic steatosis and liver injury in choline-deficient high-fat diet induced NASH mice. *Metabolism*. Published online 2017. doi:10.1016/j.metabol.2016.12.013

15. Kulinski A, Vance DE, Vance JE. A choline-deficient diet in mice inhibits neither the CDP-choline pathway for phosphatidylcholine synthesis in hepatocytes nor apolipoprotein B secretion. *J Biol Chem*. 2004;279(23):23916-23924. doi:10.1074/jbc.M312676200
16. van den Hoek AM, Verschuren L, Worms N, van Nieuwkoop A, de Ruiter C, Attema J, Menke AL, Caspers MPM, Radhakrishnan S, Salic K, Kleemann R. A Translational Mouse Model for NASH with Advanced Fibrosis and Atherosclerosis Expressing Key Pathways of Human Pathology. *Cells*. Published online 2020. doi:10.3390/cells9092014
17. van Koppen A, Verschuren L, van den Hoek AM, Verheij J, Morrison MC, Li K, Nagabukuro H, Costessi A, Caspers MPM, van den Broek TJ, Sagartz J, Kluft C, Beysen C, Emson C, van Gool AJ, Goldschmeding R, Stoop R, Bobeldijk-Pastorova I, Turner SM, Hanauer G, Hanemaaijer R. Uncovering a Predictive Molecular Signature for the Onset of NASH-Related Fibrosis in a Translational NASH Mouse Model. *Cmgh*. 2018;5(1):83-98.e10. doi:10.1016/j.jcmgh.2017.10.001
18. Morrison MC, Kleemann R, van Koppen A, Hanemaaijer R, Verschuren L. Key inflammatory processes in human NASH are reflected in Ldlr-/-.Leiden mice: A translational gene profiling study. *Front Physiol*. 2018;9(FEB). doi:10.3389/fphys.2018.00132
19. Morrison MC, Verschuren L, Salic K, Verheij J, Menke A, Wielinga PY, Iruarrizaga-Lejarreta M, Gole L, Yu W, Turner S, Caspers MPM, Martínez-Arranz I, Pieterman E, Stoop R, van Koppen A, van den Hoek AM, Mato JM, Hanemaaijer R, Alonso C, Kleemann R. Obeticholic Acid Modulates Serum Metabolites and Gene Signatures Characteristic of Human NASH and Attenuates Inflammation and Fibrosis Progression in Ldlr-/-.Leiden Mice. *Hepatol Commun*. 2018;2(12):1513-1532. doi:10.1002/hep4.1270
20. Liang W, Menke AL, Driessen A, Koek GH, Lindeman JH, Stoop R, Havekes LM, Kleemann. R, Van Den Hoek AM. Establishment of a general NAFLD scoring system for rodent models and comparison to human liver pathology. *PLoS One*. 2014;9(12). doi:10.1371/journal.pone.0115922
21. van den Hoek AM, Verschuren L, Worms N, van Nieuwkoop A, de Ruiter C, Attema J, Menke AL, Caspers MPM, Radhakrishnan S, Salic K, Kleemann R. A Translational Mouse Model for NASH with Advanced Fibrosis and Atherosclerosis Expressing Key Pathways of Human Pathology. *Cells*. 2020;9(9):2014. doi:10.3390/cells9092014
22. Liang W, Lindeman JH, Menke AL, Koonen DP, Morrison M, Havekes LM, Van Den Hoek AM, Kleemann R. Metabolically induced liver inflammation leads to NASH and differs from LPS-or IL-1β-induced chronic inflammation. *Lab Investig*. 2014;94(5):491-502. doi:10.1038/labinvest.2014.11
23. Takegoshi K, Honda M, Okada H, Takabatake R, Matsuzawa-Nagata N, Campbell JS, Nishikawa M, Shimakami T, Shirasaki T, Sakai Y, Yamashita T, Takamura T, Tanaka T, Kaneko S. Branched-chain amino acids prevent hepatic fibrosis and development of hepatocellular carcinoma in a non-alcoholic steatohepatitis mouse model. *Oncotarget*. 2017;8(11):18191-18205.

doi:10.18632/oncotarget.15304
24. *Nutrient Requirements of Laboratory Animals*.; 1995. doi:10.17226/4758
25. Gart E, Salic K, Morrison MC, Caspers M, Van Duyvenvoorde W, Heijnk M, Giera M, Bobeldijk-Pastorova I, Keijer J, Storsve AB, Hals P-A, Kleemann R, Sinclair AJ. Krill Oil Treatment Increases Distinct PUFAs and Oxylipins in Adipose Tissue and Liver and Attenuates Obesity-Associated Inflammation via Direct and Indirect Mechanisms. *Nutrients*. 2021;13:2836. doi:10.3390/nu13082836
26. Westerterp M, Van Der Hoogt CC, De Haan W, Offerman EH, Dallinga-Thie GM, Jukema JW, Havekes LM, Rensen PCN. Cholesteryl ester transfer protein decreases high-density lipoprotein and severely aggravates atherosclerosis in APOE*3-Leiden mice. *Arterioscler Thromb Vasc Biol*. 2006;26(11):2552-2559. doi:10.1161/01.ATV.0000243925.65265.3c
27. Bijland S, Rensen PCN, Pieterman EJ, Maas ACE, van der Hoorn JW, van Erk MJ, Havekes LM, van Dijk KW, Chang SC, Ehresman DJ, Butenhoff JL, Princen HMG. Perfluoroalkyl sulfonates cause alkyl chain length-dependent hepatic steatosis and hypolipidemia mainly by impairing lipoprotein production in APOE*3-leiden CETP mice. *Toxicol Sci*. 2011;123(1):290-303. doi:10.1093/toxsci/kfr142
28. Princen HMG, Van Duyvenvoorde W, Buytenhek R, Van Der Laarse A, Van Poppel G, Gevers Leuven JA, Van Hinsbergh VWM. Supplementation With Low Doses of Vitamin E Protects LDL From Lipid Peroxidation in Men and Women. *Arterioscler Thromb Vasc Biol*. 1995;15(3):325-333. doi:10.1161/01.ATV.15.3.325
29. Salic K, Gart E, Seidel F, Verschuren L, Caspers M, van Duyvenvoorde W, Wong KE, Keijer J, Bobeldijk-Pastorova I, Wielinga PY, Kleemann R. Combined Treatment with L-Carnitine and Nicotinamide Riboside Improves Hepatic Metabolism and Attenuates Obesity and Liver Steatosis. *Int J Mol Sci*. 2019;20(18). doi:10.3390/IJMS20184359
30. Mueller AM, Kleemann R, Gart E, van Duyvenvoorde W, Verschuren L, Caspers M, Menke A, Krömmelbein N, Salic K, Burmeister Y, Seilheimer B, Morrison MC. Cholesterol Accumulation as a Driver of Hepatic Inflammation Under Translational Dietary Conditions Can Be Attenuated by a Multicomponent Medicine. *Front Endocrinol (Lausanne)*. 2021;12. doi:10.3389/fendo.2021.601160
31. Love MI, Huber W, Anders S. Moderated estimation of fold change and dispersion for RNA-seq data with DESeq2. *Genome Biol*. 2014;15(12):1-21. doi:10.1186/s13059-014-0550-8
32. Krämer A, Green J, Pollard J, Tugendreich S. Causal analysis approaches in Ingenuity Pathway Analysis. *Bioinformatics*. 2014;30(4):523-530. doi:10.1093/BIOINFORMATICS/BTT703
33. Gart E, Duyvenvoorde W van, Toet K, Caspers MPM, Verschuren L, Nielsen MJ, Leeming DJ, Lima ES, Menke A, Hanemaaijer R, Keijer J, Salic K, Kleemann R, Morrison MC. Butyrate Protects against Diet-Induced NASH and Liver Fibrosis and Suppresses Specific Non-Canonical TGF-β Signaling Pathways in Human Hepatic Stellate Cells. *Biomedicines*. 2021;9(12):1954. doi:10.3390/BIOMEDICINES9121954
34. White PJ, Newgard CB. Branched-chain amino acids in disease. *Science (80-)*. 2019;363(6427):582-583. doi:10.1126/science.aav0558
35. Cianflone K, Zhang ZJ, Vu H, Kohen-Avramoglu R, Kalant D, Sniderman AD. The effect of individual amino acids on ApoB100 and Lp(a) secretion by HepG2 cells. *J*

Biol Chem. 1996;271(46):29136-29145. doi:10.1074/jbc.271.46.29136

36. García-Berumen CI, Ortiz-Avila O, Vargas-Vargas MA, Del Rosario-Tamayo BA, Guajardo-López C, Saavedra-Molina A, Rodríguez-Orozco AR, Cortés-Rojo C. The severity of rat liver injury by fructose and high fat depends on the degree of respiratory dysfunction and oxidative stress induced in mitochondria. *Lipids Health Dis*. 2019;18(1). doi:10.1186/S12944-019-1024-5
37. van den Hoek AM, de Jong JCBC, Worms N, van Nieuwkoop A, Voskuilen M, Menke AL, Lek S, Caspers MPM, Verschuren L, Kleemann R. Diet and exercise reduce pre-existing NASH and fibrosis and have additional beneficial effects on the vasculature, adipose tissue and skeletal muscle via organ-crosstalk. *Metabolism*. 2021;124:154873. doi:10.1016/J.METABOL.2021.154873
38. Fernandez-Marcos PJ, Auwerx J. Regulation of PGC-1α, a nodal regulator of mitochondrial biogenesis. *Am J Clin Nutr*. 2011;93(4):884S. doi:10.3945/AJCN.110.001917
39. Gao J, Schatton D, Martinelli P, Hansen H, Pla-Martin D, Barth E, Becker C, Altmueller J, Frommolt P, Sardiello M, Rugarli EI. CLUH regulates mitochondrial biogenesis by binding mRNAs of nuclear-encoded mitochondrial proteins. *J Cell Biol*. 2014;207(2):213. doi:10.1083/JCB.201403129
40. Jeon SM. Regulation and function of AMPK in physiology and diseases. *Exp Mol Med 2016 487*. 2016;48(7):e245-e245. doi:10.1038/emm.2016.81
41. Jiang LQ, de Castro Barbosa T, Massart J, Deshmukh AS, Löfgren L, Duque-Guimaraes DE, Ozilgen A, Osler ME, Chibalin A V., Zierath JR. Diacylglycerol kinase-δ regulates AMPK signaling, lipid metabolism, and skeletal muscle energetics. *Am J Physiol - Endocrinol Metab*. 2016;310(1):E51. doi:10.1152/AJPENDO.00209.2015
42. Sahini N, Borlak J. Recent insights into the molecular pathophysiology of lipid droplet formation in hepatocytes. *Prog Lipid Res*. 2014;54(1):86-112. doi:10.1016/J.PLIPRES.2014.02.002
43. Scorletti E, Carr RM. A new perspective on NAFLD: focusing on lipid droplets. *J Hepatol*. Published online November 15, 2021. doi:10.1016/J.JHEP.2021.11.009
44. Mulder P, Liang W, Wielinga P, Verschuren L, Toet K, Havekes L, van den Hoek A, Kleemann R. Macrovesicular steatosis is associated with development of lobular inflammation and fibrosis in diet-induced non-alcoholic steatohepatitis (NASH). *Inflamm Cell Signal*. Published online 2015. doi:10.14800/ics.804
45. Koliaki C, Szendroedi J, Kaul K, Jelenik T, Nowotny P, Jankowiak F, Herder C, Carstensen M, Krausch M, Knoefel WT, Schlensak M, Roden M. Adaptation of Hepatic Mitochondrial Function in Humans with Non-Alcoholic Fatty Liver Is Lost in Steatohepatitis. *Cell Metab*. 2015;21(5):739-746. doi:10.1016/j.cmet.2015.04.004
46. Tedesco L, Corsetti G, Ruocco C, Ragni M, Rossi F, Carruba MO, Valerio A, Nisoli E. A specific amino acid formula prevents alcoholic liver disease in rodents. *Am J Physiol Gastrointest Liver Physiol*. 2018;314(5):G566-G582. doi:10.1152/AJPGI.00231.2017
47. Lyu K, Zhang Y, Zhang D, Kahn M, ter Horst KW, Rodrigues MRS, Gaspar RC, Hirabara SM, Luukkonen PK, Lee S, Bhanot S, Rinehart J, Blume N, Rasch MG, Serlie MJ, Bogan JS, Cline GW, Samuel VT, Shulman GI. A Membrane-Bound Diacylglycerol Species Induces PKCε-Mediated Hepatic Insulin Resistance. *Cell Metab*. 2020;32(4):654-664.e5. doi:10.1016/J.CMET.2020.08.001

48. Li Y, Xu S, Mihaylova MM, Zheng B, Hou X, Jiang B, Park O, Luo Z, Lefai E, Shyy JYJ, Gao B, Wierzbicki M, Verbeuren TJ, Shaw RJ, Cohen RA, Zang M. AMPK Phosphorylates and Inhibits SREBP Activity to Attenuate Hepatic Steatosis and Atherosclerosis in Diet-induced Insulin Resistant Mice. *Cell Metab*. 2011;13(4):376. doi:10.1016/J.CMET.2011.03.009
49. Tahri-Joutey M, Andreoletti P, Surapureddi S, Nasser B, Cherkaoui-Malki M, Latruffe N. Mechanisms Mediating the Regulation of Peroxisomal Fatty Acid Beta-Oxidation by PPARα. *Int J Mol Sci*. 2021;22(16). doi:10.3390/IJMS22168969
50. Hotamisligil GS. Inflammation and metabolic disorders. *Nature*. 2006;444(7121):860-867. doi:10.1038/nature05485
51. McDonald B, Pittman K, Menezes GB, Hirota SA, Slaba I, Waterhouse CCM, Beck PL, Muruve DA, Kubes P. Intravascular danger signals guide neutrophils to sites of sterile inflammation. *Science (80-)*. 2010;330(6002):362-366. doi:10.1126/SCIENCE.1195491/SUPPL_FILE/MCDONALD.SOM.PDF
52. Meyer A, Laverny G, Bernardi L, Charles AL, Alsaleh G, Pottecher J, Sibilia J, Geny B. Mitochondria: An organelle of bacterial origin controlling inflammation. *Front Immunol*. 2018;9(APR):536. doi:10.3389/FIMMU.2018.00536/BIBTEX
53. Liang W, Lindeman JH, Menke AL, Koonen DP, Morrison M, Havekes LM, van den Hoek AM, Kleemann R. Metabolically induced liver inflammation leads to NASH and differs from LPS- or IL-1β-induced chronic inflammation. *Lab Invest*. 2014;00(November 2013):1-12. doi:10.1038/labinvest.2014.11
54. Hwang S, Yun H, Moon S, Cho YE, Gao B. Role of Neutrophils in the Pathogenesis of Nonalcoholic Steatohepatitis. *Front Endocrinol (Lausanne)*. 2021;12. doi:10.3389/FENDO.2021.751802
55. Jang C, Oh SF, Wada S, Rowe GC, Liu L, Chan MC, Rhee J, Hoshino A, Kim B, Ibrahim A, Baca LG, Kim E, Ghosh CC, Parikh SM, Jiang A, Chu Q, Forman DE, Lecker SH, Krishnaiah S, Rabinowitz JD, Weljie AM, Baur JA, Kasper DL, Arany Z. A branched-chain amino acid metabolite drives vascular fatty acid transport and causes insulin resistance. *Nat Med*. 2016;22(4):421-426. doi:10.1038/NM.4057
56. Nishimura J, Masaki T, Arakawa M, Seike M, Yoshimatsu H. Isoleucine prevents the accumulation of tissue triglycerides and upregulates the expression of PPARalpha and uncoupling protein in diet-induced obese mice. *J Nutr*. 2010;140(3):496-500. doi:10.3945/JN.109.108977
57. McGarrah RW, Zhang GF, Christopher BA, Deleye Y, Walejko JM, Page S, Ilkayeva O, White PJ, Newgard CB. Translational Physiology: Dietary branched-chain amino acid restriction alters fuel selection and reduces triglyceride stores in hearts of Zucker fatty rats. *Am J Physiol - Endocrinol Metab*. 2020;318(2):E216. doi:10.1152/AJPENDO.00334.2019
58. Newgard CB, An J, Bain JR, Muehlbauer MJ, Stevens RD, Lien LF, Haqq AM, Shah SH, Arlotto M, Slentz CA, Rochon J, Gallup D, Ilkayeva O, Wenner BR, Yancy WS, Eisenson H, Musante G, Surwit RS, Millington DS, Butler MD, Svetkey LP. A branched-chain amino acid-related metabolic signature that differentiates obese and lean humans and contributes to insulin resistance. *Cell Metab*. 2009;9(4):311-326. doi:10.1016/J.CMET.2009.02.002
59. Nagata C, Nakamura K, Wada K, Tsuji M, Tamai Y, Kawachi T. Branched-chain amino acid intake and the risk of diabetes in a Japanese community: the Takayama

study. *Am J Epidemiol*. 2013;178(8):1226-1232. doi:10.1093/AJE/KWT112
60. Lee J, Vijayakumar A, White PJ, Xu Y, Ilkayeva O, Lynch CJ, Newgard CB, Kahn BB. BCAA Supplementation in Mice with Diet-induced Obesity Alters the Metabolome Without Impairing Glucose Homeostasis. *Endocrinology*. 2021;162(7). doi:10.1210/ENDOCR/BQAB062
61. Woo SL, Yang J, Hsu M, Yang A, Zhang L, Lee RP, Gilbuena I, Thames G, Huang J, Rasmussen A, Carpenter CL, Henning SM, Heber D, Wang Y, Li Z. Effects of branched-chain amino acids on glucose metabolism in obese, prediabetic men and women: a randomized, crossover study. *Am J Clin Nutr*. 2019;109(6):1569-1577. doi:10.1093/AJCN/NQZ024
62. Liu R, Li H, Fan W, Jin Q, Chao T, Wu Y, Huang J, Hao L, Yang X. Leucine Supplementation Differently Modulates Branched-Chain Amino Acid Catabolism, Mitochondrial Function and Metabolic Profiles at the Different Stage of Insulin Resistance in Rats on High-Fat Diet. *Nutrients*. 2017;9(6). doi:10.3390/NU9060565
63. Tobias DK, Clish C, Mora S, Li J, Liang L, Hu FB, Manson JAE, Zhang C. Dietary Intakes and Circulating Concentrations of Branched-Chain Amino Acids in Relation to Incident Type 2 Diabetes Risk among High-Risk Women with a History of Gestational Diabetes Mellitus. *Clin Chem*. 2018;64(8):1203. doi:10.1373/CLINCHEM.2017.285841
64. Woo SL, Yang J, Hsu M, Yang A, Zhang L, Lee RP, Gilbuena I, Thames G, Huang J, Rasmussen A, Carpenter CL, Henning SM, Heber D, Wang Y, Li Z. Effects of branched-chain amino acids on glucose metabolism in obese, prediabetic men and women: a randomized, crossover study. *Am J Clin Nutr*. 2019;109(6):1569-1577. doi:10.1093/AJCN/NQZ024
65. Ruocco C, Segala A, Valerio A, Nisoli E. Essential amino acid formulations to prevent mitochondrial dysfunction and oxidative stress. *Curr Opin Clin Nutr Metab Care*. 2021;24(1):88-95. doi:10.1097/MCO.0000000000000704
66. Honda T, Ishigami M, Luo F, Lingyun M, Ishizu Y, Kuzuya T, Hayashi K, Nakano I, Ishikawa T, Feng GG, Katano Y, Kohama T, Kitaura Y, Shimomura Y, Goto H, Hirooka Y. Branched-chain amino acids alleviate hepatic steatosis and liver injury in choline-deficient high-fat diet induced NASH mice. *Metabolism*. 2017;69:177-187. doi:10.1016/J.METABOL.2016.12.013
67. Chen KH, Chen YL, Tang HY, Hung CC, Yen TH, Cheng ML, Shiao MS, Chen JK. Dietary Leucine Supplement Ameliorates Hepatic Steatosis and Diabetic Nephropathy in db/db Mice. *Int J Mol Sci*. 2018;19(7). doi:10.3390/IJMS19071921
68. Arakawa M, Masaki T, Nishimura J, Seike M, Yoshimatsu H. The effects of branched-chain amino acid granules on the accumulation of tissue triglycerides and uncoupling proteins in diet-induced obese mice. *Endocr J*. Published online 2011. doi:10.1507/endocrj.K10E-221
69. Sunny NE, Kalavalapalli S, Bril F, Garrett TJ, Nautiyal M, Mathew JT, Williams CM, Cusi K. Cross-talk between branched-chain amino acids and hepatic mitochondria is compromised in nonalcoholic fatty liver disease. *Am J Physiol - Endocrinol Metab*. 2015;309(4):E311-E319. doi:10.1152/ajpendo.00161.2015
70. Nakanishi C, Doi H, Katsura K, Satomi S. Treatment with L-valine ameliorates liver fibrosis and restores thrombopoiesis in rats exposed to carbon tetrachloride. *Tohoku J Exp Med*. 2010;221(2):151-159. doi:10.1620/tjem.221.151

71. Chalasani N, Vuppalanchi R, Rinella M, Middleton MS, Siddiqui MS, Barritt AS, Kolterman O, Flores O, Alonso C, Iruarrizaga-Lejarreta M, Gil-Redondo R, Sirlin CB, Zemel MB. Randomised clinical trial: a leucine-metformin-sildenafil combination (NS-0200) vs placebo in patients with non-alcoholic fatty liver disease. *Aliment Pharmacol Ther*. 2018;47(12):1639-1651. doi:10.1111/apt.14674
72. Bruckbauer A, Banerjee J, Fu L, Li F, Cao Q, Cui X, Wu R, Shi H, Xue B, Zemel MB. A Combination of Leucine, Metformin, and Sildenafil Treats Nonalcoholic Fatty Liver Disease and Steatohepatitis in Mice. *Int J Hepatol*. 2016;2016. doi:10.1155/2016/9185987
73. Richardson NE, Konon EN, Schuster HS, Mitchell AT, Boyle C, Rodgers AC, Finke M, Haider LR, Yu D, Flores V, Pak HH, Ahmad S, Ahmed S, Radcliff A, Wu J, Williams EM, Abdi L, Sherman DS, Hacker TA, Lamming DW. Lifelong restriction of dietary branched-chain amino acids has sex-specific benefits for frailty and life span in mice. *Nat Aging 2020 11*. 2021;1(1):73-86. doi:10.1038/s43587-020-00006-2
74. Yu D, Richardson NE, Green CL, Spicer AB, Murphy ME, Flores V, Jang C, Kasza I, Nikodemova M, Wakai MH, Tomasiewicz JL, Yang SE, Miller BR, Pak HH, Brinkman JA, Rojas JM, Quinn WJ, Cheng EP, Konon EN, Haider LR, Finke M, Sonsalla M, Alexander CM, Rabinowitz JD, Baur JA, Malecki KC, Lamming DW. The adverse metabolic effects of branched-chain amino acids are mediated by isoleucine and valine. *Cell Metab*. 2021;33(5):905-922.e6. doi:10.1016/J.CMET.2021.03.025
75. White PJ, Lapworth AL, An J, Wang L, McGarrah RW, Stevens RD, Ilkayeva O, George T, Muehlbauer MJ, Bain JR, Trimmer JK, Brosnan MJ, Rolph TP, Newgard CB. Branched-chain amino acid restriction in Zucker-fatty rats improves muscle insulin sensitivity by enhancing efficiency of fatty acid oxidation and acyl-glycine export. *Mol Metab*. 2016;5(7):538-551. doi:10.1016/J.MOLMET.2016.04.006
76. Fontana L, Cummings NE, Arriola Apelo SI, Neuman JC, Kasza I, Schmidt BA, Cava E, Spelta F, Tosti V, Syed FA, Baar EL, Veronese N, Cottrell SE, Fenske RJ, Bertozzi B, Brar HK, Pietka T, Bullock AD, Figenshau RS, Andriole GL, Merrins MJ, Alexander CM, Kimple ME, Lamming DW. Decreased consumption of branched chain amino acids improves metabolic health. *Cell Rep*. 2016;16(2):520. doi:10.1016/J.CELREP.2016.05.092
77. van den Hoek AM, Verschuren L, Worms N, van Nieuwkoop A, de Ruiter C, Attema J, Menke AL, Caspers MPM, Radhakrishnan S, Salic K, Kleemann R. A Translational Mouse Model for NASH with Advanced Fibrosis and Atherosclerosis Expressing Key Pathways of Human Pathology. *Cells*. 2020;9(9):1-21. doi:10.3390/cells9092014
78. Petersen MC, Shulman GI. Roles of Diacylglycerols and Ceramides in Hepatic Insulin Resistance. *Trends Pharmacol Sci*. 2017;38(7):649-665. doi:10.1016/j.tips.2017.04.004
79. Samuel VT, Shulman GI. Mechanisms for insulin resistance: Common threads and missing links. *Cell*. 2012;148(5):852-871. doi:10.1016/j.cell.2012.02.017
80. Petersen MC, Vatner DF, Shulman GI. Regulation of hepatic glucose metabolism in health and disease. *Nat Rev Endocrinol*. 2017;13(10):572. doi:10.1038/NRENDO.2017.80
81. Gray N, Lawler NG, Yang R, Morillon AC, Gay MCL, Bong SH, Holmes E, Nicholson JK, Whiley L. A simultaneous exploratory and quantitative amino acid and biogenic amine metabolic profiling platform for rapid disease phenotyping via UPLC-QToF-

MS. *Talanta*. 2021;223(Pt 2). doi:10.1016/J.TALANTA.2020.121872
82. Tremblay F, Marette A. Amino acid and insulin signaling via the mTOR/p70 S6 kinase pathway. A negative feedback mechanism leading to insulin resistance in skeletal muscle cells. *J Biol Chem*. 2001;276(41):38052-38060. doi:10.1074/JBC.M106703200
83. Bishop CA, Schulze MB, Klaus S, Weitkunat K. The branched-chain amino acids valine and leucine have differential effects on hepatic lipid metabolism. *FASEB J*. 2020;34(7):9727-9739. doi:10.1096/FJ.202000195R

Supplemental information

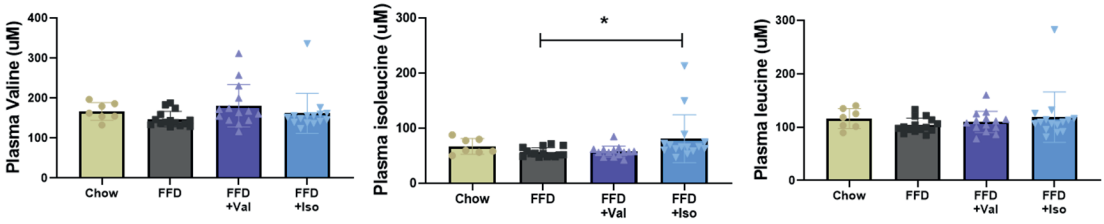

***Supplemental figure 1**. Plasma BCAAs concentrations of valine, leucine and isoleucine measured by LC-MS at t=38 weeks in 5h-fasting plasma. An * asterisk indicates significant difference compared to the FFD control group with p<0.05. Data shown are mean ± SD.*

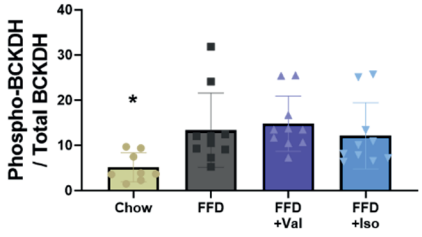

***Supplemental figure 2**. Phosphorylated-BCKDH/total-BCKDH protein ratio normalized for tubulin analyzed with Western blots at t=38 weeks. An * asterisk indicates significant difference compared to the FFD control group with p<0.05. Data shown are mean ± SD.*

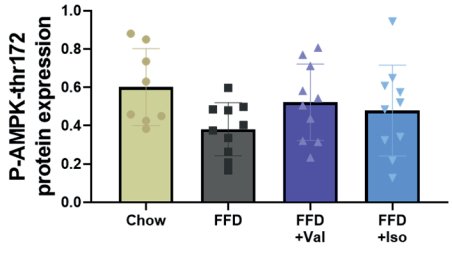

***Supplemental figure 3**. Phosphorylated-AMPK normalized for tubulin protein expression analyzed with Western blots at t=38 weeks. An * asterisk indicates significant difference compared to the FFD control group with p<0.05. Data shown are mean ± SD.*

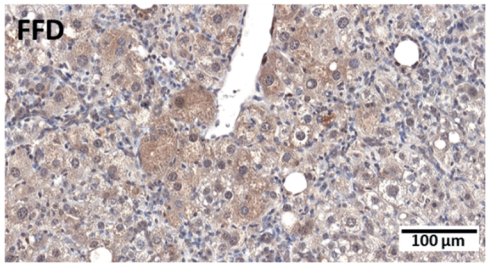

Supplemental figure 4. *Illustrative photomicrographs of 4-HNE-positive immunoreactivity in enlarged hepatocytes.*

CHAPTER

6

Diet-independent correlations between bacteria and dysfunction of gut, adipose tissue, and liver: a comprehensive microbiota analysis in feces and mucosa of the Ileum and colon in obese mice with NAFLD

Eveline Gart, Everton Souto Lima, Frank Schuren,
Christa G. F. de Ruiter, Joline Attema, Lars Verschuren, Jaap Keijer,
Kanita Salic, Martine C. Morrison and Robert Kleemann

Int J Mol Sci. 2018 Dec 20;20(1):1.
doi: 10.3390/ijms20010001. PMID: 30577415; PMCID: PMC6337295.

Abstract

Development of non-alcoholic fatty liver disease (NAFLD) is linked to obesity, adipose tissue inflammation, and gut dysfunction, all of which depend on diet. So far, studies have mainly focused on diet-related fecal microbiota changes, but other compartments may be more informative on host health. We present a first systematic analysis of microbiota changes in the ileum and colon using multiple diets and investigating both fecal and mucosal samples. Ldlr−/−.Leiden mice received one of three different energy-dense (ED)-diets (*n* = 15/group) for 15 weeks. All of the ED diets induced obesity and metabolic risk factors, altered short-chain fatty acids (SCFA), and increased gut permeability and NAFLD to various extents. ED diets reduced the diversity of high-abundant bacteria and increased the diversity of low-abundant bacteria in all of the gut compartments. The ED groups showed highly variable, partially overlapping microbiota compositions that differed significantly from chow. Correlation analyses demonstrated that (1) specific groups of bacteria correlate with metabolic risk factors, organ dysfunction, and NAFLD endpoints, (2) colon mucosa had greater predictive value than other compartments, (3) correlating bacteria differed per compartment, and (4) some bacteria correlated with plasma SCFA levels. In conclusion, this comprehensive microbiota analysis demonstrates correlations between the microbiota and dysfunctions of gut, adipose tissue, and liver, independent of a specific disease-inducing diet.

1. Introduction

Non-alcoholic fatty liver disease (NAFLD) has become a major health problem worldwide [1]. Ample evidence shows that an increased intake of calories from saturated fat and carbohydrates such as sucrose and fructose contribute to the development of NAFLD [2,3]. Furthermore, important drivers of the disease are dysmetabolism (e.g., dyslipidemia, hyperinsulinemia), white adipose tissue (WAT) inflammation [4], and gut dysfunction [5,6]. Gut dysfunction includes dysbiosis, alterations of microbiota-derived metabolites such as short-chain fatty acids (SCFAs), and increased gut permeability [7]. Together, these dysfunctions are thought to propel the progression of NAFLD from the relative benign hepatic lipid accumulation (steatosis) toward non-alcoholic steatohepatitis (NASH), which is the severe stage of NAFLD that is characterized by steatosis and liver inflammation [8].

The reported alterations of the gut microbiota in obese and NAFLD/NASH patients are typically based on the analysis of the fecal colonic microbiota, which is an easily accessible gut site. However, it is known that different bacteria dominate in the various regions of the intestinal tract [9,10], and that the microbiota of the fecal and mucosal compartment is composed of different bacteria [11]. Hence, it is possible that an analysis of specific gut microbial compartments may be more informative on host health than the conventional analysis, which is solely based on fecal microbiota. However, a systematic analysis of multiple microbial compartments of the gut in relation to obesity and NAFLD endpoints has not been performed to date.

In the present study, we examined microbiota changes evoked by energy-dense (ED) diets in the colon and ileum during obesity-associated NAFLD development. In the colon and ileum, fecal and mucosal compartments were analyzed by 16S rRNA gene sequencing. We complemented this with the analysis of SCFAs, which constitute potential mediators between the microbiota and host health. We studied NAFLD development in Ldlr−/−.Leiden mice through an established translational model for NAFLD/NASH [12–14]. Upon the feeding of ED diets, these mice developed metabolic dysfunction and features of human NAFLD (obesity, dyslipidemia, insulin resistance, WAT inflammation, hepatic steatosis, lobular inflammation, and fibrosis) [12].

Since diets can alter microbiota composition [15], we evaluated the generic effects of three different ED diets containing macronutrients that are frequently present in human diets, i.e., diets rich in saturated fat (butter or lard), as well as rapidly metabolizable carbohydrates (fructose and sucrose). These three diets were compared with a reference chow-fed group, which did not develop obesity and NAFLD. The chosen approach allowed us to investigate general diet-independent changes in specific gut microbial compartments that inform on readouts of metabolic dysfunction and NAFLD development (e.g., fat mass, WAT inflammation, gut permeability, macrovesicular steatosis, hepatic inflammation). We demonstrate that specific bacteria correlate with these readouts, independent of the NAFLD-inducing diet used, and that these correlations differ between gut compartments and involve different bacteria in different compartments.

2. Materials and Methods

2.1. Animals, Diets, and Study Design

Ethics approval: Approval was granted by the ethics committee on animal experiments (approval reference number DEC-3682,11 December 2014) and the institutional animal welfare body (approval reference number TNO-136, 29 March 2016)).

All of the animal experiments were performed in accordance with the Animal Care and Use Committee of The Netherlands Organization of Applied Research (TNO), Leiden, the Netherlands. All of the mice were group-housed (four to five mice per cage) in Macrolon cages in clean-conventional animal rooms in the American Association for Accreditation of Laboratory Animal Care (AAALAC)-accredited animal facility at TNO Leiden (relative humidity 50–60%, temperature ~21 °C, light cycle 07:00 to 19:00) and had *ad libitum* access to food and water. Male Ldlr−/−.Leiden mice were obtained from the breeding facility of TNO Metabolic Health Research, Leiden, the Netherlands, and were kept on a low-fat control diet (chow; Sniff-R/M-V1530, Uden, the Netherlands, containing 23 kcal% protein (soy and cereal grains), 67 kcal% carbohydrate (mainly starch), 9 kcal% fat (grain cereals and soy products) and 4.9 *w*/*w*% fiber) until the start of the study (six weeks of age). The mice were then matched into four groups (n = 15/group) based on body weight and blood glucose. The first group remained on chow, while the other groups were switched to energy-dense (ED) diet regimens, as shown in Table 1. For a total of 15 weeks, groups of mice were fed a butter fat with fructose diet (BF; D16032401, Research Diets Inc., New Brunswick, USA; with 14 kcal% protein, 44 kcal% carbohydrate (mainly fructose), and 41 kcal% butter fat, 5.1 *w*/*w*% fiber) or a lard fat with sucrose diet (LS; D12451, Research Diets Inc.; with 20 kcal% protein, 35 kcal% carbohydrate (mainly sucrose), 45 kcal% lard fat, 5.8 *w*/*w*% fiber), or the same LS diet with 10% fructose in the drinking water (LS+FW). Body weight was measured at set intervals, and body composition was determined using echoMRI. After 12 weeks, gut permeability was analyzed using an FD4 test. In week 15, five-hour fasted tail blood plasma (Ethylenediaminetetraacetic acid; EDTA) was collected to measure cholesterol, TG, glucose, insulin, ALT, and SCFAs. After 15 weeks, five hour-fasted animals were terminated by gradual fill CO_2 asphyxiation, and a terminal blood sample (for EDTA plasma) was collected by cardiac puncture. Isolated liver and epididymal adipose tissue were fixed in formalin and paraffin-embedded for histological analysis. At sacrifice, microbiota from four different regions of the intestinal tract were sampled, i.e., the feces were collected and the mucosa was scraped in both the colon and ileum.

Table 1. Diet composition.

	Chow	BF	LS	LS+FW
Fat	9% kcal (Cereal grains and soy)	41% kcal (Butter fat)	45% kcal (Lard)	Same as LS
Protein	24% kcal (Soy and cereal grains)	14% kcal (Casein)	20% kcal (Casein)	Same as LS
Carbohydrate	67% kcal (Starch)	44% kcal (Fructose)	35% kcal (Sucrose)	Same as LS
Cholesterol	-	-	-	-
kcal/gram	3.2 kcal/g	4.5 kcal/g	4.7 kcal/g	Same as LS
Fiber	4.9% *w*/*w*	5.1% *w*/*w*	5.8% *w*/*w*	Same as LS
Drink	Water	Water	Water	10% *w*/*v* fructose in water

Ldlr−/−.Leiden mice were fed Chow, butter fat–fructose (BF), lard fat–sucrose (LS) or a diet with LS and fructose water (LS+FW) for 15 weeks (*n* = 15/diet grp). (-) = not present; (*w*/*w*) = weight per weight; (*w*/*v*) weight per volume; (% kcal) = percent of energy.

2.2. Blood Chemistry

Plasma lipids (cholesterol and TGs), ALT levels, and insulin were assessed in a fasted (five-hour) blood sample (100 µL, tail incision). Plasma total cholesterol and TGs were measured spectrophotometrically with enzymatic assays (Roche diagnostics, Almere, the Netherlands) according to the manufacturer's instructions. Plasma ALT levels were measured by reflectance photometry (Reflotron-Plus system, Roche diagnostics,). Blood glucose was measured during blood sampling using a hand-held glucose analyzer (Freestyle Disectronic, Vianen, the Netherlands). Plasma insulin levels were determined by ELISA (Mercodia, Uppsala, Sweden).

Plasma SCFAs were analyzed using ultra performance liquid chromatography (UPLC, Ultimate 3000 UPLC system, Thermo Scientific, Waltham, MA, USA) coupled to high-resolution mass spectrometry (HR-MS, Q-Exactive mass spectrometer equipped with an electro-spray ionization probe (Thermo Scientific)). Briefly, plasma was mixed with MilliQ water and deuterated internal standard solution was added. Subsequently, three M of zinc sulfate solution was used to precipitate proteins. After vortexing and centrifugation, the supernatant was used for derivatization with glycidyltrimethylammonium chloride solution (diluted in 100 mM of Tris-HCl buffer pH = 7.2) which was incubated for 90 min at 70 °C. After derivatization, the SCFAs were separated on an Acquity HSS T3 column (150 × 2.1 mm, 1.8 µm; Waters Corporation, Milford, MA, USA) using a mobile phase gradient from 99.5% mobile phase A (0.1% formic acid in MilliQ) to 100% mobile phase B (0.1% formic acid in

acetonitrile). Mass detection was carried out using electrospray ionization in the positive mode (spray voltage three kV, scan range m/z 150–700).

2.3. Histological Analysis of Adipose Tissue and Liver

Paraffin-embedded cross sections (five-µm thick) of gonadal WAT were stained with hematoxylin-phloxine-saffron to blindly score the number of crown-like structures (CLS) in three non-overlapping fields (100× magnification) per mouse and data were expressed as number of CLS/mm^2 [4]. Histopathological analysis of NAFLD was performed on five-µm thick hematoxylin-eosin stained cross-sections of the medial lobe. NAFLD was scored blindly by a board-certified pathologist using an adapted grading method for human NASH [12,49]. Briefly, two cross-sections per mouse were examined to assess the level of macrovesicular steatosis relative to the hepatocyte area, which was expressed as a percentage. Hepatic inflammation was evaluated by counting the number of inflammatory cell aggregates per field at a 100× magnification [12,50] in five non-overlapping fields per mouse, and expressed as the average number of cell aggregates per mm^2.

2.4. FD4 Gut Permeability Assay

In vivo gut permeability was assessed by measuring the ability of the relatively impermeant fluorescein isothiocyanate-labelled dextran (three to five kDa FD4; Sigma, St. Louis, MO, USA) to cross from the intestinal lumen into the circulation, which is a test employed in human [51] and rodent studies [52,53]. Mice were fasted for four hours, after which a baseline blood sample was taken by tail incision. Then, FD4 was administered by oral gavage (900 mg/kg) and four hours later, a second blood sample was taken to determine the plasma concentration of FD4 using a fluorometer (FLUOstar Galaxy, BMG labtech, Offenburg, Germany). The baseline blood sample was used to correct for autofluorescence.

2.5. Statistical Analysis

Data is presented as mean ± standard error of the mean (SEM). Significance of differences between the control diet (chow) and the ED diet groups were tested using a one-way ANOVA with Dunnett's post hoc test. Differences with $p \leq 0.05$ were considered to be statistically significant. The statistics of the microbiota data analysis is described below.

2.6. Gut Microbiota Analysis

2.6.1. Collection and DNA Isolation:

Microbiota samples from both the colon and ileum collected from the feces or mucosa were collected at the end of the study and frozen immediately at −80 °C. Samples were mechanically homogenized and genomic DNA was isolated using the AGOWA mag mini kit (DNA Isolation Kit, AGOWA, Berlin, Germany) according to the manufacturer's instructions.

2.6.2. Metagenomic Sequencing and Data Analysis:

A fragment of the 16S rRNA gene (~270 bp), spanning the V4 hypervariable regions, was amplified by PCR within 30 cycles using F515/R806 primers. Seventeen purified PCR

products were paired-end sequenced on an Illumina MiSeq platform (Illumina, Eindhoven, The Netherlands). The sequences were classified by the RDP-II Naïve Bayesian Classifier ('Wang method') [54]. In addition, taxa that were not observed in at least 5% of the samples or had a total count of less than five were removed. Microbiota data analysis and visual representation was performed with R [55]: To address differences in sequencing depth and heteroscedasticity, the data was normalized by DESeq^2 using the variance stabilization transformation [56]. Community profiles were analyzed on the genus level, compared by Bray–Curtis dissimilarity and visualized in non-metric multidimensional scaling (NMDS) plots. The minimum-entropy decomposition algorithm, which clusters 16S rRNA gene amplicons in a sensitive manner, was used to calculate the Shannon index, Pielou evenness index, and the tail-statistic for alpha diversity on the sequence level with the vegan package in R [57]. Significance of differences in diversity between chow and the ED diets was tested using a one-way ANOVA with Dunnett's post hoc test. Statistical permutation tests were performed to compare composition level differences [58–60] with the phyloseq GraphTest package in R [61]. Correlation analysis between the microbiota composition and histological and functional readouts of NAFLD development were performed with regularized canonical correlation analysis (rCCA analysis) [62] using MixOmics in R [63].

3. Results

3.1. All ED Diets Resulted in NAFLD in the Context of Obesity, White Adipose Tissue Dysfunction, and Gut Dysfunction

After 15 weeks, all of the ED diets induced hepatic steatosis, as shown in Figure 1A. More specifically, quantitative histopathological analysis revealed that a butter fat with fructose diet (BF), lard fat with sucrose diet (LS), and the same LS diet with 10% fructose in the drinking water (LS+FW) induced extensive macrovesicular steatosis (Figure 1B) relative to chow-fed controls (0.0 ± 0.0% in chow; 19.3 ± 2.8% in BF, $p < 0.001$; 22.1 ± 3.5%, $p < 0.001$ in LS; 24.8 ± 1.9% in LS+FW, $p < 0.001$). Hepatic inflammation, which was expressed as number of inflammatory aggregates per mm^2 (Figure 1C), was induced by all of the ED diets in varying degrees, which reached statistical significance in BF-fed mice (3.4 ± 0.5 per mm^2, $p < 0.001$). Furthermore, plasma levels of the liver damage marker alanine aminotransferase (ALT) were significantly increased in BF; while in LS, a slight (non-significant) increase was observed, and levels were significantly increased in LS+FW (Table 2).

These characteristics of liver dysfunction were observed in the context of an obese phenotype with pronounced hyperinsulinemia, hypertriglyceridemia, and hypercholesterolemia (Table 2). Body weight was significantly increased relative to the chow-fed controls after 15 weeks on all of the ED diets. Blood glucose on the ED diets did not significantly differ from the chow-fed controls; however, insulin was markedly elevated, with all the ED reaching statistical significance in the LS and LS+FW diets indicating a reduction in insulin sensitivity (Table 2). Furthermore, plasma cholesterol and triglycerides (TG) levels were higher in the ED diet groups, and BF was the strongest inducer of dyslipidemia (Table 2).

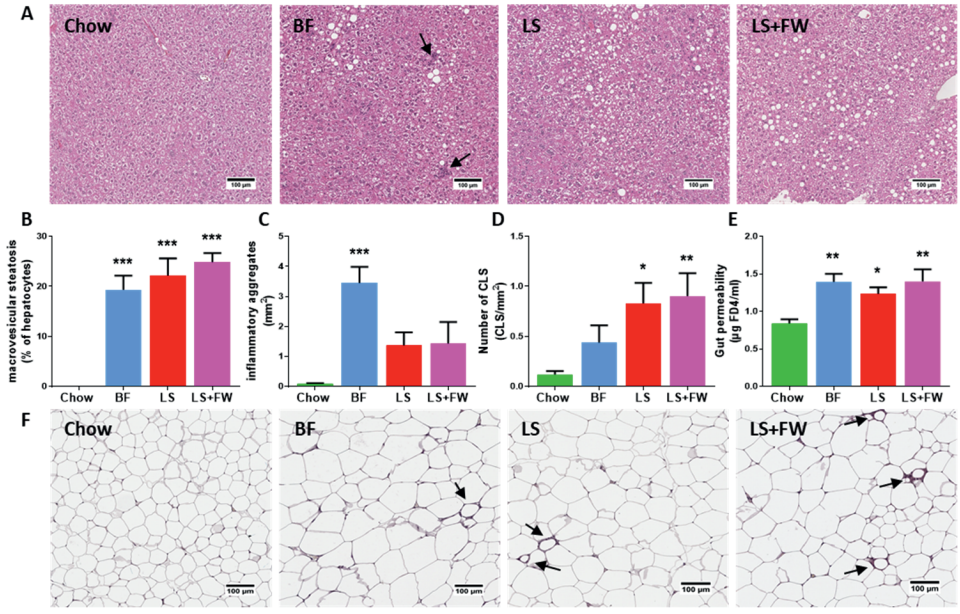

Figure 1. *Different energy-dense diets induced liver and white adipose tissue (WAT) dysfunction, and was associated with increased gut permeability. (**A**) Representative photomicrographs of HE-stained liver sections of chow, butter fat–fructose (BF), lard fat–sucrose (LS), and a diet with LS and fructose water (LS+FW); arrows indicate inflammatory aggregates. Histological quantification of (**B**) macrovesicular steatosis and (**C**) inflammatory aggregates per mm² in the liver and (**D**) crown-like structures (CLS) per mm² in WAT. (**E**) Functional gut permeability analysis using a fluorescein isothiocyanate-labeled dextran (FD4) assay. (**F**) Representative photomicrographs of hematoxylin-phloxine-saffron-stained gonadal WAT sections, arrows indicate CLS. Data are presented as mean ± SEM, * $p \leq 0.05$ or ** $p \leq 0.01$, or *** $p \leq 0.001$ compared to the chow control group.*

In line with the observed increase in body weight, total fat mass was significantly increased on the ED diets (Table 2) compared with the control diet. In addition to this increase in adipose tissue mass, quantitative histological analysis of inflammation in the gonadal white adipose tissue depot (representative images shown in Figure 1F) demonstrated that the number of CLS in the BF group was comparable to chow (Figure 1D) (0.1 ± 0.0 in chow; 0.4 ± 0.2 in BF, $p = 0.45$). By contrast, treatment with LS and LS+FW resulted in pronounced CLS formation in WAT (0.8 ± 0.2, $p = 0.02$; 0.9 ± 0.2, $p = 0.03$).

Table 2. Metabolic parameters. ALT: alanine aminotransferase.

	Chow	BF	LS	LS+FW
Body weight (g)	29.1 ± 2.2	34.5 ± 3.8**	37.8 ± 6.0***	40.1 ± 5.1***
Total caloric intake (kcal/day)	11.0 ± 0.7	11.7 ± 1.1	11.5 ± 0.5	12.6 ± 0.8
Total fat mass (g)	3.7 ± 1.0	9.1 ± 1.9***	11.8 ± 4.0***	13.4 ± 4.8***
Plasma cholesterol (mM)	8.9 ± 1.8	50.9 ± 10.9***	20.3 ± 6.2***	24.3 ± 10.8***
Plasma triglycerides (mM)	1.6 ± 0.4	10.3 ± 2.4***	4.9 ± 1.9***	4.5 ± 2.6***
Plasma insulin (ng/ml)	1.3 ± 0.6	4.2 ± 1.2	4.6 ± 2.1*	8.0 ± 6.8*
Blood glucose (mM)	7.2 ± 1.0	6.3 ± 0.9	7.6 ± 2.1	7.7 ± 1.5**
ALT (U/L)	32.6 ± 7.3	139.7 ± 76.4***	78.9 ± 50.0	137.1 ± 99.3***

Data are presented as mean ± SD, * $p \leq 0.05$ or ** $p \leq 0.01$ or *** $p \leq 0.001$ compared to chow.

In addition, gut barrier function measured with an fluorescein isothiocyanate-labeled dextran (FD4) assay for gut permeability (Figure 1E) was significantly elevated on BF, LS, and LS+FW relative to chow (0.8 ± 0.1 in chow; 1.4 ± 0.1 in BF, $p < 0.001$; 1.2 ± 0.1, $p = 0.04$ in LS; 1.4 ± 0.2 in LS+FW, $p < 0.001$). Furthermore, the plasma levels of gut-derived metabolites (SCFAs) were quantified by high-performance LC-MS (Table 3). These metabolites may be potential bioactive mediators in host health, and 90% are absorbed from the gut [16]; therefore, their plasma levels may be more informative than conventionally studied fecal levels. Plasma levels of the SCFA propionate were markedly elevated in LS-fed mice only, while acetate and butyrate were reduced in BF and LS+FW. Plasma levels of the SCFAs isobutyrate, methylbutyrate, isovalerate, and valerate (also known as the isoacid SCFAs) were all significantly increased in LS and LS+FW.

Collectively, these data show that all of the ED diets induced NAFLD in varying degrees of severity in the context of obesity, WAT inflammation, and gut dysfunction.

Table 3. Plasma levels of gut-derived metabolites (short-chain fatty acids, or SCFAs).

	Chow	BF	LS	LS+FW
Acetate (nM)	5966.6 ± 874.1	4828.2 ± 891.8**	6468.3 ± 1361.3	4977.9 ± 810.9**
Butyrate (nM)	123.7 ± 67.1	55.6 ± 14.4**	142.3 ± 90.7	45.8 ± 7.3**
Propionate (nM)	257.8 ± 103.3	310.8 ± 127.1	464.6 ± 214.9**	388.3 ± 171.6
Isobutyrate (nM)	33.5 ± 7.3	45.7 ± 11.6	88.9 ± 42.7***	57.6 ± 12.2*
Methylbutyrate (nM)	36.6 ± 8.5	46.9 ± 8.7	81.9 ± 34.6***	54.8 ± 8.9*
Isovalerate (nM)	26.9 ± 4.6	33.3 ± 7.7	66.7 ± 16.7***	60.9 ± 19.8***
Valerate (nM)	10.8 ± 5.7	19.9 ± 11.8	36.4 ± 14.4***	23.7 ± 10.2**

*Data are presented as mean ± SD, * $p \leq 0.05$, or ** $p \leq 0.01$, or *** $p \leq 0.001$ compared to chow.*

3.2. Global Analysis of Fecal and Mucosal Microbiota Composition in Colon and Ileum

To investigate whether the observed diet-induced metabolic dysfunction in liver, white adipose tissue, and gut may be linked to changes in bacterial colonization in specific gut compartments, we performed a 16S rRNA gene microbiota analysis of the fecal and mucosal compartments of both the colon and ileum.

First, we investigated whether these four gut compartments differ in their colonization using permutation tests, which enable the statistical testing of differences between the groups. This analysis revealed a clear difference in microbiota composition between the colon and ileum (Figure 2A, $p < 0.05$), which is consistent with their different physiological roles. Furthermore, we observed significant differences between the mucosal and the fecal compartments in both regions of the gut (Figure 2B, colon $p < 0.05$; Figure 2C, ileum $p < 0.05$).

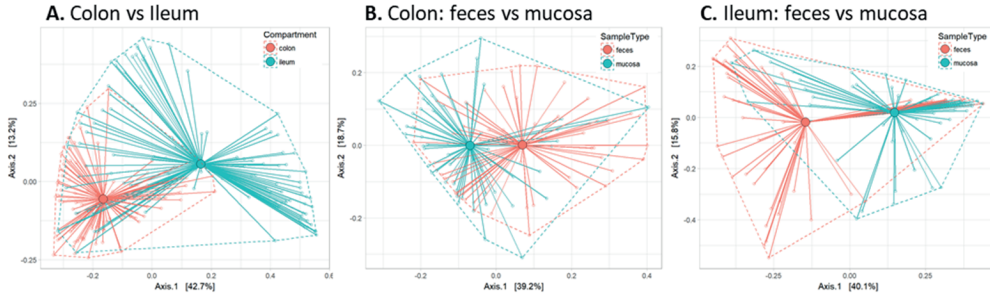

Figure 2. *Refined microbiota analysis reveals marked composition differences between the gut compartments. Permutation tests were used to calculate statistical differences in microbiota composition, and group distances were visualized between (**A**) the colon and ileum, (**B**) colon feces and mucosa, and (**C**) ileum feces and mucosa.*

Next, we investigated whether the microbiota composition was affected by ED feeding and whether there were differences in microbiota composition between the three ED diet groups, in which the dissimilarity in composition was visualized with non-metric multidimensional scaling analysis (NMDS). This NMDS plot (Figure 3) demonstrated that the chow animals formed a discrete cluster, in which ileum feces differed the most from the other compartments. The microbiota composition of the ED diet groups was clearly different from that of the chow diet group (i.e., did not overlap with the chow cluster), and showed pronounced variation with no clear separation of the different ED diets. Similarly to what was observed in chow-fed animals, the ileum feces compartment was the most dissimilar and most variable in comparison with the other compartments. These observations were statistically confirmed by permutation tests, which revealed that the microbiota composition of the chow group clearly differed from the other groups in all of the compartments ($p = 0.002$) (see also Figure S1), whereas the composition of the ED diets was statistically comparable in all of the compartments (Figure 4; colon feces $p = 0.09$, colon mucosa $p = 0.32$, ileum feces $p = 0.60$, ileum mucosa $p = 0.07$).

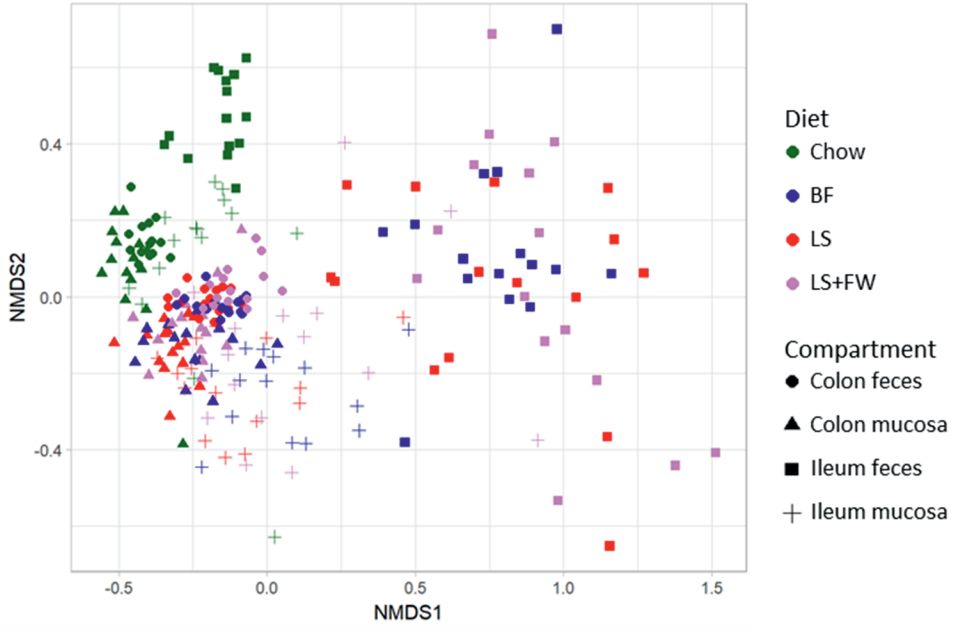

Figure 3. *Effects of the non-alcoholic fatty liver disease (NAFLD)-inducing energy-dense diets on microbiota composition of the colon and ileum in both the feces and mucosa. 16S rRNA gene sequencing analysis was performed on the luminal and mucosal contents of both the ileum and colon, and was used to visualize microbiota ordination with non-metric multidimensional scaling (NMDS) using the Bray–Curtis index. Complementary statistical analysis were performed with permutation tests and visualized in the previous figure to show the differences in microbiota composition between gut compartments. The following figure shows the differences in microbiota composition between the energy-dense diets.*

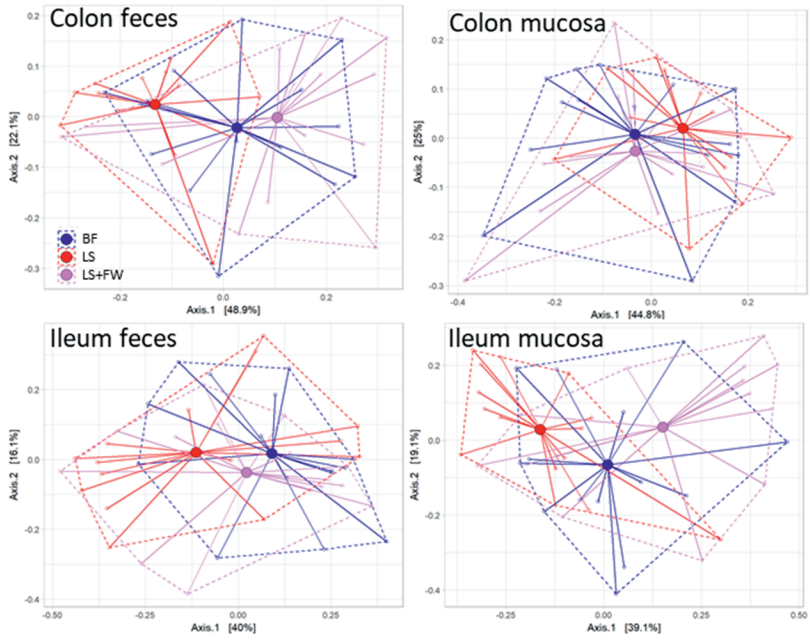

Figure 4. *Microbiota composition between the energy-dense diets was comparable in all of the gut compartments. Permutation tests were used to calculate statistical differences in microbiota composition, and group distances were visualized between ED diets in the colon feces, colon mucosa, ileum feces, and ileum mucosa.*

To gain more insight into how the microbiota of the ED diets differed from those of the chow-fed controls, we next investigated the effects of the NAFLD-inducing diets on microbiota diversity using the Shannon index (sensitive to high-abundant bacteria) and tail-statistic analysis (sensitive to low-abundant bacteria). The Shannon index analysis demonstrated that the ED diets consistently reduced the microbiota diversity of high-abundant bacteria in all of the compartments that were studied (Figure 5A), which reached statistical significance by BF in colon feces, ileum feces, and ileum mucosa ($p = 0.01$; $p < 0.001$; and $p = 0.02$), LS only in the ileum feces ($p < 0.001$), and LS+FW in all of the compartments ($p < 0.001$; $p < 0.001$; $p < 0.001$; and $p < 0.001$). This reduction in diversity was more pronounced in the feces than in the mucosa in both the colon and ileum, suggesting a more robust microbiota in the mucosal compartments compared with feces. Complementary to this analysis, the Pielou evenness index was calculated, which represents species evenness (Figure S2). A high number indicates that an equal number of bacteria belong to each species, while a low number indicates the presence of dominant species. The results of the Pielou evenness index show a similar trend as the Shannon index, and confirm that the ED diets reduce species diversity. In contrast, the tail-statistic analysis showed that the diversity of low-abundant bacteria was increased by the ED diets in all of the compartments (Figure 5B) ($p < 0.001$ for all of the ED diets in all of the gut compartments). These results suggest that abundant bacteria decreased, while low abundant bacteria increased on the ED diets.

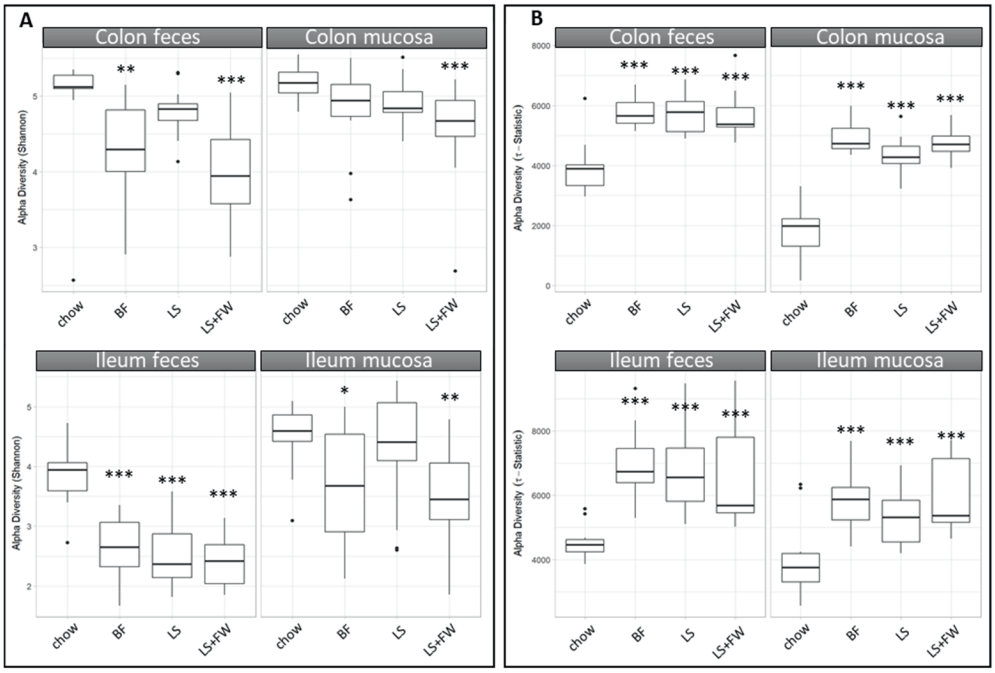

Figure 5. *All of the energy-dense (ED) diets reduced diversity in high-abundant bacteria and increased diversity in low-abundant bacteria in all of the gut compartments. 16S rRNA gene sequencing analysis was performed on the luminal and mucosal contents of both the ileum and colon, and was used to calculate alpha diversity using the (**A**) Shannon index (sensitive for high-abundant bacteria) and (**B**) the tail statistic (sensitive for low-abundant bacteria). Data are presented as mean ± SD, * p ≤ 0.05, ** p ≤ 0.01, or *** p ≤ 0.001 compared to chow.*

In order to study general disease-associated microbiota changes, independent of the specific ED diet used, we investigated the microbiota abundance on the genus level in all four gut compartments using heat maps as a visualization tool (Figure 6). These heatmaps illustrate that several of the top most abundant genera increased in abundance on all of the ED diets, independent of the gut microbial compartment, including *Lactococcus, Allobaculum, Bifidobacterium, Clostridium sensu stricto*, and *Clostridium_XI*.

Altogether, these analyses show that there were significant differences in composition between the gut microbial compartments studied, and that the three NAFLD-inducing ED diets resulted in a microbiota composition that is significantly different from chow, but did not differ between the ED diets, thus allowing us to study diet-independent disease-associated changes in the microbiota composition.

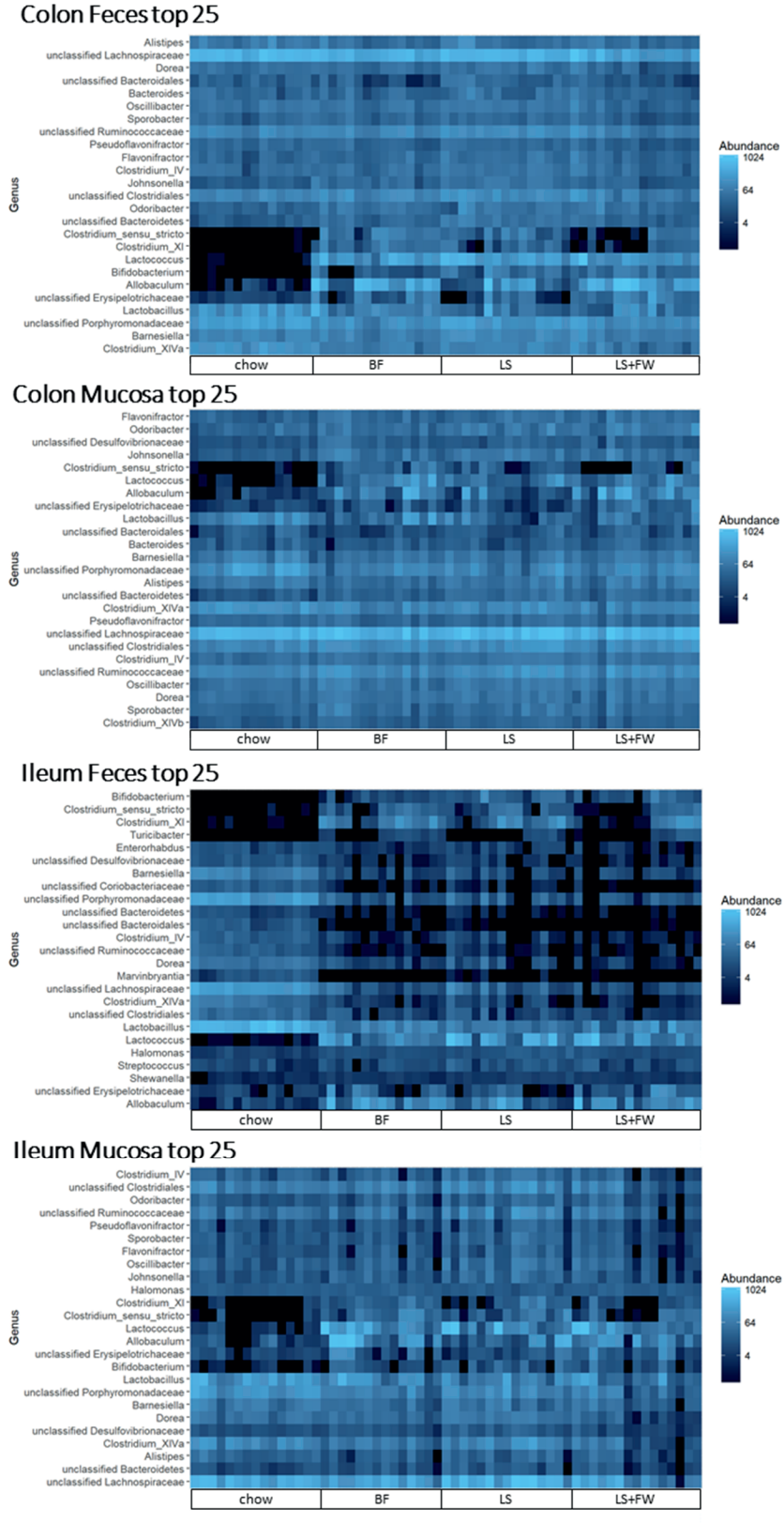
Colon Feces top 25
Alistipes
unclassified Lachnospiraceae
Dorea
unclassified Bacteroidales
Bacteroides
Oscillibacter
Sporobacter
unclassified Ruminococcaceae
Pseudoflavonifractor
Flavonifractor
Clostridium_IV
Johnsonella
unclassified Clostridiales
Odoribacter
unclassified Bacteroidetes
Clostridium_sensu_stricto
Clostridium_XI
Lactococcus
Bifidobacterium
Allobaculum
unclassified Erysipelotrichaceae
Lactobacillus
unclassified Porphyromonadaceae
Barnesiella
Clostridium_XIVa
Genus
chow
BF
LS
LS+FW
Abundance
1024
64
4
Colon Mucosa top 25
Flavonifractor
Odoribacter
unclassified Desulfovibrionaceae
Johnsonella
Clostridium_sensu_stricto
Lactococcus
Allobaculum
unclassified Erysipelotrichaceae
Lactobacillus
unclassified Bacteroidales
Bacteroides
Barnesiella
unclassified Porphyromonadaceae
Alistipes
unclassified Bacteroidetes
Clostridium_XIVa
Pseudoflavonifractor
unclassified Lachnospiraceae
unclassified Clostridiales
Clostridium_IV
unclassified Ruminococcaceae
Oscillibacter
Dorea
Sporobacter
Clostridium_XIVb
Genus
chow
BF
LS
LS+FW
Abundance
1024
64
4
Ileum Feces top 25
Bifidobacterium
Clostridium_sensu_stricto
Clostridium_XI
Turicibacter
Enterorhabdus
unclassified Desulfovibrionaceae
Barnesiella
unclassified Coriobacteriaceae
unclassified Porphyromonadaceae
unclassified Bacteroidetes
unclassified Bacteroidales
Clostridium_IV
unclassified Ruminococcaceae
Dorea
Marvinbryantia
unclassified Lachnospiraceae
Clostridium_XIVa
unclassified Clostridiales
Lactobacillus
Lactococcus
Halomonas
Streptococcus
Shewanella
unclassified Erysipelotrichaceae
Allobaculum
Genus
chow
BF
LS
LS+FW
Abundance
1024
64
4
Ileum Mucosa top 25
Clostridium_IV
unclassified Clostridiales
Odoribacter
unclassified Ruminococcaceae
Pseudoflavonifractor
Sporobacter
Flavonifractor
Oscillibacter
Johnsonella
Halomonas
Clostridium_XI
Clostridium_sensu_stricto
Lactococcus
Allobaculum
unclassified Erysipelotrichaceae
Bifidobacterium
Lactobacillus
unclassified Porphyromonadaceae
Barnesiella
Dorea
unclassified Desulfovibrionaceae
Clostridium_XIVa
Alistipes
unclassified Bacteroidetes
unclassified Lachnospiraceae
Genus
chow
BF
LS
LS+FW
Abundance
1024
64
4

Figure 6. *Diet-independent changes of the microbiota composition after 15 weeks of energy-dense diet treatment. 16s rRNA gene sequencing analysis was performed on the luminal and mucosal contents of both the ileum and colon, and the abundance of the 25 most dominant genera were expressed in a heat map.*

3.3. Microbiota Composition Associations with NAFLD Disease Endpoints

Next, we investigated whether there are correlations between the microbiota composition and histological and functional readouts of metabolic dysfunction and NAFLD development (body weight, fat mass, WAT inflammation, gut permeability, macrovesicular steatosis, hepatic inflammation) or plasma levels of gut-derived metabolites (SCFAs: acetate, propionate, butyrate, methylbutyrate, isobutyrate isovalerate, and valerate), independent of the specific ED diet that was employed. For this, we performed a comprehensive regularized canonical correlation analysis (rCCA), which allows the study of relationships between sets of variables. This analysis revealed that correlations exist between the gut microbiota composition and histological and functional readouts in all of the compartments that were studied (Table 4). The strength of this correlation (expressed in the cross-validation score (CV score), which is a total (weighted) correlation score, where a higher score implies a stronger relation) was highest for the colon mucosa (CV scores of 0.71 for endpoints and 0.62 for metabolites), while colon feces (the typically used sampling compartment) showed weaker correlations (CV scores of 0.56 and 0.43 for endpoints and metabolites, respectively). In contrast, in the fecal compartment of the ileum, both the endpoints and metabolites correlated better (CV scores of 0.60 and 0.62, respectively) than the mucosal compartment (CV scores of 0.52 and 0.41, respectively).

Table 4. Correlation strength.

		Histological and Functional Readouts	Metabolites
Colon	Feces	0.56	0.43
	Mucosa	0.71	0.62
Ileum	Feces	0.60	0.62
	Mucosa	0.52	0.41

Data represents cross-validation score (CV score) from the regularized canonical correlation analysis (rCCA).

Consistent with our previous finding that each compartment exhibited a different microbiota composition, bacteria with the strongest correlations differed, to a large extent, in each of the compartments. However, correlation analysis between microbiota and histological and functional readouts showed strong positive correlations for *Allobaculum* and *Bifidobacterium*, and strong negative correlations for the *Roseburia* and *Anaerostipes* bacteria, in all of the compartments (Figure 7A). Interestingly, correlation analysis between the microbiota and plasma levels of gut-derived metabolites (Figure 7B) revealed that the

bacteria that positively correlated with disease readouts (indicating an unfavorable metabolic state) also positively correlated with the isoacid SCFAs (isobutyrate, methylbutyrate, isovalerate, and valerate).

Altogether, we identified diet-independent correlations between specific bacteria and the histological and functional readouts of NAFLD development, in which the strongest correlations were found for the colon mucosa compartment.

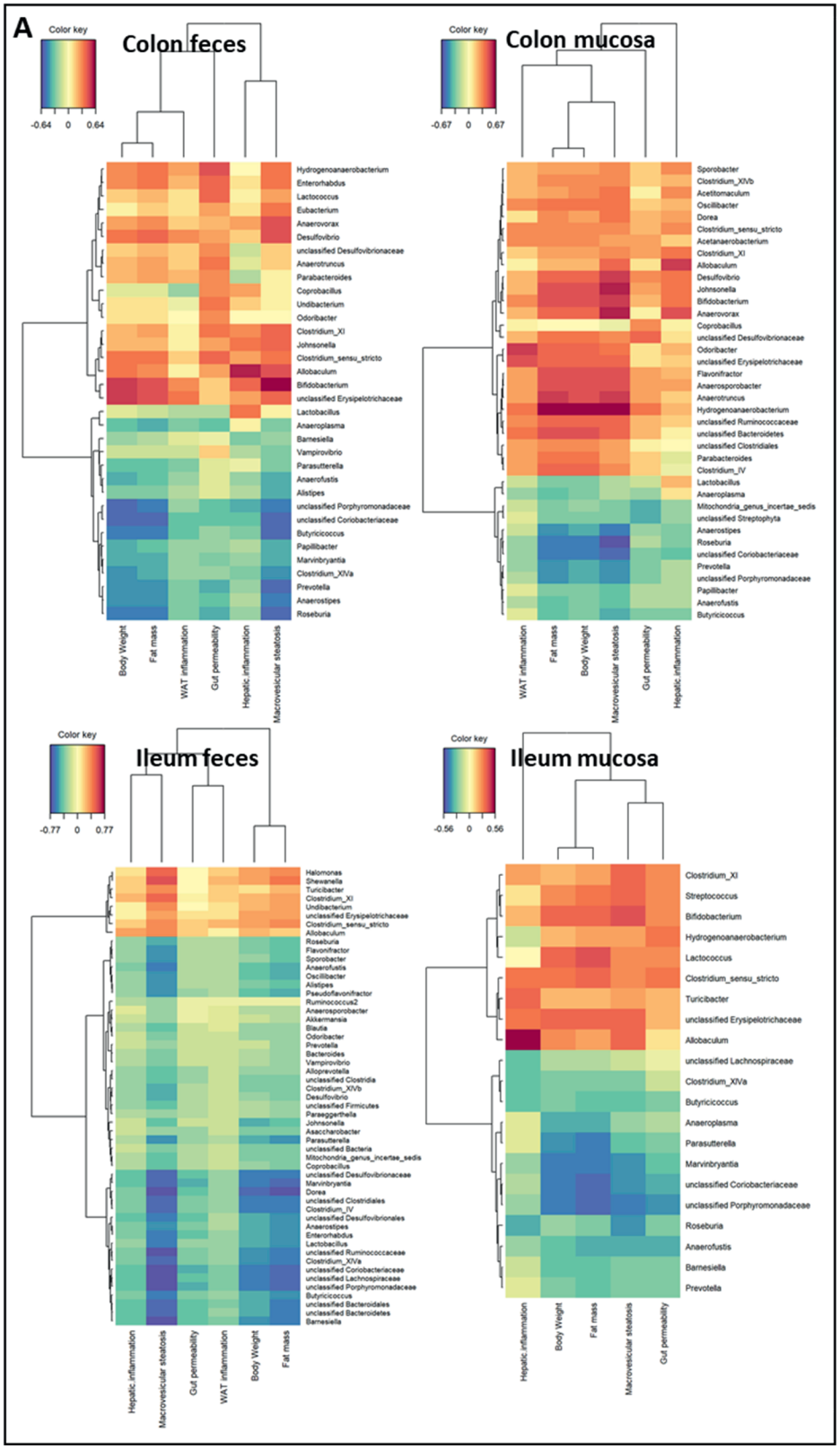
A
Color key
-0.64 0 0.64
Colon feces
Hydrogenoanaerobacterium
Enterorhabdus
Lactococcus
Eubacterium
Anaerovorax
Desulfovibrio
unclassified Desulfovibrionaceae
Anaerotruncus
Parabacteroides
Coprobacillus
Undibacterium
Odoribacter
Clostridium_XI
Johnsonella
Clostridium_sensu_stricto
Allobaculum
Bifidobacterium
unclassified Erysipelotrichaceae
Lactobacillus
Anaeroplasma
Barnesiella
Vampirovibrio
Parasutterella
Anaerofustis
Alistipes
unclassified Porphyromonadaceae
unclassified Coriobacteriaceae
Butyricicoccus
Papillibacter
Marvinbryantia
Clostridium_XIVa
Prevotella
Anaerostipes
Roseburia
Body Weight
Fat mass
WAT inflammation
Gut permeability
Hepatic inflammation
Macrovesicular steatosis
Color key
-0.67 0 0.67
Colon mucosa
Sporobacter
Clostridium_XlVb
Acetitomaculum
Oscillibacter
Dorea
Clostridium_sensu_stricto
Acetanaerobacterium
Clostridium_XI
Allobaculum
Desulfovibrio
Johnsonella
Bifidobacterium
Anaerovorax
Coprobacillus
unclassified Desulfovibrionaceae
Odoribacter
unclassified Erysipelotrichaceae
Flavonifractor
Anaerosporobacter
Anaerotruncus
Hydrogenoanaerobacterium
unclassified Ruminococcaceae
unclassified Bacteroidetes
unclassified Clostridiales
Parabacteroides
Clostridium_IV
Lactobacillus
Anaeroplasma
Mitochondria_genus_incertae_sedis
unclassified Streptophyta
Anaerostipes
Roseburia
unclassified Coriobacteriaceae
Prevotella
unclassified Porphyromonadaceae
Papillibacter
Anaerofustis
Butyricicoccus
WAT inflammation
Fat mass
Body Weight
Macrovesicular steatosis
Gut permeability
Hepatic inflammation
Color key
-0.77 0 0.77
Ileum feces
Halomonas
Shewanella
Turicibacter
Clostridium_XI
Undibacterium
unclassified Erysipelotrichaceae
Clostridium_sensu_stricto
Allobaculum
Roseburia
Flavonifractor
Sporobacter
Anaerofustis
Oscillibacter
Alistipes
Pseudoflavonifractor
Ruminococcus2
Anaerosporobacter
Akkermansia
Blautia
Odoribacter
Prevotella
Bacteroides
Vampirovibrio
Alloprevotella
unclassified Clostridia
Clostridium_XlVb
Desulfovibrio
unclassified Firmicutes
Paraeggerthella
Johnsonella
Asaccharobacter
Parasutterella
unclassified Bacteria
Mitochondria_genus_incertae_sedis
Coprobacillus
unclassified Desulfovibrionaceae
Marvinbryantia
Dorea
unclassified Clostridiales
Clostridium_IV
unclassified Desulfovibrionales
Anaerostipes
Enterorhabdus
Lactobacillus
unclassified Ruminococcaceae
Clostridium_XIVa
unclassified Coriobacteriaceae
unclassified Lachnospiraceae
unclassified Porphyromonadaceae
Butyricicoccus
unclassified Bacteroidales
unclassified Bacteroidetes
Barnesiella
Hepatic inflammation
Macrovesicular steatosis
Gut permeability
WAT inflammation
Body Weight
Fat mass
Color key
-0.56 0 0.56
Ileum mucosa
Clostridium_XI
Streptococcus
Bifidobacterium
Hydrogenoanaerobacterium
Lactococcus
Clostridium_sensu_stricto
Turicibacter
unclassified Erysipelotrichaceae
Allobaculum
unclassified Lachnospiraceae
Clostridium_XIVa
Butyricicoccus
Anaeroplasma
Parasutterella
Marvinbryantia
unclassified Coriobacteriaceae
unclassified Porphyromonadaceae
Roseburia
Anaerofustis
Barnesiella
Prevotella
Hepatic inflammation
Body Weight
Fat mass
Macrovesicular steatosis
Gut permeability

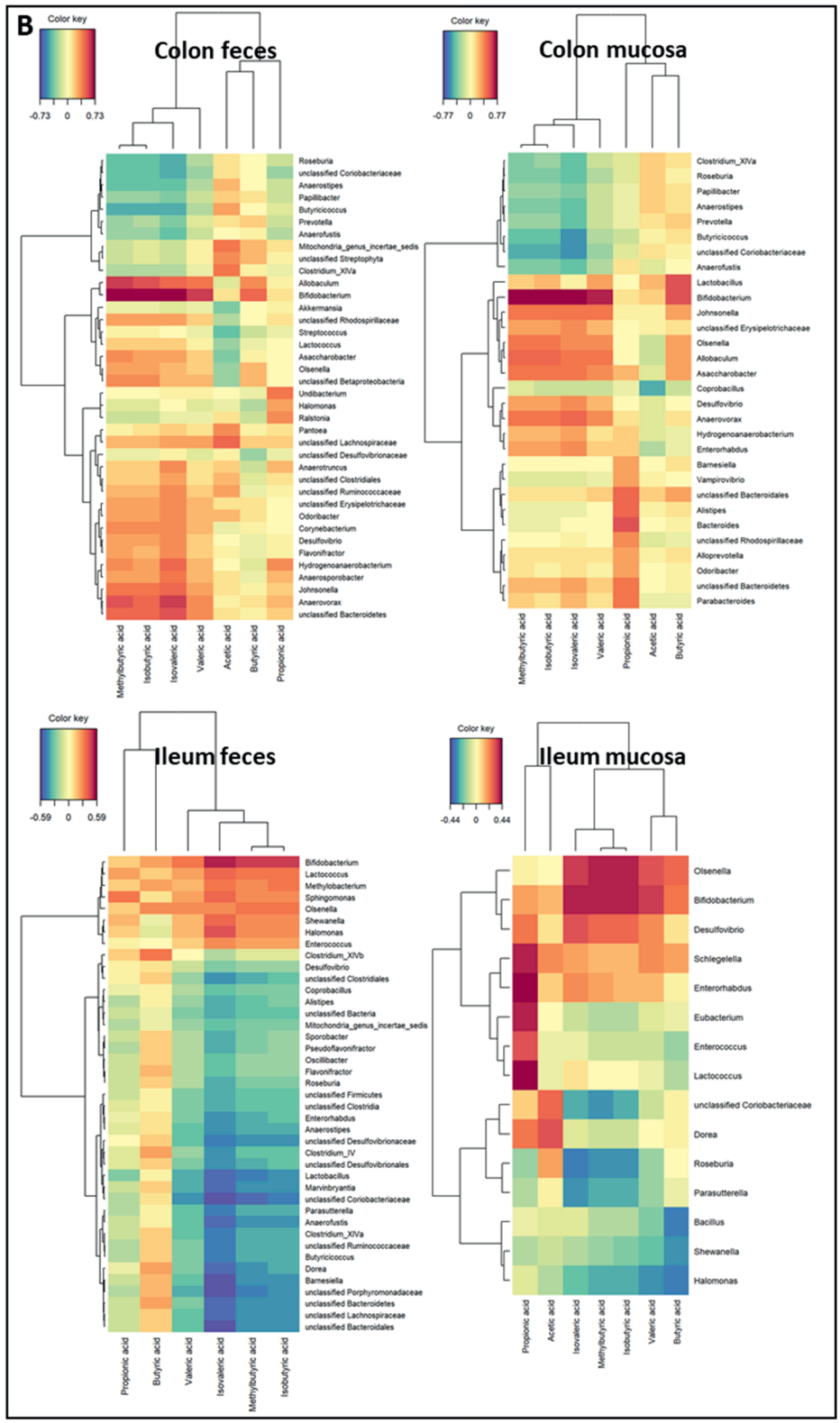
B
Color key
-0.73 0 0.73
Colon feces
Roseburia
unclassified Coriobacteriaceae
Anaerostipes
Papillibacter
Butyricicoccus
Prevotella
Anaerofustis
Mitochondria_genus_incertae_sedis
unclassified Streptophyta
Clostridium_XIVa
Allobaculum
Bifidobacterium
Akkermansia
unclassified Rhodospirillaceae
Streptococcus
Lactococcus
Asaccharobacter
Olsenella
unclassified Betaproteobacteria
Undibacterium
Halomonas
Ralstonia
Pantoea
unclassified Lachnospiraceae
unclassified Desulfovibrionaceae
Anaerotruncus
unclassified Clostridiales
unclassified Ruminococcaceae
unclassified Erysipelotrichaceae
Odoribacter
Corynebacterium
Desulfovibrio
Flavonifractor
Hydrogenoanaerobacterium
Anaerosporobacter
Johnsonella
Anaerovorax
unclassified Bacteroidetes
Methylbutyric acid
Isobutyric acid
Isovaleric acid
Valeric acid
Acetic acid
Butyric acid
Propionic acid
Color key
-0.77 0 0.77
Colon mucosa
Clostridium_XIVa
Roseburia
Papillibacter
Anaerostipes
Prevotella
Butyricicoccus
unclassified Coriobacteriaceae
Anaerofustis
Lactobacillus
Bifidobacterium
Johnsonella
unclassified Erysipelotrichaceae
Olsenella
Allobaculum
Asaccharobacter
Coprobacillus
Desulfovibrio
Anaerovorax
Hydrogenoanaerobacterium
Enterorhabdus
Barnesiella
Vampirovibrio
unclassified Bacteroidales
Alistipes
Bacteroides
unclassified Rhodospirillaceae
Alloprevotella
Odoribacter
unclassified Bacteroidetes
Parabacteroides
Methylbutyric acid
Isobutyric acid
Isovaleric acid
Valeric acid
Propionic acid
Acetic acid
Butyric acid
Color key
-0.59 0 0.59
Ileum feces
Bifidobacterium
Lactococcus
Methylobacterium
Sphingomonas
Olsenella
Shewanella
Halomonas
Enterococcus
Clostridium_XlVb
Desulfovibrio
unclassified Clostridiales
Coprobacillus
Alistipes
unclassified Bacteria
Mitochondria_genus_incertae_sedis
Sporobacter
Pseudoflavonifractor
Oscillibacter
Flavonifractor
Roseburia
unclassified Firmicutes
unclassified Clostridia
Enterorhabdus
Anaerostipes
unclassified Desulfovibrionaceae
Clostridium_IV
unclassified Desulfovibrionales
Lactobacillus
Marvinbryantia
unclassified Coriobacteriaceae
Parasutterella
Anaerofustis
Clostridium_XIVa
unclassified Ruminococcaceae
Butyricicoccus
Dorea
Barnesiella
unclassified Porphyromonadaceae
unclassified Bacteroidetes
unclassified Lachnospiraceae
unclassified Bacteroidales
Propionic acid
Butyric acid
Valeric acid
Isovaleric acid
Methylbutyric acid
Isobutyric acid
Color key
-0.44 0 0.44
Ileum mucosa
Olsenella
Bifidobacterium
Desulfovibrio
Schlegelella
Enterorhabdus
Eubacterium
Enterococcus
Lactococcus
unclassified Coriobacteriaceae
Dorea
Roseburia
Parasutterella
Bacillus
Shewanella
Halomonas
Propionic acid
Acetic acid
Isovaleric acid
Methylbutyric acid
Isobutyric acid
Valeric acid
Butyric acid

Figure 7. *Diet-independent correlations between the microbiota and NAFLD-associated readouts or gut-derived metabolites. Regularized canonical correlation analysis (rCCA analysis) results were visualized in a heat map for positive (red) and negative (blue) correlations between the microbiota composition and (**A**) histological and functional readouts of non-alcoholic fatty liver disease (NAFLD) development or (**B**) gut-derived metabolites for each gut compartment analyzed. Correlations with CV scores >0.03 are shown.*

4. Discussion

The objective of the present study was to investigate whether there are generic changes in specific gut microbial compartments that correlate with metabolic risk factors, organ dysfunction, and NAFLD endpoints, independent of the specific energy-dense diet (ED diet) that was used to induce disease. We demonstrated that all of the ED diets induced obesity and NAFLD during 15 weeks of ED diet feeding, but the severity of liver pathology, WAT dysfunction, and gut dysfunction varied between the individual ED diets. Microbiota composition analysis revealed significant differences between the gut compartments, but not between the ED diets. The diversity of highly abundant bacteria decreased, while the diversity of low-abundant bacteria increased on the ED diets. Independent of the type of ED diet used, we identified correlations between certain bacteria and readouts of metabolic dysfunction and NAFLD development, and correlating bacteria differed per gut compartment. The colon mucosa had the greatest predictive value when compared with the other compartments. Interestingly, plasma levels of SCFAs (isoacids) may function as a possible reflective marker of disease-associated microbiota changes and a less beneficial metabolic state.

We found that all of the ED diets that were used induced NAFLD, but diets differed with respect to the severity of liver pathology that was induced. The pronounced induction of liver inflammation with BF cannot be explained by an increase in caloric intake or gut permeability in this group, because the other ED diets had a comparable caloric intake and developed a similar level of gut permeability. Thus, it is likely that hepatic inflammation in BF is a consequence of the quality of calories, i.e., a macronutrient-mediated effect. One possible explanation may be the difference in the type of carbohydrates in the ED diets; the BF diet only contains fructose, while LS and LS+FW are high in sucrose (i.e., consisting of both fructose and glucose). Furthermore, fructose intake was higher (1.3 g of fructose/day) in animals on the BF diet than in the other ED diet groups (0.5 g/day in LS and 0.9 g/day in LS+FW). Studies have shown that while both fructose and glucose are able to induce hepatic steatosis and steatohepatitis [17], liver injury is typically much worse in fructose-treated mice [17,18], which is in line with the findings herein. Another possible explanation for the pronounced hepatic inflammation observed with BF is the fat source of the diet: BF contains butter fat, while LS and LS+FW contain lard. Butter fat contains more saturated fat than lard, and saturated fatty acids (SFA) have been shown to induce liver inflammation [19,20].

The choice of the diet was made based on previous studies with these diets (unpublished data), and the knowledge that these diets would induce different levels of obesity, adipose tissue inflammation, and NAFLD pathology in this mouse model. Furthermore, many NASH studies use experimental diets that are difficult to translate to human diets, because experimental diets are supplemented with supraphysiological levels

of cholesterol (e.g., 2% *w/w* cholesterol) or experimental diets with extremely high fat content are used (e.g., >50% energy from fat). The diets that were used in this study were not supplemented with dietary cholesterol, and contained a level of dietary fat that can also be found in traditional diets, for instance those of Finland and Greece ([21] and references therein). A recent study showed that the LS diet employed herein results in a plasma metabolome and a liver transcriptome disease profile that recapitulates the metabolome and gene expression profile of NASH patients [13,22], which supports the use of such diets, the more so because more extreme diets did not induce human-like gene expression changes [23].

The NAFLD-inducing ED diets also significantly altered the composition of the microbiota relative to chow. However, the composition within the ED diet groups was very variable, and there was no significant difference between the three ED diets in microbiota composition. These findings may seem unexpected, since dietary macronutrient composition is thought to be a very important determinant of microbiota composition [15,24]. However, earlier studies did not compare the total microbiota composition between diet treatments, but rather focused on specific bacterial changes by macronutrients [25–28]. Other reasons for the absence of significant differences between the ED diets used herein may be a) that not all of the macronutrients were changed (e.g., the protein source was casein in all of the ED diets) and b) that the relative content of each macronutrient (e.g., protein, carbohydrate, fat) was comparable among the ED diets. Consistent with this view, the macronutrient composition of the chow-control diet did markedly differ from the ED diets, and chow-fed mice also had a microbiota that significantly differed from the ED diets.

The diversity of the microbiota was also similarly affected by the three ED diets, with a reduction in the diversity of high abundant bacteria in all of the gut compartments. These findings are consistent with previous findings using high-fat diets in both humans [29,30] and mice [30,31]. Yet, while these studies only focus on the fecal compartment, we now also show that this reduction in diversity also occurs in the mucosal compartments of the ileum and colon. Conversely, we observed an increase in the diversity of low-abundant bacteria. This is in line with studies that focused on microbiota abundance during aging [32,33], which is accompanied by a general decline in health status and metabolic disease development. These studies, together with our observations, indicate that the reduction in diversity of high-abundant bacteria is a generic pattern in all gut compartments during metabolic disease development. Together with an increase in the diversity of low-abundant bacteria, this may serve as an indicator of an unfavorable metabolic state. In addition, we observed that the mucosal microbiota composition was more stable in terms of diversity than the fecal compartment, which may be a consequence of the functional differences between gut compartments [34,35]. The mucosal microbiota is in closer proximity to the gut barrier; therefore, it is assumed that these bacteria (and their metabolites) are in more direct contact with the host than the fecal microbiota [36].

A strength of this study is that we used three different NAFLD-inducing ED diets, allowing us to study correlations between the microbiota and NAFLD that are not dependent on one specific disease-inducing diet. We found that there are correlations

between the microbiota and readouts of metabolic dysfunction and NAFLD development, which were strongest for the colon mucosa. Remarkably, we observed a strong positive correlation of *Bifidobacterium* with NAFLD-associated readouts, suggesting an adverse role. The observed positive correlation between *Bifidobacterium* and NAFLD endpoints may be related to specific strains of *Bifidobacterium*, as shown by Yin et al. [37] in a rat model of HFD obesity. The authors found that body weight development upon *Bifidobacterium* treatment is strain-dependent, suggesting that different strains may affect energy metabolism and fat distribution in a different way. Furthermore, an open label pilot trial in adult human subjects with NAFLD (*n* = four) showed that participants treated with the probiotic VSL#3 (which also contains *Bifidobacterium*) experienced a significant increase in liver fat after four months, and this was reversed in three subjects after washout [38]. The authors concluded that the results of this trial did not support their hypothesis (probiotics would reduce hepatic steatosis in humans). Notably, the effect of HFD on *Bifidobacterium* abundance also varies among studies, because some studies report an increased abundance upon HFD feeding [25], while others report a reduction in its abundance [30,39]. Similarly, the role of *Lactobacillus* is unclear: Jiang et al. showed that the abundance of *Lactobacillus* was increased in the microbiota of NAFLD patients [40], suggesting a role in disease development, whereas probiotic treatment with *Lactobacillus* has been associated with beneficial effects in clinical NAFLD trials [6]. Hence, associative findings should be treated with caution, and even correlations should be interpreted carefully. The positive correlations between bacteria and endpoints on the genera level that were observed in our study indicate a tight relationship between gut microbiota and NAFLD development, yet follow-up intervention studies with specific species (e.g., *Bifidobacterium* strains as in Yin et al. [37]) are necessary to define the disease-augmenting or disease-attenuating role of particular bacteria to demonstrate their causal role. It is possible that the composition of bacterial species that underlie a correlation on genera level may change in response to an intervention (and remain unnoticed on genera level), but may result in an altered production of metabolites and altered gut functioning.

We found that increased gut permeability positively correlated with higher levels of the *Hydrogenoanaerobacterium* in the colon feces and mucosa. In this study, we measured gut permeability after four hours of fasting, which is a time span that mainly reflects colonic permeability based on time-resolved analyses with the tracer (FD4) used herein [41]. Associations between gut permeability and *Hydrogenoanaerobacterium* have not been reported before. However, *Hydrogenoanaerobacterium* is increased in fecal microbiota in both obese mice [42] and humans [43], which is consistent with our findings.

Interestingly, our correlation analyses revealed that bacteria that were positively correlated with disease-associated readouts were also strongly positively correlated with the isoacid SCFAs (isobutyrate, methylbutyrate, isovalerate, and valerate) of which physiological effects have hardly been investigated so far. Isoacids are a product of protein fermentation by the microbiota, for which branched-chain amino acids (positively associated with insulin resistance and metabolic disease development [44,45]) are one of the sources to synthesize them [46]. Hence, the elevated plasma isoacids levels that were

observed herein may indicate enhanced protein fermentation, which is associated with the production of potential toxic by-products, and has been linked to intestinal disease [47,48].

Taken together, this first systematic analysis of different gut microbial compartments demonstrates with three different ED diets that a limited group of bacteria correlates with NAFLD endpoints. The comprehensive analysis of multiple gut compartments indicates that the colon mucosa may have added value above other compartments when it comes to prediction of the metabolic health state of organs such as the liver. Lastly, generic changes were observed in all of the compartments regarding microbiota diversity and changes in plasma SCFAs (isoacids), which may be used as a marker of the metabolic state.

Acknowledgments: We would like to thank Marijke Voskuilen, Anne Schwerk and Martien Caspers for their excellent technical assistance.

References

1. Estes, C.; Anstee, Q.M.; Arias-Loste, M.T.; Bantel, H.; Bellentani, S.; Caballeria, J.; Colombo, M.; Craxi, A.; Crespo, J.; Day, C.P.; et al. Modeling NAFLD disease burden in China, France, Germany, Italy, Japan, Spain, United Kingdom, and United States for the period 2016–2030. *J. Hepatol.* **2018**, doi:10.1016/j.jhep.2018.05.036.
2. Abdelmalek, M.; Suzuki, A.; Guy, C.; Unalp-Arida, A.; Colvin, R.; Johnson, R. D.A. Increased fructose consumption is associated with fibrosis severity in patients with nonalcoholic fatty liver disease. *Hepatology* **2011**, *51*, 1961–1971, doi:10.1002/hep.23535.INCREASED.
3. Jang, C.; Hui, S.; Lu, W.; Cowan, A.J.; Morscher, R.J.; Lee, G.; Liu, W.; Tesz, G.J.; Birnbaum, M.J.; Rabinowitz, J.D. The Small Intestine Converts Dietary Fructose into Glucose and Organic Acids. *Cell Metab.* **2018**, *27*, 351–361, doi:10.1016/j.cmet.2017.12.016.
4. Mulder, P.; Morrison, M.C.; Wielinga, P.Y.; Van Duyvenvoorde, W.; Kooistra, T.; Kleemann, R. Surgical removal of inflamed epididymal white adipose tissue attenuates the development of non-alcoholic steatohepatitis in obesity. *Int. J. Obes.* **2016**, *40*, 675–684, doi:10.1038/ijo.2015.226.
5. Boursier, J.; Mueller, O.; Barret, M.; Machado, M.; Fizanne, L.; Araujo-Perez, F.; Guy, C.D.; Seed, P.C.; Rawls, J.F.; David, L.A.; et al. The severity of nonalcoholic fatty liver disease is associated with gut dysbiosis and shift in the metabolic function of the gut microbiota. *Hepatology* **2016**, *63*, 764–775, doi:10.1002/hep.28356.
6. Altamirano-Barrera, A.; Uribe, M.; Chávez-Tapia, N.C.; Nuño-Lámbarri, N. The role of the gut microbiota in the pathology and prevention of liver disease. *J. Nutr. Biochem.* **2018**, *60*, 1–8, doi:10.1016/j.jnutbio.2018.03.006.
7. Boursier, J.; Diehl, A.M. Nonalcoholic Fatty Liver Disease and the Gut Microbiome. *Clin. Liver Dis.* **2016**, *20*, 263–275, doi:10.1016/j.cld.2015.10.012.
8. Lonardo, A.; Nascimbeni, F.; Targher, G.; Bernardi, M.; Bonino, F.; Bugianesi, E.; Casini, A.; Gastaldelli, A.; Marchesini, G.; Marra, F.; et al. AISF position paper on nonalcoholic fatty liver disease (NAFLD): Updates and future directions. *Dig. Liver Dis.* **2017**, *49*, 471–483, doi:10.1016/j.dld.2017.01.147.
9. Korpela, K. Diet, Microbiota, and Metabolic Health: Trade-Off Between Saccharolytic and Proteolytic Fermentation. *Annu. Rev. Food Sci. Technol.* **2018**, *9*, doi:10.1146/annurev-food-030117-012830.
10. Aron-Wisnewsky, J.; Doré, J.; Clement, K. The importance of the gut microbiota after bariatric surgery. *Nat. Rev. Gastroenterol. Hepatol.* **2012**, *9*, 590–598, doi:10.1038/nrgastro.2012.161.
11. Rangel, I; Sundin, J.; Fuentes, S.; Repsilber, D.; de Vos, W.M.; Brummer, R.J. The relationship between faecal-associated and mucosal-associated microbiota in irritable bowel syndrome patients and healthy subjects. *Aliment. Pharmacol. Ther*. **2015**, *42*, 1211–1221, doi:10.1111/apt.13399.
12. Liang, W.; Menke, A.L.; Driessen, A.; Koek, G.H.; Lindeman, J.H.; Stoop, R.; Havekes, L.M.; Kleemann, R.; van den Hoek, A.M. Establishment of a general NAFLD scoring system for rodent models and comparison to human liver pathology. *PLoS ONE* **2014**,

9, doi:10.1371/journal.pone.0115922.

13. Morrison, M.C.; Kleemann, R.; van Koppen, A.; Hanemaaijer, R.; Verschuren, L. Key inflammatory processes in human NASH are reflected in Ldlr$^{-/-}$.Leiden mice: A translational gene profiling study. *Front. Physiol.* **2018**, *9*, doi:10.3389/fphys.2018.00132.
14. van Koppen, A.; Verschuren, L.; van den Hoek, A.M.; Verheij, J.; Morrison, M.C.; Li, K.; Nagabukuro, H.; Costessi, A.; Caspers, M.P.; van den Broek, T.J.; et al. Uncovering a Predictive Molecular Signature for the Onset of NASH-Related Fibrosis in a Translational NASH Mouse Model. *CMGH* **2018**, *5*, 83–98, doi:10.1016/j.jcmgh.2017.10.001.
15. Graf, D.; Di Cagno, R.; Fåk, F.; Flint, H.J.; Nyman, M.; Saarela, M.; Watzl, B. Contribution of diet to the composition of the human gut microbiota. *Microb. Ecol. Health Dis.* **2015**, *26*, 1–11, doi:10.3402/mehd.v26.26164.
16. den Besten, G.; van Eunen, K.; Groen, A.K.; Venema, K.; Reijngoud, D.-J.; Bakker, B.M. The role of short-chain fatty acids in the interplay between diet, gut microbiota, and host energy metabolism. *J. Lipid Res.* **2013**, *54*, 2325–2340, doi:10.1194/jlr.R036012.
17. Pickens, M.K.; Ogata, H.; Soon, R.K.; Grenert, J.P.; Maher, J.J. Dietary fructose exacerbates hepatocellular injury when incorporated into a methionine-choline-deficient diet. *Liver Int.* **2010**, *30*, 1229–1239, doi:10.1111/j.1478-3231.2010.02285.x.
18. Ishimoto, T.; Lanaspa, M.A.; Rivard, C.J.; Roncal-Jimenez, C.A.; Orlicky, D.J.; Cicerchi, C.; McMahan, R.H.; Abdelmalek, M.F.; Rosen, H.R.; Jackman, M.R.; et al. High-fat and high-sucrose (western) diet induces steatohepatitis that is dependent on fructokinase. *Hepatology* **2013**, *58*, 1632–1643, doi:10.1002/hep.26594.
19. Morrison, M.C.; Mulder, P.; Stavro, P.M.; Suárez, M.; Arola-Arnal, A.; Van Duyvenvoorde, W.; Kooistra, T.; Wielinga, P.Y.; Kleemann, R. Replacement of dietary saturated fat by PUFA-rich pumpkin seed oil attenuates non-alcoholic fatty liver disease and atherosclerosis development, with additional health effects of virgin over refined oil. *PLoS ONE* **2015**, doi:10.1371/journal.pone.0139196.
20. Kiziltas, S. Toll-like receptors in pathophysiology of liver diseases. *World J. Hepatol.* **2016**, *8*, 1354–1369, doi:10.4254/wjh.v8.i32.1354.
21. Liang, W.; Lindeman, J.H.; Menke, A.L.; Koonen, D.P.; Morrison, M.; Havekes, L.M.; Van Den Hoek, A.M.; Kleemann, R. Metabolically induced liver inflammation leads to NASH and differs from LPS-or IL-1β-induced chronic inflammation. *Lab. Investig.* **2014**, *94*, 491–502, doi:10.1038/labinvest.2014.11.
22. Morrison, M.C.; Verschuren, L.; Salic, K.; Verheij, J.; Menke, A.; Wielinga, P.Y.; Iruarrizaga-Lejarreta, M.; Gole, L.; Yu, W.M.; Turner, S.; et al. Obeticholic Acid Modulates Serum Metabolites and Gene Signatures Characteristic of Human NASH and Attenuates Inflammation and Fibrosis Progression in Ldlr$^{-/-}$.Leiden Mice. *Hepatol. Commun.* **2018**, doi:10.1002/hep4.1270/suppinfo.
23. Teufel, A.; Itzel, T.; Erhart, W.; Brosch, M.; Wang, X.Y.; Kim, Y.O.; von Schönfels, W.; Herrmann, A.; Brückner, S.; Stickel, F.; Dufour, J.F. Comparison of Gene Expression Patterns Between Mouse Models of Nonalcoholic Fatty Liver Disease and Liver Tissues From Patients. *Gastroenterology* **2016**, doi:10.1053/j.gastro.2016.05.051.

24. Tidjani Alou, M.; Lagier, J.C.; Raoult, D. Diet influence on the gut microbiota and dysbiosis related to nutritional disorders. *Hum. Microbiome J.* **2016**, *1*, 3–11, doi:10.1016/j.humic.2016.09.001.
25. Neyrinck, A.M.; Possemiers, S.; Druart, C.; Van de Wiele, T.; De Backer, F.; Cani, P.D.; Larondelle, Y.; Delzenne, N.M. Prebiotic effects of wheat Arabinoxylan related to the increase in bifidobacteria, roseburia and bacteroides/prevotella in diet-induced obese mice. *PLoS ONE* **2011**, doi:10.1371/journal.pone.0020944.
26. Brinkworth, G.D.; Noakes, M.; Clifton, P.M.; Bird, A.R. Comparative effects of very low-carbohydrate, high-fat and high-carbohydrate, low-fat weight-loss diets on bowel habit and faecal short-chain fatty acids and bacterial populations. *Br. J. Nutr.* **2009**, doi:10.1017/S0007114508094658.
27. Russell, W.R.; Gratz, S.W.; Duncan, S.H.; Holtrop, G.; Ince, J.; Scobbie, L.; Duncan, G.; Johnstone, A.M.; Lobley, G.E.; Wallace, R.J.; et al. High-protein, reduced-carbohydrate weight-loss diets promote metabolite profiles likely to be detrimental to colonic health. *Am. J. Clin. Nutr.* **2011**, doi:10.3945/ajcn.110.002188.
28. Aguirre, M.; Eck, A.; Koenen, M.E.; Savelkoul PHM, Budding, A.E.; Venema, K. Diet drives quick changes in the metabolic activity and composition of human gut microbiota in a validated in vitro gut model. *Res. Microbiol.* **2016**, doi:10.1016/j.resmic.2015.09.006.
29. David, L.A.; Maurice, C.F.; Carmody, R.N.; Gootenberg, D.B.; Button, J.E.; Wolfe, B.E.; Ling, A.V.; Devlin, A.S.; Varma, Y.; Fischbach, M.A.; et al. Diet rapidly and reproducibly alters the human gut microbiome. *Nature* **2014**, *505*, 559–563, doi:10.1038/nature12820.
30. Mulders, R.J.; de Git, K.C.G.; Schéle, E.; Dickson, S.L.; Sanz, Y.; Adan, R.A.H. Microbiota in obesity: Interactions with enteroendocrine, immune and central nervous systems. *Obes. Rev.* **2018**, doi:10.1111/obr.12661.
31. De Wit, N.; Derrien, M.; Bosch-Vermeulen, H.; Oosterink, E.; Keshtkar, S.; Duval, C.; de Vogel-van den Bosch, J.; Kleerebezem, M.; Müller, M.; van der Meer, R. Saturated fat stimulates obesity and hepatic steatosis and affects gut microbiota composition by an enhanced overflow of dietary fat to the distal intestine. *AJP Gastrointest. Liver Physiol*. 2012, 303, G589–99, doi:10.1152/ajpgi.00488.2011.
32. Vaiserman, A.M.; Koliada, A.K.; Marotta, F. Gut microbiota: A player in aging and a target for anti-aging intervention. *Ageing Res. Rev.* **2017**, *35*, 36–45, doi:10.1016/j.arr.2017.01.001.
33. O'Toole, P.W.; Jeffery, I.B. Gut microbiota and aging. *Science* **2015**, *350*, 1214–1215, doi:10.1126/science.aac8469.
34. Cornick, S.; Tawiah, A.; Chadee, K. Roles and regulation of the mucus barrier in the gut. *Tissue Barriers* **2015**, doi:10.4161/21688370.2014.982426.
35. Li, H.; Limenitakis, J.P.; Fuhrer, T.; Geuking, M.B.; Lawson, M.A.; Wyss, M.; Brugiroux, S.; Keller, I.; Macpherson, J.A.; Rupp, S.; et al. The outer mucus layer hosts a distinct intestinal microbial niche. *Nat. Commun.* **2015**, *6*, doi:10.1038/ncomms9292.
36. Tang, M.S.; Poles, J.; Leung, J.M.; Wolff, M.J.; Davenport, M.; Lee, S.C.; Lim, Y.A.; Chua, K.H.; Loke, P.N.; Cho, I. Inferred metagenomic comparison of mucosal and fecal

microbiota from individuals undergoing routine screening colonoscopy reveals similar differences observed during active inflammation. *Gut Microbes* **2015**, doi:10.1080/19490976.2014.1000080.

37. Yin, Y.N.; Yu, Q.F.; Fu, N.; Liu, X.W.; Lu, F.G. Effects of four Bifidobacteria on obesity in high-fat diet induced rats. *World J. Gastroenterol.* **2010**, doi:10.3748/wjg.v16.i27.3394.
38. Solga, S.F.; Buckley, G.; Clark, J.M.; Horska, A.; Diehl, A.M. The effect of a probiotic on hepatic steatosis. *J. Clin. Gastroenterol.* **2008**, *42*, 1117–1119, doi:10.1097/MCG.0b013e31816d920c.
39. Liu, Y.; Gibson, G.R.; Walton, G.E. Impact of high fat diets, prebiotics and probiotics on gut microbiota and immune function, with relevance to elderly populations. *Nutr. Aging* **2016**, *3*, 171–192, doi:10.3233/NUA-150058.
40. Jiang, W.; Wu, N.; Wang, X.; Chi, Y.; Zhang, Y.; Qiu, X.; Hu, Y.; Li, J.; Liu, Y. Dysbiosis gut microbiota associated with inflammation and impaired mucosal immune function in intestine of humans with non-alcoholic fatty liver disease. *Sci. Rep.* **2015**, doi:10.1038/srep08096.
41. Woting, A.; Blaut, M. Small Intestinal Permeability and Gut-Transit Time. *Nutrients* **2018**, *10*, 685, doi:10.3390/nu10060685.
42. Jung, M.J.; Lee, J.; Shin, N.R.; Kim, M.S.; Hyun, D.W.; Yun, J.H.; Kim, P.S.; Whon, T.W.; Bae, J.W. Chronic Repression of mTOR Complex 2 Induces Changes in the Gut Microbiota of Diet-induced Obese Mice. *Sci. Rep.* **2016**, doi:10.1038/srep30887.
43. Mathur, R.; Amichai, M.; Chua, K.S.; Mirocha, J.; Barlow, G.M.; Pimentel, M. Methane and hydrogen positivity on breath test is associated with greater body mass index and body fat. *J. Clin. Endocrinol. Metab.* **2013**, doi:10.1210/jc.2012-3144.
44. Boursier, J.; Diehl AM a. Implication of gut microbiota in nonalcoholic fatty liver disease. *PLoS Pathog.* **2015**, *11*, e1004559, doi:10.1371/journal.ppat.1004559.
45. Newgard, C.B. Interplay between lipids and branched-chain amino acids in development of insulin resistance. *Cell Metab.* **2012**, *15*, 606–614, doi:10.1016/j.cmet.2012.01.024.
46. Beck, H.C. Branched-chain fatty acid biosynthesis in a branched-chain amino acid aminotransferase mutant of Staphylococcus carnosus. *FEMS Microbiol. Lett.* **2005**, doi:10.1016/j.femsle.2004.11.041.
47. Windey, K.; de Preter, V.; Verbeke, K. Relevance of protein fermentation to gut health. *Mol. Nutr. Food Res.* **2012**, *56*, 184–196, doi:10.1002/mnfr.201100542.
48. Jakobsdottir, G.; Bjerregaard, J.H.; Skovbjerg, H.; Nyman, M. Fasting serum concentration of short-chain fatty acids in subjects with microscopic colitis and celiac disease: No difference compared with controls, but between genders. *Scand. J. Gastroenterol.* **2013**, doi:10.3109/00365521.2013.786128.
49. Kleiner, D.E.; Brunt, E.M. Nonalcoholic fatty liver disease: Pathologic patterns and biopsy evaluation in clinical research. *Semin. Liver Dis.* **2012**, *32*, 3–13, doi:10.1055/s-0032-1306421.
50. Schoemaker, M.H.; Kleemann, R.; Morrison, M.C.; Verheij, J.; Salic, K.; van Tol, E.A.; Kooistra, T.; Wielinga, P.Y. A casein hydrolysate based formulation attenuates obesity

and associated nonalcoholic fatty liver disease and atherosclerosis in Ldlr$^{-/-}$.Leiden mice. *PLoS ONE* **2017**, *12*, doi:10.1371/journal.pone.0180648.
51. Nejdfors, P.; Ekelund, M. Intestinal permeability in humans is increased after radiation therapy 2000.
52. Patel, R.M.; Myers, L.S.; Kurundkar, A.R.; Maheshwari, A.; Nusrat, A.; Lin, P.W. Probiotic bacteria induce maturation of intestinal claudin 3 expression and barrier function. *Am. J. Pathol.* **2012**, *180*, 626–635, doi:10.1016/j.ajpath.2011.10.025.
53. Dong, C.X.; Zhao, W.; Solomon, C.; Rowland, K.J.; Ackerley, C.; Robine, S.; Holzenberger, M.; Gonska, T.; Brubaker, P.L. The intestinal epithelial insulin-like growth factor-1 receptor links glucagon-like peptide-2 action to gut barrier function. *Endocrinology* **2014**, *155*, 370–379, doi:10.1210/en.2013-1871.
54. Wang, Q.; Garrity, G.M.; Tiedje, J.M.; Cole, J.R. Naïve Bayesian classifier for rapid assignment of rRNA sequences into the new bacterial taxonomy. *Appl. Environ. Microbiol.* **2007**, *73*, 5261–5267, doi:10.1128/AEM.00062-07.
55. McMurdie, P.J.; Holmes, S. Phyloseq: An R Package for Reproducible Interactive Analysis and Graphics of Microbiome Census Data. *PLoS ONE* **2013**, *8*, doi:10.1371/journal.pone.0061217.
56. Love, M.I.; Huber, W.; Anders, S. Moderated estimation of fold change and dispersion for RNA-seq data with DESeq2. *Genome Biol.* **2014**, *15*, doi:10.1186/s13059-014-0550-8.
57. Oksanen, J. *Vegan: Community Ecology Package*, Version 1.17-2; R Package 2010. Available online: http://cran.r-project.org (accessed on 7 May 2018).
58. Friedman, J.H.; Rafsky, L.C. Multivariate Generalizations of the Wald-Wolfowitz and Smirnov Two-Sample Tests. *Ann. Stat.* **1979**, *7*, 697–717, doi:10.1214/aos/1176344722.
59. Schilling, M.F. Multivariate two-sample tests based on nearest neighbors. *J. Am. Stat. Assoc.* **1986**, *81*, 799–806, doi:10.1080/01621459.1986.10478337.
60. Methods, B.; Tests, P. Bootstrap Methods and Permutation Tests. *Introd. Pract. Stat.* **2005**, *5*, 1–70.
61. Fukuyama, J.; Holmes, S. phyloseqGraphTest: Graph-Based Permutation Tests for Microbiome Data. R Package Version 0.0.2. 2018. Available online: https://cran.r-project.org/package=phyloseqGraphTest (accessed on 7 May 2018).
62. Rencher, A.C. Canonical Correlation. *Methods Multivar. Anal.* **2003**, 361–379, doi:10.1002/0471271357.ch11.
63. Lê Cao, González, I. KA, Déjean, S. MixOmics: Omics Data Integration Project. 2011. Available online: http://www. math. univ-toulouse. fr/~ biostat/mixOmics (accessed on 7 May 2018).

Supplementary information

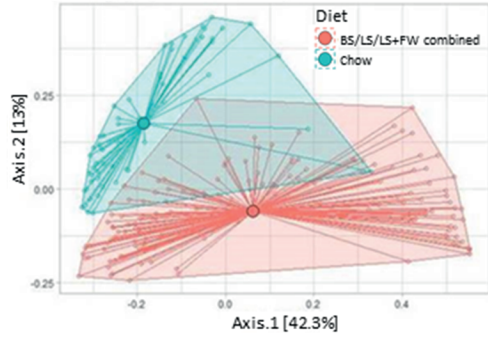

Figure S1. Microbiota composition of chow differs from the ED diets. Permutation tests were used to calculate statistical differences in microbiome composition and group distances were visualized between chow and all ED diets.

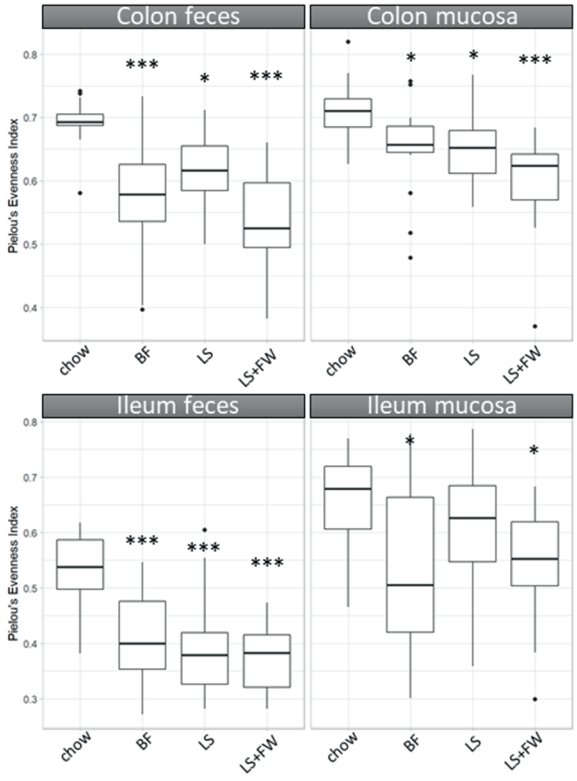

Figure S2. All ED diets reduced species evenness in all gut compartments. 16S rRNA gene sequencing analysis was performed on the luminal and mucosal contents of both the ileum and colon and was used to calculate Pielou's Evenness Index. Data are presented as mean ± SD,*p≤0.05 or **p≤0.01 or ***p≤0.001 compared to chow.

CHAPTER

7

The human milk oligosaccharide 2'-fucosyllactose alleviates liver steatosis, ER stress and insulin resistance by reducing hepatic diacylglycerols and improved gut permeability in obese Ldlr- /-.Leiden mice

Eveline Gart, Kanita Salic, Martine C. Morrison, Martin Giera, Joline Attema, Christa de Ruiter, Martien Caspers, Frank Schuren, Ivana Bobeldijk-Pastorova, Marianne Heer, Yan Qin and Robert Kleemann

Front Nutr. 2022 Jun 17;9:904740.
doi: 10.3389/fnut.2022.904740. PMID: 35782914; PMCID: PMC9248376.

Abstract

Non-alcoholic fatty liver disease (NAFLD) is a complex multifactorial disorder that is associated with gut dysbiosis, enhanced gut permeability, adiposity and insulin resistance. Prebiotics such as human milk oligosaccharide 2'-fucosyllactose are thought to primarily improve gut health and it is uncertain whether they would affect more distant organs. This study investigates whether 2'-fucosyllactose can alleviate NAFLD development in manifest obesity. Obese hyperinsulinemic Ldlr-/-.Leiden mice, after an 8 week run-in on a high-fat diet (HFD), were treated with 2'-fucosyllactose by oral gavage until week 28 and compared to HFD-vehicle controls. 2'-fucosyllactose did not affect food intake, body weight, total fat mass or plasma lipids, but significantly decreased circulating pro-inflammatory factor MCP-1/CCL2. 2'-fucosyllactose altered the fecal microbiota composition which was paralleled by a suppression of HFD-induced gut permeability at t=12 weeks. 2'-fucosyllactose significantly attenuated the development of NAFLD by reducing microvesicular steatosis. These hepatoprotective effects were supported by upstream regulator analyses showing that 2'-fucosyllactose activated ACOX1 (involved in lipid catabolism), while deactivating SREBF1 (involved in lipogenesis). Furthermore, 2'-fucosyllactose suppressed ATF4, ATF6, ERN1, and NUPR1 all of which participate in endoplasmic reticulum stress. 2'-fucosyllactose reduced fasting insulin concentrations and HOMA-IR, which was corroborated by decreased intrahepatic diacylglycerols. In conclusion, long-term supplementation with 2'-fucosyllactose can counteract the detrimental effects of HFD on gut dysbiosis and gut permeability and attenuates the development of liver steatosis. The observed reduction in intrahepatic diacylglycerols provides a mechanistic rationale for the improvement of hyperinsulinemia and supports the use of 2'-fucosyllactose to correct dysmetabolism and insulin resistance.

Graphical abstract

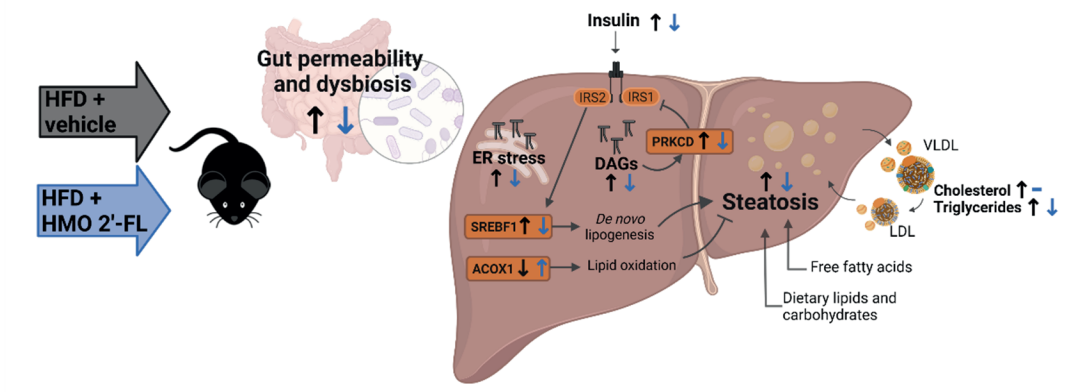

1. Introduction

Increased energy intake, particularly from diets rich in sucrose and saturated fat, leads to the development of obesity which is frequently associated with intrahepatic lipid accumulation (steatosis), an early hallmark of non-alcoholic fatty liver disease (NAFLD) [1]. NAFLD is a complex multifactorial disorder that is linked to microbial dysbiosis, gut permeability, and insulin resistance (IR) [1], all of which are considered to be drivers of disease progression. In the liver, triacylglycerols (TAGs) start to accumulate when the rates of hepatic lipid uptake and production exceed the rates of lipid oxidation and export (via VLDL particles). Insulin resistance is accompanied by hyperinsulinemia, which can drive hepatic lipid accumulation by stimulating *de novo* lipogenesis via the transcriptional master regulator SREBP1c [2]. At the same time, specific lipids may build up in the liver, which can exacerbate hepatic IR thereby creating a vicious circle [3]. Critical molecules that directly participate in the development of insulin resistance at tissue level are lipids such as diacylglycerols (DAGs), which are intermediate products of triacylglycerols (TAGs) synthesis [3]. In contrast to TAGs – which are considered to be a safe storage form of lipids – DAGs are bioactive lipids that have been shown to directly interfere in insulin signaling. Conversely, treatments that lower DAGs can improve IR [3].

Prebiotics are nondigestible food ingredients such as complex oligosaccharides [4]. It is thought that these nondigestible oligosaccharides can provide a health benefit to the host by promoting the growth or activity of specific microorganisms in the gut, for instance by stimulating the growth of Bifidobacterium genera [5]. A recent meta-analysis showed that treatment with prebiotics can improve liver integrity markers such as ALT in NAFLD patients, suggesting an effect of prebiotics beyond the gut on the liver, which plays an essential role in whole-body metabolism [6]. 2'-fucosyllactose (2'-FL) is the most prevalent human milk oligosaccharide (HMO) present in human breast milk, and has been reported to protect against pathogens [7]. Furthermore, it can stimulate the growth of beneficial gut bacteria [8] and attenuate ethanol-induced liver damage in a rodent model [9]. Putative effects of HMO 2'-FL on NAFLD have not been studied so far, and it is unknown whether 2'-FL can reduce NAFLD pathology development in a therapeutic setting, i.e. when obesity, dyslipidemia (high VLDL/LDL) and hyperinsulinemia are already manifest at the start of 2'-FL supplementation.

To study the putative hepatoprotective effects of HMO 2'-FL under conditions of hyperinsulinemia, dyslipidemia and obesity we used Ldlr-/-.Leiden mice, a high fat diet (HFD)-inducible model of NAFLD/NASH that recapitulates phenotypical and molecular disease profiles of NAFLD patients [10–12]. After a run-in of 8 weeks on HFD, obese hyperinsulinemic mice received 2'-FL by oral gavage and were compared to HFD-control mice receiving saline. After a total treatment period of 20 weeks, liver histology was studied in conjunction with lipidomics and transcriptomics to gain insight into the metabolic processes that are affected in the liver.

2. Materials and Methods

2.1 Animal experiment

Male Ldlr-/-.Leiden mice were bred and housed in the American Association for Accreditation of Laboratory Animal Care (AAALAC)-accredited animal facility at TNO (Leiden, the Netherlands). They were group-housed (four to five mice per cage) in Macrolon type 2L cages in a clean-conventional animal room (relative humidity 55 ± 10, temperature 20-24°C, light cycle 07:00 to 19:00) with ad libitum access to food and water. To induce obesity, mice were fed a HFD (D12451, Research Diets Inc., New Brunswick, USA; containing 20 kcal% protein, 35 kcal% carbohydrate, 45 kcal% mainly from lard fat) as reported previously [13] and mice on standard rodent chow (Sniff-R/M-V1530, Uden, the Netherlands) were used as a reference.

After a run-in of 8 weeks on HFD, obese hyperinsulinemic mice were matched into 2 groups based on body weight, blood glucose, plasma cholesterol and triglycerides concentrations. One group of mice was treated with 2'-fucosyllactose (2'-FL) by oral gavage twice daily (750 mg/kg/day) until week 28, and compared with the HFD + vehicle controls receiving twice daily oral saline (n=18/group). An experimental outline is provided in Figure 1. Blood samples, gut permeability (by FD4 tests) and body composition (by EchoMRI) were longitudinally analyzed during the study. Fecal samples were collected from individual mice for 16S microbiota profiling. Mice were terminated in week 28 by gradual-fill CO_2 asphyxiation. At sacrifice, livers and other organs were isolated and immediately snap-frozen in liquid N_2 and/or fixed in formalin as previously described [14].

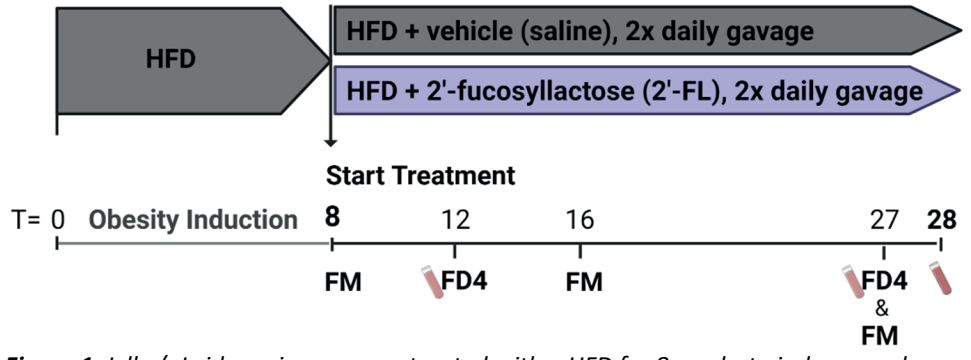

Figure 1: *Ldlr-/-.Leiden mice were pretreated with a HFD for 8 weeks to induce an obese phenotype with hyperinsulinemia. These mice were then divided into 2 groups. One group of mice was treated with 2'-fucosyllactose (2'-FL) by oral gavage twice daily (750 mg/kg/day) until week 28, and subsequently compared with HFD + vehicle control mice receiving twice daily saline (n=18/group). At week 8, 16 and 27 feces were collected for 16S microbiota profiling (fecal microbiota; FM). Blood samples were taken at week 12 and 27 for gut permeability measurements (FD4) and in week 28 sacrifice plasma was collected.*

2.2 Gut permeability and microbiota composition analysis

An *in vivo* FD4 assay was used to measure functional gut permeability as described previously [15]. In short, plasma concentrations of FITC-labeled dextran (three to five kDa FD4; Sigma, St. Louis, MO, USA) were determined after 4 hours of FD4 administration via oral gavage, indicative of paracellular permeability of the intestinal barrier.

Feces were collected from individual mice in week 8 (pre-treatment), as well as at t=16 weeks and t=27 weeks. These fecal samples were mechanically homogenized and genomic DNA was isolated using the AGOWA Mag mini kit (DNA Isolation Kit, AGOWA, Berlin, Germany) according to the manufacturer's instructions. Microbiota composition was determined using an established PCR-based amplification method of the hypervariable region V4 a fragment of 16S rRNA as described previously [14]. Subsequent bioinformatical analyses of the dynamical changes in microbiota composition and the microorganisms (on genera level) were analyzed over time as detailed in [14].

2.3 Blood chemistry

Fasting (5h) blood samples were taken from the tail vein to prepare EDTA plasma. Blood glucose was determined during blood sampling using a hand-held glucometer (Freestyle Freedom Light, Abbott Laboratories, Lake Bluff, IL, USA). Plasma insulin, leptin, adiponectin, cholesterol, triacylglycerols, ALT, CK-18M30 were determined as described [16]. ELISA assays were used to measure plasma serum amyloid A (SAA; KMA0021 Thermo Fisher Scientific, Waltman, USA), MCP-1/CCL2 (DY479 R&D, Minneapolis, USA), MIF (DY1978 R&D, Fetuin A (DY1563 R&D) and LPS binding protein (LPB; HK205-02 Hycult Biotech, Uden, the Netherlands) according to manufacturer's protocol.

Lipoprotein profiles were analyzed by first separating lipoproteins in fractions using fast protein liquid chromatography (FPLC) with an AKTA apparatus (Pharmacia, Roosendaal, the Netherlands), as previously described [17,18]. Subsequently, total cholesterol and triacylglycerols were measured in the fractions collected for profiling with enzymatic assays (Roche diagnostics, Basel, CHF) [19–21].

2.4 Liver biochemistry and histology

Liver biopsies (2.5 mg) were homogenized and processed to extract lipids. Lipids were quantified with the Lipidyzer platform as previously described [22,23]. Lipids were grouped into classes (triacylglycerols (TAGs), diacylglycerols (DAGs), monoacylglycerols, free fatty acids, cholesteryl esters, phosphatidylcholines, phosphatidylethanolamines, sphingolipids, ceramides etc.). The concentrations of the lipids were expressed as nmol/mg tissue.

Histopathological analyses of liver steatosis, hepatocellular hypertrophy and inflammation were performed on 3-µm-thick hematoxylin-eosin-stained cross sections of the medial lobe using a standardized method for rodent liver histopathology based on the human NAS scoring system [24]. The cross-sectional liver area was assessed by a board-certified pathologist to determine the percentage area with microvesicular steatosis and macrovesicular steatosis as well as the area with abnormally enlarged cells (hypertrophy) essentially as detailed in [25]. Lobular inflammation was assessed by counting the number of inflammatory aggregates which were expressed per mm^2 as reported [25].

2.5 Gene expression analysis using next-generation sequencing (NGS) and subsequent pathway analysis

RNA was isolated from livers (n=18 HFD+ vehicle and n=18 HFD + 2'-FL) using RNA-Bee (Bio-Connect, Huissen, the Netherlands) and purified using PureLink RNA Mini Kit (Thermo Fisher Scientific). RNA concentration was determined and RNA quality was assessed as reported in [16]. Strand-specific messenger RNA sequencing libraries for the Illumina (Illumina NovaSeq6000, San Diego, CA) platform were generated Paired-End 150 bp for approximately 20 million Paired-End reads per sample at Genomescan (Leiden, the Netherlands). The sequences were filtered, trimmed and subjected to a QC procedure as described previously [26]. These files were then merged and aligned to the reference genome "Mus_musculus.GRCm38.gencode.vM19". To count the read mapping frequency per gene Htseq-count 0.6.1p1 was used, and resulting count files (GSE195862 -while under review this data on the public repository GEO remains in private status. This data is accessible using the following code: cnivsauyjfuthut. Once the manuscript is accepted for publication we will change the status to public so no code is necessary anymore) served as input for the differentially expressed genes (DEGs) analysis using the DESeq2-method [27]. DEGs were used as an input for upstream regulator and pathway analysis through Ingenuity Pathway Analysis (IPA) [28]. IPA uses gene expression data of all known downstream target genes to predict activation or deactivation of an upstream regulator or pathway as reported [25]. Positive Z-scores ($Z \geq 2$) indicate an enhanced activity of an upstream regulator while negative Z-scores ($Z \leq -2$) indicate a reduced activity of an upstream regulator [25], while the P-value indicates significant enrichment of the target genes downstream of a regulator.

2.6 Statistics

The present study tested the null hypothesis that 2'-FL does not improve disease parameters relative to saline controls (HFD + vehicle). All statistical analyses were performed using SPSS Version 25 (SPSS Inc., Chicago, IL, USA). Normal distribution of variables was analyzed with the Shapiro-Wilk test, assuming normality at $p>0.05$. For normally distributed variables, and independent sample t-test was used (1-sided). In case the data was not normally distributed, a Mann-Whitney test was used (1-sided). Gut permeability data from multiple time points (t=12 and t=27) was analyzed with a 2-way ANOVA. Correlation analyses were performed by Spearman's rank correlation analysis. P-values <0.05 were considered statistically significant. Data are represented as means ± SD. IPA analysis to determine differentially expressed genes were based on Fisher's exact test ($\alpha = 0.01$).

3. Results

3.1 HMO 2'-FL does not affect adiposity or metabolic parameters

Ldlr-/-.Leiden mice with a starting body weight of 27.0 ± 2.0 gram were fed an energy-dense HFD during an 8-week run-in period to induce obesity (41.5 ± 4.2 grams). The weight gain on HFD was found to be about 3-fold higher than on a chow diet (chow mice weigh on average 31.6 ± 3.2 grams). After 8 weeks the intervention was started and mice received either 2'-FL or vehicle control until week 28. During the entire study, the average food intake was comparable between the two groups (Table 1). At t=28 weeks, both groups gained a comparable body weight, fat mass and lean mass. Visceral adiposity, reflected by the mass of epididymal (eWAT) and mesenteric (mWAT) adipose tissue depots, was also comparable

between the groups, as was the weight of the subcutaneous depot (sWAT). Consistent with this, the plasma concentrations of the adipokines leptin and adiponectin were consistent with an obese phenotype and were not affected by 2'-FL compared to the HFD + vehicle controls. Markers associated with inflammation including plasma MCP-1/CCL2 was significantly decreased with 2'-FL, while plasma MIF, SAA and Fetuin A were comparable in 2'-FL and HFD + vehicle treated controls. Plasma total cholesterol and triacylglycerol (TAG) levels were comparable between the groups. Lipoprotein profile analysis showed that cholesterol confined to apoB-containing (V)LDL sized particles was comparable, while TAGs confined to (V)LDL-sized particles were somewhat reduced in the 2'-FL group (Figure 2).

Table 1. Body composition, energy intake and metabolic and inflammatory parameters.

	HFD + vehicle	HFD + 2'-FL
Average food intake (g/day)	2.5 ± 0.2	2.6 ± 0.3
Body weight (g)	46.8 ± 4.2	47.4 ± 4.7
Fat mass (g)	19.5 ± 3.1	19.9 ± 3.6
Fat mass (%)	42.5 ± 4.2	42.5 ± 4.0
Lean mass (g)	26.2 ± 2.1	26.6 ± 3.6
eWAT (g)	2.2 ± 0.4	2.4 ± 0.6
mWAT (g)	1.0 ± 0.3	0.9 ± 0.3
sWAT (g)	2.6 ± 0.7	2.5 ± 0.6
Plasma leptin (ng/ml)	48.4 ± 13.5	46.4 ± 10.5
Plasma adiponectin (µg/ml)	9.9 ± 3.5	10.0 ± 2.8
Plasma MCP-1/CCL2 (pg/ml)	15.7 ± 8.7	9.6 ± 4.0*
Plasma MIF (µg/ml)	32.0 ± 14.5	22.1 ± 14.9
Plasma SAA (µg/ml)	18.8 ± 4.6	19.5 ± 4.1
Plasma Fetuin A (µg/ml)	46.1 ± 7.7	44.4 ± 10.8
Plasma cholesterol (mM)	31.0 ± 7.8	29.9 ± 8.4
Plasma triacylglycerol (mM)	6.5 ± 2.4	5.8 ± 2.6

eWAT= epididymal white adipose tissue, mWAT= mesenteric white adipose tissue and sWAT = subcutaneous white adipose tissue. Data are presented as mean ± SD.

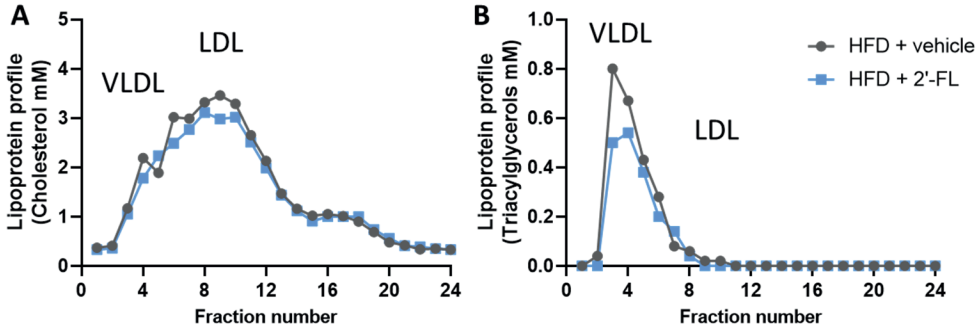

***Figure 2**. Lipoprotein profiles were analyzed in fasting plasma (pooled from n=18 mice per treatment group) by fast protein liquid chromatography (FPLC). The plasma is fractionated and lipoprotein particles are collected in the respective fractions. In these fractions, (**A**) cholesterol and (**B**) triglyceride concentrations were analyzed and plotted as profiles, which demonstrate changes in lipoprotein particles to which the plasma lipids are associated with.*

3.2 2'-FL supplementation reduces liver steatosis

Plasma concentrations of ALT, a liver integrity marker associated with NAFLD development, tended to be decreased with 2'-FL (p=0.07), while CK18-M30 and total liver weight was not altered compared to the HFD + vehicle controls (Table 2). Subsequent histological analysis of NAFLD in liver cross-sections demonstrated that 2'-FL reduced the total steatotic area with borderline significance (-19%; p=0.051). This prompted us to perform a more refined analysis of steatosis subtypes, i.e. macrovesicular and microvesicular steatosis, the former being associated with lobular inflammation [29], the latter being associated with mitochondrial dysfunction and oxidative stress [30]. Remarkably, 2'-FL did not affect macrovesicular steatosis, and its anti-steatotic effect was almost fully attributable to a suppression of microvesicular steatosis (-32%; P<0.05) (Figure 3). This hepatoprotective effect was further supported by an effect on hepatocellular hypertrophy, i.e. the liver area covered with abnormally enlarged cells (-32%; P<0.05) (Table 2). The number of inflammatory aggregates reflecting lobular inflammation was unaffected (Table 2).

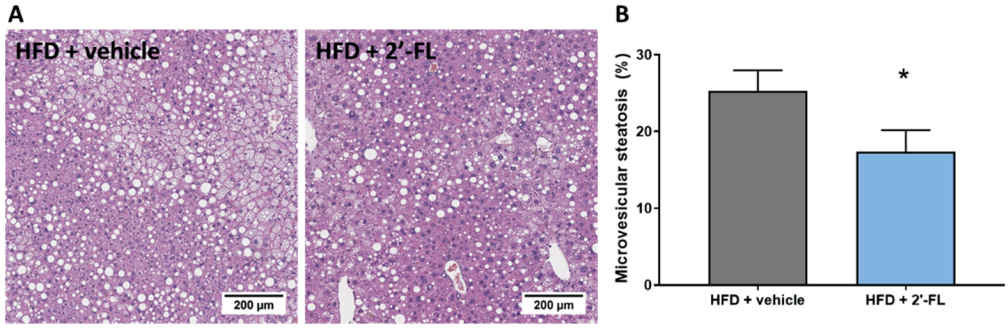

Figure 3. *Human milk oligosaccharide 2'-FL reduced the accumulation of lipids in small lipid droplets referred to as microvesicular steatosis.* ***A****) representative images* ***B****) percentage of hepatic cross-section affected with microvesicular steatosis. Data is from n=18 mice per treatment group shown as mean ± SEM, *p<0.05.*

Table 2. Liver integrity markers, liver weight and NAFLD score after 28 weeks.

	HFD + vehicle	HFD + 2'-FL
Plasma ALT (U/L)	210.8 ± 95.3	163.7 ± 85.9
Plasma CK18-M30 (U/mL)	305.6 ± 67.1	334.7 ± 82.4
Liver weight (g)	2.6 ± 0.7	2.5 ± 0.6
Total steatosis (%)	47.4 ± 16.2	38.1 ± 17.3$^{p=0.051}$
Macrovesicular steatosis (%)	22.1 ± 7.5	20.8 ± 8.1
Hepatocellular hypertrophy (%)	30.6 ± 15.4	21.1 ± 14.0*
Inflammatory aggregates (per mm2)	6.8 ± 16.9	3.9 ± 9.7

*Asterisks indicate a significant difference relative to HFD + vehicle control (*p<0.05). Data shown as mean ± SD.*

3.3 2'-FL modulates upstream regulators involved in lipid metabolism and ER stress

To gain more insight into the effects of 2'-FL on metabolic processes in the liver, a genome-wide gene expression analysis was performed using NGS and datasets were analyzed with Ingenuity Pathway Analysis (IPA). IPA predicts the activation state of critical upstream regulators (e.g. signaling molecules, transcription factors) based on the expression pattern of their downstream genes. Consistent with the development of steatosis in the HFD group, important upstream regulators involved in lipid catabolism (peroxisomal acyl-CoA oxidase 1 (ACOX1), AMP kinase (AMPK) and mitochondrial biogenesis (PPARGC1a) were all inactivated with HFD (Table 3). 2'-FL counteracted this HFD effect and specifically reactivated ACOX1 indicating that 2'-FL supplementation enhanced beta-oxidation. Furthermore, the activity of sterol regulatory element-binding transcription factor 1 (SREBF1), a positive regulator of fatty acid synthesis genes, was suppressed by 2'-FL which is in line with reduced plasma insulin levels and the observed lowering of TAG in (V)LDL particles. In addition, HFD elevated the activity of protein kinase C delta (PRKCD) which impairs insulin signaling, and this activation was counter regulated with 2'-FL. Since PRKCD can be activated by DAGs, a decreased activity also suggests a lower amount of intrahepatic DAGs with 2'-FL. Several regulators associated with endoplasmic reticulum (ER) stress, e.g. ATF4, ATF6, ERN1, NUPR1, were activated with HFD indicating increased ER stress in the control group. 2'-FL significantly attenuated the effects of HFD, indicating an overall suppression of the ER stress response. Altogether, the NGS analyses support an improvement of hepatic lipid handling by 2'-FL that is accompanied by beneficial effects on the ER stress response. Consistent with these upstream regulator effects, the canonical pathway 'Nrf2-mediated oxidative stress response' was attenuated with 2'-FL (Z= -1.6 , $p<0.05$) (supplemental table 1).

Table 3. Upstream regulator analysis of factors controlling metabolic homeostasis in the liver.

	HFD + vehicle vs Chow		HFD + 2'-FL vs HFD + vehicle	
	Z-score	**p-value**	**Z-score**	**p-value**
ACOX1	-5.8	0.000	2.2	0.037
AMPK	-2.2	0.000	N/A	1.000
ATF4	1.9	0.000	-2.6	0.000
ATF6	0.5	0.007	-1.9	0.000
ERN1	0.9	0.037	-2.4	0.009
NRF1	-0.9	0.000	0.6	0.000
NUPR1	2.8	0.000	-1.2	0.005
PPARGC1A	-4.2	0.000	0.1	0.005
PRKCD	3.8	0.000	-2.4	0.011
SREBF1	0.2	0.000	-1.7	0.005

The activity of an upstream regulator was predicted based on gene expression changes of all downstream target genes. A negative Z-score indicates inhibition of the respective regulator or pathway (green color) and a positive Z-score indicates activation (red color). The p-value < 0.05 in grey indicates significant enrichment of the target genes downstream of a regulator, i.e. that more downstream genes are affected than can be expected by chance. N/A indicates an insufficient number of differentially expressed genes to predict the activation state of an upstream regulator.

We next investigated effects exerted by 2'-FL supplementation during the experiment that may explain the reduced development of liver steatosis, with particular emphasis on gut permeability and insulin resistance.

3.4 2'-FL modulates microbiota and improves gut permeability

Orally administered FITC-labeled dextran (FD4) was used to measure the functional integrity of the gut. The amount of FD4 retrieved in plasma in Ldlr-/-.Leiden mice on chow was 1.2 ± 0.5 mg/mL (not shown). At t=12 weeks, HFD feeding resulted in an increased gut permeability and this HFD effect was strongly attenuated with 2'-FL (-55%; $p<0.05$), i.e. after only 4 weeks of 2'-FL supplementation (Figure 4A). The effect of 2'-FL on gut permeability was not observed anymore at week 27 with the FD4 test, while plasma LPB were significantly decreased with 2'-FL after 28 weeks (Figure 4B).

To investigate whether the reduced gut permeability during the development of NAFLD was associated with specific changes in microbiota composition, 16S sequencing was performed on feces collected prior to the intervention (at t=8 weeks) and at time points close to the FD4 tests. Permutation tests enabled the statistical testing of differences in entire microbiota composition between experimental groups, and showed that, prior to the 2'-FL intervention, the HFD + vehicle and HFD + 2'-FL groups were comparable as expected. The similarity of their microbiota composition is visualized in an NMDS plot (Figure 4C) showing a great overlap between the groups at t=8 weeks. While the microbiota of the HFD + vehicle remained stable during the study, 2'-FL significantly altered the microbiota composition as revealed by a marked shift to the right at t=16 weeks, indicating a higher dissimilarity relative to respective controls early during the intervention. Towards the end of the study, at t=27 weeks, the microbiota composition was still significantly different from the HFD-controls, however the dissimilarity was smaller as the dots shifted back in the direction of the HFD controls. In addition to these shifts on the level of the entire microbiome, analysis of specific genera over time demonstrated that 2'-FL gradually increased the Bifidobacterium content over time (Figure 4D). Altogether, 2'-FL transiently reduced gut permeability and led to pronounced changes of fecal microbiota composition during the time in which NAFLD developed.

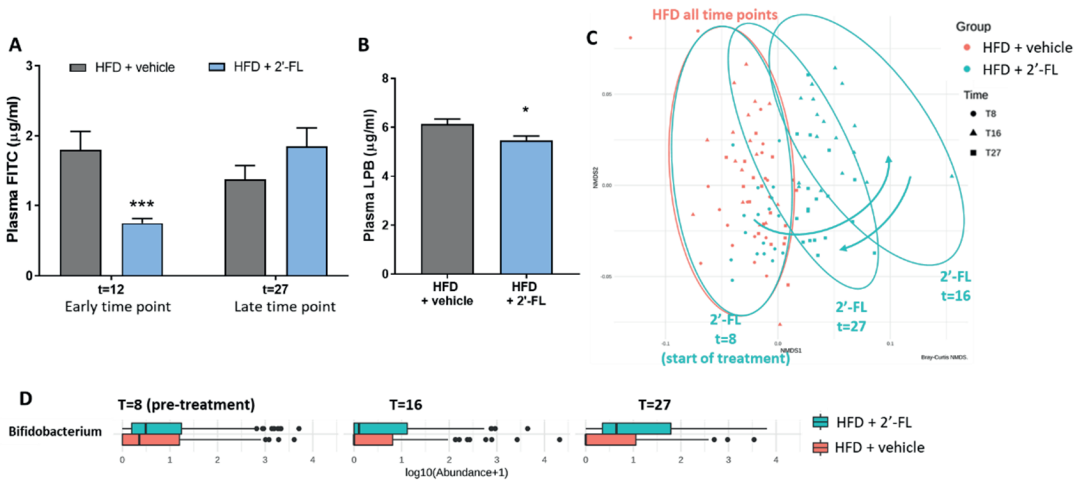

Figure 4. *Human milk oligosaccharide 2'-FL improves gut permeability during early NAFLD development. (**A**) Gut permeability measured by FITC-labeled dextran at an early (at t = 12 w) and late (at t = 27 w) time point of the disease process equaling 4 and 19 weeks of 2'-FL supplementation, respectively. (**B**) Plasma LPS-binding protein (LBP) measured in week 28 of the study. Data is from n = 18 mice per treatment group presented as mean ± SEM, *p < 0.05, ***p < 0.001 compared to HFD + vehicle. (**C**) Fecal microbiota composition was analyzed by 16S sequencing and composition changes over time were visualized by non-metric multidimensional scaling (NMDS) using the Bray-Curtis index. Every dot represents the microbiota composition of one mouse. A greater distance between dots indicates more dissimilarity. Blue arrows indicate 2'-FL induced microbiota composition shifts. (**D**) Fecal Bifidobacterium abundance over time.*

3.5 2'-FL lowers hyperinsulinemia and HOMA-IR and reduces liver diacylglycerols

In the fasting state, blood glucose is mainly (~90%) derived from the liver [31]. Fasting blood glucose at the end of the treatment period was not affected by 2'-FL (Table 4). By contrast, fasting plasma insulin concentrations, which increased strongly in response HFD feeding (from 1.6 ± 0.6 ng/mL at the start of the experiment to 12.5 ± 5.1 ng/mL), were significantly lowered by 2'-FL. Also, insulin resistance assessed by HOMA-IR was significantly reduced in the 2'-FL group, suggesting improved insulin action in livers of 2'-FL fed mice.

We therefore analyzed the concentrations of diacylglycerols (DAGs) in the liver as this lipid species blocks insulin action at the level of its receptor, an effect that can be dissociated from inflammation-mediated IR [3]. In response to HFD feeding, liver DAGs in the HFD + vehicle-treated group were 9.4 ± 4.4 nmol/mg liver and thus markedly elevated compared to littermates on chow (2.6 ± 0.8 nmol/mg liver; not shown). The HFD-induced accumulation of intrahepatic DAGs was significantly suppressed by 2'-FL, which is consistent with a reduction of HOMA-IR by 2'-FL relative to vehicle control (Figure 5A). The relationship between fasting plasma insulin concentrations and intrahepatic DAGs was further supported by a significant correlation between the two parameters (Figure 5B).

Altogether, 2'-FL attenuated gut permeability and IR thereby providing a rationale for the reduction of NAFLD development.

Table 4. Glucose, insulin and insulin resistance (HOMA-IR) after 28 weeks.

	HFD + vehicle	HFD + 2'-FL
Blood glucose (mmol/l)	7.9 ± 0.8	8.1 ± 1.2
Plasma insulin (ng/ml)	12.5 ± 5.1	9.1 ± 4.0*
HOMA-IR	110.2 ± 49.8	83.7 ± 41.5*

*Asterisk indicates a significant difference relative to the HFD + vehicle control group (*p<0.05). Data shown as mean ± SD.*

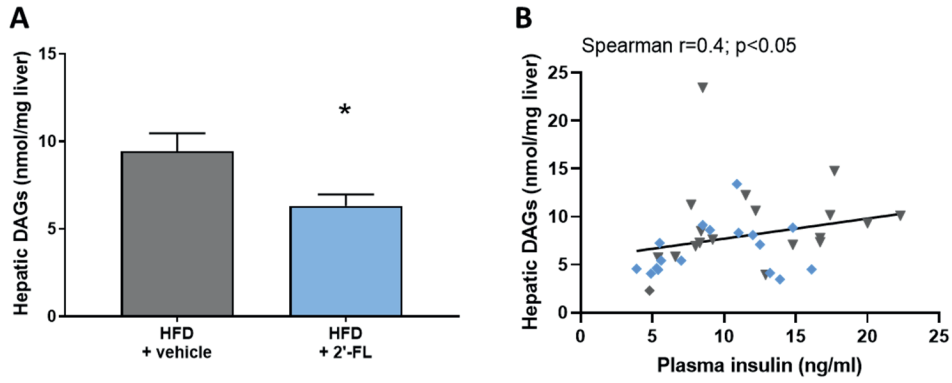

Figure 5. Human milk oligosaccharide 2'-FL reduced **A**) total intrahepatic diacylglycerols (DAGs). **B**) Total DAGs correlated with fasting plasma insulin concentrations. Data is from n=18 mice per treatment group shown as mean ± SEM, *p<0.05.

4. Discussion

In the current study we investigated the potential hepatoprotective effects of the human milk oligosaccharide 2'-fucosyllactose (2'-FL) in a therapeutic setting, i.e. we started its supplementation when obesity, dyslipidemia and hyperinsulinemia were already manifest. Long-term supplementation (20 weeks) with 2'-FL counteracted the detrimental effects of HFD feeding on dysbiosis and gut permeability, which was accompanied by an increase in the abundance of Bifidobacterium. In the liver, 2'-FL specifically suppressed the accumulation of lipids in small intracellular droplets, so-called microvesicular steatosis. These hepatoprotective effects were supported by functional transcriptome analysis demonstrating improved lipid handling (by activating the peroxisomal enzyme ACOX1 and deactivating the transcription factor SREBF1). Improved hepatic lipid handling by 2'-FL was accompanied by beneficial effects on the ER/cellular stress response because 2'-FL counter-regulated HFD-dependent induction of ATF4, ATF6, ERN1, NUPR1 and the 'Nrf2-mediated oxidative stress response' pathway. Moreover, 2'-FL significantly reduced fasting insulin concentrations and HOMA-IR, an observation that is mechanistically supported by

a significant decrease in intrahepatic bioactive DAGs and deactivation of PKC-delta which has been shown to block insulin signaling upon binding to DAGs [3,32].
The current study is the first to investigate the effect of long-term supplementation with 2'-FL on NAFLD development and demonstrates hepatoprotective effects independent of changes on body weight, food intake or plasma lipids. The absence of an effect on body weight and food intake is in line with short-term studies (6-8 weeks) that used comparably low doses of 2'-FL (1% and 2% w/v) as herein (2.5% w/w) [33]. In these short-term studies only the higher doses of 2'-FL (5% and 10% w/v) decreased body weight, which was also associated with a lowering of caloric intake [33,34]. In line with our findings, no major effect on plasma lipids was observed in a meta-analysis of other types of prebiotic treatments in ultrasound- or biopsy-confirmed NAFLD patients [6].
The supplementation of 2'-FL in diet-induced obese and hyperinsulinemic mice resulted in significantly lower microvesicular steatosis. In general, hepatic steatosis occurs when hepatic uptake and production of lipids is higher than the combined lipid export via VLDL and lipid oxidation. As TAGs confined to VLDL were slightly reduced in this study, it appears that 2'-FL did apparently *not* stimulate hepatic lipid export to reduce steatosis. Our observation rather suggests that 2'-FL may improve lipid utilization by increasing fatty acid oxidation and/or decreasing *de novo* lipogenesis. Indeed functional transcriptomic analysis demonstrated that 2'-FL specifically activated ACOX1, the rate-limiting enzyme in peroxisomal beta oxidation [35,36] with an important role in lipid catabolism. At the same time 2'-FL deactivated SREBF1, the transcriptional master regulator of *de novo* lipogenesis [2], which is itself positively regulated by insulin. Fasting insulin levels were strongly increased with HFD and attenuated by 2'-FL, which is consistent with the observed activation/deactivation of SREBF1. This is particularly relevant for the situation in NAFLD patients, in which it has also been demonstrated that hyperinsulinemia as a consequence of IR is a key driver of *de novo* lipogenesis [37]. Moreover, insulin plays also an important role in regulation of fatty acid fluxes to the liver because it inhibits TAG lipolysis in adipose tissue [38]. Under conditions of peripheral IR however, the fluxes of fatty acids from extrahepatic organs to the liver can increase markedly because insulin is no longer able to put the brakes on lipolysis [3]. These peripheral effects in the adipose organ, together with an excessive dietary intake of carbohydrates and lipids further promotes the development of liver steatosis. The observed reductions in fasting insulin and HOMA-IR with 2'-FL are in line with results from a human study, in which increased serum concentrations of 2'-FL during pregnancy tended to be consistently negatively associated with insulin levels [39].
The strong association between IR and NAFLD development has been linked to the involvement of bioactive lipids like DAGs in the etiology of the disease. DAGs can directly impair the insulin receptor (INSR) activity via recruitment of Protein kinase C delta (PRKCD) [3]. Protein kinase C members are enzymes that are able to interact with lipids and affect cellular signaling cascades including insulin receptor signaling through kinase activity, a mechanism which occurs in various organs including liver and adipose tissue. PRKCD interacts with membrane-bound DAGs and blocks insulin signaling at the level of its receptor thereby promoting IR development [32]. Under conditions of IR glucose uptake from the

circulation is impaired and so is the synthesis of glycogen [1]. In a state of hepatic IR, in which insulin-mediated activation of glycogen synthase is thus impaired, dietary glucose moieties will be redirected into the *de novo* lipogenesis pathway thereby further promoting lipid accumulation in NAFLD [1]. The reduction of hyperinsulinemia and associated hepatic SREBF1 activity observed herein, indicate that hepatic insulin signaling may be improved with 2'-FL, supported by the significant reduction of hepatic DAG. Separate studies with dedicated sacrifice conditions are required to investigate putative effects on insulin signaling in more detail.

Another potential beneficial effect of 2'-FL which may have contributed to the decrease in steatosis is the counter regulation of several important factors associated with ER stress such as ATF4, ATF6, ERN1, NUPR1 indicating an overall attenuation of the ER stress response. The endoplasmic reticulum (ER) is an organelle that synthesizes, folds and secretes various proteins, among which are proteins to enable secretion of hepatic lipids. Thus, HFD-evoked ER stress can result in impaired protein folding and function, which can diminish lipid mobilization and thereby exacerbating the accumulation of intrahepatic lipids [40]. Interestingly, one of the primary sites of DAG synthesis is in the ER [41] and accumulated DAGs in the ER were identified as key signaling molecules that cause disruption of the endomembrane system of the ER ultimately leading to induction of aforementioned factors implicated in ER stress [42], which is consistent with the HFD effects herein. It is thus amenable that the observed intrahepatic DAG accumulation upon HFD feeding is tightly associated with the induction of an ER stress response. 2'-FL lowered intrahepatic DAGs which may explain the counter-regulatory effect on the upstream regulators involved in the ER-stress response. This effect together with the improvement in lipid handling (i.e. activation of ACOX1 and deactivation of SREBF1) would reduce the export of lipids from the liver (as VLDL) and could therefore explain the slightly reduced triglyceride content in VLDL particles observed in the lipoprotein profile analysis. The ER stress-inducing effects of HFD may contribute to mitochondrial dysfunction also in another way because proper mitochondrial functioning (e.g. the Krebs cycle) relies on mitochondrial uptake of calcium from the ER [42,43] which is disturbed under conditions of metabolic stress [44]. Taken together, the combination of functional transcriptomics analysis with lipidomics for quantification of DAG concentrations in the same tissue provides a mechanistic rationale for the improvements in steatosis with 2'-FL and supports our histological observations in liver.

Besides the effects of 2'-FL on the liver we also showed that this prebiotic attenuated HFD-induced gut dysbiosis, in particular at the early time point (week 12). A pronounced microbiota dissimilarity was observed at week 16 and this was associated with a transient improvement of *in vivo* gut permeability during NAFLD development. In line with observations made in obese children treated with 2'-FL for 8-weeks, which resulted in increased intestinal abundance of Bifidobacterium [45], we also observed a gradual increase in Bifidobacterium over time. It is noteworthy, because 2'-FL seems to create a condition that facilitates persistent growth of Bifidobacterium while the total microbiome composition shifted back in the direction of HFD controls, possibly due to the very long

period of experimental HFD feeding of more than 6 months and the associated severe metabolic stress. The observed effects on gut permeability are consistent with other rodent studies which reported that preventive 2'-FL treatment for 6-8 weeks in HFD fed animals led to changes in the gut microbiota composition [33] and gut barrier function using ex vivo gut transplants [34]. Microbiota dysbiosis and disturbed gut permeability are thought to be drivers of NASH pathology and reportedly precede the pathological manifestation of NAFLD [13,14,46]. Gut permeability has even been associated with the severity of NAFLD [47,48]. The observed beneficial effects on the gut (permeability, microbiota shift and increased Bifidobacterium) with 2'-FL may therefore have contributed to the attenuation of NAFLD.
A limitation of the current study is that we did not sacrifice a group of mice at 8 weeks, the time point at which interventions were started which would have enabled us to assess NAFLD development prior to treatment to determine potential regression of histological features. Intrinsic to the set-up of the study, using oral administration of 2'-FL, we cannot distinguish whether the effects on liver or gut are direct, e.g. via 2'-FL itself or metabolites formed from 2'-FL, or more indirect, i.e. mediated via other metabolites that do not directly stem from 2'-FL but are produced by the altered microbiota as a whole. Consequently, the study design does also not allow investigation of the exact molecular mechanisms that mediate gut permeability effects, but this has been studied by others: 2'-FL directly increased expression of tight junction expression proteins, involved in the regulation of gut barrier integrity, in LPS-treated Caco2 cells [49] and directly diminished LPS-induced inflammation in human enterocytes [50] and Caco2 cells [49]. Indirect effects of 2'-FL have been demonstrated by using 2'-FL derived bacterial metabolites, which attenuated paracellular permeability of FITC-dextran's in Caco2 monolayers and upregulated the expression of tight junction proteins in a gut-on-a-chip model generated from human gut tissue biopsies [51]. Taken together, both direct and indirect effects of 2'-FL on the gut may have contributed to the observed beneficial effects of 2'-FL.
In conclusion, we provide evidence that 2'-FL can exert effects beyond the gut and can affect more distant organs like the liver in which it improved lipid handling and reduced obesity-associated steatosis. The observed reduction of specific bioactive lipids in the liver, DAGs, constitutes an important finding because this class of lipids affects insulin signaling, is implicated in ER stress and contributes to the dysmetabolic state that causes insulin resistance. Hyperinsulinemia correlated with intrahepatic DAGs, and 2'-FL treatment reduced DAGs as well as HOMA-IR and mediators of ER stress. The improvement in microvesicular steatosis with 2'-FL is supported by improved lipid catabolism and suppression of *de novo* lipogenesis signaling pathways. Thus specific HMOs such as 2'-FL may constitute a means to correct gut dysfunction, dysmetabolism and insulin resistance, all of which drive the development of metabolic diseases including NAFLD.

Acknowledgments

We thank Dr. Aswin Menke for technical support and histological evaluations.

Reference list

[1] Loomba R, Friedman SL, Shulman GI. Mechanisms and disease consequences of nonalcoholic fatty liver disease. Cell 2021;184:2537–64. https://doi.org/10.1016/j.cell.2021.04.015.

[2] Ferré P, Foufelle F. Hepatic steatosis: a role for de novo lipogenesis and the transcription factor SREBP-1c. Diabetes Obes Metab 2010;12 Suppl 2:83–92. https://doi.org/10.1111/J.1463-1326.2010.01275.X.

[3] Petersen MC, Shulman GI. Roles of Diacylglycerols and Ceramides in Hepatic Insulin Resistance. Trends Pharmacol Sci 2017;38:649–65. https://doi.org/10.1016/j.tips.2017.04.004.

[4] Barile D, Rastall RA. Human milk and related oligosaccharides as prebiotics. Curr Opin Biotechnol 2013;24:214–9. https://doi.org/10.1016/J.COPBIO.2013.01.008.

[5] He C, Man H, Guowei S, Qi M, Tao Q. Effect of prebiotics on growth of Bifidobacterium bifidum. Proc 2011 Int Conf Hum Heal Biomed Eng HHBE 2011 2011:981–4. https://doi.org/10.1109/HHBE.2011.6028988.

[6] Loman BR, Hernández-Saavedra D, An R, Rector RS. Prebiotic and probiotic treatment of nonalcoholic fatty liver disease: a systematic review and meta-analysis. Nutr Rev 2018;76:822–39. https://doi.org/10.1093/NUTRIT/NUY031.

[7] Newburg DS, Ruiz-Palacios GM, Altaye M, Chaturvedi P, Meinzen-Derr J, de Lourdes Guerrero M, et al. Innate protection conferred by fucosylated oligosaccharides of human milk against diarrhea in breastfed infants. Glycobiology 2004;14:253–63. https://doi.org/10.1093/GLYCOB/CWH020.

[8] Mezoff EA, Hawkins JA, Ollberding NJ, Karns R, Morrow AL, Helmrath MA. The human milk oligosaccharide 2'-fucosyllactose augments the adaptive response to extensive intestinal. Am J Physiol - Gastrointest Liver Physiol 2016;310:G427. https://doi.org/10.1152/AJPGI.00305.2015.

[9] Zhou R, Llorente C, Cao J, Gao B, Duan Y, Jiang L, et al. Deficiency of Intestinal α1-2-fucosylation Exacerbates Ethanol-Induced Liver Disease in Mice. Alcohol Clin Exp Res 2020;44:1842. https://doi.org/10.1111/ACER.14405.

[10] van den Hoek AM, Verschuren L, Worms N, van Nieuwkoop A, de Ruiter C, Attema J, et al. A Translational Mouse Model for NASH with Advanced Fibrosis and Atherosclerosis Expressing Key Pathways of Human Pathology. Cells 2020. https://doi.org/10.3390/cells9092014.

[11] van Koppen A, Verschuren L, van den Hoek AM, Verheij J, Morrison MC, Li K, et al. Uncovering a Predictive Molecular Signature for the Onset of NASH-Related Fibrosis in a Translational NASH Mouse Model. Cmgh 2018;5:83-98.e10. https://doi.org/10.1016/j.jcmgh.2017.10.001.

[12] Morrison MC, Kleemann R, van Koppen A, Hanemaaijer R, Verschuren L. Key inflammatory processes in human NASH are reflected in Ldlr-/-.Leiden mice: A translational gene profiling study. Front Physiol 2018;9. https://doi.org/10.3389/fphys.2018.00132.

[13] Morrison MC, Gart E, van Duyvenvoorde W, Snabel J, Nielsen MJ, Leeming DJ, et al. Heat-Inactivated Akkermansia muciniphila Improves Gut Permeability but Does Not Prevent Development of Non-Alcoholic Steatohepatitis in Diet-Induced Obese Ldlr−/−.Leiden Mice. Int J Mol Sci 2022;23:1–17. https://doi.org/10.3390/ijms23042325.

[14] Gart E, Lima ES, Schuren F, Ruiter CGF De, Attema J, Verschuren L, et al. Diet-Independent Correlations between Bacteria and Dysfunction of Gut , Adipose Tissue , and Liver : A Comprehensive Microbiota Analysis in Feces and Mucosa of the Ileum and Colon in Obese Mice with NAFLD. Int J Mol Sci 2019:1–20. https://doi.org/10.3390/ijms20010001.

[15] Salic K, Gart E, Seidel F, Verschuren L, Caspers M, van Duyvenvoorde W, et al. Combined Treatment with L-Carnitine and Nicotinamide Riboside Improves Hepatic Metabolism and Attenuates Obesity and Liver Steatosis. Int J Mol Sci 2019;20. https://doi.org/10.3390/IJMS20184359.

[16] Gart E, Duyvenvoorde W van, Toet K, Caspers MPM, Verschuren L, Nielsen MJ, et al. Butyrate Protects against Diet-Induced NASH and Liver Fibrosis and Suppresses Specific Non-Canonical TGF-β Signaling Pathways in Human Hepatic Stellate Cells. Biomedicines 2021;9:1954. https://doi.org/10.3390/BIOMEDICINES9121954.

[17] Westerterp M, Van Der Hoogt CC, De Haan W, Offerman EH, Dallinga-Thie GM, Jukema JW, et al. Cholesteryl ester transfer protein decreases high-density lipoprotein and severely aggravates atherosclerosis in APOE*3-Leiden mice. Arterioscler Thromb Vasc Biol 2006;26:2552–9. https://doi.org/10.1161/01.ATV.0000243925.65265.3c.

[18] Bijland S, Rensen PCN, Pieterman EJ, Maas ACE, van der Hoorn JW, van Erk MJ, et al. Perfluoroalkyl sulfonates cause alkyl chain length-dependent hepatic steatosis and hypolipidemia mainly by impairing lipoprotein production in APOE*3-leiden CETP mice. Toxicol Sci 2011;123:290–303. https://doi.org/10.1093/toxsci/kfr142.

[19] Dewey FE, Gusarova V, Dunbar RL, O'Dushlaine C, Schurmann C, Gottesman O, et al. Genetic and Pharmacologic Inactivation of ANGPTL3 and Cardiovascular Disease. N Engl J Med 2017;377:211–21. https://doi.org/10.1056/nejmoa1612790.

[20] Kooistra T, Verschuren L, De Vries-Van Der Weij J, Koenig W, Toet K, Princen HMG, et al. Fenofibrate reduces atherogenesis in ApoE*3Leiden mice: Evidence for multiple antiatherogenic effects besides lowering plasma cholesterol. Arterioscler Thromb Vasc Biol 2006;26:2322–30. https://doi.org/10.1161/01.ATV.0000238348.05028.14.

[21] Verschuren L, Kleemann R, Offerman EH, Szalai AJ, Emeis SJ, Princen HMG, et al. Effect of low dose atorvastatin versus diet-induced cholesterol lowering on atherosclerotic lesion progression and inflammation in apolipoprotein E*3-Leiden transgenic mice. Arterioscler Thromb Vasc Biol 2005;25:161–7. https://doi.org/10.1161/01.ATV.0000148866.29829.19.

[22] Loef M, Von Hegedus JH, Ghorasaini M, Kroon FPB, Giera M, Ioan-Facsinay A, et al. Reproducibility of Targeted Lipidome Analyses (Lipidyzer) in Plasma and

Erythrocytes over a 6-Week Period. Metabolites 2021;11:1–11. https://doi.org/10.3390/METABO11010026.

[23] Ghorasaini M, Mohammed Y, Adamski J, Bettcher L, Bowden JA, Cabruja M, et al. Cross-Laboratory Standardization of Preclinical Lipidomics Using Differential Mobility Spectrometry and Multiple Reaction Monitoring. Anal Chem 2021;93:16369–78. https://doi.org/10.1021/ACS.ANALCHEM.1C02826/SUPPL_FILE/AC1C02826_SI_002.XLSX.

[24] Liang W, Menke AL, Driessen A, Koek GH, Lindeman JH, Stoop R, et al. Establishment of a general NAFLD scoring system for rodent models and comparison to human liver pathology. PLoS One 2014;9. https://doi.org/10.1371/journal.pone.0115922.

[25] Gart E, Salic K, Morrison MC, Caspers M, van Duyvenvoorde W, Heijnk M, et al. Krill oil treatment increases distinct pufas and oxylipins in adipose tissue and liver and attenuates obesity-associated inflammation via direct and indirect mechanisms. Nutrients 2021;13. https://doi.org/10.3390/nu13082836.

[26] Mueller AM, Kleemann R, Gart E, van Duyvenvoorde W, Verschuren L, Caspers M, et al. Cholesterol Accumulation as a Driver of Hepatic Inflammation Under Translational Dietary Conditions Can Be Attenuated by a Multicomponent Medicine. Front Endocrinol (Lausanne) 2021;12. https://doi.org/10.3389/fendo.2021.601160.

[27] Love MI, Huber W, Anders S. Moderated estimation of fold change and dispersion for RNA-seq data with DESeq2. Genome Biol 2014;15:1–21. https://doi.org/10.1186/s13059-014-0550-8.

[28] Krämer A, Green J, Pollard J, Tugendreich S. Causal analysis approaches in Ingenuity Pathway Analysis. Bioinformatics 2014;30:523–30. https://doi.org/10.1093/BIOINFORMATICS/BTT703.

[29] Mulder P, Liang W, Wielinga P, Verschuren L, Toet K, Havekes L, et al. Macrovesicular steatosis is associated with development of lobular inflammation and fibrosis in diet-induced non-alcoholic steatohepatitis (NASH). Inflamm Cell Signal 2015. https://doi.org/10.14800/ics.804.

[30] Fromenty B, Pessayre D. Impaired mitochondrial function in microvesicular steatosis effects of drugs, ethanol, hormones and cytokines. J Hepatol 1997;26:43–53. https://doi.org/10.1016/S0168-8278(97)80496-5.

[31] Petersen MC, Vatner DF, Shulman GI. Regulation of hepatic glucose metabolism in health and disease. Nat Rev Endocrinol 2017;13:572. https://doi.org/10.1038/NRENDO.2017.80.

[32] Samuel VT, Shulman GI. Mechanisms for insulin resistance: Common threads and missing links. Cell 2012;148:852–71. https://doi.org/10.1016/j.cell.2012.02.017.

[33] Lee S, Goodson M, Vang W, Kalanetra K, Barile D, Raybould H. 2'-Fucosyllactose Supplementation Improves Gut-Brain Signaling and Diet-Induced Obese Phenotype and Changes the Gut Microbiota in High Fat-Fed Mice. Nutrients

2020;12. https://doi.org/10.3390/NU12041003.
[34] Lee S, Goodson ML, Vang W, Rutkowsky J, Kalanetra K, Bhattacharya M, et al. Human milk oligosaccharide 2'-fucosyllactose supplementation improves gut barrier function and signaling in the vagal afferent pathway in mice. Food Funct 2021;12:8507–21. https://doi.org/10.1039/D1FO00658D.
[35] Tahri-Joutey M, Andreoletti P, Surapureddi S, Nasser B, Cherkaoui-Malki M, Latruffe N. Mechanisms Mediating the Regulation of Peroxisomal Fatty Acid Beta-Oxidation by PPARα. Int J Mol Sci 2021;22. https://doi.org/10.3390/IJMS22168969.
[36] Wang L, Zhu X, Sun X, Yang X, Chang X, Xia M, et al. FoxO3 regulates hepatic triglyceride metabolism via modulation of the expression of sterol regulatory-element binding protein 1c. Lipids Health Dis 2019;18:1–12. https://doi.org/10.1186/S12944-019-1132-2/FIGURES/5.
[37] Smith GI, Shankaran M, Yoshino M, Schweitzer GG, Chondronikola M, Beals JW, et al. Insulin resistance drives hepatic de novo lipogenesis in nonalcoholic fatty liver disease. J Clin Invest 2020;130:1453. https://doi.org/10.1172/JCI134165.
[38] Chakrabarti P, Kim JY, Singh M, Shin Y-K, Kim J, Kumbrink J, et al. Insulin Inhibits Lipolysis in Adipocytes via the Evolutionarily Conserved mTORC1-Egr1-ATGL-Mediated Pathway. Mol Cell Biol 2013;33:3659. https://doi.org/10.1128/MCB.01584-12.
[39] Jantscher-Krenn E, Treichler C, Brandl W, Schönbacher L, Köfeler H, Van Poppel MNM. The association of human milk oligosaccharides with glucose metabolism in overweight and obese pregnant women. Am J Clin Nutr 2019;110:1335–43. https://doi.org/10.1093/AJCN/NQZ202.
[40] Zhang XQ, Xu CF, Yu CH, Chen WX, Li YM. Role of endoplasmic reticulum stress in the pathogenesis of nonalcoholic fatty liver disease. World J Gastroenterol 2014;20:1768. https://doi.org/10.3748/WJG.V20.I7.1768.
[41] Finck BN, Hall AM. Does Diacylglycerol Accumulation in Fatty Liver Disease Cause Hepatic Insulin Resistance? Biomed Res Int 2015;2015. https://doi.org/10.1155/2015/104132.
[42] Li D, Yang SG, He CW, Zhang ZT, Liang Y, Li H, et al. Excess diacylglycerol at the endoplasmic reticulum disrupts endomembrane homeostasis and autophagy. BMC Biol 2020;18:1–15. https://doi.org/10.1186/S12915-020-00837-W/FIGURES/6.
[43] Bravo R, Gutierrez T, Paredes F, Gatica D, Rodriguez AE, Pedrozo Z, et al. Endoplasmic reticulum: ER stress regulates mitochondrial bioenergetics. Int J Biochem Cell Biol 2012;44:16. https://doi.org/10.1016/J.BIOCEL.2011.10.012.
[44] Gordaliza-Alaguero I, Cantó C, Zorzano A. Metabolic implications of organelle–mitochondria communication. EMBO Rep 2019;20:e47928. https://doi.org/10.15252/EMBR.201947928.
[45] Fonvig CE, Amundsen ID, Vigsnæs LK, Sørensen N, Frithioff-Bøjsøe C, Christiansen M, et al. Human Milk Oligosaccharides Modulate Fecal Microbiota and Are Safe for Use in Children With Overweight: A Randomized Controlled Trial. J Pediatr

Gastroenterol Nutr 2021;73:408–14. https://doi.org/10.1097/MPG.0000000000003205.

[46] Wang X, Xia J, Jiang C. Role of gut microbiota in the development of non-alcoholic fatty liver disease. Liver Res 2019;3:25–30. https://doi.org/10.1016/J.LIVRES.2019.01.006.

[47] Luther J, Garber JJ, Khalili H, Dave M, Bale SS, Jindal R, et al. Hepatic Injury in Nonalcoholic Steatohepatitis Contributes to Altered Intestinal Permeability. Cell Mol Gastroenterol Hepatol 2015;1:222. https://doi.org/10.1016/J.JCMGH.2015.01.001.

[48] De Munck TJI, Xu P, Verwijs HJA, Masclee AAM, Jonkers D, Verbeek J, et al. Intestinal permeability in human nonalcoholic fatty liver disease: A systematic review and meta-analysis. Liver Int 2020;40:2906–16. https://doi.org/10.1111/LIV.14696.

[49] Li A, Zhang C, Chi H, Han X, Ma Y, Zheng J, et al. 2'-Fucosyllactose promotes Lactobacillus rhamnosus KLDS 8001 to repair LPS-induced damage in Caco-2 cells. J Food Biochem 2022:e14059. https://doi.org/10.1111/JFBC.14059.

[50] He YY, Liu SB, Kling DE, Leone S, Lawlor NT, Huang Y, et al. The human milk oligosaccharide 2'-fucosyllactose modulates CD14 expression in human enterocytes, thereby attenuating LPS-induced inflammation. Gut 2016;65:33–46. https://doi.org/10.1136/GUTJNL-2014-307544.

[51] Šuligoj T, Vigsnæs LK, Van den Abbeele P, Apostolou A, Karalis K, Savva GM, et al. Effects of Human Milk Oligosaccharides on the Adult Gut Microbiota and Barrier Function. Nutrients 2020;12:1–21. https://doi.org/10.3390/NU12092808.

CHAPTER

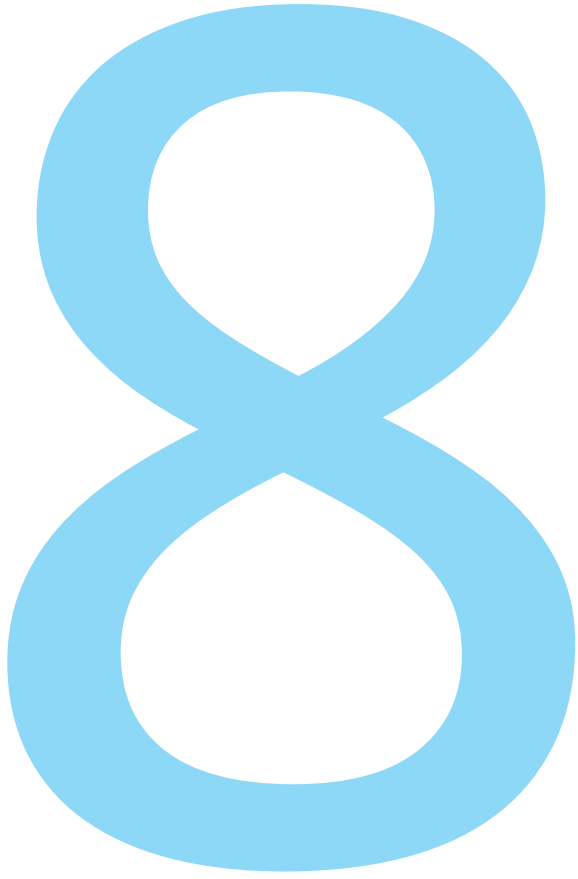

Butyrate protects against diet-induced NASH and liver fibrosis and suppresses specific non-canonical TGF-β signaling pathways in human hepatic stellate cells

Eveline Gart, Wim van Duyvenvoorde, Karin Toet, Martien P. M. Caspers, Lars Verschuren, Mette Juul Nielsen, Diana Julie Leeming, Everton Souto Lima, Aswin Menke, Roeland Hanemaaijer, Jaap Keijer, Kanita Salic, Robert Kleemann and Martine C. Morrison

Biomedicines. 2021 Dec 20;9(12):1954.
doi: 10.3390/biomedicines9121954. PMID: 34944770; PMCID: PMC8698820.

Abstract

In obesity-associated non-alcoholic steatohepatitis (NASH), persistent hepatocellular damage and inflammation are key drivers of fibrosis, which is the main determinant of NASH-associated mortality. The short-chain fatty acid butyrate can exert metabolic improvements and anti-inflammatory activities in NASH. However, its effects on NASH-associated liver fibrosis remain unclear. Putative antifibrotic effects of butyrate were studied in Ldlr-/-.Leiden mice fed an obesogenic diet (HFD) containing 2.5% (*w*/*w*) butyrate for 38 weeks and compared with a HFD-control group. Antifibrotic mechanisms of butyrate were further investigated in TGF-β-stimulated primary human hepatic stellate cells (HSC). HFD-fed mice developed obesity, insulin resistance, increased plasma leptin levels, adipose tissue inflammation, gut permeability, dysbiosis, and NASH-associated fibrosis. Butyrate corrected hyperinsulinemia, lowered plasma leptin levels, and attenuated adipose tissue inflammation, without affecting gut permeability or microbiota composition. Butyrate lowered plasma ALT and CK-18M30 levels and attenuated hepatic steatosis and inflammation. Butyrate inhibited fibrosis development as demonstrated by decreased hepatic collagen content and Sirius-red-positive area. In TGF-β-stimulated HSC, butyrate dose-dependently reduced collagen deposition and decreased procollagen1α1 and PAI1 protein expression. Transcriptomic analysis and subsequent pathway and upstream regulator analysis revealed deactivation of specific non-canonical TGF-β signaling pathways Rho-like GTPases and PI3K/AKT and other important pro-fibrotic regulators (e.g., YAP/TAZ, MYC) by butyrate, providing a potential rationale for its antifibrotic effects. In conclusion, butyrate protects against obesity development, insulin resistance-associated NASH, and liver fibrosis. These antifibrotic effects are at least partly attributable to a direct effect of butyrate on collagen production in hepatic stellate cells, involving inhibition of non-canonical TGF-β signaling pathways.

Graphical abstract

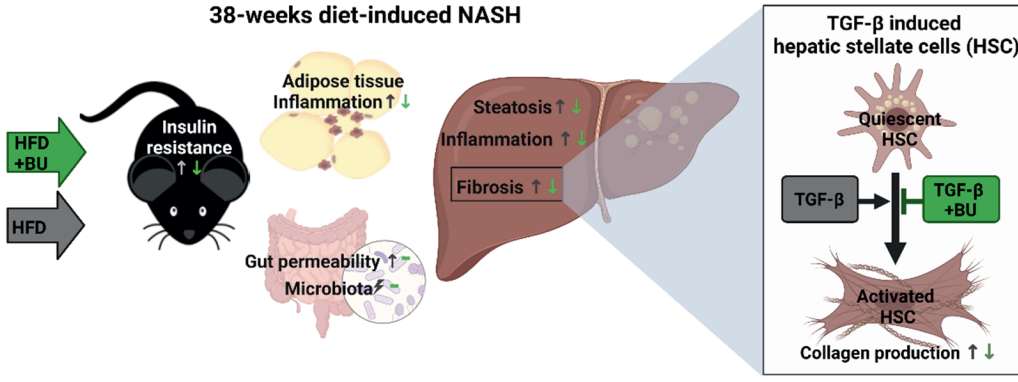

1. Introduction

Liver fibrosis is a result of chronic liver damage for which non-alcoholic steatohepatitis (NASH) is one of the main causal factors [1,2]. Excessive food intake from energy-dense diets can induce hepatic lipids deposition (steatosis) which can progress to NASH (steatosis and inflammation) and fibrosis [3]. NASH-associated liver fibrosis is closely related to obesity, dyslipidemia, insulin resistance, white adipose tissue (WAT) inflammation, and gut dysfunction (increased gut permeability and changes in microbiota composition), all of which are drivers of disease progression [4,5]. To date, no approved treatment for liver fibrosis is available and little is known about how fibrosis development can be attenuated.

Liver fibrosis is characterized by excessive accumulation of extracellular matrix (ECM) proteins such as collagens [6]. Hepatic stellate cells (HSCs) are the main producers of these ECM proteins and therefore play a central role in liver fibrosis. During liver injury, transforming growth factor β (TGF-β) is the most potent fibrogenic cytokine and a key regulator in promoting HSC activation [7]. In response to TGF-β, the canonical signaling pathway (involving SMADs) and non-canonical signaling pathways (i.e., ERK, JNK/p38, Rho-like GTPases, PI3K/AKT) promote HSC activation [8]. The activation of these signaling pathways by TGF-β stimulates trans-differentiation of quiescent HSC to undergo a transcriptional and morphological program into proliferative HSCs that produce excessive amounts of ECM proteins.

Butyrate (BU) is a short-chain fatty acid that is produced by bacterial fermentation of dietary fibers in the colon and has been shown to have beneficial metabolic effects [9–14]. In humans, BU has been studied non-specifically and indirectly (by using probiotics and prebiotics to affect gut microbiota composition, which could potentially increase endogenous colonic butyrate production), which demonstrated that BU, in concert with other pre/pro-biotic induced changes, has satiety-increasing and body weight-reducing effects ([15] and references therein). These observations have been confirmed in rodents, where dietary supplementation with BU was shown to reduce food intake and attenuate body weight gain [16]. BU has also been shown to improve liver steatosis and inflammation [12,17,18]; however, it is unclear if these effects are secondary to its anti-obesogenic effects, or result from a direct effect of BU on these processes. Furthermore, while BU has been shown to improve many of the metabolic dysregulations that underlie development of inflammation and fibrosis in the liver, it is unknown whether BU can also reduce development of fibrosis in the context of obesity-associated NASH.

To study the potential anti-fibrotic effects of butyrate we used a well-established translational mouse model for diet-induced NASH and liver fibrosis: high-fat diet (HFD)-fed Ldlr-/-.Leiden mice. Under translational dietary conditions (i.e., using a HFD with a macronutrient composition and cholesterol content comparable to human diets)[17], these mice develop NASH with fibrosis in the context of obesity, insulin resistance, adipose tissue inflammation, and gut dysfunction, as is typical for many NASH patients [18]In addition, these mice express underlying disease pathways relevant for human NASH, as demonstrated by recent transcriptomics, metabolomics, and proteomics studies [18,19]. To gain mechanistic insight into potential direct anti-fibrotic effects of BU, we performed in vitro studies with primary human HSCs.

2. Materials and Methods

2.1. Animal Experiment

The animal experiment was performed according to the standards of the Animal Care and Use Committee and ethically approved by an independent Animal Welfare Body (IVD TNO; approval number 3682/TNO-245). The ARRIVE guidelines were also adhered to. Ldlr-/-.Leiden male mice (94% C57BL/6J and 6% 129S1 genetic background) obtained from our breeding stock were group-housed (four to five mice per cage) in Macrolon cages in clean conventional animal rooms (relative humidity 50%–60%, temperature ~21°C, light cycle 07:00 to 19:00) in the American Association for Accreditation of Laboratory Animal Care (AAALAC)-accredited animal facility at TNO (Leiden, the Netherlands) with ad libitum access to food and water. Mice were matched into three groups of 15 mice per group based on body weight, plasma cholesterol and triglycerides, and blood glucose, which was the number of mice required to detect statistical differences in liver fibrosis. Two groups of mice (n = 15 each) were fed a high-fat diet (HFD; D12451, Research Diets Inc., New Brunswick, USA; containing 20 kcal% protein, 35 kcal% carbohydrate, 45 kcal% lard fat), or HFD+BU, in which HFD was supplemented with 2.5% sodium butyrate (303410 Sigma Aldrich, Steinheim, Germany). A reference group remained on standard laboratory chow (n = 15), a low-fat control diet (chow; Sniff-R/M-V1530, Uden, the Netherlands). The total treatment period was 38 weeks, during which the mice developed obesity- and insulin resistance-associated liver fibrosis [18,20], which was the main endpoint of this study.

Blood samples were collected via the tail vein from 5 hour-fasted mice, and body weight, food intake, and body composition measurements using echo-MRI were acquired at set intervals during the study. Gut permeability was analyzed after 37 weeks of dietary treatment, and after 38 weeks mice were sacrificed by gradual-fill CO_2 asphyxiation after a 5 h fast. A terminal blood sample was collected via cardiac puncture, organs (liver and adipose tissue) were isolated and immediately snap-frozen in liquid N_2 and/or fixed in formalin, and the mucosal microbiota was collected from the ileum and the colon as previously described [4].

2.2. Blood Chemistry

Analysis of cholesterol, triglycerides, insulin, alanine amine transferase (ALT), tissue inhibitor of metalloproteinases 1 (TIMP-1) in EDTA plasma, and whole blood glucose was performed as described previously [4]. LPS-binding protein (LBP) was measured in plasma with an ELISA kit following the manufacturer's instructions (HK-205, Hycult Biotech, Uden, the Netherlands). The ECM-remodeling biomarkers PRO-C3 and PRO-C4, for type III and type IV collagen formation [21,22], and C4M and C6M to assess metalloproteinase-mediated degradation of type IV and type VI collagen, respectively [23,24], were measured in serum using competitive ELISAs (Nordic Bioscience, Herlev, Denmark).

2.3. Adipose Tissue Histopathology Analysis

Adipose tissue inflammation was assessed as described previously [17]. In short, the number of crown-like structures (CLS) were scored in hematoxylin-phloxine-saffron stained epididymal WAT (eWAT) and mesenteric WAT (mWAT) cross sections in three non-overlapping fields (100×magnification) per mouse. The number of adipocytes in the same fields were analyzed using Adiposoft [25] to express the number of CLS/1000 adipocytes.

2.4. Gut Permeability and Microbiota Composition Analysis

Gut permeability was assessed with an FD4 gut permeability assay, which assesses the ability of fluorescein isothiocyanate-labelled dextran (3–5 kDa FD4; Sigma, St. Louis, MO, USA) to leak through the intestinal lumen into the circulation, as described previously [4].

Microbiota DNA was isolated from mucosal samples of both the colon and ileum using the AGOWA Mag Mini kit (DNA Isolation Kit, AGOWA, Berlin, Germany), according to the manufacturer's instructions. Metagenomic sequencing of the 16s rRNA gene spanning the v4 hypervariable region and data analysis was performed as reported previously [4].

2.5. Liver Histopathology and Biochemistry

Liver histopathology was scored using a standardized method for rodents that is based on the human NAS scoring system [26] in hematoxylin-Eosin-stained (HE) cross sections of the medial lobe. Hepatic fibrosis was analyzed in Sirius-red stained cross sections of the sinister lobe. Total steatosis, i.e., the sum of macrovesicular and microvesicular steatosis, hypertrophy (abnormally enlarged hepatocytes), and fibrosis for each mouse was determined as a percentage of total liver section affected. Hepatic inflammation was quantified by counting the number of inflammatory aggregates in five non-overlapping fields per mouse at 100× magnification (field of view 4.15 mm^2) and expressed as the number of aggregates per mm^2.

In addition, inflammatory chemokines were measured in liver biopsies homogenized in a 50 mmol/L Tris-HCL pH 7.4, 150 mmol/L NaCL, 5 mmol/L CaCl2, 1% Triton X-100 lysis buffer. Intrahepatic chemokines CCL3, CCL5, CXCL1, and CXCL10 were measured with a Quanterix chemokine panel according to the manufacturer's protocol (Mouse 4-Plex Developer Kit; 100A-0497 Rev 01; Quanterix, MA, USA) on a SP-X Quanterix machine. Protein concentrations were measured with the BCA Protein Assay Kit (Thermo Fisher Scientific, Waltham, MA, USA) to determine chemokines per mg of protein.

Hepatic total collagen content was quantified based on hydroxyproline residues obtained from acid hydrolysis (QZBtiscol, Quickzyme, Leiden, the Netherlands) of the sinister lobe, and protein concentrations were measured in the same hydrolysates (QZBtotprot, Quickzyme) according to the manufacturer's instructions.

2.6. Primary Human Hepatic Stellate Cell Experiments, Gene Expression Analysis, and Protein Expression Using Western Blot Analysis

Primary human hepatic stellate cells (HSC) (BioIVT, West Sussex, UK) were seeded on fibronectin-coated (Roche, Woerden, The Netherlands) 24-well culture plates and maintained overnight in stellate cell medium (STECM) supplemented with 2% (*v*/*v*) fetal bovine serum (FBS), 1% (*v*/*v*) antibiotic solution, and 1% (*v*/*v*) stellate cell growth supplement (all HSC seeding medium materials were from ScienCell, Carlsbad, CA, USA). HSC were incubated for 4 days in STECM supplemented with 1% (*v*/*v*) FBS and 1% (*v*/*v*) antibiotic solution with or without TGF-β1 (2 ng/mL; rh-TGFB1 R&D systems, Minneapolis, USA), and TGF-β1 co-treated with BU (sodium butyrate, Sigma Aldrich; the same as was used in the animal experiment), acetate (sodium acetate, Sigma Aldrich), or caproate (sodium hexanoate, Sigma Aldrich).

Cytotoxicity was determined in triplicate per condition in conditioned medium using the CyQUANT LDH cytotoxicity assay (Invitrogen, Eugene, OR, USA), according to the manufacturer's instructions. The cell-matrix fraction was hydrolyzed in 6M HCL and used for determination of collagen protein concentration based on hydroxyproline residues (QZBtiscol, Quickzyme) and total cell protein concentrations (QZBtotprot, Quickzyme), following the manufacturer's instructions. Total protein levels were used to correct the collagen concentration per sample. Human procollagen 1α1 and plasminogen activator inhibitor 1 (PAI1) protein expression (R&D Systems, Abingdon, UK) were measured in conditioned medium collected after 24 h of stimulation.

In addition, next-generation sequencing was performed in RNA samples extracted from n = 6 unstimulated; n = 8 TGF-β; n = 8 TGF-β+BU conditioned HSC. RNA was isolated using the RNAqeous Microkit (Thermo Fisher Scientific) and RNA concentrations were determined spectrophotometrically, as described in [17]. The NEBNext Ultra II Directional RNA Library Prep Kit for Illumina (New England BioLabs, Ipswich, MA, USA) was used to process the samples, following the manufacturer's instructions. Strand-specific messenger RNA sequencing libraries were clustered, and sequenced on a NovaSeq6000 system (paired-end 20M reads/sample, Illumina, San Diego, CA, USA) at Genomescan (Leiden, the Netherlands). The quality was checked with the Illumina data analysis pipeline RTA3.4.4 and Bcl2fastq v2.20, and filtered and trimmed using TRIMMOMATIC software. These trimmed files were merged and aligned to the reference genome (Homo_sapiens.GRCh38.gencode.v29) using the STAR 2.5 algorithm with default settings. Next, Htseq-count 0.6.1p1 was used to count the read mapping frequency per gene, resulting in count files (GSE179395) which served as input for the differentially expressed genes (DEGs) analysis using the Deseq2-method [27]. DEGs ($p < 0.0001$ and Z-score > 1.3) were used as an input for pathway analysis through Ingenuity Pathway Analysis (IPA) [28]. Based on gene expression of all known downstream target genes, IPA predicted activation or deactivation of an upstream regulator, as reported in [17].

Protein expression of cMyc was analyzed using western blot analysis. HSC from each condition (two pools of three wells per condition) were collected by scraping in ice cold lysis buffer [29], and protein content was determined (BCA Protein Assay Kit, Thermo Fisher Scientific). Protein samples (10 µg) were prepared, separated, and blotted, as

previously described in [29]. The blotting membranes were treated with block buffer for 1 h (5% (*w*/*v*) milk powder in tris-buffered saline with 0.1% Tween 20 (TBST)) and incubated overnight in at 4 °C in block buffer with either the primary antibody targeting cMyc (#9402–1:2000 *v*/*v*; Cell Signaling, Leiden, the Netherlands) or the loading control vinculin (#4650–1:1000 *v*/*v*, Cell Signaling). The next day, blots were washed in TBST and incubated for 1 h in block buffer with the secondary antibody (#7074S-1:2000 *v*/*v*; Cell Signaling). Blots were washed again and treated with SuperSignal West Femto (Thermo Fisher Scientific) to visualize protein bands. Blots were analyzed with a ChemiDoc Touch Imaging system (Bio-Rad) and band intensities were normalized to vinculin.

2.7. Statistics

Statistical analysis was performed with IBM SPSS statistics version 25.0 (SPSS Inc., Chicago, IL, USA). Data were tested for normality with the Shapiro-Wilk test and for equal variance with Levene's test ($\alpha = 0.05$). Normally distributed data with equal variance was tested with an one-way analysis of variance (ANOVA) with a Dunnet's post hoc test (HFD was the control group for in vivo data, TGF-β condition was the control group for in vitro data). The Kruskal–Wallis test with a Mann–Whitney post hoc test was performed for data that were not normally distributed or had equal variance.

3. Results

3.1. Butyrate Attenuates HFD-Induced Obesity, Improves Metabolic Risk Factors, and Reduces Adipose Tissue Inflammation

Long-term HFD feeding over 38 weeks significantly increased body weight relative to chow, while energy intake was comparable in the HFD and chow group. The observed increase in body weight with HFD was associated with a higher food efficiency (body weight gain per kcal consumed) in the HFD group (Table 1). Treatment with BU reversed these HFD-induced effects as observed by a decrease in body weight and energy intake (Table 1). Moreover, food efficiency was lowered compared with HFD, indicating that BU has additional positive effects on body weight, independent of energy intake (Table 1). HFD feeding increased plasma cholesterol and triglycerides, which were unaffected by BU. Glucose levels were comparable in all groups, while fasting insulin concentrations were strongly increased by HFD feeding and significantly lowered with BU, reaching insulin concentrations below those observed in chow (Table 1).

Table 1. Body composition and metabolic risk factors.

	Chow	HFD	HFD + BU
Body weight (g)	42.4 ± 6.3 ***	56.5 ± 3.9	45.3 ± 4.4 ***
Average energy intake (kcal/mouse/day)	12.7 ± 0.5	13.4 ± 0.3	11.6 ± 0.5 **
Average food efficiency (mg BW gain/kcal)	3.85 ± 1.72 ***	7.54 ± 1.14	5.73 ± 0.86 ***
Cholesterol (mM)	9.3 ± 2.2 ***	34.4 ± 6.4	35.7 ± 7.5
Triglycerides (mM)	1.7 ± 0.6 ***	5.5 ± 2.1	6.3 ± 2.5
Glucose (mM)	7.1 ± 1.1	6.6 ± 0.9	6.6 ± 1.2
Insulin (ng/mL)	9.3 ± 16.4 *	20.3 ± 11.1	8.1 ± 4.2 *
Leptin (ng/mL)	25.3 ± 13.3 ***	59.2 ± 16.0	39.3 ± 9.5 ***
Adiponectin (ug/mL)	7.2 ± 1.2 *	6.1 ± 1.6	6.2 ± 0.8

*BW = body weight. Data are presented as mean ± SD, * $p < 0.05$, ** $p < 0.01$, *** $p < 0.001$ vs. the HFD control group.*

The observed increase in fat mass with HFD was accompanied by alterations in plasma adipokine concentrations, i.e., leptin was increased and adiponectin decreased. BU reduced plasma leptin concentrations with no effect on adiponectin (Table 1), suggesting a beneficial effect on adipose tissue. Quantitative histological analysis of inflammation in epididymal and mesenteric white adipose tissue (WAT) depots demonstrated that the number of crown-like structures (CLS) was increased by HFD in both WAT depots (Figure 1A–D). BU lowered the number of CLS in both WAT depots, in line with the reduction in proinflammatory plasma leptin level.

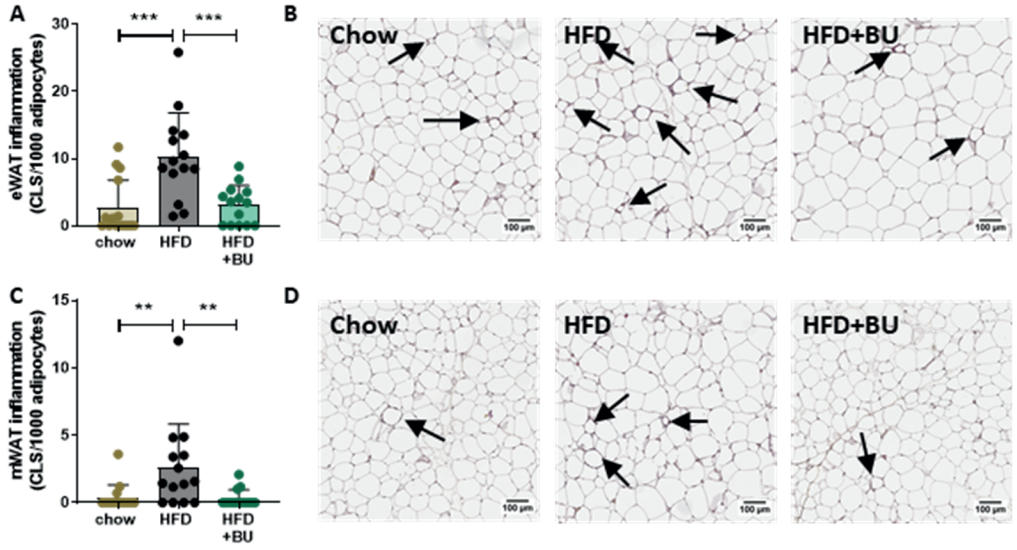

Figure 1. *Butyrate reduced white adipose tissue inflammation (WAT). The number of inflammatory crown-like structures (indicated with arrows) were scored in (**A**) epididymal WAT (eWAT), and shown in (**B**) the representative images of eWAT inflammation. Inflammation was also scored in (**C**) mesenteric WAT (mWAT and shown in (**D**)) the respective images representing mWAT inflammation. Data are presented as mean ± SD, ** p < 0.01, *** p < 0.001 vs. the HFD control group.*

3.2. Butyrate Did Not Affect the HFD-Induced Increase in Gut Permeability or Changes in Microbiota Composition

To determine whether these metabolic improvements with BU may be associated with beneficial effects in the gut, we performed a functional gut permeability test, measured plasma LPS-binding protein (LPB) concentrations, and performed a 16S rRNA microbiota composition analysis. Gut permeability was increased with HFD and unaffected by BU (Figure 2A). Similarly, plasma concentrations of the LPB were increased with HFD and not altered by BU (Figure 2B). Microbiota composition analysis was performed in the mucosal compartments of both the colon and ileum. Permutation tests which enable the statistical testing of differences in microbiota composition between experimental groups showed that HFD feeding altered both ileum (p = 0.002) and colon (p = 0.002) colonization relative to chow, as presented in Figure 2C. An overview of the significantly different genera between the experimental groups are provided in Supplementary Figures S1–3. BU did not affect microbiota composition compared with HFD in colon (p = 0.234) and was affected only the abundance of three genera in ileum (p = 0.048), as visualized in Figure 2C by the extensive overlap between HFD and butyrate-fed mice.

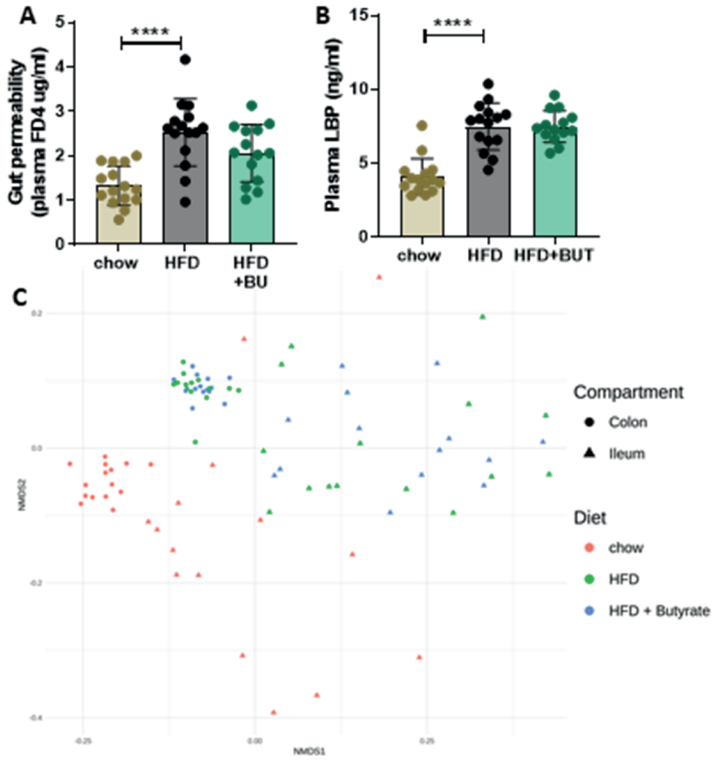

Figure 2. *Butyrate does not affect gut permeability and microbiota composition. (**A**) Functional gut permeability fluorescein isothiocyanate-labeled dextran (FD4) assay. (**B**) Plasma LPS binding protein (LBP) concentrations. Data are presented as mean ± SD, **** $p < 0.0001$ vs. the HFD control group. (**C**) 16S rRNA gene analysis was performed to study the microbiota composition in fecal and mucosal compartments of both the colon and ileum. These changes in microbiota composition were visualized by non-metric multidimensional scaling (NMDS) using the Bray–Curtis index, in which every dot represents the microbiota composition of one mouse and the distance between dots represent how (dis)similar the microbiota composition is between these mice.*

Taken together, in the context of an obese phenotype with pronounced hyperinsulinemia, hyperlipidemia, WAT, and gut dysfunction, BU decreased body weight, WAT inflammation, and reversed hyperinsulinemia. All of these beneficial BU effects seem to be independent of the gut microbiota composition or gut permeability as these were largely unaffected by BU.

3.3. Butyrate Protected Mice against NASH Development

Liver weight was increased in control mice on an HFD, whereas BU-fed mice were protected from the HFD-induced liver weight gain (Figure 3A). Levels of the circulating liver damage markers ALT and CK18-M30 were increased with HFD and were lowered by BU (Figure 3B,C). To investigate the effect on the liver in more detail, liver cross sections were

analyzed for histopathological features of NASH (Figure 3D). Steatosis was hardly present in the chow-fed mice, whereas HFD-fed mice developed pronounced steatosis with equal induction of macrovesicular (Figure 3E) and microvesicular steatosis (Figure 3F). BU significantly reduced steatosis observed by a similar reduction in both macrovesicular and microvesicular steatosis. Consistent with this, HFD increased the cross-sectional area covered with abnormally enlarged hepatocytes, which was attenuated with BU (Figure 3G). Hepatic inflammation was practically absent in chow-fed mice, and HFD strongly increased the number of inflammatory aggregates. BU significantly suppressed the number of inflammatory aggregates (Figure 3H). These anti-inflammatory effects were confirmed by analyzing hepatic chemokine concentrations. HFD increased hepatic CCL3 (MIP1a) and CCL5 (RANTES), which were significantly decreased with butyrate (Figure 3I,J). HFD feeding also significantly increased CXCL1 (KC) and CXCL10 (IP-10), which were not affected by butyrate (Supplemental Figure S4). Altogether, HFD feeding resulted in a pronounced increase in steatosis and inflammation in the liver, which was strongly attenuated by BU.

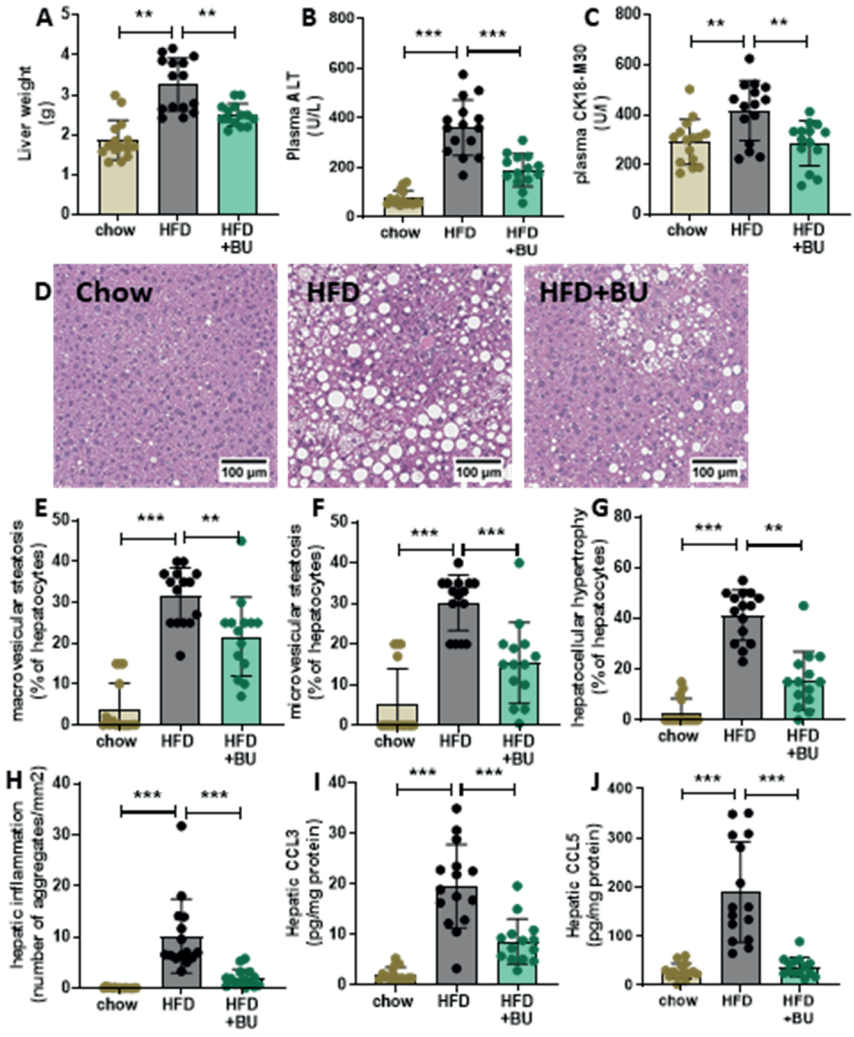

Figure 3. *Butyrate reduced plasma liver damage markers, steatosis, and hepatic inflammation in 38-week HFD-fed animals. (**A**) Liver weight, (**B**) plasma liver damage maker ALT, and (**C**) CK18-m30. (**D**) Representative images of hematoxylin-eosin stained liver sections analyzed for (**E**) macrovesicular steatosis, (**F**) microvesicular steatosis, (**G**) hepatocellular hypertrophy, and (**H**) hepatic inflammation, supported by hepatic chemokine concentrations (**I**) CCL3 and (**J**) CCL5, expressed per mg protein. Data are presented as mean ± SD, ** p < 0.01, *** p < 0.001 vs. the HFD control group.*

3.4. Butyrate Reduced Liver Fibrosis

HFD feeding strongly increased the alpha smooth muscle cell actin (αSMA)-positive area in liver cross sections, which is a marker for activated hepatic stellate cell (HSC), the main collagen-producing cells in the liver. BU tended to lower this HFD-induced αSMA positive area (Figure 4A). In line with this data, HFD significantly increased the hepatic

collagen content as demonstrated in freshly prepared liver homogenates (Figure 4B). In BU-fed mice hepatic collagen content was significantly lower, indicating that BU-fed mice were protected against HFD-induced liver fibrosis (Figure 4B). This was confirmed by histopathological analysis of fibrosis, which showed that HFD increased the Sirius-red-positive area and BU fully blunted this induction (Figure 4C). Development of liver fibrosis was accompanied by significant increases in circulating tissue inhibitor of metalloproteinase 1 (TIMP1) and ECM remodeling markers of pericellular fibrosis, PRO-C4 and C6M (Supplementary Table S1). BU did not significantly affect TIMP1 or ECM turnover biomarkers.

Thus, BU-fed mice were not only protected against NASH development but also showed strongly reduced fibrosis, which was not reflected by the measured circulating ECM remodeling markers.

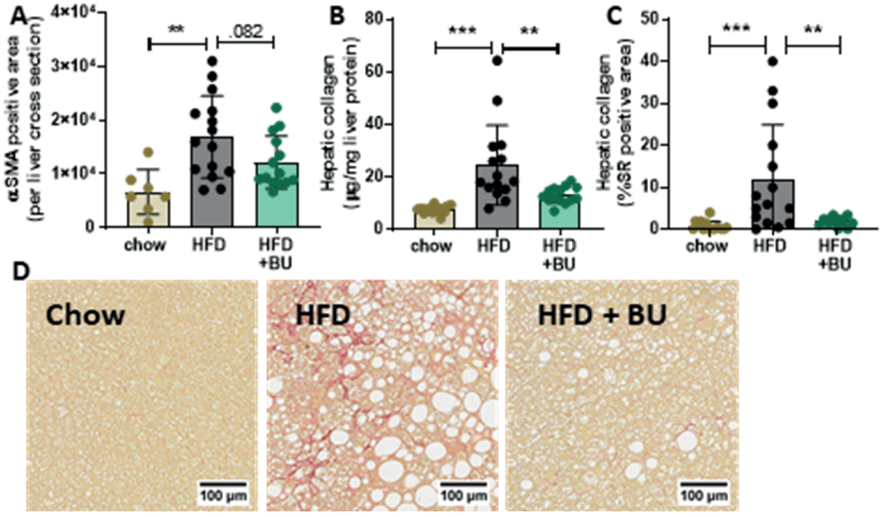

Figure 4. *Butyrate decreased liver fibrosis in 38-week HFD-fed animals. (**A**) Alpha-smooth muscle cell actin (αSMA) immunoreactive positive area in liver cross sections, (**B**) hepatic collagen content measured in liver homogenates, (**C**) Sirius-red (SR) positive area of (**D**) Sirius-red stained cross-sections (representative images). Data are presented as mean ± SD, ** p < 0.01, *** p < 0.001 vs. the HFD control group.*

3.5. Butyrate Directly Reduced TGF-β-Induced Collagen Production in Primary Human Hepatic Stellate Cells

To further elucidate the mechanisms underlying these antifibrotic effects, we studied BU treatment effects on collagen production by hepatic stellate cells (HSC) in vitro, followed by a transcriptomics analysis to assess modulation of underlying pathways and regulators. After defining an optimal dose for BU in cell viability assays (Supplemental Figure S5), TGF-β-stimulated primary human HSC treated with 1mM BU demonstrated a consistent strong reduction of TGF-β-induced collagen deposition showing that BU has direct anti-fibrotic effects in HSC (Figure 5A). This was further confirmed by reduced procollagen1α1

levels in conditioned culture medium from BU-treated cells, suggesting that the observed collagen decrease is a result of reduced collagen synthesis (Figure 5B). In addition, BU significantly attenuated TGF-β-induced protein expression of the stellate cell activation marker PAI1, which demonstrates that BU inhibited activation of HSC into proliferative fibrogenic myofibroblasts (Figure 5C). In line with this, a reduction was observed in gene expression of HSC activation markers (e.g., ACTA2 encoding for αSMA, SERPINE1 encoding for PAI1, ELN) (Table 2). These anti-fibrotic effects were found to be specific and dose-dependent for the SCFA butyrate, since other SCFAs did not affect collagen deposition in TGF-β-stimulated HSC (Supplemental Figure S6).

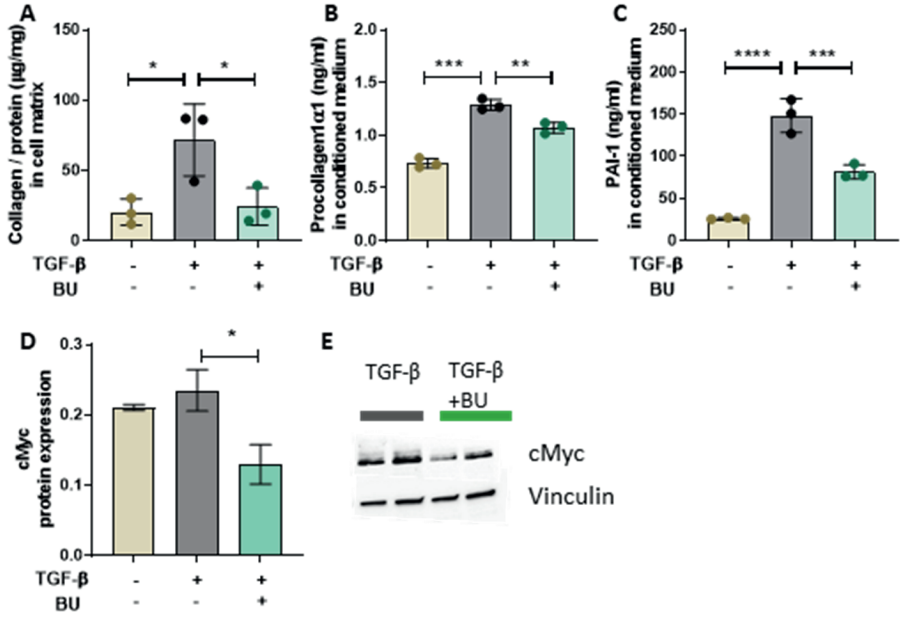

Figure 5. *Butyrate directly decreased TGF-β induced fibrosis in primary human hepatic stellate cells. (**A**) Collagen content in the cell matrix, (**B**) procollagen1a1 protein expression, and (**C**) PAI-1 protein expression in conditioned medium. Western blot analysis was used to determine (**D**) cMyc protein expression normalized for vinculin protein expression. (**E**) Representative images of the western blot bands. Data are presented as mean ± SD, * p < 0.05, ** p < 0.01, *** p < 0.001, ****p<0.0001 compared with the TGF-β control group.*

Table 2. Gene expression analysis in primary human stellate cells.

	TGF-β vs. Unstimulated		BU+TGF-β vs. TGF-β	
Gene Name:	**2logR**	**P-value**	**2logR**	**P-value**
Myofibroblast markers				
ACTA2	4.28	0.000	−1.15	0.000
SERPINE1	2.03	0.000	−0.37	0.000
ELN	2.13	0.000	−1.40	0.000
CDH11	1.43	0.000	−1.45	0.000
DES	0.70	0.007	1.62	0.000
VIM	−0.02	0.682	0.79	0.000
PALLD	2.29	0.000	−0.27	0.000
TPM1	3.24	0.000	0.13	0.002
CFL1	0.62	0.000	−0.26	0.000
COL1A1	0.63	0.000	−0.05	0.402

Changes in gene expression of myofibroblast markers indicative for hepatic stellate cell activation. Gene expression changes are expressed in 2log fold-change (2logR), red indicates upregulation in gene expression, green indicates downregulation, and significant changes are marked in grey.

To gain mechanistic insight into these anti-fibrotic effects of BU, we performed a subsequent upstream regulator analysis on the gene expression data. As expected, TGF-β strongly activated the TGF-β receptor and canonical pathway signaling downstream of the TGF-β receptor (Table 3). Although a number of these factors were significantly enriched by BU treatment, most of the upstream regulators did not reach the cut-off value for consistent activation or inactivation—indicating that attenuation of TGF-β induced fibrosis by BU is not mediated via modification of the canonical TGF-β signaling pathway (Table 3). Importantly, TGF-β also activated non-canonical pathways downstream of the TGF-β receptor (involving ERK, JNK/P38, Rho-like GTPases and PI3K/AKT). BU did not affect the pathways via ERK and JNK/P38, but consistently deactivated the non-canonical signaling routes mediated by Rho-like GTPases and PI3K/AKT/MYC. Of note, BU did not exert its effect on one particular component of these pathways, but tended to simultaneously inactivate multiple of its components. Furthermore, BU also reduced TGF-β-induced activation of the Hippo signaling pathway (YAP/TAZ), a critical pathway in liver fibrosis [30]. To confirm our observations on protein level we performed a western blot analysis on cMyc protein expression. In line with the upstream regulator analysis we found that TGF-β non-significantly increased cMyc expression, whereas butyrate significantly decreased cMyc protein expression (Figure 5D,E).

Table 3. Upstream regulator analysis in primary human stellate cells.

	TGF-β vs. Unstimulated		BU+TGF-β vs. TGF-β	
Upstream Regulator:	**Z-Score**	**P-value**	**Z-Score**	**P-value**
TGF-β signaling				
TGFB1	9.7	0.000	1.5	0.000
TGFB2	5.1	0.000	−0.4	0.002
TGFB3	5.6	0.000	−0.7	0.000
TGFBR1	2.6	0.000	−0.2	0.030
TGFBR2	1.8	0.000	−0.1	0.000
TGFBR3	−1.0	0.026	N/A	N/A
Canonical TGF-β signaling				
SMAD1	0.4	0.000	0.7	0.003
SMAD2	4.5	0.000	N/A	1.000
SMAD3	2.8	0.000	2.0	0.014
SMAD4	3.5	0.000	1.3	0.002
SMAD7	−1.5	0.000	−0.9	0.002
SMAD2/3/4	2.6	0.001	N/A	1.000
SMAD1/5/9	N/A	1.000	N/A	0.022
Non-canonical TGF-β signaling via ERK				
RAS	2.9	0.000	0.9	0.000
RAF	0.2	0.000	0.5	0.000
MAP2K1	1.6	0.000	2.1	0.000
ERK	3.0	0.000	3.1	0.000
CAV1	1.3	0.000	1.6	0.000
via JNK/p38				
MAP3K7	0.6	0.000	N/A	1.000
JNK	3.4	0.000	0.0	0.000
MAPK11	0.6	0.030	2.4	0.120
MAPK13	−0.8	0.039	1.3	0.037
MAPK14	1.4	0.000	2.7	0.000
AP1	2.2	0.000	2.7	0.026
via Rho-like GTPases				
RHOA	1.2	0.001	−1.0	0.001
ROCK	1.5	0.000	−0.9	0.000
CDC42	N/A	1.000	N/A	1.000
RAC1	2.7	0.000	N/A	1.000
PAK1	1.4	0.006	−1.0	0.019
PAK2	−0.3	0.000	−1.6	0.006
via PI3K/AKT				
AKT	3.3	0.000	0.2	0.000

PTEN	−2.0	0.000	1.2	0.000
GSK3B	0.6	0.011	−1.1	0.042
MDM2	N/A	1.000	−0.7	0.008
MYC	2.2	0.000	−6.2	0.000
MTORC1	0.7	0.003	N/A	1.000
HIPPO signaling				
YAP1	2.5	0.000	−2.1	0.000
WWTR1	0.8	0.000	−1.8	0.000

The activity of an upstream regulator was calculated based on gene expression changes of all downstream target genes. A Z-score < −2 indicates inhibition of the respective regulator or pathway (green color) and Z > 2 indicates activation (red color). The p-value < 0.05 in grey indicates significant enrichment of the target genes downstream of a regulator, i.e., that more downstream genes are affected than can be expected by chance. N/A indicates an insufficient number of differentially expressed genes to predict the activation state of an upstream regulator.

In conclusion, BU specifically and dose-dependently decreased collagen synthesis in TGF-β stimulated HSC by attenuating activation of HSC into proliferative fibrogenic myofibroblasts. Gene expression analysis indicated that BU deactivated non-canonical TGF-ß signaling pathways involving Rho-like GTPases and PI3K/AKT/MYC, confirmed by western blot analysis for cMyc protein expression, providing a rationale for its antifibrotic effects.

4. Discussion

The objective of this long-term BU supplementation study was to investigate potential anti-fibrotic effects of BU in the context insulin-resistance-associated obesity. Indeed, mice fed BU for 38 weeks were protected against obesity-associated WAT inflammation, hyperinsulinemia, and NASH, and BU strongly suppressed development of liver fibrosis. These anti-fibrotic effects were supported by in vitro experiments in HSC demonstrating that BU directly and dose-dependently inhibited TGF-β induced collagen production.

This long-term dietary treatment study of 38 weeks allowed the examination of NASH-associated liver fibrosis. We demonstrated that BU-fed mice were protected against liver fibrosis development as hepatic collagen content and Sirius-red-positive area were decreased. The anti-fibrotic effects of BU observed in vivo were further substantiated by a dose-dependent reduction in collagen production by BU in an in vitro fibrosis model using TGF-β induced primary human HSC. Quiescent HSC comprise 10% of the liver and, in response to chronic liver injury, HSC will be activated and expand to approximately 15% of the total liver cells [31], concomitant with a major upregulation of hepatic collagen production. Importantly, only the SCFA BU—but not other SCFAs—lowered collagen deposition, indicating that the anti-fibrotic effect is specific for BU. NGS gene expression analysis demonstrated that HSC activation was attenuated with butyrate (e.g., SERPINE1 encoding for PAI1 and ACTA2 encoding for αSMA) [32,33], supported by a decrease in PAI1 protein expression in the HSC, and also in vivo by the αSMA staining in the livers of the mice. Subsequent pathway and upstream regulator analysis on the NGS data showed that BU did

not affect canonical TGF-β signaling, but rather inactivated specific non-canonical pathways Rho-like GTPases and PI3K/AKT. RhoA and Rock GTPases promote nuclear localization and activation of YAP/TAZ to stimulate fibrosis [34], as observed in TGF-β stimulated HSC, and BU counteracted this effect. Suppression of YAP/TAZ activation by BU may be of particular importance because YAP/TAZ has been shown to sense ECM stiffness and to promote ECM production in a self-sustaining feedforward loop [34]. Interestingly, it was very recently shown that PAI-1 protein expression is mainly determined by the YAP/TAZ signaling pathway [35]. Therefore, the reduction of PAI-1 protein expression shown with butyrate in the present study confirms the predicted observed reduction in the Hippo signaling pathway (YAP/TAZ signaling) on the protein level. Also of note is the pronounced deactivation of MYC upon BU treatment, as confirmed by a decrease in cMyc protein expression with western blot analysis, since this has been demonstrated to be a marker of liver fibrosis [36] and overexpression of MYC alone induces HSC activation [37].

The observed NASH-attenuating effects are in line with findings in other rodent models that rely on the use of supraphysiological levels of cholesterol to induce liver inflammation [38,39] or methionine-choline-deficient diet models [40], which both focus on a very specific aspect of disease development. In this study, we used a model that makes use of translational dietary conditions (with a macronutrient composition and a natural cholesterol content similar to human diets) [17] and reflects the multiple organ dysfunction that is characteristic of NASH in humans [3,18]. Under these translational experimental conditions, we demonstrated that BU supplementation protects against diet-induced obesity, WAT inflammation, hyperinsulinemia, NASH, and liver fibrosis. These findings with BU cannot be merely ascribed to a reduction in caloric intake as food efficiency calculations showed that BU decreased the body weight increase per consumed calorie. Li et al. demonstrated that BU modestly increased fat oxidation in metabolic organs such as brown adipose tissue and muscle tissue [16], which may contribute to the observed weight loss independent of food intake. In line with this, the observed anti-fibrotic effects of BU can also not be linked directly to the reduction in energy intake, as demonstrated by a comparison of historical data from HFD-fed Ldlr-/-.Leiden control mice (Supplemental Figure S7)—which showed no difference in fibrosis development between mice with 'normal' energy intake (comparable to the HFD control group in the current study) and mice with 'low' energy intake (comparable to the HFD+BU group in the current study).

The pronounced hepatoprotective effects by BU seem to be mediated independent of the gut, as BU did not affect gut permeability or microbiota composition. It is possible that BU in the current study did not reach the colon, since absorption of SCFAs such as BU already takes place in the stomach [41] and ileum [42–44]. In line with this notion, studies using higher BU supplementation concentrations did report changes in fecal [9,40] or cecal [16] microbiota composition. Changes in microbiota composition are typically based on the fecal microbiota composition since it is easily accessible. However, we have previously shown that the colon mucosal site has better predictive value for metabolic dysfunction and NAFLD development [4]. Moreover, a reasonable assumption is that bacteria in the mucosal layer are in closer proximity to the gut barrier and therefore in more direct contact with the host than the fecal microbiota. Changes in functional gut

permeability with BU in the context of metabolic overload induced NASH have not been studied yet to our knowledge, though increased gut barrier protein expression with butyrate has been reported [9]. Attenuation of gut permeability has been studied in the context of acute infections [45], stroke [46], and atherosclerosis models [47]. The experimental conditions employed in the present study (i.e., long-term HFD treatment with chronic low-grade inflammation) deviate from these models and it is possible that in other (more severe conditions) BU has different effects. Additionally, differences may be attributable to the higher butyrate dosages used in other studies.

BU attenuated WAT inflammation associated with an improvement in adipokine secretion, i.e., lowering of circulating proinflammatory leptin in line with previous observations [48]. Ikejima et al. demonstrated that sinusoidal endothelial cells and Kupffer cells both express functional leptin receptors and, when studied in vitro, respond to leptin with increased expression of TGF-β [49], the main pro-fibrotic cytokine. Furthermore, leptin has also been described to directly stimulate HSC activation in vitro [50]. The observed anti-inflammatory effect in WAT and lowered circulating leptin levels in the current study could therefore also indirectly have contributed to the attenuation of hepatic inflammation and liver fibrosis with BU.

A limitation of the current in vivo study is that it does not allow investigation of body weight-independent effects of BU. Nevertheless, the food-efficiency calculations and results from the in vitro experiments do provide an indication that BU has additional (direct) beneficial effects on top of the observed anti-obesogenic effects. These may be further investigated in future studies that include a pair-fed control group. In addition, as mentioned above, butyrate that is supplemental to the diet can already be absorbed in the upper intestinal tract and its effects are therefore not directly comparable to the effects of microbially produced BU, which is absorbed in the colon (and most likely becomes available systemically at lower doses than those used herein). However, the route of administration chosen here does allow direct and specific investigation of the effects of BU, while studies using fermentable fibers to increase microbial butyrate production indirectly will always be confounded by other fiber-induced effects.

In conclusion, we demonstrate that in the context of an obese phenotype with multiple-organ dysfunction and insulin resistance, BU protected mice against diet-induced NASH and liver fibrosis development. The anti-fibrotic effects of BU may at least in part be explained by direct inhibition of collagen synthesis in hepatic stellate cells involving suppression of specific non-canonical TGF-β signaling pathways Rho-like GTPases and PI3K/AKT, and other important pro-fibrotic regulators (e.g., YAP/TAZ, MYC).

Acknowledgments: We would like to thank Jessica Snabel, Christa G. F. de Ruiter and Joline Attema for assistance with coordination and conduct of the animal studies. We also greatly appreciate Haysam Mohamed Magdy Ahmed for his assistance during the cell culture experiments and thoughtful discussions.

References

1. Pelusi, S.; Cespiati, A.; Rametta, R.; Pennisi, G.; Mannisto, V.; Rosso, C.; Baselli, G.; Dongiovanni, P.; Fracanzani, A.L.; Badiali, S.; et al. Prevalence and Risk Factors of Significant Fibrosis in Patients With Nonalcoholic Fatty Liver Without Steatohepatitis. *Clin. Gastroenterol. Hepatol.* **2019**, *17*, 2310-2319.e6.
2. Vilar-Gomez, E.; Calzadilla-Bertot, L.; Wai-Sun Wong, V.; Castellanos, M.; Aller-de la Fuente, R.; Metwally, M.; Eslam, M.; Gonzalez-Fabian, L.; Alvarez-Quiñones Sanz, M.; Conde-Martin, A.F.; et al. Fibrosis Severity as a Determinant of Cause-Specific Mortality in Patients With Advanced Nonalcoholic Fatty Liver Disease: A Multi-National Cohort Study. *Gastroenterology* **2018**.
3. Brown, G.T.; Kleiner, D.E. Histopathology of nonalcoholic fatty liver disease and nonalcoholic steatohepatitis. *Metabolism.* 2016, *65*, P1080-P1086.
4. Gart, E.; Lima, E.S.; Schuren, F.; Ruiter, C.G.F. De; Attema, J.; Verschuren, L.; Keijer, J.; Salic, K.; Morrison, M.C. Diet-Independent Correlations between Bacteria and Dysfunction of Gut , Adipose Tissue , and Liver : A Comprehensive Microbiota Analysis in Feces and Mucosa of the Ileum and Colon in Obese Mice with NAFLD. 1–20.
5. Loomba, R.; Friedman, S.L.; Shulman, G.I. Mechanisms and disease consequences of nonalcoholic fatty liver disease. *Cell* **2021**, *184*, 2537–2564.
6. Baiocchini, A.; Montaldo, C.; Conigliaro, A.; Grimaldi, A.; Correani, V.; Mura, F.; Ciccosanti, F.; Rotiroti, N.; Brenna, A.; Montalbano, M.; et al. Extracellular matrix molecular remodeling in human liver fibrosis evolution. *PLoS One* **2016**, *11*, e0151736.
7. Dewidar, B.; Soukupova, J.; Fabregat, I.; Dooley, S. TGF-β in Hepatic Stellate Cell Activation and Liver Fibrogenesis: Updated. *Curr. Pathobiol. Rep.* **2015**, *3*, 291–305.
8. Zhang, Y.E. Non-Smad pathways in TGF-β signaling. *Cell Res.* 2009, *19*, 128–139.
9. Zhou, D.; Pan, Q.; Xin, F.Z.; Zhang, R.N.; He, C.X.; Chen, G.Y.; Liu, C.; Chen, Y.W.; Fan, J.G. Sodium butyrate attenuates high-fat diet-induced steatohepatitis in mice by improving gut microbiota and gastrointestinal barrier. *World J. Gastroenterol.* **2017**, *23*, 60–75.
10. Sun, B.; Jia, Y.; Hong, J.; Sun, Q.; Gao, S.; Hu, Y.; Zhao, N.; Zhao, R. Sodium butyrate ameliorates high-fat diet-induced NAFLD through PPARα-mediated activation of β oxidation and suppression of inflammation. *J. Agric. Food Chem.* **2018**, *66*, 7633–7642.
11. Canfora, E.E.; Jocken, J.W.; Blaak, E.E. Short-chain fatty acids in control of body weight and insulin sensitivity. *Nat. Rev. Endocrinol.* **2015**, *11*, 577–591.
12. Mattace Raso, G.; Simeoli, R.; Russo, R.; Iacono, A.; Santoro, A.; Paciello, O.; Ferrante, M.C.; Canani, R.B.; Calignano, A.; Meli, R. Effects of Sodium Butyrate and Its Synthetic Amide Derivative on Liver Inflammation and Glucose Tolerance in an Animal Model of Steatosis Induced by High Fat Diet. *PLoS One* **2013**, *8*, 1–13.
13. Arnoldussen, I.A.C.; Wiesmann, M.; Pelgrim, C.E.; Wielemaker, E.M.; Van Duyvenvoorde, W.; Amaral-Santos, P.L.; Verschuren, L.; Keijser, B.J.F.; Heerschap, A.; Kleemann, R.; et al. Butyrate restores HFD-induced adaptations in brain function and metabolism in mid-adult obese mice. *Int. J. Obes.* **2017**, *41*, 935–944.
14. Bouter, K.E.C.; Bakker, G.J.; Levin, E.; Hartstra, A. V.; Kootte, R.S.; Udayappan, S.D.;

Katiraei, S.; Bahler, L.; Gilijamse, P.W.; Tremaroli, V.; et al. Differential metabolic effects of oral butyrate treatment in lean versus metabolic syndrome subjects article. *Clin. Transl. Gastroenterol.* **2018**, *9*, 155.

15. Cerdó, T.; García-Santos, J.A.; Bermúdez, M.G.; Campoy, C. The role of probiotics and prebiotics in the prevention and treatment of obesity. *Nutrients* **2019**, *11*, 635.
16. Li, Z.; Yi, C.X.; Katiraei, S.; Kooijman, S.; Zhou, E.; Chung, C.K.; Gao, Y.; Van Den Heuvel, J.K.; Meijer, O.C.; Berbée, J.F.P.; et al. Butyrate reduces appetite and activates brown adipose tissue via the gut-brain neural circuit. *Gut* **2018**.
17. Mueller, A.M.; Kleemann, R.; Gart, E.; van Duyvenvoorde, W.; Verschuren, L.; Caspers, M.; Menke, A.; Krömmelbein, N.; Salic, K.; Burmeister, Y.; et al. Cholesterol Accumulation as a Driver of Hepatic Inflammation Under Translational Dietary Conditions Can Be Attenuated by a Multicomponent Medicine. *Front. Endocrinol. (Lausanne).* **2021**, *12*.
18. Morrison, M.C.; Verschuren, L.; Salic, K.; Verheij, J.; Menke, A.; Wielinga, P.Y.; Iruarrizaga-Lejarreta, M.; Gole, L.; Yu, W.; Turner, S.; et al. Obeticholic Acid Modulates Serum Metabolites and Gene Signatures Characteristic of Human NASH and Attenuates Inflammation and Fibrosis Progression in Ldlr-/-.Leiden Mice. *Hepatol. Commun.* **2018**, *2*, 1513–1532.
19. van Koppen, A.; Verschuren, L.; van den Hoek, A.M.; Verheij, J.; Morrison, M.C.; Li, K.; Nagabukuro, H.; Costessi, A.; Caspers, M.P.M.; van den Broek, T.J.; et al. Uncovering a Predictive Molecular Signature for the Onset of NASH-Related Fibrosis in a Translational NASH Mouse Model. *Cmgh* **2018**, *5*, 83-98.e10.
20. van den Hoek, A.M.; de Jong, J.C.B.C.; Worms, N.; van Nieuwkoop, A.; Voskuilen, M.; Menke, A.L.; Lek, S.; Caspers, M.P.M.; Verschuren, L.; Kleemann, R. Diet and exercise reduce pre-existing NASH and fibrosis and have additional beneficial effects on the vasculature, adipose tissue and skeletal muscle via organ-crosstalk. *Metabolism* **2021**, *124*, 154873.
21. Nielsen, M.J.; Nedergaard, A.F.; Sun, S.; Veidal, S.S.; Larsen, L.; Zheng, Q.; Suetta, C.; Henriksen, K.; Christiansen, C.; Karsdal, M.A.; et al. The neo-epitope specific PRO-C3 ELISA measures true formation of type III collagen associated with liver and muscle parameters. *Am. J. Transl. Res.* **2013**, *5*, 303–315.
22. Leeming, D.J.; Nielsen, M.J.; Dai, Y.; Veidal, S.S.; Vassiliadis, E.; Zhang, C.; He, Y.; Vainer, B.; Zheng, Q.; Karsdal, M.A. Enzyme-linked immunosorbent serum assay specific for the 7S domain of collagen type IV (P4NP 7S): A marker related to the extracellular matrix remodeling during liver fibrogenesis. *Hepatol. Res.* **2012**, *42*, 482–493.
23. Sand, J.M.; Larsen, L.; Hogaboam, C.; Martinez, F.; Han, M. Larsen, M.R.; Nawrocki, A.; Zheng, Q.; Karsdal, M.A.; Leeming, D.J. MMP Mediated Degradation of Type IV Collagen Alpha 1 and Alpha 3 Chains Reflects Basement Membrane Remodeling in Experimental and Clinical Fibrosis-Validation of Two Novel Biomarker Assays. *PLoS One* **2013**, *8*, 84934.
24. Skovgård Veidal, S.; Karsdal, M.A.; Vassiliadis, E.; Nawrocki, A.; Larsen, M.R.; Nguyen, H.T.; Hägglund, P; Luo, Y.; Zheng, Q.; Vainer, B.; Leeming, D.J. MMP Mediated Degradation of Type VI Collagen Is Highly Associated with Liver Fibrosis-Identification and Validation of a Novel Biochemical Marker Assay. *PLoS ONE* **2011**,

6, e24753
25. Galarraga, M.; Campión, J.; Munõz-Barrutia, A.; Boqué, N.; Moreno, H.; Martínez, J.A.; Milagro, F.; Ortiz-de-Solórzano, C. Adiposoft: Automated software for the analysis of white adipose tissue cellularity in histological sections. *J. Lipid Res.* **2012**. *53*, 2791–2796.
26. Liang, W.; Menke, A.L.; Driessen, A.; Koek, G.H.; Lindeman, J.H.; Stoop, R.; Havekes, L.M.; Kleemann., R.; Van Den Hoek, A.M. Establishment of a general NAFLD scoring system for rodent models and comparison to human liver pathology. *PLoS One* **2014**, *9*.
27. Love, M.I.; Huber, W.; Anders, S. Moderated estimation of fold change and dispersion for RNA-seq data with DESeq2. *Genome Biol.* **2014**, *15*.
28. Krämer, A.; Green, J.; Pollard, J.; Tugendreich, S. Causal analysis approaches in Ingenuity Pathway Analysis. *Bioinformatics* **2014**, *30*, 523–530.
29. Gart, E.; Salic, K.; Morrison, M.C.; Caspers, M.; Van Duyvenvoorde, W.; Heijnk, M.; Giera, M.; Bobeldijk-Pastorova, I.; Keijer, J.; Storsve, A.B.; et al. Krill Oil Treatment Increases Distinct PUFAs and Oxylipins in Adipose Tissue and Liver and Attenuates Obesity-Associated Inflammation via Direct and Indirect Mechanisms. *Nutrients* **2021**, *13*, 2836.
30. Mannaerts, I.; Leite, S.B.; Verhulst, S.; Claerhout, S.; Eysackers, N.; Thoen, L.F.R.; Hoorens, A.; Reynaert, H.; Halder, G.; Van Grunsven, L.A. The Hippo pathway effector YAP controls mouse hepatic stellate cell activation. *J. Hepatol.* **2015**, *63*, 679–688.
31. Kisseleva, T.; Cong, M.; Paik, Y.H.; Scholten, D.; Jiang, C.; Benner, C.; Iwaisako, K.; Moore-Morris, T.; Scott, B.; Tsukamoto, H.; et al. Myofibroblasts revert to an inactive phenotype during regression of liver fibrosis. *Proc. Natl. Acad. Sci. U. S. A.* **2012**. *109*, 9448–9453.
32. Ghosh, A.K.; Vaughan, D.E. PAI-1 in Tissue Fibrosis. *J. Cell. Physiol.* **2012**, *227*, 493.
33. Noguchi, R.; Kaji, K.; Namisaki, T.; Moriya, K.; Kawaratani, H.; Kitade, M.; Takaya, H.; Aihara, Y.; Douhara, A.; Asada, K.; et al. Novel oral plasminogen activator inhibitor.1 inhibitor TM5275 attenuates hepatic fibrosis under metabolic syndrome via suppression of activated hepatic stellate cells in rats. *Mol. Med. Rep.* **2020**, *22*, 2948–2956.
34. Noguchi, S.; Saito, A.; Nagase, T. Molecular Sciences YAP/TAZ Signaling as a Molecular Link between Fibrosis and Cancer. **2018**, *19*, 3674.
35. Higgins, C.E.; Tang, J.; Higgins, S.P.; Gifford, C.C.; Mian, B.M.; Jones, D.M.; Zhang, W.; Costello, A.; Conti, D.J.; Samarakoon, R.; et al. The Genomic Response to TGF-β1 Dictates Failed Repair and Progression of Fibrotic Disease in the Obstructed Kidney. *Front. Cell Dev. Biol.* **2021**, *9*, 1716.
36. Shen, Y.; Miao, N.; Wang, B.; Xu, J.; Gan, X.; Xu, D.; Zhou, L.; Xue, H.; Zhang, W.; Yang, L.; et al. c-Myc promotes renal fibrosis by inducing integrin αv-mediated transforming growth factor-β signaling. *Kidney Int.* **2017**, *92*, 888–899.
37. Nevzorova, Y.A.; Hu, W.; Cubero, F.J.; Haas, U.; Freimuth, J.; Tacke, F.; Trautwein, C.; Liedtke, C. Overexpression of c-myc in hepatocytes promotes activation of hepatic stellate cells and facilitates the onset of liver fibrosis. *Biochim. Biophys. Acta - Mol. Basis Dis.* **2013**, *1832*, 1765–1775.
38. Baumann, A.; Jin, C.J.; Brandt, A.; Sellmann, C.; Nier, A.; Burkard, M.; Venturelli, S.;

Bergheim, I. Oral supplementation of sodium butyrate attenuates the progression of non-alcoholic steatohepatitis. *Nutrients* **2020**.

39. Jin, C.J.; Sellmann, C.; Engstler, A.J.; Ziegenhardt, D.; Bergheim, I. Supplementation of sodium butyrate protects mice from the development of non-alcoholic steatohepatitis (NASH). *Br. J. Nutr.* **2015**, *114*, 1745–1755.
40. Ye, J.; Lv, L.; Wu, W.; Li, Y.; Shi, D.; Fang, D.; Guo, F.; Jiang, H.; Yan, R.; Ye, W.; et al. Butyrate Protects Mice Against Methionine–Choline-Deficient Diet-Induced Non-alcoholic Steatohepatitis by Improving Gut Barrier Function, Attenuating Inflammation and Reducing Endotoxin Levels. *Front. Microbiol.* **2018**, *9*, 1–16.
41. Saunder, D.R. ABSORPTION OF SHORT-CHAIN FATTY ACIDS IN HUMAN STOMACH AND RECTUM. *Nutr. Res.* **1991**, *8*, 55.
42. Schmitt, M.G.; Soergel, K.H.; Wood, C.M.; Steff, J.J. *Absorption of Short-Chain Fatty Acids from the Human Ileum*. Dig. Dis. Sci. 1977, 22, 340–347.
43. Gill, R.K.; Saksena, S.; Alrefai, W.A.; Sarwar, Z.; Goldstein, J.L.; Carroll, R.E.; Ramaswamy, K.; Dudeja, P.K. Expression and membrane localization of MCT isoforms along the length of the human intestine. *Am. J. Physiol. - Cell Physiol.* **2005**, *289*, C846–C852.
44. Guilloteau, P.; Martin, L.; Eeckhaut, V.; Ducatelle, R.; Zabielski, R.; Van Immerseel, F. From the gut to the peripheral tissues: The multiple effects of butyrate. *Nutr. Res. Rev.* **2010**, *23*, 366–384.
45. Han, X.; Song, H.; Wang, Y.; Sheng, Y.; Chen, J. Sodium butyrate protects the intestinal barrier function in peritonitic mice. *Int. J. Clin. Exp. Med.* **2015**, *8*, 4000–4007.
46. Wang, H.; Song, W.; Wu, Q.; Gao, X.; Li, J.; Tan, C.; Zhou, H.; Zhu, J.; He, Y.; Yin, J. Fecal Transplantation from db/db Mice Treated with Sodium Butyrate Attenuates Ischemic Stroke Injury. *Microbiol. Spectr.* **2021**, *9*, e00042-21.
47. Bai, H.-B.; Yang, P.; Zhang, H.-B.; Liu, Y.-L.; Fang, S.-X.; Xu, X.-Y. [Short-chain fatty acid butyrate acid attenuates atherosclerotic plaque formation in apolipoprotein E-knockout mice and the underlying mechanism]. *Sheng Li Xue Bao* **2021**, *73*, 42–50.
48. Pelgrim, C.E.; Franx, B.A.A.; Snabel, J.; Kleemann, R.; Arnoldussen, I.A.C.; Kiliaan, A.J. Butyrate reduces HFD-induced adipocyte hypertrophy and metabolic risk factors in Obese LDLr-/-.Leiden mice. *Nutrients* **2017**, *9*, 714.
49. Ikejima, K.; Takei, Y.; Honda, H.; Hirose, M.; Yoshikawa, M.; Zhang, Y.-J.; Lang, T.; Fukuda, T.; Yamashina, S.; Kitamura, T.; et al. Leptin receptor–mediated signaling regulates hepatic fibrogenesis and remodeling of extracellular matrix in the rat. *Gastroenterology* **2002**, *122*, 1399–1410.
50. Choi, S.S.; Syn, W.K.; Karaca, G.F.; Omenetti, A.; Moylan, C.A.; Witek, R.P.; Agboola, K.M.; Jung, Y.; Michelotti, G.A.; Diehl, A.M. Leptin promotes the myofibroblastic phenotype in hepatic stellate cells by activating the Hedgehog pathway. *J. Biol. Chem.* **2010**, *285*, 36551–36560.

Supplementary information

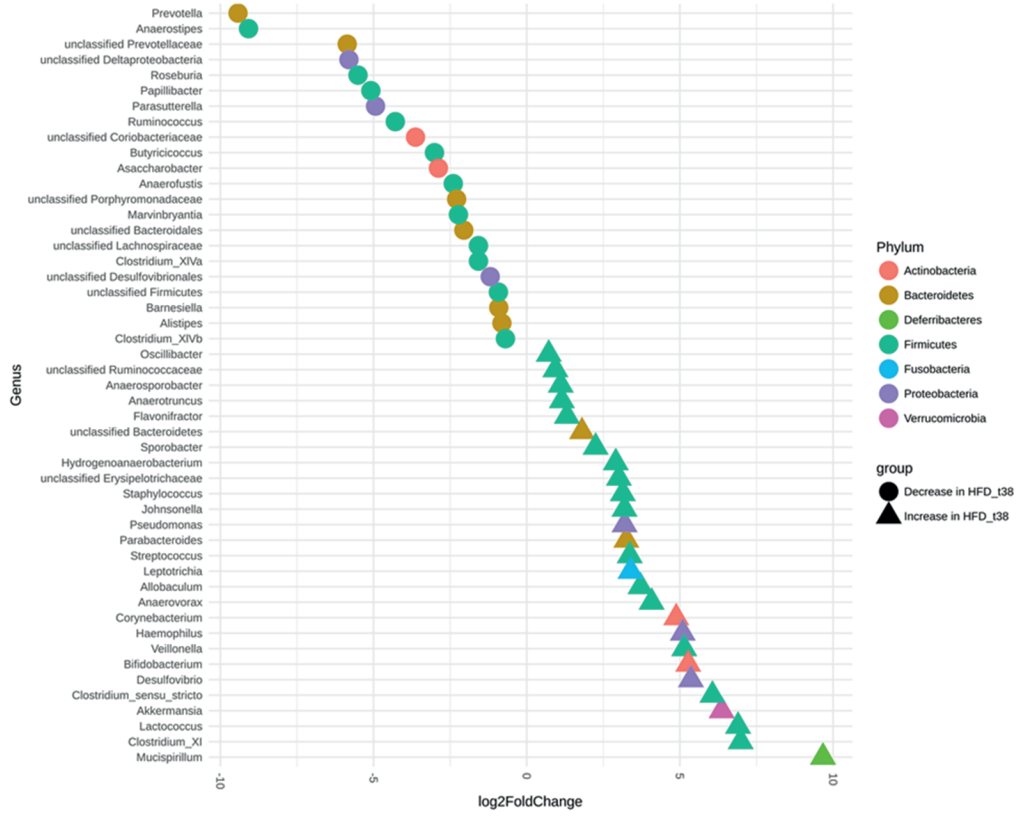

Supplemental figure 1: List of genera in the colon mucosa *of which the presence was significantly affected upon HFD feeding compared to chow-fed mice and expressed on a log-2fold scale.*

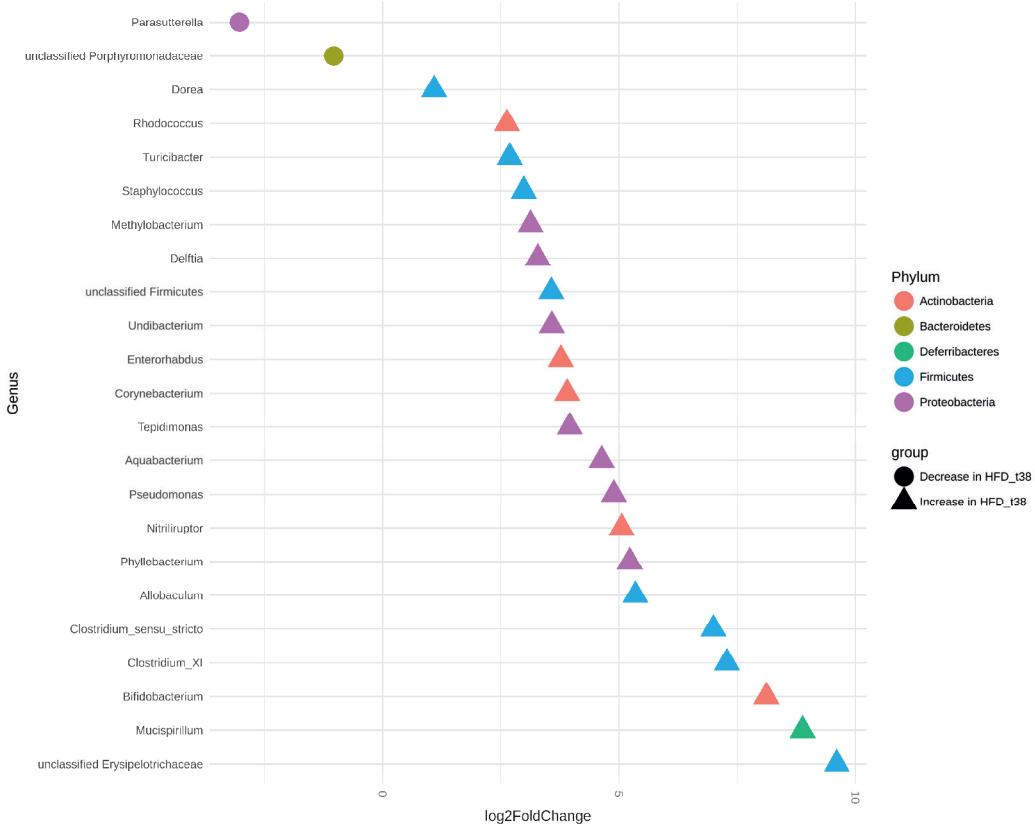

Supplemental figure 2: Genera expressed in the mucosal layer of the ileum *of which the presence was significantly affected upon HFD feeding compared to chow-fed mice and expressed on a log2fold scale.*

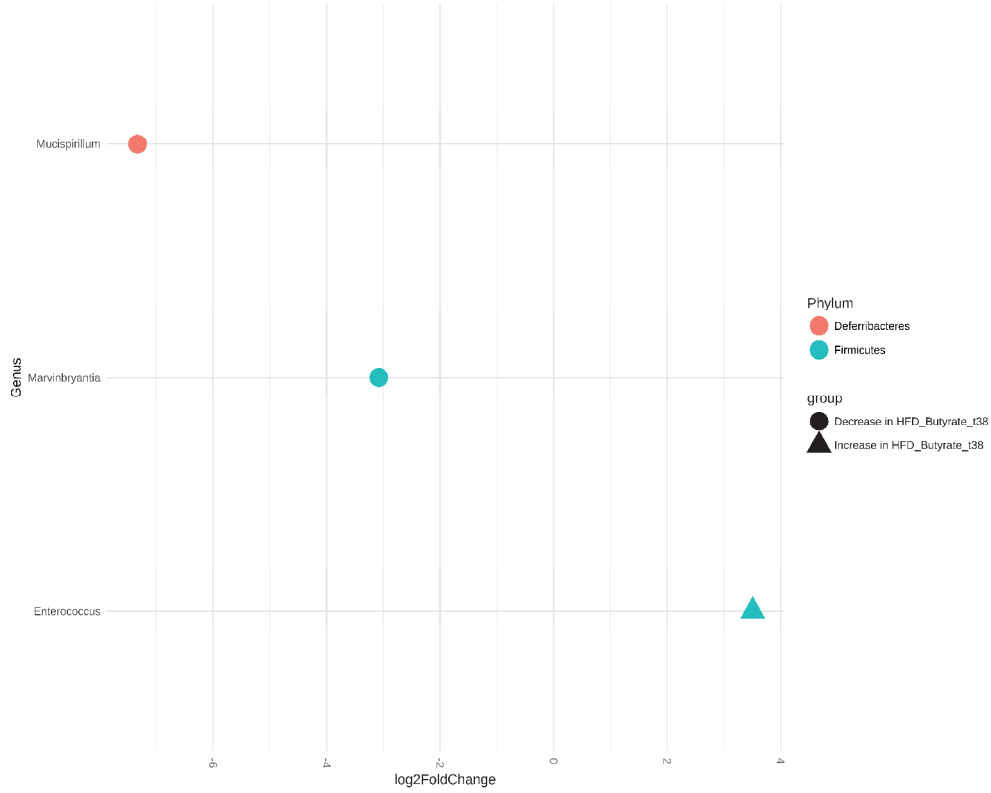

Supplemental figure 3: Genera expressed in the mucosal layer of the ileum *of which the presence was significantly affected upon BU feeding compared to HFD-fed mice and expressed on a log2fold scale.*

Supplementary Table 1: Circulating extracellular matrix remodeling markers

	Chow	HFD	HFD+BU
TIMP1 (ng/ml)	2.6 ± 1.0***	4.6 ± 1.2	3.9 ± 0.6
PRO-C3 (ng/ml)	11.0 ± 5.0	14.0 ± 7.2	18.5 ± 5.3
PRO-C4 (ng/ml)	131.7 ± 25.2*	200.5 ± 63.3	192.0 ± 50.6
C4M (ng/ml)	4.4 ± 1.3	5.2 ± 1.4	4.9 ± 1.0
C6M (ng/ml)	4.0 ± 1.5*	7.2 ± 3.3	5.8 ± 1.9

*Data are presented as mean ± SD, *p<0.05, **p<0.01, ***p<0.001 compared to the HFD-control group.*

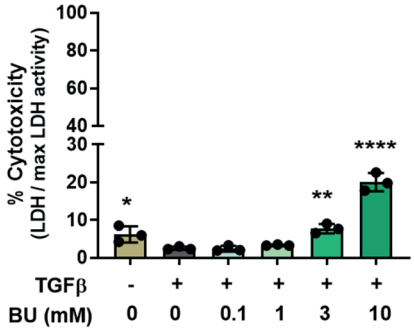

Supplemental figure 4: Cytotoxicity of different BU dosages *was calculated as a percentage based on maximum LDH activity in cell supernatant. Data is presented as mean with SD , *p<0.05, **p<0.01, ***p<0.001 compared to the TGF-B control group (In grey).*

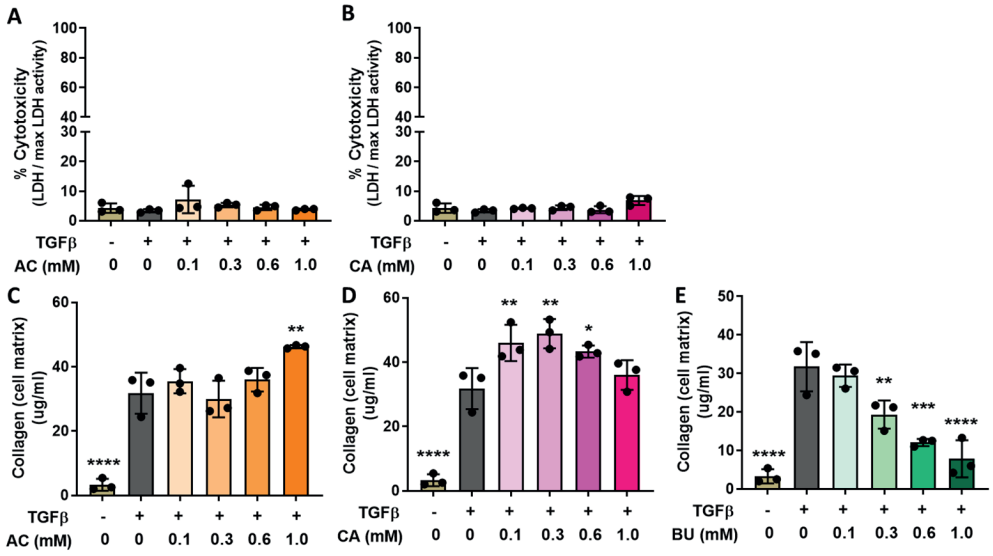

Supplemental figure 5: Effect of short chain fatty acids acetate (AC), caproate (CA) and butyrate (BU) on TGF-β induced fibrosis in primary human hepatic stellate cells.
*Cytotoxicity percentage based on maximum LDH activity in cell supernatant of cells treated with **A**) AC and **B**) CA. Also collagen content in the cell matrix was measured in cells treated with different dosages of **C**) AC, **D**) CA and **E**) BU. Data is presented as mean with SD , *p<0.05, **p<0.01, ***p<0.001 compared to the TGF-B control group (In grey).*

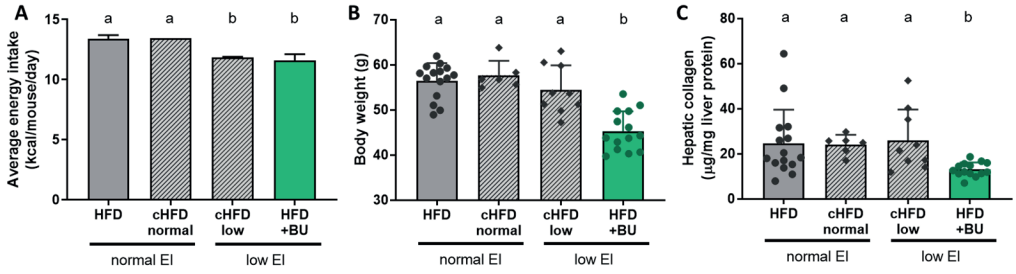

Supplemental figure 6: Association between energy intake and liver fibrosis. *Historical data from Ldr-/-.Leiden mice fed HFD for 38 weeks (the same as in the current study) – grouped according to energy intake: cHFD normal = comparable energy intake to the HFD group in the current experiment; cHFD low = comparable energy intake to HFD+BU in the current experiment.* ***A****) Average energy intake,* ***B****) body weight and* ***C****) hepatic collagen content. Data are presented as mean ± SD, a indicates no significant differences, whereas b indicates a significant difference with p<0.05.*

CHAPTER

Propionic acid and not caproic acid, attenuates non-alcoholic steatohepatitis and improves (cerebro) vascular functions in obese Ldlr-/-.Leiden mice

Anouk C. Tengeler, Eveline Gart, Maximilian Wiesmann,
Ilse A. C. Arnoldussen, Wim van Duyvenvoorde, Marloes Hoogstad,
Pieter J. Dederen, Vivienne Verweij, Bram Geenen, Tamas Kozicz,
Robert Kleemann, Martine C. Morrison, Amanda J. Kiliaan

FASEB J. 2020 Jul;34(7):9575-9593.
doi: 10.1096/fj.202000455R. PMID: 32472598.

Abstract

The obesity epidemic increases interest to elucidate impact of short-chain fatty acids on metabolism, obesity, and the brain. We investigated effects of propionic acid (PA) and caproic acid (CA) on metabolic risk factors, liver and adipose tissue pathology, brain function, structure (by MRI), and gene expression, during obesity development.
Ldlr-/-.Leiden mice received 16-weeks either a high-fat diet (HFD) to induce obesity, or chow as reference group. Next, obese HFD-fed mice were treated 12 weeks with 1) HFD+CA (CA), 2) HFD+PA (PA) and compared to HFD controls.
PA reduced body weight and systolic blood pressure, lowered fasting insulin levels, and reduced HFD-induced liver macrovesicular steatosis, hypertrophy, inflammation, and collagen content. PA increased the amount of glucose transporter type 1-positive cerebral blood vessels, reverted cerebral vasoreactivity and HFD-induced effects in microstructural gray and white matter integrity of optic tract, and somatosensory and visual cortex. PA and CA also reverted HFD-induced effects in functional connectivity between visual and auditory cortex. However, PA mice were more anxious in open field, and showed reduced activity of synaptogenesis and glutamate regulators in hippocampus. Therefore, PA treatment should be used with caution even though positive metabolic, (cerebro)vascular, and brain structural and functional effects were observed.

1. Introduction

The prevalence of obesity has increased considerately worldwide over the past decades (1). Obesity is associated with ectopic fat accumulation, dyslipidemia, hyperinsulinemia and it promotes the development of non-alcoholic fatty liver disease (NAFLD) (2). NAFLD encompasses a spectrum of liver disease, ranging from simple steatosis to the more severe stage of non-alcoholic steatohepatitis (NASH). NASH is characterized by steatosis and lobular inflammation (3, 4), and can progress to liver fibrosis (5). Other than modifying lifestyle factors, for instance weight loss through dietary advice and physical activity, no approved pharmacological therapy is yet available for NASH.

In addition to the dysfunction of peripheral metabolic organs, obesity is also associated with mitochondrial dysfunction and alterations in brain structure and cognitive dysfunction (6, 7). Obesity-associated changes in white matter have been reported in numerous studies (8-10) and effects on the cerebrovasculature, i.e. decreased cerebral vasoreactivity and glucose transporter 1 (GLUT-1) expression, a marker for vascular endothelium cells and vascular health (11, 12).

Short-chain fatty acids (SCFAs) have already shown some beneficial effects on obesity development. For example, CA has been reported to have possible antilipogenic effects (13-16). Moreover, a small-scale clinical study showed that an elevation of colonic PA levels was associated with reduced weight gain and reductions in liver lipids (17). In rodent studies, PA has been shown to protect against-diet induced obesity (18-21). Furthermore, elevated PA levels were associated with reduced visceral adiposity and steatohepatitis in obese mice that were treated with fructo-oligosaccharides (22).

Herein, we investigated whether CA and PA can attenuate the development of HFD-induced obesity and associated NASH, liver fibrosis and associated brain dysfunction on functional and structural level. To do so, we used the low-density lipoprotein receptor knockout (Ldlr-/-).Leiden mice which develop dyslipidemia, hyperinsulinemia, obesity, NASH, liver fibrosis and hypertension in conjunction with brain dysfunction in a period of about 30 weeks on HFD (6, 23). PA and CA were administered as dietary supplement in a therapeutic setting, i.e., after a 16-weeks run-in to establish obesity.

2. Materials and Methods

2.1 Mice, diets and study design

Male Ldlr$^{-/-}$.Leiden mice were obtained from a specific pathogen-free breeding stock at TNO Metabolic Health Research (Leiden, the Netherlands) and were housed in the Preclinical Imaging Center (PRIME) at the Animal Research Facility, Radboudumc Nijmegen, the Netherlands. Mice were group-housed in digital ventilated cages (DVC; Tecniplast S.P.A., Buguggiate (VA) Italy) in which locomotor activity of the mice can be tracked 24 hrs/day. Mice were housed in conventional animal rooms (relative humidity 50–60%, temperature 21°C, light cycle 7 a.m. – 7 p.m.), 2-3 mice per cage with *ad libitum* access to food and water. All animal experiments were carried out in accordance with international European ethical standards (European Directive 2010/63/EU) and were approved by the TNO Animal Welfare Body (Permit number: TNO-345) and the Veterinary Authority of the Radboud university medical center (Radboudumc; Permit number: RU-DEC 2017-0063-002). All applicable (inter)national, and institutional guidelines for the care and use of animals were followed and are reported herein in accordance with the ARRIVE guidelines (24).

The study design of this experiment is shown in Figure 1A. From weaning at 3 weeks of age onwards, all groups received a standard chow diet (9.0% kcal fat, 58.0% carbohydrates and 33.0% kcal protein Sniff R/M-H diet V1530, Sniff Spezialdiäten GmbH, Soest, Germany). At 15 weeks of age, mice were divided into 4 experimental groups (N=15 per group) that were matched for body weight prior to treatment. Mice in group 1 were kept on the chow diet, and mice in group 2-4 were switched to an HFD (45.0% kcal fat, 35.0% carbohydrates and 20.0% kcal protein, D12451, Research Diets Inc, New Brunswick, USA) with anise. From 31 weeks of age until the end of the study (for a total of 12 weeks), group 3 HFD was supplemented with 2.5% w/w CA (CA mice), and group 4 with 2.5% w/w PA (PA mice).

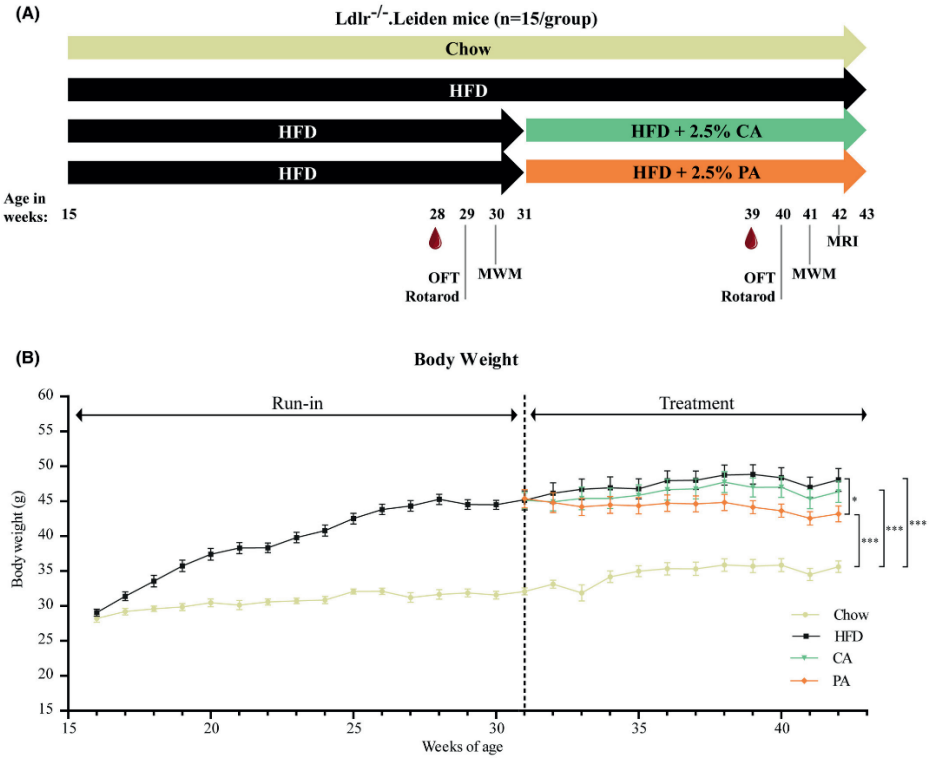

Figure 1. *Study design and body weight. (A) Study design. From 15 to 30 weeks of age, Ldlr-/- mice received either a chow diet or an HFD diet. At 31 weeks of age CA and PA treatment started. Systolic blood pressure was measured, and plasma samples were collected (see droplet). Behavior and cognition were assessed, and MRI-experiments were performed. In week 43, all mice were sacrificed via cervical dislocation followed by decapitation. (B) Body weight. An HFD supplemented with CA or PA started at 31 weeks of age. Reference mice were kept on chow. HFD: high-fat diet; PA: propionic acid; CA: caproic acid; OFT: Open Field test; MWM: Morris water maze. Data are presented as mean ± SEM. *p<0.05; ***p<0.001. N=14 (HFD) or N=15 (chow, CA, PA) mice per group.*

Food intake at cage level and individual body weight were monitored weekly. Blood samples were collected before and after 8 weeks of treatment. Systolic blood pressure, cognition with the Morris water maze test (MWM), behavior in an Open Field Test and motor skills with the Rotarod experiment were assessed before treatment and after 9-10 weeks of treatment. Brain function and structure were measured using magnetic resonance imaging (MRI) after 11 weeks of treatment. After 12 weeks, mice were sacrificed via cervical dislocation followed by decapitation.

2.2 Plasma measurements

Blood samples were collected after 5h fast via tail vein bleeding to determine whole blood glucose, and for isolation of EDTA plasma in which total cholesterol, triglycerides, serum amyloid A (SAA) and insulin were determined as described previously (23).

2.3 Systolic blood pressure
SBP was measured using a computerized and warmed tail-cuff plethysmography device (IITC Life Scientific Instruments, Woodland Hill, CA, USA). One trial, consisting of ten measurements, was used to habituate the mice to the restrainer and acclimatize the animals to the complete procedure. SBP was then measured for a total of 20 measurements, in two trials on two consecutive days and expressed as mean SBP in millimeter of mercury (mmHg).

2.4 Liver histological and biochemical analyses
The liver was isolated and weighed. Development of NAFLD was analyzed in the medial liver lobe in 3 µm liver hematoxylin-eosin (HE) stained sections by a board-certified pathologist using a well-established rodent NASH scoring method adapted from the human NAFLD activity score (NAS) (23, 25). Briefly, the level of total steatosis or hypertrophy (abnormally enlarged hepatocytes) per mouse was expressed as a percentage of the total liver section affected. Hepatic inflammation was quantified by counting the number of inflammatory aggregates in 5 fields per mouse at 100x magnification (field of view 4.15 mm^2) and expressed as the number of foci per mm^2.
The sinister lobe was snap-frozen in liquid nitrogen and stored at -80 °C for biochemical analyses. Hepatic total collagen content was determined with a hydroxyproline assay (Quickzyme, Leiden, the Netherlands) and protein with a total protein assay (Quickzyme) according to manufacturer's instructions. The hepatic ketone body β-hydroxybutyrate was measured with a colorimetric assay kit (Cayman chemical, Michigan, USA) and protein content was assayed with (Pierce BCA protein assay kit, Thermo Fisher Scientific, Waltham, USA) in an assay buffer containing protease inhibitors (100 mg/ml) following the manufacturer's protocol.
Liver lipids were determined in a 100 mg/ml phosphate-buffered saline homogenate following the Bligh and Dyer method (26), then separated by high-performance thin-layer chromatography on silica gel plates. Subsequently, the lipids were stained as described previously (23), and analyzed with ChemiDoc Touch Imaging System (Bio-Rad, Hercules, USA). Liver triglyceride (TG), cholesterol ester (CE) and free cholesterol (FC) content was quantified using Image-lab version 5.2.1 software (Bio-Rad, Hercules, USA) and expressed per mg liver protein. In the same liver homogenates, the glycogen content was determined according to manufacturer's protocol (MAK016 Glycogen assay kit, Sigma-Aldrich, Steinheim, Germany).

2.5 White adipose tissue (WAT) analyses
Gonadal (gWAT), mesenteric (mWAT) and subcutaneous (sWAT) WAT depots were isolated, weighed, and 5 µm paraffin embedded sections were stained with hematoxylin-phloxine-saffron and scanned for digital analysis (Aperio AT2, Leica Biosystems, Amsterdam, the Netherlands). Size of adipose cells were analyzed using Adiposoft (27) an open-source automated plug-in for the image processing package Fiji (28) for ImageJ (29). Inflammation was quantified by counting the number of crown-like structures (CLS; the histological hallmark of adipose tissue inflammation (30) in the same fields used for adipocyte size analysis and expressed as number of CLS per 1000 adipocytes.

2.6 Digital Ventilated Cages (DVC)
Mice were housed in DVC cages (2-3 mice per cage) during the experiment to study locomotor activity 24hrs/day. Activity was monitored via 12 electrodes underneath the home-cage, as described previously (31, 32). For analysis of the processed results, we used activity data of two days and two nights before the start of the interventions, and two days and two nights at the end of the experiment. Activity measures were corrected for the number of mice per cage.

2.7 Rotarod
To study sensory-motor integration mice were placed on a rotating rod (3.18 cm in diameter; IITC Inc., Woodland Hills, CA, USA) and their ability to remain on the device was recorded as latency to fall. First, mice were accustomed to the task by placing them on a stationary rod for one minute followed by a test trial at 10 rpm. Next, four accelerating trials with intervals of 30 min were performed (4 to 40 rpm) with a maximum duration of 300 seconds.

2.8 Open field
Explorative behavior and locomotion were assessed in the open field test. Mice were placed individually in a square open field (45 cm x 45 cm x 30 cm) with transparent Plexiglas walls, and recorded for 10 min. Locomotion and explorative behavior were automatically calculated with EthoVision XT10.1 (Noldus, Wageningen, The Netherlands).

2.9 Morris water maze
The Morris water maze (MWM) was used to examine long-term memory and spatial learning abilities. During the acquisition phase, the mice were trained to find the platform in a circular pool (diameter 108 cm) that was filled with water (21–22°C), made opaque by adding milk powder. The platform (diameter 8 cm) was submerged 1 cm below the water surface and located in the North-East quadrant of the pool. Mice performed 4 acquisition trials per day starting from four different positions (South, North, East, West; maximal swimming time 120 s; 30 s on the platform; inter-trial interval 60 min) during 4 consecutive days. Visual cues were present on the four walls surrounding the pool at a distance of 0.5 m. All trials were recorded and latency to find the platform (s) was used as a measure for spatial learning. Mice performed a single probe trial at the end of day 4 of acquisition, in which the platform was removed from the pool.
During this probe trial, the mice were allowed to swim freely for 120 s. Trials were recorded and analyzed with EthoVision XT 10.1.

2. 10 Functional and structural brain experiments using Magnetic Resonance Imaging (MRI)
All MRI measurements were performed using an 11.7-T BioSpec Avance III small animal MR system (Bruker BioSpin, Ettlingen, Germany). Isoflurane (Abbott Animal Health, Abbott Park, IL, USA) was used for anesthesia (3.5% for induction and ~1.7% for maintenance) in a 1:2 oxygen and air mixture). Imaging parameters can be found in Table S1.
Arterial spin labeling (ASL) was assessed to indicate cerebral blood flow (CBF) levels using an established ASL method with flow-sensitive alternating inversion recovery (FAIR) technique (33). To induce vasoconstriction, the normal 1:2 oxygen-air mixture was changed to a 3:0 oxygen and air mixture. CBF values from both conditions were used to

evaluate the ability of the cerebrovasculature to adapt from a normal condition to a vasoconstrictive condition, which is referred to as cerebral vasoreactivity (34). Cerebral vasoreactivity was calculated by subtraction of the vasoconstriction CBF from the normal CBF values, and this was then divided by the sum of the normal and vasoconstrictive CBF values. To calculate regional CBF we used the same protocol as described previously (35). CBF was measured in the total brain, cortex, thalamus (an important brain structure for relaying motor signals to the cortex) and the hippocampus (an important brain structure for memory consolidation).

To investigate white and gray matter integrity in the brain, diffusion tensor imaging (DTI) was employed as described (36, 37). Fractional anisotropy is a marker of the degree of myelination and fiber density of white matter, while mean diffusivity characterizes an inverse measure of the membrane density (38). These scalars were measured in several manually selected white matter and gray matter areas: fornix and corpus callosum, and regions in the left and right hemisphere: auditory cortex, hippocampus, motor cortex, optic tract, somatosensory cortex, visual cortex, caudate putamen, anterior commissure, amygdala, external capsule, fimbria, forceps minor, and internal capsule (39).

Resting-state functional MRI (rs-fMRI) acquisition was performed to assess functional connectivity between specific regions of interest (ROI) that support multiple cognitive and motor processes: dorsal hippocampus, ventral hippocampus, auditory cortex, motor cortex, somatosensory cortex and visual cortex. Functional connectivity between ROIs was calculated from the blood oxygen level-dependent (BOLD) time series using total and partial correlation analyses as previously described (40). Partial correlations accentuates the direct connectivity between two ROI while it regresses the temporal BOLD signal from all other ROIs (40)(41).

2.11 Enzymatic mitochondrial activity analysis in brain tissue

A homogenate of snap-frozen cerebellum (N=8 randomly selected animals per treatment group) was made with a glass-glass potter tube in SEF buffer (0.25 M sucrose, 2 mM K-EDTA, 10 mM phosphate buffer, pH 7.4) to obtain a 5% w/v homogenate. The homogenized samples were centrifuged at 600g for 10 minutes at 2 °C and the supernatant underwent three freeze-thaw cycles to adequately permeabilize the mitochondria. Enzyme activities of the individual complexes of the respiratory chain (complex I, II, III and IV), citrate synthase (CS) and Succinate cytochrome C oxidoreductase (SCC) were measured spectrophotometrically on a KoneLab 20XT analyzer (Thermo Scientific, Waltham, MA, USA), following previously described methods (42, 43). Enzyme activities were normalized to CS activity (a marker for the number of mitochondria (44)).

2.12 Quantitative real-time polymerase chain reaction

Snap-frozen hippocampi were used for mRNA level analysis using quantitative real-time polymerase chain reaction (qRT-PCR) of post-synaptic density-95 (PSD-95) and synaptophysin (SYP-1), as previously described (45). Glyceraldehyde 3-phosphate dehydrogenase (GAPDH) and β2-microglobulin (B2M) were used as reference genes. To determine the threshold cycle (CT) values, the StepOne Software version 2.2.2 was used. CT values were normalized against the average of the two reference genes and transformed to the comparative CT values using the Pfaffl method (46).

2.13 Gene expression analysis using the NanoString Neuroinflammation panel

The isolated hippocampal RNA, as used previously for qRT-PCR, concentration was measured spectrophotometrically using a NanoDrop 1000 (Isogen Life Science, De Meern, Netherlands). To assess the quality of the isolated RNA, the 2100 Bioanalyzer (Agilent Technologies, Amstelveen, Netherlands) was used. Molecular barcodes from the nCounter Neuroinflammation panel (XT-CSO-MNROI1-12) code set, included 770 genes and 13 internal reference genes for normalization. The isolated RNA (25ng/ul sample) was used to make a reporter code set master mix and samples from chow, HFD and PA were incubated for 24h at 65°C for hybridization following the manufacturers protocol. Hybridized samples were then loaded on to an nCounter cartridge and run on the nCounter SPRINT (NanoString Technologies, Seattle, WA, USA) to measure barcode signals. nSolver 4.0 (NanoString Technologies, USA) was used to analyze the geometric mean of internal reference genes was used to compute the reference normalization factor. Internal references with a count below background levels or outside the 0.10–10.0 range normalization factor were excluded. Herein internal reference Asb10 average count fell below background levels and Xpnpep1 was affected by our treatment, and both had to be excluded from the analyses. Normalized gene expression data were used for gene enrichment analysis across pathways and biological processes with the Ingenuity Pathway Analysis (IPA). The upstream regulator analysis tool of IPA was used to assess the activity of upstream regulators as reported (47). Briefly, the gene expression levels of all known target genes of an upstream regulator of interest were analyzed together. A Z-score less than -2 indicates a significantly reduced transcriptional activity, while a Z-score greater than 2 indicates significant activation based on the direction of gene expression changes of target genes as reported in translational studies (23).

2.14 Immunohistochemistry on brain tissue

The left brain hemisphere was immersion-fixated overnight at 4°C in 4% paraformaldehyde in 0.1 M PBS, and subsequently stored at 4°C in 0.1 M PBS with 0.01% sodium azide. Coronal frozen brain sections (−60°C) were cut in 8 series of 30-µm-thick sections that were used for diaminobenzidine-nickel (DAB-Ni) immunohistochemical (IHC) staining purposes. IHC was performed using standard free-floating labeling procedures, using the protocol described in other studies (34, 45, 48).

Brain sections were stained for doublecortin (DCX) as marker for immature neurons (neurogenesis) using polyclonal goat anti-doublecortin (1:8000; sc-8066 Santa Cruz Biotechnology Inc., Santa Cruz, CA, USA). Glucose transporter 1 (GLUT-1) stainings were used to quantify the amount of glucose transporters on brain blood vessels (indication for blood vessel wall integrity) with GLUT-1 polyclonal rabbit anti-GLUT1 (1:80,000; Chemicon International Inc., Temecula, CA, United States). To assess activated microglia (measure for neuroinflammation) ionized calcium-binding adapter molecule 1 (IBA-1) was stained with polyclonal goat anti-IBA1 (1:8000, Abcam, Cambridge, United Kingdom). Secondary antibodies donkey anti-goat biotin (1:1500; Jackson ImmunoResearch, West Grove, PA, USA) and donkey anti-rabbit biotin (1:1500; Jackson ImmunoResearch) were used.

DCX-positive cells were quantified in the hippocampus (-1.97 mm posterior to bregma) in three successive sections per mouse. Stained brain regions were counted at 40x magnification by 2 independent observers using a Zeiss Axioscop microscope equipped with hardware and software of MBF Bioscience (Williston, VT, USA). GLUT-1 and IBA-1 positive (+) DAB-Ni immunohistochemistry was scored using ImageJ, in sections

photographed with an Axio Imager A2 (Zeiss Germany). Measurements of IBA-1 and GLUT-1 density were defined as the area covered with either 1) relative IBA-1+ or GLUT-1+ staining, or 2) IBA-1+ or GLUT-1+ staining per mm^2, all in the cortex, thalamus and hippocampus (bregma -1.97 mm). In addition, the intensity of the GLUT-1 staining was calculated by subtracting the mean particle intensity from 255 (49). Intensity was quantified using ImageJ, in the same regions mentioned above.

2.15 Statistics

The upstream regulators were analyzed using the upstream regulator analysis tool of IPA. All other data were analyzed using IBM SPSS for Windows 25.0 software (SPSS Inc., Chicago, IL, USA), and are expressed as mean ± SEM.

Parameters that were measured at multiple separate time points (i.e., body weight, caloric intake, and the acquisition of the MWM) were analyzed using repeated measures ANOVA with Bonferroni correction for multiple comparisons. The post hoc Dunnett's multiple comparison two-sided t-test was used to compare treatment groups to the HFD control group. In addition, significant effects were also compared to the chow group using the same Dunnett's post hoc test. These results are described in Table S2. To compare treatment groups to the HFD control group and the chow control group, the post hoc Dunnett's multiple comparison two-sided t-test was used. When a significant interaction between diet and time was present, the data were split for the concerning factor and analyzed again with repeated measures ANOVA. All other data (behavioral tests, imaging, biochemistry) were analyzed using multivariate ANOVA with Bonferroni correction for multiple comparisons (normally distributed) followed by Dunnett's multiple comparison two-sided t-test, or Kruskal–Wallis test (not normally distributed data) followed by a post hoc Mann–Whitney U test to compare groups to the HFD and chow group. Statistical outliers were removed from the dataset. The number of mice that was considered an outlier per test is described in Table S3.

3. Results

3.1 PA attenuates HFD-induced obesity independent of food intake

During the 16-week run-in period, HFD-treated mice gained significantly more weight than the reference mice on chow (Figure 1B). After 12 weeks of treatment these weight gain differences persisted with HFD-fed mice being significantly heavier than chow-fed mice. Body weight attenuating effects were not observed for CA, whereas PA markedly attenuated HFD-induced body weight gain. Average caloric intake was slightly lower in HFD compared to chow (Table 1). Caloric intake between HFD, CA and PA did not differ.

Table 1. **Metabolic parameters at the end of the experiment**

	Chow	*HFD*	*CA*	*PA*
Body weight (g)	35.61± 0.83	48.04± 1.62***	46.35± 1.54	43.17± 1.13[&]
Caloric intake[1] *(kcal/day/mouse)*	13.77± 0.68	11.52± 0.67*	11.96± 0.45	11.68± 0.24
Cholesterol (mM)	7.36± 0.46	34.78± 2.95***	32.53± 2.64	30.94± 2.16
Triglycerides (mM)	1.71± 0.16	5.70± 0.80***	5.38± 0.89	4.52± 0.94
Glucose (mM)	6.89± 0.33	6.65± 0.34	6.87± 0.21	7.19± 0.14
Insulin(ng/ml)	2.25± 0.47	4.68± 0.63**	4.07± 0.47	3.23± 0.31[&]
SBP (mmHg)	107.33± 2.15	126.79± 1.43***	122.27± 2.81	116.93± 1.53[&]
SAA (ug/ml)	11.30± 0.67	26.94± 2.14***	26.24± 1.67	21.38± 1.45

*[1]Average food intake during the 12-week treatment period. *p<0.05, ** p<0.01, *** p<0.001 compared to control. [&]p<0.05 compared to HFD. Data are presented as Mean ± SEM.*

3.2 PA attenuated metabolic risk factors and systolic blood pressure

We next examined the effects of the treatments on metabolic risk factors (Table 1). Plasma cholesterol and triglyceride concentrations were increased by HFD , and this was not affected by CA or PA. Glucose levels were comparable in all groups (Table 1). Insulin levels were significantly increased by HFD. CA did not affect plasma insulin, while PA reduced the HFD-induced increase in plasma insulin levels.

Obesity-associated hypertension was assessed by measuring SBP before and after treatment. HFD-fed mice had a significantly higher SBP than chow-fed mice before the start of CA and PA treatment and this difference persisted until the end of the experiment. CA had no significant effect on SBP, whereas PA lowered the HFD-induced increase in SBP (Table 1).

Plasma concentrations of SAA, an inflammatory marker produced by inflamed adipose tissue and liver (50), were low on chow, and significantly increased by HFD. SAA was unchanged by CA treatment, and PA treatment tended to reduce the HFD-induced increase in SAA levels (p=0.056).

3.3 PA treatment reduces HFD-induced liver steatosis, inflammation and collagen content

We next studied the liver, which is the first organ SCFAs pass after absorption from the intestine. Liver weight increased on HFD (Figure 2A) and was not affected by CA or PA. HE-stained liver cross-sections were analyzed for histopathological features of NAFLD (Figure 2B). Macrovesicular steatosis (Figure 2C) was hardly present in the chow group, whereas the HFD-fed mice developed pronounced macrovesicular steatosis. CA treatment did not

affect macrovesicular steatosis. In contrast, PA treatment significantly reduced HFD-induced macrovesicular steatosis. Microvesicular steatosis was also increased in HFD-fed animals (Figure 2D), with no effect of CA and a trend reduction by PA (p=0.08). The cross-sectional area that was covered with abnormally enlarged hepatocytes (hepatocellular hypertrophy; Figure 2E) was strongly increased by HFD and this HFD-induced increase was significantly reduced by PA only. Inflammatory aggregates were practically absent on chow (Figure 2F), whereas HFD livers showed a high number of inflammatory aggregates. CA did not significantly affect the number of inflammatory aggregates. However, PA reduced the HFD-induced number of inflammatory aggregates.

Hepatic collagen content was determined as a measure of fibrosis (Figure 2G). The hepatic collagen content was markedly increased by HFD. Liver fibrosis was not affected by CA, while PA decreased hepatic collagen content.

Histopathological analyses were supplemented by measurement of liver lipids, β-hydroxybutyrate and glycogen in liver homogenates. Liver lipid analysis of cholesteryl esters (CE), triglycerides (TG) and free cholesterol (FC), showed that CE and TG increased pronouncedly on HFD (Figure 2H). CA did not alter any of the liver lipids, whereas PA lowered the HFD-induced CE levels. The concentrations of β-hydroxybutyrate, a ketone body that is formed during beta-oxidation of lipids, were not affected by CA and PA (Figure 2I). Since hepatic steatosis and insulin resistance are associated with impairment of glycogen synthesis (51), we quantified hepatic glycogen levels (Figure 3J). HFD reduced glycogen levels relative to chow. The HFD-induced reduction in glycogen levels was partly prevented by CA and PA treatment.

Collectively, these data show that CA had no effect on liver pathology whereas the attenuating effects of PA on obesity and metabolic risk factors were paralleled by pronounced reductions in NASH and fibrosis.

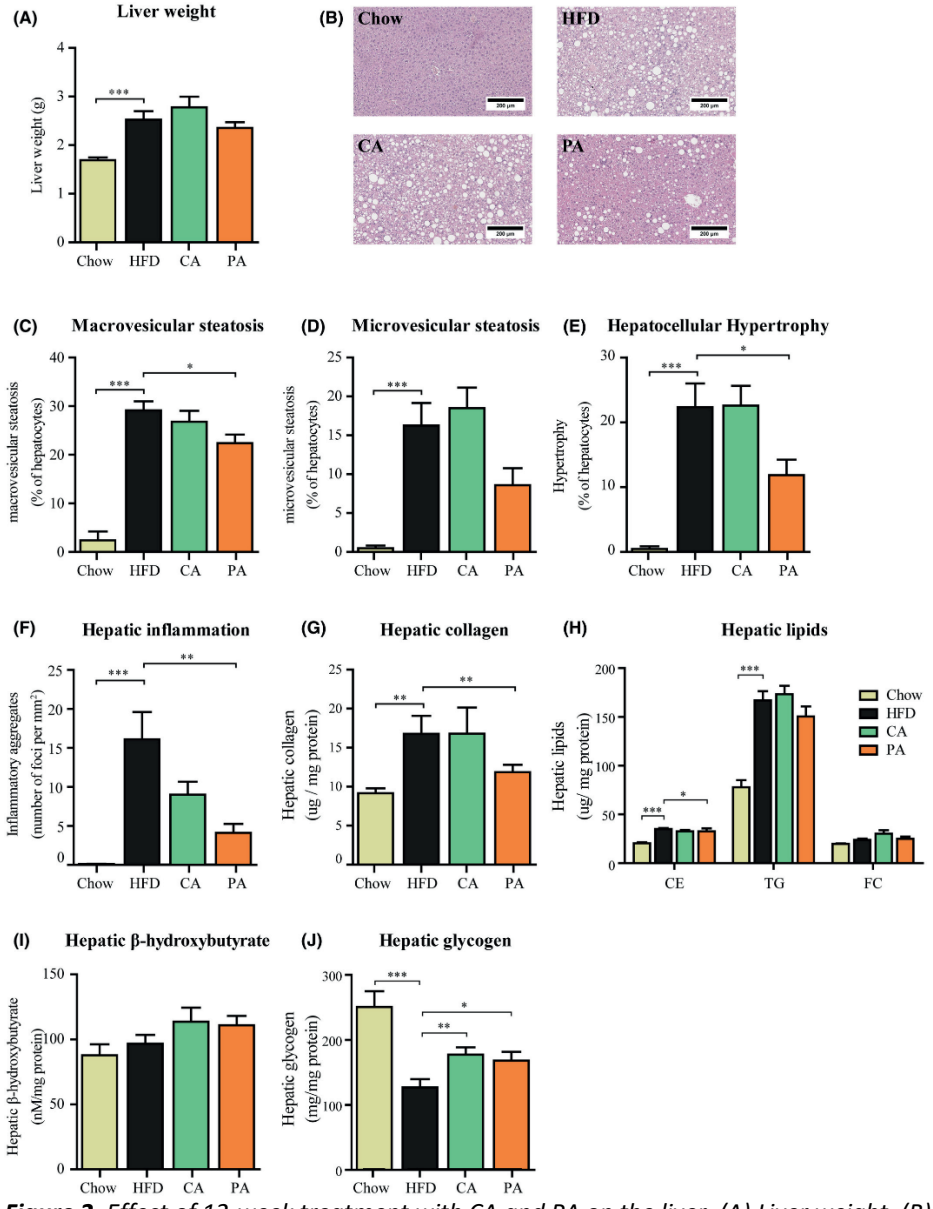

Figure 2. *Effect of 12-week treatment with CA and PA on the liver. (A) Liver weight, (B) representative images of hematoxylin-eosin stained liver sections, (C) macrovesicular steatosis, (D) microvesicular steatosis, (E) hepatocellular hypertrophy and (F) hepatic inflammation. Liver homogenates were analyzed for G) collagen content, (H) cholesteryl esters (CE), triglycerides (TG) and free cholesterol (FC), (I) ketone body ß-hydroxybutyrate as marker for the rate of ß-oxidation and (J) glycogen. HFD: high-fat diet; PA: propionic acid; CA: caproic acid. Data are presented as mean ± SEM, * p<0.05 or ** p<0.01 or *** p<0.001 compared to HFD.*

3.4 PA reduced subcutaneous fat mass and increased the frequency of small adipocytes
Next, we determined whether the observed reduction in body weight with PA was accompanied by an effect on adiposity, adipocyte morphology and inflammation in different fat depots (Figure 3). sWAT, gWAT and mWAT weight were increased by HFD treatment (Figure 3A-3C). CA did not affect the mass of these depots, while PA significantly reduced WAT mass relative to HFD and non-significantly lowered mWAT mass relative to HFD (p=0.08).
Relative to chow, HFD feeding resulted in a shift towards an increased frequency of hypertrophic adipocytes in all three depots (% of adipocytes > 8000 μm^2; Figure 3D-3F) with a concomitant reduction in small adipocytes (% of adipocytes < 2000 μm^2). Only PA was able to affect these HFD-induced changes, with an increased frequency of small adipocytes in sWAT (2000-4000 μm^2) and reduced frequency of hypertrophic adipocytes in mWAT (>8000 μm^2). WAT inflammation, as quantified by the number of crown-like structures (CLS) was practically absent on chow (Figure 3G-3I). HFD-feeding increased the number of CLS relative to chow in gWAT and mWAT. CA and PA treatment did not affect CLS counts in these depots relative to HFD.
Taken together, PA had a modest effect on adiposity in sWAT but did not reduce WAT inflammation in sWAT, gWAT or mWAT.

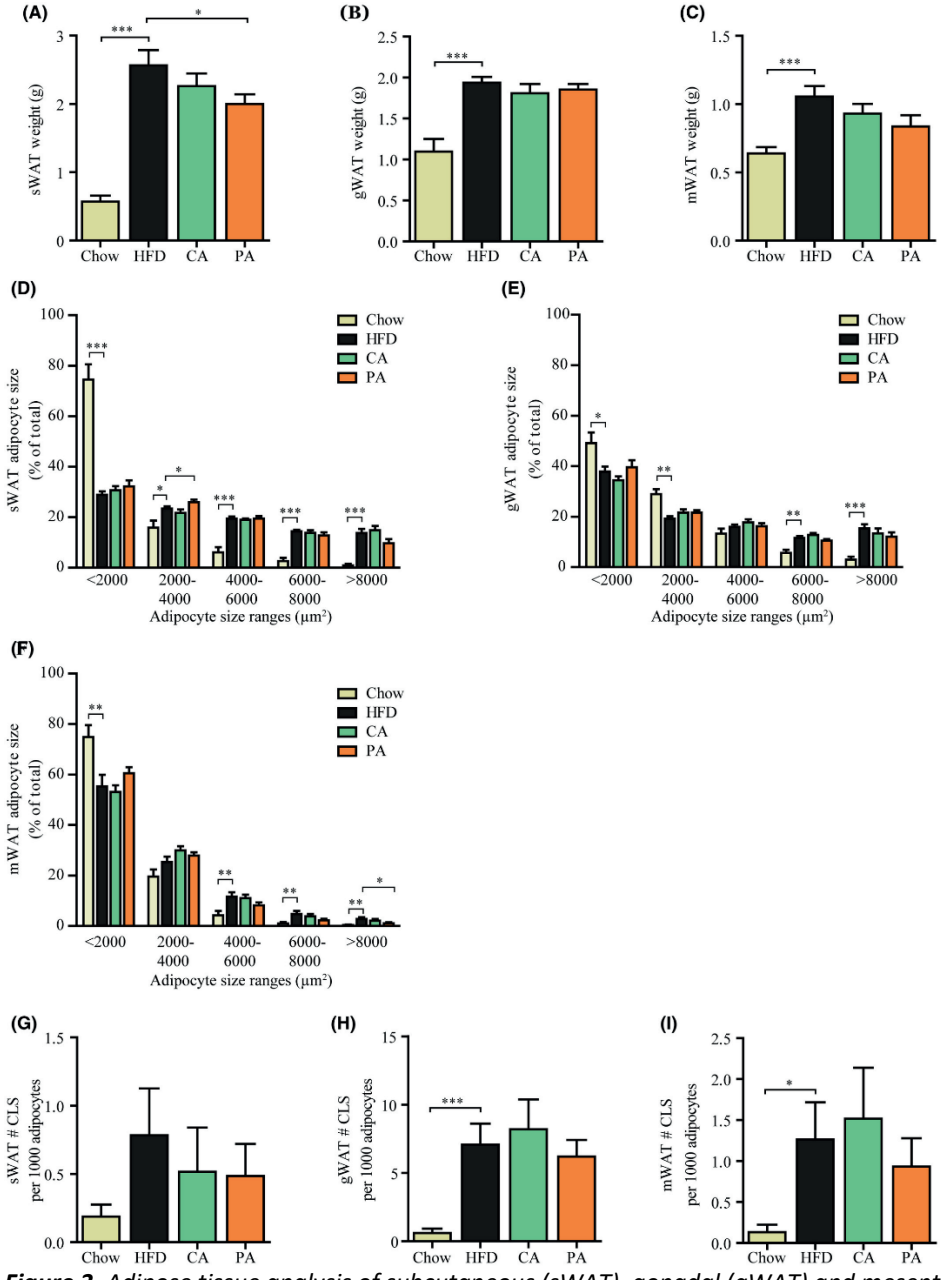

***Figure 3**. Adipose tissue analysis of subcutaneous (sWAT), gonadal (gWAT) and mesenteric (mWAT) depots after 12 weeks of CA and PA treatment: (A) sWAT (B) gWAT and (C) mWAT weight. Distribution of adipocyte sizes in (D) sWAT, (E) gWAT and (F) mWAT. Number of crown-like structures (CLS) per 1000 adipocytes in (G) sWAT, (H) gWAT and (I) mWAT. HFD: high-fat diet; PA: propionic acid; CA: caproic acid. Data are presented as mean ± SEM, * p<0.05 or ** p<0.01 or *** p<0.001 compared to HFD control.*

3.5 CA and PA do not affect behavior or spatial memory

Motor coordination was studied with the Rotarod. HFD-fed mice had a lower latency to fall compared to the chow-fed mice before the start of the interventions (Figure S1A). At the end of the experiment, HFD still had a lower latency to fall off the rod compared to chow mice and this was not affected by CA or PA (Figure 4A).

We did not find differences in exploration or locomotion activity in the open field test before the start of the interventions (Figure S1B) and at the end of the experiment (Figure 4B). However, PA mice spent less time in the periphery and more time in the corners of the open field than chow mice (Figure 4B) whereas frequency of entering the corners did not differ between groups. This suggests increased anxiety in PA mice. In addition, PA mice showed lower walking velocity and reduced total distance moved than chow mice (Figure S1C-S1D; Table S2), although no differences between groups were observed in home cage activity during the day or night as monitored in the DVC before the start of the interventions and at the end of the experiment (Figure S2A-S2B).

Spatial learning and memory of the mice were tested with the MWM test. All mice learned to find the hidden platform and showed a significant learning effect between day 1-2, day 1-3, and day 1-4 during the acquisition phase before the start of the treatments (Figure 4C). When the MWM was repeated after 10 weeks of treatment, we similarly found that mice were still able to find the hidden platform after 25-54 sec with no differences between the treatment groups. Next, a probe test was performed in which the platform of the MWM was removed. No significant effects between treatment groups were observed at the start of the intervention (Figure S1E-S1G) and at the end of the experiment in mean swimming velocity, the frequency to visit the former platform location, or time spent in the former platform location (Figure 4D-F).

Collectively, these behavioral experiments show that CA and PA were not able to reverse the HFD-induced reduced motor coordination in the rotarod test. Exploration activity and spatial learning and memory were not affected by HFD-feeding and were not affected by CA and PA treatment.

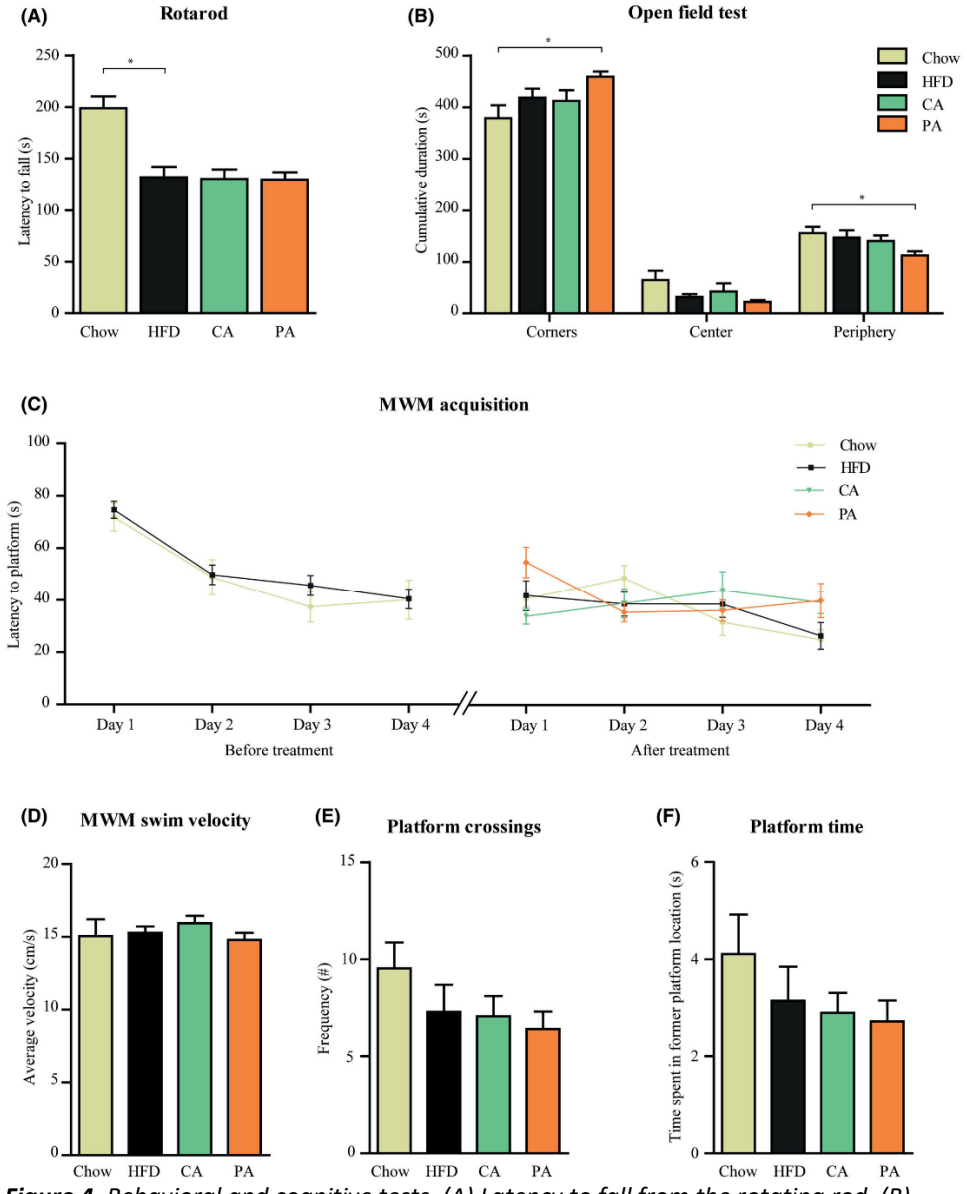

Figure 4. *Behavioral and cognitive tests. (A) Latency to fall from the rotating rod. (B) Cumulative duration (s) spent in corners, periphery and center in the open field test. (C) Acquisition test of the Morris water maze (MWM) before and after treatment. The latency to find the platform was measured on 4 consecutive days. (D) Mean swim velocity, (E) frequency of crossing the former platform location, and (F) total time spent at the former platform location during the probe test of the MWM. HFD: high-fat diet; PA: propionic acid; CA: caproic acid. Data are presented as mean ± SEM, * p<0.0. Open field test: N=14 (chow and HFD) or N=15 (CA and PA) per group. MWM and Rotarod: N=14 (HFD) or N=15 (chow, CA, PA) mice per group.*

3.6 PA treatment reverts HFD-induced changes in cerebral vasoreactivity

Effects on cerebrovasculature were assessed by measurement of CBF in the cortex, thalamus and hippocampus under normal and vasoconstrictive conditions. These two parameters were then used to calculate cerebral vasoreactivity a measure of the ability to respond to vasoconstrictive stimuli. CBF under normal and vasoconstrictive conditions did not differ between groups in any of the regions assessed (Figure 5A and 5B). While HFD (relative to chow) and CA (relative to HFD) had no effect on cerebral vasoreactivity, PA significantly improved cerebral vasoreactivity in the cortex and hippocampus (Figure 5C) and reverted cerebral vasoreactivity to chow levels.

Immunohistochemical stainings were performed to assess neurogenesis (DCX), neuroinflammation (IBA-1), and cerebrovascular integrity (GLUT-1). No differences between groups were observed in the number of DCX+ cells in the hippocampus (Figure S3A). Furthermore, no differences between groups were observed in the amount of IBA-1+ staining or relative IBA-1+ positive area in the cortex, hippocampus or thalamus (Figure S3B-S3C). HFD-fed mice had a smaller relative GLUT-1+ area in the thalamus than chow-fed mice (Figure 5D). CA had no effect, whereas PA increased the GLUT-1+ area and the number of GLUT-1+ particles per mm^2 measures for blood vessel density, in the hippocampus (Figure 5D and 5E). The number of GLUT-1+ particles per mm^2 was even higher than in chow mice. GLUT-1 intensity, reflecting the amount of GLUT-1 transporters, was not affected by HFD (compared to chow) or CA (compared to HFD). However, we observed a trend toward an increased GLUT-1 intensity in PA mice compared to HFD in the cortex ($p=0.06$) and hippocampus ($p=0.08$). GLUT-1 intensity in PA mice was even higher than in chow mice in the hippocampus (Figure S3D).

In summary, PA reduces cerebrovascular activity in the hippocampus and cortex to chow levels and increases the number of GLUT-1+ particles per mm^2, reflecting vascular density, and GLUT-1 intensity, a marker for the amount of GLUT-1 transporters, in the hippocampus (52).

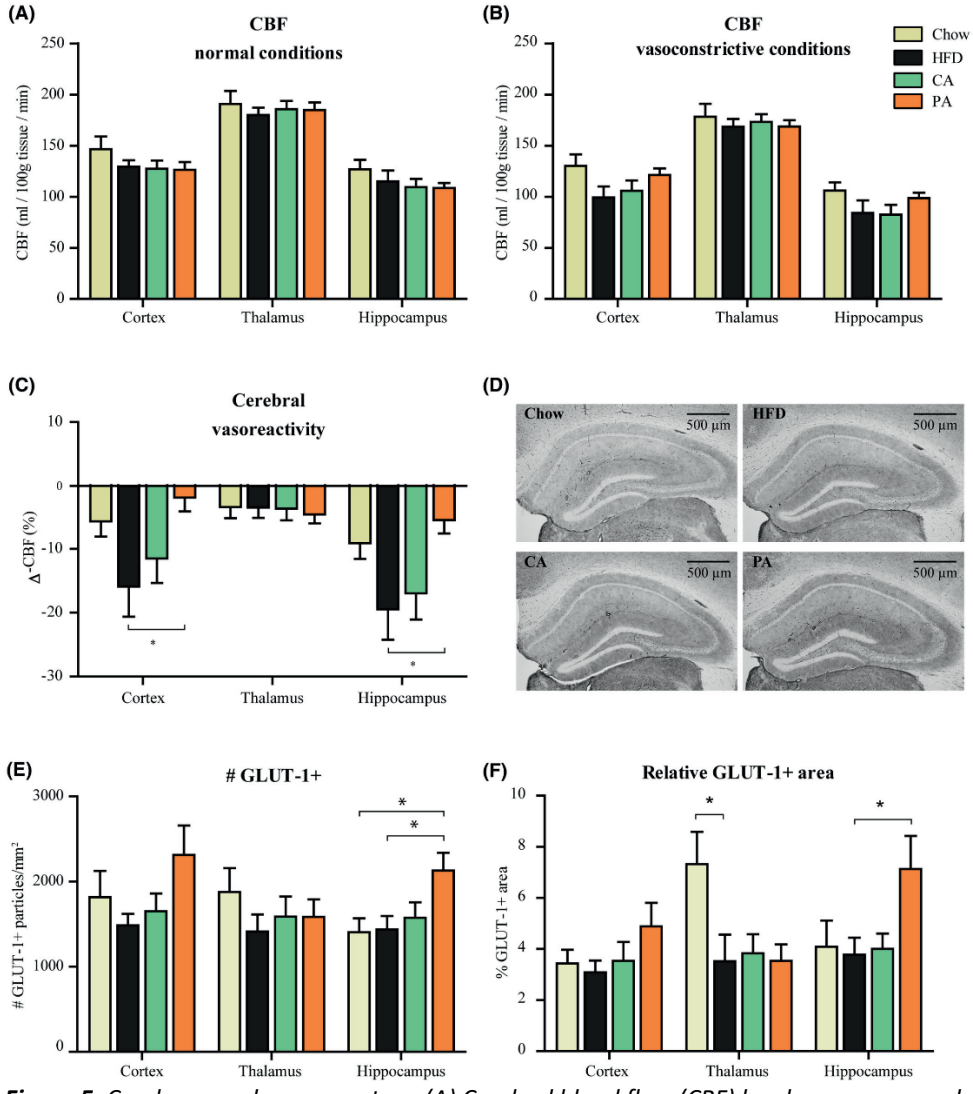

Figure 5. *Cerebrovascular parameters. (A) Cerebral blood flow (CBF) levels were assessed under normal conditions; and (B) under vasoconstrictive conditions in the cortex, hippocampus and thalamus. (C) Cerebral vasoreactivity was measured using normal and vasoconstrictive CBF, as a measure of ability to respond to vasoconstrictive stimuli (D) Representative images of GLUT-1 staining in Chow, HFD, CA and PA mice (5× objective, scale bar represents 500 µm). (E) Quantification of the relative GLUT-1+ area, and (F) amount of GLUT-1+ particles per mm2 in the cortex, hippocampus and thalamus. HFD: high-fat diet; PA: propionic acid; CA: caproic acid; CBF: cerebral blood flow; GLUT-1: glucose transporter type 1. Data are presented as mean ± SEM, * p<0.05 or ** p<0.01 or # p<0.08. CBF: N=14 (chow and CA), N=13 (HFD) and N=15 (PA). GLUT-1: N=14 (HFD), N=14 (chow, CA) or N=15 (PA) mice per group.*

3.7 PA reverts HFD-induced effects in functional connectivity and microstructural gray and white matter integrity

To gain insight into functional and microstructural brain changes in HFD-induced obesity and the effects of CA and PA thereupon, mitochondrial enzyme activity analysis, rs-fMRI and DTI were performed.

Cerebellar mitochondrial CS enzyme activity was comparable in all groups and the activity of complexes (I – IV) were unaffected by the treatments (Figure S4).

Functional connectivity was assessed by rs-fMRI using total and partial correlation analyses. Here, we observed no differences in functional connectivity, as analyzed with total correlations (Figure S5). Partial correlation highlights the direct connectivity between two regions. A reduction in partial functional connectivity was observed between the visual and auditory cortex in HFD mice compared to chow mice ($p<0.001$; Figure 6A and 6B). CA and PA had no effect on functional connectivity compared to HFD. However, the functional connectivity of CA and PA mice was comparable to chow mice ($p>0.05$), suggesting that CA and PA were able to revert the HFD-induced effects in functional connectivity.

Next, DTI was used to assess gray and white matter integrity in several brain regions. The FA was higher in HFD mice than in chow-fed mice in the somatosensory cortex ($p<0.05$) and visual cortex. No effects of CA or PA on the HFD-induced increase in FA levels in these brain regions were observed. However, FA levels of PA mice were comparable to chow, indicating that PA reverted the HFD-induced effects in the somatosensory cortex and visual cortex. Furthermore, HFD and CA had no effects on the FA in the hippocampus and motor cortex, but PA-treated mice had a significantly lower FA in the hippocampus and motor cortex (Figure 6C) than HFD mice. The FA in these regions in PA mice was comparable to chow.

The mean diffusivity (MD) in the hippocampus, motor cortex, somatosensory cortex and visual cortex were not affected by HFD (relative to chow), CA and PA (relative to HFD) (Figure 6D). MD in the optic tract was significantly lower in HFD-fed animals than in chow-fed animals (Figure 6D). CA and PA did not affect MD relative to HFD in any of the regions assessed. However, MD did not differ between PA-fed mice and chow mice in the optic tract, suggesting that PA reverted the HFD-induced effects on the MD in this region.

Taken together, CA and PA were able to revert the HFD-induced effects in functional connectivity between the visual and auditory cortex. PA altered microstructural gray matter integrity in the hippocampus and motor cortex, but this was not significant when compared to chow. In addition, PA reverted the HFD-induced effects in the somatosensory cortex, visual cortex and optic tract.

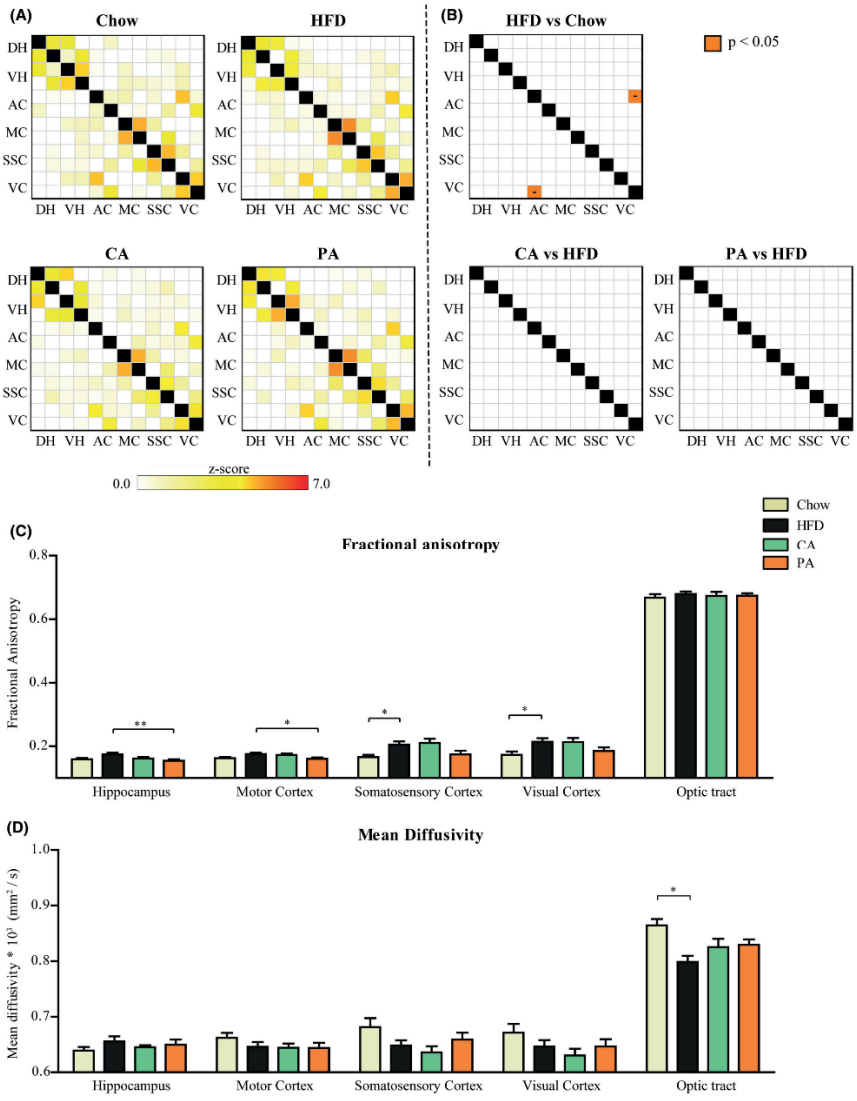

Figure 6. *Connectivity between brain regions and white matter integrity. (A) Partial correlation matrixes of the Chow, HFD, CA, and PA experimental groups. The selected brain regions (dorsal hippocampus (DH), ventral hippocampus (VH), auditory cortex (AC), motor cortex (MC), somatosensory cortex (SSC) and visual cortex (VC) are subdivided in left hemisphere (first row) and right hemisphere (second row). A higher Z-score (red) indicates a stronger functional connectivity. (B) Statistical analysis of functional connectivity between HFD and chow, CA and HFD, and PA and HFD. Minus (-) symbols in the matrix indicate whether the connectivity was decreased. Orange: p<0.05). (C) Differences in fractional anisotropy, and (D) mean diffusivity between the experimental groups in the hippocampus, motor cortex, somatosensory cortex and visual cortex. Data are presented as mean ± SEM, * p<0.05, ** p<0.01. N=14 (HFD) or N=15 (chow, CA, PA) mice per group.*

3.8 PA affects genes and upstream regulators involved in synaptogenesis and inflammation

Hippocampal gene expression was studied using qRT-PCR and a multiplex neuroinflammation panel. Post synaptic density marker *Psd95* mRNA levels did not differ between the experimental groups (Figure 7A). Also, no differences between chow, HFD and CA mice were observed in synaptophysin (*Syp1*) mRNA levels. A trend toward reduced expression of synaptophysin in the hippocampus was observed in mice that received PA ($p=0.055$; Figure 7B), however, this was not significant when compared to chow.

A more extensive gene profiling analysis using a neuroinflammation panel followed by an upstream regulator analysis and an enrichment analysis across biological pathways confirmed this effect. There were no significant changes in predicted activation state of upstream regulators between chow and HFD (Figure 7C; signaling downstream of IFNG and STAT1 was significantly enriched in HFD but did not reach the cut-off value for relevant inhibition or activation). PA inhibited specific upstream regulators important in synaptogenesis relative to HFD (e.g., GH1, WNT3A, VEGFA, BDNF, EGF, JUN; Figure 8C). PA also attenuated signaling of the N-methyl-D-aspartate (NMDA) receptor a post-synaptic glutamate receptor involved in excitatory neurotransmission, important for synaptic plasticity and memory function. In addition, PA inhibited inflammatory pathways downstream of e.g., IL-1, IL-1B, IL17A, Il-33, CXCL12. The above findings are supported by canonical pathway analysis showing significant inhibition of synaptogenesis and glutamate receptor signaling, neuroinflammation and lipopolysaccharide (LPS)-stimulated mitogen-activated kinase (MAPK) signaling pathways by PA.

Altogether, we found that PA treatment showed anti-inflammatory effects and reduced synaptogenesis and synaptic plasticity signaling.

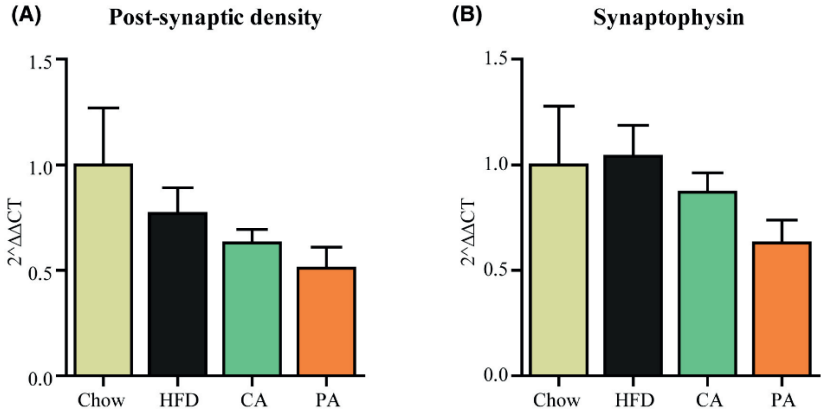

(C) Upstream regulator gene expression analysis

	HFD vs Chow		PA vs HFD	
Upstream regulator	Z-score	p-value	Z-score	p-value
Inflammatory signalling				
IL1	N/A	1.000	-2.2	0.003
IL1B	N/A	1.000	-1.8	0.000
IL17A	N/A	1.000	-2.4	0.000
IL33	N/A	1.000	-2.0	0.016
IFNG	0.2	0.001	-1.5	0.000
Ige	N/A	1.000	-2.4	0.002
STAT1	0.0	0.000	-2.1	0.000
CXCL12	N/A	1.000	-2.0	0.008
TLR4	N/A	0.037	-2.0	0.000
IRF1	N/A	0.008	-2.0	0.001
CHUK	N/A	0.001	-1.8	0.000
TGFB1	N/A	1.000	-1.5	0.000
Synaptic plasticity				
BDNF	N/A	1.000	-1.7	0.000
VEGFA	N/A	1.000	-2.0	0.000
EGF	N/A	1.000	-1.9	0.000
JUN	N/A	1.000	-2.2	0.000
STAT1	0.0	0.000	-2.1	0.000
GH1	N/A	1.000	-2.0	0.001
WNT3A	N/A	1.000	-1.9	0.000
NTRK2	N/A	1.000	-1.8	0.000
N-methyl-D-aspartate	N/A	1.000	-2.4	0.000
NMDA Receptor	N/A	1.000	-2.0	0.000
AMPA receptor	N/A	1.000	N/A	0.039

***Figure 7**. Hippocampal synaptophysin, post-synaptic density and upstream regulators. (A) Post-synaptic density-95 and (B) Synaptophysin mRNA expression levels in the hippocampus. N=14 (HFD) or N=15 (chow, CA, PA) mice per group. (C) Changes in upstream regulators are predicted from changes in transcription factors or key regulators with a Z-score. Z < -2 indicates a relevant inhibition (shown in green) and Z > 2 indicates a relevant activation. Significant changes with Z < -1.96 are shown in light green. N/A indicates an insufficient number of differentially expressed genes to link gene effects to an upstream regulator. The p-value indicates significant enrichment of the genes downstream of a regulator. N=8 per group. Data are presented as mean ± SEM*

Discussion

The present study examined potential health effects of PA and CA treatment on obesity-induced liver fibrosis as well as brain function and structure. Such effects have, to our knowledge, not been investigated so far and, and in case of CA, there are no published studies in rodent models of diet-induced obesity, dysmetabolism and inflammation.

In the present study, CA treatment showed no significant effects on body weight, plasma lipids and metabolic risk factors as well as on liver steatosis. Interestingly, HFD treatment strongly lowered hepatic glycogen content, and both CA and PA significantly prevented this reduction indicating an effect of both CA and PA on liver metabolism. A reduction in hepatic glycogen content appears to be indicative of a defect in liver metabolism, impaired liver function, and hepatic insulin resistance as reported by others (53, 54), an effect that has not been reported earlier in the HFD-fed Ldlr-/-.Leiden model of NASH. The hepatic glycogen augmenting effect of CA was paralleled by an insignificant reduction of lobular inflammation (by about 50%), whereas similar increases of hepatic glycogen with PA were associated with a reduction in liver inflammation. Because hepatic glycogen content is usually not determined in rodent studies of NAFLD/NASH, it is unclear whether the two effects are related to each other. It is well established that chronic tissue inflammation can impair insulin signaling thereby contributing to hepatic insulin resistance. It is thus possible that the observed increase in hepatic glycogen, the formation of which requires insulin signaling, is secondary to a possible inflammation-quenching effect of CA.

In contrast to CA, PA treatment prevented further HFD-induced weight gain independent of food intake. The attenuating effect on body weight as well as the reduction in plasma insulin levels observed here, are in line with the study of Lin *et al.* in which a similar dose of 2.2% w/w PA was used (21).
In addition, we observed that HFD increases SBP, a finding that is consistent with earlier studies (6, 55). PA-treatment was able to reduce the HFD-induced increased SBP, which is in line with observations in two other mouse models (56) and may be attributable to PA-induced endothelium-dependent vasodilation, as has been previously reported in tail arteries (57). Since high SBP is associated with high body weight (58); and cognitive decline in humans (59), the observed effects of PA on SBP and body weight may reduce the risk for cognitive decline.

The attenuating effects of PA treatment on obesity and metabolic risk factors are associated with a reduction in hepatic steatosis, accompanied by a reduction in hepatic cholesterol ester content. These findings are in line with a previous study which showed reduced intrahepatic lipid accumulation in NAFLD patients (assessed by magnetic resonance imaging) upon increased colonic PA levels (17) and with *in vitro (60, 61)* and *in vivo* (18) studies which show inhibition of lipid synthesis by PA. An alternative explanation for the observed antisteatotic effects of PA could be a stimulation of β-oxidation by PA, as has been previously reported in a short term mouse study (18). However we did not observe any effect of PA on hepatic β-hydroxybutyrate, a marker for β-oxidation, indicating that this pathway is not of major importance in the current study. Discrepancies between our findings and those of den Besten *et al.* could be due to differences in mouse

strain and diet, lower dosage of PA used in our study (2.5% w/w), the therapeutic setting used here or the difference in methods used to measure β-oxidation.

PA also showed pronounced effects on hepatic inflammatory aggregates and collagen content, showing that PA can reduce development of NASH and liver fibrosis. To the best of our knowledge we are the first to comprehensively study the effects of PA on liver steatosis, inflammation and fibrosis. Anti-inflammatory effects of PA have been reported previously for other organs and pathologies, such as acute leukemia (62), cardiovascular disease (56, 63) and inflammatory bowel disease (64) although the underlying mechanisms remain unclear.

To assess effects of PA and CA on behavior and cognition, we performed behavioral and cognitive tests. We found that HFD-fed mice had reduced motor coordination in the rotarod test. CA and PA could not reverse this effect. PA mice spent more time in the corners of the open field test than chow mice, suggesting that PA mice were more anxious than chow-fed mice. Increased anxiety-like behavior after PA administration has been reported in other studies as well (65-67). Exploration activity and spatial learning and memory were not affected by HFD, CA or PA. Other studies found cognitive deficits, increased motor activity, and impaired spatial memory in rats that were given PA (68-70). However, these rats were given PA via intracerebroventricular injections with a relatively high dosage (4 µl of 0.26 M) of PA.

We measured cerebral vasoreactivity, a measure of ability to respond to vasoconstrictive stimuli, to study the effects of PA and CA on cerebrovascular health. Overall, the cerebral vasoreactivity levels that we detected, are similar to those found in another study (34). The cerebral vasoreactivity levels in the cortex and hippocampus were low in HFD compared to chow, albeit not significant. HFD-induced obesity is associated with cerebrovascular remodeling (71, 72), an active process of structural changes of the vessel wall (73). These structural changes to the vasculature can result in a decreased diameter of the blood vessels, and can lead to an exaggerated response to vasoconstrictive stimuli (74). Hypertension can induce hyperperfusion of (brain) tissue, which is then followed by remodeling of the vasculature (74). Moreover, hypertension and obesity are associated with rarefaction (a loss of capillaries and arterioles), which further contributes to vascular remodeling (74, 75). In line with this, the relative GLUT-1+ area in the thalamus was decreased in HFD mice compared to chow. GLUT-1 is selectively expressed in the cerebral capillary endothelium, and is used as a marker for cerebrovascular integrity (34). This indicates that HFD is able to affect cerebrovascular integrity.
PA reverted HFD-induced effects on cerebrovascular activity in the hippocampus and cortex to chow levels. This adapted cerebral vasoreactivity is in line with the increased hippocampal GLUT-1, and may explain the effects of PA on cerebral hemodynamics. Together, this suggests that PA is able to revert HFD-induced vascular remodeling.

We revealed that PA reversed the HFD-induced effect mainly in different components of the visual system, i.e. the visual cortex and the optic tract. HFD decreased functional connectivity between the visual cortex and the auditory cortex, an effect that was reversed by CA and PA. On the other hand, HFD mice had a higher FA in cortical regions,

i.e., the visual and somatosensory cortex, and a lower MD in the optic tract compared to chow mice. PA treatment reduced FA in the visual and somatosensory cortex, and increased MD in the optic tract, which could suggest that PA reversed the HFD-induced effects back to chow or prevented further changes upon start of PA treatment. Recent studies by Medic *et al.* and Ou *et al.*, described positive associations between white matter integrity and increased adiposity (76, 77). In addition, we revealed possible negative effects of PA on synaptogenesis in the hippocampus. Gene expression analysis in the hippocampus showed that synaptic signaling was reduced and associated with a reduction of glutamate signaling and upstream regulator NMDA in PA mice. Neuronal glutamate signaling is vital for the encoding of information, the formation and retrieval of memories, spatial recognition and the maintenance of consciousness (78). NMDA receptors are involved in myelinating processes, and consistent herewith, NMDA receptor antagonists, like memantine and MK801, have shown a decrease in FA in the hippocampus of rats (79, 80).

In conclusion, we found that PA exerted pronounced positive effects on metabolic risk factors and attenuated the development of HFD induced NASH and liver fibrosis. PA also decreased the systolic blood pressure and reverted cerebral vasoreactivity. PA reverted HFD-induced effects in functional connectivity and microstructural gray and white matter integrity to chow levels, however PA also increased anxiety-like behavior and reduced regulation of synaptogenesis in the hippocampus. Therefore, caution should be used when considering PA as treatment, even though positive effects on metabolism, (cerebro)vasculature, and on both brain structure and function were observed.

Acknowledgments
We thank the bio-technicians at TNO Metabolic Health Research and at the Animal Research Facility of the Radboud university medical center for taking excellent care of the mice. We also thank Andor Veltien, Sjaak van Asten, and Tim Emmerzaal for their great scientific support.

References

1. Ng, M., Fleming, T., et al. (2014) Global, regional, and national prevalence of overweight and obesity in children and adults during 1980-2013: a systematic analysis for the Global Burden of Disease Study 2013. *Lancet* **384**, 766-781
2. Burhans, M. S., Hagman, D. K., Kuzma, J. N., Schmidt, K. A., and Kratz, M. (2018) Contribution of Adipose Tissue Inflammation to the Development of Type 2 Diabetes Mellitus. *Compr Physiol* **9**, 1-58
3. Kitade, H., Chen, G., Ni, Y., and Ota, T. (2017) Nonalcoholic Fatty Liver Disease and Insulin Resistance: New Insights and Potential New Treatments. *Nutrients* **9**
4. Friedman, S. L., Neuschwander-Tetri, B. A., Rinella, M., and Sanyal, A. J. (2018) Mechanisms of NAFLD development and therapeutic strategies. *Nat Med* **24**, 908-922
5. Bataller, R., and Brenner, D. A. (2005) Liver fibrosis. *J Clin Invest* **115**, 209-218
6. Arnoldussen, I. A. C., Wiesmann, M., Pelgrim, C. E., Wielemaker, E. M., van Duyvenvoorde, W., Amaral-Santos, P. L., Verschuren, L., Keijser, B. J. F., Heerschap, A., Kleemann, R., Wielinga, P. Y., and Kiliaan, A. J. (2017) Butyrate

restores HFD-induced adaptations in brain function and metabolism in mid-adult obese mice. *Int J Obes (Lond)* **41**, 935-944
7. de Mello, A. H., Costa, A. B., Engel, J. D. G., and Rezin, G. T. (2018) Mitochondrial dysfunction in obesity. *Life Sci* **192**, 26-32
8. Pannacciulli, N., Del Parigi, A., Chen, K., Le, D. S., Reiman, E. M., and Tataranni, P. A. (2006) Brain abnormalities in human obesity: a voxel-based morphometric study. *Neuroimage* **31**, 1419-1425
9. van Bloemendaal, L., Ijzerman, R. G., Ten Kulve, J. S., Barkhof, F., Diamant, M., Veltman, D. J., and van Duinkerken, E. (2016) Alterations in white matter volume and integrity in obesity and type 2 diabetes. *Metab Brain Dis* **31**, 621-629
10. Uranga, R. M., and Keller, J. N. (2019) The Complex Interactions Between Obesity, Metabolism and the Brain. *Front Neurosci* **13**, 513
11. Hurr, C., Patik, J. C., Kim, K., and Brothers, R. M. (2017) Blunted cerebral vascular responsiveness to hypercapnia in obese individuals. *Exp Physiol* **102**, 1300-1308
12. Jais, A., Solas, M., Backes, H., Chaurasia, B., Kleinridders, A., Theurich, S., Mauer, J., Steculorum, S. M., Hampel, B., Goldau, J., Alber, J., Forster, C. Y., Eming, S. A., Schwaninger, M., Ferrara, N., Karsenty, G., and Bruning, J. C. (2016) Myeloid-Cell-Derived VEGF Maintains Brain Glucose Uptake and Limits Cognitive Impairment in Obesity. *Cell* **165**, 882-895
13. Mar Rodriguez, M., Perez, D., Javier Chaves, F., Esteve, E., Marin-Garcia, P., Xifra, G., Vendrell, J., Jove, M., Pamplona, R., Ricart, W., Portero-Otin, M., Chacon, M. R., and Fernandez Real, J. M. (2015) Obesity changes the human gut mycobiome. *Sci Rep* **5**, 14600
14. Patrone, V., Vajana, E., Minuti, A., Callegari, M. L., Federico, A., Loguercio, C., Dallio, M., Tolone, S., Docimo, L., and Morelli, L. (2016) Postoperative Changes in Fecal Bacterial Communities and Fermentation Products in Obese Patients Undergoing Bilio-Intestinal Bypass. *Front Microbiol* **7**, 200
15. Rial, S. A., Ravaut, G., Malaret, T. B., Bergeron, K. F., and Mounier, C. (2018) Hexanoic, Octanoic and Decanoic Acids Promote Basal and Insulin-Induced Phosphorylation of the Akt-mTOR Axis and a Balanced Lipid Metabolism in the HepG2 Hepatoma Cell Line. *Molecules* **23**
16. Akpa, M. M., Point, F., Sawadogo, S., Radenne, A., and Mounier, C. (2010) Inhibition of insulin and T3-induced fatty acid synthase by hexanoate. *Lipids* **45**, 997-1009
17. Chambers, E., Viardot, A., Psichas, A., Morrison, D., Murphy, K., Zac-Varghese, S., MacDougall, K., Preston, T., Tedford, C., Bell, J., Thomas, E., Mt-Isa, S., Ashby, D., Dhillo, W., Bloom, S., Morley, W., Clegg, S., and Frost, G. (2015) Effects of elevating colonic propionate on liver fat content in overweight adults with non-alcoholic fatty liver disease: a pilot study. *Proceedings of the Nutrition Society* **74**
18. den Besten, G., Bleeker, A., Gerding, A., van Eunen, K., Havinga, R., van Dijk, T. H., Oosterveer, M. H., Jonker, J. W., Groen, A. K., Reijngoud, D.-J., and Bakker, B. M. (2015) Short-Chain Fatty Acids Protect Against High-Fat Diet-Induced Obesity via a PPARgamma-Dependent Switch From Lipogenesis to Fat Oxidation. *Diabetes* **64**, 2398-2408
19. De Vadder, F., Kovatcheva-Datchary, P., Goncalves, D., Vinera, J., Zitoun, C., Duchampt, A., Backhed, F., and Mithieux, G. (2014) Microbiota-generated

metabolites promote metabolic benefits via gut-brain neural circuits. *Cell* **156**, 84-96

20. Chambers, E. S., Preston, T., Frost, G., and Morrison, D. J. (2018) Role of Gut Microbiota-Generated Short-Chain Fatty Acids in Metabolic and Cardiovascular Health. *Curr Nutr Rep* **7**, 198-206
21. Lin, H. V., Frassetto, A., Kowalik, E. J., Jr., Nawrocki, A. R., Lu, M. M., Kosinski, J. R., Hubert, J. A., Szeto, D., Yao, X., Forrest, G., and Marsh, D. J. (2012) Butyrate and propionate protect against diet-induced obesity and regulate gut hormones via free fatty acid receptor 3-independent mechanisms. *PLoS One* **7**, e35240
22. Takai, A., Kikuchi, K., Ichimura, M., Tsuneyama, K., Moritoki, Y., Matsumoto, K., Tsunashima, H., Onda, T., Kuniyoshi, N., Nariyama, T., Ohyatsu, S., Kubota, J., Nagumo, K., Sato, S., Hara, M., and Miyakawa, H. (2020) Fructo-oligosaccharides ameliorate steatohepatitis, visceral adiposity, and associated chronic inflammation via increased production of short-chain fatty acids in a mouse model of non-alcoholic steatohepatitis. *BMC Gastroenterol* **20**, 46
23. Morrison, M. C., Verschuren, L., Salic, K., Verheij, J., Menke, A., Wielinga, P. Y., Iruarrizaga-Lejarreta, M., Gole, L., Yu, W.-M., Turner, S., Caspers, M. P. M., Martinez-Arranz, I., Pieterman, E., Stoop, R., van Koppen, A., van den Hoek, A. M., Mato, J. M., Hanemaaijer, R., Alonso, C., and Kleemann, R. (2018) Obeticholic Acid Modulates Serum Metabolites and Gene Signatures Characteristic of Human NASH and Attenuates Inflammation and Fibrosis Progression in Ldlr-/-.Leiden Mice. *Hepatol Commun* **2**, 1513-1532
24. Kilkenny, C., Browne, W. J., Cuthi, I., Emerson, M., and Altman, D. G. (2012) Improving bioscience research reporting: the ARRIVE guidelines for reporting animal research. *Vet Clin Pathol* **41**, 27-31
25. Liang, W., Menke, A. L., Driessen, A., Koek, G. H., Lindeman, J. H., Stoop, R., Havekes, L. M., Kleemann, R., and van den Hoek, A. M. (2014) Establishment of a general NAFLD scoring system for rodent models and comparison to human liver pathology. *PLoS One* **9**, e115922
26. Bligh, E. G., and Dyer, W. J. (1959) A rapid method of total lipid extraction and purification. *Can J Biochem Physiol* **37**, 911-917
27. Galarraga, M., Campion, J., Munoz-Barrutia, A., Boque, N., Moreno, H., Martinez, J. A., Milagro, F., and Ortiz-de-Solorzano, C. (2012) Adiposoft: automated software for the analysis of white adipose tissue cellularity in histological sections. *Journal of lipid research* **53**, 2791-2796
28. Schindelin, J., Arganda-Carreras, I., Frise, E., Kaynig, V., Longair, M., Pietzsch, T., Preibisch, S., Rueden, C., Saalfeld, S., Schmid, B., Tinevez, J.-Y., White, D. J., Hartenstein, V., Eliceiri, K., Tomancak, P., and Cardona, A. (2012) Fiji: an open-source platform for biological-image analysis. *Nat Methods* **9**, 676-682
29. Schneider, C. A., Rasband, W. S., and Eliceiri, K. W. (2012) NIH Image to ImageJ: 25 years of image analysis. *Nat Methods* **9**, 671-675
30. Mulder, P., Morrison, M. C., Wielinga, P. Y., van Duyvenvoorde, W., Kooistra, T., and Kleemann, R. (2016) Surgical removal of inflamed epididymal white adipose tissue attenuates the development of non-alcoholic steatohepatitis in obesity. *Int J Obes (Lond)* **40**, 675-684

31. Pernold, K., Iannello, F., Low, B. E., Rigamonti, M., Rosati, G., Scavizzi, F., Wang, J., Raspa, M., Wiles, M. V., and Ulfhake, B. (2019) Towards large scale automated cage monitoring - Diurnal rhythm and impact of interventions on in-cage activity of C57BL/6J mice recorded 24/7 with a non-disrupting capacitive-based technique. *PLoS One* **14**, e0211063
32. Giles, J. M., Whitaker, J. W., Moy, S. S., and Fletcher, C. A. (2018) Effect of Environmental Enrichment on Aggression in BALB/cJ and BALB/cByJ Mice Monitored by Using an Automated System. *J Am Assoc Lab Anim Sci*
33. Wiesmann, M., Zerbi, V., Jansen, D., Lutjohann, D., Veltien, A., Heerschap, A., and Kiliaan, A. J. (2017) Hypertension, cerebrovascular impairment, and cognitive decline in aged AbetaPP/PS1 mice. *Theranostics* **7**, 1277-1289
34. Arnoldussen, I. A. C., Zerbi, V., Wiesmann, M., Noordman, R. H. J., Bolijn, S., Mutsaers, M. P. C., Dederen, P. J. W. C., Kleemann, R., Kooistra, T., van Tol, E. A. F., Gross, G., Schoemaker, M. H., Heerschap, A., Wielinga, P. Y., and Kiliaan, A. J. (2016) Early intake of long-chain polyunsaturated fatty acids preserves brain structure and function in diet-induced obesity. *J Nutr Biochem* **30**, 177-188
35. Zerbi, V., Jansen, D., Wiesmann, M., Fang, X., Broersen, L. M., Veltien, A., Heerschap, A., and Kiliaan, A. J. (2014) Multinutrient diets improve cerebral perfusion and neuroprotection in a murine model of Alzheimer's disease. *Neurobiol Aging* **35**, 600-613
36. Zerbi, V., Wiesmann, M., Emmerzaal, T. L., Jansen, D., Van Beek, M., Mutsaers, M. P. C., Beckmann, C. F., Heerschap, A., and Kiliaan, A. J. (2014) Resting-state functional connectivity changes in aging apoE4 and apoE-KO mice. *J Neurosci* **34**, 13963-13975
37. Harsan, L.-A., Paul, D., Schnell, S., Kreher, B. W., Hennig, J., Staiger, J. F., and von Elverfeldt, D. (2010) In vivo diffusion tensor magnetic resonance imaging and fiber tracking of the mouse brain. *NMR Biomed* **23**, 884-896
38. Alexander, A. L., Lee, J. E., Lazar, M., and Field, A. S. (2007) Diffusion tensor imaging of the brain. *Neurotherapeutics* **4**, 316-329
39. Paxinos, G., and Franklin, K. (2001) Paxinos and Franklin's the Mouse Brain in Stereotaxic Coordinates.
40. Zerbi, V., Wiesmann, M., Emmerzaal, T. L., Jansen, D., Van Beek, M., Mutsaers, M. P., Beckmann, C. F., Heerschap, A., and Kiliaan, A. J. (2014) Resting-state functional connectivity changes in aging apoE4 and apoE-KO mice. *J Neurosci* **34**, 13963-13975
41. Wiesmann, M., Zinnhardt, B., Reinhardt, D., Eligehausen, S., Wachsmuth, L., Hermann, S., Dederen, P. J., Hellwich, M., Kuhlmann, M. T., Broersen, L. M., Heerschap, A., Jacobs, A. H., and Kiliaan, A. J. (2017) A specific dietary intervention to restore brain structure and function after ischemic stroke. *Theranostics* **7**, 493-512
42. Janssen, A. J., Trijbels, F. J., Sengers, R. C., Smeitink, J. A., van den Heuvel, L. P., Wintjes, L. T., Stoltenborg-Hogenkamp, B. J., and Rodenburg, R. J. (2007) Spectrophotometric assay for complex I of the respiratory chain in tissue samples and cultured fibroblasts. *Clin Chem* **53**, 729-734

43. Emmerzaal, T. L., Rodenburg, R. J., Tanila, H., Verweij, V., Kiliaan, A. J., and Kozicz, T. (2018) Age-Dependent Decrease of Mitochondrial Complex II Activity in a Familial Mouse Model for Alzheimer's Disease. *J Alzheimers Dis* **66**, 75-82
44. Srere, P. A. (1969) [1] Citrate synthase: [EC 4.1.3.7. Citrate oxaloacetate-lyase (CoA-acetylating)].
45. Janssen, C. I. F., Zerbi, V., Mutsaers, M. P. C., de Jong, B. S. W., Wiesmann, M., Arnoldussen, I. A. C., Geenen, B., Heerschap, A., Muskiet, F. A. J., Jouni, Z. E., van Tol, E. A. F., Gross, G., Homberg, J. R., Berg, B. M., and Kiliaan, A. J. (2015) Impact of dietary n-3 polyunsaturated fatty acids on cognition, motor skills and hippocampal neurogenesis in developing C57BL/6J mice. *J Nutr Biochem* **26**, 24-35
46. Pfaffl, M. W. (2001) A new mathematical model for relative quantification in real-time RT-PCR. *Nucleic Acids Res* **29**, e45
47. Liang, W., Tonini, G., Mulder, P., Kelder, T., van Erk, M., van den Hoek, A. M., Mariman, R., Wielinga, P. Y., Baccini, M., Kooistra, T., Biggeri, A., and Kleemann, R. (2013) Coordinated and interactive expression of genes of lipid metabolism and inflammation in adipose tissue and liver during metabolic overload. *PLoS One* **8**, e75290
48. Wiesmann, M., Roelofs, M., van der Lugt, R., Heerschap, A., Kiliaan, A. J., and Claassen, J. A. (2017) Angiotensin II, hypertension and angiotensin II receptor antagonism: Roles in the behavioural and brain pathology of a mouse model of Alzheimer's disease. *J Cereb Blood Flow Metab* **37**, 2396-2413
49. Vani, K., Sompuram, S. R., Schaedle, A. K., Balasubramanian, A., Pilichowska, M., Naber, S., Goldsmith, J. D., Chang, K. G., Noubary, F., and Bogen, S. A. (2017) The Importance of Epitope Density in Selecting a Sensitive Positive IHC Control. *J Histochem Cytochem* **65**, 463-477
50. Uhlar, C. M., and Whitehead, A. S. (1999) Serum amyloid A, the major vertebrate acute-phase reactant. *Eur J Biochem* **265**, 501-523
51. Samuel, V. T., Liu, Z.-X., Qu, X., Elder, B. D., Bilz, S., Befroy, D., Romanelli, A. J., and Shulman, G. I. (2004) Mechanism of hepatic insulin resistance in non-alcoholic fatty liver disease. *The Journal of biological chemistry* **279**, 32345-32353
52. Choeiri, C., Staines, W., and Messier, C. (2002) Immunohistochemical localization and quantification of glucose transporters in the mouse brain. *Neuroscience* **111**, 19-34
53. Wagner, J., Fillebeen, C., Haliotis, T., Charlebois, E., Katsarou, A., Mui, J., Vali, H., and Pantopoulos, K. (2019) Mouse models of hereditary hemochromatosis do not develop early liver fibrosis in response to a high fat diet. *PLoS One* **14**, e0221455
54. Xu, H., Zhou, Y., Liu, Y., Ping, J., Shou, Q., Chen, F., and Ruo, R. (2016) Metformin improves hepatic IRS2/PI3K/Akt signaling in insulin-resistant rats of NASH and cirrhosis. *J Endocrinol* **229**, 133-144
55. de Montgolfier, O., Pouliot, P., Gillis, M. A., Ferland, G., Lesage, F., Thorin-Trescases, N., and Thorin, E. (2019) Systolic hypertension-induced neurovascular unit disruption magnifies vascular cognitive impairment in middle-age atherosclerotic LDLr(-/-):hApoB(+/+) mice. *Geroscience*
56. Bartolomaeus, H., Balogh, A., Yakoub, M., Homann, S., Marko, L., Hoges, S., Tsvetkov, D., Krannich, A., Wundersitz, S., Avery, E. G., Haase, N., Kraker, K.,

Hering, L., Maase, M., Kusche-Vihrog, K., Grandoch, M., Fielitz, J., Kempa, S., Gollasch, M., Zhumadilov, Z., Kozhakhmetov, S., Kushugulova, A., Eckardt, K.-U., Dechend, R., Rump, L. C., Forslund, S. K., Muller, D. N., Stegbauer, J., and Wilck, N. (2019) Short-Chain Fatty Acid Propionate Protects From Hypertensive Cardiovascular Damage. *Circulation* **139**, 1407-1421

57. Natarajan, N., Hori, D., Flavahan, S., Steppan, J., Flavahan, N. A., Berkowitz, D. E., and Pluznick, J. L. (2016) Microbial short chain fatty acid metabolites lower blood pressure via endothelial G protein-coupled receptor 41. *Physiol Genomics* **48**, 826-834
58. Seravalle, G., and Grassi, G. (2017) Obesity and hypertension. *Pharmacol Res* **122**, 1-7
59. Lopez, O. L., Jagust, W. J., Dulberg, C., Becker, J. T., DeKosky, S. T., Fitzpatrick, A., Breitner, J., Lyketsos, C., Jones, B., Kawas, C., Carlson, M., and Kuller, L. H. (2003) Risk factors for mild cognitive impairment in the Cardiovascular Health Study Cognition Study: part 2. *Arch Neurol* **60**, 1394-1399
60. Demigne, C., Morand, C., Levrat, M. A., Besson, C., Moundras, C., and Remesy, C. (1995) Effect of propionate on fatty acid and cholesterol synthesis and on acetate metabolism in isolated rat hepatocytes. *Br J Nutr* **74**, 209-219
61. Wright, R. S., Anderson, J. W., and Bridges, S. R. (1990) Propionate inhibits hepatocyte lipid synthesis. *Proc Soc Exp Biol Med* **195**, 26-29
62. Bindels, L. B., Porporato, P., Dewulf, E. M., Verrax, J., Neyrinck, A. M., Martin, J. C., Scott, K. P., Buc Calderon, P., Feron, O., Muccioli, G. G., Sonveaux, P., Cani, P. D., and Delzenne, N. M. (2012) Gut microbiota-derived propionate reduces cancer cell proliferation in the liver. *Br J Cancer* **107**, 1337-1344
63. Li, M., van Esch, B., Wagenaar, G. T. M., Garssen, J., Folkerts, G., and Henricks, P. A. J. (2018) Pro- and anti-inflammatory effects of short chain fatty acids on immune and endothelial cells. *Eur J Pharmacol* **831**, 52-59
64. Tedelind, S., Westberg, F., Kjerrulf, M., and Vidal, A. (2007) Anti-inflammatory properties of the short-chain fatty acids acetate and propionate: a study with relevance to inflammatory bowel disease. *World J Gastroenterol* **13**, 2826-2832
65. Foley, K. A., Ossenkopp, K.-P., Kavaliers, M., and Macfabe, D. F. (2014) Pre- and neonatal exposure to lipopolysaccharide or the enteric metabolite, propionic acid, alters development and behavior in adolescent rats in a sexually dimorphic manner. *PLoS One* **9**, e87072
66. Wah, D. T. O., Ossenkopp, K.-P., Bishnoi, I., and Kavaliers, M. (2019) Predator odor exposure in early adolescence influences the effects of the bacterial product, propionic acid, on anxiety, sensorimotor gating, and acoustic startle response in male rats in later adolescence and adulthood. *Physiol Behav* **199**, 35-46
67. Shams, S., Foley, K. A., Kavaliers, M., MacFabe, D. F., and Ossenkopp, K.-P. (2019) Systemic treatment with the enteric bacterial metabolic product propionic acid results in reduction of social behavior in juvenile rats: Contribution to a rodent model of autism spectrum disorder. *Dev Psychobiol* **61**, 688-699
68. Shultz, S. R., MacFabe, D. F., Ossenkopp, K.-P., Scratch, S., Whelan, J., Taylor, R., and Cain, D. P. (2008) Intracerebroventricular injection of propionic acid, an

enteric bacterial metabolic end-product, impairs social behavior in the rat: implications for an animal model of autism. *Neuropharmacology* **54**, 901-911
69. MacFabe, D. F., Cain, N. E., Boon, F., Ossenkopp, K.-P., and Cain, D. P. (2011) Effects of the enteric bacterial metabolic product propionic acid on object-directed behavior, social behavior, cognition, and neuroinflammation in adolescent rats: Relevance to autism spectrum disorder. *Behav Brain Res* **217**, 47-54
70. MacFabe, D. F., Cain, D. P., Rodriguez-Capote, K., Franklin, A. E., Hoffman, J. E., Boon, F., Taylor, A. R., Kavaliers, M., and Ossenkopp, K.-P. (2007) Neurobiological effects of intraventricular propionic acid in rats: possible role of short chain fatty acids on the pathogenesis and characteristics of autism spectrum disorders. *Behav Brain Res* **176**, 149-169
71. Deutsch, C., Portik-Dobos, V., Smith, A. D., Ergul, A., and Dorrance, A. M. (2009) Diet-induced obesity causes cerebral vessel remodeling and increases the damage caused by ischemic stroke. *Microvasc Res* **78**, 100-106
72. Deng, J., Zhang, J., Feng, C., Xiong, L., and Zuo, Z. (2014) Critical role of matrix metalloprotease-9 in chronic high fat diet-induced cerebral vascular remodelling and increase of ischaemic brain injury in mice. *Cardiovasc Res* **103**, 473-484
73. Renna, N. F., de Las Heras, N., and Miatello, R. M. (2013) Pathophysiology of vascular remodeling in hypertension. *Int J Hypertens* **2013**, 808353
74. Jennings, J. R., and Zanstra, Y. (2009) Is the brain the essential in hypertension? *NeuroImage* **47**, 914-921
75. Sorop, O., Olver, T. D., van de Wouw, J., Heinonen, I., van Duin, R. W., Duncker, D. J., and Merkus, D. (2017) The microcirculation: a key player in obesity-associated cardiovascular disease. *Cardiovasc Res* **113**, 1035-1045
76. Medic, N., Kochunov, P., Ziauddeen, H., Ersche, K. D., Nathan, P. J., Ronan, L., and Fletcher, P. C. (2019) BMI-related cortical morphometry changes are associated with altered white matter structure. *Int J Obes (Lond)* **43**, 523-532
77. Ou, X., Andres, A., Pivik, R. T., Cleves, M. A., and Badger, T. M. (2015) Brain gray and white matter differences in healthy normal weight and obese children. *J Magn Reson Imaging* **42**, 1205-1213
78. Daikhin, Y., and Yudkoff, M. (2000) Compartmentation of brain glutamate metabolism in neurons and glia. *J Nutr* **130**, 1026S-1031S
79. Sekar, S., Jonckers, E., Verhoye, M., Willems, R., Veraart, J., Van Audekerke, J., Couto, J., Giugliano, M., Wuyts, K., Dedeurwaerdere, S., Sijbers, J., Mackie, C., Ver Donck, L., Steckler, T., and Van der Linden, A. (2013) Subchronic memantine induced concurrent functional disconnectivity and altered ultra-structural tissue integrity in the rodent brain: revealed by multimodal MRI. *Psychopharmacology (Berl)* **227**, 479-491
80. Wu, H., Wang, X., Gao, Y., Lin, F., Song, T., Zou, Y., Xu, L., and Lei, H. (2016) NMDA receptor antagonism by repetitive MK801 administration induces schizophrenia-like structural changes in the rat brain as revealed by voxel-based morphometry and diffusion tensor imaging. *Neuroscience* **322**, 221-233

Supplemental information

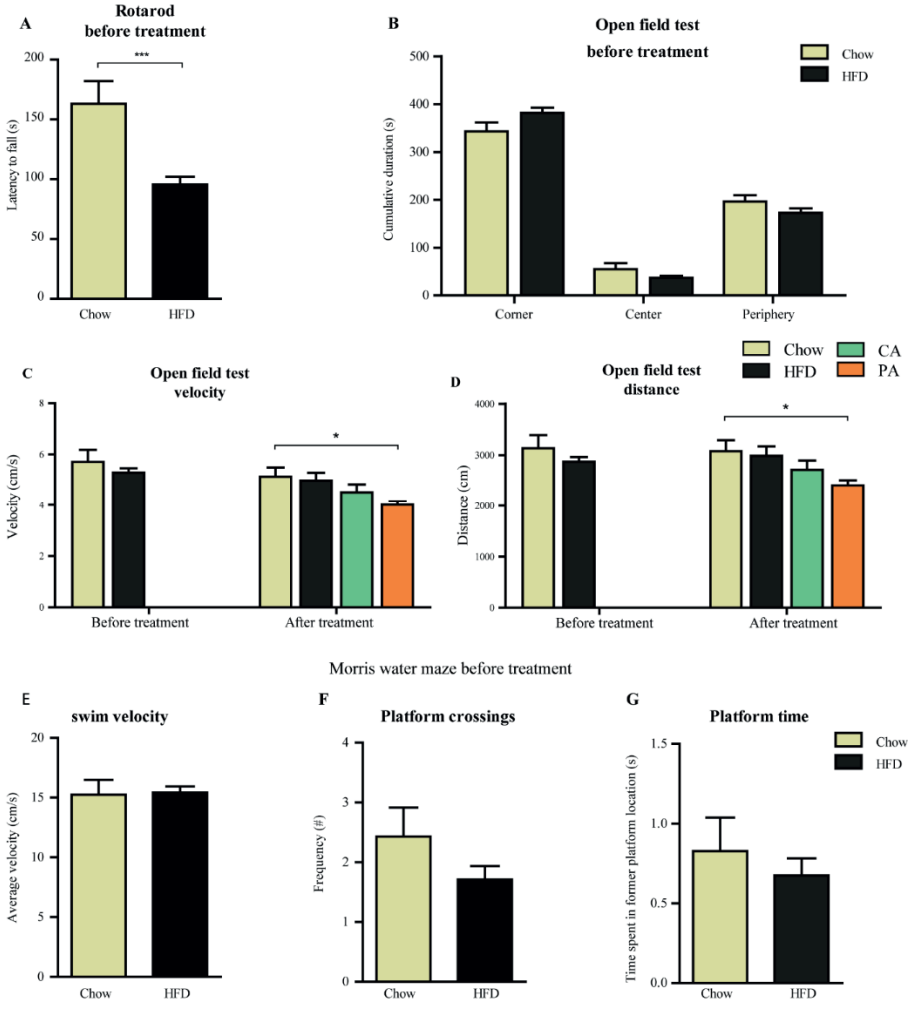

Figure S1. Behavioral and cognitive tests before the start of the interventions. (A) *Latency to fall from the rotating rod.* ***(B)*** *Cumulative duration (s) spent in corners, periphery and center in the open field test.* ***(C)*** *Walk velocity, and* ***(D)*** *total distance moved in the open field test before treatments and at the end of the experiment.* ***(E)*** *Mean swim velocity,* ***(F)*** *frequency of crossing the former platform location, and* ***(G)*** *total time spent at the former platform location during the probe test of the MWM. HFD: high-fat diet. Data are presented as mean ± SEM, * p< 0.05; *** p<0.001. Before treatment: N = 15 (chow); N= 45 (HFD). After treatment: N=14 (chow and HFD) or N=15 (CA and PA) per group.*

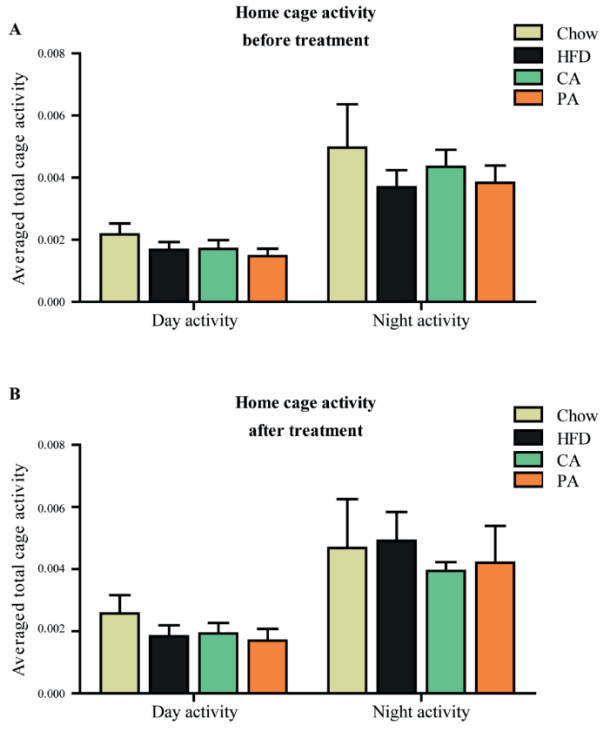

Figure S2. Home-cage activity. *Averaged total cage activity during the day (left) and night (right).* ***(A)*** *Averaged home cage activity during two days before start of the treatments and* ***(B)*** *averaged home cage activity during two days at the end of the experiment. Activity was corrected for the number of mice per cage (N=3 or N=2); 5 cages per treatment.*

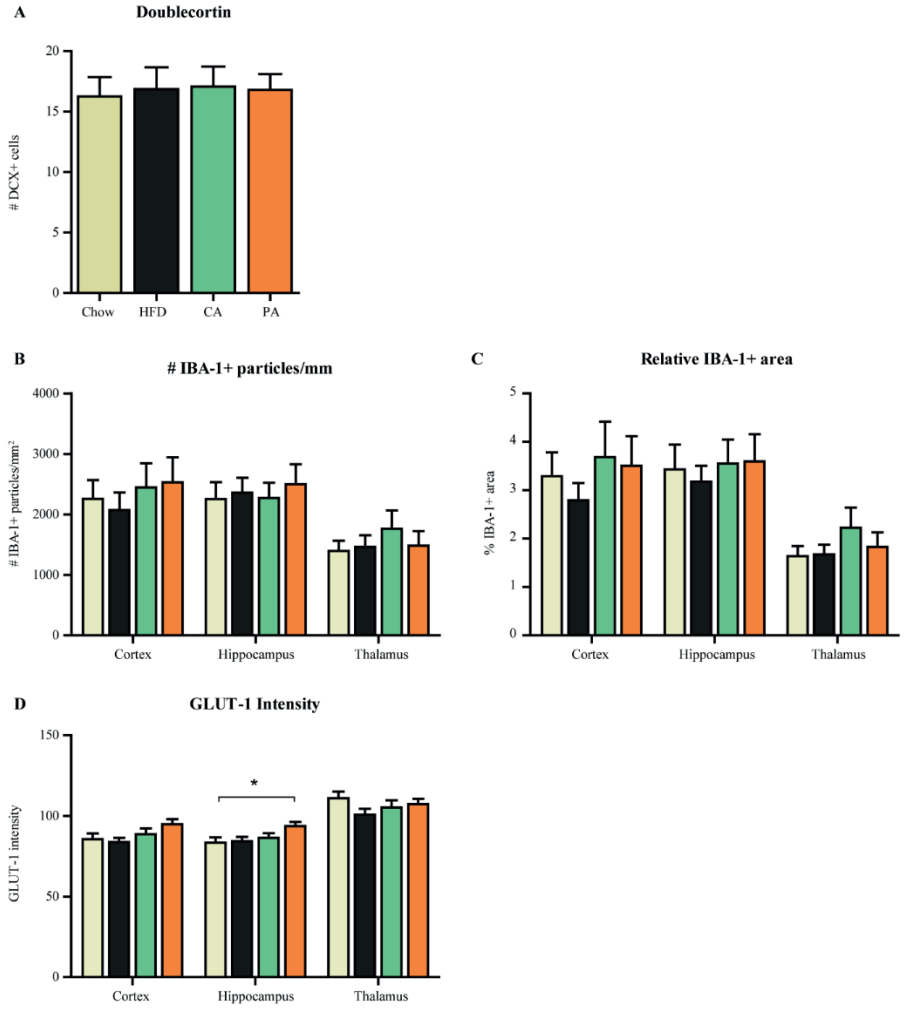

Figure S3. Immunohistochemical stainings. (A) *Number of DCX+ cells in the hippocampus.* ***(B)*** *Quantification of the amount of IBA-1+ particles per mm² and* ***(C)*** *the relative IBA-1+ area in the cortex, hippocampus and thalamus.* ***(D)*** *GLUT-1 intensity in the cortex, hippocampus and thalamus. DCX: N=14 (chow and HFD) and N=15 (CA and PA). IBA: N=14 (chow, HFD, CA) and N=15 (PA). GLUT-1: N=14 (HFD), N=14 (chow, CA) or N=15 (PA) mice per group.*

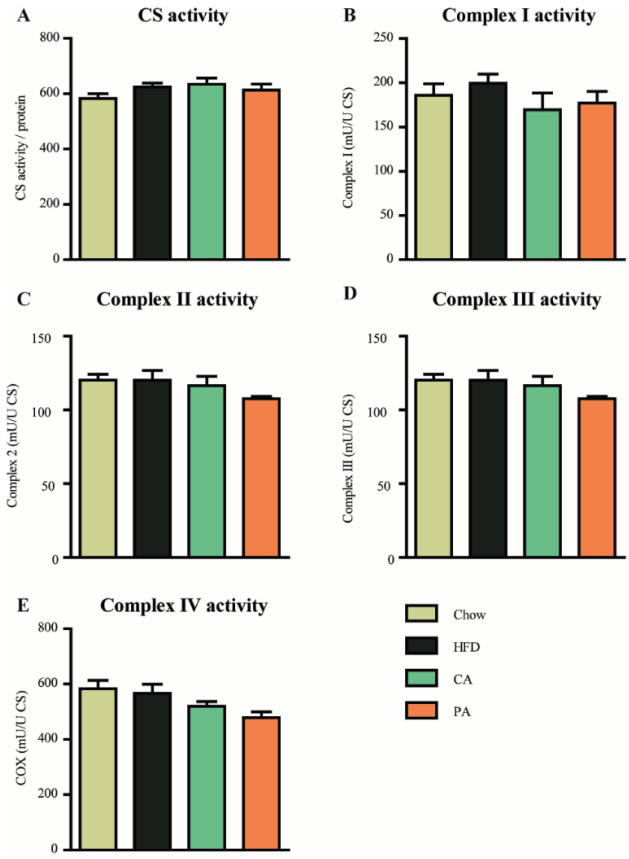

Figure S4. Activity of mitochondrial complexes. (A) *Citrate synthase,* ***(B)*** *Complex I,* ***(C)*** *complex II,* ***(D)*** *complex III, and* ***(E)*** *COX (complex IV) activity. N= 8 mice per group. Data are presented as mean ± SEM.*

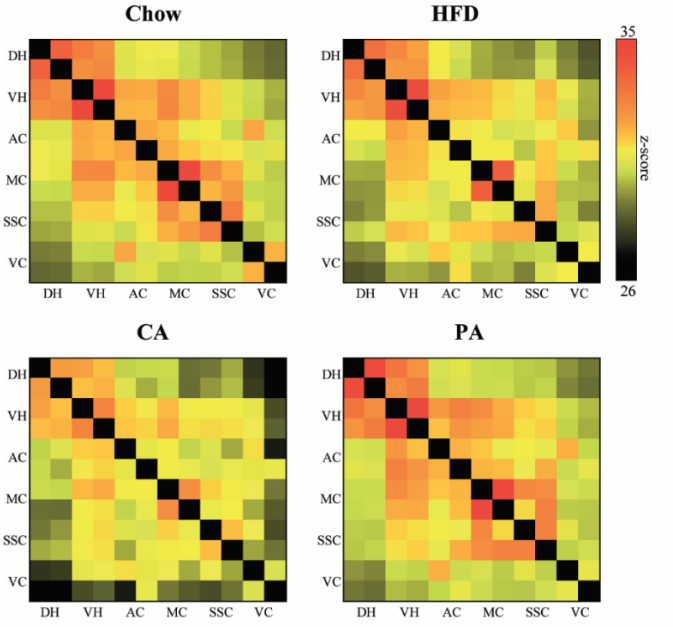

Figure S5. Resting-state functional connectivity based on total correlation analyses. *Total correlation matrixes of the Chow, HFD, CA, and PA experimental groups. The selected brain regions (dorsal hippocampus (DH), ventral hippocampus (VH), auditory cortex (AC), motor cortex (MC), somatosensory cortex (SSC) and visual cortex (VC) are subdivided in left hemisphere (first row) and right hemisphere (second row). A higher Z-score (red) indicates a stronger functional connectivity. N=14 (HFD) or N=15 (chow, CA, PA) mice per group.*

Table S1. List of parameters used in MRI experiments

	Anatomical T2*	**ASL**	**DTI**	**rs-fMRI**
Imaging method	GE	FAIR-ASL	4-shot spin-echo PI	Spin-echo EPI
Echo time (ms)	7.35	10.8	21.0	10.0
Repetition time (s)	0.86	12.0	7.75	1.80
Image matrix (pixel x pixel)	512x512	128x96	128x128	96x96
Field-of-view (mm)	40x40	25x25	20x20	25x25
Spatial resolution (µm/pixel)	78x78x500	195x260x 1000	156x156x500	260x260x500
Number of slices	20x3	16	20	20
Total acquisition time (min)	8	12	35	10

Table S2. Summary of results compared to chow.

Parameter	**Results**
Body weight	↑ in all groups
Caloric intake	↓ in all groups

Systolic blood pressure		↑ in all groups
Plasma measurements	Cholesterol	↑ in all groups
	Triglyceride	↑ in all groups
	Glucose	No effects
	Insulin	↑ in all groups
	Serum Amyloid A	↑ in all groups
Liver	Liver weight	↑ in all groups
	Macrovesicular steatosis	↑ in all groups
	Microvesicular steatosis	↑ in all groups
	Hepatocellular hypertrophy	↑ in all groups
	Inflammatory aggregates	↑ in all groups
	Collagen	↑ in all groups
	Cholesteryl esters	↑ in all groups
	Triglycerides	↑ in all groups
	Glycogen	↑ in all groups
White adipose tissue	sWAT weight	↑ in all groups
	gWAT weight	↑ in all groups
	mWAT weight	↑ in all groups
	CLS sWAT	No effects
	CLS gWAT	↑ in all groups
	CLS mWAT	↑ in all groups
Rotarod	Latency to fall	↑ in all groups
Open field	Velocity	↓ in PA mice
	Distance moved	↓ in PA mice
	Time spent in corners, center and periphery	↑ in PA mice (corners); ↓ in PA mice (periphery); no effects for the center duration
	Frequency of visiting the corners, periphery and center	No effects
Home cage activity		No effects
Morris water maze		No effects
Immunohistochemical stainings	# GLUT-1+	↑ in PA mice in hippocampus
	% GLUT-1+	↓ in all groups in the thalamus
	# IBA-1+	No effects
	% IBA-1+	No effects
Cerebral blood flow	Normal	No effects
	Vasoconstriction	No effects
	Vasoreactivity	Reduced to chow levels in PA mice
rs-fMRI	Partial connectivity	↓ in HFD between the visual and auditory cortex; reverted to chow levels in PA and CA mice

DTI	FA	Somatosensory cortex	↑ in HFD and CA mice; reverted to chow levels in PA mice
		Visual cortex	↑ in HFD and CA mice; reverted to chow levels in PA mice
		Hippocampus	No effects
		Motor cortex	No effects
	MD	Optic tract	↓ in HFD; reverted to chow levels in PA mice
qRT-PCR	*Psd95*		No effects
	Syp1		No effects

Table S3. Statistical outliers which were removed from the dataset per test

Test	Statistical outliers per experimental group				Reason
	Chow	HFD	CA	PA	
Open Field Test (OFT)	1				Freezing behavior
Cerebral blood flow (CBF)	1	1	1		Scans showed motion and/or echo planar imaging artifacts
Diffusion tensor imaging (DTI)	1		1	1	Scans showed motion and/or echo planar imaging artifacts
Resting-state fMRI (rsfMRI)	2		1		Scans showed motion and/or echo planar imaging artifacts
GLUT-1	1	2	1		Artifacts in region of interest
IBA-1	1	1	1		Artifacts in region of interest
DCX	1				Artifacts in region of interest

CHAPTER

10

General discussion

Non-alcoholic fatty liver disease (NAFLD) is a complex disease that is characterized by multiple metabolic dysfunctions, affecting several cells types within the liver as well as in other metabolic organs. The high number of NAFLD patients and the lack of available treatment options form a major concern. The lack of treatment options has multiple reasons, including the fact that NAFLD development is still incompletely understood, persistent difficulties in diagnosis and monitoring of disease progression, and a low public awareness of the disease. A better characterization of the metabolic dysfunctions underlying NAFLD development as well as exploration of alternative treatment approaches are warranted in view of the high societal burden of NAFLD. This resulted in the overall aim of my thesis, which was to gain more insight into the metabolic dysfunction that underlies obesity-associated NAFLD.

The first specific aim of my thesis was to unravel the sequence of metabolic dysfunctions during NAFLD development in liver, gut and adipose tissue and identify relevant metabolites released by these organs. In **chapter 2,** we addressed this first aim and demonstrated that metabolic dysfunction in the liver manifests as an early accumulation of specific bioactive lipids (e.g. diacylglycerols and ceramides), which can directly promote insulin resistance. Additional hits that can promote hepatic inflammation and fibrosis were also observed, including the accumulation of intrahepatic free cholesterol, free fatty acids (FFA) and oxidative stress-induced 4-hydroxynonenal. In this chapter, we also underlined the importance of distant organs in NAFLD development. The dysfunction of the visceral epididymal white adipose tissue (WAT) depot, characterized by hypertrophy and inflammation, was evident before NASH and liver fibrosis were fully developed. In contrast, the mesenterial WAT depot and the subcutaneous WAT depot developed hypertrophy slower with minimal inflammation. In the gut, microbiota dysbiosis as well as increased gut permeability precede the development of NASH and liver fibrosis. Circulating factors secreted from these tissues could be mediators of disease development as they were altered early in NAFLD development (e.g. leptin, FFA, bile acids). In this chapter, we also underlined the translational value of Ldlr-/-.Leiden mice as NAFLD model. When fed a high-fat diet, these mice developed for example obesity, dyslipidemia and insulin resistance, essentially as observed in obese NAFLD patients. The results from this chapter indicated that early changes in distant organs and associated circulating factors may play a role in NAFLD development. Hence, new strategies aiming at prevention or attenuation of NAFLD development should not be limited to the liver, but should also focus on correcting dysmetabolism and inflammation in other organs that can affect metabolic homeostasis in the liver.

The second specific aim of this thesis was to study the potential of several nutritional treatments as a multiple organ treatment approach in NAFLD. In **chapter 3,** we demonstrated that the combination of L-carnitine and nicotinamide riboside, but not their monotreatment, significantly attenuated obesity, hepatic steatosis, and oxidative-stress-induced lipid peroxidation, and exerts beneficial effects on metabolic pathways in the liver. The results from this study demonstrated the remarkable impact of combining nutrients as a treatment. They also stress the importance of studying new treatment combinations to identify novel preventative and curative treatments for NAFLD.

Next, in **chapter 4,** we showed that long-term krill oil treatment attenuated inflammation in both adipose tissue and the liver based on histological, lipidomics and gene expression analyses in these tissues, which also provided a new mechanistic rationale for the health effects observed. Moreover, results from this study suggest that the way how fat is stored can impact organ function, by either adapting the spatial distribution of fat inside one fat storage depot as well as by changing the type of fatty acids, with either pro- or anti-inflammatory potency, that are stored.
In **chapter 5** we showed that nutritional interventions using the individual branched chain amino acids (BCAAs) valine and isoleucine were both able to attenuate manifest NAFLD in a therapeutic setting. Both interventions corrected liver diacylglycerols, gene expression of metabolic processes in association with improvements in intrahepatic inflammatory proteins. All these effects were more pronounced for isoleucine than for valine.
In conclusion, results from the interventions studied in this thesis demonstrate a proof of principle that nutritional treatment strategies could be a relevant tool to correct multiple metabolic dysfunctions in multiple organs. The data indicate that nutritional interventions are applicable in early stages to prevent disease development or even as intervention to reduce manifest NAFLD.

Our third and final specific aim was to further investigate gut-WAT-liver crosstalk during NAFLD development. In **chapter 6,** we identified bacteria that correlated with organ dysfunction independent of the type of energy dense diet used to induce NAFLD. More specifically, we showed that the colon mucosa composition has the greatest predictive value for distant organ dysfunction compared with other compartments (colon feces, ileum mucosa or feces).
Next, in **chapter 7,** we demonstrated that the prebiotic 2'-fucosyllactose, which alters microbiota composition and improved gut function, has effects beyond the gut with improvements in liver steatosis. Specifically, the treatment lowered intrahepatic DAGs which was associated with a reduction in insulin resistance, indicative of systemic health effects.
In the last two chapters, inter-organ cross-talk was studied by testing the effects of directly supplementing microbiota-derived metabolites (short-chain fatty acids (SCFA) butyrate, propionate and caproate) on multiple organs during NAFLD development. In **chapter 8** dietary supplementation with butyrate protected against the development of obesity-associated WAT inflammation, hyperinsulinemia, hepatic inflammation and it strongly suppressed the development of liver fibrosis. Additional in vitro experiments demonstrated direct anti-fibrotic effects specifically for butyrate, while similar concentrations of acetate and caproate could not achieve this. Further differences in bioactivity between SCFAs were found in **chapter 9.** In this chapter we explored interorgan crosstalk beyond the gut-WAT-liver axis in NAFLD. We found that propionate, but not caproate improved functional connectivity between brain areas, structural integrity and anti-inflammatory signaling, while the animals were also more anxious and reduced synaptogenesis signaling. In the liver also propionate, but not caproate was able to attenuate non-alcoholic steatohepatitis (NASH). The data in these last two chapters demonstrated that not all SCFA exert similar effects.
Taken together, we have shown that targeting the gut via the microbiota or microbiota-derived metabolites has beneficial effects beyond the gut. Underlining the importance of

inter organ crosstalk in NAFLD development showing that this may be used in the development of new strategies aiming at prevention or attenuation of NAFLD.

Lipids in NAFLD – location, quality, quantity or all?

In this thesis, we demonstrated that lipids play a very important role in the development of NAFLD. For example, the location of fat mass storage matters in the development of NAFLD. In **chapter 2** we demonstrated that the visceral epididymal WAT depot starts to dysfunction early, displaying hypertrophy and inflammation, and can promotes lipid- and/or inflammatory-induced insulin resistance. Following this, it can be assumed that the visceral fat will mainly contribute to the early fat accumulation in the liver. FFA release from adipose tissue, stimulated under insulin resistance conditions, is the major source (~60%) of intrahepatic triglyceride synthesis [1]. These triglycerides account for approximately 70% of total liver fat measured after 38 weeks of HFD-induced NAFLD as shown in **chapter 2**. The observation of early visceral WAT dysfunction without subcutaneous WAT dysfunction during NAFLD development is in line with findings in NAFLD patients [2–5]. In humans, the prevalence and severity of NAFLD is higher in men compared to woman, at least before woman reach menopause [6]. Male subjects store fat more in visceral depots, whereas females store more fat in the subcutaneous depot [6]. After menopause woman have an increased risk of developing NAFLD, which is in part due to a redistribution of body fat, shifting to the visceral depots [6].

Lipid storage within a cell is located in a lipid droplet, dynamic organelles located in the cytosol [7]. The accumulation of lipid droplets in the cell is thought to be the result of an imbalance between the process of lipid storage and utilization [7]. In the last few years the basic biology of lipid droplet dynamics is being unraveled, however still much is unknown about how lipid droplet physiology relates to NAFLD progression. The liver is not a fat storage organ such as the adipose tissue, thus the accumulation of lipid droplets within hepatocytes is a key pathological feature [8]. In **chapter 2** we demonstrated that in the liver large lipid droplets (macrovesicular steatosis) and small lipid droplets (microvesicular steatosis) develop simultaneously during NAFLD progression. Previous studies have reported that macrovesicular steatosis is associated with lobular inflammation [9], while microvesicular steatosis is associated with mitochondrial dysfunction and oxidative stress [10]. In this thesis we also found that the distribution of lipids within one organ may alter its function. In **chapter 7** we found that 2'-fucosyllactose treatment specifically lowered microvesicular steatosis, which was associated with improvements in endoplasmic reticulum stress and lipid metabolism signaling pathways in the liver. In addition, tissue specific response in lipid storage seem important, i.e. in adipose tissue fat can also be stored in multiple smaller adipocytes or in larger hypertrophic adipocytes (**chapter 4**). Krill oil stimulated adipogenesis and promoted fat storage in a larger number of smaller adipocytes, which may have limited adipocyte expansion and prevented them from reaching their maximum size. This is considered to be a favorable form of lipid storage in adipose tissue, as it has been reported that adipocyte size is an important determinant of adipokine and cytokine secretion [11]. Increased size of adipocytes are associated with a shift towards higher secretion of proinflammatory adipokines and cytokines, which stimulate the infiltration of immune cells [12,13]. In **chapter 4** the beneficial effects in function of the adipose tissue were independent of energy intake, as the diets were

isocaloric and krill oil did not lower body weight. Taken together, the distribution of the lipids over the cells in one organ seem to be a determinant of cell function and development of tissue inflammation.

Not only, where lipids are stored is important for organ function but also the lipid composition can play an important role in the development of NALFD. The growing research in bioactive lipids, in association with advancement of lipidomic technologies, demonstrate that the role of lipids go beyond essential components of cell membranes and energy substrate [14]. Findings in this thesis support this notion, In **chapter 4,** krill oil supplementation altered the composition of lipids in liver and adipose tissue, with a shift towards an increase in omega-3 PUFAs and a reduction of omega-6 PUFAs and associated oxylipins. This change in lipid composition was associated with a lower inflammatory tone in the liver and WAT. In **chapter 2,** we demonstrated that NAFLD is linked with changes in intrahepatic lipid composition. Moreover, many intrahepatic bioactive lipids, including cholesterol, FFA and diacylglycerols, accumulated in the early development of NAFLD. For cholesterol and FFA it has been shown that these lipids can directly activate inflammatory signaling pathways [15–17]. The findings suggests a potential lipid-based mechanism for the progression towards organ inflammation, NASH. Besides inflammation, bioactive lipids such as diacylglycerols have been shown to be causally implicated in the development of insulin resistance [18]. This observation is supported by our data in **chapter 7**, in which HFD-induced hyperinsulinemia was associated with the accumulation of intrahepatic DAGs. Nutritional intervention with 2'-fucosyllactose (**chapter 7**) and BCAAs valine and isoleucine (**chapter 5**) demonstrated that a lowering of DAGs was associated with parallel improvements in plasma insulin. Lastly, the impact of specific lipids on organ function has been shown by the supplementation of gut-derived lipid metabolites such as SCFA butyrate (**chapter 8**), as well as for propionate and caproate (**chapter 9**). Specifically for butyrate, we demonstrated direct antifibrotic effects via non-canonical TGF-β signaling pathways. Measurement of bioactive lipids are currently of great interest, which in part has been driven by the great advances in lipidomic technologies including improved selectivity and sensitivity, and lower detection limits [19]. Many of the bioactive lipids are often very low in concentration, but as discussed in this thesis these low abundant species (e.g. oxylipins and diacylglycerols) can greatly impact organ function. Future advances in lipidomic analyses are being made in the development of enrichment analysis, which will allow association with molecular mechanism in metabolic lipid pathways based on lipid composition [20]. Unfortunately, the annotation of lipids is currently the main challenge and bottleneck of advances in integrative lipidomic analyses [20]. In conclusion, in this thesis we demonstrated that the quality of lipids consumed and their impact on lipid composition of an organ has benefits, independent of the amount of fat ingested.

Lastly, the quantity of lipids matters. Total lipid lowering has consistently been demonstrated to result in a proportional degree of liver histology improvements [21,22]. This is in line with our findings with nutritional interventions like butyrate (**chapter 8**) and the combined L-carnitine and nicotinamide riboside treatment (**chapter 3**), which were both able to lower body weight, body fat mass and improve liver histology. A recent meta-analysis of seven human trials including 346 subjects demonstrated that a 30% liver fat reduction based on non-invasive magnetic resonance imaging –estimated proton density

fat fraction analysis is associated with higher odds of histological NASH resolution without worsening fibrosis [23]. This was supported by a recent study, demonstrating that a 30% intrahepatic lipid lowering increased the odds of a ≥1 stage improvement in fibrosis [24]. In line with these findings, the butyrate treatment in **chapter 8** resulted in a lowering of macrovesicular steatosis with at least 10% and microvesicular steatosis with 15%, this strong lowering of intrahepatic lipids indeed associated with reduced liver fibrosis development.

Taken together, lipid location, quality and quantity all matter in the development of metabolic dysfunctions and are all potential targets to attenuate NAFLD development. We demonstrated a proof of principle that nutritional treatments can help to avoid weight gain, supports weight loss and have multiple organ function benefits, besides intrahepatic lipid lowering. The remarkable improvements with the nutritional interventions on multiple organ metabolic function should seriously be considered as treatment option in NAFLD. Combinations of treatments should not be limited to pharmaceutical drugs, but also the combination with nutritional interventions should be used as multi-organ treatment approach to attenuate NAFLD. Pharmaceutical drugs should be an addition to, rather than a substitute for, nutritional and lifestyle interventions in metabolic diseases.

Oxidative metabolism in NAFLD

The lipid overflow in NAFLD challenges the function of the hepatocyte. To combat the metabolic overload and to reduce intrahepatic fat accumulation, one major pathway to achieve this is the oxidative metabolism of fatty acids in peroxisomes and mitochondria [25]. In obese insulin resistance subjects, oxidative metabolism appears to be upregulated. Higher fatty acid oxidation has been demonstrated with radionuclide ^{11}C-palmitate non-invasively imaged with a positron emission tomography scan [26], as well as stable isotope tracers [27]. In the early obese insulin resistant state this increase in oxidative metabolism may be an adaptive response to handle the metabolic overload. An overflow of lipids and increased oxidative lipid metabolism inevitably leads to an excessive formation of by-products, reactive oxygen species (ROS). These ROS are signalling molecules and are not necessarily bad [28], as long as they are transiently present. To ensure a short presence of these ROS species, several mechanism have evolved to neutralize the ROS molecules, so-called anti-oxidant defence systems [29]. However, constant metabolic overload is associated with loss of mitochondrial function, including loss of oxidative capacity and anti-oxidant defenses, which promotes the development of lipid accumulation in association with oxidative stress as steatosis proceeds to NASH [30].

Our findings in the HFD-fed Ldlr-/-.Leiden mice suggest a similar course of disease progression, since the oxidative stress-induced lipid peroxidation marker 4-HNE was significantly elevated from 16 weeks onwards in HFD-fed mice (**chapter 2**). Moreover, in **chapter 3,** supplementation with L-carnitine and nicotinamide riboside was not able to prevent the initial body weight gain, however, at a later phase when oxidative stress was increased and mitochondrial function was potentially declining, HFD-induced obesity was attenuated by the combination treatment. In addition, transcriptomics data of long-term energy-dense diet fed Ldlr-/-.Leiden mice demonstrate that pathways involved in lipid oxidation were downregulated, including deactivation of upstream regulators PPARA, ACOX1, PGC1a. Anti-obesogenic nutritional interventions, including the combination of L-

carnitine and nicotinamide riboside (**chapter 3**), the BCAAs valine and isoleucine (**chapter 5**), 2'-fucosyllactose (**chapter 7**) and butyrate (**chapter 8**) were able to reverse energy-dense diet-induced effects on lipid metabolism.
The lowering of the mitochondrial oxidative capacity could be an acquired defect in the transition to NASH that further exacerbates steatosis and ROS production, or it could be a protective adaptive mechanism aiming to limit ROS production from mitochondrial lipid oxidation.

Evolutionary perspective on obesity-associated metabolic diseases
Nowadays in the Western society, food is abundant and is rich in fat and sugars. In addition, there is lack of physical activity, which in part may be attributable to major shifts from manual labor jobs to office jobs and technological advances [31]. These environmental changes are reflected in the large increase in the prevalence of obesity and metabolic-associated diseases such as NAFLD [32]. Although it is well recognized that obesity-associated metabolic diseases are modulated by the environment, there is also still debate about the potential evolutionary roots of metabolic control [33]. The main causes of death during the major part of human history were infection and starvation [34]. Due to these circumstances human evolution favored pathways dedicated to the inflammatory response to fence of pathogens and adaptation to nutrient availability, e.g. by efficient storage, to fulfill energy needs for survival [33].
Nowadays, insulin resistance is considered a deleterious condition associated with obesity and one of the driving factors of NAFLD [35]. However, since this mechanism is such a well preserved adaptative response, it suggests that insulin resistance is a beneficial process for species survival. Indeed, insulin resistance is thought to be an example of an evolutionary preserved mechanism in humans and many other species, [36] because it could serve as a tool to prepare for winter and survive the months during which little food was available. Primitive humans in times when food was available could first store their energy surplus in adipose tissue until a maximum is reached, which can subsequently lead to adipose tissue dysfunction and insulin resistance [37]. Under the insulin resistant state lipolysis inhibition is lost in the adipose tissue, causing an overflow of fatty acids to the liver [37]. In addition, the hyperinsulinemia in the insulin resistance continues to stimulate hepatic fatty acid synthesis in the liver, as insulin continues to induce *de novo* lipogenesis via the transcriptional master regulator SREBP1C [17]. These mechanisms thus allows an increase fat storage during insulin resistance to prepare for times of food scarcity. However, in the obese situation due to chronic metabolic overload the consistent promotion of adiposity under insulin resistance becomes detrimental and can lead to NASH and liver fibrosis. In **chapter 2, 4** and **5** insulin resistance was associated with high activation of SREBP1C in the liver and plays a role in the increase of hepatic lipid accumulation and NAFLD development. The close association between insulin resistance and NAFLD encompasses a complex interplay between bioactive lipids, inflammatory, genetic and environmental factors. As such, targeting insulin resistance could be a cornerstone for the clinical management of NAFLD. We demonstrated that nutritional interventions of valine, isoleucine (**chapter 5**) or 2'-fucosyllactose (**chapter 7**) were able to decrease intrahepatic DAGs and this was associated with a lowering of fasting plasma insulin. These treatment strategies aiming at the root cause, i.e. at lipid and/or inflammation induced insulin resistance, are favorable over pharmacological treatments

that aim at increasing insulin (i.e. supplying exogenous insulin, sulfonylureas or DPP-4 inhibitors) for type 2 diabetes patients. The hyperinsulinemia induced by these pharmacological treatments is essentially forcing even more glucose into the already fuel-overflowing cell in these obese patients.

Another example of an evolutionary mechanism that contributes to preserve fat stores is the uricase mutation [38]. Uricase normally catabolizes uric acid, however due to evolutionary mutations its function is lost in humans [38]. Uric acid is a product of purine metabolism including AMP. High fructose levels increase AMP levels and consequently increase uric acid [39,40]. Increased intracellular levels of uric acid are associate with more fat accumulation, potentially via two mechanisms that basically inhibit upregulation of fat oxidation 1) inhibition of AMPK [38] and 2) decreased mitochondrial function [38]. Thus the progressive loss of uricase activity and subsequent high uric acid levels allowed our ancestors to accumulate fat via the metabolism of fructose (e.g. from fruit that is abundantly available during the summer months) for survival of harsh winters [38]. The first step in fructose metabolism is the phosphorylation of fructose by ketohexokinase, for which ATP is utilized and this enzymatic reaction consequently lowers intracellular ATP levels [38]. Normally ATP levels are replenished by activating AMP protein-activated kinase (AMPK), however in the obese insulin resistant state, AMPK is deactivated [41].

It has also been suggested that obesity, insulin resistance and associated metabolic diseases are the result of deleterious mutations and genetic drift, rather than ingrained adaptive mechanisms [33]. Several key genes involved in the regulation of lipid metabolism in hepatocytes are the strongest genetic predictors of NAFLD [42]. One example is polymorphisms in the patatin-like phospholipase domain-containing 3 (PNPLA3) gene, which are associated with higher risk in NAFLD development [43]. The enzyme encoded by PNPLA3 hydrolyses triglycerides, while polymorphisms makes the enzyme inactive and results in triglyceride accumulation and predisposes for advanced liver disease [43]. Hyperinsulinemia in insulin resistance has a strong effect on exacerbating NAFLD in individuals with PNPLA3 polymorphisms [43,44]. These genetic discoveries suggest a close relationship between insulin resistance and the worsening of NAFLD. If the genetics of the control of body weight and insulin resistance were better understood, NAFLD management interventions could be more tailored to an individual based on his or her individual genetic profile.

Concluding remarks and future perspectives

In this thesis, we provided new insights regarding the dynamics of metabolic dysfunctions in multiple organs during NAFLD development. These data indicated that early metabolic dysfunction in distant organs and associated circulating factors may play a role in NAFLD development. This notion is supported by our treatments that targeted the gut via the microbiota or microbiota-derived metabolites and had beneficial effects beyond the gut. Together the data suggest that new treatment strategies aiming at prevention or attenuation of NAFLD development should not be limited to the liver, but should also focus on correcting dysmetabolism and inflammation in other organs that can affect metabolic homeostasis in the liver. These insights regarding NAFLD pathogenesis could be

crucial to define the foundation for future disease management and development of new treatments.

At present no treatment options exist for NAFLD patients, thus currently medical care is limited to changes in lifestyle which have not lessened the ever growing rate of NAFLD. In this thesis, we tested novel nutritional strategies in preclinical studies, of which many show the potential to attenuate a variety of metabolic dysfunctions that underlies NAFLD development. More importantly, many of the nutritional treatments were able to course-correct multiple metabolic dysfunctions in different organs. From the tested treatments in this thesis, butyrate demonstrated the most advanced health benefits in adipose tissue, on metabolic risk factors and reduced liver fibrosis, thus butyrate would be the most interesting to try in combinations with other treatment strategies in NAFLD. Nonetheless, butyrate was given before NAFLD was present and our results thus mainly demonstrate its preventive potential. 2'-fucossyllactose corrected gut dysfunctions in the context of obesity, while also improving insulin resistance, suggesting potential benefits for correction of early NAFLD dysfunctions. These benefits may be strengthened by using a combination intervention approach with for example isoleucine as the most potent BCAA or combined L-carnitine and nicotinamide riboside that reduced adiposity in WAT and/or liver in the context of obesity-associated NAFLD. Anti-obesogenic treatments currently have shown the greatest potential to reduce late-stage NAFLD, including inflammation and fibrosis [23,24]. These later stages will perhaps also still benefit from combining anti-obesogenic treatments with krill oil, which primarily improved tissue inflammation. The mechanisms of nutritional targets are pleiotropic, thus in case of combination treatments it remains to be seen whether they actually target different mechanisms that could potentially reinforce each other. For example, The combination of L-carnitine and nicotinamide riboside achieved anti-obesogenic effects, which were not observed in the respective monotreatments. Nonetheless, it is also possible that some interventions will overlap in their action to achieve the observed benefits in NAFLD development. This might be the case for the differences observed in valine and isoleucine intervention, as the health effects overlapped, but were more pronounced with isoleucine. Taken together, in light of complementary action it may be worthwhile to consider combinations of nutrients that improve (lipid) metabolism (e.g. butyrate or isoleucine) with those that attenuate inflammation (e.g. krill oil) to restore multi-organ function. The results of the preclinical studies in this thesis demonstrate the remarkable impact of nutrients alone or in combination as a treatment for NAFLD. However, they still need to be proven in the clinical setting. In humans, butyrate has been tested in small and short-term (e.g. 4 weeks) clinical trials, in which butyrate was able to improve insulin sensitivity in lean subjects but not in individuals with metabolic syndrome [45]. Another nutritional treatment that is making the first steps to being tested in humans is krill oil, which is currently being done in NAFLD patients. It will be interesting to see in the next few years if more nutritional concepts will be tested and if they have merit to be integrated in a combination treatment approach against NAFLD development.

Taken together, in this thesis we provided insight in the multi-organ metabolic dysfunctions during NAFLD development. These metabolic dysfunctions were targeted with a variety of novel nutritional intervention approaches to study their potential to attenuate NAFLD. Because of the complex mechanisms and multiple organs that are

affected in NAFLD, it seems unlikely that a single drug will be sufficient to effectively treat most patients. In support of this, current monotherapies for NAFLD have indeed failed in clinical trials [46]. Moreover, it is becoming increasingly clear that there are different subtypes of NASH patients. This is evident for instance from the fact that therapeutics appear to work only in a subset of patients (for instance in 27% of patients with liver biopsy confirmed NASH demonstrated NASH resolution in a phase 2 clinical trial with Resmetirom [47]). Also, efforts based on extensive metabolomics analyses in large patient groups (N=535 NASH patients [48], and n= 1099 NAFLD/NASH patients [49]) show that there are distinct patient groups. In the absence of any pharmacological treatment option in NAFLD, nutritional treatment approaches with both preventive and intervention potential to restore multi-organ metabolic homeostasis should be seriously considered to reduce the ever rising burden of NAFLD. Hence, the nutritional strategies that we investigated in this thesis corrected metabolic derangements in multiple organs simultaneously to restore organ function. This more holistic approach differs from a classical pharmacological 'one-target approach' and often liver-centric in NAFLD. Hence, the combination of therapies with different but complementary mechanisms of actions such as nutritional interventions used in this thesis should be considered in the prevention and treatment of NAFLD.

References

1. Donnelly, K.L.; Smith, C.I.; Schwarzenberg, S.J.; Jessurun, J.; Boldt, M.D.; Parks, E.J. Sources of fatty acids stored in liver and secreted via lipoproteins in patients with nonalcoholic fatty liver disease. *J. Clin. Invest.* **2005**, *115*, 1343–1351.
2. Stanhope, K.L.; Schwarz, J.M.; Keim, N.L.; Griffen, S.C.; Bremer, A.A.; Graham, J.L.; Hatcher, B.; Cox, C.L.; Dyachenko, A.; Zhang, W.; et al. Consuming fructose-sweetened, not glucose-sweetened, beverages increases visceral adiposity and lipids and decreases insulin sensitivity in overweight/obese humans. *J. Clin. Invest.* **2009**.
3. Mirza, M.S. Obesity, Visceral Fat, and NAFLD: Queryingthe Role of Adipokines in the Progression ofNonalcoholic Fatty Liver Disease. *ISRN Gastroenterol.* **2011**, *2011*, 1–11.
4. Fain, J.N.; Madan, A.K.; Hiler, M.L.; Cheema, P.; Bahouth, S.W. Comparison of the release of adipokines by adipose tissue, adipose tissue matrix, and adipocytes from visceral and subcutaneous abdominal adipose tissues of obese humans. *Endocrinology* **2004**, *145*, 2273–2282.
5. Longo, M.; Zatterale, F.; Naderi, J.; Parrillo, L.; Formisano, P.; Raciti, G.A.; Beguinot, F.; Miele, C. Adipose tissue dysfunction as determinant of obesity-associated metabolic complications. *Int. J. Mol. Sci.* **2019**.
6. Lonardo, A.; Nascimbeni, F.; Ballestri, S.; Fairweather, D.L.; Win, S.; Than, T.A.; Abdelmalek, M.F.; Suzuki, A. Sex Differences in NAFLD: State of the Art and Identification of Research Gaps. *Hepatology* **2019**, *70*, 1457.
7. Gluchowski, N.L.; Becuwe, M.; Walther, T.C.; Farese, R. V. Lipid droplets and liver disease: from basic biology to clinical implications. *Nat. Rev. Gastroenterol. Hepatol.* **2017**, *14*, 343.
8. Fraile, J.M.; Palliyil, S.; Barelle, C.; Porter, A.J.; Kovaleva, M. Non-Alcoholic Steatohepatitis (NASH) – A Review of a Crowded Clinical Landscape, Driven by a Complex Disease. *Drug Des. Devel. Ther.* **2021**, *15*, 3997.
9. Mulder, P.; Liang, W.; Wielinga, P.; Verschuren, L.; Toet, K.; Havekes, L.; van den Hoek, A.; Kleemann, R. Macrovesicular steatosis is associated with development of lobular inflammation and fibrosis in diet-induced non-alcoholic steatohepatitis (NASH). *Inflamm. Cell Signal.* **2015**.
10. Fromenty, B.; Pessayre, D. Impaired mitochondrial function in microvesicular steatosis effects of drugs, ethanol, hormones and cytokines. *J. Hepatol.* **1997**, *26*, 43–53.
11. Skurk, T.; Alberti-Huber, C.; Herder, C.; Hauner, H. Relationship between Adipocyte Size and Adipokine Expression and Secretion. *J. Clin. Endocrinol. Metab.* **2007**, *92*, 1023–1033.
12. Skurk, T.; Alberti-Huber, C.; Herder, C.; Hauner, H. Relationship between adipocyte size and adipokine expression and secretion. *J. Clin. Endocrinol. Metab.* **2007**, *92*, 1023–1033.
13. Morrison, M.C.; Kleemann, R. Role of macrophage migration inhibitory factor in obesity, insulin resistance, type 2 diabetes, and associated hepatic co-morbidities: A comprehensive review of human and rodent studies. *Front. Immunol.* **2015**, *6*.
14. Vázquez, L.; Corzo-Martínez, M.; Arranz-Martínez, P.; Barroso, E.; Reglero, G.;

Torres, C. Bioactive Lipids. *Ref. Ser. Phytochem.* **2019**, 467–527.
15. Georgiadi, A.; Kersten, S. Mechanisms of Gene Regulation by Fatty Acids. *Adv. Nutr.* **2012**, *3*, 127.
16. Samstad, E.O.; Niyonzima, N.; Nymo, S.; Aune, M.H.; Ryan, L.; Bakke, S.S.; Lappegård, K.T.; Brekke, O.-L.; Lambris, J.D.; Damås, J.K.; et al. Cholesterol Crystals Induce Complement-Dependent Inflammasome Activation and Cytokine Release. *J. Immunol.* **2014**, *192*, 2837–2845.
17. Marí, M.; Caballero, F.; Colell, A.; Morales, A.; Caballeria, J.; Fernandez, A.; Enrich, C.; Fernandez-Checa, J.C.; García-Ruiz, C. Mitochondrial free cholesterol loading sensitizes to TNF- and Fas-mediated steatohepatitis. *Cell Metab.* **2006**, *4*, 185–198.
18. Petersen, M.C.; Shulman, G.I. Mechanisms of Insulin Action and Insulin Resistance. *Physiol. Rev.* **2018**, *98*, 2133.
19. Liakh, I.; Pakiet, A.; Sledzinski, T.; Mika, A. Methods of the Analysis of Oxylipins in Biological Samples. *Molecules* **2020**, *25*.
20. Belhaj, M.R.; Lawler, N.G.; Hoffman, N.J. Metabolomics and Lipidomics: Expanding the Molecular Landscape of Exercise Biology. *Metabolites* **2021**, *11*.
21. Koutoukidis, D.A.; Koshiaris, C.; Henry, J.A.; Noreik, M.; Morris, E.; Manoharan, I.; Tudor, K.; Bodenham, E.; Dunnigan, A.; Jebb, S.A.; et al. The effect of the magnitude of weight loss on non-alcoholic fatty liver disease: A systematic review and meta-analysis. *Metabolism.* **2021**, *115*.
22. Koutoukidis, D.A.; Jebb, S.A.; Tomlinson, J.W.; Cobbold, J.F.; Aveyard, P. Association of Weight Changes With Changes in Histological Features and Blood Markers in Nonalcoholic Steatohepatitis. *Clin. Gastroenterol. Hepatol.* **2022**, *20*, e538–e547.
23. Stine, J.G.; Munaganuru, N.; Barnard, A.; Wang, J.L.; Kaulback, K.; Argo, C.K.; Singh, S.; Fowler, K.J.; Sirlin, C.B.; Loomba, R. Change in MRI-PDFF and Histologic Response in Patients With Nonalcoholic Steatohepatitis: A Systematic Review and Meta-Analysis. *Clin. Gastroenterol. Hepatol.* **2021**, *19*, 2274-2283.e5.
24. Tamaki, N.; Munaganuru, N.; Jung, J.; Yonan, A.Q.; Loomba, R.R.; Bettencourt, R.; Ajmera, V.; Valasek, M.A.; Behling, C.; Sirlin, C.B.; et al. Clinical utility of 30% relative decline in MRI-PDFF in predicting fibrosis regression in non-alcoholic fatty liver disease. *Gut* **2022**, *71*, 983–990.
25. Schrader, M.; Costello, J.; Godinho, L.F.; Islinger, M. Peroxisome-mitochondria interplay and disease. *J. Inherit. Metab. Dis.* 2015.
26. Iozzo, P.; Bucci, M.; Roivainen, A.; Någren, K.; Järvisalo, M.J.; Kiss, J.; Guiducci, L.; Fielding, B.; Naum, A.G.; Borra, R.; et al. Fatty acid metabolism in the liver, measured by positron emission tomography, is increased in obese individuals. *Gastroenterology* **2010**, *139*, 846-856.e6.
27. Sunny, N.E.; Parks, E.J.; Browning, J.D.; Burgess, S.C. Excessive Hepatic Mitochondrial TCA Cycle and Gluconeogenesis in Humans with Nonalcoholic Fatty Liver Disease. *Cell Metab.* **2011**, *14*, 804.
28. Sinenko, S.A.; Starkova, T.Y.; Kuzmin, A.A.; Tomilin, A.N. Physiological Signaling Functions of Reactive Oxygen Species in Stem Cells: From Flies to Man. *Front. Cell Dev. Biol.* **2021**, *9*, 1994.
29. Chen, Z.; Tian, R.; She, Z.; Cai, J.; Li, H. Role of oxidative stress in the pathogenesis of nonalcoholic fatty liver disease. *Free Radic. Biol. Med.* **2020**, *152*, 116–141.

30. Morris, E.M.; Rector, R.S.; Thyfault, J.P.; Ibdah, J.A. Mitochondria and Redox Signaling in Steatohepatitis. *Antioxid. Redox Signal.* **2011**, *15*, 485.
31. Kapoor, G.; Chauhan, P.; Singh, G.; Malhotra, N.; Chahal, A. Physical Activity for Health and Fitness: Past, Present and Future. *J. Lifestyle Med.* **2022**, *12*, 9.
32. Riazi, K.; Azhari, H.; Charette, J.H.; Underwood, F.E.; King, J.A.; Afshar, E.E.; Swain, M.G.; Congly, S.E.; Kaplan, G.G.; Shaheen, A.A. The prevalence and incidence of NAFLD worldwide: a systematic review and meta-analysis. *Lancet Gastroenterol. Hepatol.* **2022**, *7*, 851–861.
33. Genné-Bacon, E.A. Thinking Evolutionarily About Obesity. *Yale J. Biol. Med.* **2014**, *87*, 99.
34. Fernández-Real, J.M.; Ricart, W. Insulin resistance and inflammation in an evolutionary perspective: The contribution of cytokine genotype/phenotype to thriftiness. *Diabetologia* **1999**, *42*, 1367–1374.
35. Loomba, R.; Friedman, S.L.; Shulman, G.I. Mechanisms and disease consequences of nonalcoholic fatty liver disease. *Cell* **2021**, *184*, 2537–2564.
36. Soeters, M.R.; Soeters, P.B. The evolutionary benefit of insulin resistance. *Clin. Nutr.* **2012**, *31*, 1002–1007.
37. Tsatsoulis, A.; Mantzaris, M.D.; Bellou, S.; Andrikoula, M. Insulin resistance: An adaptive mechanism becomes maladaptive in the current environment — An evolutionary perspective. *Metab. - Clin. Exp.* **2013**, *62*, 622–633.
38. Kratzer, J.T.; Lanaspa, M.A.; Murphy, M.N.; Cicerchi, C.; Graves, C.L.; Tipton, P.A.; Ortlund, E.A.; Johnson, R.J.; Gaucher, E.A. Evolutionary history and metabolic insights of ancient mammalian uricases. *Proc. Natl. Acad. Sci. U. S. A.* **2014**, *111*, 3763–3768.
39. Lanaspa, M.A.; Sanchez-Lozada, L.G.; Choi, Y.J.; Cicerchi, C.; Kanbay, M.; Roncal-Jimenez, C.A.; Ishimoto, T.; Li, N.; Marek, G.; Duranay, M.; et al. Uric Acid Induces Hepatic Steatosis by Generation of Mitochondrial Oxidative Stress: POTENTIAL ROLE IN FRUCTOSE-DEPENDENT AND -INDEPENDENT FATTY LIVER*. *J. Biol. Chem.* **2012**, *287*, 40732.
40. Cicerchi, C.; Li, N.; Kratzer, J.; Garcia, G.; Roncal-Jimenez, C.A.; Tanabe, K.; Hunter, B.; Rivard, C.J.; Sautin, Y.Y.; Gaucher, E.A.; et al. Uric acid-dependent inhibition of AMP kinase induces hepatic glucose production in diabetes and starvation: evolutionary implications of the uricase loss in hominids. *FASEB J.* **2014**, *28*, 3339.
41. Ruderman, N.B.; Carling, D.; Prentki, M.; Cacicedo, J.M. AMPK, insulin resistance, and the metabolic syndrome. *J. Clin. Invest.* **2013**, *123*, 2764.
42. Palma, R.; Pronio, A.; Romeo, M.; Scognamiglio, F.; Ventriglia, L.; Ormando, V.M.; Lamazza, A.; Pontone, S.; Federico, A.; Dallio, M. The Role of Insulin Resistance in Fueling NAFLD Pathogenesis: From Molecular Mechanisms to Clinical Implications. *J. Clin. Med.* **2022**, *11*.
43. Jornayvaz, R.; Gabriel-Medina, P.; Ferrer-Costa, R.; Rodriguez-Frias, F.; Ciudin, A.; Augustin, S.; Rivera-Esteban, J.; Pericàs, J.M.; Selva, D.M. Influence of Type 2 Diabetes in the Association of PNPLA3 rs738409 and TM6SF2 rs58542926 Polymorphisms in NASH Advanced Liver Fibrosis. **2022**.
44. Luukkonen, P.K.; Qadri, S.; Lehtimäki, T.E.; Juuti, A.; Sammalkorpi, H.; Penttilä, A.K.; Hakkarainen, A.; Orho-Melander, M.; Arola, J.; Yki-Järvinen, H. The PNPLA3-I148M Variant Confers an Antiatherogenic Lipid Profile in Insulin-resistant

Patients. *J. Clin. Endocrinol. Metab.* **2021**, *106*, e300–e315.
45. Bouter, K.E.C.; Bakker, G.J.; Levin, E.; Hartstra, A. V.; Kootte, R.S.; Udayappan, S.D.; Katiraei, S.; Bahler, L.; Gilijamse, P.W.; Tremaroli, V.; et al. Differential metabolic effects of oral butyrate treatment in lean versus metabolic syndrome subjects article. *Clin. Transl. Gastroenterol.* **2018**, *9*.
46. Ratziu, V.; Friedman, S.L. Why do so many NASH trials fail? *Gastroenterology* **2020**.
47. Harrison, S.A., Bashir, M., Moussa, S. E., McCarty, K., Pablo Frias, J., Taub, R., & Alkhouri, N. Effects of Resmetirom on Noninvasive Endpoints in a 36-Week Phase 2 Active Treatment Extension Study in Patients With NASH. *Hepatol. commun.* **2021**. 5(4), 573–588.
48. Morrison MC, Verschuren L, Salic K, Verheij J, Menke A, Wielinga PY, Iruarrizaga-Lejarreta M, Gole L, Yu W, Turner S, Caspers MPM, Martínez-Arranz I, Pieterman E, Stoop R, van Koppen A, van den Hoek AM, Mato JM, Hanemaaijer R, Alonso C, Kleemann R. Obeticholic Acid Modulates Serum Metabolites and Gene Signatures Characteristic of Human NASH and Attenuates Inflammation and Fibrosis Progression in Ldlr-/-.Leiden Mice. *Hepatol Commun*., **2018**.
49. Martínez-Arranz I, Bruzzone C, Noureddin M, Gil-Redondo R, Mincholé I, Bizkarguenaga M, Arretxe E, Iruarrizaga-Lejarreta M, Fernández-Ramos D, Lopitz-Otsoa F, Mayo R, Embade N, Newberry E, Mittendorf B, Izquierdo-Sánchez L, Smid V, Arnold J, Iruzubieta P, Castaño YP, Krawczyk M, Marigorta UM, Morrison MC, Kleemann R, Martín-Duce A, Hayardeny L, Vitek L, Bruha R, Fuente RA de la, Crespo J, Romero-Gomez M, Banales JM, Arrese M, Cusi K, Bugianesi E, Klein S, Lu SC, Anstee QM, Millet O, Davidson NO, Alonso C, Mato JM. Metabolic subtypes of patients with NAFLD exhibit distinctive cardiovascular risk profiles. *Hepatol.* **2022**.

Appendices

Summary

About the author

- Curriculum Vitae
- List of publications
- Overview of completed training activities

Dankwoord

Summary

Non-alcoholic fatty liver disease (NAFLD) is characterized by excessive fat accumulation in the liver. A healthy human liver contains little to no fat. If fat accumulates over 5% of the liver this is considered pathological as is the case in NAFLD. The excess fat in the liver affects liver cell function, causing damage and cell death. This can eventually lead to inflammation of the liver, a progressive condition called non-alcoholic steatohepatitis (NASH). This chronic damage can lead to scar formation and loss of liver function, the stage of disease when evident scarring is present is called liver fibrosis. It can take decades for NAFLD to develop, at first it is often asymptomatic, but it can be life-threatening in the advanced stages of disease. NAFLD is a serious disease; it currently affects 25-30% of the adult population, is the most common cause of liver transplants in young adults (<50 years of age) and is a leading cause of liver-related morbidity and mortality. NAFLD is prone to develop in obese persons that consume more energy (fat and sugars) than the body can handle. This chronic liver disease is strongly associated with the metabolic syndrome, a disorder characterized by increased blood lipid levels, and high insulin levels (reflective of insulin resistance).

The liver is a key metabolic organ that regulates energy homeostasis for our body, providing and regulating energy to tissues. For the liver to function properly it integrates signals from and sends out signals to other metabolic organs such as the adipose tissue, the gut, and the gut microbiota. Dysfunction of these other metabolic organs is thought to be involved in the development of NAFLD, which would make NALFD a multiple-organ disease. However, the complex multiple-organ pathophysiology disease is still incompletely understood. The lack of insight in temporal development and metabolic dysfunctions that underlie NAFLD development contribute to the fact that at present no approved treatments for NAFLD are available. As a consequence, NAFLD is currently considered to be a disease of unmet medical need, with an urgent requirement for innovative treatment strategies to correct the metabolic dysfunctions that underlie NAFLD development.

To study and diagnose NAFLD development over time in humans is very difficult as it would require routine tissue biopsies that are invasive, often painful, and not without risk. Therefore, we used a mouse model which has been developed to mimic human physiology and develops NAFLD when fed a surplus of calories similar to NAFLD patients. An advantage of the mouse model is that the disease develops much faster than in humans, in a matter of weeks instead of decades. This NAFLD mouse model allowed us to study crosstalk between organs over time and to assess the effect of innovative treatments in NAFLD. In addition, we used liver cell experiments to study more direct mechanisms of action of interventions.

In this thesis, we first aimed to unravel the sequence of metabolic dysfunctions events, in the liver, the gut and its microbiota, the adipose tissue and by measuring circulating factors secreted by these organs during NAFLD development in **chapter 2**. Results from this study demonstrate that dysfunction of a specific adipose tissue depot and the gut

precede development of NASH and liver fibrosis and thus may contribute to NAFLD development. Hence, new treatment strategies aiming at NAFLD development should not be limited to the liver. In addition, we underline the translational value of metabolic dysfunctions observed in our mouse model to those reported in humans.
With the insight into the temporal dynamics and chronology of these processes our second aim was to test innovative concepts that could potentially attenuate NAFLD development. These treatments either targeted processes in the liver directly, the white adipose tissue or the gut and its microbiota, or a combination of these to restore organ homeostasis.
In **chapter 3**, we used two nutritional supplements L-carnitine and nicotinamide riboside, which are considered to be 'fat burners' and are therefore thought to protect against the accumulation of fat in the liver. We demonstrated that the combination of L-carnitine and nicotinamide riboside, but not the individual treatments, reduced the accumulation of fat in the liver.
In **chapter 4**, we studied the effect of krill oil, a dietary supplement rich in specific lipids called omega-3 fatty acids, which humans cannot synthesize and must be obtained from diet. Omega-3 fatty acids were thought to have anti-inflammatory effects and to be beneficial against the development of the metabolic syndrome. We demonstrated that long-term krill oil treatment altered fat storage to a more favorable fat distribution, in more smaller fat cells (larger cells tend to secrete more proinflammatory factors). In addition, we used an advanced analysis platform to measure the concentrations of specific bioactive lipid metabolites in adipose and liver tissues. This analysis demonstrated that krill oil changed the composition of bioactive lipids involved in the inflammatory process. Indeed, krill oil created a more anti-inflammatory environment in both adipose tissue and the liver, which was confirmed with gene expression analysis in both tissues. Taken together, this chapter provided new insights into the mechanisms of action of health benefits from krill oil.
In **chapter 5**, two essential branched-chain amino acids, valine and isoleucine, were studied as an intervention treatment in established NAFLD. Previously a mix of amino acids containing valine and isoleucine was found to have beneficial effects on lipid metabolism. We demonstrated that individual treatment with each of the branched-chain amino acids valine or isoleucine (the latter having the most pronounced effects) was able to decrease lipid accumulation and inflammation in the liver.

Our final aim was to study organ crosstalk in NAFLD development, including the gut, adipose tissue, liver and to a smaller extent the brain.
In **chapter 6**, we studied correlations between (dys)function of the gut, adipose tissue and liver with the gut microbiota composition. We found that specifically the microbiota composition in the mucosa has more predictive value for organ function than the more often studied and more easily accessible fecal microbiota. It is possible that mucosal microbiota is more informative due to the closer proximity to the host and more constant and direct interaction of regulating the gut barrier.
In **chapter 7**, we studied the effects of prebiotic 2'-fucosyllactose. This prebiotic is a complex sugar that humans are not able to digest, but that can be digested by our gut microbiota. 2'-fucosyllactose and its metabolites have previously been shown to promote the growth of specific microbiota species and has been associated with improvements in

local gut health. Since the microbiota and gut can play a role in NAFLD development we studied whether 2'-FL could have beneficial effects on the liver. Indeed, we found that 2'-FL not only improved gut health but also directly reduced fat accumulation in the liver. More importantly, 2'-FL was able to reduce the accumulation of a specific lipid called diacylglycerol, which has been shown to play a causal role in insulin resistance. In line with this, we also found that the lowering of diacylglycerol in the liver was associated with lower insulin levels, indicative for improvements in insulin resistance.
In the last two chapters we tested the effects of supplementation with specific microbiota metabolites, called short chain fatty acids (SCFA). These SCFA are normally produced by our microbiota during breakdown of food in our gut. In **chapter 8**, we demonstrated that direct dietary supplementation of the SCFA butyrate was able to reduce NAFLD and liver fibrosis development. This effect seemed to be independent of the gut as the gut microbiota composition was largely unaffected and there was no effect on a gut permeability assay. The mechanism of action of the anti-fibrotic effect of butyrate was studied in cell experiments, in which we demonstrated that butyrate was able to directly inhibit the activation of cells that are responsible for the production of scar tissue/fibrosis in the liver. These effects were specific and dose dependent for butyrate, but not other SCFA such as acetate and caproate. Gene expression analysis on these cells allowed us to identify specific signaling pathways that are involved in the anti-fibrotic effects of butyrate.
In **chapter 9**, we explored the effects of a second SCFA intervention using propionate and caproate on NAFLD development and obesity-associated neuropathological changes. We found that caproate had no effects. In contrast, propionate improved functional connectivity between brain areas, structural integrity and anti-inflammatory signaling, while the animals were also more anxious and reduced signaling of cell structure formation that allows chemical signals between brain cells. Moreover, propionate had positive effects on metabolic risk factors, including lowering of blood pressure, fat mass reduction and in the liver propionate was able to attenuate inflammation and fibrosis development.

In conclusion, we provide new insights into the dynamics of metabolic dysfunctions in multiple organs during NAFLD development. These insights underline the importance of inter-organ crosstalk in the development of new strategies aiming to prevent or attenuate NAFLD. The metabolic dysfunctions were targeted with a variety of novel nutritional intervention approaches to study their potential to attenuate NAFLD. The results of these studies demonstrate the remarkable impact of nutrients alone or in combination as a treatment for NAFLD.

Curriculum Vitae

Eveline Gart was born on 1 April 1993 in Barendrecht. After finishing her pre-university education at the Dalton Lyceum Barendrecht, she started studying Biomedical Sciences at the Leiden University Medical Center (LUMC) in 2012.

As part of her Bachelor degree, she performed a research internship at the cell biology department of the LUMC. In this internship she studied the potential transport function of double-cortin like (DCL) in the suprachiasmatic nucleus in relation to the regulation of the circadian rhythm in this area of the brain.

After obtaining her bachelor's degree in Biomedical Sciences, she started with her Master degree of Biomedical Sciences and followed an interdisciplinary minor Brain and Cognition. As part of her Master degree, she performed two research internships, the first internship at the endocrinology department (LUMC) in which she investigated the role of the circadian rhythm of corticosterone (cortisol in humans) in regulating metabolism in brown adipose tissue. Her second internship was performed at the department of Metabolic Health Research at TNO in which she investigated side effects of tyrosine kinase inhibitors (TKIs) on plasma lipids. In this internship she also studied potential underlying mechanisms of these side effects using radioisotope labeling studies. In the same year she also wrote a review on the relationship between circadian rhythm and plasma lipids.

Eveline started her PhD in 2017 at the department of Human and Animal Physiology at Wageningen in a joint project with the department of Metabolic Health Research at TNO. During her PhD she designed and performed several preclinical studies as part of the Public-Private-Partnership ProLiver (in collaboration with companies such as Pfizer, AKER biomarine, Heel GmbH, BASF and Quickzyme). A part of the results from this research are presented in this thesis (see list of publications appendices for a complete overview of (co)authored articles). During her PhD, Eveline successfully participated in the educational program of the Graduate School VLAG (see overview of completed training activities appendices).

List of publications

1) Hoeke G, Wang Y, van Dam AD, Mol IM, Gart E, Klop HG, van den Berg SM, Pieterman EH, Princen HMG, Groen AK, Rensen PCN, Berbée JFP, Boon MR. Atorvastatin accelerates clearance of lipoprotein remnants generated by activated brown fat to further reduce hypercholesterolemia and atherosclerosis. Atherosclerosis. 2017 Dec;267:116-126. doi: 10.1016/j.atherosclerosis.2017.10.030. Epub 2017 Oct 26. PMID: 29121499.
2) Jacobs SAH, Gart E, Vreeken D, Franx BAA, Wekking L, Verweij VGM, Worms N, Schoemaker MH, Gross G, Morrison MC, Kleemann R, Arnoldussen IAC, Kiliaan AJ. Sex-Specific Differences in Fat Storage, Development of Non-Alcoholic Fatty Liver Disease and Brain Structure in Juvenile HFD-Induced Obese Ldlr-/-.Leiden Mice. Nutrients. 2019 Aug 10;11(8):1861. doi: 10.3390/nu11081861. PMID: 31405127; PMCID: PMC6723313.
3) Gart E, Souto Lima E, Schuren F, de Ruiter CGF, Attema J, Verschuren L, Keijer J, Salic K, Morrison MC, Kleemann R. Diet-Independent Correlations between Bacteria and Dysfunction of Gut, Adipose Tissue, and Liver: A Comprehensive Microbiota Analysis in Feces and Mucosa of the Ileum and Colon in Obese Mice with NAFLD. Int J Mol Sci. 2018 Dec 20;20(1):1. doi: 10.3390/ijms20010001. PMID: 30577415; PMCID: PMC6337295.
4) Salic K*, Gart E*, Seidel F, Verschuren L, Caspers M, van Duyvenvoorde W, Wong KE, Keijer J, Bobeldijk-Pastorova I, Wielinga PY, Kleemann R. Combined Treatment with L-Carnitine and Nicotinamide Riboside Improves Hepatic Metabolism and Attenuates Obesity and Liver Steatosis. Int J Mol Sci. 2019 Sep 5;20(18):4359. doi: 10.3390/ijms20184359. PMID: 31491949; PMCID: PMC6770226.
*shared first authorship.
5) Tengeler AC*, Gart E*, Wiesmann M, Arnoldussen IAC, van Duyvenvoorde W, Hoogstad M, Dederen PJ, Verweij V, Geenen B, Kozicz T, Kleemann R, Morrison MC, Kiliaan AJ. Propionic acid and not caproic acid, attenuates nonalcoholic steatohepatitis and improves (cerebro) vascular functions in obese $Ldlr^{-/-}$ .Leiden mice. FASEB J. 2020 Jul;34(7):9575-9593. doi: 10.1096/fj.202000455R. Epub 2020 May 30. PMID: 32472598.
*shared first authorship.
6) Mueller AM, Kleemann R, Gart E, van Duyvenvoorde W, Verschuren L, Caspers M, Menke A, Krömmelbein N, Salic K, Burmeister Y, Seilheimer B, Morrison MC. Cholesterol Accumulation as a Driver of Hepatic Inflammation Under Translational Dietary Conditions Can Be Attenuated by a Multicomponent Medicine. Front Endocrinol (Lausanne). 2021 Mar 18;12:601160. doi: 10.3389/fendo.2021.601160. PMID: 33815271; PMCID: PMC8014004.
7) Gart E, Salic K, Morrison MC, Caspers M, van Duyvenvoorde W, Heijnk M, Giera M, Bobeldijk-Pastorova I, Keijer J, Storsve AB, Hals PA, Kleemann R. Krill Oil Treatment Increases Distinct PUFAs and Oxylipins in Adipose Tissue and Liver and Attenuates Obesity-Associated Inflammation via Direct and Indirect Mechanisms. Nutrients. 2021 Aug 18;13(8):2836. doi: 10.3390/nu13082836. PMID: 34444996; PMCID: PMC8401900.
8) Gart E, van Duyvenvoorde W, Toet K, Caspers MPM, Verschuren L, Nielsen MJ, Leeming DJ, Souto Lima E, Menke A, Hanemaaijer R, Keijer J, Salic K, Kleemann R, Morrison MC. Butyrate Protects against Diet-Induced NASH and Liver Fibrosis and Suppresses Specific

Non-Canonical TGF-β Signaling Pathways in Human Hepatic Stellate Cells. Biomedicines. 2021 Dec 20;9(12):1954. doi: 10.3390/biomedicines9121954. PMID: 34944770; PMCID: PMC8698820.

9) Morrison MC, Gart E, Duyvenvoorde WV, Snabel J, Nielsen MJ, Leeming DJ, Menke A, Kleemann R. Heat-Inactivated Akkermansia muciniphila Improves Gut Permeability but Does Not Prevent Development of Non-Alcoholic Steatohepatitis in Diet-Induced Obese Ldlr-/-.Leiden Mice. Int J Mol Sci. 2022 Feb 19;23(4):2325. doi: 10.3390/ijms23042325. PMID: 35216439; PMCID: PMC8878538.
10) Gart E, Salic K, Morrison MC, Giera M, Attema J, de Ruiter C, Caspers M, Schuren F, Bobeldijk-Pastorova I, Heer M, Qin Y, Kleemann R. The Human Milk Oligosaccharide 2'-Fucosyllactose Alleviates Liver Steatosis, ER Stress and Insulin Resistance by Reducing Hepatic Diacylglycerols and Improved Gut Permeability in Obese Ldlr-/-.Leiden Mice. Front Nutr. 2022 Jun 17;9:904740. doi: 10.3389/fnut.2022.904740. PMID: 35782914; PMCID: PMC9248376.
11) Gart E, van Duyvenvoorde W, Caspers MPM, van Trigt N, Snabel J, Menke A, Keijer J, Salic K, Morrison MC, Kleemann R. Intervention with isoleucine or valine corrects hyperinsulinemia and reduces intrahepatic diacylglycerols, liver steatosis, and inflammation in Ldlr-/-.Leiden mice with manifest obesity-associated NASH. FASEB J. 2022 Aug;36(8):e22435. doi: 10.1096/fj.202200111R. PMID: 35830259.
12) Gart E, Duyvenvoorde W, Snabel JM, de Ruiter C, Attema J, Caspers MPM, Lek S, van Heuven B, Speksnijder AGCL, Giera M, Menke A, Salic K, Bence KK, Tesz GJ, Keijer J, Kleemann R, Morrison MC. Translational characterization of the temporal dynamics of metabolic dysfunctions in liver, adipose tissue and the gut during diet-induced NASH development in Ldlr-/-.Leiden mice. Heliyon. 2023 Feb 24;9(3):e13985. doi: 10.1016/j.heliyon.2023.e13985. PMID: 36915476; PMCID: PMC10006542.

Overview of completed training activities

Discipline-specific activities
Energy metabolism and body composition in nutrition and health research (VLAG)
Gut-liver axis monothematic conference (EASL)
Muscle clocks and diabetes (NIN)
European nutrition conference (FENS)
NAFLD summit (EASL)
International liver conference (EASL)
Fatty Liver Disease and multi-system complications (Keystone)
The liver meeting (AASLD)
The International Society for the Study of Fatty Acids and Lipids congress (ISSFAL)
International conference on fatty liver (EASL)
Inter Organ Crosstalk in Non-Alcoholic Steatohepatitis (Keystone Symposia)
ProLiver consortium meetings (TNO)

General courses
Scientific artwork – Adobe illustrator & photoshop (WUR library)
Introduction to R (VLAG)
Applied statistics (VLAG)
Efficient writing strategies (Wageningen into languages)
Brain friendly working and writing (WGS)
Reviewing a scientific manuscript (WUR library)
PhD week (VLAG)

Other activities
Writing of PhD research proposal
Weekly Tuesday morning department meeting at HAP or TNO
Coordination of the TNO Metabolic Health Research science meetings

Dankwoord

The end! Na ruim 4 jaar werk aan mijn PhD project is het nu tot een einde gekomen met dit boekje. Heel veel mensen hebben hieraan bijgedragen en ik wil daarom graag eindigen met een woord van dank.

Allereerst wil ik graag mijn (co-)promotoren Martine, Jaap en Robert bedanken.

Martine en **Robert**, wat ben ik blij dat ik jullie als begeleiders heb getroffen. **Martine**, jouw input was absoluut onmisbaar voor de totstandkoming van dit proefschrift. Ik heb de samenwerking met jou altijd als buitengewoon plezierig ervaren. Het enthousiasme voor onderzoek en hoe je hierover kan vertellen zijn inspirerend. Bedankt dat ik altijd bij je terecht kan om te sparren en het vertrouwen dat je mij hebt gegeven. **Robert**, dankjewel voor al je creatieve ideeën en je kritische, maar constructieve feedback. Door jou ben ik gegroeid als wetenschapper. Al vroeg heb je mij iets heel belangrijks meegegeven, om te proberen los te laten wat anderen denken, wat dogma's zijn, wat concepten zijn of denkbeelden waarin mensen blijven hangen, als iedereen hetzelfde vindt wordt het één grote zelf-bewieroking van hoe prachtig alles is. Je vrolijkheid en enthousiasme over onderzoek inspireren mij. Ik heb genoten van onze brainstormsessies en interessante theorieën van alle podcasts die je deelde! Beste **Jaap,** ondanks dat we elkaar niet vaak zagen heb ik onze samenwerking erg prettig ervaren. Bedankt voor de discussies, alle ideeën en frisse blik op mijn onderzoeksresultaten!

Leden van mijn thesis committee**, prof. dr. Eric Hazebroek**, **prof. dr. A.J. Han Moshage, dr. H.A.M. Rick Mutsaers** en **dr. Debby PY Koonen** dank jullie wel voor de tijd en moeite om mijn thesis te lezen en deze met mij te bediscussiëren voor mijn promotie.

Every one of the ProLiver team, thank you for the pleasant partnership, your interest and support over the years. In het bijzonder wil ik nog **Ivana**, **Robert O, Elsbet** en **Kanita** bedanken voor de fijne samenwerking, mede door jullie organisatie en inzet is het ProLiver consortium een groot succes geworden. **Kanita**, ik wil jou ook heel erg bedanken voor de begeleiding en de leerzame momenten aan het begin van mijn promotie traject. Ik bewonder je keuze om een andere weg in te slaan!

Alle (oud) collega's van TNO wil ik bedanken voor de samenwerking en ontzettend leuke tijd die ik heb gehad tijdens mijn promotieonderzoek. Door jullie gezelligheid ga ik nog altijd met veel plezier naar werk. Daarnaast natuurlijk heel erg veel dank voor al jullie bijdragen aan de studies en de manuscripten die de basis vormen van dit proefschrift, zonder jullie zou dit proefschrift niet bestaan. **Marianne, Elsbet,** en **Hans** wat gaat de tijd toch snel! Dank jullie wel voor de mooie kans die jullie mij hebben gegeven om bij TNO te starten, en de allerleukste stage ervaring. Jullie zorgden er zo voor dat ik ruim vier jaar geleden een vliegende start kon maken met mijn promotietraject. Dankjewel **Elsbet** dat ik altijd bij jou terecht kon met vragen en voor al je hulp bij mijn experimenten. Nog altijd geldt: zolang je maar doet wat Elsbet zegt dat moet, komt het allemaal wel goed!

Wim, vanaf dag één van mijn promotie heb jij mij wegwijs gemaakt bij het uitvoeren van alle dierstudies voor ProLiver. Dankjewel voor al je hulp en ondersteuning, jouw positieve energie maakt mij altijd vrolijk! **Marianne, Nicole** en **Nanda**, dank jullie wel voor de ervaring om in de aller gezelligste kamer van TNO te zitten voordat we overgingen naar een kantoortuin. Ook dank voor de hulp om mijn bloedsuikerniveau wat op te krikken met de snoep pot. **Jessica**, ik bewonder jouw werklust en efficiëntie in experimenten draaien, jouw tips hebben veel geholpen bij het opzetten en uitvoeren van mijn experimenten. **Karin en Roeland,** dank voor jullie begeleiding in de wondere wereld van het celkweken en aanstekelijke enthousiasme voor onderzoek doen. **Christa, Joline, Anita, Simone, en Marijke** dank jullie wel voor al jullie lab support, maar ook alle gezellige momenten binnen en buiten het lab. **Aswin** heel erg bedankt voor jouw enthousiasme en inzichten in de histopathologie, jouw hulp bij levers scoren was essentieel voor veel van de hoofdstukken in dit boekje waarvoor ik je eeuwig dankbaar ben. Verder bedank ik **Anita, Reinout, Geurt en Arianne** voor alle input tijdens bureaustoelgesprekken en koffiepauzes! **Everton**, **Martien en Lars** heel erg bedankt voor al jullie hulp bij de microbiota en genexpressie analyses die een belangrijk onderdeel vormen van de manuscripten in dit boekje. Lieve Adri, de koffiepauzes zonder jou levensavonturen zijn niet hetzelfde, we gaan je missen bij TNO!

Lieve “Jeugd van TNO”**, Nikki**, **Florine**, **José** en **Jelle**, dank jullie wel voor alle gezelligheid en support bij de laatste loodjes van mijn eigen promotie traject, mede-aios jullie gaan er ook komen! Nikki, mede door jou heb ik de eerste stap gewaagd om bij TNO te beginnen, bedankt voor jouw top advies. Het is altijd gezellig om met jou samen te werken en dank voor alle hulp bij mijn experimenten. Ik ben ontzettend blij dat jij een van mijn paranimfen wilt zijn. Florine, it is always fun when you are around and I admire your positive energy you bring with you. José, de laatste tijd ben jij mijn vaste buurvrouw en mede AIO in de kantoortuin, de gezellige bureaustoelgesprekken en jouw humor maken het nooit saai om naast jou te werken. Ik voel me vereerd dat jij een van mijn paranimfen wilt zijn.

Ook wil ik mijn collega’s in de kantoortuin bedanken waarmee ik misschien niet direct heb samengewerkt, maar die ik dagelijks zag in de wandelgangen en het koffie apparaat. Dank jullie wel voor alle gezelligheid, zowel op de werkvloer, de borrels en feestjes.

Everyone at HAP, even though I was not often there you always made me feel welcome. In het bijzonder wil ik **Corine en Irene** heel erg bedanken voor jullie interesse en behulpzaamheid vanuit Wageningen tijdens mijn PhD traject.

Ook buiten het werk zijn verschillende mensen een grote energiebron voor me geweest tijdens mijn promotietraject. Lieve meiden van de middelbare school, **Roosmarijn, Esther, Tessa, Sophie, Savannah, Conny, Merve, Mubbecel en Aicha,** ook al zitten we inmiddels verspreid binnen of buiten Nederland ben ik blij met jullie vriendschap. Wat we ook doen het is altijd gezellig met jullie en ik hoop dat we nog heel veel mooie momenten uit ons leven met elkaar gaan delen. Bedankt voor jullie belangstelling, dit is dus waar ik de afgelopen jaren mee bezig ben geweest.

Anamarija en Julia, mijn allerliefste sportmaatjes, dank voor alle gezellige uurtjes naast het werk. Jullie zijn heel belangrijk geweest om even los te komen van mijn PhD, om vervolgens weer met frisse moed verder te gaan!

Ook de steun, interesse en liefde vanuit mijn familie is voor mij van onschatbare waarde geweest.

Lieve **Martijn**, jij weet mij altijd aan het lachen te maken, ik ben enorm trots dat jij mijn grote broer bent! Lieve **Denise**, ik had me geen leukere schoonzus kunnen wensen. Lieve **oudjes, pap en mam**, er zijn geen woorden genoeg om jullie te bedanken voor jullie vertrouwen in mij, en alle liefde en steun die jullie mij hebben gegeven. Mam, extra dank voor jouw luisterend oor en je goede adviezen, jij wist mij altijd te helpen met alles te relativeren. Lieve **Sven**, jij hebt alles van dichtbij meegemaakt. Jou wil ik bedanken voor je eindeloze begrip en flexibiliteit tijdens dit traject. Ik ben blij en dankbaar dat ik jou aan mijn zijde heb, voor je hulp en vertrouwen dat jij mij geeft!

Bedankt allemaal!

The studies presented in this thesis were performed at the Gaubius Laboratory of TNO, Leiden, the Netherlands. The research was in part financially supported by the public-private partnership (PPP) ProLiver, a collaboration project that is co-funded by a PPP Allowance made available by Health~Holland, Top Sector Life Sciences & Health, to stimulate public-private partnerships. The studies were also supported by TNO Research Programs Food and Nutrition and Biomedical Health (PMC 9 and PMC 13).

The printing of this thesis was kindly supported by TNO, Metabolic Health Research, the Daan Traas fonds and Human and Animal Physiology, Wageningen University and Research.

Cover design by Stefanie van den Herik - Herikmedia

Printed by ProefschriftMaken on FSC-certified paper